NUREG/CR-5407
SAND93-0234

Assessment of the Impact of Degraded Shear Wall Stiffnesses on Seismic Plant Risk and Seismic Design Loads

Prepared by
E. W. Klamerus, M. P. Bohn/SNL
J. J. Johnson, A. P. Asfura, D. J. Doyle/EQE

Sandia National Laboratories
Operated by
Sandia Corporation

EQE Engineering, Inc.

Prepared for
U.S. Nuclear Regulatory Commission

AVAILABILITY NOTICE

Availability of Reference Materials Cited in NRC Publications

Most documents cited in NRC publications will be available from one of the following sources:

1. The NRC Public Document Room, 2120 L Street, NW., Lower Level, Washington, DC 20555-0001

2. The Superintendent of Documents, U.S. Government Printing Office, Mail Stop SSOP, Washington, DC 20402-9328

3. The National Technical Information Service, Springfield, VA 22161

Although the listing that follows represents the majority of documents cited in NRC publications, it is not intended to be exhaustive.

Referenced documents available for inspection and copying for a fee from the NRC Public Document Room include NRC correspondence and internal NRC memoranda; NRC bulletins, circulars, information notices, inspection and investigation notices; licensee event reports; vendor reports and correspondence; Commission papers; and applicant and licensee documents and correspondence.

The following documents in the NUREG series are available for purchase from the GPO Sales Program: formal NRC staff and contractor reports, NRC-sponsored conference proceedings, international agreement reports, grant publications, and NRC booklets and brochures. Also available are regulatory guides, NRC regulations in the *Code of Federal Regulations*, and *Nuclear Regulatory Commission Issuances*.

Documents available from the National Technical Information Service include NUREG-series reports and technical reports prepared by other Federal agencies and reports prepared by the Atomic Energy Commission, forerunner agency to the Nuclear Regulatory Commission.

Documents available from public and special technical libraries include all open literature items, such as books, journal articles, and transactions. *Federal Register* notices, Federal and State legislation, and congressional reports can usually be obtained from these libraries.

Documents such as theses, dissertations, foreign reports and translations, and non-NRC conference proceedings are available for purchase from the organization sponsoring the publication cited.

Single copies of NRC draft reports are available free, to the extent of supply, upon written request to the Office of Administration, Distribution and Mail Services Section, U.S. Nuclear Regulatory Commission, Washington, DC 20555-0001.

Copies of industry codes and standards used in a substantive manner in the NRC regulatory process are maintained at the NRC Library, 7920 Norfolk Avenue, Bethesda, Maryland, for use by the public. Codes and standards are usually copyrighted and may be purchased from the originating organization or, if they are American National Standards, from the American National Standards Institute, 1430 Broadway, New York, NY 10018.

NUREG/CR-5407
SAND93-0234

Assessment of the Impact of Degraded Shear Wall Stiffnesses on Seismic Plant Risk and Seismic Design Loads

Manuscript Completed: January 1994
Date Published: February 1994

Prepared by
E. W. Klamerus, M. P. Bohn, Sandia National Laboratories
J. J. Johnson, A. P. Asfura, D. J. Doyle, EQE Engineering

Sandia National Laboratories
Albuquerque, NM 87185

EQE Engineering, Inc.
44 Montgomery Street
San Francisco, CA 94104

Prepared for
Division of Engineering
Office of Nuclear Regulatory Research
U.S. Nuclear Regulatory Commission
Washington, DC 20555-0001
NRC FIN A1851

ABSTRACT

Test results sponsored by the USNRC have shown that reinforced shear wall (Seismic Category I) structures exhibit stiffnesses and natural frequencies that are smaller than those calculated in the design process. The USNRC has sponsored Sandia National Laboratories to perform an evaluation of the effects of the reduced frequencies on several existing seismic Probabilistic Risk Assessments (PRAs) in order to determine the seismic risk implications inherent in these test results. This report presents the results for the reevaluation of the seismic risk for three nuclear power plants: the Peach Bottom Atomic Power Station, the Zion Nuclear Power Plant, and Arkansas Nuclear One - Unit 1 (ANO-1).

Increases in core damage frequencies for seismic initiated events at Peach Bottom were 25 to 30 percent (depending on whether LLNL or EPRI hazard curves were used). At the ANO-1 site, the corresponding increases in plant risk were 10 percent (for each set of hazard curves). Finally, at Zion, there was essentially no change in the computed core damage frequency when the reduction in shear wall stiffness was included.

In addition, an evaluation of deterministic "design-like" structural dynamic calculations with and without the shear stiffness reductions was made. Deterministic loads calculated for these two cases typically increased on the order of 10 to 20 percent for the affected structures.

CONTENTS

CONTENTS (continued)

FIGURES

FIGURES (Continued)

TABLES

TABLES

ACKNOWLEDGEMENTS

The authors would like to thank our program manager, Dr. Roger Kenneally, U.S. Nuclear Regulatory Commission for his continuing support of this work in providing an effective liaison with Los Alamos National Laboratory and the ASCE Working Group on Shear Wall Stiffnesses, and in obtaining draft material for us in a timely fashion. We would also like to express our appreciation to Dr. Joel G. Bennett and Dr. Charles R. Farrar of Los Alamos National Laboratory for their active assistance in providing us with their test results and interpreting their results for us in light of the goals of this project. Finally, we would like to express our special appreciation to Berlinda Gonzales for her skilled and conscientious production of this report.

EXECUTIVE SUMMARY

The U.S. Nuclear Regulatory Commission has been sponsoring tests at Los Alamos National Laboratory on the dynamic response of Seismic Category I reinforced concrete shear wall structures. As test results accumulated, it became clear that there was a significant difference between as-calculated and measured shear wall stiffnesses and frequencies, and that these differences existed both in static and dynamic tests. For very low level tests, measured frequencies were found to range between 50% and 100% of the computed values. During simulated earthquake tests, measured frequencies were found to further decrease as the earthquake level increased. The observed differences between calculated and measured stiffnesses and frequencies represents a potentially important issue in the seismic design and safety of nuclear power plants.

In order to assess the importance of this "frequency difference" issue the U.S. Nuclear Regulatory Commission funded Sandia National Laboratories to reevaluate several existing seismic PRAs by modeling and incorporating the effects of the frequency reductions. This report presents the results for the reevaluation of the seismic risk for three nuclear power plants: the Peach Bottom Atomic Power Station, the Zion Nuclear Power Plant, and Arkansas Nuclear One - Unit 1 (ANO-1).

The three sites were chosen to reflect a reasonably broad range of plant and site conditions. Two types of PWRs (ANO-1 and Zion) and one BWR (Peach Bottom) were selected. These particular plants were selected because seismic PRAs had already been performed on these plants, and all structural models and Boolean plant system logic equations were available (or could be easily developed by extension of existing work). These site choices also reflected a broad range of physical site conditions. That is, Peach Bottom is a hard rock site. ANO-1 is characterized by very stiff soil. Finally, the Zion site is a layered soil site having 110 feet of soil overlaying bedrock.

In this study we developed a shear wall stiffness degradation model based on experimental results from tests performed at Los Alamos National Laboratory. This model predicts the reduction in stiffness of shear walls as a function of shear stress. It includes an initial reduction in shear stiffness to 75% of theoretical, with further decreases in stiffness for shear stresses above 150 psi.

For each site, a suite of earthquakes was selected (appropriate to the site) and dynamic response analyses using the suite of earthquakes were performed. These dynamic response analyses were performed in iterative fashion, in which the method of successive approximations was used to incorporate the reduction in stiffness with calculated shear stress for each wall. In each case, the dynamic response analyses were performed at at least three different earthquake levels (corresponding roughly to 1 SSE, 3 SSE, and 5 SSE). These calculations, performed with and without shear wall stiffness reduction, provided the basis for estimating the

impact of the reduction in shear wall stiffness on the responses of the various floor slabs within the buildings. From these calculations, new loads and responses were computed, from which two sets of probabilities of structural and component failures were determined. Applying these two sets of probabilities (with and without stiffness reduction) to the PRA accident sequence calculations will result in two different core damage frequencies, which can then be compared to estimate the effect of reduced stiffnesses.

First and foremost, the impact of the reduction in shear wall stiffness on computed core damage frequency was found to be very plant specific. The largest impact occurs for those plants in which certain critical equipment is located in structures which experience a significant increase in response with reduction in shear wall stiffness. For example, increases in mean core damage frequencies at Peach Bottom were 25 to 30 percent (depending on whether LLNL or EPRI hazard curves were used). At the ANO-1 site, the corresponding increases in plant risk were 10 percent (for each set of hazard curves). Although these might appear to be a significant increase in core damage frequency, they are small in a PRA context. Finally, at Zion, there was essentially no change in the computed core damage frequency when a reduction in shear wall stiffness was included.

A second conclusion is that (at any given site) the impact of the reduction of shear wall stiffness is very much structure specific, and is likely to vary amongst the important structures at the site. The largest increase in response occurs for structures which have natural modes of vibration with frequencies in the 7 to 12 Hz range.

Finally, an evaluation of deterministic "design-like" structural dynamic calculations with and without the shear stiffness reductions was made. Deterministic loads calculated for these two cases typically increased on the order of 10 to 20 percent for the affected structures. In general, this increase is felt to be a reasonable upper bound to the expected changes in loads for a deterministic design calculation, because the reduction in shear wall stiffness with stress is relatively small at the stresses which are experienced by these structures at design earthquake levels. Thus, a general conclusion is that the calculated increase in shear wall loads from a deterministic "design-like" calculation at the SSE (approximately 10 to 20 percent) is well within the bounds of typical conservatism built into the design calculational process and into the design code allowables. Hence these studies do not indicate the need for any design re-analysis for typical shear wall structures at current nuclear power plants.

1.0 INTRODUCTION

The U.S. Nuclear Regulatory Commission has been sponsoring a program at Los Alamos National Laboratory (the Seismic Category I Structures Program) which is investigating the dynamic response of Seismic Category I reinforced concrete shear wall structures (exclusive of containments) subjected to seismic loads beyond their design basis. This work has been a combined analytical and experimental effort. Testing has been performed on isolated shear walls and on scale models of a diesel generator building (1/30 and 1/10 scale) and an auxiliary building (1/42 and 1/14 scale) as reported in References 1 through 4. Later, tests were performed on simpler box type models called TRG structures as reported in References 5 through 10.

In these test programs, both free vibration and small amplitude excitation tests have been performed, as well as subjecting the model to a set of (scaled) recorded earthquake time history (the 1940 N-S El Centro corrected record) simulations. The amplitude of the simulated earthquake time history was increased in steps for successive tests, to assess the effects of peak ground acceleration on response.

By 1986, as test results accumulated, it became clear that there was a significant difference existing between calculated shear wall stiffnesses and those inferred from both static and dynamic tests. In particular, for low level static and dynamic tests, measured frequencies were found to be 50 to 80 percent of the computed values. During the simulated earthquake time history tests, measured structure frequencies were found to decrease with increased levels of excitation, and reductions in stiffnesses down to as much as 25 percent of the calculated stiffness values were measured, which corresponds to a reduction in structural frequencies of up to 50 percent.

The observed differences between calculated and measured stiffnesses and frequencies represent a potentially important issue relative to the seismic design and safety of nuclear power plants, for the following reasons:

a. In the typical PWR and BWR power plant, most of the safety injection systems and piping, the emergency on-site power systems and the control room itself are located in shear wall Seismic Category I structures, and these structures have (calculated) fixed base frequencies typically in the 5 Hz to 20 Hz range.

b. Based on the LANL tests, and depending on the level and frequency content of the earthquake time history and the local soil conditions, these structures could have effective frequency reductions of up to 50 percent, i.e., in the range of 2.5 Hz to 10 Hz.

c. Most broad band strong motion recorded earthquake accelerograms have the majority of their energy in the 2 Hz to 8 Hz range. Thus if the structure has an effective frequency in this band,

the excitation of the structure would be greater than was considered in the design of the structure. Both the loads experienced by the structural members and in-structure floor acceleration spectra would be increased.

d. Since the (calculated) in-structure floor response spectra which are used to design and qualify safety equipment have been based on calculated structural stiffnesses and frequencies, it is possible that certain safety equipment could experience greater seismic loads than were specified for qualification.

Thus, this "frequency difference" issue has potentially important implications with respect to power plant operation during seismic events.

In order to assess the importance of this "frequency difference" issue, the U.S. NRC has funded Sandia National Laboratories to reevaluate three existing seismic PRAs incorporating the effects of the frequency reduction issue. As part of this work, analytical models for reduction in frequency will be developed from the LANL data. Finally, in addition to the probabilistic reevaluations, design-type deterministic calculations of plant response will be made for each of the three plants to assess the potential impact of the frequency reduction issue on the design of structures and on the floor spectra used in the equipment qualification process.

In 1989, a preliminary evaluation was performed for the Peach Bottom Atomic Power Station [Reference 11]. The amount of stiffness reduction used in this preliminary report was based only on the early LANL test results. Later, when all of the TRG-type structures were tested and results finalized, the reduction in stiffness was not as large as the early tests exhibited. However, there was still some significant reductions, especially at higher levels of nominal base shear stress.

A final stiffness reduction model was then chosen for re-analysis of the three plants, based on the latest LANL results and other similar tests. This model, and how it was arrived at, is discussed in chapter three. This new model is less conservative than the one used in the preliminary report, therefore it was necessary to re-analyze Peach Bottom using this updated model.

The three plants chosen for reevaluation using a reduced stiffness include both a Boiling Water Reactor (BWR) and two Pressurized Water Reactors (PWRs) in order to assess the effect of plant type on stiffness reduction. In addition, both a soil site and two rocks sites were chosen to be analyzed in order to assess the effect of soil-structure interaction on the plant response. The three plants chosen for this study are the Peach Bottom Atomic Power Station, Zion Nuclear Power Plant, and Arkansas Nuclear One - Unit 1. The results of the reevaluation for these three plants is discussed in chapter four.

2.0 THE SEISMIC PRA PROCESS AND POTENTIAL IMPACTS FROM THE "STIFFNESS REDUCTION" ISSUE

In this section, we present an overview of the seismic PRA calculational process, and identify points where incorporation of reduced (and degrading) structural stiffnesses would affect the risk results. Selected LANL test results are used to illustrate the potential effects of these frequency reductions.

Figure 2-1 illustrates schematically the general seismic PRA calculational procedure. The six steps are listed below:

1. Determine the local earthquake hazard.

2. Identify accident scenarios for the plant which lead to core damage (initiating events and event trees).

3. Determine failure modes for the plant safety and support systems (fault trees).

4. Determine fragilities (probabilistic failure criteria) for the important structures and components.

5. Determine the responses (accelerations or forces) of all structures and components (for each earthquake level).

6. Compute the frequency of core damage using the information from Steps 1 through 5.

Each of these steps and their relationship to the frequency reduction issues are described below.

2.1 Hazard Curve

The earthquake hazard at a given power plant site is characterized by a frequency plot which gives the probability of exceedance (per year) of different peak ground accelerations. Figure 2-2 shows this so-called hazard curve for the Zion Nuclear Power Plant, located at Zion, Illinois.

For a given site, this curve is derived from a combination of recorded earthquake data, estimated earthquake magnitudes of known events for which no data are available, review of local geological investigations, and use of expert judgment from seismologists and geologists familiar with the region in question. The region around the site (say within 100 km) is divided into zones, each zone having an (assumed) uniform mean rate of earthquake occurrence. This mean occurrence rate is determined from the historical record, as is the distribution of earthquake magnitudes. Then, for the region under consideration, an attenuation law is determined which relates the ground acceleration at the site to the ground acceleration at the earthquake source, as a function of the earthquake magnitude. The uncertainty in the attenuation law is specified by the standard deviation of the data (from which the law was derived) about the mean attenuation

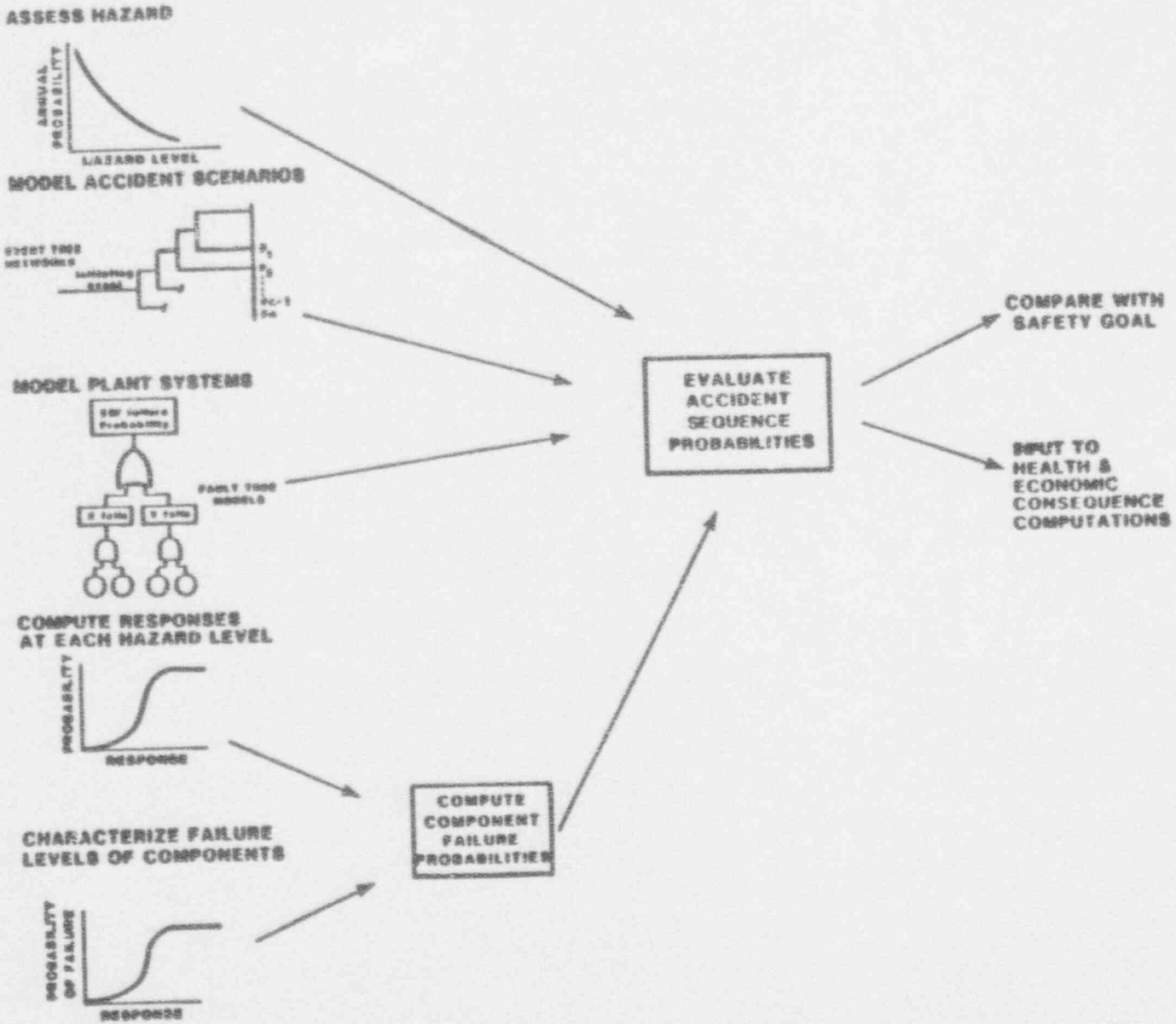

Figure 2-1 General Procedure for Analysis of Risk Due to Seismic Events

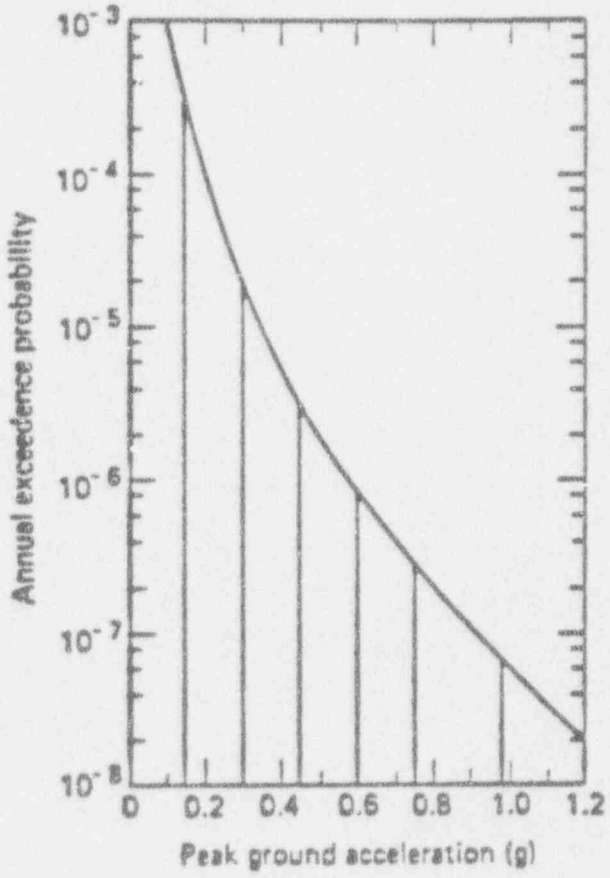

Figure 2-2 Seismic Hazard Curve for the Zion Site

curve. These four pieces of information (zonation, mean occurrence rate and magnitude distribution for each zone, and attenuation law) are then combined statistically to compute the hazard curve.

The low level of seismic activity and the lack of instrument records make it difficult to carry out seismic hazard analyses for the central and eastern United States using historical data alone. To augment the data base, current methodologies make use of the judgment of experts familiar with the area under consideration.

Expert opinion is solicited on input parameters for both the earthquake occurrence model and the ground motion (attenuation) model. Questions directed to experts cover the following areas: (1) the configuration of seismic source zones, (2) the maximum magnitude or intensity earthquake expected in each zone, (3) the earthquake activity rate and occurrence statistics associated with each zone, and (4) appropriate methods for predicting ground motion attenuation in the zones from an earthquake of a given size at a given distance.

Using the information provided by the experts, seismic hazard evaluations for the site are performed. The hazard results obtained using each expert's input are combined into a family of hazard estimates, often using some method of weighting.

The uncertainty in the seismic hazard at a site is represented by a family of hazard curves (with judgmentally assigned weights) or in a distributional form, with curves corresponding to different confidence levels depicted. Figure 2-3 illustrates a family of weighted curves, while Figure 2-4 shows a distributional presentation. Either format is suitable for propagation of uncertainty to obtain a probabilistic distribution of the computed core damage frequency.

To complete the description of the seismic hazard at the site, a ground motion input spectrum must be available. This is the spectra used in the design of the plant structures, and is commonly a broad band spectra scaled to the safe shutdown earthquake (SSE) level approved for the plant site. Alternatively, a site-specific spectra may be used. Typical broad band site-independent spectra used in existing plants are the Housner, Modified Housner, Newmark-Blume-Kapur or the Newmark-Hall spectra. In designing the plant, one or more time histories are generated which envelope the prescribed design spectra and these time histories (scaled to the OBE or SSE) are used to determine building loads as well as in-structure response spectra, which are used as the basis for specifying equipment qualification requirements.

In the risk requantifications to be performed in this program, the site design spectra used in the original PRA would be utilized in the median centered form used in the original seismic PRA. In general, a plant design spectrum is constructed such that there is a high confidence (often 84 percent) that the spectrum will not be exceeded. By contrast, in a seismic PRA, one needs a best-estimate median-centered input spectra, and an estimate of the uncertainty distribution of the spectra about that

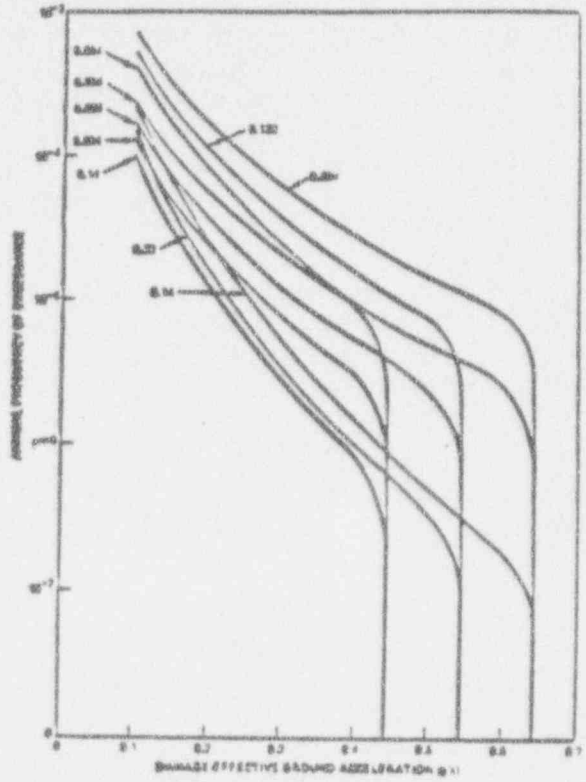

Figure 2-3 Typical Discrete Family of Hazard Curves

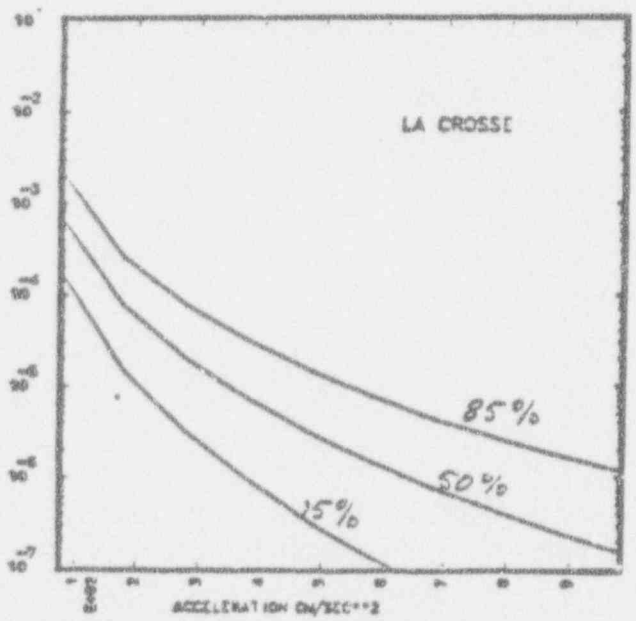

Figure 2-4 Typical Distributional Presentation of Hazard Curve Uncertainty

median. Hence, the original design ground motion input spectra must be scaled to a best estimate spectra. The point here is that, in these requantifications, the same scaling of design spectra to median centered spectra will be used as in the original seismic PRA, so direct comparability will be maintained.

2.2 Event Trees and Initiating Events

In the event of an earthquake or any other abnormal condition in a nuclear power plant, the plant safety systems act to bring the plant to a safe shutdown condition. In this step of the risk analysis process, the possible paths that a nuclear plant would follow are identified, given that an earthquake-related event has occurred which causes shutdown. These paths involve an initiating event and a success or failure designation for systems affecting the course of events, and are referred to as accident sequences.

2.3 Fault Trees

To determine failure modes for the plant safety systems, fault tree methodology is used. This methodology systematically identifies all groups of components in a system which, if they failed simultaneously, would result in failure of that system.

Construction of a fault tree begins by identifying the immediate causes of system failure. Each of these causes is then examined for more fundamental causes, until one has constructed a downward branching tree, at the bottom of which are failures not further reducible, i.e., failures of mechanical or electrical components due to all causes such as structural failure, human error, maintenance outage, etc. These lowest order failures on the fault tree are called basic events. Basic events due to seismic ground motions, random failures, human error, and test and maintenance outages are all to be included in the seismic analysis.

The main difference between an internal event fault tree for a safety system and an external event fault tree is that in an external event fault tree, consideration must be given to the physical location of the components, because the physical location determines the acceleration the component experiences, as well as to what extent secondary failures could be important. Examples of secondary failures are component failure caused by local masonry wall collapse or a high temperature/steam environment from a broken steam line. Hence, in performing the seismic analyses, the locations of all important pieces of equipment must be determined.

In general, the event trees and fault trees are combined (using Boolean logic and truncation as necessary) to obtain the accident sequences which define paths to core damage. Each accident sequence has the form

$$ACC_i = C_1 \cup C_2C_3 \cup C_4C_5C_6 \ldots$$

where the C_i are component failure probabilities, and "U" denotes the

logical Boolean "or" operator. Each group of component failures $C_iC_j \ldots C_k$ denotes the logical "and" of the failure events, and each such group is called a cutset. If all components in a cutset fail, then by construction, the accident sequence occurs, and core damage occurs. The frequency (per year) of the core damage associated with each particular accident sequence is determined by the conditional failure probabilities of the components in the cutsets (given that an earthquake of a certain size has occurred) integrated over the hazard curve (which provides the frequency that an earthquake exceeding any particular size will occur in any given year).

In this risk requantification effort, it is optimal to use the seismic accident sequences as defined in the original seismic PRA. However, this is the first point in the requantification process where the "frequency difference" issue can have an impact. In defining the accident sequences in the original seismic PRA, the analyst has "solved" the event trees by substituting into the logical fault trees, and in this process, only dominant component failures are kept. Otherwise, the resulting solution is prohibitively large and a full solution impossible to obtain. Thus, if the inclusion of the "frequency difference" issue results in increasing the failure probabilities of certain components which were dropped from the original seismic PRA accident sequences, then the requantification analyst will have no direct way of incorporating the now important component failures into the accident sequences for requantification. The analyst has recourse to several approaches to alleviate this situation, depending on the type of seismic PRA being requantified and some re-evaluation of the plant logic Boolean expressions may be required. In any event, it is important to note that the "frequency difference" issue may introduce new cutsets into the existing accident sequences.

2.4 Seismic Structural Responses

In general, one must obtain median (best estimate) spectral accelerations and their associated variability (both random and modeling uncertainties) for each component in the accident sequences as well as median loads and their variability for the critical walls and diaphragms of the buildings involving the NSSS and the safety systems. These response distributions are combined with the fragility distributions (as described below) so as to compute the failure probability of each component or structure as a function of PGA.

As a first step, it is necessary to obtain (from the FSAR and amendments) the underlying soil conditions and embedment depths. Second, it is necessary to obtain the structural design reports which summarize the lateral load resisting members and fixed or flexible based natural frequencies. These structural reports should contain the masses, stiffness description, and soil springs used in the original design analysis.

The effects of shallow or inhomogeneous soil conditions require analyses using the SHAKE code [12] in conjunction with previously generated results and approximate rules such as those of Roesset [13] to determine the

foundation input motion. Analyses are usually performed for several earthquake levels, and strain-dependent soil properties are determined in the process.

Finally, one computes the floor slab accelerations using a model (often a simple lumped mass beam element model) of the structure and foundation. One available approach uses the CLASSI code [14]. This code takes a fixed base eigensystem model of the structure (available from the design reports) and input-specified frequency-dependent soil impedances and computes the structural response (as well as variation in structural response if desired). The cost of running CLASSI is not great provided the structural model is available and soil impedances can be estimated.

In order to obtain a good estimate of the median acceleration response, analyses for a suite of (at least) ten time histories should be performed. Further, since the variation of the median response with earthquake level is required, these analyses should be performed at three peak ground acceleration levels (1SSE, 3SSE and 5SSE) as a minimum.

Impact of the "Frequency Difference" Issue on Seismic Structural Responses

The "frequency difference" issue can have a direct impact on the computed responses (structural loads, floor accelerations and in-structure floor response spectra). The extent of the impact, however, can be affected by soil-structure interaction, as will be discussed later.

Consider first the typical results of the LANL tests which constitute the "frequency difference" issue. These will be illustrated by test results for the 1/10 scale model of a diesel generator building (test series CERL-1). This is a two-story model as shown in Figure 2-5. As given in Reference 4, the results of static and free vibration tests showed the model to have a virgin (uncracked) lowest lateral vibration natural frequency of around 53 to 54 Hz. This same physical model was subjected to simulated (scaled) 1940 El Centro N-S time histories as base input motion, with each seismic test having a larger value of peak acceleration. The model failed by shear at the first floor shear wall on the eleventh test. The test series, input accelerations and measured frequencies of the model are shown in Table 2-1 (from Table VII of Reference [3]).

When these results were scaled up to the full size diesel generator building, a lowest natural frequency of 7.5 to 8.8 Hz was predicted. Figure 2-6 shows the variation in lowest frequency of the full size diesel generator building, versus (scaled up) base peak acceleration. A reduction in lowest frequency from about 8 Hz down to 3.5 Hz over the acceleration range of 0.15 g to 2.6 g is observed.

Figure 2-7 shows the damping ratios inferred from these same tests. As detailed in Reference 4, the inferred damping ratios are in the range of 5 to 8 percent up to 1 g (for the full size structure) and tend to increase for higher peak acceleration levels above 1 g.

Finally, consider Figures 2-8 through 2-10 which give response spectra

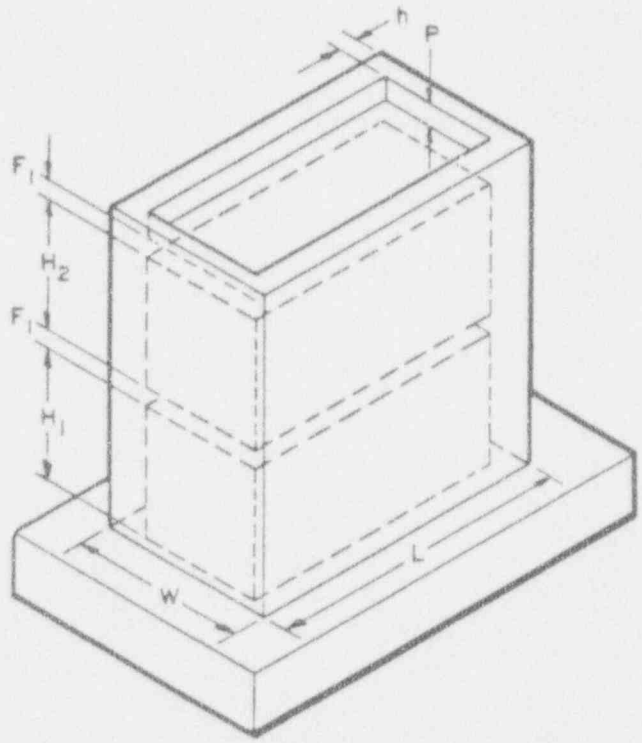

	h, F_1, F_2	W	L	H_1 & H_2	P	Wt/STORY*(lb)
1/30 SCALE	1 in.	10 in.	18 in.	7.25 in.	1 in.	47.7
1/10 SCALE	3 in.	30 in.	54 in.	21.75 in.	3 in.	1286
PROTOTYPE	30 in.	25 ft	45 ft	18 ft, 1.5 in.	30 in.	1,286,000

*BASE NOT INCLUDED

Figure 2-5 Diesel Generator Building, Model and Prototype [3]

Table 2-1

CERL Test Sequence

(Two-storied Structures, Simulated Seismic, with Added Mass)

Structure	Test (No.)	Input Level Y_{pk}(g)	Measured First Mode Frequency f_1(Hz)	Remarks
CERL #1	1	0.7	54	1
1/10-Scale	2	1.2	54	
CERL	3	2.0	51	
	4	2.7	50	
	5	3.5	49	
	6	4.7	49	
	7	7.0	44	
	8	9.0	41	
	9	10.0	38	
	10	12.0	24	
	11	16.0	--	2

Remarks:

1. Low-level tests with no mass added prededed this test.
2. Structure failed by shear of first-story wall.

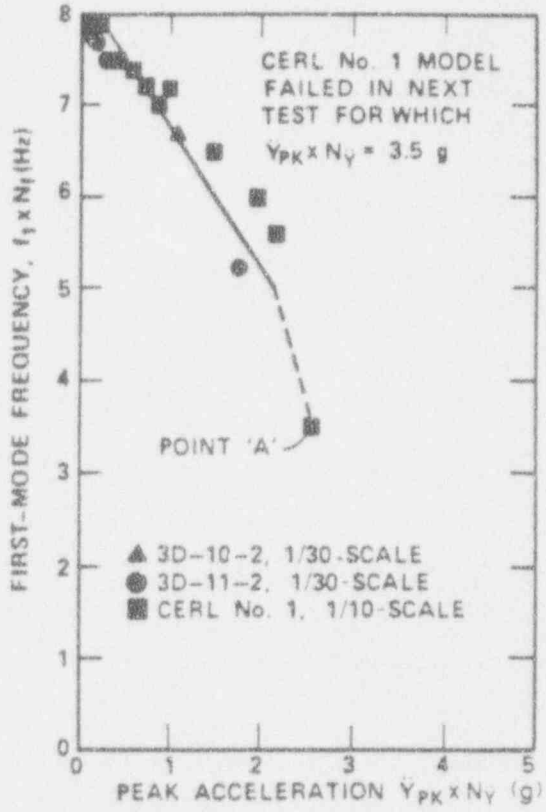

NOTES:

FOR 1/30-SCALE, $N_f = 1/11.8$, $N_{\ddot{Y}} = 1/4.6$

FOR 1/10-SCALE, $N_f = 1/6.8$, $N_{\ddot{Y}} = 1/4.6$

EXAMPLE:

AT POINT 'A' CERL TEST No.1

$f_{1_{PROT.}} = 24 \times 1/6.8 = 3.5$ Hz

$\ddot{Y}_{PK_{PROT.}} = 12 \times 1/4.6 = 2.6$ g

Figure 2-6 Variation in First Mode Frequency [3]

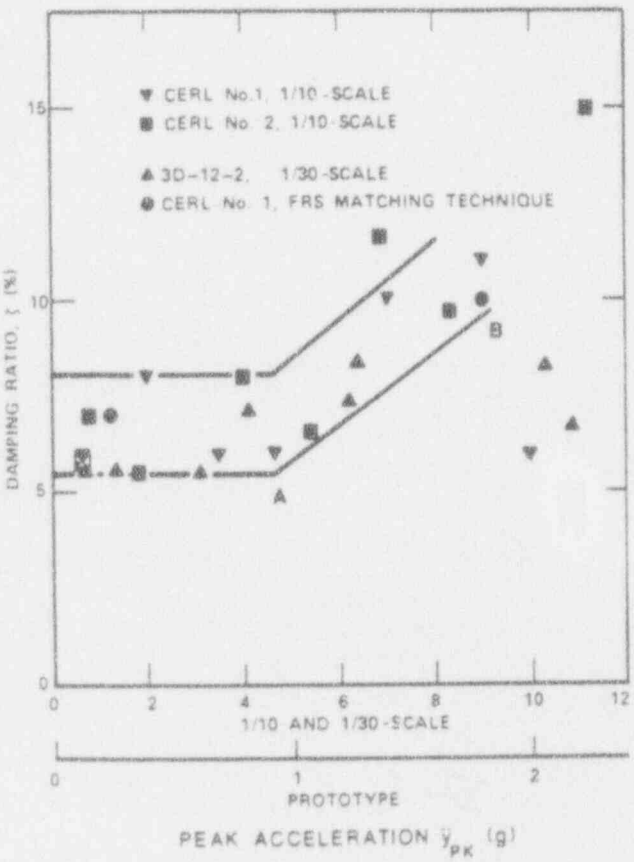

Figure 2-7 Measured Damping Ratios [3]

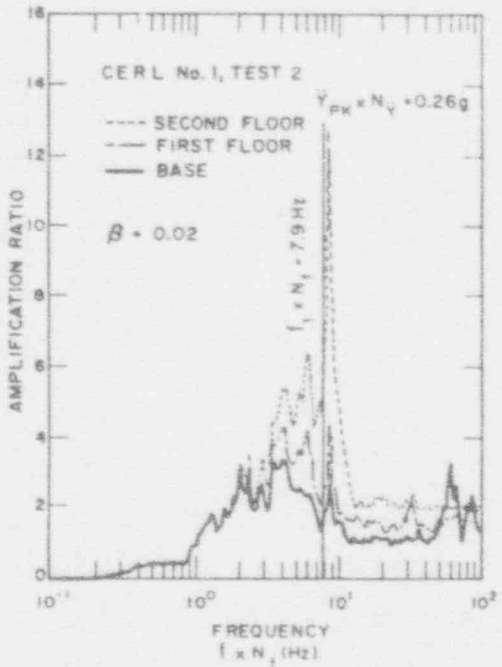

Figure 2-8 Floor Response Spectra: Y_{pk}/N_y = 0.26g [3]

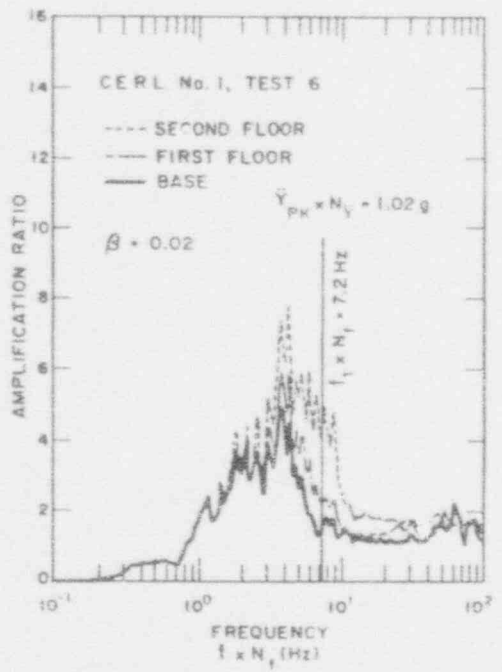

Figure 2-9 Floor Response Spectra: Y_{pk}/N_y = 1.02g [3]

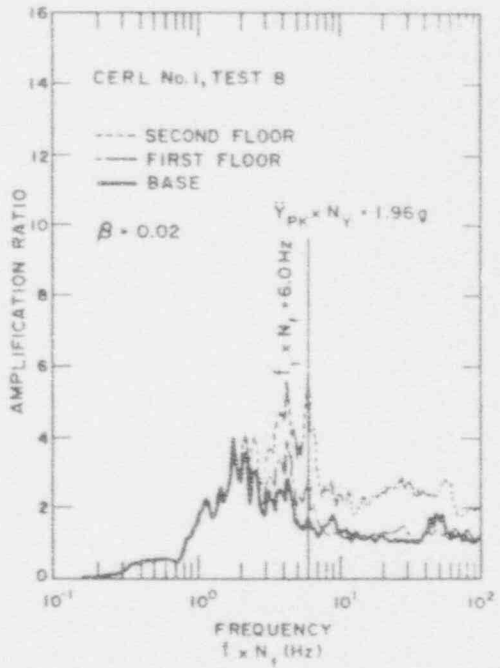

Figure 2-10 Floor Response Spectra: Y_{pk}/N_y = 1.96g [3]

scaled to the full size diesel generator building (obtained by scaling up the measured response time histories from the same series of tests). The base input peak ground accelerations are 0.26 g, 1.02 g and 1.96 g, respectively. If the tested specimen behaved in a linear fashion, the shape of the spectra would be the same for different input peak acceleration levels. The amplitude of acceleration at any frequency would be directly proportional to the input peak acceleration. However, due to the degradation in natural frequency, the shape of the spectra changes with increasing input acceleration levels (the frequency dropping from 7.9 Hz to 7.2 Hz to 6.0 Hz, respectively).

In each plot, the spectra for the base, the first, and the second (highest) floors are shown. Consider a piece of equipment having its own natural frequency in the 8 to 10 Hz range mounted on the second floor. (Many electrical cabinets have frequencies in this range.) From Figure 2-8, for this frequency range the component sees a peak amplification ratio of about 12.6, which implies a peak acceleration of 12.6 x 0.26 g = 3.28 g. The amplification ratios at 1.02 g and 1.96 g in Figures 2-9 and 2-10, however, are about 5 and 2.8, respectively. So as the base excitation increases, this component sees proportionately less acceleration. The probability of failure will be less than predicted using spectral accelerations scaled by 12.6 (based on the initial, nondegraded structural frequency). Thus, if this component plays an important role in determining the frequency of core melt, then the total core melt frequency would decrease when the structural frequency degradation was included.

By contrast, consider a second component, again on the second floor, having its own resonant frequency in the 4 to 5 Hz range. From Figures 2.8 through .10 the corresponding amplification ratios are approximately 5.0, 8.0 and 5.0. Thus this component experiences proportionately higher accelerations at 1.02 g than at either 0.26 g or 1.96 g input peak accelerations. And the conditional probabilities of failure are higher (near 1.02 g) than would be predicted with linear scaling of spectral accelerations scaled by 5.0 (based on the initial, nondegraded structural frequency). In this case, the total core damage frequency would increase.

Thus, it can be seen that incorporating the "frequency difference" issue into the calculation of structural response can potentially increase or decrease the probability of component failure, and similarly potentially increase or decrease the total core damage frequency (relative to risk based on nondegrading structure frequencies and design-based initial natural frequencies).

2.5 Building Fragilities

As part of determining the seismic risk, it is necessary to determine failure criteria for all critical components in the safety systems. Besides functional failure of these critical components, one must consider the possibility that the buildings enclosing the critical components may fail and secondarily cause component failure. If a floor slab or wall collapses onto a pump or valve, the latter has a high probability of

failure. More likely is the possibility that the walls or floor slabs will be so cracked and spalled that bolts anchoring critical equipment will pull out, and components will then fail by excessive motion. Thus, an essential part of developing fragility relations for a power plant is the development of failure criteria for those buildings housing critical components.

General Approach

Inasmuch as no actual tests to failure of typical nuclear power plant buildings exist, it is necessary to base the development of the building fragilities on a comparison of analytically calculated loads with experimentally determined wall, slab, and beam capacities. The starting point for this comparison is to have available a dynamic structural analysis of the building under consideration, which provides estimates of dynamic response (in-structure accelerations; forces in walls, slabs, and beams; etc.) for a specified free-field ground motion. This analysis can be based on design calculations or on a best-estimate analysis. In terms of building fragilities, the important results are the amplitude and distribution of the forces and moments in structural members conditional on the specified free-field ground motion. From this load response information and an assessment of the load capacities of the members, their fragility functions are developed.

Fragility functions relate probability of failure to a single parameter. Examples are support point accelerations of a component and moment in a piping system. The parameter is typically a measure of the excitation or response of the item of interest. For building fragilities, one first considers structural elements, e.g., shear walls. The failure of the structural element is described by loads in the member (e.g., shear force in a shear wall), with consideration given to other simultaneously acting loads. This fragility parameter coincides with a response parameter which describes response conditional on the occurrence of an earthquake described by the seismic hazard curve. Convolution of the two yields the probability of failure of the item of interest.

Typically, fragility functions are developed for structural elements of importance, first, in terms of forces in the members, e.g., shear force in a shear wall. Subsequently, the fragility parameter are transformed to an in-structure floor acceleration for computational convenience. Structural member forces are correlated with floor accelerations, and the acceleration at a node point in the structure is selected as the fragility response parameter.

Failure of a structural element or building is thus described by a fragility parameter. For example, this parameter may be the acceleration, the internal stress, or the applied load.

Fragility functions for a structural element or building are assumed to take the form:

$$V_F = V \cdot F_S \cdot F_\mu \qquad (1)$$

where,

V_F = fragility parameter at failure (e.g., shear force in wall),

V = reference value of fragility parameter at a known earthquake level (e.g., the SSE),

F_S = factor relating the actual strength capacity to the calculated (best estimate) load, and

F_μ = factor accounting for inelastic energy absorption capability of the structure or structural element.

If no structural analysis is performed to determine the best-estimate load, then F_S is computed using the design loads, which are usually quite conservative. In this case, an extra factor is added, and the fragility function takes the form

$$V_F = V \cdot F_S \cdot F_\mu \cdot F_R \qquad (2)$$

where

F_R = additional factor accounting for conservatisms in the design analysis from which the reference value of V was determined; if best estimate probabilistic response calculations are performed, $F_R = 1$.

The strength factor, F_S, is computed by

$$F_S = \frac{V_{ult} - V_{normal}}{V_{seismic}} \qquad (3)$$

where V_{ult} is the capacity of the member in terms of load, V_{normal} is the load due to normal conditions assumed to act simultaneously with the earthquake (dead weight, thermal, pressure, etc.), and $V_{seismic}$ is the load at the reference level earthquake. The factor F_S ratios up the load or response in Eq. (2) to the actual ultimate load capacity. Figure 2.11 shows a typical nonlinear load-deflection curve. The linearly extrapolated V_{ult} is shown schematically.

For members that behave in a brittle fashion, V_{ult} is the load at failure. However, many members behave in a ductile manner, and a significant degree of nonlinearity occurs before failure. Figure 2-11 shows this schematically. To account for this nonlinear behavior before failure, a ductility factor or inelastic energy absorption factor, F_μ, is developed and applied. F_μ is applied to reduce the linearly calculated response or, alternatively, to increase the capacity as described by the fragility parameter. Development of F_μ is based on parameter studies involving a large number of nonlinear analyses of relatively simple systems of varying

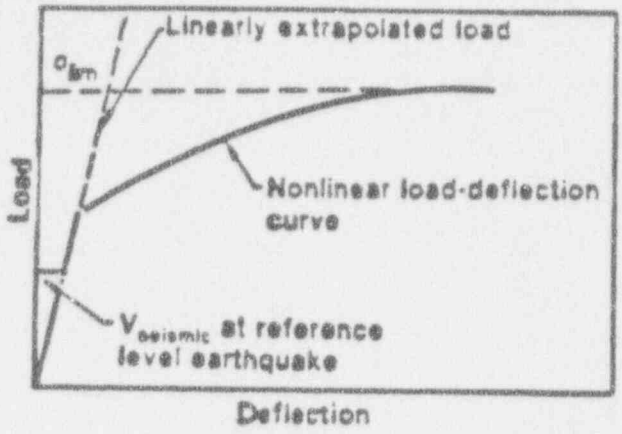

Figure 2-11 Typical Monotonic Stress-Deflection Curve

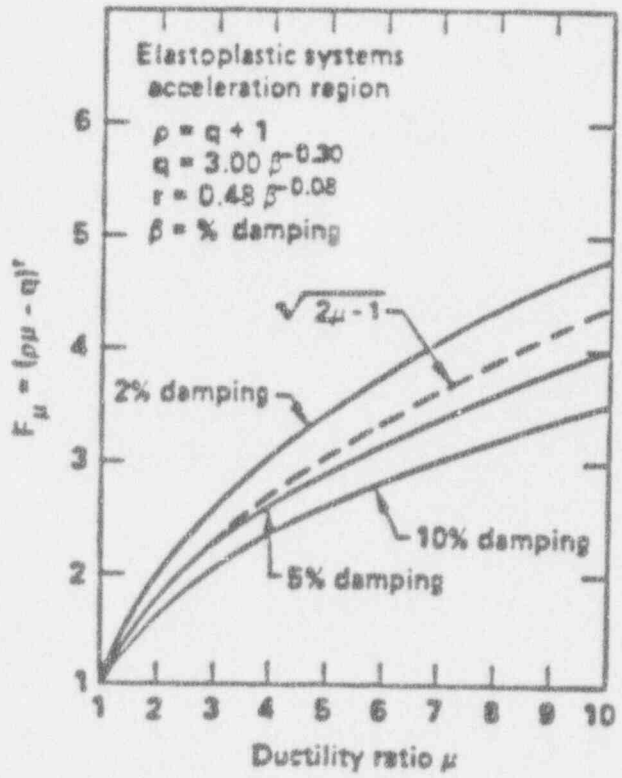

Figure 2-12 Relationship of Ductility Ratio and Damping Factor on Ductility Factor

frequency characteristics, damping, and available ductility. An early model for F_μ, taken from the work of Newmark-Riddell [15] is shown in Figure 2-12, in which F_μ is only a function of ductility and (weakly) damping. More recently, Kennedy et al have correlated F_μ values with duration and damageability potential of different types of earthquake accelerograms [Reference 16]. Because failure is not deterministic, the factors in Eq. (1) and (2) are subject to uncertainty. These factors are treated as random variables, and uncertainties are explicitly included. Lognormal distributions are usually assumed for F_S, F_μ, and F_R, which are assumed to be independent variables. Consequently, V_F is lognormally distributed and

$$\hat{V}_F = \hat{V} \cdot \hat{F}_S \cdot \hat{F}_\mu \cdot \hat{F}_R \tag{4}$$

$$\beta_F^2 = \beta_S^2 + \beta_\mu^2 + \beta_R^2 \tag{5}$$

where the symbol $\hat{}$ indicates the median and β denotes the log-standard deviation. The two variables $\hat{V}_F$ and β_F define the distribution of the fragility parameter, V_F, and

$$V_F = \hat{V}_F \varepsilon \tag{6}$$

where ε is a random variable with median of unity and log-standard deviation, β_F, given by Eq. (5)

Modeling and Random Uncertainties

Uncertainty in the calculation of the fragility can be separated into two categories, random uncertainty and modeling uncertainty. Random uncertainty is that part of the total variance which results from inherent randomness in the system, which cannot be reduced by additional data or analysis. Random uncertainty is variability induced by the earthquake motion. By contrast, modeling uncertainty is that part of the total variance which results from our model or representation of the phenomenon. Modeling uncertainties can be reduced by use of improved models, additional tests, etc.

It is possible to separate the effects of random and modeling uncertainties by estimating the variances in the term F_S and F_μ separately. Thus, we estimate

$$\beta_S^2 = \beta_S^{R\,2} + \beta_S^{u\,2} \tag{7}$$

$$\beta_\mu = \beta_\mu^{R\,2} + \beta_\mu^{u\,2} \tag{8}$$

in which each β^R is the variance due to random uncertainty and each β^μ is the variance due to modeling uncertainty. Thus, Eq. (6) can be generalized to

$$V_F = V_F \, \varepsilon_R \, \varepsilon_u \qquad (9)$$

where ε_u is a lognormal random variable with unit median and log-standard deviation

$$\beta^{u\,2} = \beta_s^{u\,2} + \beta_\mu^{u\,2} \qquad (10)$$

which accounts for all the modeling uncertainty, and ε_R is a lognormal random variable with unit median and log-standard deviation

$$\beta^{R\,2} = \beta_s^{R\,2} + \beta_\mu^{R\,2} \qquad (11)$$

which accounts for all the inherent random uncertainty.

The formulation in Eq. (9) allows us to put upper and lower bounds on the location of the median V_F by thinking of it as a random variable with variance which is the variance caused by modeling uncertainties alone. Hence, using the lognormal distribution for ε_u, we can get upper and lower values of the median corresponding to prescribed probabilities of non-exceedance, and thus plot the fragility relation in terms of a median (ε_u=1.0) curve and fragility curves based a 95% confidence and 5% confidence level of nonexceedance medians as shown in Figure 2-13. In general, a single fragility curve corresponding to any desired confidence level can be easily generated.

Impact of Frequency Difference Issue on Structural Fragilities

In order to requantify a seismic PRA to evaluate the impact of the "frequency difference" issue on the calculated seismic risk, the building frequencies (fixed base) will be reduced consistently with the LANL test results, and these reductions will impact the structural fragility values as shown below.

(i) Case A Building Responses Re-analyzed

Ideally, new best estimate loads (at several earthquake pga levels) would be computed. In these calculations, the reduced or effective building natural frequencies would be used for the (fixed-base) beam element model. This process was briefly described in Section 2.4. Inclusion of "reduced" building frequencies (as a function of pga) would change the computed median shear wall loads, floor accelerations and floor spectra. The new shear wall loads would be used to compute a new strength factor F_s using equation 4. The uncertainty in the frequency reduction would contribute to the uncertainty in F_s.

This approach should be considered when significant soil-structure interaction effects are present, for significant shifts in the natural frequency of the combined building-soil model could either mask or enhance the effect of the reduced building frequency.

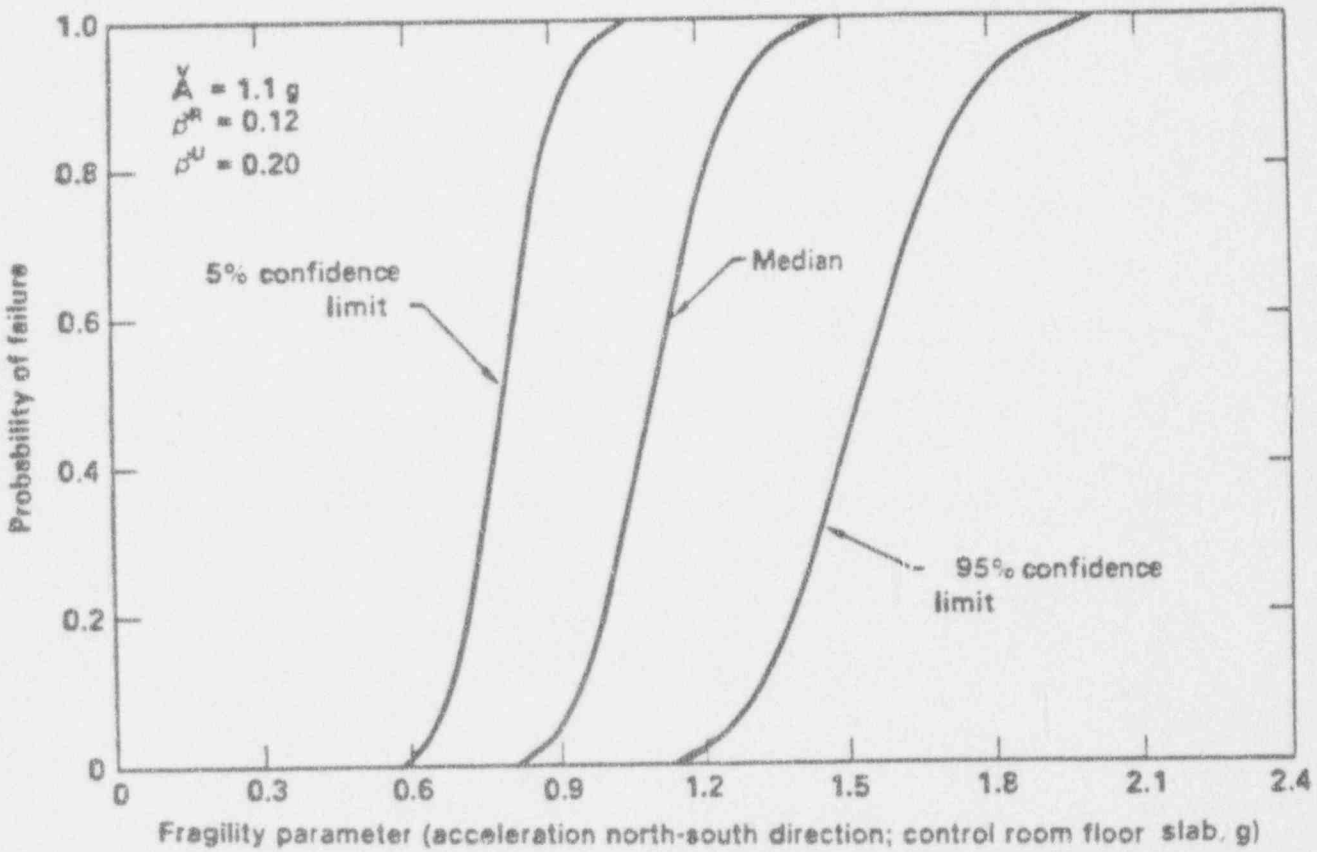

Figure 2-13 Lognormal Family of Fragility Curves

(ii) Case B No Building Response Re-analysis

If no building response reanalysis were possible (due to lack of models or budget etc.) one can still include the effects of fixed base structure degradation, but in a more uncertain fashion. Here, one would have to estimate new shear wall loads based on using judgement or other analytical experience to reflect the degraded structural frequencies. In this case, the F_S would be based on the design calculations, and a significant factor F_R (with associated uncertainty) would be included to account for the bias and uncertainty due to the soil structure interaction effects. (Of course, if the building is founded on rock, and soil structure interaction effects are minimal or negligible, the frequency difference effect can be added to the original building fragility derivation directly).

2.6 Component Fragilities

Plant-specific component fragilities can be represented in the same way as structural fragilities, i.e., in terms of a median, M_F, a random uncertainty β_{FR} and a modeling uncertainty β_{Fu}. A sample fragility curve is shown in Figure 2-14. The ordinate gives the conditional probability that failure has occurred given a base acceleration corresponding to the value of the abcissa. The fragility parameter is usually the floor spectral acceleration computed at the natural frequency of the component.

Fragilities for specific components are derived (ideally) from fragility tests on a shaker table using an input time history compatible with the floor response spectra for the floor on which the component is mounted. When dealing with large components which cannot be tested, the fragility curve is derived by analysis, that is, the design calculations for the component are scaled up to a (presumed) failure level and uncertainties are prescribed using expert judgement. This latter approach is typically used for components whose important failure modes are structural damage rather than functional failure. Finally, for components whose dominant failure mode is functional, but for which no fragility test data are available, recourse is taken to the equipment qualification tests, and expert judgement is used to estimate the margin to failure over the qualification test results. Examples of fragility calculations by each of these methods is given in Reference 15.

Given that one has derived a response distribution (in terms of median response M_R, random uncertainty β_{RR} and modeling uncertainty β_{Ru} as a function of pga as described in Section 2.4, one can de-condition the fragility curve, i.e., derive the component fragility curve in terms of the site pga, using

$$P_F(pga) = \int F_{frag}(r) f_{resp}(r;pga)dr \qquad (12)$$

where

F_{frag} = cumulative fragility probability distribution,

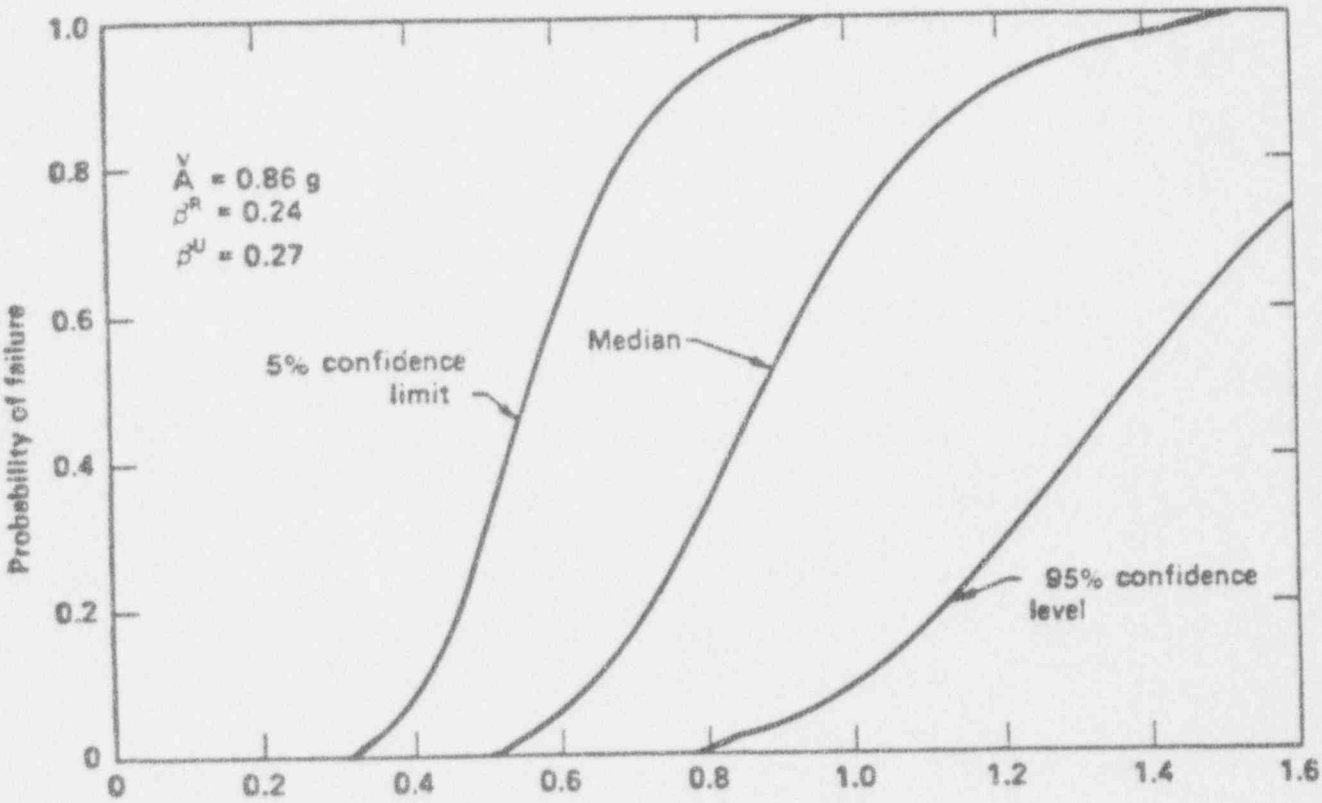

Figure 2-14 Typical Component Fragility Curve

f_{resp} = response probability density function conditional on pga, and

r = local response.

An alternative approach to equation (12), often used in industry-sponsored seismic PRAs, is to assume the fragility to be a lognormal variable in terms of pga directly, in the same fashion as was illustrated for structural fragilities. As before, one assumes the fragility curve to be given by

$$A_F = \hat{A}\ \varepsilon_R \varepsilon_u \qquad (13)$$

where

A_F = peak ground acceleration at failure,

$\hat{A}$ = median pga at failure, and

$\varepsilon_R, \varepsilon_u$ = lognormal random variables with unit median and uncertainties β_R and β_u (random and modeling) respectively.

Given a probabilistic description of both the local response and the component fragilities in terms of local response, one can easily derive the fragility relation in terms of pga so as to be compatible with any existing seismic PRA. Alternatively, one can reverse the process to derive local fragilities given the derivation of the fragility in terms of peak ground acceleration, provided relationships between local and peak ground accelerations are available.

A generic data base of fragility functions for seismically induced failures was developed in the SSMRP [27]. The generic categories and the corresponding fragility medians and uncertainties used are shown in Tables 2-2 and 2-3.

Impact of "Frequency Difference" Issue on Component Fragilities

The effect of reducing the building (fixed base) natural frequencies on the component fragilities comes into play entirely through the floor spectra for the equipment mounting point. The fragility derivation (whether based on fragility test, analysis or qualification test extrapolation) is modified to include the new spectra. Since spectra no longer scale directly with pga, the (non-linear) variation of spectral acceleration with pga must be included, although this is straightforward.

2.7 Integration of Seismic Risk and Uncertainty Analysis

Once all component fragilities and responses are known for several earthquake pga levels, one computes the failure frequency of each component in the accident sequences. If fragilities and responses are assumed to be lognormal variables, one uses:

Table 2-2

Generic Component Categories

Fragility Category	Component Class	Typical Components	Frequency (Hz)
1	LOSP	Ceramic Insulators	ZPA
2	Relays		5-10
3	Circuit Breakers		5-10
4	Batteries		ZPA
5	Battery Racks		ZPA
6	Inverters		5-10
7	Transformers	4 kV to 480 V and 480 to 120 V	10
8	Motor Control Centers	Control for ESF Pumps and Valves	5-10
9	Aux. Relay Cabinets		5-10
10	Switchgear (Including Transformers, Buses and Breakers)	416 V and 480 V	5-10
11	Cable Trays		ZPA
12	Control Panels and Racks	RPS Process Control	5-10
13	Local Instruments	Misc. Pressure & Temperature Sensors	5-35
14	Diesel Generators	4160 ac Emergency Power Units	22
15	Horizontal Motors	Motor-Generator Sets	ZPA
16	Motor-Driven Pumps and Compressors	AFWS, RHR, SIS, Charging Pumps, Lube Oil Pumps, Diesel Starting Compressors	7
17	Large Vertical, Centrifugal Pumps (Motor-Drive)	Service Water Pumps	5
18	Large Motor-Operated Valves (10")		ZPA
19	Small Motor-Operated Valves (10")		ZPA
20	Large Pneumatic/Hydraulic Valves	Includes MSIV, ADP, and PORV	ZPA
21	Large Check and Relief Valves		ZPA
22	Miscellaneous Small Valves (8")		ZPA
23	Large Horizontal Vessels & Heat Exchangers	Pressurizer Relief Tank, CCW Heat Exchangers	ZPA
24	Small to Medium Heat Exchangers and Vessels	Boron Injection Tank	20
25	Large Vertical Storage Vessels with Formed Heads	RHR Heat Exchanger, Accumulator Tank	ZPA
26	Large Vertical Flat-Bottomed Storage Tanks	CST, RWST	
27	Air Handling Units	Containment Fan Coolers	5

Table 2-3

Generic Component Fragilities, in Units of Gravity (g)

Category	Generic Component	Median*	β_U	β_R
1	Ceramic Insulators	0.25	0.25	0.25
2	Relays	3.00	0.48	0.75
3	Circuit Breakers	7.63	0.48	0.74
4	Batteries	0.80	0.40	0.39
5	Battery Racks	2.29	0.31	0.39
6	Inverters	2.00	0.26	0.35
7	Dry Transformers	8.80	0.28	0.30
8	Motor Control Centers	7.63	0.48	0.74
9	Auxiliary Relay Cabinets	7.63	0.48	0.74
10	Switchgear	6.43	0.29	0.66
11	Cable Trays	2.23	0.34	0.19
12	Control Panels and Racks	11.50	0.48	0.74
13	Local Instruments	7.68	0.20	0.35
14	Diesel Generators	1.00	0.25	0.31
15	Horizontal Motors	12.10	0.27	0.31
16	Motor-Driven Pumps and Compressors	2.80	0.25	0.27
17	Large Vertical Centrifugal Pumps	2.21	0.22	0.32
18	Large Motor-Operated Valves (10 in.)	6.50	0.26	0.60
19	Small Motor-Operated Valves (10 in.)	3.83	0.26	0.35
20	Large Pneumatic/Hydraulic Valves	6.50	0.26	0.35
21	Large Relief, Manual, and Check Valves	8.90	0.20	0.35
22	Miscellaneous Small Valves	12.50	0.33	0.43
23	Large Horizontal Vessels and Heat Exchangers	3.0	0.30	0.53
24	Small to Medium Vessels and Heat Exchangers	1.84	0.25	0.45
25	Large Vertical Vessels With Formed Heads	1.46	0.20	0.35
26	Large Vertical Tanks With Flat Bottoms	0.45	0.25	0.35
27	Air Handling Units	6.90	0.27	0.61

R = Random Uncertainty.

U = Systematic Uncertainty.

*All medians in terms of spectral acceleration at 5% damping.

$$P_f(pga) = \Phi\left[\frac{\ln \frac{m_F}{m_R}}{\sqrt{\beta_F^2 + \beta_R^2}}\right] \qquad (14)$$

where Φ is the standard N(0,1) normal cumulative distribution function. This equation gives the failure frequency as a function of pga since, as described in Section 2.4, the median response values are functions of pga. Note that the result of applying (14) at various pga levels gives the component fragility analogous to the form in equation (13) as used in the engineering factor approach.

After all component failure frequencies are known, the accident sequences

$$Acc_i(pga) = C_1 \cup C_2C_3 \cup C_4C_5C_6 \ldots$$

can be evaluated as a function of pga. When computing the cutset frequencies, seismically induced correlation may need to be taken into account. Finally, the (unconditional) frequency of the accident sequences is obtained by integration over the hazard curve, using

$$P(Acc_i) = \int Acc_i(pga)\, f_{hazard}(pga)\, d(pga) \qquad (15)$$

where

$P(Acc_i)$ = total (unconditional) accident sequence frequency,

Acc_i = cumulative distribution function for accident sequence, and

f_{hazard} = probability density function of hazard curve.

Equation (15) is often replaced by discrete integration.

3.0 MODELING STIFFNESS REDUCTION

3.1 Previous Experimental Results

Starting in 1980, the U.S. Nuclear Regulatory Commission sponsored Los Alamos National Laboratory to perform a combined experimental/analytical series of tests for investigating the behavior of nuclear concrete shear wall structures [Refs. 1-4]. Initially, 1/30 scale, 1-inch thick, isolated shear wall structures constructed with micro-concrete were tested both statically and dynamically. Later, three-dimensional box-like structures that represented idealized diesel generator and auxiliary buildings were tested. These were also micro-concrete scale models that ranged from 1/10 to 1/42 and wall thicknesses ranging from 1 inch to 3 inches. One of the most important and consistent conclusions from these early tests was that measured stiffnesses were lower than theoretical stiffnesses by a factor of about 4, or 25% of theoretical. This would imply that structural frequencies would be only 50% of what would be otherwise determined analytically.

This observed difference between calculated and measured stiffnesses and frequencies could represent a potentially important issue in the design of nuclear power plants. This is due to two major factors. First, most safety related equipment is located in Seismic Category I structures which typically have predicted fixed base natural frequencies in the 5 Hz to 20 Hz range. If the frequency reduction was as large as 50%, then these structures could have actual frequencies in the 2 Hz to 10 Hz range. Most broad band strong motion earthquake time histories have the majority of their energy in the 2 Hz to 8 Hz range. Therefore, the excitation of the structure could be much greater than was considered in the original design. Both the loads experienced by the structural members and in-structure floor acceleration spectra would be increased. The second important factor to consider is that safety related equipment could experience greater seismic loads due to a shift in the floor spectra near the equipment natural frequency.

Later, LANL tested several box type shear wall structures titled TRG structures, [Refs. 5-10] using both conventional concrete and microconcrete in order to show scalability between microconcrete and "real" concrete. Some of the earlier models had cracks that developed before testing and results are therefore inconclusive. However, TRG-4 and TRG-5 were full scale models with wall thicknesses of 6 and 4 inches respectively and tested in a quasi-static load cycle manner. These were felt to be two of the more reliable specimens that were tested and exhibited stiffnesses that were almost identical to theory until first cracking. For TRG-4, first cracking occurred when a Nominal Base Shear Stress (NBSS) of 131 psi was reached. For TRG-5, first cracking occurred at a NBSS of 167 psi. Figure 3-1 shows the degradation in stiffness as a function of the NBSS for increasing applied loads on TRG-4 and TRG-5. Later, other TRG structures were tested dynamically, however, because of unexpected rocking motion in the shaker table, measured frequencies from accelerometers were inaccurate. However, stiffnesses inferred from strain gages mounted on the specimens, showed little or no stiffness reduction prior to cracking.

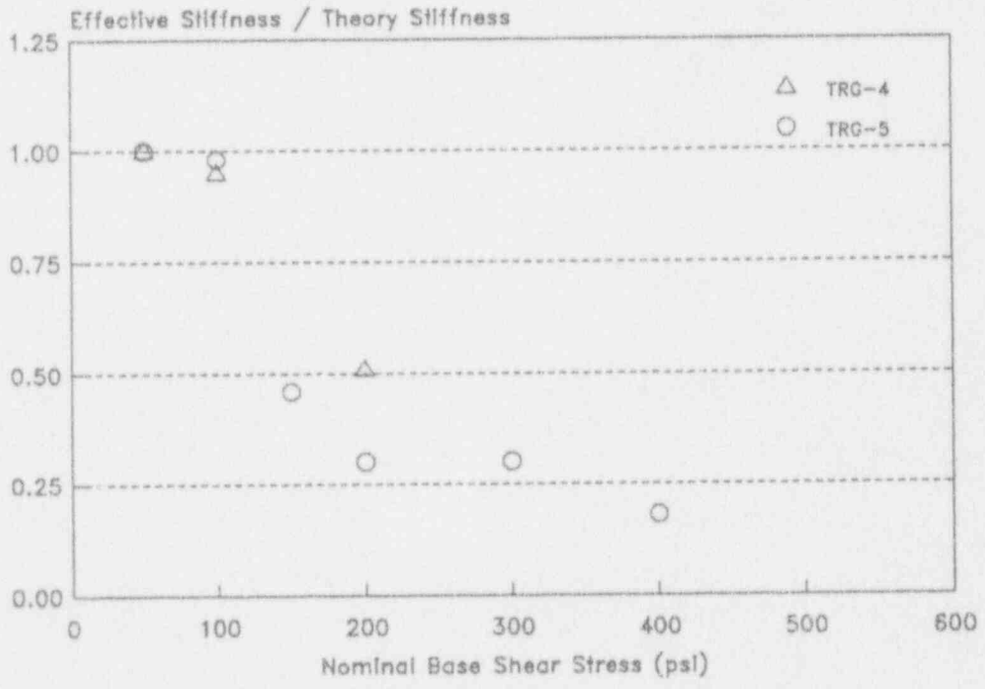

Figure 3-1: TRG-4 and TRG-5 Stiffness Reductions

While these tests were being performed at LANL, an ASCE Working Group was assembled to study the stiffness reduction issue. In May 1988 Professor Mete Sozen, University of Illinois, gave a presentation to the Working Group on data he had assembled on earthquake response of reinforced concrete structures over the years. Professor Sozen's presentation centered around data from Japan, from the University of Illinois and from others that are plotted in Figures 3-2 to 3-4. These results are documented in Refs. [17-22]. Sozen argued that these data show that there is clearly a large variation in the expected value of the stiffness from a concrete shear wall, and not all measured results can be attributed to experimental error.

The TRG results from LANL and Prof. Sozen clearly show there is a difference between theoretical stiffnesses using uncracked section properties and experimentally tested stiffnesses of concrete shear wall structures. Although not as low as 25%, in most cases, initial stiffnesses are usually between 50% and 100% of theoretical, which implies frequencies would be between 70% and 100%. In addition, most test data taken at higher excitation levels or higher shear stresses, also show even further reductions in stiffness.

3.2 Stiffness Reduction Model

To determine a stiffness reduction model for concrete shear walls to be used in the analysis of measuring plant risk and margin for this program, all the information above was incorporated. The first stiffness reduction model developed for this program had a very high initial stiffness reduction and further reduction was based on the PGA at the base of the structure analyzed. This model was developed only from the early test results at LANL and later proved to be much too conservative at low earthquake levels and was not applicable to all concrete structures. When later test results showed stiffness reduction as a function of shear stress, it was decided this would be much more accurate and could be used for any reinforced concrete structure as long as shear stress levels could be determined.

From the results presented in the previous section, an initial reduction of 25%, or 75% of the original theoretical stiffness, was chosen to be used until first cracking for the stiffness reduction model. After cracking occurs the stiffness was chosen to be 50% of the analytical stiffness. This was selected primarily from data taken from the LANL tests on TRG structures. In these tests cracking usually occurred at shear stress levels of about 150 psi. This also corresponds to the shear cracking capacity of most high strength concrete, using the ACI formula $v_c = 2*(f_c')^{1/2}$. At higher stress levels the stiffness continues to decrease until only 10% of the initial stiffness remains and this is assumed to occur at about 500 psi NBSS.

The resulting stiffness reduction model selected from this data and applied in this program is shown in Figure 3-5. As can be seen, the amount of stiffness reduction is a function of the nominal base shear

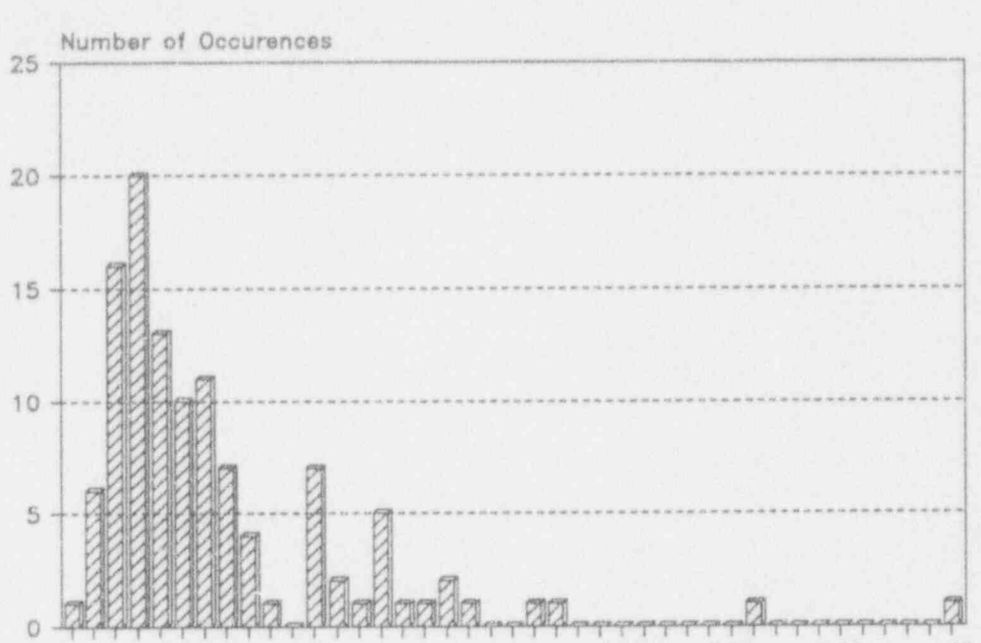

Figure 3-2: Histogram of Initial Stiffnesses presented to the ASCE Working Group by Dr. Mete Sozen, University of Illinois.

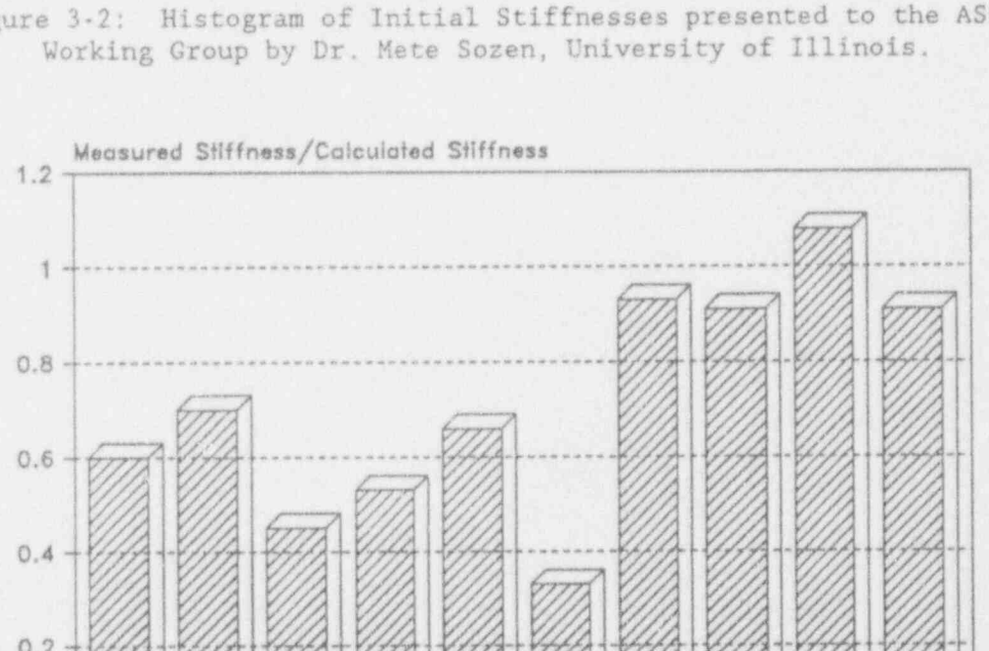

Figure 3-3: Additional data on Initial Stiffnesses taken by Japanese Investigators and presented to the ASCE Working Group.

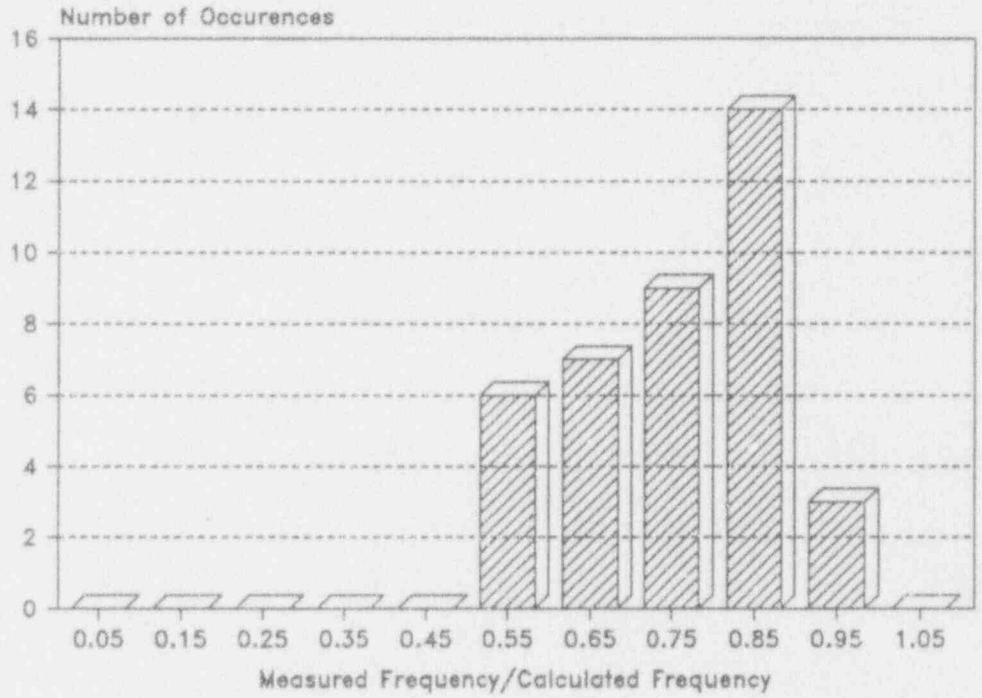

Figure 3-4: Histogram of Frequency Reductions presented to the ASCE Working Group by Dr. Mete Sozen, University of Illinois.

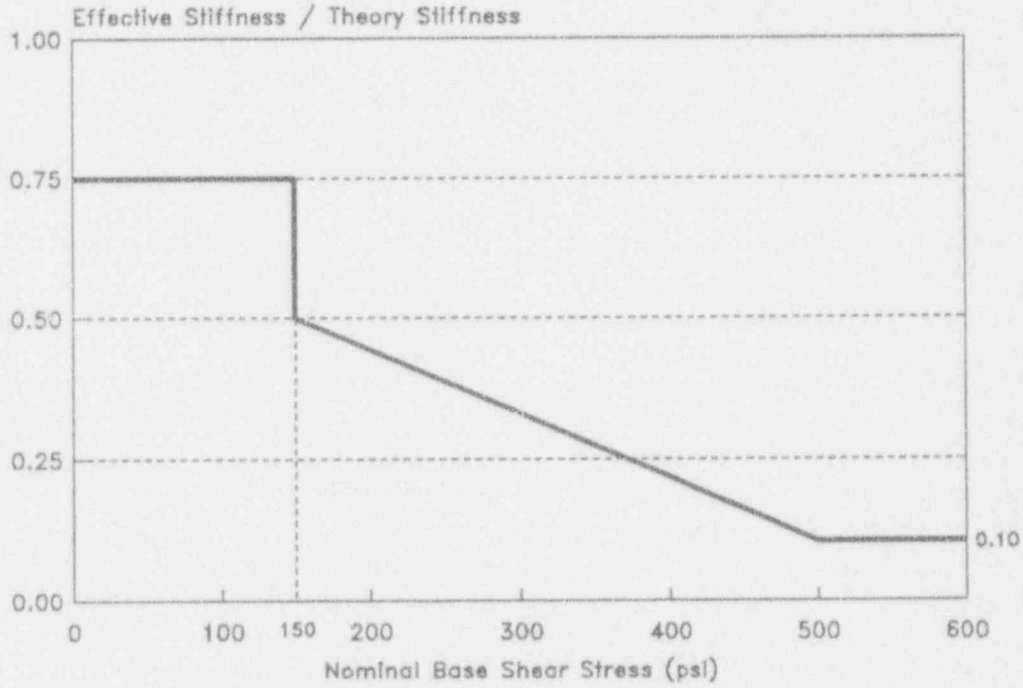

Figure 3-5: Stiffness Reduction Model

stress in the concrete shear wall. At low stress levels, below 150 psi, all concrete shear walls are reduced in stiffness to 75%. This will almost always be the case for earthquakes up to and including the SSE. However, when analyzing a structure beyond the SSE, stresses will eventually exceed 150 psi. When this occurs the structure must be re-analyzed using only 50% of the initial stiffness for concrete walls that exceeded 150 psi NBSS. Again the resulting shear stress will probably not equal 150 psi, therefore, one must iterate until the amount of stiffness used results in a NBSS corresponding to the model in Fig. 3-5. However, in the structural models analyzed thus far, convergence usually occurs after only a few iterations. At high stress levels, above 500 psi, all stiffnesses will be 10% and no further iteration is necessary. However, this level of stress only occurs at very high earthquake levels, which are in most cases beyond the range where most of the seismic risk occurs.

4.0 PLANT SPECIFIC RESULTS

4.1 Peach Bottom

4.1.1 Background

A detailed seismic risk assessment was performed for the Peach Bottom plant as part of the NRC sponsored NUREG-1150 program [23]. This analysis utilized dynamic response calculations for all important structures, a generic seismic fragility data base for components, and detailed component fragility derivations for a number of components identified during the plant visit as falling outside the generic data base. Point estimates and mean values of accident sequence and core damage frequencies were obtained using a Monte Carlo approach.

The Peach Bottom Atomic Power Station (PBAPS) is located on the western shore of Conowingo Pond, formed by the backwater of Conowingo dam, 9 miles downstream on the Susquehanna River. The plant is 38 miles N-NE of Baltimore, Maryland, and 63 miles W-SW of Philadelphia, Pennsylvania.

The twin BWR units (Peach Bottom Units 2 and 3) of Philadelphia Electric Company are each rated at 1,065 MW. The reactor and generator for both these units were supplied by General Electric Corporation. Bechtel was the Architect/Engineer/Constructor. The plants began commercial operation in 1974. Unit 1 is a 40 MW decommissioned HTGR and is now in a mothball status. Based on the Peach Bottom Final Safety Analysis Report [24], a horizontal peak ground acceleration of 0.12g was defined for the SSE.

4.1.2 Summary of Input

In order to perform a seismic PRA, the following pieces of information must first be obtained: First, the local earthquake hazard, usually in the form of seismic hazard curves with uncertainty bounds or weighting factors, must be determined. Second, the accident sequences which lead to core damage must be identified. Third, the failure modes for the plant safety and support systems must also be determined. Forth, the fragilities of all important structures and components must be determined. Fifth, the location of components and level of seismic response at that location for a given level of seismic input, must be determined.

To begin with, the seismic hazard curves at Peach Bottom were taken from the NRC-sponsored Eastern and Central United States Seismic Characterization Program [25]. A second set of hazard curves were obtained from the commercial power industry-sponsored Electrical Power Research Institute's Seismic Hazard Methodology Development program for the Eastern United States [26]. Figure 4-1 shows the mean hazard curves taken from these two programs. The median, 15% and 85% hazard curves for both these programs are shown along with the means, in Appendix A of this report. The median curve and the mean curve were input, and random realizations for the Monte Carlo study were generated assuming a lognormal distribution for any given peak ground acceleration.

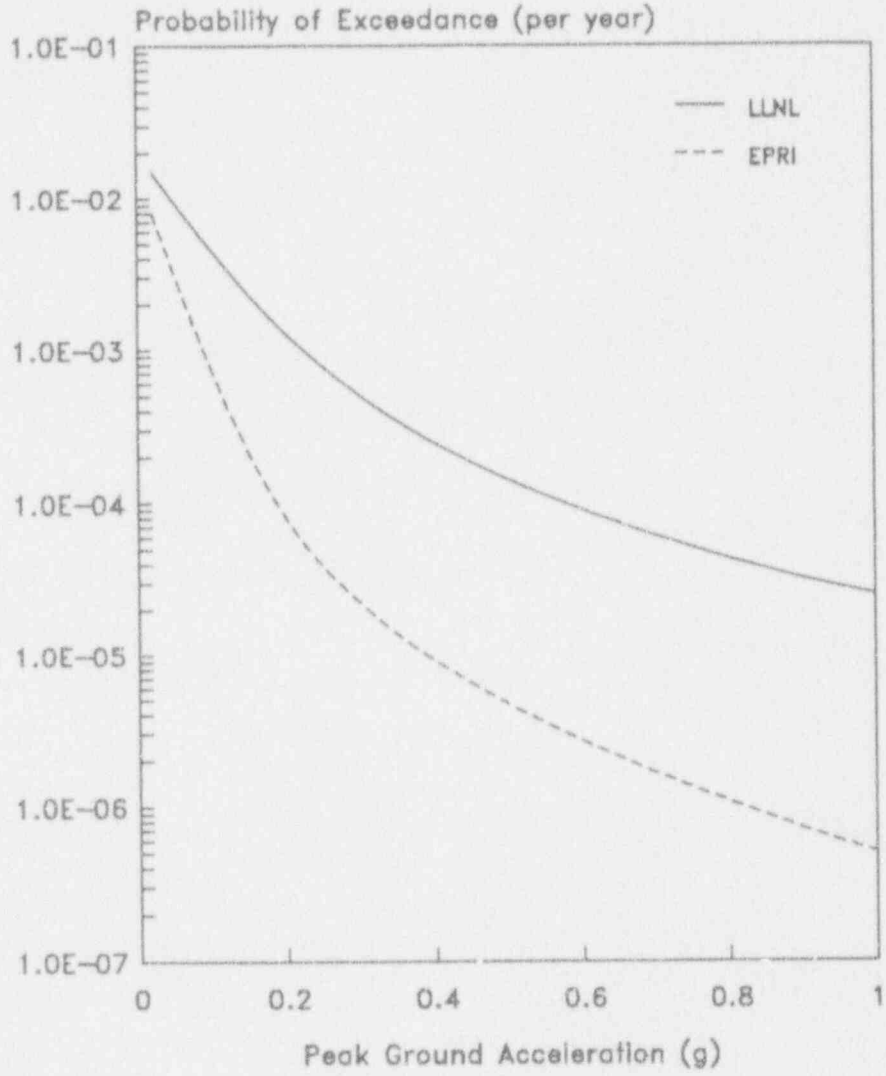

Figure 4-1 Peach Bottom Mean Hazard Curves

A detailed description of the plant safety systems at Peach Bottom is fully outlined in Appendix A of this report. The event trees developed for the internal event analyses in the NUREG-1150 program were used directly. After screening, a total of 22 accident sequences corresponding to the seven initiating events were evaluated in the NUREG-1150 external events and also in this study and are fully explained in Appendix A of this report.

The probability of each individual component failures is dependent on two factors, the seismic fragility of the component and the amount of response experienced by the component during a given peak ground acceleration. The fragility for each vital component is given either a generic fragility or is computed on a plant specific basis if no generic fragility is applicable. At Peach Bottom, the Reactor Building, Radwaste/Turbine Building, Diesel Generator Building, Circulating Water Pump Structure, and Emergency Cooling Towers all required development of structural fragilities including reduced stiffnesses. The structural fragilities for these structures using original stiffnesses were developed in the original NUREG-1150 program. The RWST, CST, 4kV switchgear, Diesel Generator Day tank and HPCI room cooler all required plant specific fragilities and are shown along with the structural fragilities in Table 4-1. The component fragilities, both site specific and generic, were not altered for the reduced stiffness case.

The amount of response (acceleration or force) experienced by each component at each earthquake level is next determined. First, the actual location of each component must be determined and related to a certain floor elevation of the building it is located within. After a dynamic time history analysis of each structure is run, building responses in terms of peak ground acceleration are developed. These are described in the next section and are the last piece of information needed to perform a seismic PRA.

4.1.3 Building Responses

Five independent building models were generated at Peach Bottom: the Reactor/Containment Building, the Radwaste-Turbine Building, the Circulating Water Pump House, the Diesel Generator Building, and the Emergency Cooling Tower structure. These were analyzed in order to determine the final degraded models for each applicable SSE level and to determine maximum probabilistic structure responses of both original and degraded models.

The models mentioned above are referred to herein as the original models since the element stiffnesses are those of the undegraded buildings. For the shear wall degradation study, at each of the applicable SSE levels (1, 2, 3, 5, 6, and 7 depending on the structure) the shear area of the beams representing the concrete walls was reduced according to the shear stiffness degradation curve defined in Section 3.2. In this way stiffnesses associated with bending and axial deformations were not affected.

Table 4-1

Summary of Site Specific Fragilities for Peach Bottom

Structure or Component	Failure Element	Original[1] A_m(g)	B_R	B_U	Reduced[2] A_m(g)	B_R	B_U	Effect of Failure
Reactor Building	N-S Shear Walls	1.5	0.16	0.27	1.6	0.17	0.28	Vessel Rupture Initiating Event
Radwaste/Turbine Building	Roof Diaphragm	1.4	0.10	0.23	1.2	0.11	0.24	Cause SBO and loss of all actuation. Modeled as initiating event, and failure event in LOCA sequences.
Radwaste/Turbine Building	N-S Shear Walls	1.5	0.13	0.25	1.6	0.15	0.26	
Diesel Generator Building	E-W Shear Walls	2.3	0.06	0.21	2.3	0.07	0.21	Negligible
Circulating Water Pump Structure	N-S Shear Walls	2.5	0.11	0.28	2.2	0.13	0.29	Negligible
Emergency Cooling Towers	Columns El. 153' to El. 163'	0.55	0.11	0.21	No change			Basic event in ESW system. Screened out due to redundancy.
Turbine Building	-	0.5	0.11	0.21	No change			Fails PCS, ECW pump cables, instrument air, and condensate system. Modeled as a failure event in T1, T3 and LOCA sequences.
Watertight Dike	Surrounds CST	1.0	0.04	0.17	No change			Failure mode of CST. screened out due to redundancy.
4KV Switchgear	Anchor weld failure	3.3	0.15	0.25	No change			Loss of function
DG Day Tank	Anchorage failure	0.95	0.15	0.20	No change			Loss of supply
HPCI Room Cooler	Weld Failure	3.42	0.15	0.25	No change			Loss of function
Condensate Storage Tank	Anchorage	Fragility Based on Dike						
RWST	Unanchored	Not on Fault Trees						

1. These fragilities are based on loads from analyses using original stiffnesses.

2. These fragilities are based on loads from analyses including shear wall stiffness degradation.

3. B_R and B_U do not include response variability.

The responses calculated from the simulations are combined to estimate median responses conditional on the occurrence of an earthquake described by the hazard curve parameter, i.e., peak ground acceleration.

From these response spectra (generated with and without stiffness reduction effects) at the various pga levels (0.12g-0.84g), one can construct plots of any particular spectral acceleration response (at any point in the structures being modeled) as a function of pga. The difference between these plots shows the effect of stiffness reduction directly. This was done for the locations of all equipment modeled on the accident sequence expressions (for the spectral acceleration corresponding to the equipment of interest).

A sample of the resulting plots of response point spectral accelerations versus peak ground acceleration for responses corresponding to critical components are shown on Figures 4-2 thru 4-6 for both original and reduced stiffnesses. It can be seen that a nearly linear relation exists up to peak ground accelerations of 0.36g or 3 SSE. However, at higher earthquake levels, a linear fit is often unappropriate, particularly for the reduced stiffness responses. Therefore, a quadratic fit was made for each of the response curves in the form:

$$M(PGA) = F_1(1.0 + F_2 PGA)PGA$$

where F_1 is essentially the initial slope of the response curve, and F_2 is the multiple that determines the rate of increase or decrease in response. For a response versus pga that remains linear, F_2 is equal to zero.

Figures 4-2 thru 4-6 also verify that reduced stiffness can result in a higher level of response or floor accelerations. This was most apparent in the Radwaste/Turbine building, Circulating Water Pump structure and the Emergency Cooling Towers. In the Radwaste/Turbine building at the 165' floor elevation, the spectral acceleration for frequencies in the 5-10 Hz range increased about 20% as shown in Figure 4-3. This was caused by the dominant modal frequency which was originally 9.38 Hz, shifted down to 5.95 Hz using reduced stiffnesses at 3 SSE and eventually to as low as 3.45 at 7 SSE. At these lower frequencies, the amount of input energy from the earthquake time history is higher, resulting in responses inside the building.

Similarly, the Circulating Water Pump structure experienced a dramatic increase in response at elevation 114' and 7 Hz for reduced stiffnesses above 3 SSE as shown in Figure 4-4. Again this was because the dominant modal frequency, originally 14.0 Hz, lowered to 9.95 Hz at 3 SSE using reduced stiffnesses and was only 5.89 Hz at 7 SSE. Figure 4-6 shows increased responses using reduced stiffnesses in the Emergency Cooling Towers. Again the dominant frequency dropped from 9.77 Hz to 4.78 Hz at 3 SSE and 3.59 Hz at 7 SSE.

However, the Reactor Building and Diesel Generator Building did not see great increases in response when applying reduced stiffnesses for different reasons. In the case of the Reactor Building, the walls are all

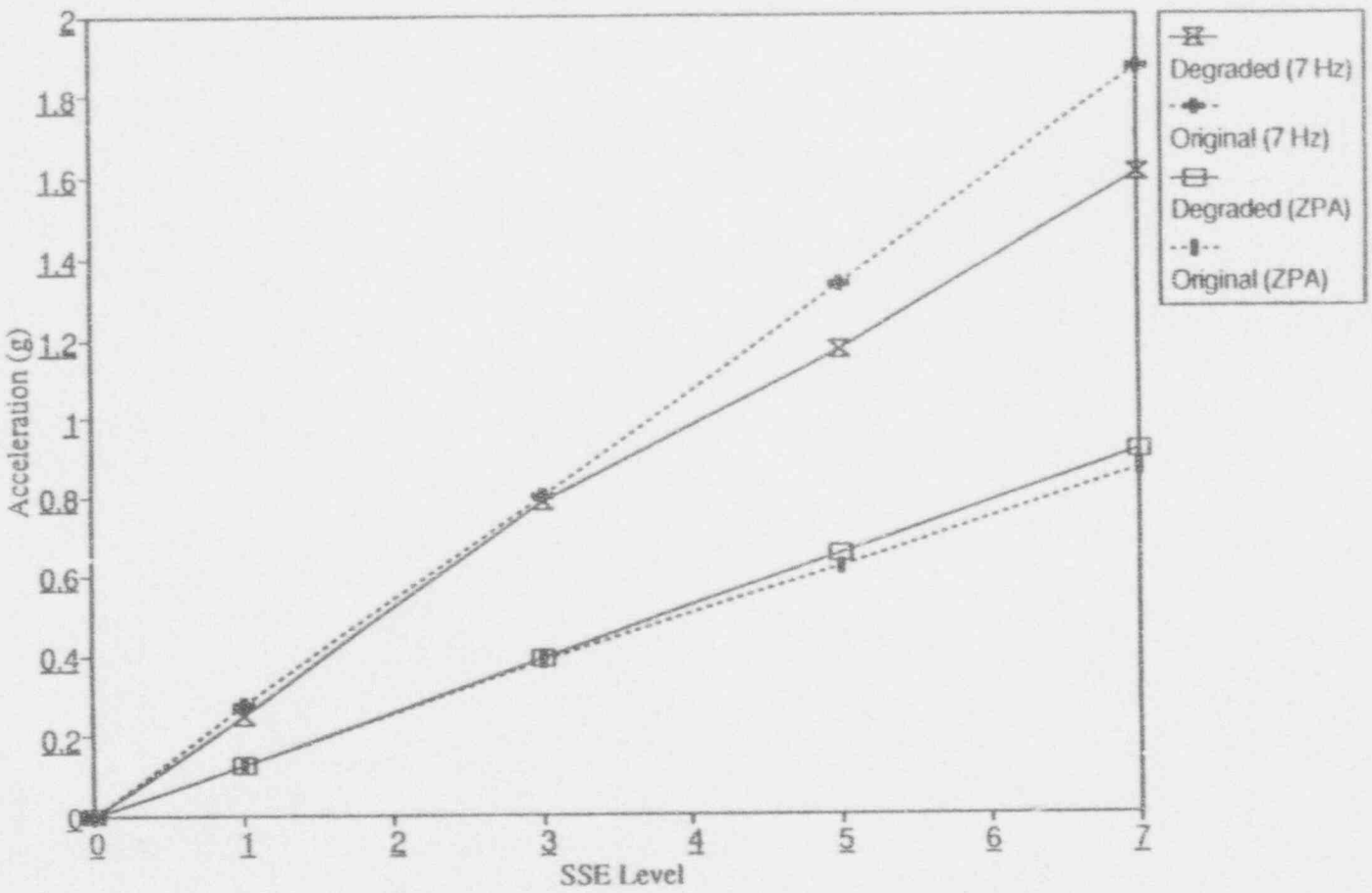

Figure 4-2 Median Responses for R/C Building, Node 2, El. 135'

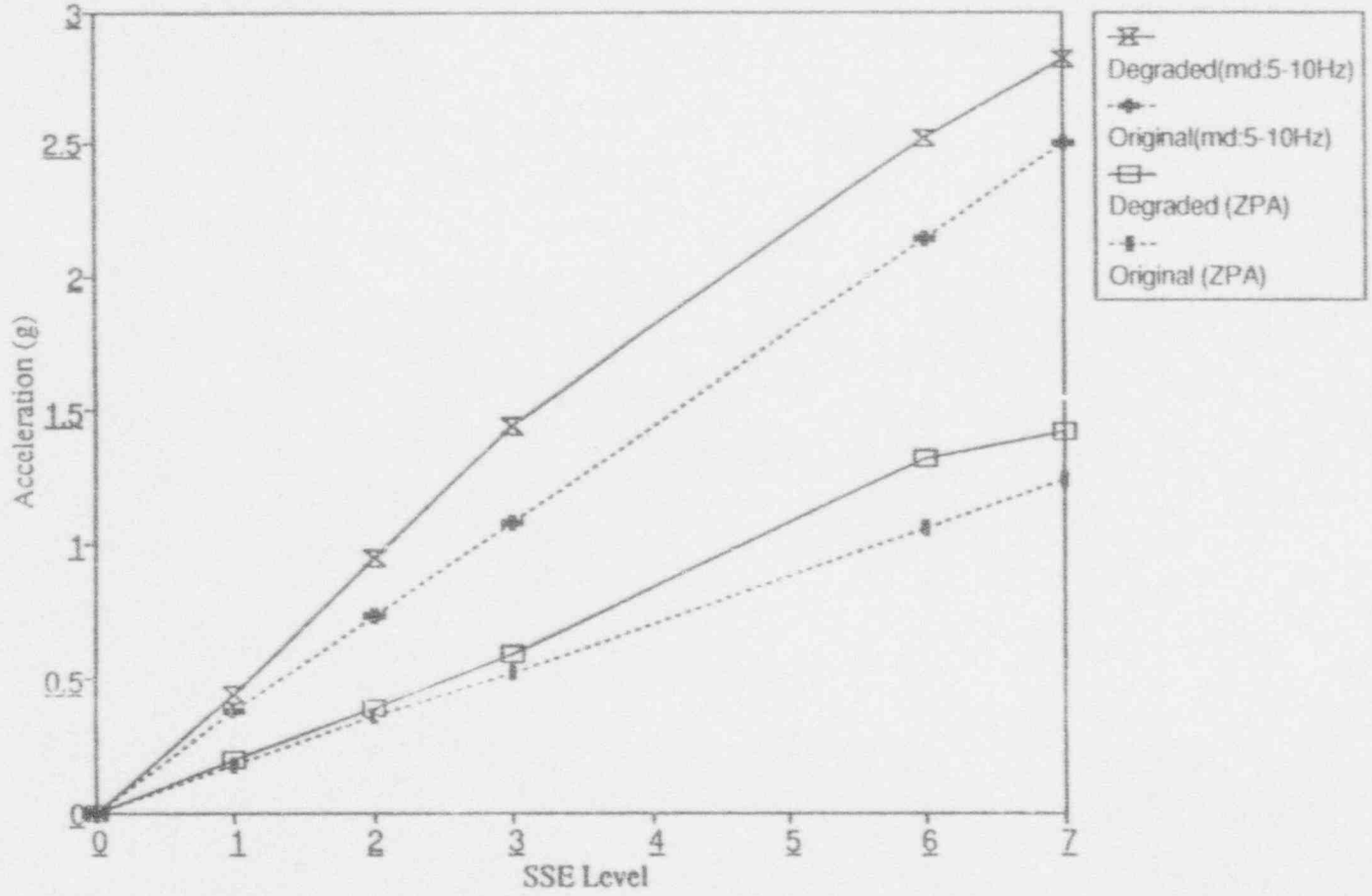

Figure 4-3 Median Responses for RWST Building, Node 12, El. 165'

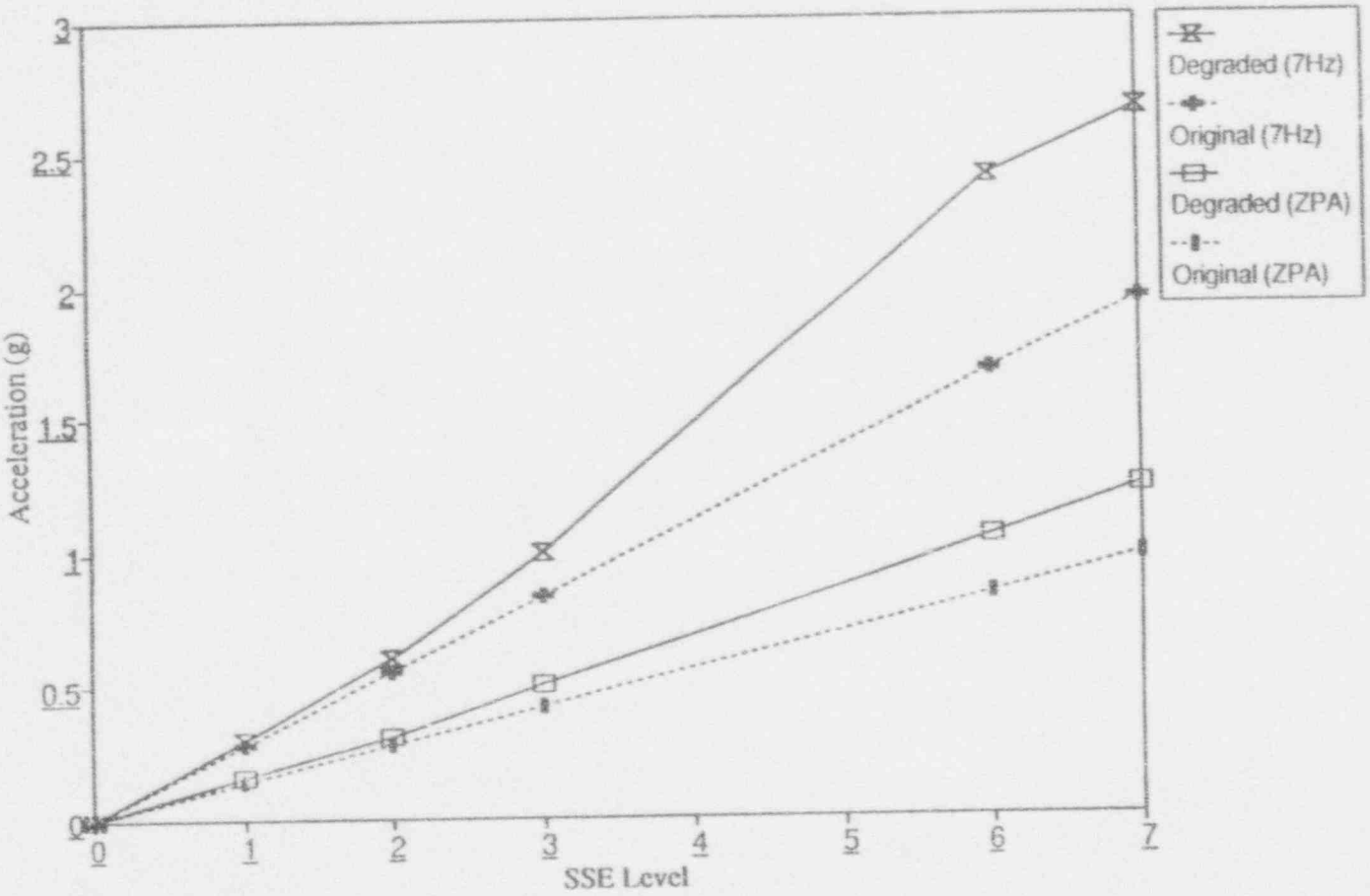

Figure 4-4 Median Responses for CWP Structure, Node 13, El. 114'

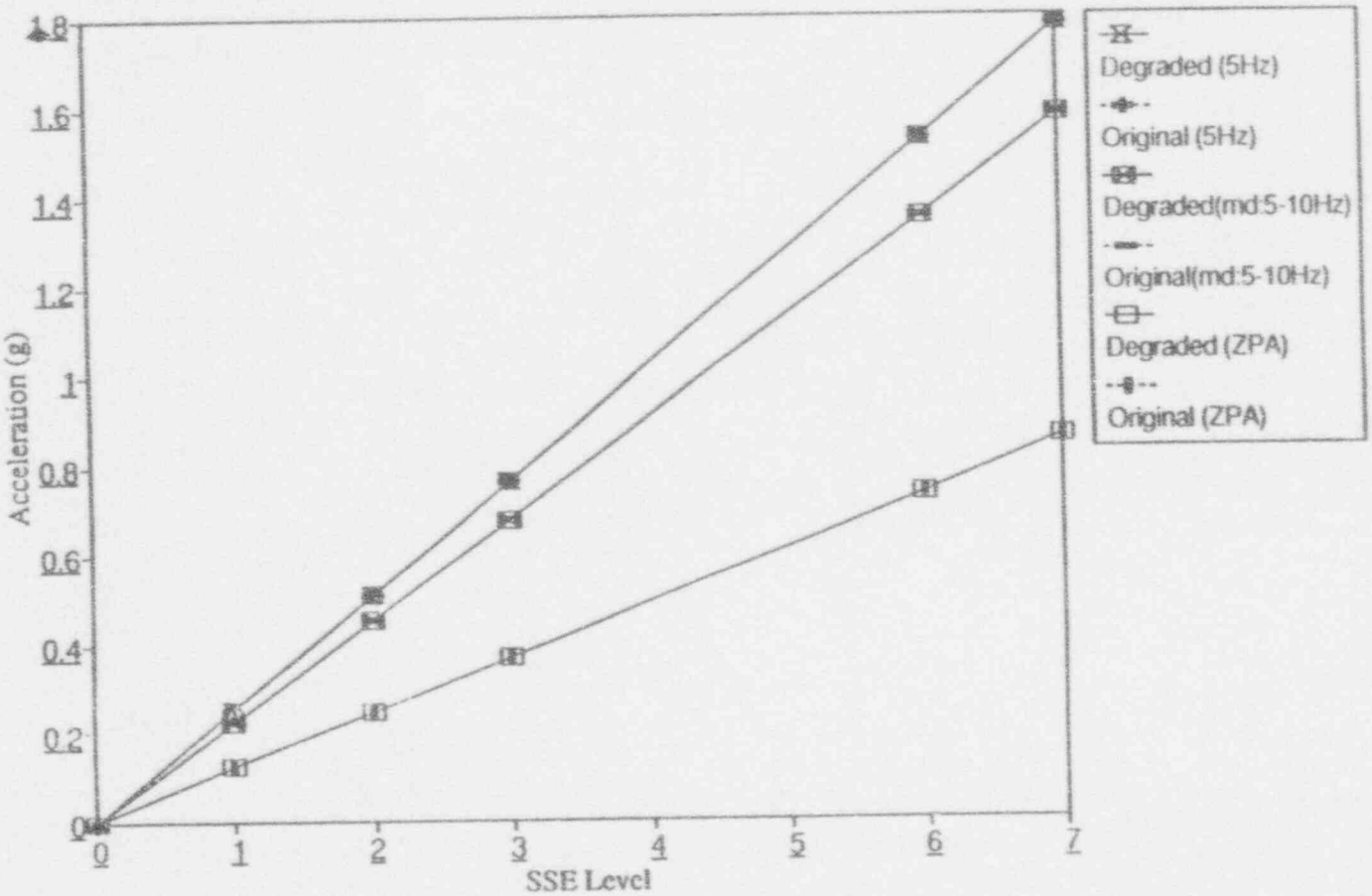

Figure 4-5 Median Responses for DG Building, Foundation, El. 127'

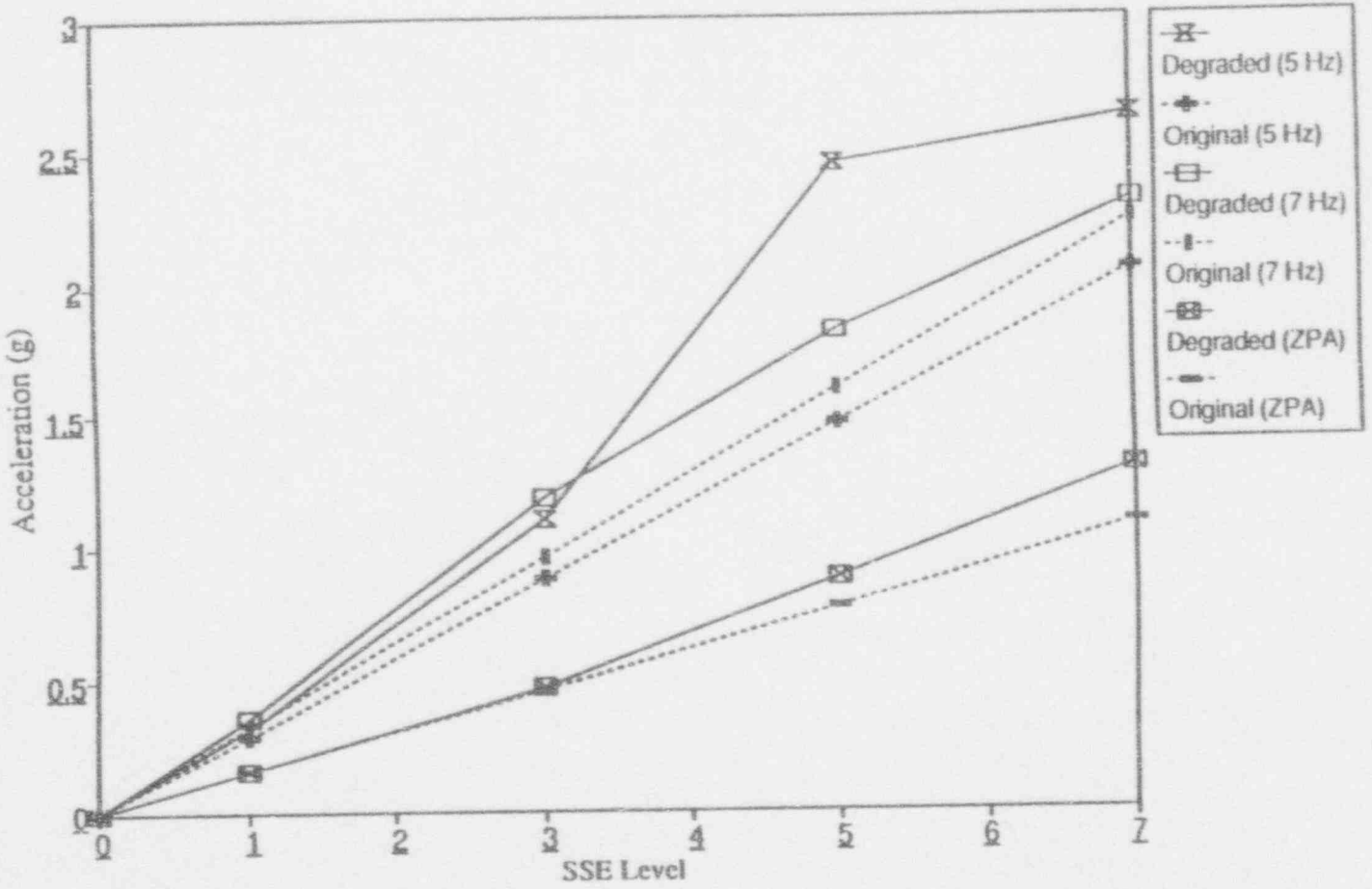

Figure 4-6 Median Responses for ECT Structure, Node 3, El. 153'

relatively thick resulting in lower stresses, thereby lessening the amount of reduction in stiffness. Also, the dominant frequency of the Reactor Building was only 7.06 Hz, which is already within the range of high earthquake intensity, further reduction will only decrease the floor responses as shown in Figure 4-2.

Figure 4-6 shows no effect when reducing the stiffnesses, this is due to the fact that this in the foundation elevation and wall stiffnesses have no effect at this level. Since this is the location of the diesel generators and all other important components inside the Diesel Generator Building, they will not see any increase in response as a result of reducing the stiffnesses.

All the computed floor responses and modal frequencies for both original and reduced stiffnesses at each earthquake level is shown in Appendix A.

4.1.4 Probabilistic Results

To evaluate the effect of including degraded shear wall stiffnesses in the seismic PRA of Peach Bottom, the accident sequences were quantified both with and without the stiffness reduction. In each case, a complete uncertainty analysis was performed on the accident sequences using a true Monte Carlo analysis.

From the accumulated values of accident sequence frequency and core damage frequency, exact statistics on their distributions are directly obtainable. The result is an estimate of the mean annual frequency of each accident sequence as well as of the total core damage plus a description of the distributions associated with these estimates. The mean core damage frequencies per year are shown below for both sets of hazard curves and with and without stiffness reduction:

	LLNL Hazard	EPRI Hazard
Original Stiffnesses	6.71E-5	2.77E-6
Reduced Stiffnesses	8.44E-5	3.58E-6

This represents an increase of between 25% and 30% in core damage frequency when reduced shear wall stiffnesses are included in a seismic PRA. The breakdown of each accident sequence contribution and the various percentile distributions for the totals are shown in Appendix A of this report.

In addition, a mean point estimate quantification (for which all random parameters were set to their mean values and a single quantification was made for each case. This allows for an efficient evaluation of each individual component's importance to the total core damage frequency and a determination of the relative contribution of different earthquake levels to the total. (Experience has shown that such mean point estimate calculations yield results which are very close to the actual mean results obtained from the full uncertainty analysis.)

Table 4-2 presents the mean point estimate core damage contributions at seven intervals over the LLNL hazard curve for each accident sequence using original stiffnesses. Table 4-3 presents the mean core damage contributions for the EPRI hazard curve and original stiffnesses. Similarly, Tables 4-4 and 4-5 present the mean point estimate contributions for both hazard curves, but using reduced stiffnesses. The right hand column in each of these tables presents the total contribution of each accident sequence to the total core damage frequency. As can be seen, the incremental contributions from the LOCA events do not become significant until the higher acceleration levels. The reactor vessel rupture sequence does not make a significant contribution until the highest PGA increment.

An important thing to note from Tables 4-2 thru 4-5 is the sum of the accident sequence contributions at each earthquake level, as shown at the bottom of each column on the table. The contributions are seen to be small at the first increment, increasing to a maximum at the forth earthquake increment, and then decreasing at higher earthquake levels. This indicates that the bulk of the risk is occurring in the range of 0.45g to 0.90g which roughly corresponds to the range of 4-7 SSE. Further, this shows that the bulk of the risk has been captured by integrating over the range 0.15g to 1.20g.

4.1.5 Deterministic Results

To assess the impact of the frequency reduction model on the deterministic design calculations for Peach Bottom, a set of "design-like" structural response calculations was performed. These "design-like" calculations do not attempt to reproduce the original design calculations, but instead, use the same parameters, such as input time history, structural damping, and material properties. However, is this study, the structural stiffnesses were varied to obtain both original stiffness results (loads and spectra) and reduced stiffness results, and could then compare the differences without actually assessing the initial design.

These calculations are as close to the original design calculation methods as could be determined from the Peach Bottom Final Safety Analysis Report [24]. A time history analysis was performed both on the original models and the reduced stiffness models using the 1952 Taft earthquake record scaled to 1 SSE (0.12g). The amount of stiffness reduction was assumed to be 25% or 0.75 * original stiffness, since 1 SSE earthquakes should always result in shear stresses below 150 psi, as they were in the probabilistic study. Structural damping was 5% for both sets of calculations.

Acceleration response spectra were generated at various nodal locations throughout all the structures comparing the undegraded response to the reduced stiffness response. An example of each structure is shown in Figures 4-7 thru 4-11. More deterministic spectras are shown in Appendix A of this report.

Table 4-2

Total Accident Sequence Frequency Increments
LLNL Seismic Hazard Curves for Peach Bottom with Original Stiffnesses

Accident Sequence	0.15-0.30g	0.30-0.45g	0.45-0.60g	0.60-0.75g	0.75-0.90g	0.90-1.05g	1.05-1.20g	Total
RVR-1	7.2E-08	6.9E-07	1.7E-06	2.5E-06	2.8E-06	2.7E-06	2.4E-06	1.3E-05
ALOCA-17	6.4E-10	3.7E-08	1.0E-07	8.2E-08	3.6E-08	1.1E-08	2.9E-09	2.7E-07
ALOCA-30	9.0E-10	2.7E-07	3.1E-06	6.9E-06	6.0E-06	3.8E-06	2.3E-06	2.2E-05
S1LOCA-25	1.5E-12	5.0E-10	3.6E-09	5.3E-09	3.5E-09	1.4E-09	4.7E-10	1.5E-08
S1LOCA-70	1.2E-10	5.4E-08	7.7E-07	1.8E-06	1.6E-06	9.7E-07	5.4E-07	5.7E-06
S1LOCA-80	7.4E-12	2.9E-09	3.6E-08	1.1E-07	1.8E-07	2.0E-07	1.6E-07	7.0E-07
S2LOCA-21	6.9E-10	3.5E-08	7.6E-08	4.8E-08	1.6E-08	3.9E-09	8.1E-10	1.8E-07
S2LOCA-42	8.8E-11	1.7E-08	1.4E-07	3.1E-07	3.8E-07	3.1E-07	2.1E-07	1.4E-06
RWT-1	1.7E-08	2.6E-07	6.4E-07	7.1E-07	5.0E-07	2.7E-07	1.3E-07	2.5E-06
RWT-2	1.8E-09	2.8E-08	6.8E-08	7.6E-08	5.4E-08	2.9E-08	1.3E-08	2.7E-07
RWT-3	3.7E-11	5.8E-10	1.4E-09	1.6E-09	1.1E-09	6.1E-10	2.8E-10	5.6E-09
RWT-4	3.7E-12	5.8E-11	1.4E-10	1.6E-10	1.1E-10	6.1E-11	2.8E-11	5.6E-10
T1-25	1.2E-11	7.3E-10	3.8E-09	6.9E-09	7.0E-09	4.9E-09	2.7E-09	2.6E-08
T1-32	1.2E-12	8.1E-12	1.7E-11	1.9E-11	1.3E-11	7.1E-12	3.1E-12	6.9E-11
T1-33	1.1E-07	3.8E-06	1.3E-05	1.1E-05	3.9E-06	1.1E-06	2.9E-07	3.2E-05
T1-36 to S2-41	1.1E-12	7.0E-11	3.6E-10	6.6E-10	6.7E-10	4.7E-10	2.6E-10	2.5E-09
T1-36 to S2-42	1.0E-13	7.3E-13	1.6E-12	1.8E-12	1.3E-12	7.1E-13	3.1E-13	6.6E-12
T1-40 to S1-70	7.1E-15	1.8E-13	2.5E-12	1.0E-11	1.8E-11	1.8E-11	1.3E-11	6.3E-11
T1-40 to S1-80	1.5E-14	7.0E-14	9.2E-14	7.2E-14	4.1E-14	1.8E-14	7.2E-15	3.1E-13
T1-43 to ALOCA-30	1.8E-13	2.1E-11	8.7E-10	9.3E-09	3.8E-08	8.7E-08	1.4E-07	2.7E-07
T3A-1 to T2-1-29	4.7E-12	1.1E-10	2.4E-10	1.5E-10	5.1E-11	1.1E-11	1.9E-12	5.7E-10
T3A-1 to T2-1-36	1.1E-12	3.6E-11	8.9E-11	6.8E-11	2.7E-11	7.1E-12	1.4E-12	2.3E-10
	2.0E-07	5.2E-06	1.9E-05	2.3E-05	1.6E-05	9.5E-06	6.2E-06	7.90E-05

Table 4-3

Total Accident Sequence Frequency Increments
EPRI Seismic Hazard Curves for Peach Bottom with Original Stiffnesses

Accident Sequence	0.15-0.30g	0.30-0.45g	0.45-0.60g	0.60-0.75g	0.75-0.90g	0.90-1.05g	1.05-1.20g	Total
RVR-1	4.8E-09	3.3E-08	6.7E-08	8.6E-08	8.8E-08	6.1E-08	6.7E-08	4.1E-07
ALOCA-17	4.3E-11	1.8E-09	3.9E-09	2.8E-09	1.1E-09	2.5E-10	8.2E-11	1.0E-08
ALOCA-30	6.0E-11	1.3E-08	1.2E-07	2.3E-07	1.9E-07	8.6E-08	6.4E-08	7.1E-07
S1LOCA-25	9.8E-14	2.4E-11	1.4E-10	1.8E-10	1.1E-10	3.3E-11	1.3E-11	5.0E-10
S1LOCA-70	7.9E-12	2.6E-09	3.0E-08	6.2E-08	5.0E-08	2.2E-08	1.5E-08	1.8E-07
S1LOCA-80	5.0E-13	1.4E-10	1.4E-09	3.9E-09	5.7E-09	4.4E-09	4.6E-09	2.0E-08
S2LOCA-21	4.6E-11	1.7E-09	3.0E-09	1.6E-09	5.0E-10	8.8E-11	2.3E-11	6.9E-09
S2LOCA-42	5.9E-12	8.2E-10	5.3E-09	1.1E-08	1.2E-08	7.1E-09	5.9E-09	4.2E-08
RWT-1	1.1E-09	1.2E-08	2.5E-08	2.4E-08	1.6E-08	6.2E-09	3.5E-09	8.8E-08
RWT-2	1.2E-10	1.3E-09	2.7E-09	2.6E-09	1.7E-09	6.6E-10	3.8E-10	9.4E-09
RWT-3	2.5E-12	2.8E-11	5.5E-11	5.4E-11	3.5E-11	1.4E-11	7.9E-12	2.0E-10
RWT-4	2.5E-13	2.8E-12	5.5E-12	5.4E-12	3.5E-12	1.4E-12	7.9E-13	2.0E-11
T1-25	7.8E-13	3.5E-11	1.5E-10	2.3E-10	2.2E-10	1.1E-10	7.6E-11	8.2E-10
T1-32	7.9E-14	3.9E-13	6.6E-13	6.4E-13	4.2E-13	1.6E-13	8.7E-14	2.4E-12
T1-33	7.4E-09	1.8E-07	4.9E-07	3.6E-07	1.2E-07	2.4E-08	8.0E-09	1.2E-06
T1-36 to S2-41	7.5E-14	3.3E-12	1.4E-11	2.2E-11	2.1E-11	1.1E-11	7.3E-12	7.9E-11
T1-36 to S2-42	6.8E-15	3.5E-14	6.3E-14	6.3E-14	4.1E-14	1.6E-14	8.7E-15	2.3E-13
T1-40 to S1-80	4.7E-16	8.6E-15	9.6E-14	3.6E-13	5.7E-13	4.1E-13	3.6E-13	1.8E-12
T1-40 to S1-80	9.8E-16	3.3E-15	3.6E-15	2.4E-15	1.3E-15	4.1E-16	2.0E-16	1.2E-14
T1-43 to ALOCA-30	1.2E-14	9.8E-13	3.4E-11	3.2E-10	1.2E-09	2.0E-09	3.8E-09	7.3E-09
T3A-1 to T2-1-29	3.1E-13	5.2E-12	9.4E-12	5.3E-12	1.6E-12	2.5E-13	5.3E-14	2.2E-11
T3A-1 to T2-1-36	7.2E-14	1.7E-12	3.5E-12	2.3E-12	8.5E-13	1.6E-13	4.0E-14	8.6E-12
	1.4E-08	2.5E-07	7.5E-07	7.9E-07	4.8E-07	2.1E-07	1.7E-07	2.67E-06

Table 4-4

Total Accident Sequence Frequency Increments
LLNL Seismic Hazard Curves for Peach Bottom with Reduced Stiffnesses

Accident Sequence	0.15-0.30g	0.30-0.45g	0.45-0.60g	0.60-0.75g	0.75-0.90g	0.90-1.05g	1.05-1.20g	Total
RVR-1	5.1E-08	5.2E-07	1.4E-06	2.1E-06	2.4E-06	2.4E-06	2.2E-06	1.1E-05
ALOCA-17	1.8E-09	8.5E-08	1.9E-07	1.3E-07	4.6E-08	1.2E-08	3.2E-09	4.7E-07
ALOCA-30	2.0E-09	5.3E-07	4.8E-06	8.1E-06	6.3E-06	4.0E-06	2.4E-06	2.6E-05
S1LOCA-25	2.5E-12	7.7E-10	4.8E-09	6.4E-09	3.9E-09	1.5E-09	4.9E-10	1.8E-08
S1LOCA-70	2.5E-10	1.0E-07	1.1E-06	2.2E-06	1.7E-06	1.0E-06	5.7E-07	6.7E-06
S1LOCA-80	3.4E-11	8.8E-09	8.6E-08	2.3E-07	3.3E-07	3.2E-07	2.5E-07	1.2E-06
S2LOCA-21	1.7E-09	7.8E-08	1.5E-07	7.7E-08	2.2E-08	4.8E-09	9.3E-10	3.3E-07
S2LOCA-42	4.0E-10	5.2E-08	3.3E-07	6.3E-07	6.8E-07	5.1E-07	3.2E-07	2.5E-06
RWT-1	7.6E-08	8.0E-07	1.5E-06	1.4E-06	9.0E-07	4.4E-07	1.9E-07	5.4E-06
RWT-2	8.1E-09	8.5E-08	1.6E-07	1.5E-07	9.6E-08	4.7E-08	2.0E-08	5.7E-07
RWT-3	1.7E-10	1.8E-09	3.4E-09	3.2E-09	2.0E-09	9.9E-10	4.3E-10	1.2E-08
RWT-4	1.7E-11	1.8E-10	3.4E-10	3.2E-10	2.0E-10	9.9E-11	4.3E-11	1.2E-09
T1-25	3.2E-11	1.4E-09	5.8E-09	8.6E-09	7.4E-09	4.4E-09	2.1E-09	3.0E-08
T1-32	1.5E-12	8.8E-12	1.7E-11	1.7E-11	1.1E-11	5.4E-12	2.2E-12	6.3E-11
T1-33	2.3E-07	7.2E-06	1.9E-05	1.2E-05	3.7E-06	9.6E-07	2.4E-07	4.3E-05
T1-36 to S2-41	3.1E-12	1.4E-10	5.5E-10	8.3E-10	7.1E-10	4.3E-10	2.1E-10	2.9E-09
T1-36 to S2-42	1.3E-13	8.0E-13	1.6E-12	1.6E-12	1.1E-12	5.4E-13	2.2E-13	6.0E-12
T1-40 to S1-70	9.0E-15	2.0E-13	2.4E-12	9.1E-12	1.4E-11	1.3E-11	8.5E-12	4.8E-11
T1-40 to S1-80	1.8E-14	7.6E-14	9.0E-14	6.4E-14	3.4E-14	1.4E-14	5.1E-15	3.0E-13
T1-43 to ALOCA-30	2.2E-13	2.3E-11	8.6E-10	8.5E-09	3.3E-08	7.3E-08	1.1E-07	2.3E-07
T3A-1 to T2-1-29	5.8E-12	1.4E-10	2.9E-10	1.7E-10	4.8E-11	9.5E-12	1.5E-12	6.6E-10
T3A-1 to T2-1-36	1.7E-12	5.2E-11	1.1E-10	7.5E-11	2.7E-11	6.3E-12	1.2E-12	2.8E-10
	3.7E-07	9.5E-06	2.8E-05	2.7E-05	1.6E-05	9.7E-06	6.3E-06	9.73E-05

Table 4-5

Total Accident Sequence Frequency Increments
EPRI Seismic Hazard Curves for Peach Bottom with Reduced Stiffnesses

Accident Sequence	0.15-0.30g	0.30-0.45g	0.45-0.60g	0.60-0.75g	0.75-0.90g	0.90-1.05g	1.05-1.20g	Total
RVR-1	3.4E-09	2.5E-08	5.3E-08	7.1E-08	7.5E-08	5.4E-08	6.1E-08	3.4E-07
ALOCA-17	1.2E-10	4.1E-09	7.6E-09	4.4E-09	1.4E-09	2.8E-10	8.9E-11	1.8E-08
ALOCA-30	1.3E-10	2.5E-08	1.9E-07	2.8E-07	1.9E-07	8.9E-08	6.8E-08	8.4E-07
S1LOCA-25	1.7E-13	3.7E-11	1.9E-10	2.2E-10	1.2E-10	3.5E-11	1.4E-11	6.1E-10
S1LOCA-70	1.6E-11	4.8E-09	4.5E-08	7.4E-08	5.2E-08	2.3E-08	1.6E-08	2.1E-07
S1LOCA-80	2.3E-12	4.2E-10	3.3E-09	7.9E-09	1.0E-08	7.2E-09	7.0E-09	3.6E-08
S2LOCA-21	1.1E-10	3.7E-09	5.7E-09	2.6E-09	6.9E-10	1.1E-10	2.6E-11	1.3E-08
S2LOCA-42	2.7E-11	2.5E-09	1.3E-08	2.2E-08	2.1E-08	1.2E-08	8.9E-09	7.9E-08
RWT-1	5.1E-09	3.8E-08	6.0E-08	4.9E-08	2.8E-08	1.0E-08	5.4E-09	2.0E-07
RWT-2	5.4E-10	4.1E-09	6.4E-09	5.2E-09	3.0E-09	1.1E-09	5.7E-10	2.1E-08
RWT-3	1.1E-11	8.5E-11	1.3E-10	1.1E-10	6.2E-11	2.2E-11	1.2E-11	4.3E-10
RWT-4	1.1E-12	8.5E-12	1.3E-11	1.1E-11	6.2E-12	2.2E-12	1.2E-12	4.3E-11
T1-25	2.2E-12	6.8E-11	2.2E-10	2.9E-10	2.3E-10	1.0E-10	6.0E-11	9.8E-10
T1-32	9.7E-14	4.2E-13	6.5E-13	5.8E-13	3.5E-13	1.2E-13	6.2E-14	2.3E-12
T1-33	1.6E-08	3.4E-07	7.2E-07	4.0E-07	1.1E-07	2.2E-08	6.8E-09	1.6E-06
T1-36 to S2-41	2.1E-13	6.5E-12	2.2E-11	2.8E-11	2.2E-11	9.6E-12	5.8E-12	9.4E-11
T1-36 to S2-42	8.4E-15	3.8E-14	6.2E-14	5.6E-14	3.4E-14	1.2E-14	6.2E-15	2.2E-13
T1-40 to S1-70	6.0E-16	9.6E-15	9.4E-14	3.1E-13	4.5E-13	3.0E-13	2.4E-13	1.4E-12
T1-40 to S1-80	1.2E-15	3.6E-15	3.5E-15	2.2E-15	1.0E-15	3.2E-16	1.4E-16	1.2E-14
T1-43 to ALOCA-30	1.5E-14	1.1E-12	3.4E-11	2.9E-10	1.0E-09	1.7E-09	3.2E-09	6.2E-09
T3A-1 to T2-1-29	3.9E-13	6.8E-12	1.1E-11	5.6E-12	1.5E-12	2.2E-13	4.2E-14	2.6E-11
T3A-1 to T2-1-36	1.1E-13	2.5E-12	4.4E-12	2.6E-12	8.3E-13	1.4E-13	3.2E-14	1.1E-11
	2.5E-08	4.5E-07	1.1E-06	9.2E-07	5.0E-07	2.2E-07	1.8E-07	3.40E-06

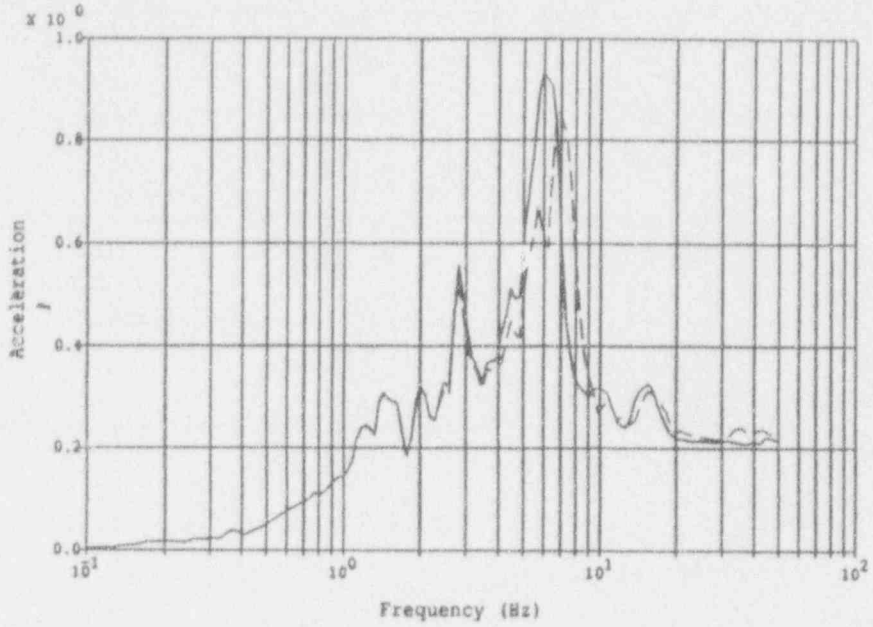

Legend:

Degraded Model
Factor = 0.75 ——————

Original Model – – – – – –

Notes:

1SSE Level, .12g PGA
Accelerations in g's
5% Spectral Damping
5% Struct. Damping

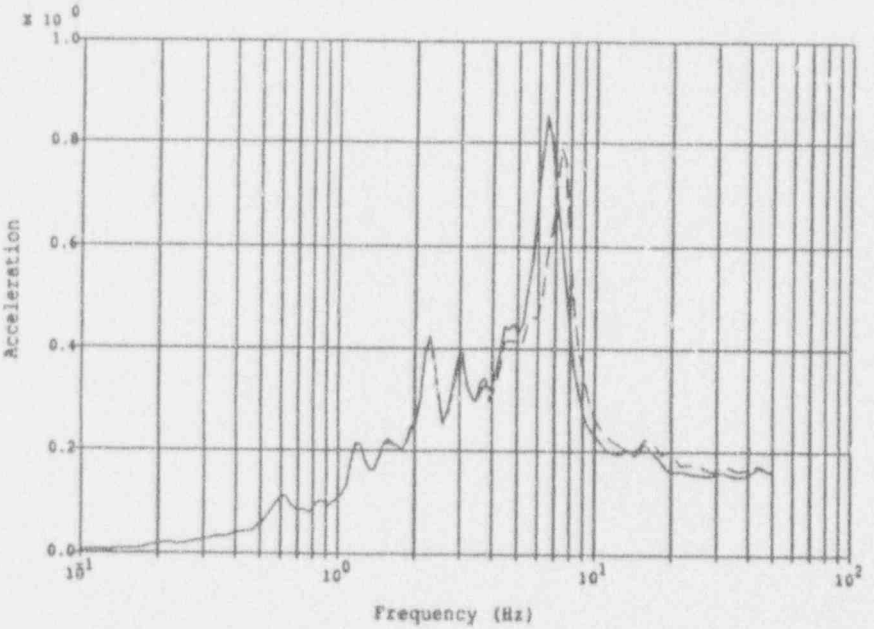

Legend:

Degraded Model
Factor = 0.75 ——————

Original Model – – – – – –

Notes:

1SSE Level, .12g PGA
Accelerations in g's
5% Spectral Damping
5% Struct. Damping

Figure 4-7 Peach Bottom Deterministic Analysis, R/C Building Node 12, Elev. 156', N-S dir. (top), E-W dir. (bottom)

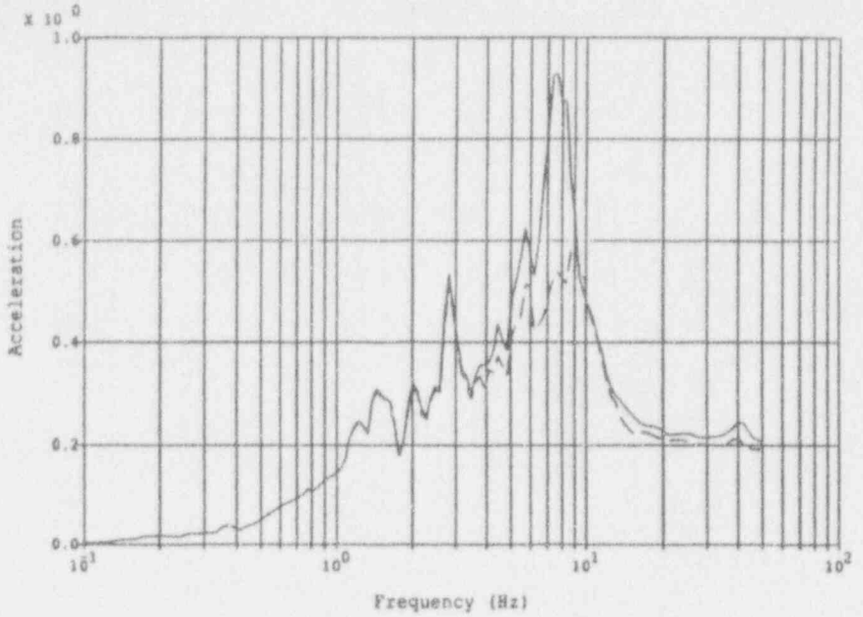

Legend:

Degraded Model
Factor = 0.75 ————————

Original Model — — — — —

Notes:

1SSE Level, .12g PGA
Accelerations in g's
5% Spectral Damping
5% Struct. Damping

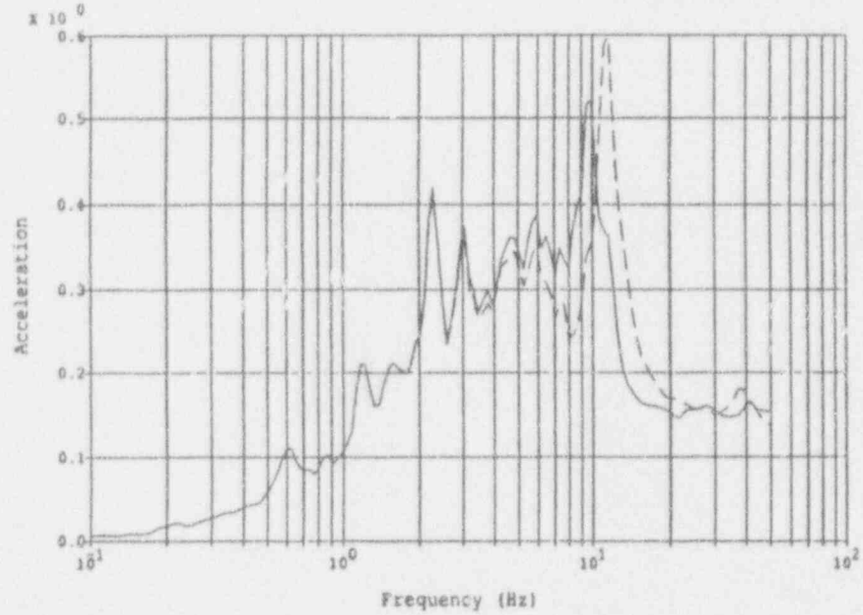

Legend:

Degraded Model
Factor = 0.75 ————————

Original Model — — — — —

Notes:

1SSE Level, .12g PGA
Accelerations in g's
5% Spectral Damping
5% Struct. Damping

Figure 4-8 Peach Bottom Deterministic Analysis, RWST Building Node 12, Elev. 165', N-S dir. (top), E-W dir. (bottom)

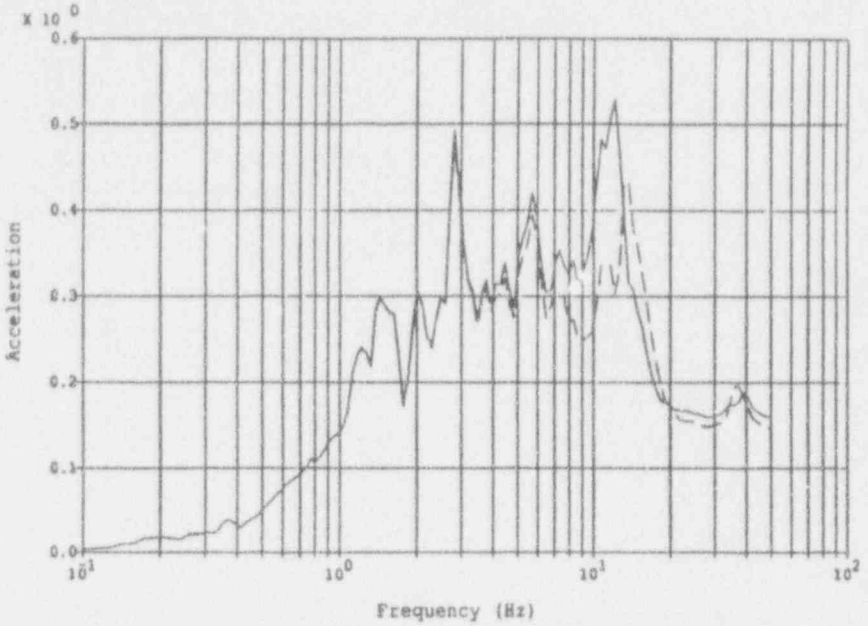

Legend:

Degraded Model
Factor = 0.75 ————————

Original Model — — — — —

Notes:

1SSE Level, .12g PGA
Accelerations in g's
5% Spectral Damping
5% Struct. Damping

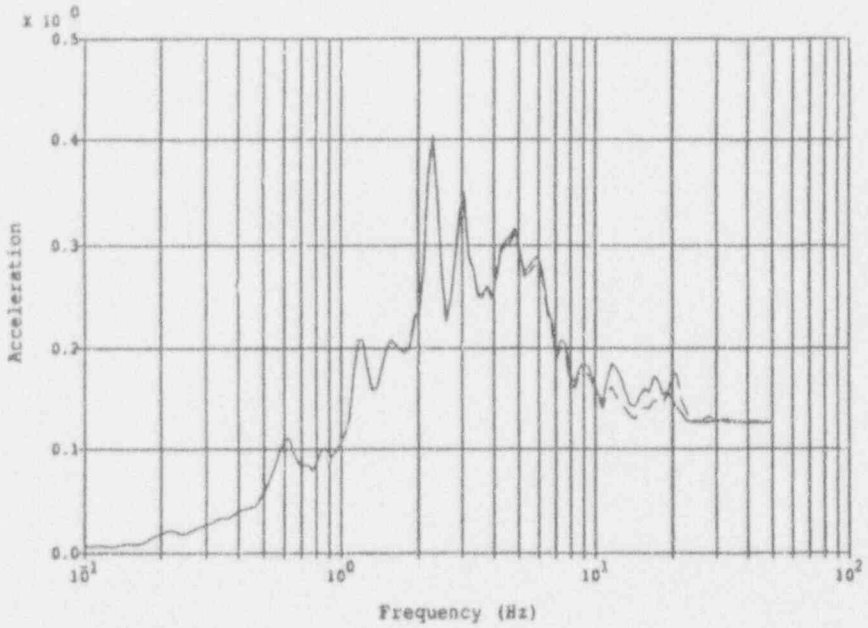

Legend:

Degraded Model
Factor = 0.75 ————————

Original Model — — — — —

Notes:

1SSE Level, .12g PGA
Accelerations in g's
5% Spectral Damping
5% Struct. Damping

Figure 4-9 Peach Bottom Deterministic Analysis, CWP Building Node 13, Elev. 114', N-S dir. (top), E-W dir. (bottom)

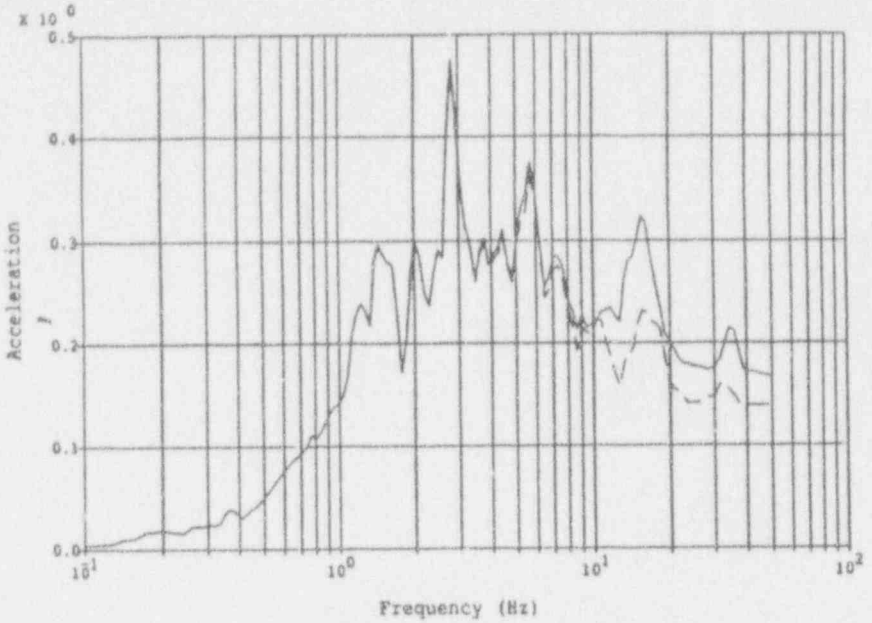

Legend:

Degraded Model
Factor = 0.75 ————————

Original Model - - - - - - -

Notes:

1SSE Level, .12g PGA
Accelerations in g's
5% Spectral Damping
5% Struct. Damping

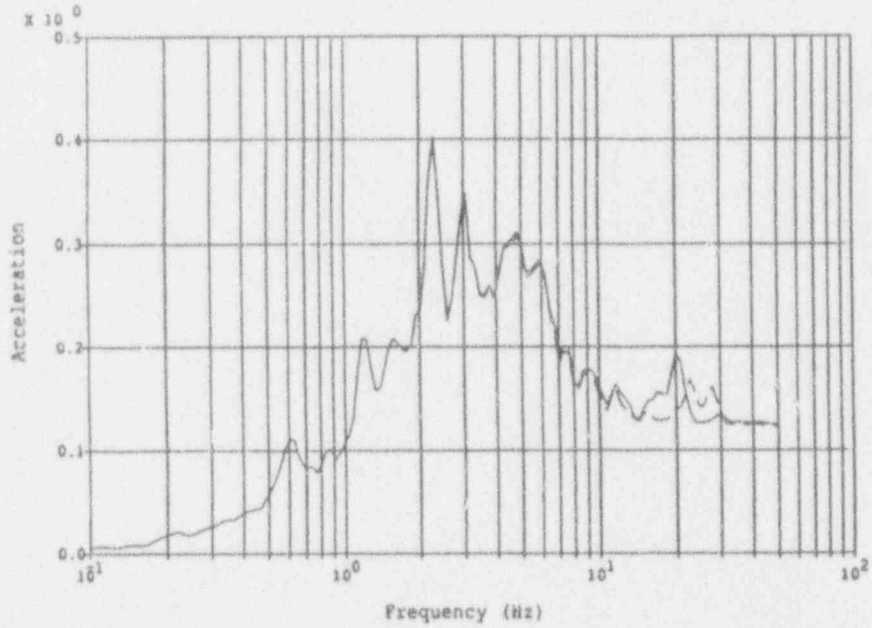

Legend:

Degraded Model
Factor = 0.75 ————————

Original Model - - - - - - -

Notes:

1SSE Level, .12g PGA
Accelerations in g's
5% Spectral Damping
5% Struct. Damping

Figure 4-10 Peach Bottom Deterministic Analysis, DG Building Node 6, Elev. 161', N-S dir. (top), E-W dir. (bottom)

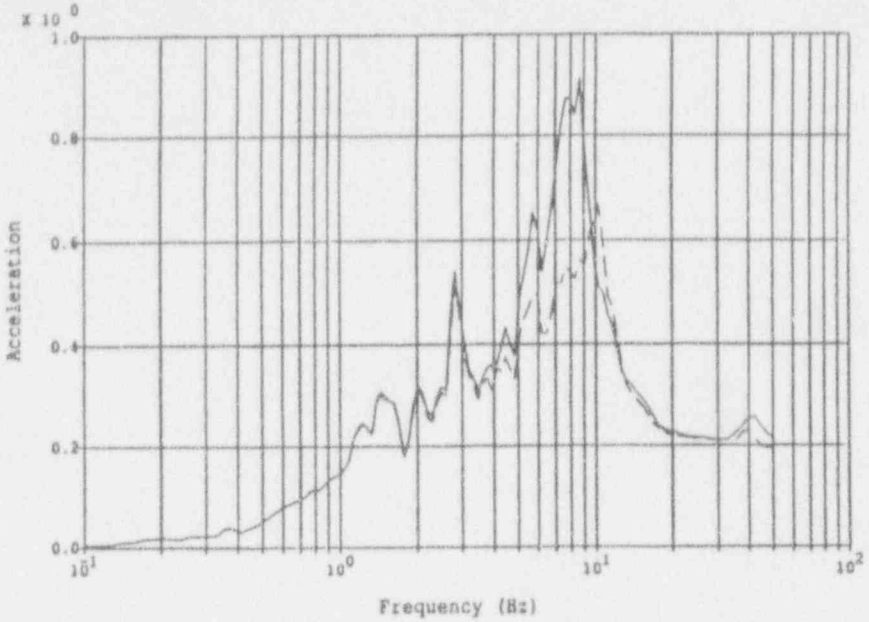

Legend:

Degraded Model
Factor = 0.75 ——————

Original Model — — — — —

Notes:

1SSE Level, .12g PGA
Accelerations in g's
5% Spectral Damping
5% Struct. Damping

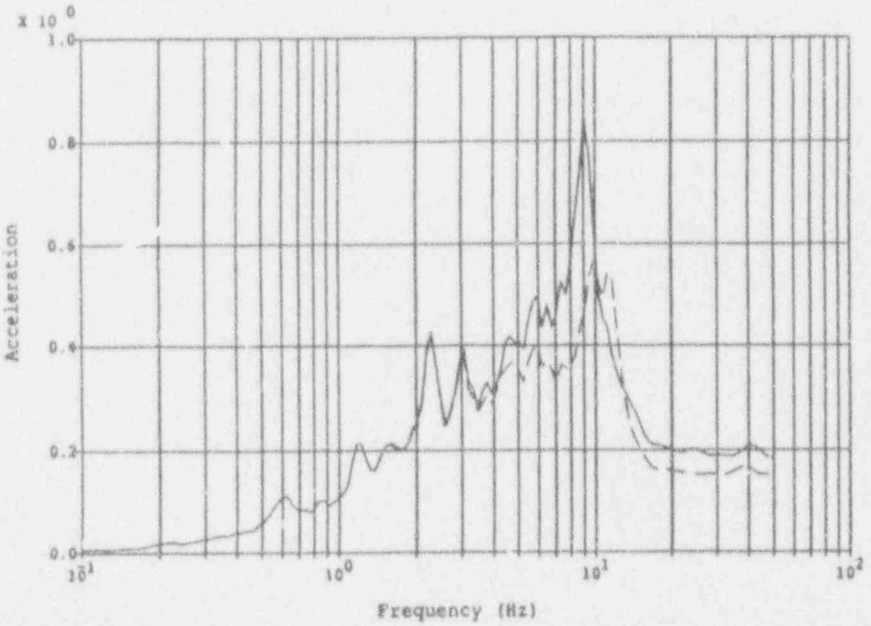

Legend:

Degraded Model
Factor = 0.75 ——————

Original Model — — — — —

Notes:

1SSE Level, .12g PGA
Accelerations in g's
5% Spectral Damping
5% Struct. Damping

Figure 4-11 Peach Bottom Deterministic Analysis, EC Towers Node 4, Elev. 168' N-S dir. (top), E-W dir. (bottom)

It can be seen from these spectra that some very significant shifts in peak values and frequencies are present. Most notably, the Emergency Cooling Towers experienced a significant shift and increase in the 7-10 Hz range in both directions as shown in Figure 4-11. In addition, the Radwaste/Turbine Building experienced a significant increase in the 6-10 Hz range in the N-S direction and a shift in the E-W direction as shown in Figure 4-8.

Tables 4-6 thru 4-10 show a comparison of story shear and moment loads listed by floor elevation (that is, the shear and moment values just under the floor slabs at these elevations) for the original and reduced stiffness models described above when subjected to the Taft earthquake scaled to 0.12g (SSE). Note that the values listed are net total forces and moments for that elevation and have not yet been distributed to the individual walls at that elevation.

In general, it can be seen that there is a maximum increase in loads of about 20% due to the stiffness reduction. Since there is very little assumed torsion in any of these structures, the same increase would apply to loads in the individual walls. Thus, from a design viewpoint, the stiffness reduction does result in a significant increase in net loads, but this increase (20%) is probably well within the range of conservatism implicit in the original design calculations.

4.1.6 Summary of Peach Bottom Analysis

Both a probabilistic and deterministic re-evaluation of the Peach Bottom Atomic Power Plant was performed using original stiffnesses and reduced stiffnesses. The probabilistic analysis consisted of re-performing a seismic PRA and adjusting the responses and structural fragilities to account for the reduced stiffnesses. This resulted in two overall core damage frequencies, one using original stiffnesses and one using reduced stiffnesses. A second set of frequencies was obtained for bounding purposes by using both the EPRI and LLNL hazard curves.

An increase of 25% and 30% (using LLNL and EPRI hazard curves respectively) in core damage frequency was observed, when reduced shear wall stiffnesses were included in a seismic PRA. This increase in core damage frequency is due primarily to the increased values of the responses for 7 Hz in the Circulating Water Pump Structure and the Emergency Cooling Water Towers. Both these responses have been increased over the case with no stiffness reduction. These responses are related to the fragilities of the Emergency Service Water pumps located in the Circulating Water Pump Structure and the Emergency Cooling Water pump located in the Emergency Cooling Water Tower. These three pumps play a critical role in providing cooling to the diesel generators in the event of loss of off-site power. Furthermore, they had a very significant risk reduction potential. That is, they were very significant contributors to the base case core damage frequency. In the recalculation of risk, their responses increased due to the frequency reduction as discussed in the last section. Thus, their failure probabilities at all earthquake levels were increased. Hence, the

Table 4-6

Forces between Floor Levels of Peach Bottom Reactor/Containment Building

Original Stiffnesses

Elev.	$Shear_X$(kip)	$Shear_Y$(kip)	$Moment_X$(kip-ft)	$Moment_Y$(kip-ft)
Externals:				
91'	16,710	13,100	1,338,000	1,642,000
119'	16,030	12,550	940,900	1,160,000
135'	13,240	10,760	751,600	928,500
165'	10,430	8,494	429,000	532,800
195'	5,224	4,179	174,100	219,800
234'	500	342	11,660	17,300
252'	248	162	5,518	8,444
Internals:				
119'	735	544	18,770	23,280
135'	670	505	10,570	12,550
145'	298	264	5,151	6,688
156'	228	197	2,488	3,631
169'	96	67	545	922
182'	81	74	963	1,056

Reduced Stiffnesses

Elev.	$Shear_X$(kip)	$Shear_Y$(kip)	$Moment_X$(kip-ft)	$Moment_Y$(kip-ft)
Externals:				
91'	17,860	13,450	1,316,000	1,715,000
119'	17,090	12,900	909,000	1,174,000
135'	13,940	10,620	724,400	915,700
165'	10,320	8,151	417,600	509,000
195'	5,130	4,109	173,000	218,300
234'	533	374	12,700	18,310
252'	265	175	5,966	9,018
Internals:				
119'	748	539	18,050	24,690
135'	684	494	9,916	13,390
145'	311	244	5,136	6,322
156'	217	188	2,759	3,699
169'	100	74	737	1,361
182'	69	59	770	902

Table 4-7

Forces between Floor Levels of Peach Bottom Radwaste/Turbine Building

Original Stiffnesses

Elev.	$Shear_X$(kip)	$Shear_Y$(kip)	$Moment_X$(kip-ft)	$Moment_Y$(kip-ft)
116'	8,490	6,176	332,800	391,500
135'	6,106	4,619	161,100	223,900
150'	4,388	3,292	92,260	128,800
165'	2,032	1,598	40,100	57,310

Reduced Stiffnesses

Elev.	$Shear_X$(kip)	$Shear_Y$(kip)	$Moment_X$(kip-ft)	$Moment_Y$(kip-ft)
116'	9,154	6,568	322,700	403,900
135'	6,456	4,977	164,100	235,100
150'	4,637	3,559	87,5[illegible]0	137,100
165'	2,183	1,453	35,34[illegible]	61,600

Table 4-8

Forces between Floor Levels of Peach Bottom
Circulating Water Pump Structure

Original Stiffnesses

Elev.	$Shear_X$(kip)	$Shear_Y$(kip)	$Moment_X$(kip-ft)	$Moment_Y$(kip-ft)
79'	6,527	5,746	151,500	159,200
88'	5,079	4,560	99,970	102,400
97'	3,564	2,996	55,760	58,840
105'	2,377	1,873	28,390	28,110
114'	267	234	4,047	4,429
114'	162	139	2,311	2,685

Reduced Stiffnesses

Elev.	$Shear_X$(kip)	$Shear_Y$(kip)	$Moment_X$(kip-ft)	$Moment_Y$(kip-ft)
79'	7,047	5,785	155,800	169,600
88'	5,437	4,646	103,200	108,300
97'	3,793	3,100	57,880	61,820
105'	2,520	1,949	29,510	29,340
114'	281	248	4,299	4,649
114'	170	146	2,437	2,809

Table 4-9

Forces between Floor Levels of Peach Bottom
Diesel Generator Building

Original Stiffnesses

Elev.	$Shear_X$(kip)	$Shear_Y$(kip)	$Moment_X$(kip-ft)	$Moment_Y$(kip-ft)
127'	1,256	1,111	30,510	36,080
151'	514	477	5,672	5,677

Reduced Stiffnesses

Elev.	$Shear_X$(kip)	$Shear_Y$(kip)	$Moment_X$(kip-ft)	$Moment_Y$(kip-ft)
127'	1,476	1,129	30,890	42,590
151'	606	480	5,688	6,793

Table 4-10

Forces between Floor Levels of Peach Bottom
Emergency Cooling Towers

Original Stiffnesses

Elev.	$Shear_X$(kip)	$Shear_Y$(kip)	$Moment_X$(kip-ft)	$Moment_Y$(kip-ft)
118′	6,205	5,758	173,900	197,000
136′	3,065	2,573	71,510	85,340
153′	1,539	1,141	29,380	38,500
168′	595	472	12,260	15,420
192′	113	91	914	1,134

Reduced Stiffnesses

Elev.	$Shear_X$(kip)	$Shear_Y$(kip)	$Moment_X$(kip-ft)	$Moment_Y$(kip-ft)
118′	5,583	6,440	206,600	184,600
136′	2,895	3,110	90,660	85,260
153′	1,615	1,481	38,530	40,510
168′	628	629	16,320	16,280
192′	119	122	1,220	1,198

inclusion of reductions in the stiffness of the structural models for the CWPS and the ECW Tower have increased the computed total core damage frequency for Peach Bottom.

The deterministic analysis also showed some increased values. Some significant shifts in peak values and frequencies were noted. Most notably, the Emergency Cooling Towers experienced a significant shift and increase in the 7-10 Hz range in both directions. In addition, the Radwaste/Turbine Building experienced a significant increase in the 6-10 Hz range in the N-S direction and a shift in the E-W direction.

Similarly, deterministic loadings (both shear and moment) experienced some increases. There was a maximum increase in loads of about 20% due to the stiffness reduction. Thus, from a design viewpoint, the stiffness reduction does result in a significant increase in net loads, but this increase (20%) is probably well within the range of conservatism implicit in the original design calculations.

4.2 Zion

4.2.1 Background

The Zion plant was selected for analyzing the potential impact of degraded shear wall stiffness on plant seismic design loads and plant seismic risk because systems models and data had been developed in the earlier NRC-sponsored Seismic Safety Margins Research Program (SSMRP), as described in Reference 27. In addition, the Zion plant was the subject of a PRA sponsored by the utility, Commonwealth Edison, Inc., as described in Reference 28. However, the present study was based entirely on the results from the SSMRP.

In the SSMRP, a seismic PRA based on five different loss of coolant accident (LOCA) break sizes and two types of transient initiators was performed, and dynamic structural models of the buildings important to safety were developed. In addition, piping models were developed for the dynamic response analysis of critical piping segments associated with five systems important to safety. Thus the models developed in the SSMRP allowed the evaluation of the impact of degraded shear wall stiffnesses on the response of important safety related piping systems.

The Zion nuclear power plant is a 1040 MWe pressurized water reactor (PWR) located on the shore of Lake Michigan north of Chicago, Illinois. Commonwealth Edison, Inc. owns and operates the facility. Zion entered commercial operation in April 1973.

The reactor vendor for Zion was Westinghouse (W). The architect/engineer was Sargent and Lundy. The design of the reactor coolant system is typical of other W plants currently in commercial operation; there are four steam generators and four reactor coolant loops. Most of the major safety system designs are also fairly typical of other W plants.

The plant is founded on a site characterized by 110 feet of soil overlying a bedrock. The top layer of soil, about 35 ft thick, consists of granular lake deposits of dense, fine-to medium sands, together with variable amounts of coarse sand and gravel. The second layer, 30 ft thick, is a cohesive, firm-to-hard glacial till. The remaining 45-ft layer of soil is a cohesionless glacial deposit of dense sands and gravel. Based on the Final Safety Analysis Report [29], a horizontal peak ground accceleration of 0.17g was defined for the SSE.

4.2.2 Summary of Input

In order to perform a seismic PRA, the following pieces of information must first be obtained: First, the local earthquake hazard, usually in the form of seismic hazard curves with uncertainty bounds or weighting factors, must be determined. Second, the accident sequences which lead to core damage must be identified. Third, the failure modes for the plant safety and support systems must also be determined. Forth, the fragilities of all important structures and components must be determined. Fifth, the location of components and level of seismic response at that location for a given level of seismic input, must be determined.

To begin with, the set of hazard curves used for this study were taken from the NRC-sponsored Eastern and Central United States Seismic Characterization Program [25]. A second set of hazard curves was obtained from the seismic PRA performed by the plant owner (Commonwealth Edison) [28]. Figure 4-12 shows the mean hazard curves taken from these two reports. The median, 15% and 85% hazard curves along with the mean for the LLNL program are shown in Appendix B of this report. The median curve and the mean curve were input, and random realizations for the Monte Carlo study were generated assuming a lognormal distribution for any given peak ground acceleration. In addition, the complete family of weighted hazard curves used in the Zion PRA are also shown in the Appendix B. This discrete family of curves (with associated confidence levels for each curve expressed as a split fraction) was used directly. That is, for each realization in the Monte Carlo uncertainty analysis, one of the discrete curves was selected by random sampling. The percentage of samples corresponding to any given hazard curve corresponds to its associated confidence level split fraction.

A detailed description of the plant safety systems at Zion are fully outlined in Appendix B of this report. The event trees developed for the original SSMRP program was used directly. Based on these trees, a total of 148 so-called "terminal event sequences" were quantified in the original SSMRP. These resulted in accident sequences with a "plant damage state" as the end point rather than "onset of core damage". Therefore, since the thrust of this project was to determine the impact of reduced shear wall stiffness on core damage frequency, the original event trees were "collapsed" down to a corresponding set of core damage event trees. This procedure and both sets of events trees are shown in Appendix B of this report.

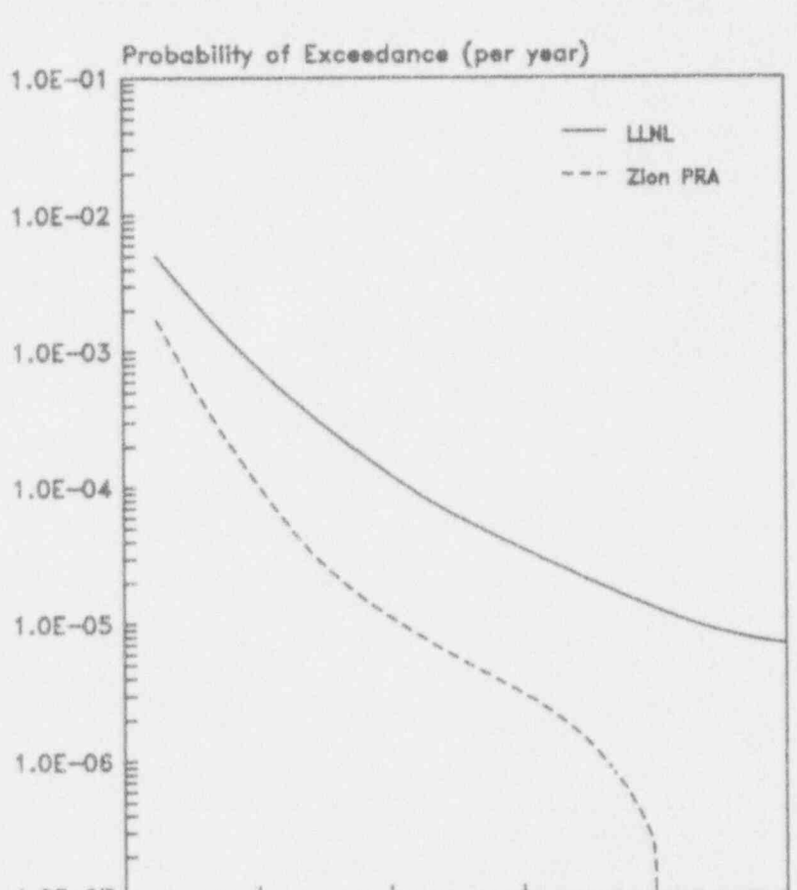

Figure 4-12 Zion Mean Hazard Curves

The probability of each individual component failure is dependent on two factors, the seismic fragility of the component and the amount of response experienced by the component during a given peak ground acceleration. The fragility for each vital component is given either a generic fragility or is computed on a plant specific basis if no generic fragility is applicable. At Zion, the Reactor Containment Building, Reactor building internal structure, and the Auxiliary/Fuel Handling/Turbine (AFT) building complex structural fragilities developed in the SSMRP were used in this analysis. The RWST, CST, reactor vessel supports, reactor coolant pump supports, and steam generator supports all required plant specific fragilities and are shown along with the structural fragilities in Table 4-11. All component fragilities, both site specific and generic, were not altered for the reduced stiffness case.

The amount of response (acceleration or force) experienced by each component at each earthquake level is next determined. First, the actual location of each component must be determined and related to a certain floor elevation of the building it is located within. After a dynamic time history analysis of each structure is run, building responses in terms of peak ground acceleration are developed. These are described in the next section and are the last piece of information needed to perform a seismic PRA.

4.2.3 Building and Piping Responses

Three distinct building models were generated for the Zion site: a reactor containment model, a reactor internal building model, and an AFT model. Ultimately, there were five structures supported on three foundations which were coupled through the soil impedances that were analyzed in order to determine the final degraded models for each SSE level and to determine maximum probabilistic structure/piping subsystem responses of both original and degraded models.

The models mentioned above are referred to herein as the original models since the element stiffnesses were those of the undegraded buildings. For the shear wall degradation study, at each SSE level (1, 3, and 5) the shear modulus G of all vertical concrete shear walls was reduced according to the shear stiffness degradation curve defined in Section 3.2. In this way, stiffnesses associated with bending and axial deformations were not affected.

The responses calculated from the simulations are combined to estimate median responses conditional on the occurrence of an earthquake described by the hazard curve parameter, i.e., peak ground acceleration.

From these response spectra (generated with and without stiffness reduction effects) at the three pga levels (0.17g, 0.51g, and 0.85g) one can construct plots of any particular spectral acceleration response (at any point in the structures being modeled) as a function of pga. The difference between these plots shows the effect of stiffness reduction directly. This was done for the locations of all equipment modeled on the

Table 4-11

Summary of Site Specific Fragilities for Zion

Structure or Element	Failure Mode	A_m(g)	B_R	B_U	Effect of Failure
Crib House	Roof Diaphragm	0.86	0.24	0.27	Fails all six service water pumps
Containment Building	Uplifting	0.70	0.40	0.40	Fails all pipes in ECCS, RHR, AFWS, CSIS, AND CSRS.
Auxiliary Building	E-W Shear Wall	2.79	0.11	0.26	Loss of electrical power and control circuits between the axuiliary building and containment building
Refuelling Water Storage Tank	Shell Buckling	3.83	0.24	0.32	Fails ECCS & Bleed and Feed Cooling
Condensate Storage Tank	Shell Buckling	0.81	0.28	0.30	Fails AFWS
Reactor Vessel	Support Failure	3.83	0.24	0.32	RVR Initiator
Reactor Coolant Pumps	Support Failure	2.64	0.24	0.37	RVR, LOCA Initiator
Steam Generators	Support Failure	2.45	0.24	0.37	RVR, LOCA Initiator
Pressurizer	Support Failure	2.00	0.21	0.34	LOCA Initiator
Reactor Core Assembly	Support Failure	2.06	0.24	0.32	ECCS Blockage

1. These fragilities are the same used in the original SSMRP analysis.

2. Median values in terms of spectral acceleration at 5% damping

3. B_R and B_U do not include response variability.

accident sequence expressions (for the spectral acceleration corresponding to the equipment of interest).

A sample of the resulting plots of response point spectral accelerations versus peak ground acceleration for responses corresponding to critical components are shown on Figures 4-13 thru 4-20 for both original and reduced stiffnesses. (Note that the spectral acceleration is identified in the caption on each plot.) It can be seen that for structural responses, a nearly linear relation exists up to peak ground accelerations of about 0.50g. Furthermore, for those curves which show some non-linearity at higher acceleration levels, a linear relation provides a conservative estimate of the local response. The piping responses however show a very irregular response. This was determined to be due to differential pipe support motions. Therefore, a bilinear response model was used to model the response of the piping relative to pga in determining core damage frequencies.

Figures 4-13 thru 4-16 show a very minor effect of the shear stiffness degradation on the median response. Also apparent from these figures is the effect of softening of the soil underlying the buildings over the range from 1 to 5 SSE. Generally, the response was not quite linear from 1 to 5 SSE, but it decreased somewhat indicating the decrease in the soil parameters affected the building response. Figures 4-17 thru 4-20 showed greater changes in responses with reduced stiffnesses. However, because both increases and decreases in response were observed, the change was again probability caused by differential pipe support motions.

4.2.4 Probabilistic Results

To evaluate the effect of including degraded shear wall stiffnesses in the seismic PRA of Zion, the accident sequences were quantified both with and without the stiffness reduction. In each case, a complete uncertainty analysis was performed on the accident sequences using a true Monte Carlo analysis.

From the accumulated values of accident sequence frequency and core damage frequency, exact stacistics on their distributions are directly obtainable. The result is an estimate of the mean annual frequency of each accident sequence as well as of the total core damage plus a description of the distributions associated with these estimates. The mean core damage frequencies per year are shown below for both sets of hazard curves and with and without stiffness reduction:

	LLNL Hazard	Zion PRA Hazard
Original Stiffnesses	5.23E-5	1.05E-5
Reduced Stiffnesses	5.20E-5	1.05E-5

There are two main reasons the overall core damage frequencies with and without stiffness reduction did not change much. One, is that responses

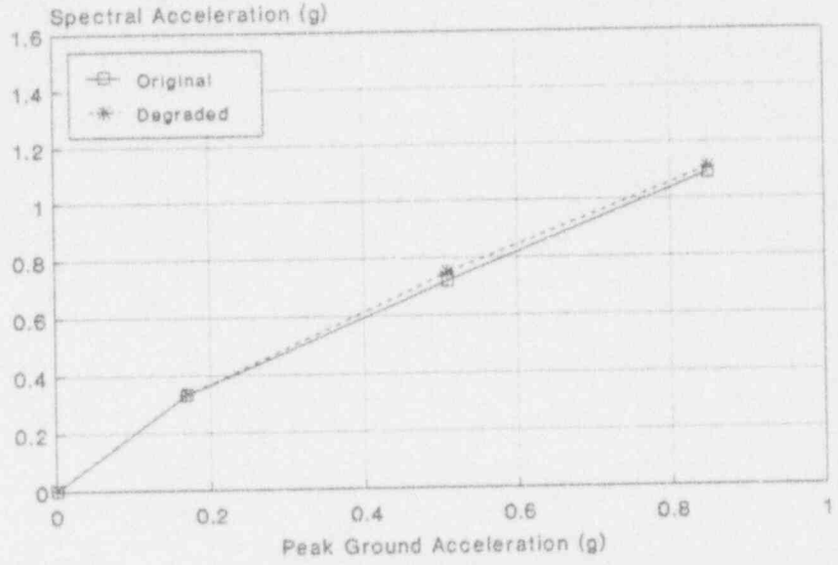

Figure 4-13 Median Responses SEISIM #11
Containment Internal Node 936 at 4 Hz

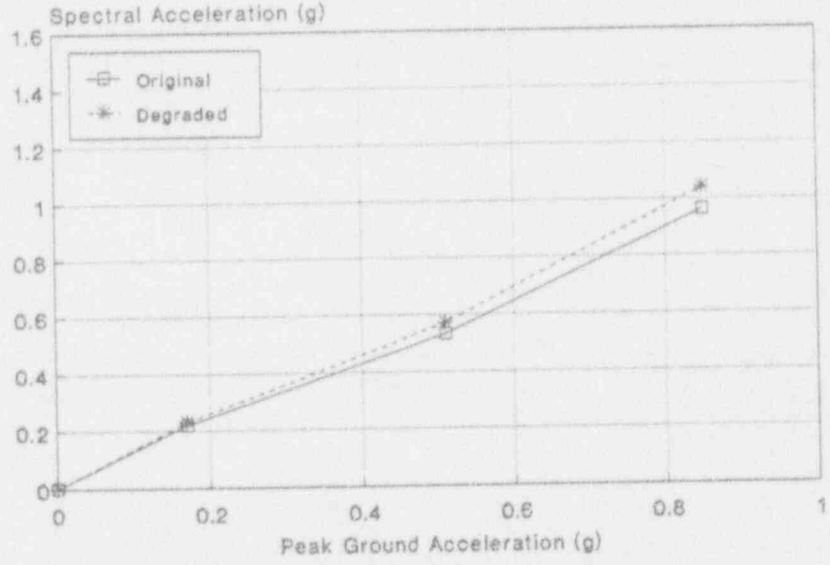

Figure 4-14 Median Responses SEISIM #12
Containment Internal Node 936 at 8 Hz

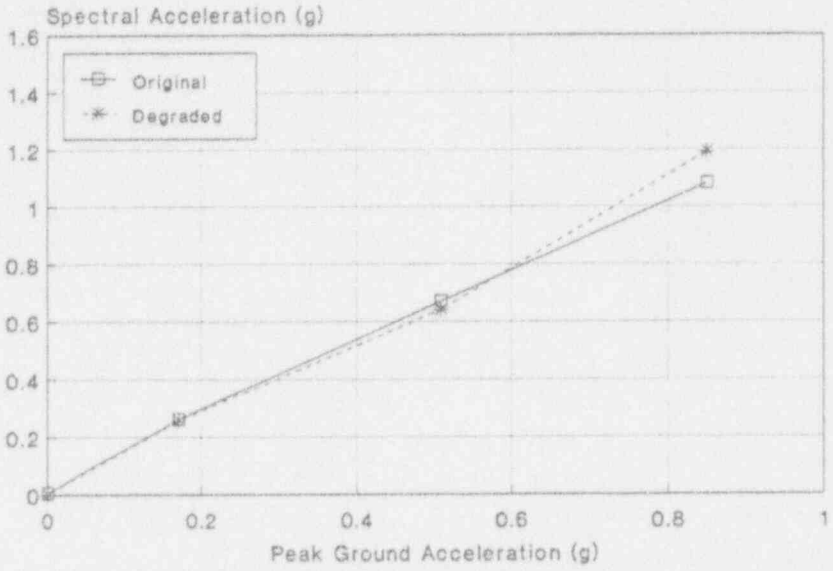

Figure 4-15 Median Responses SEISIM #308
AFT Node 2012 at 8 Hz

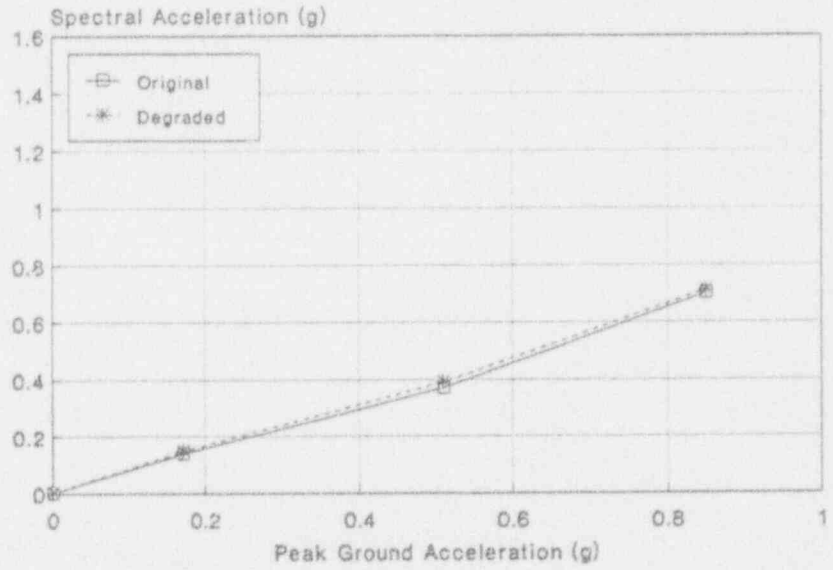

Figure 4-16 Median Responses SEISIM #310
AFT Nodes 3005 and 3006 at zpa

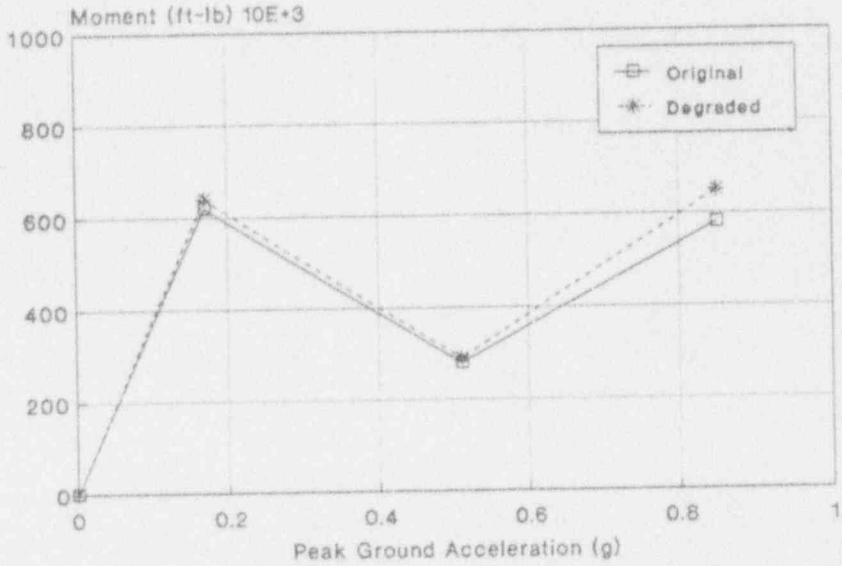

Figure 4-17 Median Responses SEISIM #87
Subsystem 1 and 2 Pipe Moments

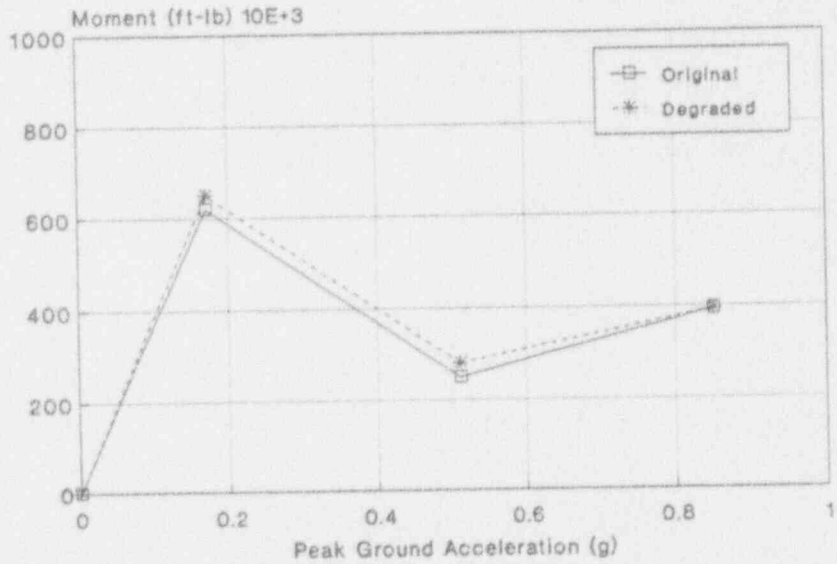

Figure 4-18 Median Responses SEISIM #120
Subsystem 2 Pipe Moments

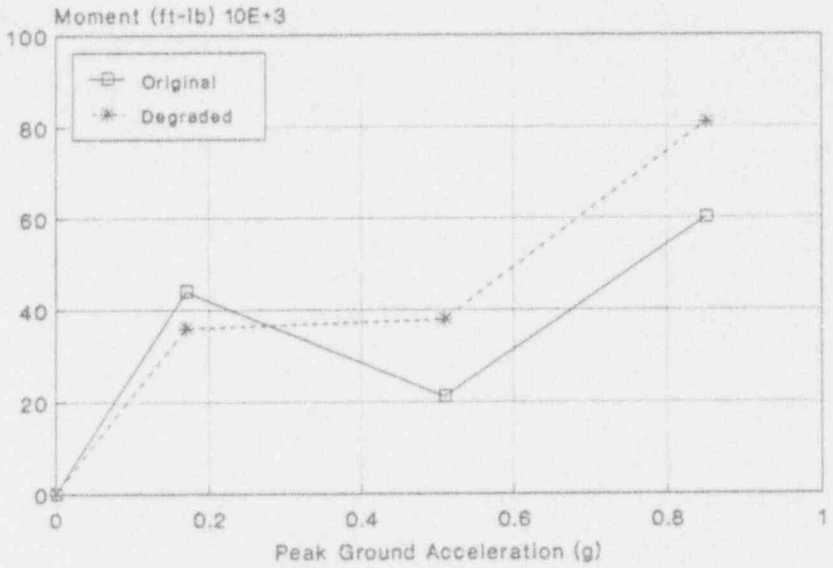

Figure 4-19 Median Responses SEISIM #284
Subsystem 6 Pipe Moments

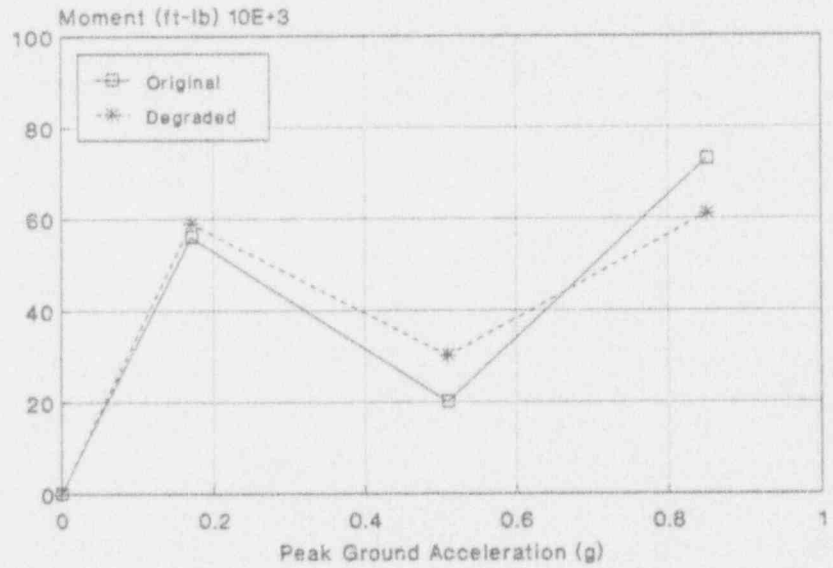

Figure 4-20 Median Responses SEISIM #285
Subsystem 6 Pipe Moments

inside to the containment building and internal structure are not being effected much by the stiffness reductions. This is because the concrete in the containment building was not reduced at all since that is not in the scope of this project and because the stiffness reductions used for this project were based on concrete shear wall tests and not concrete cylindrical containment structures. Also, the internal structure, although did see an initial stiffness reduction of 25%, saw no further reductions even at the 5*SSE level. This initial reduction only lowered the first structural frequency of the internal structure from 12.88 Hz to 12.45 Hz, which is well above the 2-8 Hz range of most earthquakes energy.

The second reason for the responses showing little change with stiffness reduction is due to the high amount of bending stiffness in the walls and flexibility of the floor slabs. It was determined that for the finite element model of the Internal Structure, 42% of the lateral flexibility came from the bending stiffness of the walls, 27% came from shear stiffness of the walls and the other 31% was coming from the floor slab, which is usually considered rigid. Since only 27% of the stiffness is due to shear and this is the only stiffness that is being reduced, it is apparent why the frequency of the Internals dropped so little. Similarly, the first structural frequency of the AFT building only dropped from 8.49 Hz to 8.10 Hz for an initial reduction of 25%. At higher pga levels, further reductions did occur in some of the walls of the AFT, but at 5*SSE the first structural frequency only dropped to 7.98 Hz. Therefore, since the frequencies are not being degraded enough the push them into the range of higher earthquake energies, the responses are not seeing much of a change.

In addition, a mean point estimate quantification (for which all random parameters were set to their mean values and a single quantification was made for each case. This allows for an efficient evaluation of each individual component's importance to the total core damage frequency and a determination of the relative contribution of different earthquake levels to the total. (Experience has shown that such mean point estimate calculations yield results which are very close to the actual mean results obtained from the full uncertainty analysis.)

Table 4-12 presents the mean point estimate core damage contributions at seven intervals over the LLNL hazard curve for each accident sequence using original stiffnesses. Table 4-13 presents the mean core damage contributions using the Zion PRA developed family of hazard curves and original stiffnesses. Similarly, Tables 4-14 and 4-15 present the mean point estimate contributions for both hazard curves, but using reduced stiffnesses. The right hand column in each of these tables presents the total contribution of each accident sequence to the total core damage frequency. As can be seen, the incremental contributions from the LOCA events do not become significant until the higher acceleration levels. The reactor vessel rupture sequence does not make a significant contribution until the higher PGA increments.

An important thing to note from Tables 4-12 thru 4-15 is the sum of the accident sequence contributions at each earthquake level, as shown at the

Table 4-12

Total Accident Sequence Frequency Increments
LLNL Seismic Hazard Curves for Zion with Original Stiffnesses

Accident Sequence	0.10-0.25g	0.25-0.40g	0.40-0.55g	0.55-0.70g	0.70-0.85g	0.85-1.00g	1.00-1.15g	Total
RVR-1	5.8E-09	8.7E-08	2.4E-07	3.6E-07	4.2E-07	4.1E-07	3.8E-07	1.9E-06
ALOCA-1	3.6E-13	3.0E-12	5.3E-12	4.9E-12	3.2E-12	1.7E-12	8.2E-13	1.9E-11
ALOCA-2	2.6E-12	2.2E-11	4.0E-11	3.7E-11	2.5E-11	1.3E-11	6.5E-12	1.5E-10
ALOCA-3	2.4E-08	2.1E-07	4.5E-07	5.7E-07	5.7E-07	4.8E-07	3.9E-07	2.7E-06
MLOCA-2	2.6E-08	1.4E-07	2.0E-07	1.7E-07	1.0E-07	5.1E-08	2.2E-08	7.2E-07
MLOCA-3	1.6E-08	9.8E-08	2.1E-07	3.1E-07	3.3E-07	2.9E-07	2.3E-07	1.5E-06
SLOCA-2	4.4E-07	2.1E-06	2.5E-06	1.6E-06	8.2E-07	3.5E-07	1.4E-07	8.0E-06
SLOCA-3	4.9E-09	1.3E-07	6.1E-07	1.0E-06	1.0E-06	7.6E-07	4.9E-07	4.0E-06
SSLOCA-2	2.2E-06	2.9E-06	1.3E-06	3.2E-07	5.2E-08	7.8E-09	1.3E-09	6.8E-06
SSLOCA-3	3.6E-09	1.5E-07	3.1E-07	1.9E-07	6.4E-08	1.7E-08	4.7E-09	7.4E-07
SSLOCA-4	9.0E-10	4.5E-08	1.4E-07	1.4E-07	7.5E-08	2.9E-08	9.0E-09	4.3E-07
SSLOCA-5	4.6E-08	5.1E-07	1.3E-06	1.4E-06	9.2E-07	4.7E-07	2.1E-07	4.8E-06
T2-2	4.6E-06	7.0E-06	5.5E-06	2.6E-06	9.7E-07	3.0E-07	8.9E-08	2.1E-05
T1-1	1.4E-15	3.0E-17	9.5E-19	3.3E-10	1.2E-11	4.8E-13	1.9E-14	3.5E-10
T1-2	2.4E-06	8.1E-07	9.6E-08	7.7E-09	5.1E-10	3.2E-11	2.0E-12	3.4E-06
	9.9E-06	1.4E-05	1.3E-05	8.7E-06	5.3E-06	3.2E-06	2.0E-06	5.61E-05

Table 4-13

Total Accident Sequence Frequency Increments
Zion PRA Seismic Hazard Curves with Original Stiffnesses

Accident Sequence	0.10-0.25g	0.25-0.40g	0.40-0.55g	0.55-0.70g	0.70-0.85g	0.85-1.00g	1.00-1.15g	Total
RVR-1	2.5E-09	1.7E-08	4.2E-08	6.1E-08	1.1E-07	0.0E+00	0.0E+00	2.3E-07
ALOCA-1	1.5E-13	6.0E-13	9.2E-13	8.2E-13	8.4E-13	0.0E+00	0.0E+00	3.3E-12
ALOCA-2	1.1E-12	4.5E-12	6.9E-12	6.3E-12	6.5E-12	0.0E+00	0.0E+00	2.5E-11
ALOCA-3	1.0E-08	4.3E-08	7.9E-08	9.6E-08	1.5E-07	0.0E+00	0.0E+00	3.8E-07
MLOCA-2	1.1E-08	2.8E-08	3.6E-08	2.9E-08	2.7E-08	0.0E+00	0.0E+00	1.3E-07
MLOCA-3	6.8E-09	2.0E-08	3.7E-08	5.2E-08	8.7E-08	0.0E+00	0.0E+00	2.0E-07
SLOCA-2	1.9E-07	4.3E-07	4.3E-07	2.8E-07	2.2E-07	0.0E+00	0.0E+00	1.5E-06
SLOCA-3	2.1E-09	2.6E-08	1.1E-07	1.7E-07	2.7E-07	0.0E+00	0.0E+00	5.7E-07
SSLOCA-2	9.4E-07	5.9E-07	2.3E-07	5.3E-08	1.4E-08	0.0E+00	0.0E+00	1.8E-06
SSLOCA-3	1.5E-09	3.0E-08	5.4E-08	3.2E-08	1.7E-08	0.0E+00	0.0E+00	1.3E-07
SSLOCA-4	3.8E-10	9.0E-09	2.4E-08	2.3E-08	1.9E-08	0.0E+00	0.0E+00	7.5E-08
SSLOCA-5	2.0E-08	1.0E-07	2.2E-07	2.3E-07	2.4E-07	0.0E+00	0.0E+00	8.1E-07
T2-2	2.0E-06	1.4E-06	9.5E-07	4.4E-07	2.5E-07	0.0E+00	0.0E+00	5.0E-06
T1-1	5.9E-16	5.9E-18	1.6E-19	5.6E-11	3.2E-12	0.0E+00	0.0E+00	5.9E-11
T1-2	1.0E-06	1.6E-07	1.7E-08	1.3E-09	1.3E-10	0.0E+00	0.0E+00	1.2E-06
	4.2E-06	2.9E-06	2.2E-06	1.5E-06	1.4E-06	0.0E+00	0.0E+00	1.21E-05

Table 4-14

Total Accident Sequence Frequency Increments
LLNL Seismic Hazard Curves for Zion with Reduced Stiffnesses

Accident Sequence	0.10-0.25g	0.25-0.40g	0.40-0.55g	0.55-0.70g	0.70-0.85g	0.85-1.00g	1.00-1.15g	Total
RVR-1	5.8E-09	8.7E-08	2.4E-07	3.6E-07	4.2E-07	4.1E-07	3.8E-07	1.9E-06
ALOCA-1	3.6E-13	3.0E-12	5.2E-12	4.8E-12	3.2E-12	1.7E-12	8.1E-13	1.9E-11
ALOCA-2	2.6E-12	2.2E-11	3.9E-11	3.7E-11	2.5E-11	1.3E-11	6.5E-12	1.5E-10
ALOCA-3	2.4E-08	2.1E-07	4.5E-07	5.7E-07	5.7E-07	4.8E-07	3.9E-07	2.7E-06
MLOCA-2	2.5E-08	1.4E-07	2.0E-07	1.7E-07	1.0E-07	5.0E-08	2.2E-08	7.1E-07
MLOCA-3	1.6E-08	9.9E-08	2.2E-07	3.1E-07	3.4E-07	2.9E-07	2.3E-07	1.5E-06
SLOCA-2	4.4E-07	2.1E-06	2.5E-06	1.6E-06	8.3E-07	3.5E-07	1.4E-07	8.0E-06
SLOCA-3	4.9E-09	1.3E-07	6.1E-07	1.0E-06	1.0E-06	7.6E-07	4.9E-07	4.0E-06
SSLOCA-2	2.2E-06	2.9E-06	1.2E-06	2.5E-07	3.3E-08	3.5E-09	3.9E-10	6.6E-06
SSLOCA-3	3.6E-09	1.4E-07	2.9E-07	1.5E-07	4.0E-08	7.5E-09	1.4E-09	6.3E-07
SSLOCA-4	9.7E-10	5.1E-08	1.6E-07	1.6E-07	9.2E-08	3.6E-08	1.2E-08	5.1E-07
SSLOCA-5	4.6E-08	5.1E-07	1.3E-06	1.4E-06	9.2E-07	4.7E-07	2.1E-07	4.8E-06
T2-2	4.7E-06	7.1E-06	5.5E-06	2.6E-06	9.7E-07	3.0E-07	8.9E-08	2.1E-05
T1-1	1.4E-15	3.0E-17	9.7E-19	3.4E-10	1.3E-11	4.9E-13	2.0E-14	3.6E-10
T1-2	2.4E-06	8.1E-07	9.6E-08	7.7E-09	5.1E-10	3.2E-11	2.0E-12	3.4E-06
	9.9E-06	1.4E-05	1.3E-05	8.6E-06	5.3E-06	3.2E-06	2.0E-06	5.59E-05

Table 4-15

Total Accident Sequence Frequency Increments
Zion PRA Seismic Hazard Curves with Reduced Stiffnesses

Accident Sequence	0.10-0.25g	0.25-0.40g	0.40-0.55g	0.55-0.70g	0.70-0.85g	0.85-1.00g	1.00-1.15g	Total
RVR-1	2.5E-09	1.7E-08	4.2E-08	6.1E-08	1.1E-07	0.0E+00	0.0E+00	2.3E-07
ALOCA-1	1.5E-13	6.0E-13	9.1E-13	8.1E-13	8.3E-13	0.0E+00	0.0E+00	3.3E-12
ALOCA-2	1.1E-12	4.4E-12	6.8E-12	6.2E-12	6.5E-12	0.0E+00	0.0E+00	2.5E-11
ALOCA-3	1.0E-08	4.3E-08	7.9E-08	9.6E-08	1.5E-07	0.0E+00	0.0E+00	3.8E-07
MLOCA-2	1.1E-08	2.8E-08	3.5E-08	2.9E-08	2.7E-08	0.0E+00	0.0E+00	1.3E-07
MLOCA-3	6.8E-09	2.0E-08	3.8E-08	5.2E-08	8.8E-08	0.0E+00	0.0E+00	2.0E-07
SLOCA-2	1.9E-07	4.3E-07	4.3E-07	2.8E-07	2.2E-07	0.0E+00	0.0E+00	1.5E-06
SLOCA-3	2.1E-09	2.6E-08	1.1E-07	1.7E-07	2.7E-07	0.0E+00	0.0E+00	5.7E-07
SSLOCA-2	9.3E-07	5.7E-07	2.1E-07	4.2E-08	8.5E-09	0.0E+00	0.0E+00	1.8E-06
SSLOCA-3	1.5E-09	2.9E-08	5.0E-08	2.5E-08	1.0E-08	0.0E+00	0.0E+00	1.2E-07
SSLOCA-4	4.1E-10	1.0E-08	2.8E-08	2.7E-08	2.4E-08	0.0E+00	0.0E+00	9.0E-08
SSLOCA-5	2.0E-08	1.0E-07	2.2E-07	2.3E-07	2.4E-07	0.0E+00	0.0E+00	8.1E-07
T2-2	2.0E-06	1.4E-06	9.5E-07	4.4E-07	2.5E-07	0.0E+00	0.0E+00	5.0E-06
T1-1	6.0E-16	6.0E-18	1.7E-19	5.8E-11	3.3E-12	0.0E+00	0.0E+00	6.1E-11
T1-2	1.0E-06	1.6E-07	1.7E-08	1.3E-09	1.3E-10	0.0E+00	0.0E+00	1.2E-06
	4.2E-06	2.9E-06	2.2E-06	1.5E-06	1.4E-06	0.0E+00	0.0E+00	1.21E-05

bottom of each column on the table. For the LLNL hazard tables, the contributions are seen to be small at the first increment, peaking at the second and third earthquake increment, and then decreasing at higher earthquake levels. This indicates that the bulk of the risk is occurring in the range of 0.25g to 0.55g which roughly corresponds to the range of 1-3 SSE. Further, this shows that the bulk of the risk has been captured by integrating over the range 0.1g to 1.15g. The Zion PRA hazard curve tables show the bulk of the risk coming from the lowest increment of 0.10g to 0.25g. However, since there hazard curves only go down to 0.10g effective pga (0.08g pga), which also corresponds to the OBE, it is not considered adequate to integrate any lower. Therefore, the same limits of integration of 0.10g to 1.15g were used in order to compare with the LLNL hazard curves results.

4.2.5 Deterministic Results

To assess the impact of the frequency reduction model on the deterministic design calculations for Zion, a set of "design-like" structural response calculations was performed. These calculations are as close to the original design calculation methods as could be determined from the Zion Final Safety Analysis Report [29]. However, we did not seek to obtain the original design calculational results themselves. Instead, we performed two sets of calculations using the FSAR guidance. The first set of calculations utilized the "design-like" models with as-calculated stiffnesses. In these "design-like" calculations, typical design damping levels were used, i.e.,

Concrete Structures	5%
Steel Structures	2%
Piping	2%

and a single time history using the 1941 El Centro earthquake record scaled to 1 SSE (0.17g) dynamic response analysis is made.

The second set of calculations used the same structural models, time history and damping levels, but incorporated a shear wall stiffness reduction appropriate to the design level earthquake (0.17g). (As before, the containment shell stiffness was not altered.) Acceleration response spectra at various nodal locations throughout all three structures comparing the undegraded response to the 75% degraded response have been plotted in Figures 4-21 and 4-22. For the reasons described previously these figures indicate only slight modifications in response in narrow frequency ranges for the degraded models.

Tables 4-16 and 4-17 show a comparison of the maximum shear stresses in selected elements for the AFT building and Reactor internal structure. In general there is a small decrease in shear stresses when reduced stiffnesses are used in the finite element models. This was primarily because structural frequencies dropped very little and may not have been enough to shift them into a higher input level on the earthquake spectra.

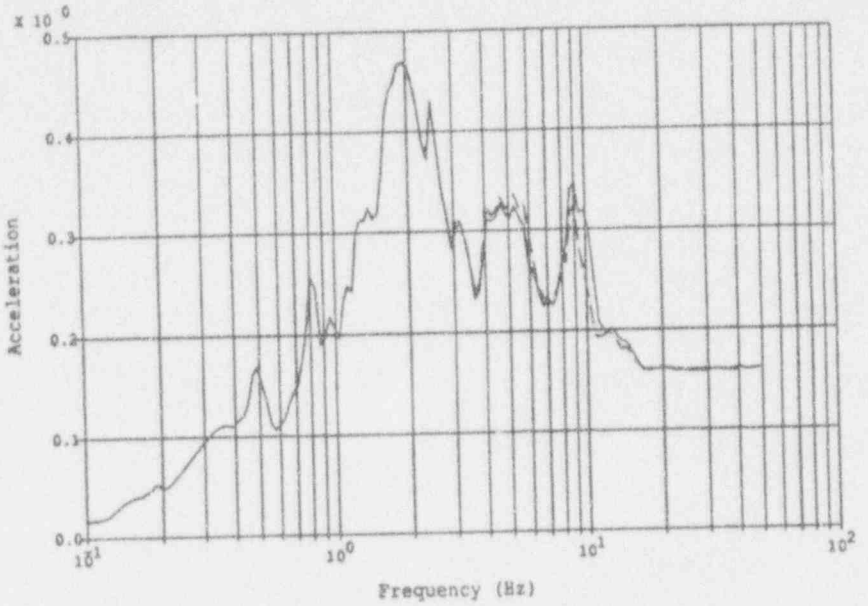

Legend:
Original Model ————————
75% Reduced Model — — — — —

Notes:
East-West Direction
Accelerations in g's
5% Spectral Damping

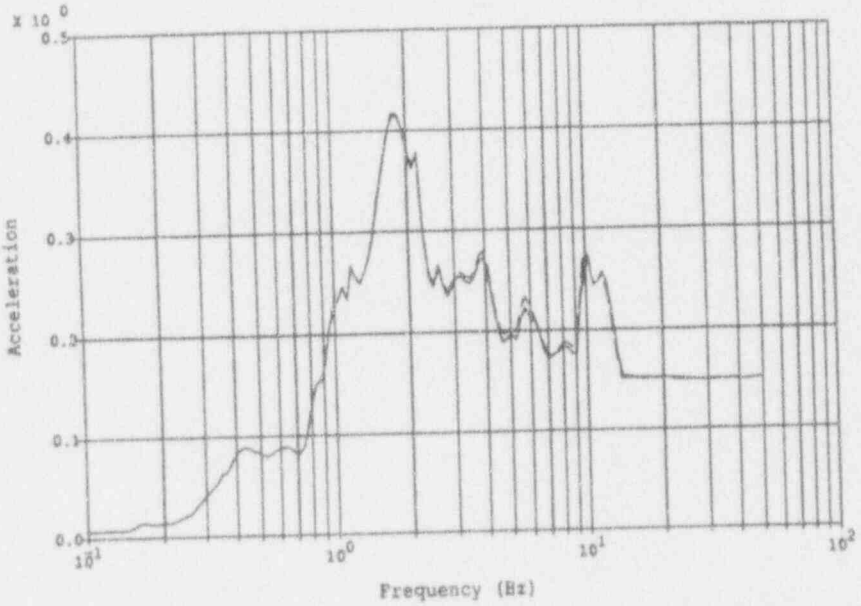

Legend:
Original Model ————————
75% Reduced Model — — — — —

Notes:
Nor-So. Direction
Accelerations in g's
5% Spectral Damping

Figure 4-21 Zion Deterministic Analysis
AFT Node 2012, El 617'

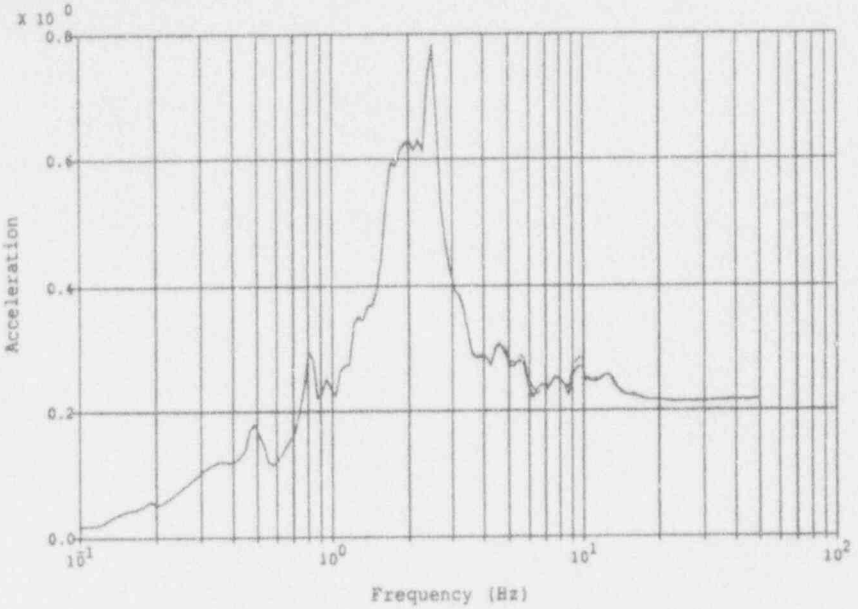

Legend:
Original Model ————————
75% Reduced Model — — — — —

Notes:
East-West Direction
Accelerations in g's
5% Spectral Damping

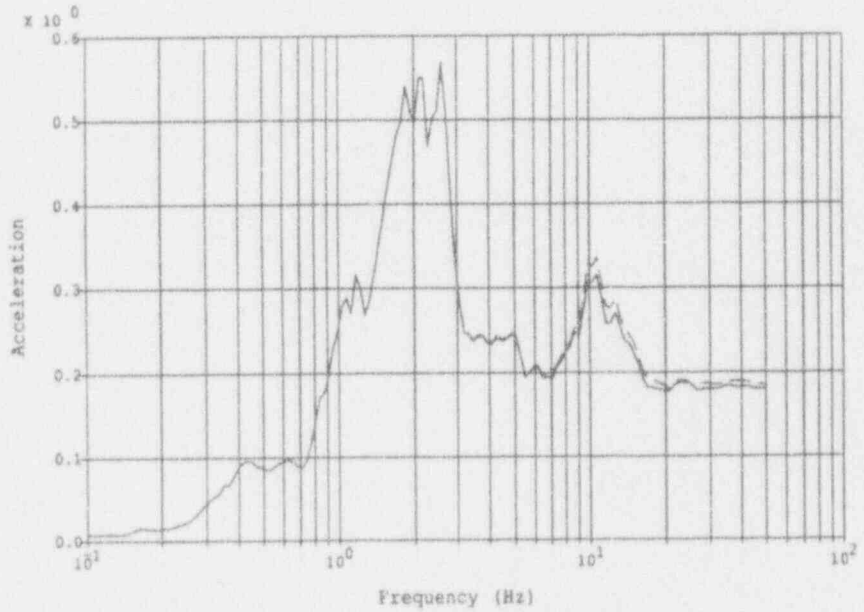

Legend:
Original Model ————————
75% Reduced Model — — — — —

Notes:
Nor-So. Direction
Accelerations in g's
5% Spectral Damping

Figure 4-22 Zion Deterministic Analysis
RCB INT Node 936, El 617'

Table 4-16

Maximum Element Stresses at Zion, Deterministic Study
Auxiliary/Fuel/Turbine Building

Original Stiffnesses

Continuous Group #	Direction	Elevation	Element	Max. Stress (psf)
1	N-S	542'-560'	30	885
			40	332
2	E-W	542'-560'	54	670
3	N-S	592'-617'	445	2,725
			452	3,148
4	E-W	592'-617'	519	21,720

Table 4-16 (Cont'd)

Maximum Element Stresses at Zion, Deterministic Study
Auxiliary/Fuel/Turbine Building

Reduced Stiffnesses

Continuous Group #	Direction	Elevation	Element	Max. Stress (psf)
1	N-S	542'-560'	30	718
			40	275
2	E-W	542'-560'	54	526
3	N-S	592'-617'	445	2,393
			452	2,686
4	E-W	592'-617'	519	18,550

Table 4-17

Maximum Element Stresses at Zion, Deterministic Study
Reactor Internals Building

Original Stiffnesses

Group #	Elevation	Element	Max. Stress (psf)
1	568'-581'	1	2,463
		7	3,425
		19	3,131
		24	2,724
2	568'-581'	25	2,971
		26	1,906
		27	1,775
		28	2,390
3	568'-581'	32	3,494
		33	2,117
		41	2,513
		42	2,028
		60	3,861
		70	2,867
		80	3,118
		87	3,749
		88	3,806
4	568'-581'	34	3,558
		35	3,309
		37	2,313
		38	653
		39	1,252
		40	2,670

Table 4-17 (cont'd)

Maximum Element Stresses at Zion, Deterministic Study
Reactor Internals Building

Reduced Stiffnesses

Group #	Elevation	Element	Max. Stress (psf)
1	568'-581'	1	2,029
		7	2,982
		19	2,708
		24	2,272
2	568'-581'	25	2,652
		26	1,638
		27	1,525
		28	2,086
3	568'-581'	32	3,172
		33	1,947
		41	2,325
		42	1,849
		60	3,272
		70	2,431
		80	2,821
		87	3,388
		88	3,397
4	568'-581'	34	3,245
		35	3,028
		37	2,019
		38	609
		39	1,128
		40	2,410

4.2.6 Summary of Zion Analysis

Both a probabilistic and deterministic re-evaluation of the Zion Nuclear Power Plant was performed using original stiffnesses and reduced stiffnesses. The probabilistic analysis consisted of re-performing a seismic PRA and adjusting the building responses to account for the reduced stiffnesses. This resulted in two overall core damage frequencies, one using original stiffnesses and one using reduced stiffnesses. A second set of core damage frequencies was obtained for bounding purposes by using both the LLNL developed hazard curves and hazard curves developed for the Zion seismic PRA.

The probabilistic re-evaluation resulted in core damage frequencies that were essentially the same when using original and reduced stiffnesses. There are two main reasons these frequencies did not change at Zion. One, is that responses inside to the containment building and internal structure are not being effected much by the stiffness reductions. This is because the concrete in the containment building was not reduced at all since that was not in the scope of this project. Also, the internal structure, although did see an initial stiffness reduction of 25% of the shear modulus, saw no further reductions even at the 5*SSE level. The second reason for the responses showing little change with stiffness reduction is due to the high amount of bending stiffness in the walls and flexibility of the floor slabs, which together provided about 70% of the lateral stiffness. Since only about 30% of the stiffness is due to shear and this is the only stiffness that is being reduced, it is apparent why the frequency of both the Reactor internal structure and AFT building dropped so little.

Similarly, the deterministic analysis showed little change when using reduced stiffnesses. Floor response spectra showed very little change, since structural frequencies were not being altered much. Shear stresses, decreased slightly when using reduced shear wall stiffnesses at Zion. This was again caused primarily by structural frequencies dropping so little they may not have been enough to shift them into a higher input level on the earthquake spectra.

4.3 ANO-1

4.3.1 Background

The ANO-1 plant was selected for analyzing the potential impacts of degraded shear wall stiffness on plant seismic design loads and plant seismic risk because systems models and data had been developed in two previous NRC-sponsored studies, namely:

a) the Interim Reliability Evaluation Program (IREP) [30], and

b) the TAP A-45 Evaluation of the Adequacy of Decay Heat Removal Systems program [31].

In the TAP-45 program, a seismic PRA based on small LOCAs and two types of transient initiators was performed, and dynamic structural models of the buildings important to safety were developed.

The Arkansas Nuclear One Unit-1 (ANO-1) nuclear power plant is an 836 MWe pressurized water reactor (PWR) located on Lake Dardanelle near Russelville, Arkansas. Arkansas Power and Light Company owns and operates the facility. ANO-1 entered commercial operation in December 1974.

The reactor vendor for ANO-1 was Babcock and Wilcox (B&W). The architect/engineer was the Bechtel Power Corporation. The design of the reactor coolant system is typical of other B&W plants currently in commercial operation; there are two once-through steam generators and four reactor coolant loops. Most of the major safety system designs are also fairly typical of other B&W plants. A horizontal peak ground acceleration of 0.20g was defined for the SSE at ANO-1.

4.3.2 Summary of Input

In order to perform a seismic PRA, the following pieces of information must first be obtained: First, the local earthquake hazard, usually in the form of seismic hazard curves with uncertainty bounds or weighting factors, must be determined. Second, the accident sequences which lead to core damage must be identified. Third, the failure modes for the plant safety and support systems must also be determined. Forth, the fragilities of all important structures and components must be determined. Fifth, the location of components and level of seismic response at that location for a given level of seismic input, must be determined.

To begin with, the seismic hazard curves at ANO-1 were taken from the NRC-sponsored Eastern and Central United States Seismic Characterization Program [25]. A second set of hazard curves were obtained from the commercial power industry-sponsored Electrical Power Research Institute's Seismic Hazard Methodology Development program for the Eastern United States [26]. Figure 4-23 shows the mean hazard curves taken from these two programs. The median, 15% and 85% hazard curves for both these programs are shown along with the means, in Appendix C of this report. The median curve and the mean curve were input, and random realizations for the Monte Carlo study were generated assuming a lognormal distribution for any given peak ground acceleration.

A detailed description of the plant safety systems at ANO-1 are fully outlined in Appendix C of this report. The event trees developed for the internal event analyses in IREP and the TAP A-45 programs were used directly. The accident sequence expressions (in terms of component failure basic events) developed in the TAP A-45 program for the small-small, small, T_2 and T_3 initiators were used directly. However, in order to perform a complete seismic PRA for this shear wall degradation study of ANO-1, accident sequences for MLOCA, LLOCA, and RVR initiating events were needed, since these were not in the scope of the TAP A-45 program. These were obtained from the sequences developed in the IREP program. Taken

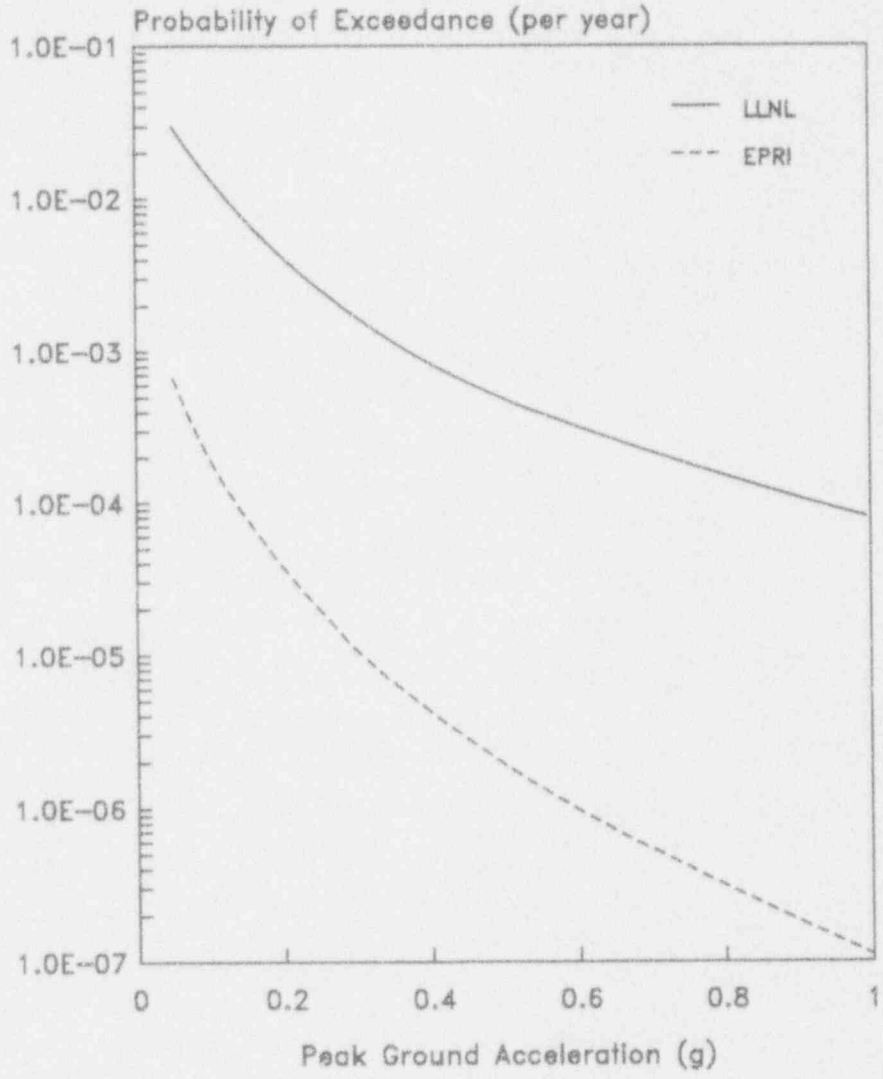

Figure 4-23 ANO-1 Mean Hazard Curves

together, a total of 21 accident sequences corresponding to the ten initiating events were evaluated in this study and are fully explained in Appendix C of this report.

The probability of each individual component failures is dependent on two factors, the seismic fragility of the component and the amount of response experienced by the component during a given peak ground acceleration. The fragility for each vital component is given either a generic fragility or is computed on a plant specific basis if no generic fragility is applicable. At ANO-1, the Reactor Buildin· iliary Building and Intake Structure required developing structural .ities for both original stiffnesses and reduced stiffnesses. The BWS., CST, 4kV and 480V busses all required plant specific fragilities and are shown along with the structural fragilities in Table 4-18. All component fragilities, both site specific and generic, were not altered for the reduced stiffness case.

The amount of response (acceleration or force) e) .ced by each component at each earthquake level is next determined. .st, the actual location of each component must be determined and related to a certain floor elevation of the building it is located within. After a dynamic time history analysis of each structure is run, building responses in terms of peak ground acceleration are developed. These are described in the next section and are the last piece of information needed to perform a seismic PRA.

4.3.3 Building Responses

Three separate buildings were modeled for ANO-1; the Reactor Building, the Auxiliary Building and the Intake Structure. All three models used in the dynamic analysis were 2-D lumped mass models taken from the original ANO-1 FSAR [32]. The material properties for these structures came directly from specimen tests that were performed during the construction of all three structures for both the concrete and reinforcing steel used. Three earthquake levels were considered and defined by their peak ground acceleration in the horizontal direction--0.20g (SSE), 0.40g (2 SSE), and 0.60g (3 SSE).

In recognition of the importance of the effects of embedment and soil-structure interaction, probabilistic respons analyses were performed on the reactor building (containment shell and ternals) and the auxiliary building to generate median responses for the seismic PRA. The methodology used is that of SMACS [33] as mplemented in the computer program CLASSI [14] utilizing the substructure approach. The substructure approach to SSI is composed of the following elements: specification of the free-field ground motion; calculation of the dynamic characteristics of the structures; determination of the foundation impedances and analysis of the coupled soil-structure system.

Soil-structure interaction and structure response variability are introduced through a limited number of parameters--soil shear modulus,

Table 4-18

Summary of Site Specific Fragilities for ANO-1

Structure or Component	Failure Element	Original[1] A_m(g)	B_R	B_U	Reduced[2] A_m(g)	B_R	B_U	Effect of Failure
Reactor Internals	N-S Shear Walls	3.3	0.06	0.21	3.0	0.06	0.21	Vessel Rupture Initiating Event
Auxiliary Building Building	N-S Shear Walls	1.5	0.09	0.23	1.4	0.10	0.23	Included in RVR initiating event leading directly core damage
Intake Structure	E-W Shear Walls	2.4	0.07	0.27	2.4	0.08	0.27	Seal LOCA with Station Blackout
4160 VAC Switchgear	Sliding & tipping due to minimal anchorage	0.7	0.4	0.30	No change			Loss of Function
480 VAC Switchgear	Sliding & tipping due to minimal anchorage	0.7	0.4	0.30	No change			Loss of Function
BWST	Buckling (Est)	1.0	0.3	0.29	No change			Loss of Supply
CST	Buckling (Est)	1.0	0.3	0.29	No change			Loss of Supply

1. These fragilities are based on loads from analyses using original stiffnesses.

2. These fragilities are based on loads from analyses including shear wall stiffness degradation.

3. B_R and B_U do not include response variability.

soil damping, structure frequency and modal damping. Variability in SSI was incorporated through modeling soil shear modulus and material damping as random variables

The responses calculated from the simulations are combined to estimate median responses conditional on the occurrence of an earthquake described by the hazard curve parameter, i.e., peak ground acceleration.

From these response spectra (generated with and without stiffness reduction effects) at the three pga levels (0.2g, 0.4g, and 0.6g), one can construct plots of any particular spectral acceleration response (at any point in the structures being modeled) as a function of pga. The difference between these plots shows the effect of stiffness reduction directly. This was done for the locations of all equipment modeled on the accident sequence expressions (for the spectral acceleration corresponding to the equipment of interest).

A sample of the resulting plots of response point spectral accelerations versus peak ground acceleration for responses corresponding to critical components are shown on Figures 4-24 thru 4-27 for both original and reduced stiffnesses. (Note that the spectral acceleration is identified in the caption on each plot.) It can be seen that a nearly linear relation exists up to peak ground accelerations of 0.60g. Furthermore, for those curves which show some non-linearity at higher acceleration levels, a linear relation provides a conservative estimate of the local response. Such behavior was first recognized in the SSMRP studies. Inasmuch as the bulk of the risk is generally due to earthquake levels only up to the 4 SSE level, it can be seen that relating local response to peak ground acceleration in a linear fashion is appropriate for the ANO-1 analysis.

Figures 4-24 thru 4-27 also verify that reduced stiffnesses can result in a higher level of response or floor acceleration. This was most apparent in the Auxiliary building where responses were as much as 20% higher at the upper floor elevations. This was primarily caused by the shifting of the 1st modal frequency down into a higher range of earthquake energies. The Auxiliary building subjected to an SSE earthquake had a fundamental frequency of about 11.2 Hz when original stiffnesses were used. Using reduced stiffnesses and the same SSE input, the frequency dropped to 10.2 Hz. Furthermore, at the highest earthquake input (3 SSE), the fundamental frequency dropped down to about 8.2 Hz.

However, the Reactor internal structure and the Intake structure did not experience as great a increase in response as did the Auxiliary Building. In the case of the Reactor internals, the fundamental frequency was 10.7 using original stiffnesses at the SSE, and only dropped to 10.0 for reduced stiffnesses at both the SSE and 2 SSE levels of input. This is because the internals are primarily made up of very thick concrete walls, resulting in lower shear stresses during an earthquake, and a delaying any significant reductions in stiffness.

Similarly, the Intake structure experienced only a small increase in response. In this case, it was the result of a much higher fundamental

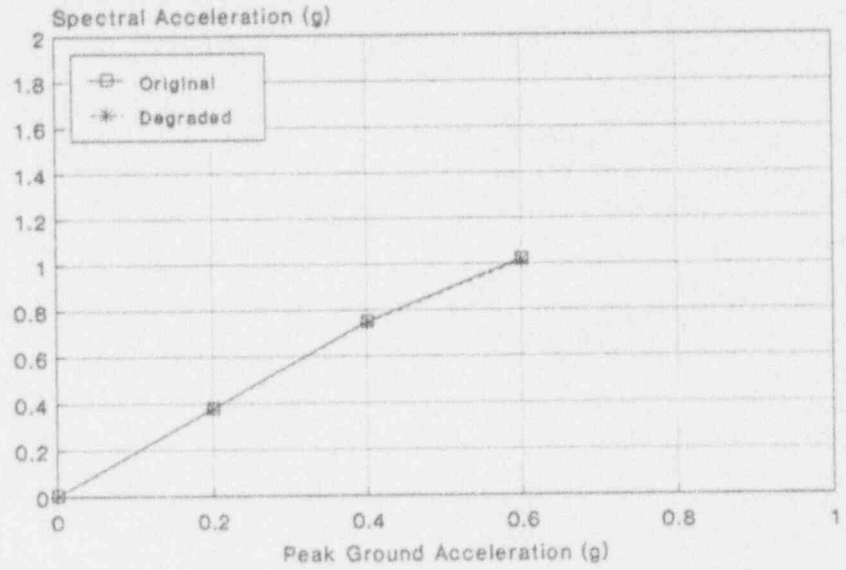

Figure 4-24 ANO-1 Median Responses Auxiliary Building El. 335', 7 Hz

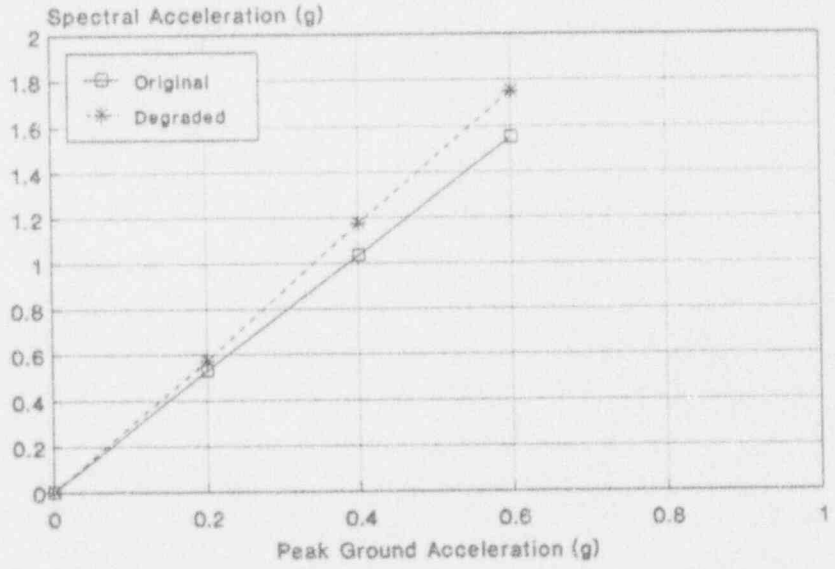

Figure 4-25 ANO-1 Median Responses Auxiliary Building El. 386', 5-10 Hz

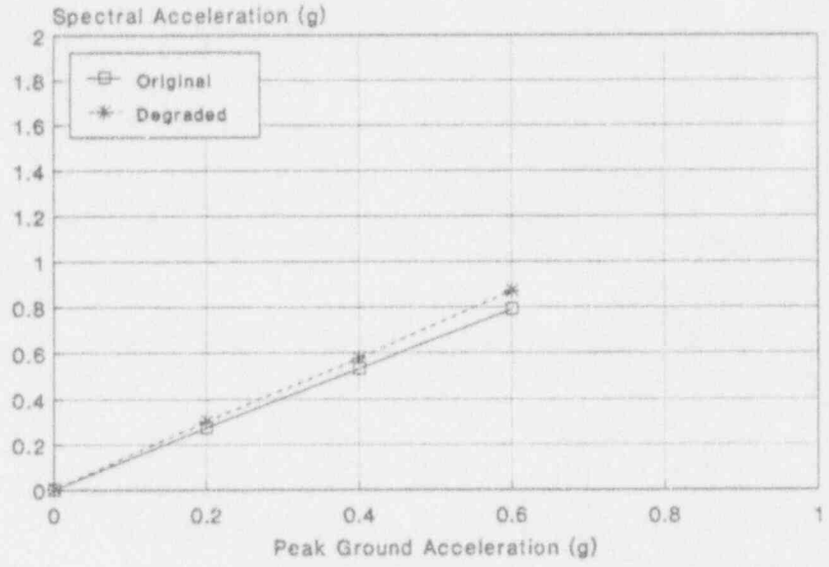

Figure 4-26 ANO-1 Median Responses Reactor Internals El. 401', ZPA

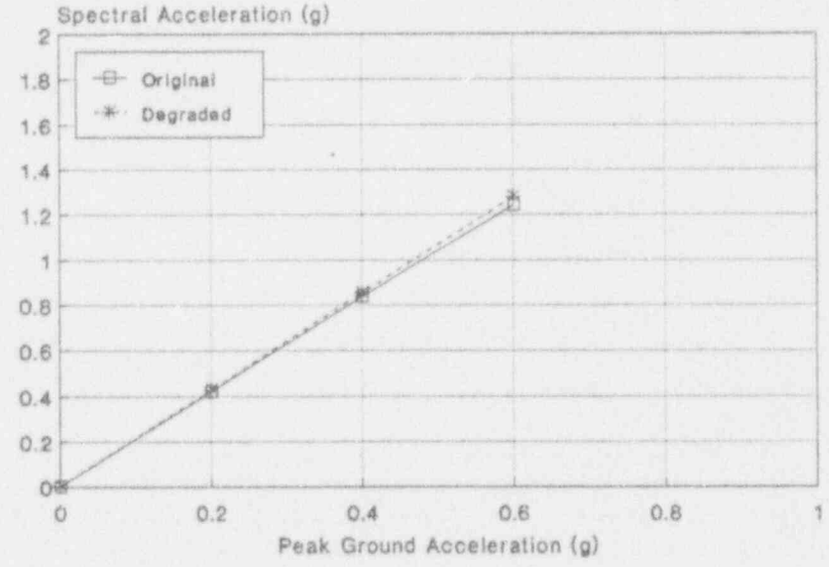

Figure 4-27 ANO-1 Median Responses Intake Structure El. 352', 5 Hz

frequency, 16 Hz using original stiffnesses at 1 SSE. After reducing the stiffnesses, the frequency only dropped to 14.7 Hz at 1 SSE, and at 3 SSE the frequency only dropped to about 13 Hz. Although this is a significant drop in frequency, the lowest level (13 Hz) is still well above most of the earthquake energies.

4.3.4 Probabilistic Results

To evaluate the effect of including degraded shear wall stiffnesses in the seismic PRA of ANO-1, the accident sequences were quantified both with and without the stiffness reduction. In each case, a complete uncertainty analysis was performed on the accident sequences using a true Monte Carlo analysis.

From the accumulated values of accident sequence frequency and core damage frequency, exact statistics on their distributions are directly obtainable. The result is an estimate of the mean annual frequency of each accident sequence as well as of the total core damage plus a description of the distributions associated with these estimates. The mean core damage frequencies per year are shown below for both sets of hazard curves and with and without stiffness reduction:

	LLNL Hazard	EPRI Hazard
Original Stiffnesses	1.07E-3	8.78E-6
Reduced Stiffnesses	1.15E-3	9.61E-6

Although the percent increase in core damage frequency due to the stiffness reduction was small (~10%), the magnitude of increase itself (8.0E-5 for LLNL and 8.3E-7 for EPRI) is quite significant. The breakdown of each accident sequence contribution and the various percentile distributions for the totals are shown in Appendix C of this report.

In addition, a mean point estimate quantification (for which all random parameters were set to their mean values and a single quantification was made for each case. This allows for an efficient evaluation of each individual component's importance to the total core damage frequency and a determination of the relative contribution of different earthquake levels to the total. (Experience has shown that such mean point estimate calculations yield results which are very close to the actual mean results obtained from the full uncertainty analysis.)

Table 4-19 presents the mean point estimate core damage contributions at seven intervals over the LLNL hazard curve for each accident sequence using original stiffnesses. Table 4-20 presents the mean core damage contributions for the EPRI hazard curve and original stiffnesses. Similarly, Tables 4-21 and 4-22 present the mean point estimate contributions for both hazard curves, but using reduced stiffnesses. The right hand column in each of these tables presents the total contribution of each accident sequence to the total core damage frequency. As can be

Table 4-19

Total Accident Sequence Frequency Increments
LLNL Seismic Hazard Curves for ANO-1 with Original Stiffnesses

Accident Sequence	0.10-0.20g	0.20-0.30g	0.30-0.40g	0.40-0.50g	0.50-0.60g	0.60-0.70g	0.70-0.80g	Total
RVR-1	3.5E-09	8.4E-08	4.6E-07	1.3E-06	2.4E-06	3.6E-06	4.5E-06	1.2E-05
A2-LOCA-1	8.7E-09	2.3E-07	7.1E-07	1.3E-06	1.7E-06	1.9E-06	1.9E-06	7.6E-06
A2-LOCA-2	1.6E-12	3.4E-10	5.4E-09	2.8E-08	8.0E-08	1.6E-07	2.5E-07	5.3E-07
M2-LOCA-1	4.2E-08	1.3E-07	7.9E-09	1.2E-10	9.4E-13	0.0E+00	0.0E+00	1.7E-07
M2-LOCA-2	1.2E-07	1.7E-06	3.6E-06	4.8E-06	5.2E-06	5.1E-06	4.6E-06	2.5E-05
M1-LOCA-1	3.5E-06	2.4E-05	3.3E-05	3.2E-05	2.8E-05	2.3E-05	1.7E-05	1.6E-04
SLOCA-1	1.8E-07	1.6E-06	4.3E-06	5.5E-06	4.6E-06	2.9E-06	1.5E-06	2.1E-05
SLOCA-2	1.3E-07	1.5E-06	4.1E-06	5.6E-06	4.8E-06	2.9E-06	1.5E-06	2.0E-05
SLOCA-3	3.5E-06	1.8E-05	1.7E-05	1.1E-05	6.3E-06	3.2E-06	1.5E-06	6.1E-05
SLOCA-4	1.4E-07	6.4E-07	5.9E-07	3.8E-07	2.1E-07	1.1E-07	5.2E-08	2.1E-06
SLOCA-5	2.7E-09	2.8E-08	2.2E-07	9.0E-07	2.0E-06	2.9E-06	3.1E-06	9.2E-06
SLOCA-7	8.5E-08	1.9E-06	8.1E-06	1.3E-05	1.3E-05	8.9E-06	5.7E-06	5.0E-05
INTK-1	7.3E-13	3.9E-10	5.5E-09	2.4E-08	5.9E-08	9.8E-08	1.3E-07	3.1E-07
SSLOCA-1	3.8E-07	3.2E-06	8.0E-06	9.8E-06	7.7E-06	4.5E-06	2.2E-06	3.6E-05
SSLOCA-2	2.6E-07	2.9E-06	7.7E-06	1.0E-05	8.0E-06	4.6E-06	2.2E-06	3.6E-05
SSLOCA-3	7.3E-06	3.6E-05	3.3E-05	2.0E-05	1.1E-05	5.0E-06	2.3E-06	1.1E-04
SSLOCA-4	2.9E-07	1.3E-06	1.1E-06	6.8E-07	3.6E-07	1.7E-07	7.7E-08	4.0E-06
SSLOCA-5	5.6E-09	5.6E-08	4.2E-07	1.6E-06	3.4E-06	4.6E-06	4.7E-06	1.5E-05
SSLOCA-7	1.8E-07	3.7E-06	1.5E-05	2.4E-05	2.1E-05	1.4E-05	8.5E-06	8.7E-05
T2-2	6.8E-06	6.4E-05	1.4E-04	1.3E-04	7.6E-05	3.7E-05	1.7E-05	4.7E-04
T3-2	3.2E-06	5.5E-06	4.0E-06	1.5E-06	4.0E-07	9.1E-08	2.1E-08	1.5E-05
	2.6E-05	1.7E-04	2.8E-04	2.7E-04	1.9E-04	1.2E-04	7.9E-05	1.14E-03

Table 4-20

Total Accident Sequence Frequency Increments
EPRI Seismic Hazard Curves for ANO-1 with Original Stiffnesses

Accident Sequence	0.10-0.20g	0.20-0.30g	0.30-0.40g	0.40-0.50g	0.50-0.60g	0.60-0.70g	0.70-0.80g	Total
RVR-1	6.3E-11	9.5E-10	3.9E-09	9.0E-09	1.4E-08	1.8E-08	2.2E-08	6.9E-08
A2-LOCA-1	1.6E-10	2.7E-09	6.1E-09	8.9E-09	1.0E-08	9.5E-09	9.3E-09	4.7E-08
A2-LOCA-2	3.0E-14	3.9E-12	4.6E-11	2.0E-10	4.8E-10	8.1E-10	1.3E-09	2.8E-09
M2-LOCA-1	7.6E-10	1.4E-09	6.7E-11	8.5E-13	5.6E-15	0.0E+00	0.0E+00	2.2E-09
M2-LOCA-2	2.2E-09	2.0E-08	3.1E-08	3.4E-08	3.1E-08	2.6E-08	2.3E-08	1.7E-07
M1-LOCA-1	6.4E-08	2.8E-07	2.8E-07	2.3E-07	1.7E-07	1.1E-07	8.6E-08	1.2E-06
SLOCA-1	3.3E-09	1.8E-08	3.6E-08	3.9E-08	2.7E-08	1.4E-08	7.4E-09	1.5E-07
SLOCA-2	2.3E-09	1.6E-08	3.5E-08	3.9E-08	2.8E-08	1.5E-08	7.4E-09	1.4E-07
SLOCA-3	6.3E-08	2.0E-07	1.5E-07	7.9E-08	3.7E-08	1.6E-08	7.5E-09	5.5E-07
SLOCA-4	2.5E-09	7.3E-09	5.0E-09	2.7E-09	1.3E-09	5.5E-10	2.6E-10	2.0E-08
SLOCA-5	4.9E-11	3.2E-10	1.9E-09	6.3E-09	1.2E-08	1.5E-08	1.5E-08	5.1E-08
SLOCA-7	1.5E-09	2.1E-08	6.9E-08	9.4E-08	7.5E-08	4.5E-08	2.8E-08	3.3E-07
INTK-1	1.3E-14	4.4E-12	4.7E-11	1.7E-10	3.5E-10	4.9E-10	6.3E-10	1.7E-09
SSLOCA-1	6.9E-09	3.7E-08	6.9E-08	6.9E-08	4.6E-08	2.3E-08	1.1E-08	2.6E-07
SSLOCA-2	4.8E-09	3.3E-08	6.6E-08	7.0E-08	4.8E-08	2.3E-08	1.1E-08	2.6E-07
SSLOCA-3	1.3E-07	4.0E-07	2.8E-07	1.4E-07	6.3E-08	2.5E-08	1.1E-08	1.1E-06
SSLOCA-4	5.3E-09	1.4E-08	9.5E-09	4.8E-09	2.1E-09	8.7E-10	3.8E-10	3.7E-08
SSLOCA-5	1.0E-10	6.4E-10	3.6E-09	1.1E-08	2.0E-08	2.3E-08	2.3E-08	8.2E-08
SSLOCA-7	3.2E-09	4.2E-08	1.3E-07	1.7E-07	1.3E-07	7.1E-08	4.2E-08	5.8E-07
T2-2	1.2E-07	7.3E-07	1.2E-06	9.1E-07	4.5E-07	1.8E-07	8.4E-08	3.7E-06
T3-2	5.8E-08	6.3E-08	3.4E-08	1.1E-08	2.4E-09	4.6E-10	1.0E-10	1.7E-07
	4.7E-07	1.9E-06	2.4E-06	1.9E-06	1.2E-06	6.3E-07	3.9E-07	8.85E-06

Table 4-21

Total Accident Sequence Frequency Increments
LLNL Seismic Hazard Curves for ANO-1 with Reduced Stiffnesses

Accident Sequence	0.10-0.20g	0.20-0.30g	0.30-0.40g	0.40-0.50g	0.50-0.60g	0.60-0.70g	0.70-0.80g	Total
RVR-1	4.0E-09	1.2E-07	6.6E-07	1.8E-06	3.3E-06	4.7E-06	5.8E-06	1.6E-05
A2-LOCA-1	1.1E-08	2.4E-07	7.1E-07	1.3E-06	1.7E-06	1.9E-06	1.8E-06	7.6E-06
A2-LOCA-2	1.6E-12	3.4E-10	5.4E-09	2.8E-08	7.9E-08	1.6E-07	2.5E-07	5.2E-07
M2-LOCA-1	4.2E-08	5.6E-08	1.3E-09	6.5E-12	0.0E+00	0.0E+00	0.0E+00	9.8E-08
M2-LOCA-2	1.7E-07	1.8E-06	3.6E-06	4.8E-06	5.2E-06	5.0E-06	4.5E-06	2.5E-05
M1-LOCA-1	4.8E-06	2.6E-05	3.3E-05	3.2E-05	2.8E-05	2.2E-05	1.7E-05	1.6E-04
SLOCA-1	1.8E-07	1.7E-06	4.7E-06	6.1E-06	4.9E-06	3.0E-06	1.5E-06	2.2E-05
SLOCA-2	1.5E-07	1.6E-06	4.4E-06	5.9E-06	4.9E-06	2.9E-06	1.5E-06	2.1E-05
SLOCA-3	4.8E-06	1.9E-05	1.7E-05	1.1E-05	6.2E-06	3.1E-06	1.5E-06	6.3E-05
SLOCA-4	1.9E-07	6.8E-07	5.9E-07	3.8E-07	2.1E-07	1.1E-07	5.0E-08	2.2E-06
SLOCA-5	2.7E-09	3.1E-08	2.6E-07	1.0E-06	2.3E-06	3.4E-06	3.5E-06	1.1E-05
SLOCA-7	1.2E-07	2.4E-06	9.4E-06	1.4E-05	1.3E-05	8.8E-06	5.6E-06	5.3E-05
INTK-1	7.3E-13	4.9E-10	5.9E-09	2.5E-08	6.1E-08	1.0E-07	1.3E-07	3.2E-07
SSLOCA-1	3.9E-07	3.4E-06	8.8E-06	1.1E-05	8.3E-06	4.7E-06	2.2E-06	3.9E-05
SSLOCA-2	3.2E-07	3.3E-06	8.4E-06	1.0E-05	8.2E-06	4.6E-06	2.2E-06	3.7E-05
SSLOCA-3	1.0E-05	3.8E-05	3.3E-05	2.0E-05	1.0E-05	5.0E-06	2.2E-06	1.2E-04
SSLOCA-4	4.0E-07	1.3E-06	1.1E-06	6.8E-07	3.6E-07	1.7E-07	7.5E-08	4.1E-06
SSLOCA-5	5.7E-09	6.3E-08	4.9E-07	1.9E-06	3.9E-06	5.4E-06	5.2E-06	1.7E-05
SSLOCA-7	2.5E-07	4.8E-06	1.8E-05	2.6E-05	2.1E-05	1.4E-05	8.4E-06	9.2E-05
T2-2	9.8E-06	8.3E-05	1.6E-04	1.4E-04	7.7E-05	3.6E-05	1.6E-05	5.2E-04
T3-2	4.6E-06	7.1E-06	4.6E-06	1.6E-06	4.0E-07	9.0E-08	2.0E-08	1.9E-05
	3.6E-05	2.0E-04	3.1E-04	2.9E-04	2.0E-04	1.3E-04	8.0E-05	1.23E-03

Table 4-22

Total Accident Sequence Frequency Increments
EPRI Seismic Hazard Curves for ANO-1 with Reduced Stiffnesses

Accident Sequence	0.10-0.20g	0.20-0.30g	0.30-0.40g	0.40-0.50g	0.50-0.60g	0.60-0.70g	0.70-0.80g	Total
RVR-1	7.1E-11	1.3E-09	5.7E-09	1.3E-08	2.0E-08	2.4E-08	2.9E-08	9.2E-08
A2-LOCA-1	2.0E-10	2.7E-09	6.1E-09	8.9E-09	1.0E-08	9.4E-09	9.1E-09	4.6E-08
A2-LOCA-2	2.9E-14	3.9E-12	4.6E-11	2.0E-10	4.7E-10	8.0E-10	1.2E-09	2.7E-09
M2-LOCA-1	7.5E-10	6.3E-10	1.1E-11	4.6E-14	0.0E+00	0.0E+00	0.0E+00	1.4E-09
M2-LOCA-2	3.0E-09	2.1E-08	3.1E-08	3.4E-08	3.1E-08	2.5E-08	2.2E-08	1.7E-07
M1-LOCA-1	8.7E-08	2.9E-07	2.8E-07	2.3E-07	1.7E-07	1.1E-07	8.4E-08	1.2E-06
SLOCA-1	3.3E-09	1.9E-08	4.0E-08	4.3E-08	3.0E-08	1.5E-08	7.4E-09	1.6E-07
SLOCA-2	2.8E-09	1.9E-08	3.8E-08	4.1E-08	2.9E-08	1.5E-08	7.2E-09	1.5E-07
SLOCA-3	8.6E-08	2.2E-07	1.5E-07	7.9E-08	3.7E-08	1.6E-08	7.3E-09	5.9E-07
SLOCA-4	3.4E-09	7.7E-09	5.0E-09	2.7E-09	1.3E-09	5.4E-10	2.5E-10	2.1E-08
SLOCA-5	5.0E-11	3.6E-10	2.2E-09	7.4E-09	1.4E-08	1.7E-08	1.7E-08	5.8E-08
SLOCA-7	2.2E-09	2.7E-08	8.0E-08	1.0E-07	7.6E-08	4.5E-08	2.8E-08	3.6E-07
INTK-1	1.3E-14	5.5E-12	5.0E-11	1.8E-10	3.6E-10	5.0E-10	6.3E-10	1.7E-09
SSLOCA-1	7.0E-09	3.9E-08	7.5E-08	7.7E-08	5.0E-08	2.4E-08	1.1E-08	2.8E-07
SSLOCA-2	5.8E-09	3.7E-08	7.1E-08	7.4E-08	4.9E-08	2.3E-08	1.1E-08	2.7E-07
SSLOCA-3	1.8E-07	4.4E-07	2.8E-07	1.4E-07	6.2E-08	2.5E-08	1.1E-08	1.1E-06
SSLOCA-4	7.2E-09	1.5E-08	9.5E-09	4.8E-09	2.1E-09	8.6E-10	3.8E-10	4.0E-08
SSLOCA-5	1.0E-10	7.1E-10	4.2E-09	1.3E-08	2.4E-08	2.7E-08	2.6E-08	9.5E-08
SSLOCA-7	4.6E-09	5.5E-08	1.5E-07	1.8E-07	1.3E-07	7.1E-08	4.2E-08	6.3E-07
T2-2	1.8E-07	9.4E-07	1.4E-06	9.8E-07	4.6E-07	1.8E-07	8.2E-08	4.2E-06
T3-2	8.4E-08	8.1E-08	3.9E-08	1.1E-08	2.4E-09	4.5E-10	1.0E-10	2.2E-07
	6.5E-07	2.2E-06	2.6E-06	2.0E-06	1.2E-06	5.3E-07	4.0E-07	9.77E-06

seen, the incremental contributions from the LOCA events do not become significant until the higher acceleration levels. The reactor vessel rupture sequence does not make a significant contribution until the highest PGA increment.

An important thing to note from Tables 4-19 thru 4-22 is the sum of the accident sequence contributions at each earthquake level, as shown at the bottom of each column on the table. The contributions are seen to be small at the first increment, increasing to a maximum at the third and forth earthquake increment, and then decreasing at higher earthquake levels. This indicates that the bulk of the risk is occurring in the range of 0.2g to 0.6g which roughly corresponds to the range of 1-3 SSE. Further, this shows that the bulk of the risk has been captured by integrating over the range 0.1g to 0.8g.

4.3.5 Deterministic Results

To assess the impact of the frequency reduction model on the deterministic design calculations for ANO-1, a set of "design-like" structural response calculations was performed. These "design-like" calculations do not attempt to reproduce the original design calculations, but instead, use the same parameters, such as input time history, structural damping, and material properties. However, is this study, the structural stiffnesses were varied to obtain both original stiffness results (loads and spectra) and reduced stiffness results, and could then compare the differences without assessing the initial design.

These calculations are as close to the original design calculation methods as could be determined from the ANO-1 Final Safety Analysis Report [29]. The first set of calculations utilized the "design-like" models with as-calculated stiffnesses. The second set of calculations used the same structural models but incorporated a frequency reduction appropriate to the design level earthquake of 1 SSE (0.2g). Structural damping was taken as 5% for both sets of calculations.

Acceleration response spectra were generated at various nodal locations throughout all the structures comparing the undegraded response to the reduced stiffness response. An example of each structure is shown in Figures 4-28 thru 4-30. More deterministic spectras are shown in Appendix C of this report.

It can be seen from these spectra that some very significant shifts in peak values and frequencies are present. Most notably, the Auxiliary Building experienced a significant increase in the 10 Hz range in both directions at the upper floor elevations. In addition, the Intake Structure experienced a significant increase in the 13 Hz range in both directions for the upper floor elevations when reduced stiffnesses were modeled.

Tables 4-23 thru 4-25 show a comparison of story shear and moment loads listed by floor elevation (that is, the shear and moment values just under

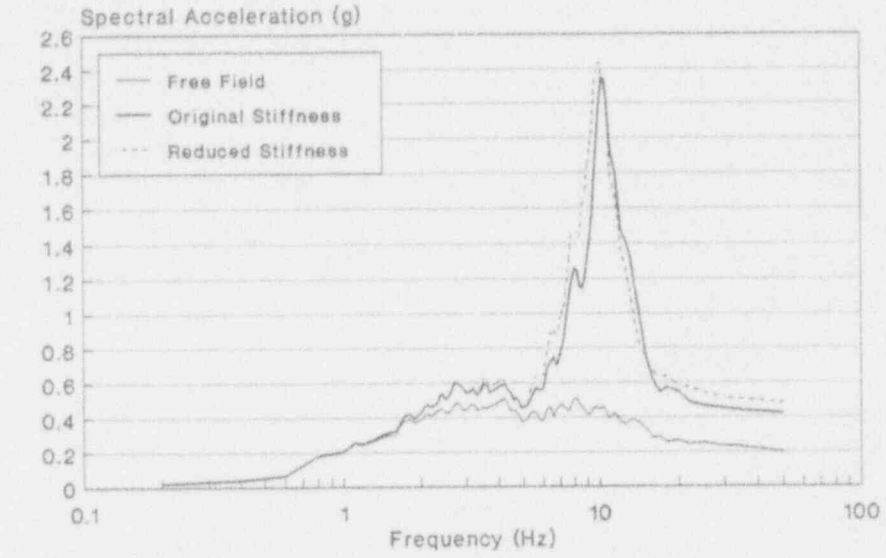

N-S Direction, El. 401'
5% Spectral Damping
PGA = 0.20g

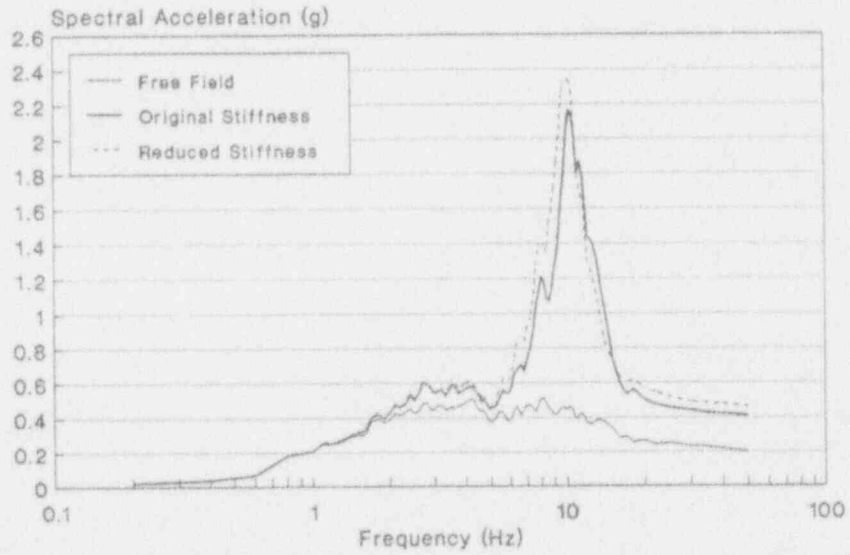

E-W Direction, El. 401'
5% Spectral Damping
PGA = 0.20g

Figure 4-28 ANO-1 Deterministic Analysis, Reactor Building, El. 401'

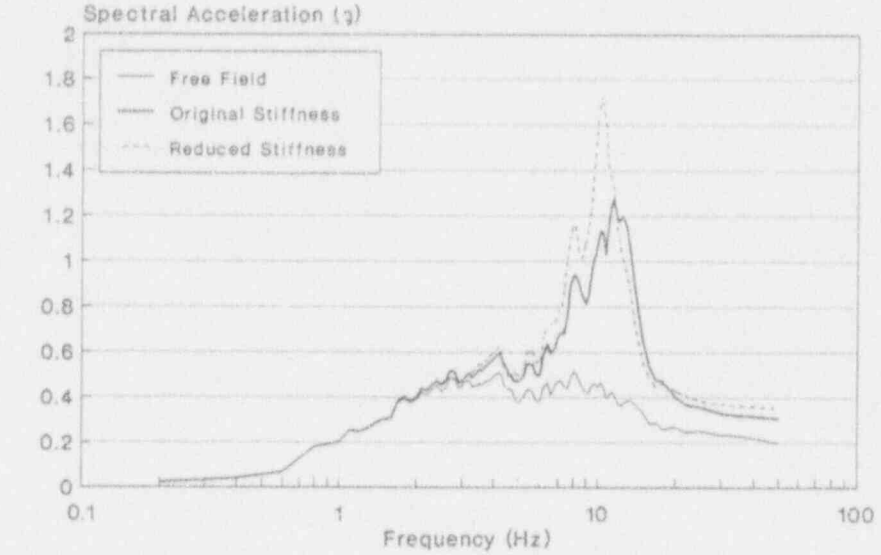

N-S Direction, El. 386'
5% Spectral Damping
PGA = 0.20g

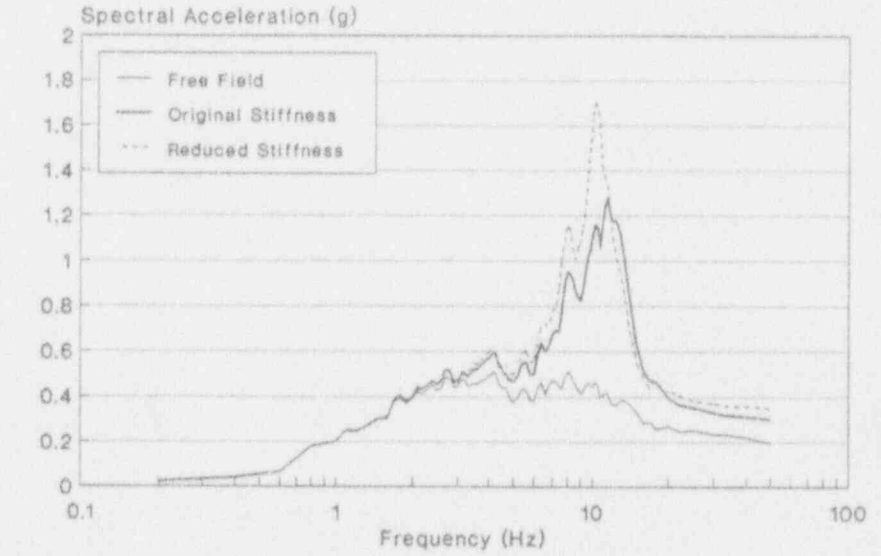

E-W Direction, El. 386'
5% Spectral Damping
PGA = 0.20g

Figure 4-29 ANO-1 Deterministic Analysis, Auxiliary Building, El. 386'

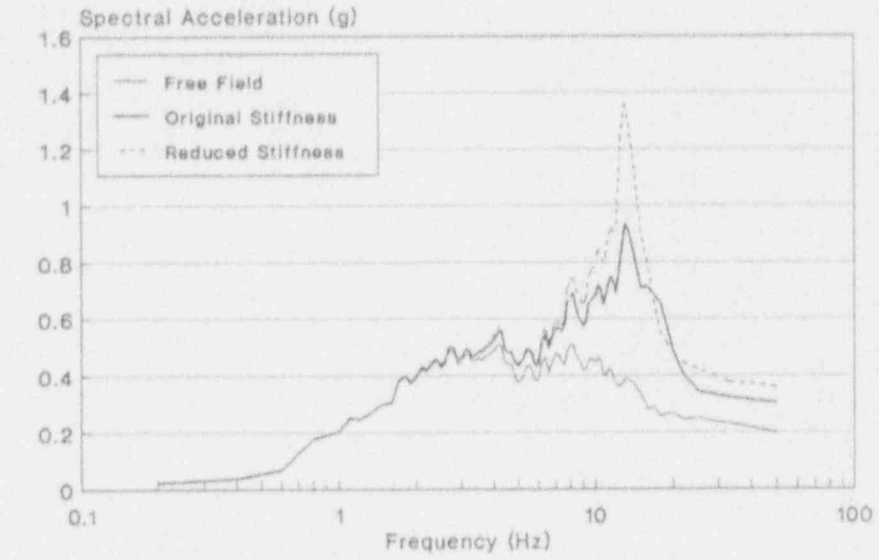

NW-SE Direction, El. 365'
5% Spectral Damping
PGA = 0.20g

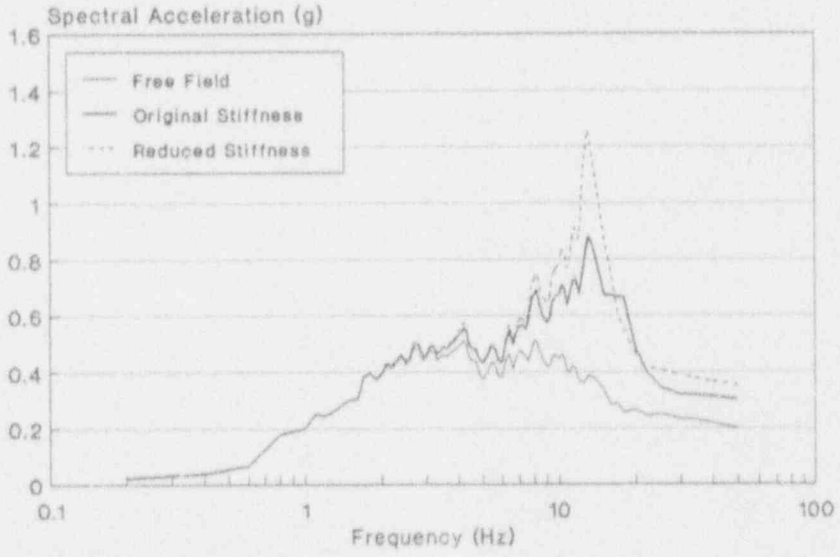

NE-SW Direction, El. 365'
5% Spectral Damping
PGA = 0.20g

Figure 4-30 ANO-1 Deterministic Analysis, Intake Structure, El. 365'

Table 4-23

Forces between Floor Levels of ANO-1 Reactor Building

Original Stiffnesses

Elev.	$Shear_X$(kip)	$Shear_Y$(kip)	$Moment_X$(kip-ft)	$Moment_Y$(kip-ft)
Internals:				
335'	261	260	12,730	12,560
357'	204	202	6,864	6,703
374'	126	121	3,404	3,275

Reduced Stiffnesses

Elev.	$Shear_X$(kip)	$Shear_Y$(kip)	$Moment_X$(kip-ft)	$Moment_Y$(kip-ft)
Internals:				
335'	298	298	14,700	14,550
357'	236	235	7,994	7,839
374'	148	143	3,991	3,848

Table 4-24

Forces between Floor Levels of ANO-1 Auxiliary Building

Original Stiffnesses

Elev.	$Shear_X$(kip)	$Shear_Y$(kip)	$Moment_X$(kip-ft)	$Moment_Y$(kip-ft)
335'	327	323	13,560	13,420
354'	241	239	7,342	7,293
371'	155	154	3,236	3,229
386'	61	61	909	914

Reduced Stiffnesses

Elev.	$Shear_X$(kip)	$Shear_Y$(kip)	$Moment_X$(kip-ft)	$Moment_Y$(kip-ft)
335'	360	358	15,030	14,980
354'	269	268	8,192	8,185
371'	173	174	3,616	3,626
386'	68	68	1,016	1,024

Table 4-25

Forces between Floor Levels of ANO-1 Intake Structure

Original Stiffnesses

Elev.	$Shear_X$(kip)	$Shear_Y$(kip)	$Moment_X$(kip-ft)	$Moment_Y$(kip-ft)
318'	77	84	2,595	2,776
333'	52	57	1,431	1,509
352'	24	23	435	418
365'	12	11	130	122

Reduced Stiffnesses

Elev.	$Shear_X$(kip)	$Shear_Y$(kip)	$Moment_X$(kip-ft)	$Moment_Y$(kip-ft)
318'	85	94	2,909	3,126
333'	59	65	1,631	1,717
352'	28	26	511	485
365'	14	13	154	143

the floor slabs at these elevations) for the original and reduced stiffness models described above when subjected to the synthetic time history at 1 SSE. Note that the values listed are net total forces and moments for that elevation and have not yet been distributed to the individual walls at that elevation.

In general, it can be seen that there is a maximum increase in loads of about 20% due to the stiffness reduction. Since there is very little assumed torsion in any of these structures, the same increase would apply to loads in the individual walls. Thus, from a design viewpoint, the stiffness reduction does result in a significant increase in net loads, but this increase (20%) is probably well within the range of conservatism implicit in the original design calculations.

4.3.6 Summary of ANO-1 Analysis

Both a probabilistic and deterministic re-evaluation of the ANO-1 Power Plant was performed using original stiffnesses and reduced stiffnesses. The probabilistic analysis consisted of re-performing a seismic PRA and adjusting the responses and structural fragilities to account for the reduced stiffnesses. This resulted in two overall core damage frequencies, one using original stiffnesses and one using reduced stiffnesses. A second set of frequencies was obtained for bounding purposes by using both the EPRI and LLNL hazard curves.

The resulting percentage increase in core damage frequency due to the stiffness reduction was small (~10%); however, the magnitude of increase itself (8.0E-5 using LLNL hazard curves) is quite significant. This increase in core damage frequency is due primarily to the increased values of response for the 5-10 Hz range of the Auxiliary building at elevations 371' and 386' respectively. These are the locations at which all the vital 480V and 4kV AC switchgear cabinets are located. Both these responses have been significantly increased over the case with no stiffness reduction. Since these switchgear cabinets still have a moderately low fragility and still contribute significantly to core damage, raising the response will result in a higher probability of losing all vital AC power and leading to a higher total core damage frequency at ANO-1.

The deterministic analysis also showed some increased values. Some shifts in floor response spectra were noted, particularly the peak spectral acceleration experienced some increases. Most notably, the Auxiliary Building experienced a significant increase in the 10 Hz range, and the Intake Structure experienced a significant increase in the 13 Hz range when reduced stiffnesses were modeled.

Similarly, deterministic loadings (both shear and moment) experienced increases. There was a maximum increase in loads of about 20% due to the stiffness reduction. Thus, from a design viewpoint, the stiffness reduction does result in a significant increase in net loads, but this increase (20%) is probably well within the range of conservatism implicit in the original design calculations.

5.0 Summary and Conclusions

In this study we developed a shear wall stiffness degradation model based on experimental results from tests performed for Los Alamos National Laboratory. This model predicts the reduction in stiffness of shear walls as a function of shear stress. This model includes an initial reduction in shear stiffness to 75% of theoretical with further decreases in stiffness for shear stresses above 150 psi.

The degradation model was used to reduce the shear modulus (G) for the shear walls in the important structures at three commercial nuclear power plant sites: ANO-1, Peach Bottom, and Zion. In this way, stiffness associated with bending and axial deformation were not affected. For each site, a suite of earthquakes was selected (appropriate to the site) and dynamic response analyses using the suite of earthquakes were performed. These dynamic response analyses were performed in iterative fashion, in which the method of successive approximations was used to incorporate the reduction in stiffness with calculated shear stress for each wall. In each case, the dynamic response analyses were performed at three different earthquake levels (corresponding roughly to 1 SSE, 3 SSE, and 5 SSE). These calculations, performed with and without shear wall stiffness reduction, provided the basis for estimating the impact of the reduction in shear wall stiffness on the responses of the various floor slabs within the buildings, and on the calculated seismic core damage frequency. In addition, deterministic "design-like" calculations (using design level damping and a single earthquake time history - the same time history used for the design of the plant) were performed to determine the effect of shear wall stiffness reduction on the design loads.

The three sites were chosen to reflect a reasonably broad range of plant and site conditions. Two types of PWRs (ANO-1 and Zion) and one BWR (Peach Bottom) were selected. These particular plants were selected because seismic PRAs had already been performed on these plants, and all structural models and Boolean logic equations were available (or could be easily developed by extension of existing work). These site choices also reflected a broad range of physical site conditions. That is, Peach Bottom is a hard rock site. ANO-1 is characterized by very stiff soil. Finally, the Zion site is a layered soil site having 110 feet of soil overlaying bedrock.

Based on these dynamic response and seismic risk analyses (as summarized in Chapter 4 and detailed in Appendices A, B, and C) a number of conclusions can be drawn as to the impact of the reduction in shear wall stiffnesses on power plant response and seismic risk.

First and foremost, the impact of the reduction in shear wall stiffness on computed core damage frequency is very plant specific. The largest impact occurs for those plants in which certain critical equipment is located in structures which experience a significant increase in response with reduction in shear wall stiffness. For example, increases in core damage frequencies at Peach Bottom were 25 to 30 percent (depending on whether LLNL or EPRI hazard curves were used). At the ANO-1 site, the

corresponding increases in plant risk were 10 percent (for each set of hazard curves). Finally, at Zion, there was essentially no change in the computed core damage frequency when a reduction in shear wall stiffness was included.

Although plant specific, it is likely that this spread in the percentage increase in seismic core damage frequency would be typical of that found at any plant. That is, it is reasonable to conclude that the increase in core damage frequency for virtually any plant would likely be less than 50 percent given our current understanding of the relationship between shear wall stiffness and shear stress. In the context of seismic probabilistic risk, 50% variations are not too significant.

The second conclusion is that (at any given site) the impact of the reduction of shear wall stiffness is very much structure specific, and is likely to vary amongst the important structures at any given site. The largest increase in response occurs for structures which have natural modes of vibration with frequencies in the 7 to 12 Hz range and for which the physical geometry is such that the stiffness of the walls is dominated by shear deformation. In these types of structures, reduction in shear wall stiffness results in a reduction in the natural frequencies of the building proportional to the square root of the shear wall stiffness. Thus these structures would have their natural frequencies reduced on the order of (typically) 10 to 30 percent. (Even though our stiffness reduction model showed reductions in shear wall stiffness down to as little as 10 percent of the original, our calculations for these three sites show that the stresses required for this level of reduction were never achieved for earthquake levels up to 5 SSE.) Thus for these types of structures experiencing a reduction in natural frequencies on the order of 10 percent to 30 percent, the effect is to increase the spectral acceleration response of the various floors because of the reduction in the dominant natural frequencies. This follows from the fact that the ground motion input spectra (which characterizes the earthquakes used in the calculational process) typically peak in the range of 4 to 8 hz. Thus the reduction in natural frequencies of these structures tends to push their response into the higher spectral acceleration region of the input ground motion spectra. The increase, however, is limited by the change in natural frequencies. Based on the sets of structures we analyzed for these three sites, the maximum increase in floor responses was on the order of 30 percent at most, and most were smaller. Thus, the effect of reduction in shear wall stiffness is not experienced uniformly by all structures at the site and for those structures that are affected, the net effect is an increase in responses on the order of 20 to 30 percent rather than orders of magnitude.

Of particular importance is the fact that, for all three plants examined, the reactor internals structure (biological shield, etc.) which are the support for the main operating floor inside the containment (upon which the reactor coolant, reactor vessel, steam generator, etc. are anchored) showed very low stresses, and as such, experienced only minimal reduction in frequency with shear wall reduction. Given the typical geometry of the concrete shear wall internal structures, this would be expected to be the

case at any typical commercial U.S. power plant. The implications are that there is negligible impact of shear wall stiffness reduction on the responses seen by the reactor vessel and the primary coolant piping, etc., and thus no change in the probability of loss of coolant events due to this effect is to be expected. This is a significant and important conclusion.

A related observation is that, for seismic PRAs, a dominant source of transients is loss of offsite power resulting from failure of ceramic insulators in the switchyard. These failures, of course, are determined only by the level of peak ground acceleration and are unaffected by shear wall reductions. Thus, the two observations taken together show that the impact of shear wall reduction on the initiating events in a seismic PRA is almost negligible. This helps to explain why the impact of the shear wall stiffness reduction on the total core damage frequency of this effect is relatively small overall.

In the process of developing fragilities for the buildings at a power plant, it is necessary to perform dynamic response calculations. Thus the reduction in shear wall stiffness can have an impact on the calculated seismic capacity of the structures. This was analyzed for two of the three plants in this study and it was found that the impact of shear wall reduction on the computed seismic capacity was not large and, in fact, was generally less than a 10 percent reduction in the median seismic capacity.

The level of modeling used in developing structural dynamic models for the structures at a specific plant can also play a role in the computed impact of shear wall reduction in stiffness. In this study, the ANO-1 and Peach Bottom structures were modeled with an interconnected set of shear beams and lumped masses representing the floor slabs, equipment and tributory wall masses. In the iterative dynamic analyses, the composite stiffness of each shear beam was changed until the reduction in shear stiffness (as a function of calculated shear stress) converged. By contrast, in the Zion analysis, detailed three-dimensional finite element models of the structures were utilized. These used plate elements for the walls and the floor slabs and a very detailed level of modeling. It was found that when very detailed finite element models were used to incorporate the effect of reduction in shear stiffness, the flexibility of the floor slabs reduced the contribution of the shear wall stiffness and thus the overall effect of reduction in shear stiffness was smaller than would be computed if a shear beam/lumped mass model were used. In fact, at Zion, the reduction in shear stiffness resulted in reductions in dominant frequencies only on the order of 10 percent. Thus one can conclude, in general, that when typical design models involving shear beams and lumped masses (and the implicit assumption of rigid floor slabs) are utilized, the effect will be to overpredict the impact of shear wall stiffness reduction on building response.

The fact that for Zion, essentially no change in seismic core damage frequency was observed was also due significantly to the fact that Zion represents a layered soil site. The small change in building fixed-base natural frequencies that results from shear wall stiffness reduction has

little effect on the frequency of the combined soil-foundation-structure system. (This is true since the soil underlying the foundations provides a relatively soft "equivalent spring" which dominates the response of the structure.) And it is these combined system natural frequencies which must shift relative to the input spectra before a significant increase in building response occurs. Thus the fact that no change in seismic core damage frequency was observed at Zion is due in small part to the increased level of modeling and in larger part due to the soil underlying the plant.

Finally, as noted above, deterministic "design-like" calculations of shear wall loads and moments were made both with and without reduction in shear wall stiffness. Deterministic loads calculated for these two cases typically increased on the order of 10 to 20 percent for the affected structures. In general, this increase is felt to be a reasonable upper bound to the expected changes in loads for a deterministic design calculation, because the reduction in shear wall stiffness with stress is relatively small at the stresses which are experienced by these structures at design earthquake levels. Thus, in general, a conclusion is that the calculated increase in shear wall loads from a deterministic "design-like" calculation at the SSE (approximately 10 to 20 percent) is well within the bounds of typical conservatism built into the design calculational process and into the design code allowables. Hence these studies do not indicate the need for any design reanalysis for typical shear wall structures at current nuclear power plants.

6.0 REFERENCES

1. E.G. Endebrock, et. al., Analysis and Tests on Small-Scale Shear Walls--FY 82 Final Report, Los Alamos National Laboratory report LA-10443-MS, NUREG/CR-4274, 1985.

2. R.C. Dove, et. al., Scale Modeling of Reinforced Concrete Category I Structures Subjected to Seismic Loading, Los Alamos National Laboratory report LA-10624-MS, NUREG/CR-4474, 1986.

3. R.C. Dove, et. al., Seismic Category I Structures Program Final Report, FY 1983-84, Los Alamos National Laboratory report LA-11013-MS, NUREG/CR-4924, 1987.

4. J.G. Bennett, et. al., Simulated Seismic Tests on 1/42- and 1/14-Scale Category I Auxiliary Buildings, Los Alamos National Laboratory report LA-11093-MS, NUREG/CR-4987, 1987.

5. J.G. Bennett, et. al., The Seismic Category I Structures Program: Results for FY 1985, Los Alamos National Laboratory report LA-11117-MS, NUREG/CR-4998, 1987.

6. J.G. Bennett, et. al., The Seismic Category I Structures Program: Results for FY 1986, Los Alamos National Laboratory report LA-11377-MS, NUREG/CR-5182, 1988.

7. C.R. Farrar, et. al., Static Load Cycle Testing of a Low-Aspect Ratio Six-Inch Wall TRG-Type Structure TRG-4-6 (1.0, 0.25), Los Alamos National Laboratory report LA-11422-MS, NUREG/CR-5222, 1989.

8. C.R. Farrar, et. al., The Seismic Category I Structures Program: Results for FY 1987, Los Alamos National Laboratory report LA-11607-MS, NUREG/CR-5369, 1990.

9. C.R. Farrar, et. al., Static Load Cycle Testing of a Low-Aspect-Ratio Four-Inch Wall, TRG-Type Structure TRG-5-4 (1.0, 0.56), Los Alamos National Laboratory report LA-11739-MS, NUREG/CR-5487, 1990.

10. C.R. Farrar, et. al., Static and Simulated Seismic Testing of the TRG-7 Through -16 Shear Wall Structures, Los Alamos National Laboratory report LA-11992-MS, NUREG/CR-5660, 1991.

11. M.P. Bohn, et. al., Assessment of Effects of Structural Response on Plant Risk: Preliminary Results for Peach Bottom Atomic Power Station, Sandia National Laboratories, SAND89-1766, July 1989.

12. P.B. Schnabel, et. al., SHAKE -- A Computer Program for Earthquake Response Analysis of Horizontally Layered Sites, Earthquake Engineering Research Center, University of California, Berkeley, CA, EERC 72-12, 1972.

13. J.M. Roesset, A Review of Soil Interaction, UCRL-15262, June 1980.

14. H.L. Wong, et. al., Soil-Structure Interaction: A Linear Continuum Mechanics Approach (CLASSI), Dept. of Civil Engineering, University of Southern California, Los Angeles, CA, CE79-03, 1980.

15. R. Riddell, et. al., Statistical Analysis of the Response of Nonlinear Systems Subjected to Earthquakes, University of Illinois, UILU-ENG 79-2016, August 1979.

16. R.P. Kennedy, et. al., Engineering Characterization and Ground Motion, NUREG/CR-3805, U.S. Nuclear Regulatory Commission Report, May 1983.

17. V. Cervenka, et. al., "Inelastic Analysis of Reinforced Concrete Panels, Part II: Experimental Verification and Application," IABSE Publications, Vol. 32-II, pp. 25-39, 1972.

18. M. Hirosawa, "Past Experimental Results on Reinforced Concrete Shear Walls and Analysis on Them [sic]," Report #6, Building Research Institute, Ministry of Construction, Tsukuba, Japan, p. 227, 1975.

19. Y. Kanoh, et. al., "Mechanical Behavior of Shear Walls with Intermediate Wall Columns," Transactions of the Japan Concrete Institute, Vol. 6, pp. 613-620, 1984.

20. R.R. Lopez, et. al., Fundamental Frequency of Reinforced Concrete Small-Scale Test Structures, Department of Civil Engineering, University of Illinois, Urbana, 1989.

21. Y. Shimizu, et. al., "Experimental Study on Repaired Reinforced Concrete Wall with Initial Cracks or with Honey Comb," Transactions of the Japan Concrete Institute, Vol. 2, pp. 415-423, 1980.

22. H. Umemura, et. al., "Aseismic Characteristics of RC Box and Cylinder Walls," Faculty of Engineering Proceedings, Department of Architecture, Tokyo University, pp. 49-54, 1977.

23. J.A. Lambright, et. al., Analysis of Core Damage Frequency: Peach Bottom Unit 2 External Events, NUREG/CR-4550, SAND86-2084, Vol. 4, Rev.1, Part 3. December 1990.

24. Peach Bottom Atomic Power Station Updated Final Safety Analysis Report Section 2.0, June 1983.

25. D.L. Bernreuter, et. al., Seismic Hazard Characterization of 69 Nuclear Plant Sites East of the Rocky Mountains, NUREG/CR-5250, October 1988.

26. Electric Power Research Institute, Seismic Hazard Methodology for the Central and Eastern United States, EPRI NP-4726, Vols 1-10, July 1986.

27. M.P. Bohn, et al., Application of the SSMRP Methodology to the Seismic Risk at the Zion Nuclear Power Plant, Lawrence Livermore National Laboratory, Livermore, CA, UCRL-53483, NUREG/CR-3428, 1983.

28. Zion Probabilistic Safety Study, prepared by Pickard, Lowe and Garrick for Commonwealth Edison, Chicago, Illinois, 1982.

29. Zion Station Updated Final Safety Analysis Report, Vol. 1, Commonwealth Edison, 1982.

30. G.J. Kolb, Interim Reliability Evaluation Program: Analysis of the Arkansas Nuclear One - Unit 1 Nuclear Power Plant, NUREG/CR-2787, SAND82-0978, Vol. 1, June 1982.

31. W.R. Cramond, et. al., Shutdown Decay Heat Removal Analysis of a Babcock and Wilcox Pressurized Water Reactor, NUREG/CR-4713, SAND86-1832, March 1987.

32. Arkansas Nuclear One - Unit 1 Nuclear Power Plant Final Safety Analysis Report, April 1971.

33. J.J. Johnson, et. al., Phase I Final Report - SMACS - Seismic Methodology Analysis Chain with Statistics (Project VIII), NUREG/CR-2015, Vol. 9, UCRL-53021, July 1981.

APPENDIX A

PEACH BOTTOM ANALYSIS

CONTENTS

A.1 INTRODUCTION

A detailed seismic risk assessment was performed for the Peach Bottom plant as part of the NRC sponsored NUREG 1150 program [A-1]. This analysis utilized dynamic response calculations for all important structures, a generic seismic fragility data base for components, and detailed component fragility derivations for a number of components identified during the plant visit as falling outside the generic data base. Point estimates and mean values of accident sequence and core damage frequencies were obtained using a Monte Carlo approach.

A.1.1 Plant Description

The Peach Bottom Atomic Power Station (PBAPS) is located on the western shore of Conowingo Pond, formed by the backwater of Conowingo dam, 9 miles downstream on the Susquehanna River. The plant is 38 miles N-NE of Baltimore, Maryland, and 63 miles W-SW of Philadelphia, Pennsylvania.

The twin BWR units (Peach Bottom Units 2 and 3) of Philadelphia Electric Company are each rated at 1,065 MW. The reactor and generator for both these units were supplied by General Electric Corporation. Bechtel acted as Architect/Engineer/Constructor. The plants began commercial operation in 1974. Unit 1 is a 40 MW decommissioned HTGR and is now in a mothball status. Based on the Peach Bottom Final Safety Analysis Report [A-2], a horizontal peak ground acceleration of 0.12g was defined for the SSE.

A.1.2 Description of Plant Systems

This section discusses the system descriptions of the major frontline and support systems important to safety. The discussion of the systems that follow includes:

a. A brief functional description of the system with reference to the one-line diagrams that were developed to indicate which components were included in the model:

b. Safety-related success criteria that were applied to the system;

c. Interfaces and safety actuation provisions between the frontline systems and the support systems.

High Pressure Coolant Injection (HPCI) System

The function of the HPCI system is to provide a makeup coolant source to the reactor vessel during accidents in which system pressure remains high.

The HPCI system consists of a single train with motor-operated valves and a turbine-driven pump. Suction is taken from either the Condensate

Storage Tank (CST) or the suppression pool (or torus). Injection to the reactor vessel is via a feedwater line. The HPCI pump is rated at 5000 gpm flow with a discharge head of 1135 psig. A simplified schematic of the HPCI system is provided by Figure A-1.

Most of the HPCI system is located in a separate room in the reactor building. Local access to the HPCI system could be affected by either containment venting or containment failure should steam be released to the reactor building area. Room cooling failure is assumed to fail the HPCI pump in 10 hours.

Reactor Core Isolation Cooling (RCIC) System

The function of the RCIC system is to provide a makeup coolant source to the reactor vessel during accidents in which system pressure remains high.

The RCIC system consists of a single train with motor-operated valves and a turbine-driven pump. Suction is taken from either the CST or the suppression pool. Injection to the reactor vessel is via a feedwater line. The RCIC pump is rated at 600 gpm flow with a discharge head of 1135 psig. A simplified schematic of the RCIC system is provided by Figure A-2.

Most of the RCIC system is located in a separate room in the reactor building. Local access to the RCIC system could be affected by either containment venting or containment failure should steam be released to the reactor building area. Room cooling failure is assumed to fail the RCIC pump in 10 hours.

Control Rod Drive (CRD) System

The CRD system was modeled as a backup source of high pressure injection. The CRD pumps take suction from the condenser hotwell in the Condensate system or the CST. A flow control station is installed downstream of the tap from the Condensate system and ties into the CRD pump suction line before the CRD suction filter. The flow control station will divert 250 gpm from the Condensate system. This will supply the CRD system with the remainder of the water being passed on to the CST. In the event that flow from the Condensate system is interrupted, the CST provides a backup source of water to ensure CRD system operability without operator action being required. A simplified schematic of the CRD system is provided by Figure A-3.

The CRD pumps, together, can achieve a flow rate of approximately 210 gpm with the reactor fully pressurized and approximately 300 gpm with the reactor depressurized. Two discharge paths are provided for the CRD pumps. One discharge path is through an air-operated valve control station. When instrument air is lost, this path is blocked. With both CRD pumps running and the reactor at nominal pressure, the second discharge path restricts flow, by means of an orifice, to approximately 180 gpm.

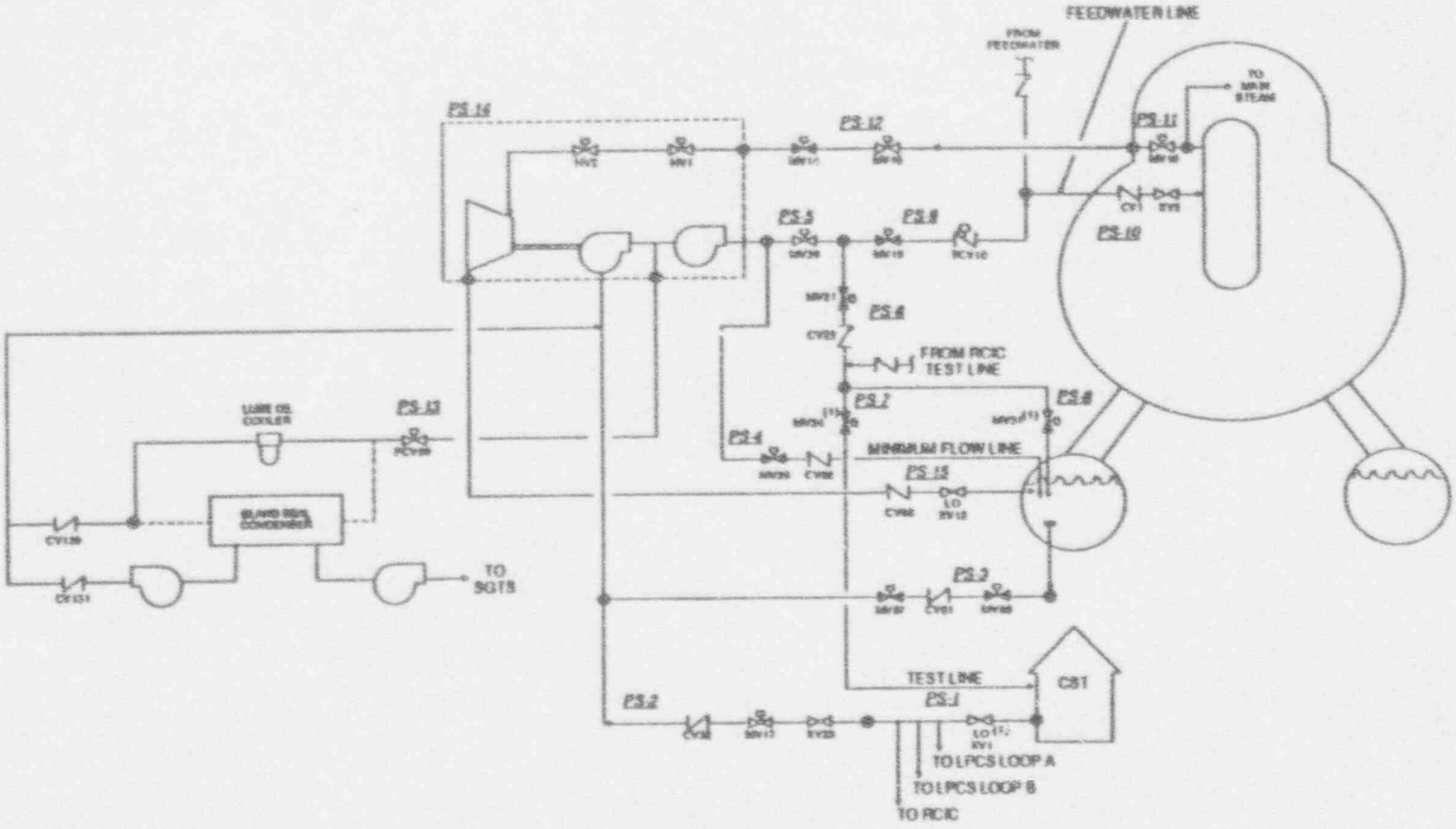

VALVE POSITIONS ARE SHOWN IN THEIR STANDBY MODE
(1) VALVE ALSO SHOWN ON RCIC SCHEMATIC

Figure A-1 High Pressure Coolant Injection System Schematic

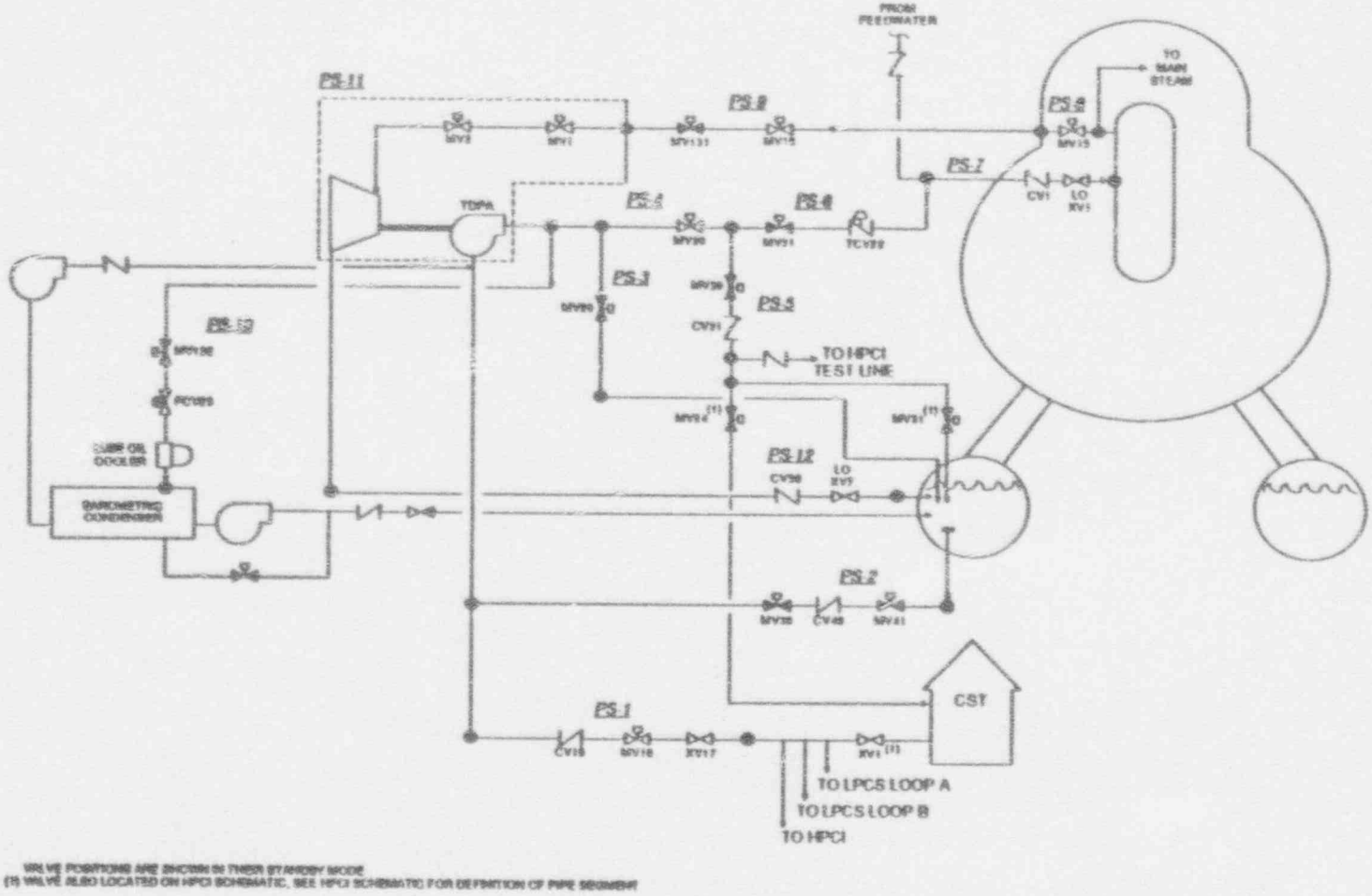

Figure A-2 Reactor Core Isolation Cooling System Schematic

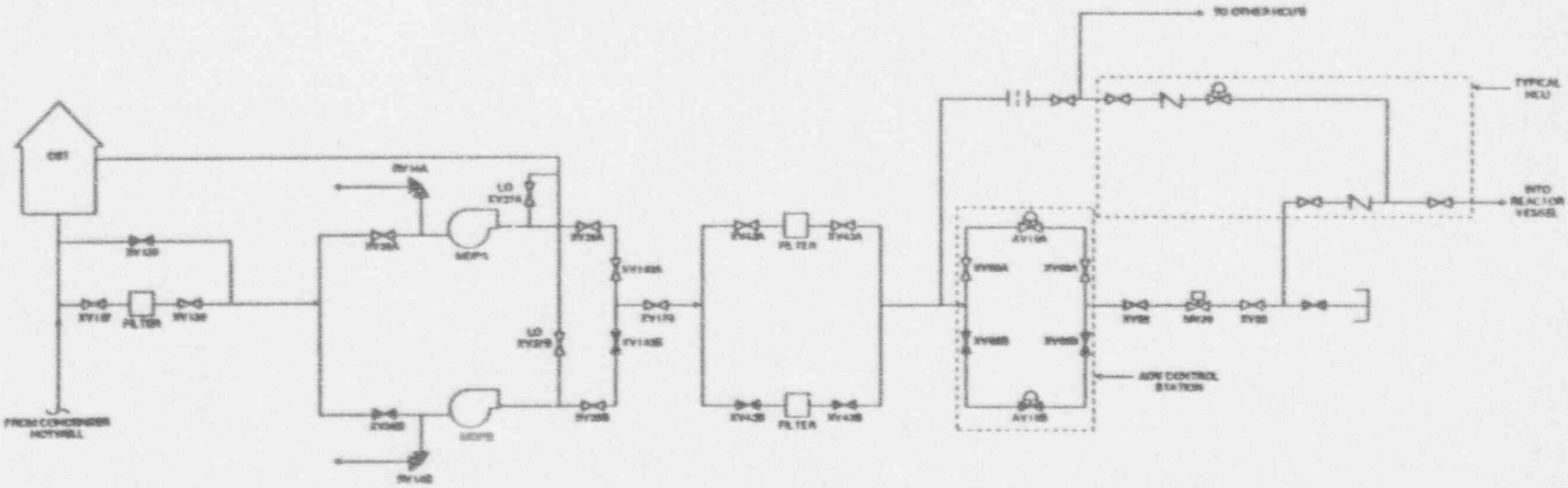

Figure A-3 Control Rod Drive System Schematic

Normally one CRD pump is running, with the suction and discharge valves to the standby pump being blocked. Should the operator be required to realign the CRD system as a sole source of early high pressure injection, the standby CRD pump must be placed into operation to achieve sufficient flow to the reactor vessel.

In general, the CRD success criteria (as a sole injection source to the reactor) requires both pumps running and one of the two discharge paths available. If some other injection system has been operating successfully for 6 or more hours following an initiator, the CRD success criteria changes to one pump running and one of two discharge paths available.

Most of the CRD system is located in the turbine building. Any physical impact of accident conditions on the ability of the CRD system to perform its function would be minimal. Since the system is located in a large open area, room cooling failure is not applicable to the CRD pumps. The CRD pumps receive no automatic initiation signals.

Automatic Depressurization System (ADS)

The ADS is designed to depressurize the primary system to a pressure at which the low pressure injection systems can inject coolant to the reactor vessel.

The ADS describes the automatic or, if required, manual operation of the ADS/SRV system to depressurize the primary system. This allows the low pressure injection systems to be used to cool the core. The Manual Depressurization system describes manual operation of the ADS/SRV system to depressurize the primary system. This allows the SDC mode of the RHR system to be used.

The ADS consists of five relief valves capable of being manually opened. Each valve discharges via a tailpipe line through a downcomer to the suppression pool. Relief valve capacity is approximately 820,000 lb/hr. A simplified schematic of the ADS is provided by Figure A-4.

The ADS is automatically initiated. The operator may manually initiate the ADS or may depressurize the reactor vessel using the six relief valves that are not connected to ADS logic. The operator can inhibit ADS operation if a spurious ADS signal occurs or if the operator desires to do so (as in an ATWS scenario). The success criterion for the ADS is three of five valves opening to depressurize the reactor.

The ADS valves are located inside the containment. ADS performance is not normally affected by accident conditions since the equipment is qualified for accident conditions and the air/nitrogen supply pressure is judged to be sufficiently high to allow valve operation under most containment conditions. However, should containment pressure be excessively high (~85 psig or greater), the valves could not be kept open since the air/nitrogen supply pressure is limited to ~85 psig based on discussions with Philadelphia Electric Company (PECO) personnel indicating the supply is orificed to that limit.

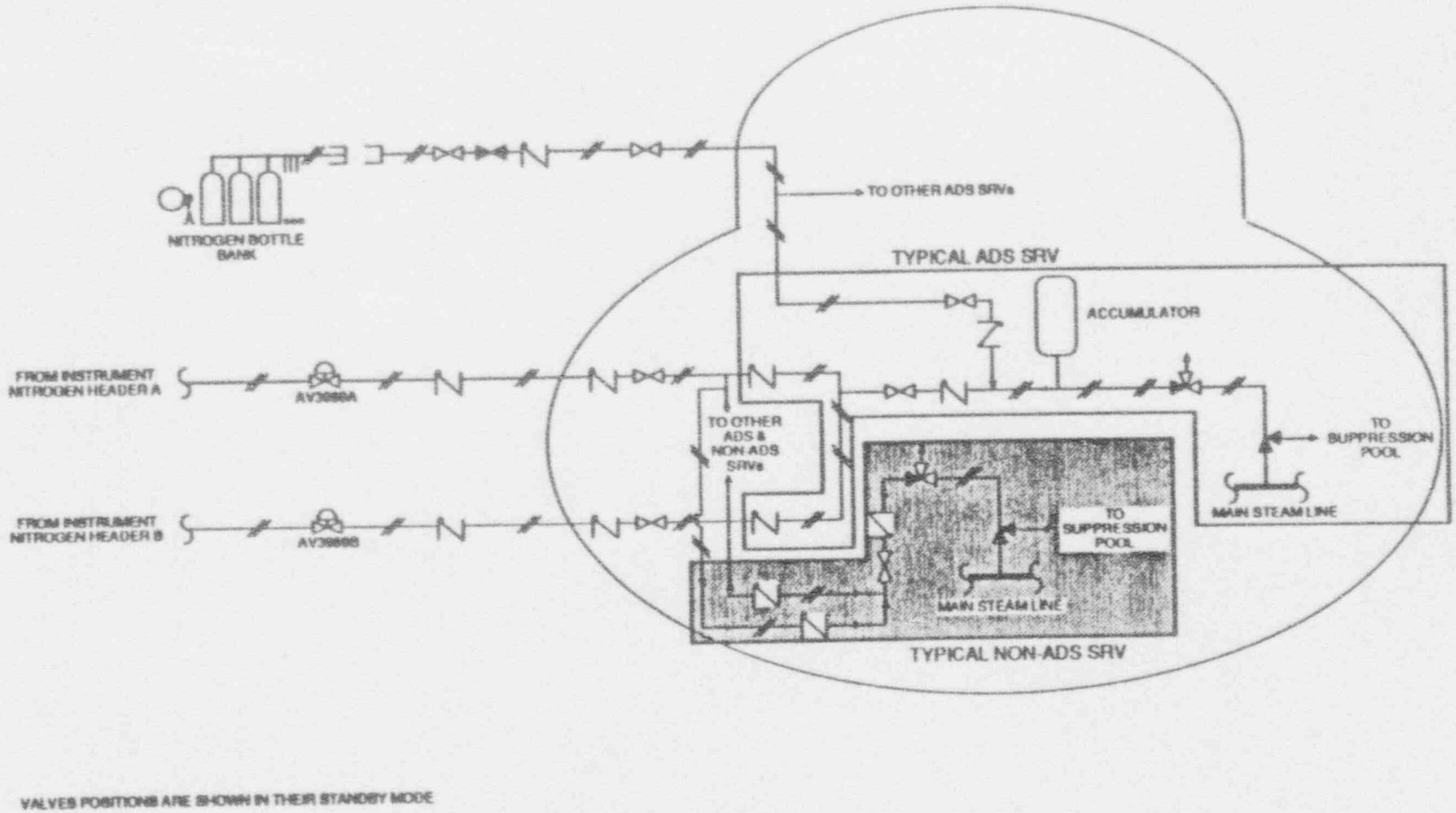

Figure A-4 Automatic and Manual Depressurization System Schematic

Low Pressure Core Spray (LPCS) System

The function of the LPCS system is to provide a makeup coolant source to the reactor vessel during accidents in which system pressure is low. The ADS can be used in conjunction with the LPCS system to attain a low enough system pressure for injection to occur.

The LPCS system is a two-loop system consisting of motor-operated valves and motor driven pumps. There are two 50-percent capacity pumps per loop, with each pump rated at 3125 gpm with a discharge head of 105 psig. The LPCS system's normal suction source is the suppression pool. Pump suction can be manually realigned to the CST. A simplified schematic of the LPCS system is provided by Figure A-5.

The LPCS system is automatically initiated and controlled. Operator intervention is required to manually start the system given an auto-start failure and to stop the system or manually control flow during an ATWS if required. The success criterion for the LPCS system is injection of flow from any two pumps to the reactor vessel.

Most of the LPCS system is located in the reactor building. Local access to the LPCS system could be affected by either containment venting or failure. Room cooling failure is assumed to fail the LPCS pumps in 10 hours.

Low Pressure Coolant Injection (LPCI) System

The function of the LPCI system is to provide a makeup coolant source to the reactor vessel during accidents in which system pressure is low. The ADS can be used in conjunction with the LPCI system to attain a low enough system pressure for injection to occur. The LPCI system is but one mode of the RHR system and, as such, shares components with other modes.

The RHR system is a two-loop system consisting of motor-operated valves and motor-driven pumps. There are two pump/heat exchanger trains per loop, with each pump rated at 10,000 gpm with a discharge head of 450 psig. Cooling water flow to the heat exchangers is not required for the LPCI mode. The LPCI suction source is the suppression pool. A simplified schematic of the LPCI (RHR) system is provided by Figure A-6.

The LPCI system is automatically initiated and controlled. Operator intervention is required to manually start the system given an auto-start failure and to stop the system or control flow during an ATWS if required. The success criterion for the LPCI system is injection of flow from any one pump to the reactor vessel.

Most of the LPCI system is located in the reactor building. Local access to the LPCI system could be affected by either containment venting or failure. Room cooling failure is assumed to fail the LPCI pumps in 10 hours.

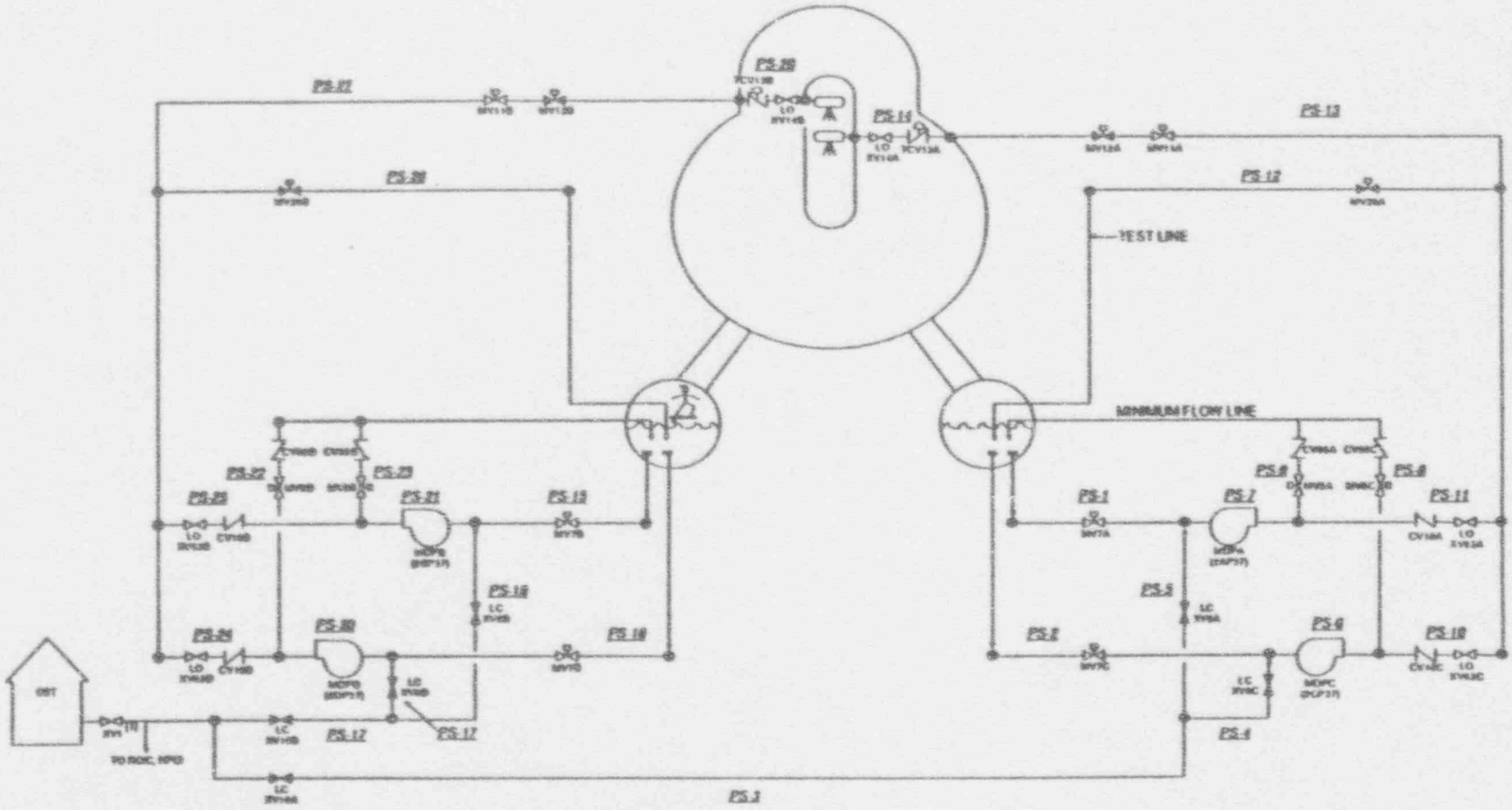

VALVE POSITIONS ARE SHOWN IN THEIR STANDBY POSITION
(1) VALVE ALSO LOCATED ON HPCI SCHEMATIC, SEE HPCI SCHEMATIC FOR DEFINITION OF PIPE SEGMENT

Figure A-5 Low Pressure Core Spray System Schematic

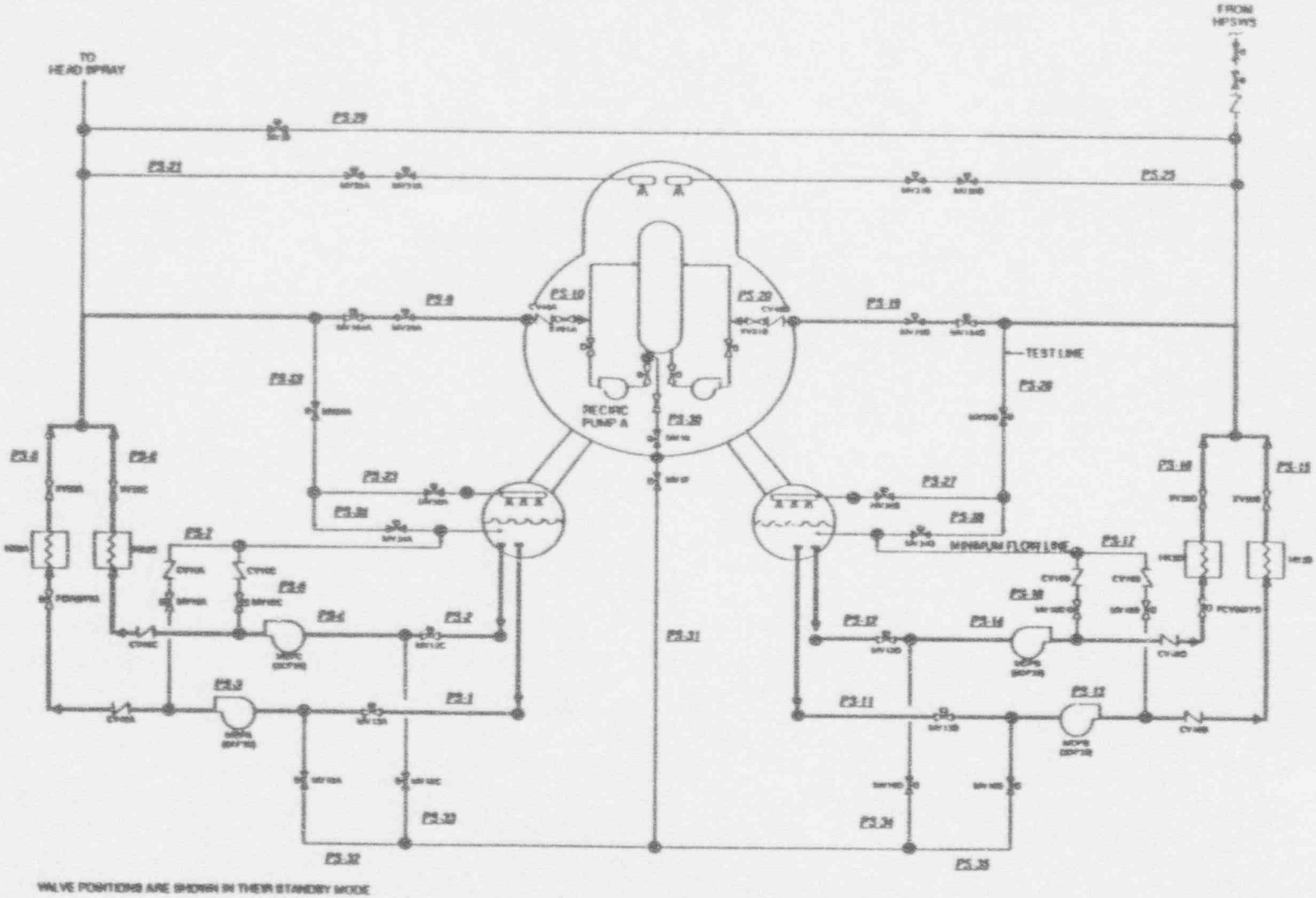

Figure A-6 Low Pressure Coolant Injection System Schematic

Residual Heat Removal: Shutdown Cooling (SDC) System

The function of the SDC system is to remove decay heat during accidents in which reactor vessel integrity is maintained. The SDC system is but one mode of the RHR system and, as such, shares components with other modes.

The RHR system is a two-loop system consisting of motor-operated valves and motor-driven pumps. There are two pump/heat exchanger trains per loop, with each pump rated at 10,000 gpm with a discharge head of 20 psid. Cooling water flow to the heat exchanger is required for the SDC mode. The SDC system suction source is one reactor recirculation pump's suction line. A simplified schematic of the SDC (RHR) system is provided by Figure A-7. The SDC system is manually initiated and controlled. The success criterion for the SDC system is injection of flow from any one pump/heat exchanger train to the reactor vessel.

Most of the SDC system is located in the reactor building. Local access to the SDC system could be affected by either containment venting or failure. Room cooling failure is assumed to fail the SDC pumps in ten hours.

Residual Heat Removal: Suppression Pool Cooling (SPC) System

The function of the SPC system is to remove decay heat from the suppression pool during accidents. The SPC system is but one mode of the RHR system and, as such, shares components with other modes.

The RHR system is a two-loop system consisting of motor-operated valves and motor-driven pumps. There are two pump/heat exchanger trains per loop, with each pump rated at 10,000 gpm with a discharge head of 20 psid. Cooling water flow to the heat exchanger is required for the SPC mode. The SPC suction source is the suppression pool. A simplified schematic of the SPC (RHR) system is provided by Figure A-8. The SPC system is manually initiated and controlled. The success criterion for the SPC system is injection of flow from any one pump/heat exchanger train to the suppression pool.

Most of the SPC system is located in the reactor building. Local access to the SPC system could be affected by either containment venting or failure. Room cooling failure is assumed to fail the RHR pumps in ten hours.

Residual Heat Removal: Containment Spray (CS) System

The function of the CS system is to suppress pressure in the drywell during accidents. The CS system is but one mode of the RHR system and, as such, shares components with other modes.

The RHR system is a two-loop system consisting of motor-operated valves and motor-driven pumps. There are two pump/heat exchanger trains per loop, with each pump rated at 10,000 gpm with a discharge head of 20 psid. Cooling water flow to the heat exchanger is required for the CS mode. The

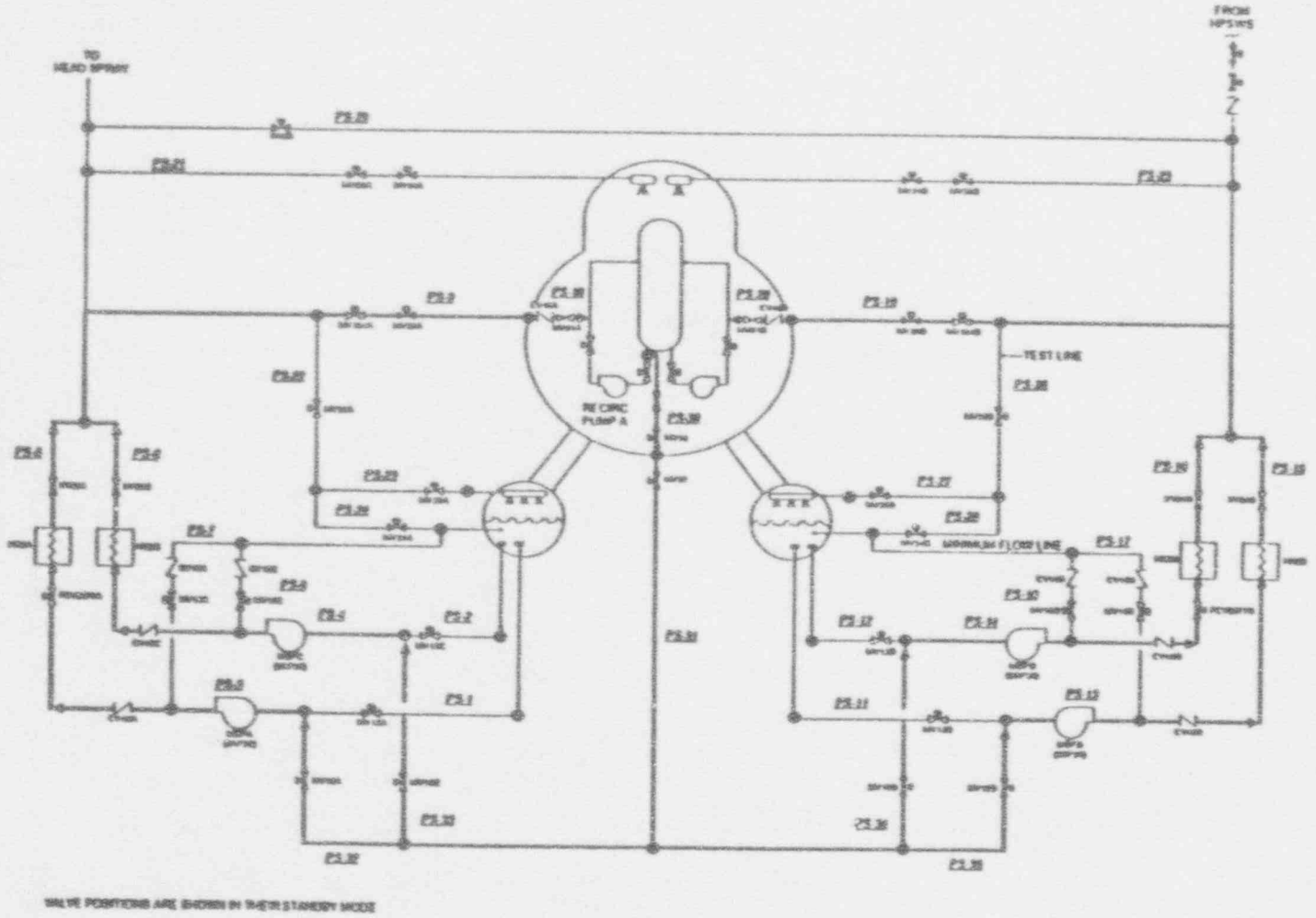

Figure A-7 Residual Heat Removal System - Shutdown Cooling Mode Schematic

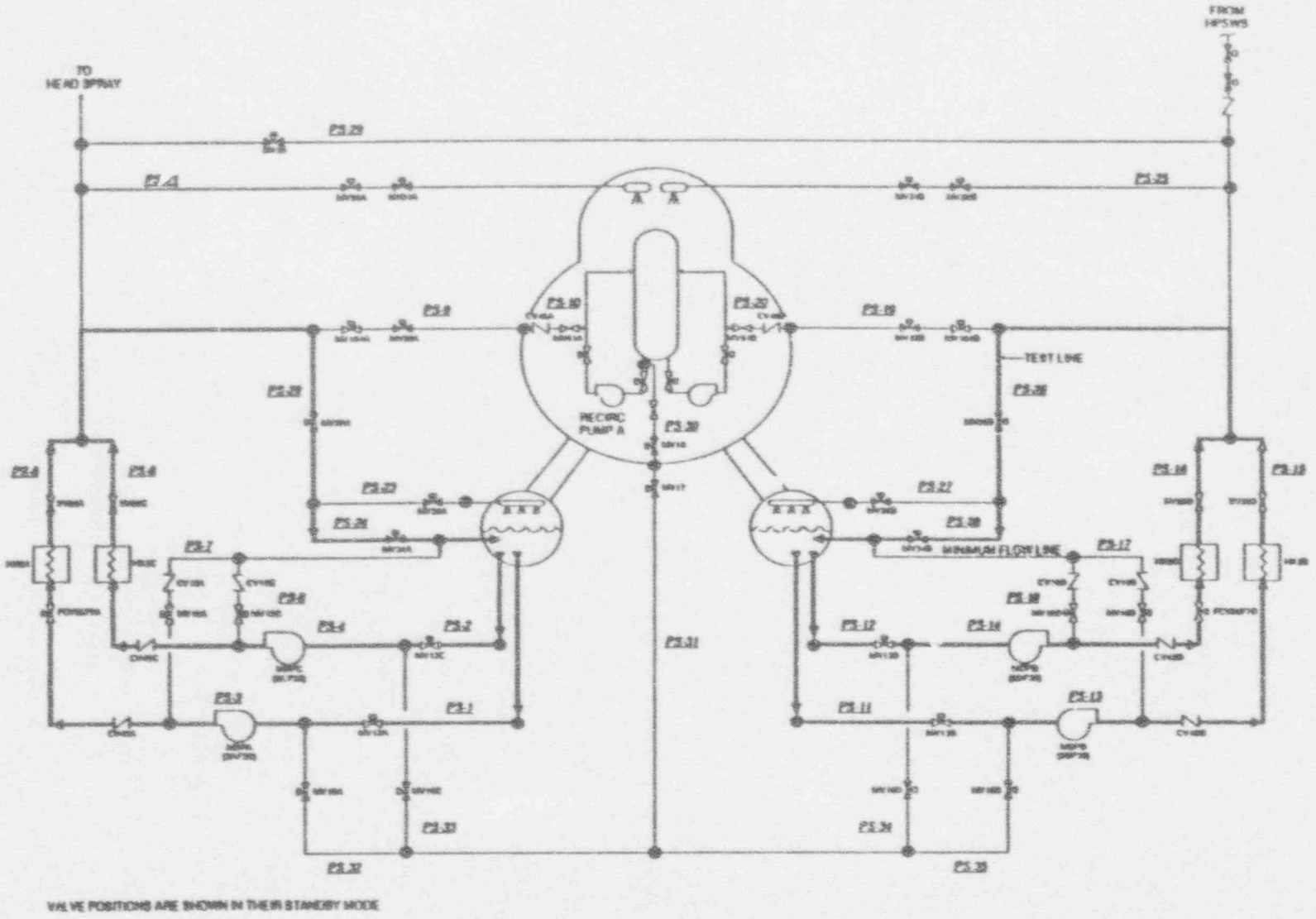

Figure A-8 Suppression Pool Cooling System Schematic

CS suction source is the suppression pool. A simplified schematic of the CS (RHR) system is provided by Figure A-9. The CS system is manually initiated and controlled. The success criterion for the CS system is injection of flow from any one pump/heat exchanger train to the spray ring.

Most of the CS system is located in the reactor building. Local access to the CS system could be affected by either containment venting or failure. Room cooling failure is assumed to fail the CS pumps in ten hours.

Electric Power System (EPS)

The EPS is designed to provide a diversity of dependable power sources which are physically isolated from each other.

The Peach Bottom station receives power from two separate offsite sources. If both offsite sources are lost, auxiliary power is supplied to both Unit 2 and Unit 3 from four onsite diesel generators shared between the two units. Loads important to plant safety are split and diversified. Station batteries provide control power for specific engineered safeguards and for other required functions when AC power is not available. A simplified schematic of the EPS is provided by Figure A-10.

Each diesel generator unit consists of a diesel engine, a generator, and the associated auxiliaries mounted on a common base. The continuous rating of the diesel generators is 2600 kW. The engine is rated for a ten percent overload for any two of every 24 hours.

There are two independent 125/250 V DC systems per unit. Each system is comprised of two 125-V batteries, each with its own charger. Each 125-V battery is a lead-calcium type with 58 cells. The chargers are full wave, silicon-controlled rectifiers. The two batteries for each unit are redundant. Loads are diversified between these systems so that each system serves loads which are identical and redundant. Power for larger loads, such as dc motor-driven pumps and valves, is supplied at 250 V from two 125-V sources. Selected batteries from Unit 2 and from Unit 3 are needed to start Diesel Generators 1, 2, 3 and 4, respectively.

Each standby diesel generator automatically starts. The diesel generator may be stopped by the operator after determining that continued operation of the diesel is not required.

Most of the EPS is located in the diesel building and in compartmentalized rooms within the reactor building. Any physical impact of accident conditions on the ability of the EPS to perform its function would be minimal. It is assumed that room cooling is not required for the ac switchgear or dc battery rooms since the heat loads are small and no sizeable heat loads are near these rooms. Diesel generators are assumed to fail in less than 30 minutes without room cooling although it is recognized that diesel performance would degrade before actual failure of the diesel and provide a warning to the operators that a problem existed. Possible recovery actions (by opening doors) could therefore take place.

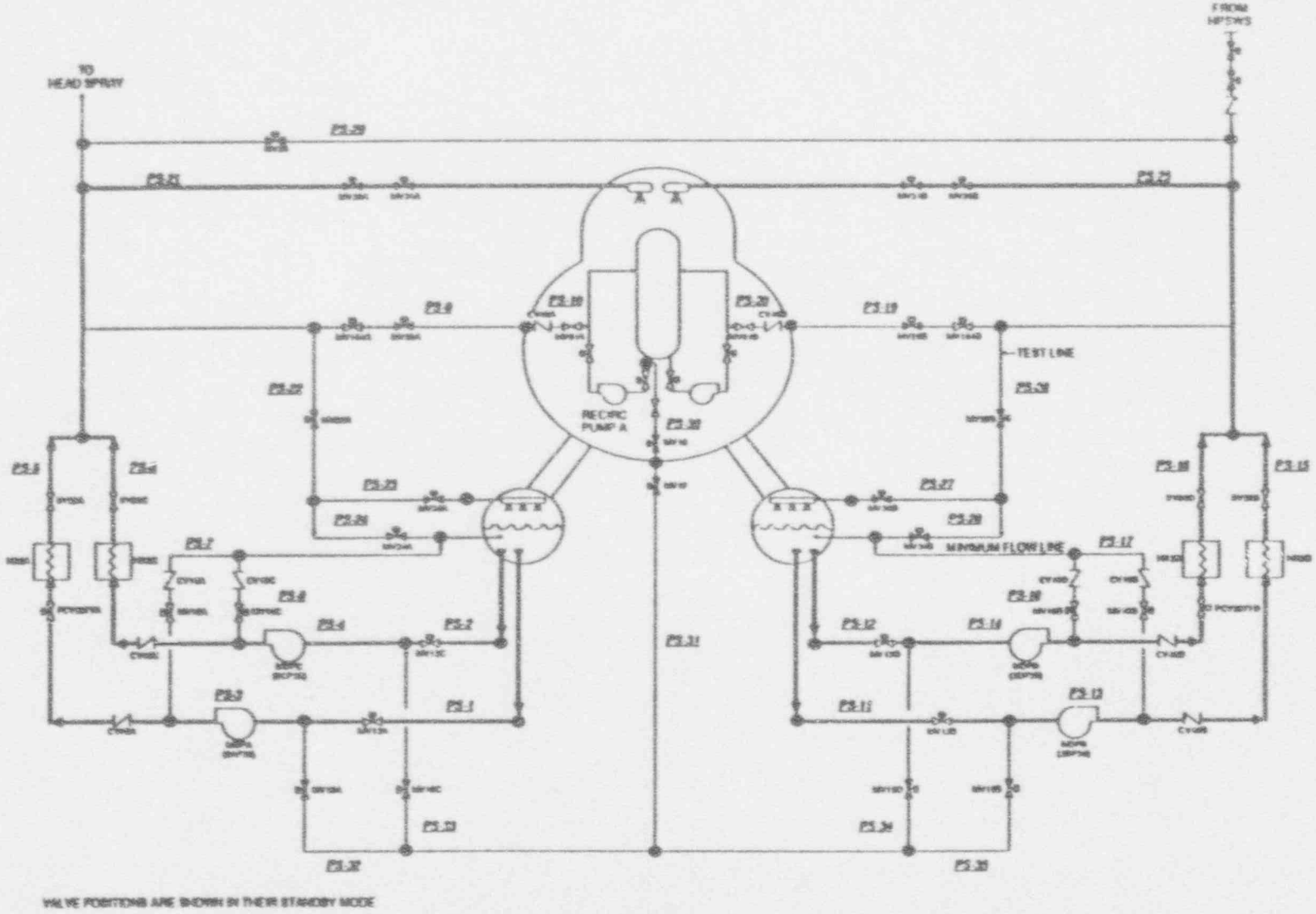

Figure A-9 Containment Spray System Schematic

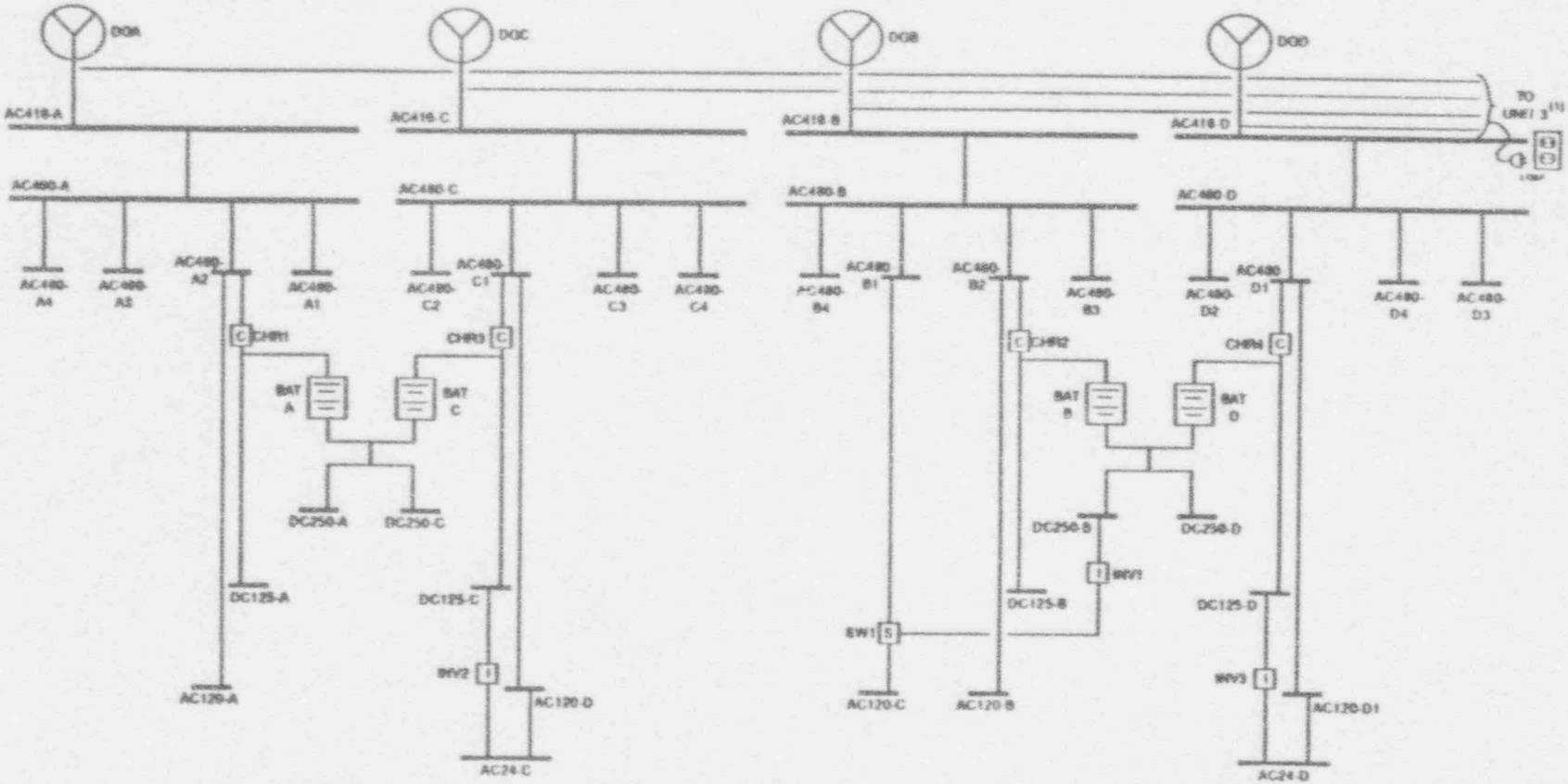

(1) GOES TO UNIT 3 BUSES (DG A, B, C, AND D ARE ARE SHARED BETWEEN UNITS 2 AND 3).

Figure A-10 Electric Power System Schematic

Complete failure of the EPS would cause a station blackout. After a total loss of ac power, dc-driven components could operate until the station batteries are depleted (estimated at about 6 hours based on PECO input).

Each standby diesel generator automatically starts on total loss of offsite power, low reactor water level, or high drywell pressure coincident with low reactor pressure. Two sources of offsite power are available to each 4-kV emergency bus. The failure of one offsite power source results in the automatic transfer to the other offsite source. When the diesel generators are demanded, essential loads are automatically sequenced onto the emergency bus. Nonessential 480 V loads are prevented from being automatically sequenced. Each diesel generator can be started locally, but can be electrically connected to its bus only from the main control room.

Emergency Service Water (ESW) System

The function of the ESW system is to provide a reliable supply of cooling water to selected equipment during a loss of offsite power event.

The ESW system is common to both Units 2 and 3. The system has two full capacity pumps installed in parallel. The normal water supply to the suction of the ESW pumps is from Conowingo pond. The pump discharge consists of two headers with service loops to the diesel-engine coolers and selected equipment coolers. The modeled components supplied with cooling water are the LPCS pumps and pump room coolers, the RHR pumps and pump room coolers, the HPCI pump room cooler, and the RCIC pump room cooler. Valves in the supply headers provide loop isolation. A common discharge header directs effluent to Conowingo pond. A simplified schematic of the ESW system is provided by Figure A-11.

The ESW pumps are vertical, single-stage, turbine types with an 8000 gpm capacity. Their normal discharge head is 96 ft and their shutoff head is 132 ft.

The cooling for all modeled equipment, with the exception of the diesel generator coolers, is normally provided by the Normal Service Water (NSW) system which operates on offsite ac power only.

Should the preferred flow paths described above be unavailable or the bay level preclude normal flow path operation, the ESW system may also be operated in conjunction with the Emergency Heat Sink (EHS) in a closed or open loop fashion. In the closed loop mode, two ESW booster pumps take return water from various coolers, boost it in pressure, and deliver the water to the emergency cooling tower structure. The booster pumps are horizontal split types, with 8000 gpm flow at a head of 100 psig. One Emergency Cooling Water (ECW) pump then takes suction from the cooling tower structure. It delivers water through a motor-operated gate valve to the ESW heat loads. The ECW pump and motor are identical to those of the ESW pumps. The only difference between the ECW pump and the ESW pumps is pump column length. While the booster pumps would normally be used in this mode, they are not required since it has been demonstrated by tests

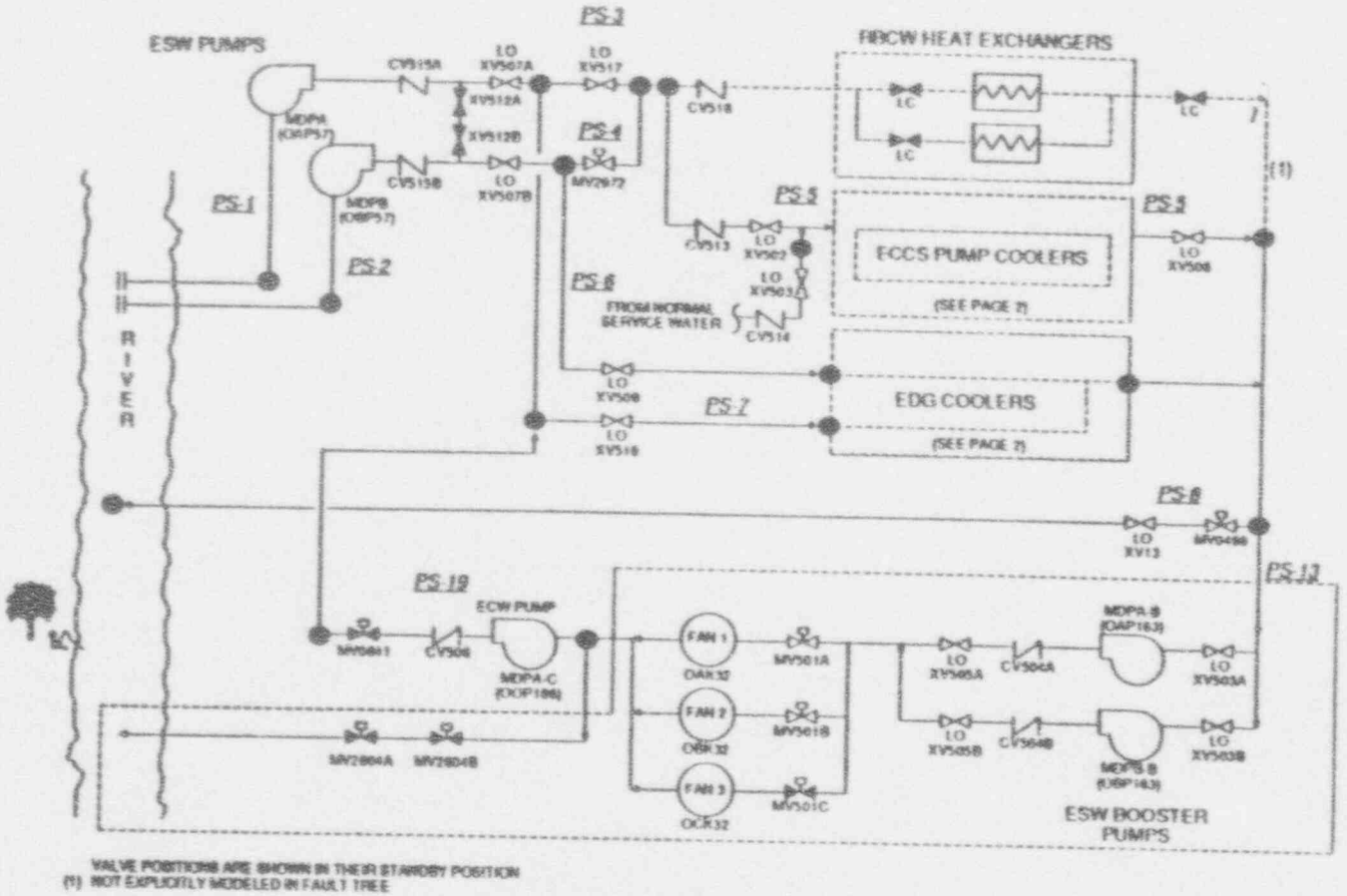

Figure A-11a Emergency Service Water System Schematic (Page 1 of 2)

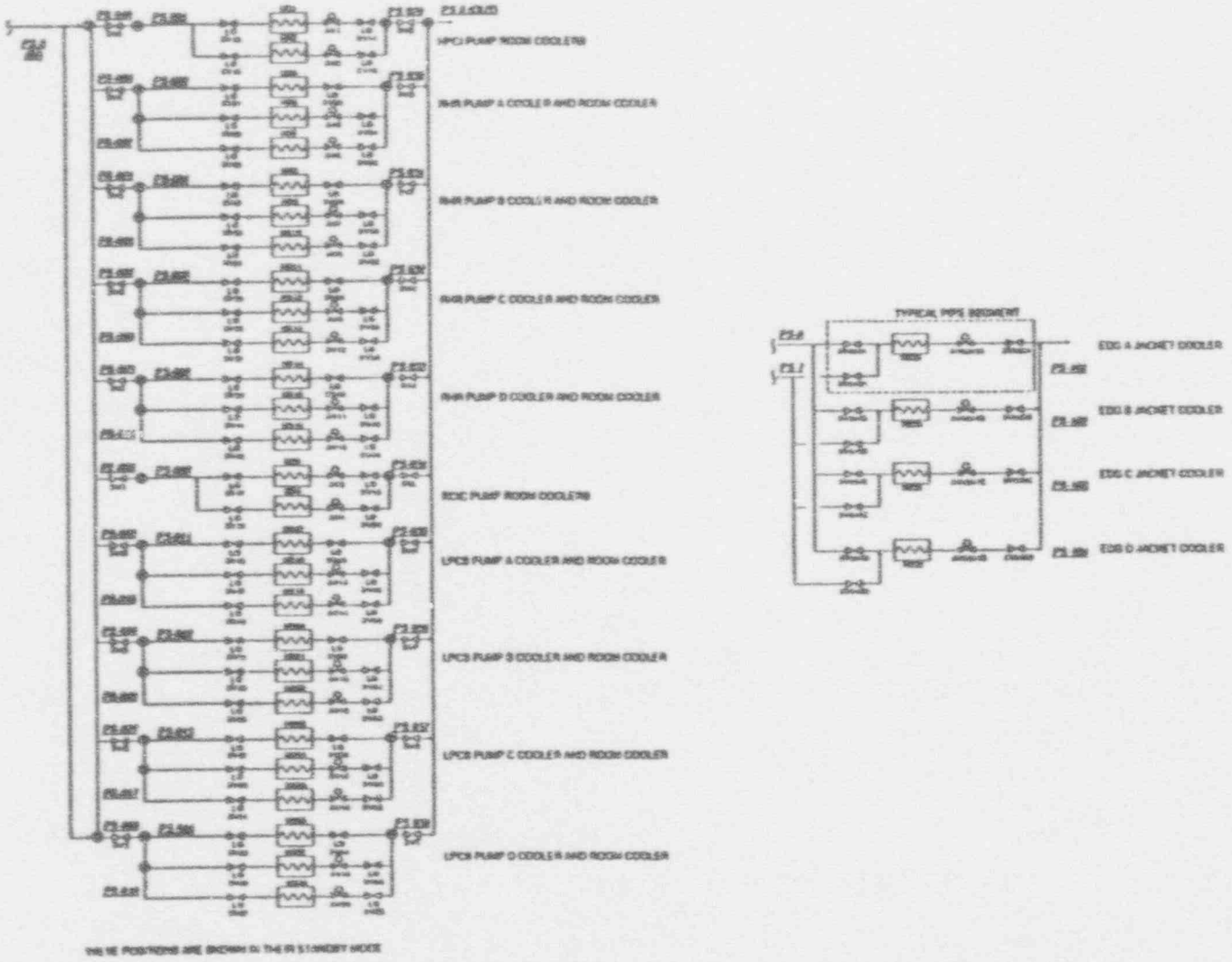

Figure A-11b Emergency Service Water System Schematic (Page 2 or 2)

that booster pump failure will not fail the cooling function of the ESW. In the open loop mode, the ECW pump delivers water from the cooling tower structure, thru the ESW loads, and back to the bay. There is sufficient water supply in the cooling tower structure to last four days; hence the open loop mode is considered a success path.

Upon system automatic initiation, the operator checks discharge pressure for the two primary ESW pumps. If discharge pressure appears normal, the operator turns off one ESW pump and the ECW pump (the ECW pump also has an automatic trip in ~45 seconds if the discharge pressure is adequate). At some later time, if the operating ESW pump trips and the standby ESW pump fails to start, the operator must manually start the ECW pump. In the EHS closed loop mode, cooling tower fans must be manually started. The success criterion for the ESW system is either of the ESW pumps or the ECW pump supplying cooling water to system heat loads.

Most of the ESW system is located in pump rooms external to the reactor and turbine buildings. Any physical impact of accident conditions on the ability of the ESW system to perform its function would be minimal. Room cooling failure is assumed not to fail the ESW pumps, ESW booster pumps, and ECW pump.

Failure of the ESW system would quickly fail operating diesel generators and potentially fail the LPCS pumps and RHR pumps. The HPCI pump and RCIC pump would fail by a loss of their room cooling 10 hours after a loss of the ESW system if other recovery actions were not taken.

Both ESW pumps and the ECW pump start on a diesel start signal or a LOCA signal (low water level/high drywell pressure). If all three pumps start successfully, the operator will shut off one ESW pump and the ECW pump. If the running ESW pump fails, the other ESW pump will receive an auto start signal on low discharge pressure.

High Pressure Service Water (HPSW) System

The HPSW system is designed to supply cooling water from the ultimate heat sink to the RHR system heat exchangers under post-accident conditions and can provide an additional source of water to the reactor vessel through a cross-tie to the RHR injection lines.

The HPSW system consists of four 4500 gpm pumps installed in parallel. The pumps are a vertical multi-stage turbine type with a discharge head of 700 ft. Each pump is sized to the design heat removal capacity of one RHR heat exchanger. Normal water supply to the suction of the pumps is from Conowingo Pond. In the EHS mode of system operation, suction and discharge comes from the emergency cooling towers. The pump discharge is split into two headers with two pumps in each header. The headers are split by a normally closed, motor-operated gate valve. Each header delivers water to two RHR heat exchangers in parallel. The pump discharge head is sufficient to maintain the HPSW system at a higher pressure than the RHR system, thus precluding leakage of radioactivity and permitting operation in conjunction with the emergency cooling towers. As an

injection source to the reactor vessel, the HPSW discharge to RHR injection lines is from the pump B/D header. This connects to the RHR header. A simplified schematic of the HPSW system is provided by Figure A-12.

The operator is required to initiate the HPSW system. To initiate the system in the RHR cooling mode, the operator must start the appropriate HPSW pump and open the appropriate motor operated discharge valve depending on which RHR heat exchanger(s) is being used. These discharge valves are arranged with one valve downstream of each of the four RHR heat exchangers. To inject water into the reactor vessel via the RHR system, the operator starts B and/or D HPSW pumps and opens M-176 and M-174.

The success criteria for the HPSW system in the RHR cooling mode is one of four pumps supplying flow to the appropriate one of four heat exchangers. This is based upon the RHR system success criteria. As a last effort injection source, either B or D pump must supply flow through the cross-tie and corresponding RHR injection line under depressurized conditions in the reactor vessel. Pump A or C can be used with operation of a cross-tie valve.

Most of the HPSW system is located in pump rooms external to the reactor and turbine buildings. Any physical impact of accident conditions on the ability of the HPSW system to perform its functions would be minimal except for the injection valves (MV-174, 176) which are in the reactor building and could be affected by harsh environments there. Room cooling failure is assumed not to fail the HPSW pumps.

Failure of the HPSW system in the RHR cooling mode would fail the RHR cooling function. Failure of the HPSW system in the injection mode would fail one source of water for reactor makeup and containment spray. The HPSW system is initiated manually, either locally or from the main control room.

Emergency Ventilation System (EVS)

The objective of the EVS is to maintain suitable temperatures in equipment rooms to preclude component failures.

The EVS cools the following: (1) standby diesel generator rooms, (2) pump structure service water pump rooms, and (3) pump rooms for the RHR, RCIC, HPCI and LPCS pumps. The pump rooms use small individual fan coolers in each room. A simplified schematic of the rest of the EVS is provided by Figure A-13.

The service water pumps, emergency switchgear, and battery rooms are assumed not to require room cooling. Pump room cooling loss for the RHR, RCIC, HPCI, and LPCS pumps is incorporated into the ESW and individual system models. Therefore, the EVS system model does not include ESW, RHR, RCIC, HPCI, and LPCS pump room cooling.

Each standby diesel generator room is provided with ventilation air supply

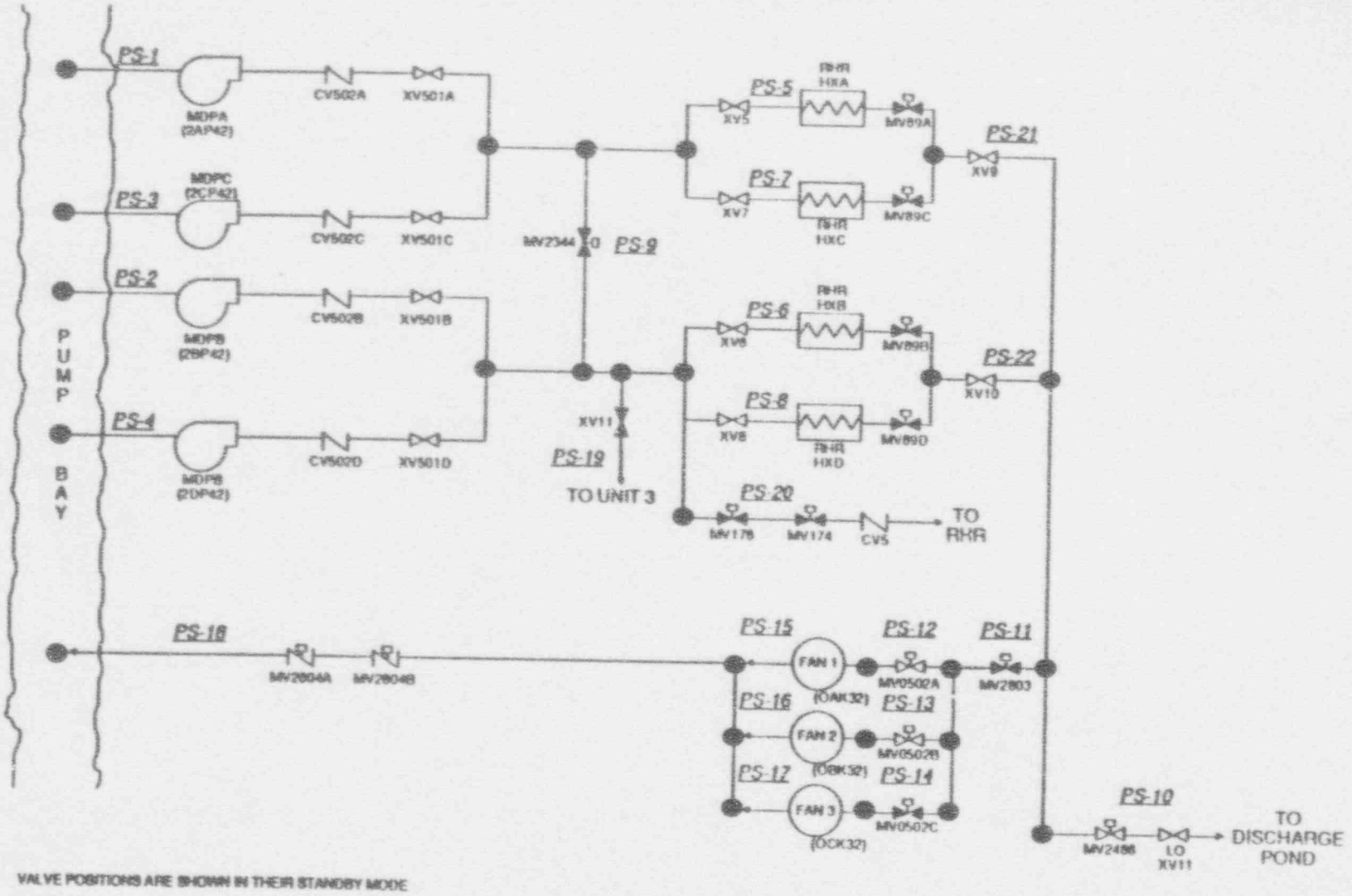

Figure A-12 High Pressure Service Water System Schematic

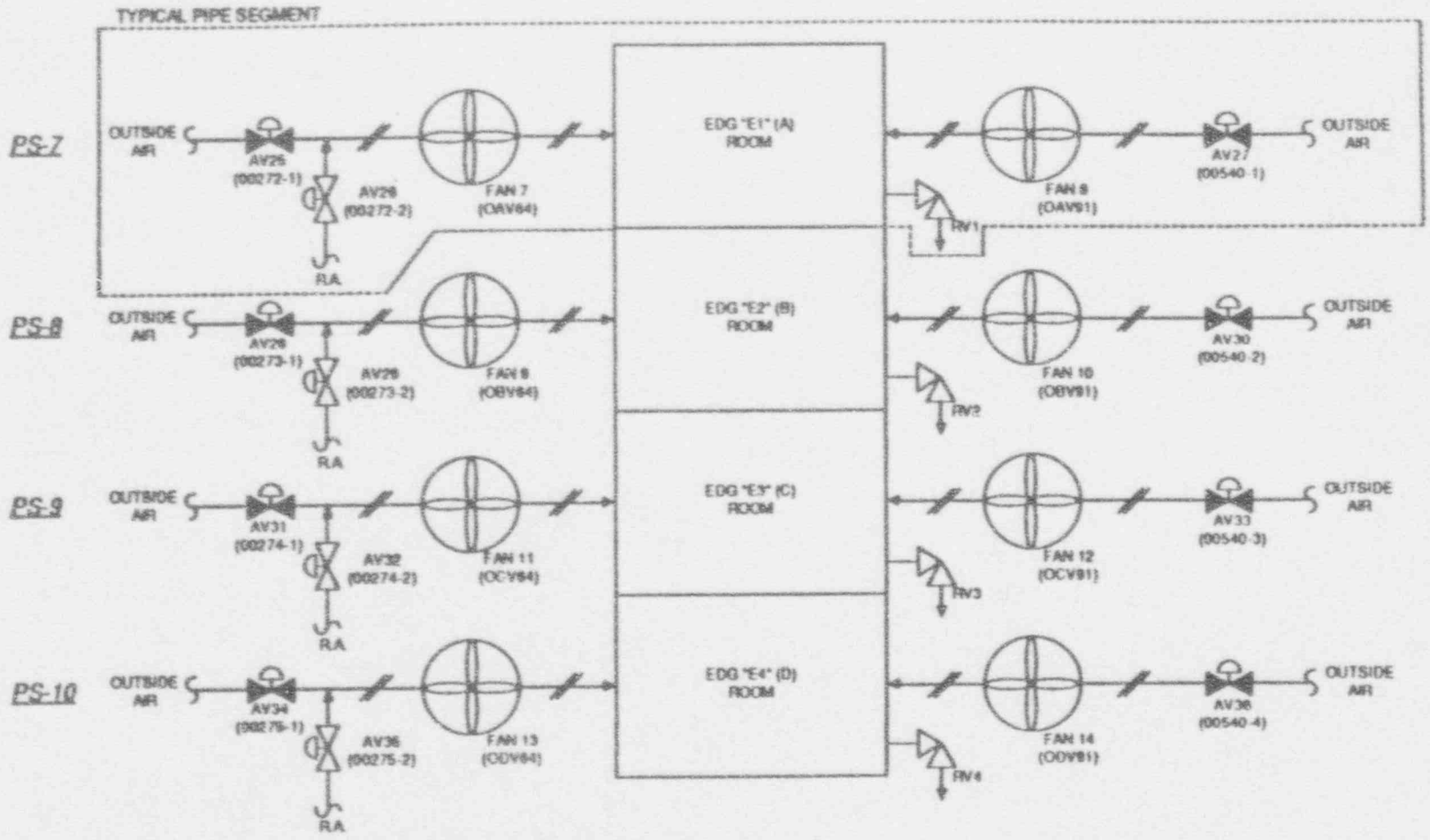

Figure A-13 Emergency Ventilation System Schematic

fans and an exhaust relief damper. Diesel generator room cooling requires operation of one of two supply fans. Any physical impact of accident conditions on the ability of the EVS to perform its function would be minimal. It is assumed that failure of the EVS would fail operating diesel generators in less than 30 minutes.

Diesel Generator Room Fans 7, 9, 11, and 13 outside air supply dampers open on 60°F fan discharge temperature and fail open on a loss of instrument air. Diesel Generator Room Fans 7, 9, 11, and 13 room air supply dampers close on 65°F fan discharge temperature and fail closed on a loss of instrument air. Dampers AV27, AV30, AV33, and AV36 open on Fans 7, 9, 11, and 13, starting signals respectively and fail open on a loss of instrument air. Fans 7, 9, 11, 13 automatically start on a diesel generator actuation signal. Fans 8, 10, 12, and 14 automatically start on an automatic start signal of Fans 7, 9, 11, and 13 respectively. Diesel generator room supply fans trip on a carbon dioxide discharge signal except when a LOCA signal is already present.

Instrument Air System (IAS)

The IAS provides a pneumatic supply to support short-term and long-term operations of safety equipment.

The IAS and Service Air System (SAS) consist of three, in parallel, air compressors supplying a common discharge header via individual air receiver tanks, piping, valves, and instrumentation. A fourth air compressor is tied into the SAS header and is common to both units. Two compressors, one IAS and one SAS, normally supply all compressed air requirements. The other IAS compressor serves in a standby capacity. A simplified schematic of the IAS is provided by Figure A-14. Shown is the tie-in with the Instrument Nitrogen System which is the preferred supply to the MSIVs and ADS/SRVs. In addition to these compressors, the IAS is constantly backed up by two diesel compressors (not shown), and can be served by the Unit 3 IAS/SAS.

Each of the three parallel compressors is a vertical, single-stage, double-acting, non-lubricated, reciprocating compressor rated at 377 SCFM at 100 psig. Each has an aftercooler, moisture separator, and air receiver tank.

The standby SAS compressor consists of a non-lubricated compressor, aftercooler, moisture separator, and two receivers. This compressor is rated at 400 scfm at 100 psig.

The IAS supplies clean, dry, oil-free air to EHV and ESW system air valves, the CRD control system, and containment venting air valves and is a backup to the Instrument Nitrogen System. When offsite power is lost, the air compressors trip. The operator is required to manually restart the air compressors when power is restored. The success criterion for the IAS is any one of the compressors supplying air to system pneumatic loads.

Any physical impact of accident conditions on the ability of the IAS to

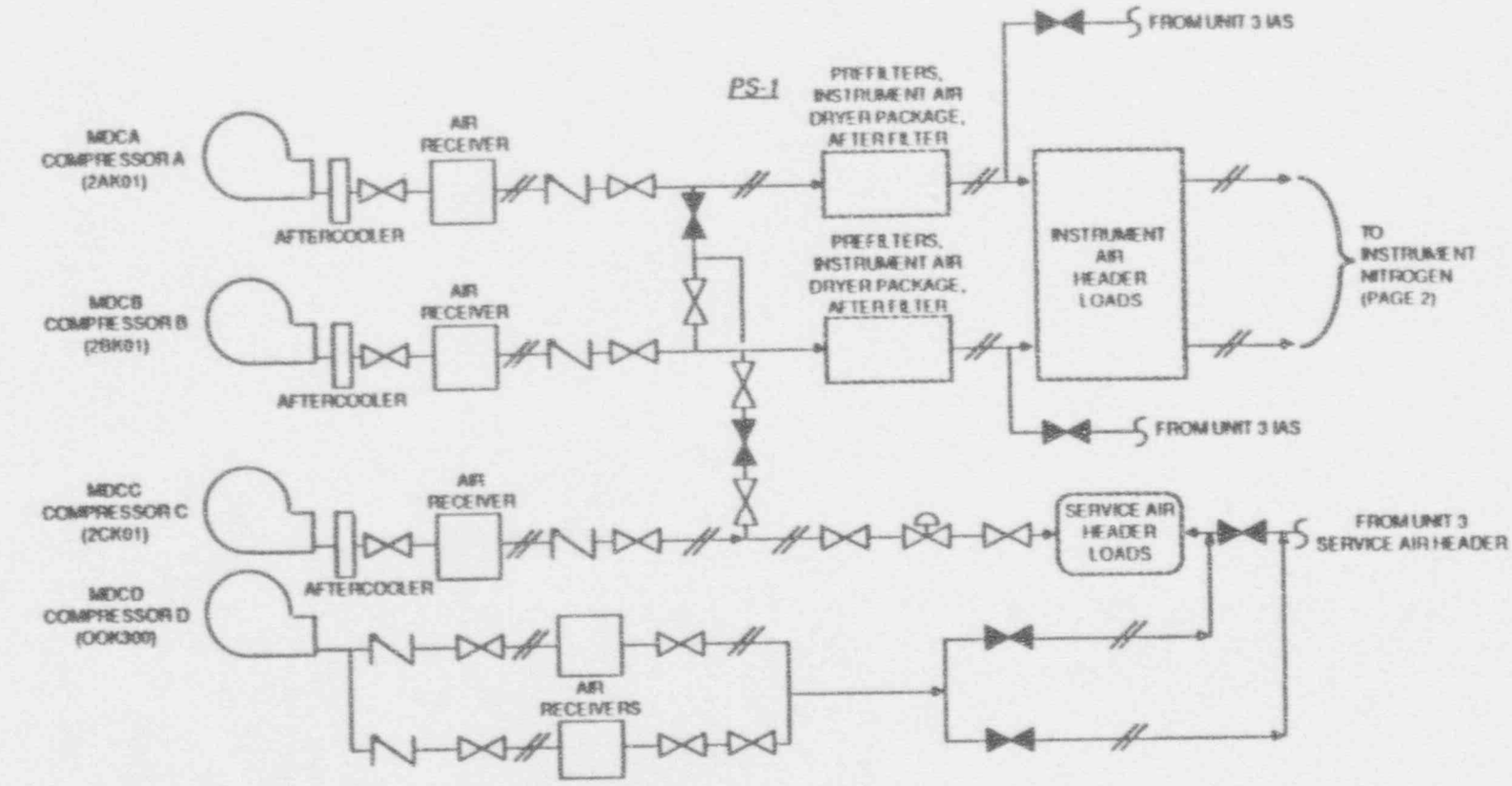

Figure A-14a Instrument Air/Nitrogen System Schematic (Page 1 of 2)

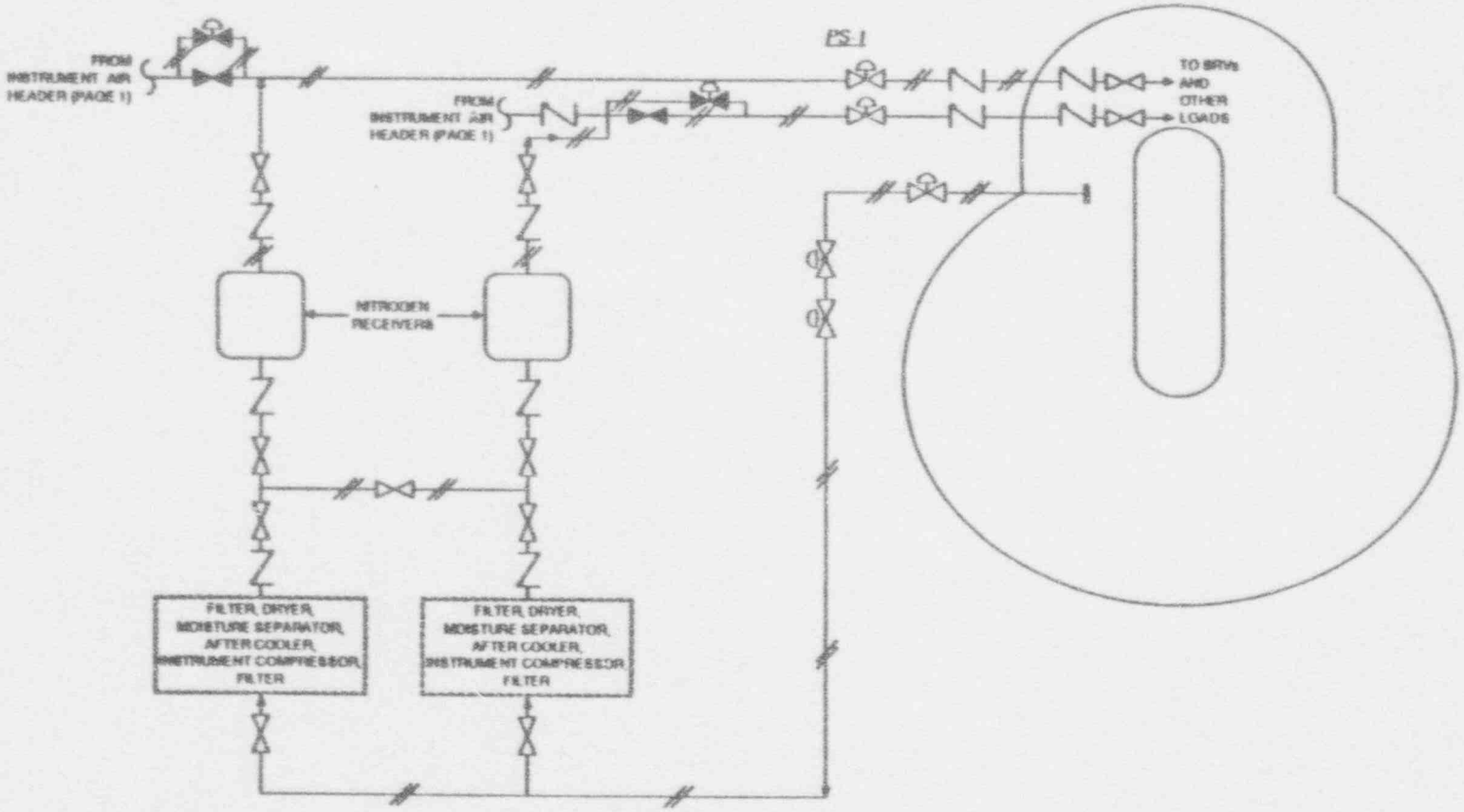

Figure A-14b Instrument Air/Nitrogen System Schematic (Page 2 of 2)

perform its functions would be minimal. Room cooling failure is assumed not to fail the IAS and SAS compressors. Even if this were to occur, the diesel compressors or Unit 3 compressors could serve the necessary loads.

Failure of the IAS does not directly fail any safety systems because (1) accumulators are on the MSIVs and ADS valves, (2) instrument nitrogen is the preferred source to the MSIVs and ADS valves, and (3) other safety systems "fail-safe" on loss of air or have dedicated air bottles.

Condensate System (CDS)

The function of the CDS system is to take condensate from the main condenser and deliver it to the reactor at an elevated temperature and pressure.

The CDS system consists of the condenser hotwell, three condensate pumps, feedwater heaters and associated piping, valves, and controls. The condenser hotwell has a working capacity of approximately 100,000 gallons. The condensate pumps provide the required head to overcome the flow and static resistance of the condensate system, and provide excess over the suction pressure requirements of the feedwater pumps. The reactor vessel must be depressurized to approximately 600 psig in order to use condensate as an injection source without the use of the feedwater pumps. Injection to the reactor vessel is via a feedwater line. The CDS pumps have a 10,870 gpm rated flow head. A simplified schematic of the CDS system is provided by Figure A-15.

The CDS system is normally running. The success criteria for the CDS system is removal of decay heat (when the reactor has tripped). This can be sufficiently accomplished with only one pump train operational. Virtually all of the CDS system is located in the turbine building.

Primary Containment Venting (PCV) System

When torus and containment sprays have failed to reduce primary containment pressure, the PCV is used to prevent a primary containment pressure limit from being exceeded.

The preferred primary containment vent paths include: (1) 2-in torus vent to the Standby Gas Treatment System (SGTS), (2) 6-in Integrated Leak Rate Test (ILRT) line from the torus, (3) 18-in torus vent path, (4) 18-in torus supply path, (5) 2-in drywell vent to the SGTS, (6) two 3-in drywell sump drain lines, (7) 6-in ILRT line from the drywell, (8) 18-in drywell vent path, and (9) 18-in drywell supply path. A simplified schematic of the PCV is provided by Figure A-16.

For decay heat loads alone it is expected that the drywell pressure rise will be relatively slow. PCV success in this case is the 6-in vent path (or larger) being operational.

Current venting procedure requires a vent path to be established if containment pressure rises to 100 psig (PECO is considering changing this

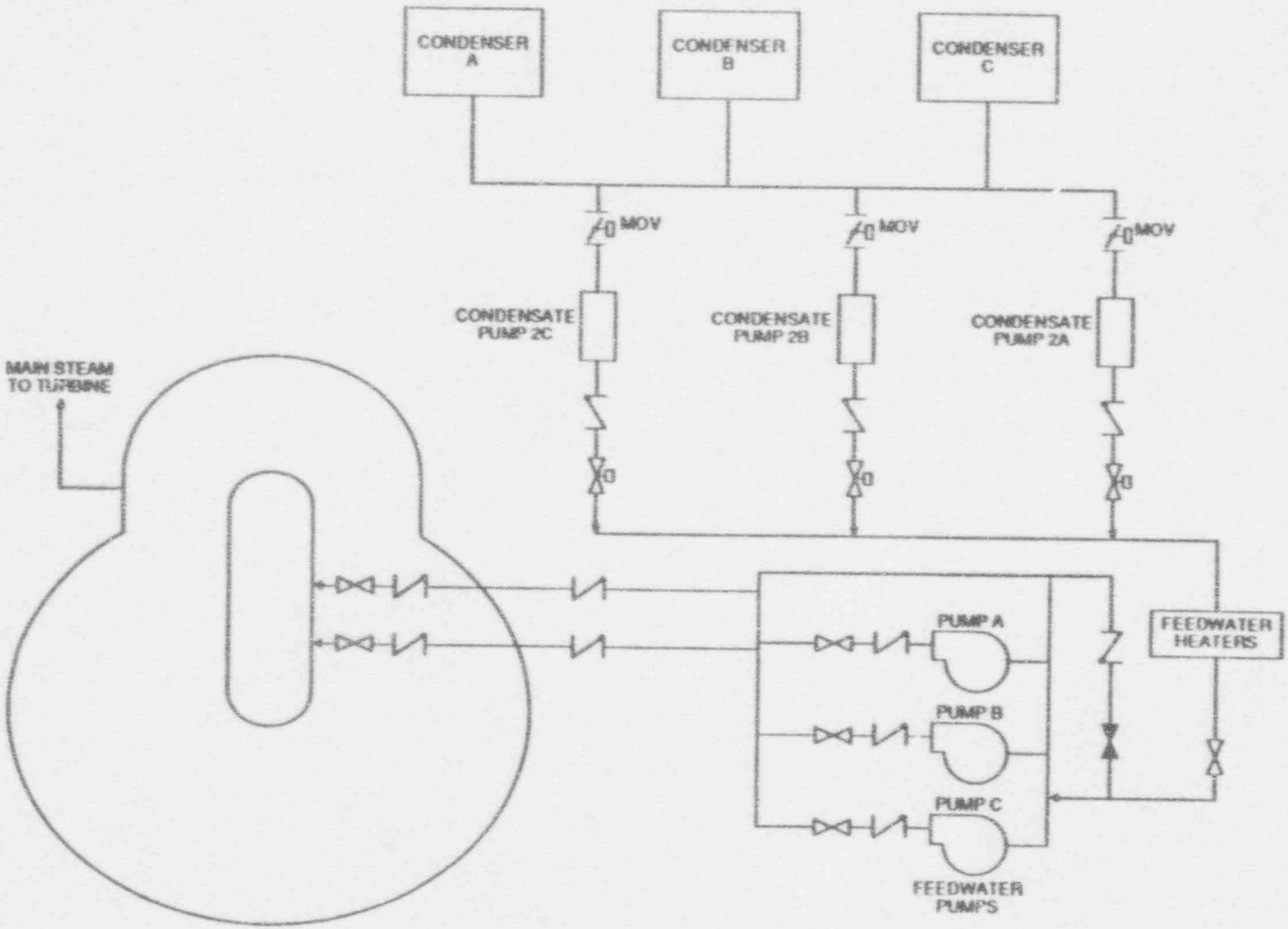

Figure A-15 Condensate System Schematic

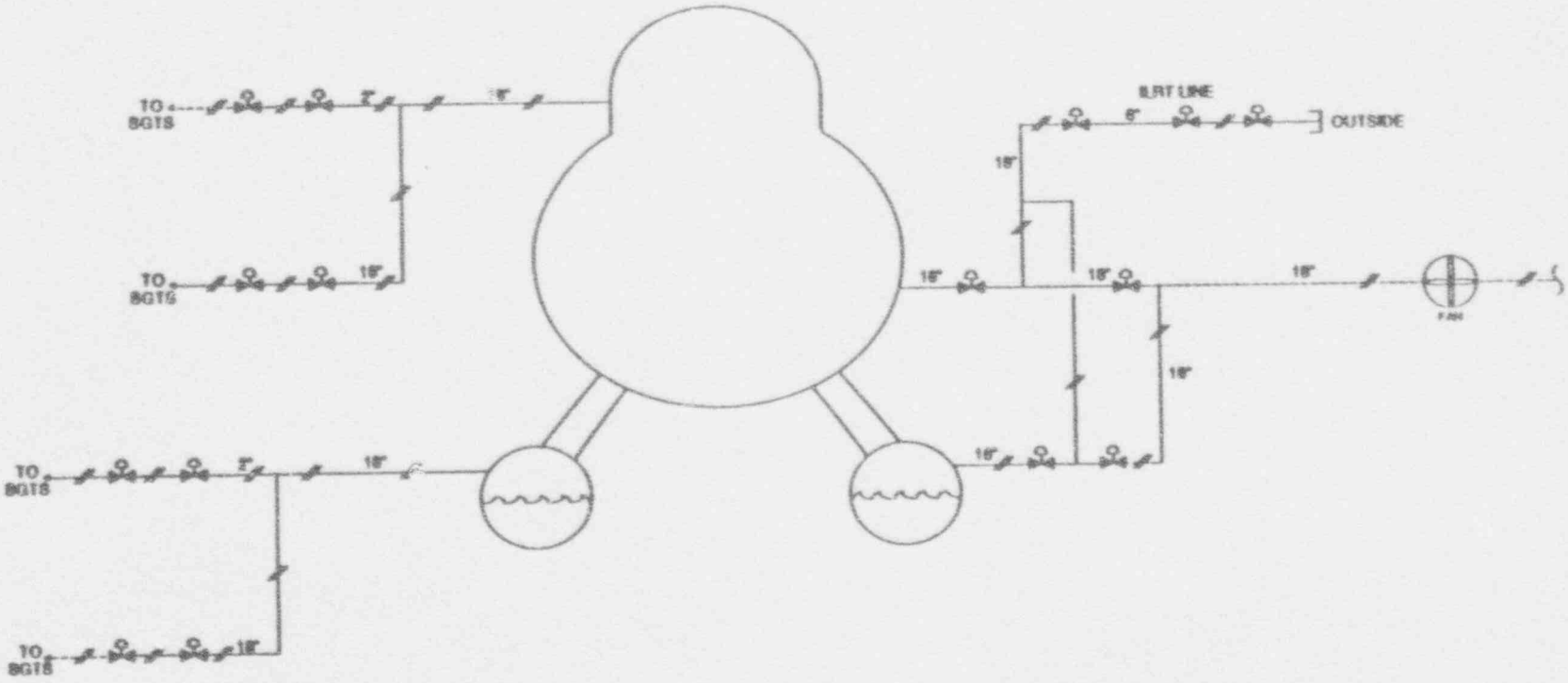

Figure A-16 Primary Containment Venting System Schemati:

to 60 psig). In the case of an ATWS, or if it can be inferred that the suppression pool is being bypassed, the operator is required to directly establish the 18-in vent paths.

Reactor Building Cooling Water (RBCW) System

The function of the RBCW system is to provide a means of cooling auxiliary plant equipment which is located primarily in the reactor building (e.g. recirculation pumps, sump coolers, radwaste, etc.). The RBCW system is a backup for cooling CRD pumps and IAS compressors and aftercoolers should the TBCW be lost.

The RBCW system is a closed loop system consisting of two full-capacity pumps, two full-capacity heat exchangers, one head tank, one chemical feed tank and associated piping, valves, and controls. The RBCW system is designed for an operating pressure of 140 psig. A simplified schematic of the RBCW system is provided by Figure A-17.

The operator uses RBCW to cool certain critical loads if the TBCW system is lost. The RBCW system usually has one pump continuously operating. Control and instrumentation is designed for remote system startup from the main control room.

The success criteria for the RBCW system is one pump and one heat exchanger train operating, providing sufficient cooling to the loads. The cooling water pumps and heat exchangers are located in the reactor building auxiliary bay. The head tank is located on the reactor building refueling floor. The specific RBCW loads are distributed throughout different areas of the plant.

Turbine Building Cooling Water (TBCW) System

The function of the TBCW system is to provide cooling water to auxiliary plant equipment associated with the power conversion system.

The TBCW system is a closed loop system consisting of two full-capacity pumps, two full-capacity heat exchangers, one head tank, one chemical fuel tank and associated piping, valves and controls. A simplified schematic of the TBCW system is provided by Figure A-18.

The TBCW system is normally running. One pump is required to supply cooling to all TBCW loads. The success criteria for TBCW is one of two pumps and either of the two heat exchangers operating. This will provide sufficient cooling to the TBCW loads.

The majority of the TCW system including the cooling water pumps, heat exchangers and associated piping, valves and controls are located on the turbine building ground floor. The specific TBCW loads are distributed throughout different areas of the plant.

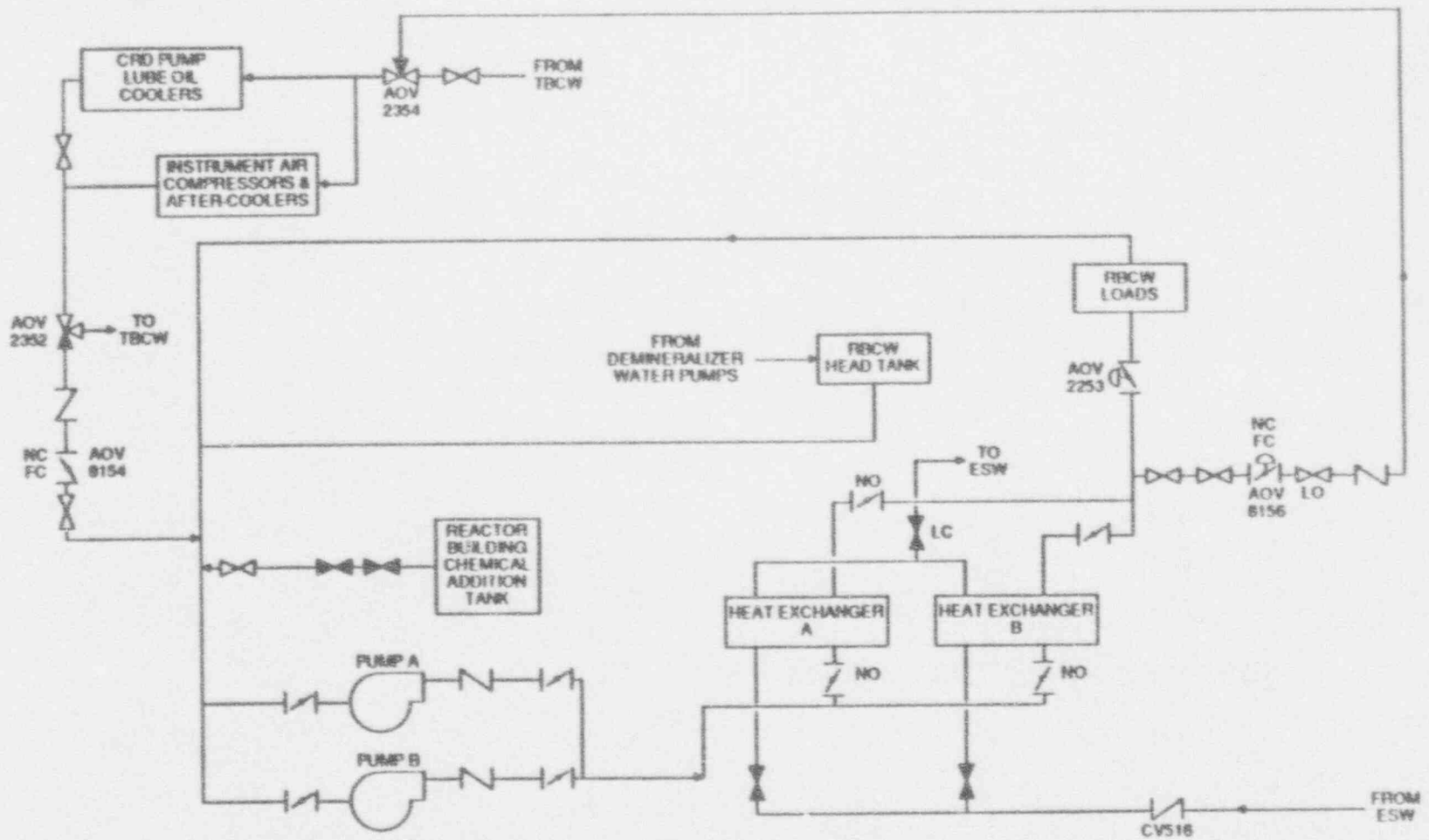

Figure A-17 Reactor Building Cooling Water System Schematic

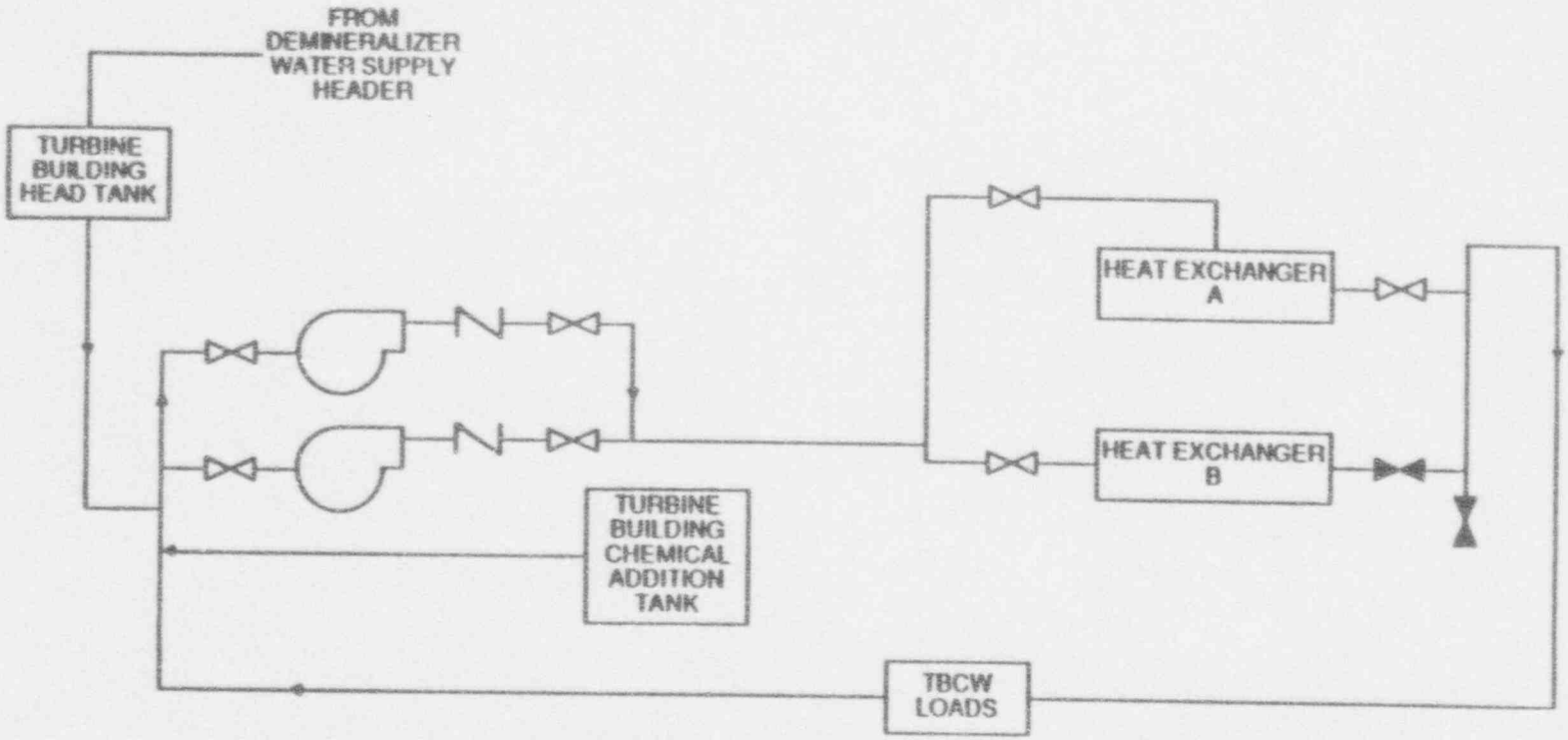

Figure A-18 Turbine Building Cooling Water System Schematic

A.2 HAZARD CURVES USED FOR PEACH BOTTOM

The hazard curves used in the NUREG-1150 PRAs were provided by the USNRC-sponsored Eastern U.S. Seismic Hazard Characterization Program [A-3]. From this program one can obtain a median hazard curve and an estimate of the distribution about the median curve. This is shown in Figure A-19 where the mean, median and the 15th percentile and 85th percentiles are shown. The distribution about the median is nearly log normal so for the NUREG-1150 analyses, a log normal distribution was fit using the median and mean hazard curves.

A second set of hazard curves was obtained from the industry-sponsored Electric Power Research Institute's Seismic Hazard Methodology Development program for the Eastern United States [A-4]. The corresponding curves are shown in Figure A-20. These were also fit with a lognormal model.

A.3 RESPONSE CALCULATIONS

This chapter will describe and summarize:

- The site and earthquake characteristics that provide the starting point in the best-estimate soil-structure analysis of the Peach Bottom structures.
- The probabilistic response analysis of the plant structures both with and without degraded shear wall stiffness, and
- The in-structure responses that define the response of components identified on the Boolean expressions for the LOCA and transient accident sequences analyzed.

A.3.1 Site Description

The Peach Bottom Nuclear Power Plant is located in Delta, Pennsylvania approximately 40 miles north of Baltimore, Maryland. The site is characterized predominantly by a Schist bedrock with shear wave velocities ranging from 8,000 to 12,000 ft/sec. The general layout of the plant is shown in Figure A-21. At the Peach Bottom Power Station the specific safety related components are housed in the Reactor/Containment Building, the Radwaste-Turbine Building, the Circulating Water Pump House, the Diesel Generator Building, and the Emergency Cooling Tower structure denoted as RB, RWTB, CWP, DG, and ECT respectively.

A.3.2 Earthquake Definition

The initial step in performing a probabilistic response analysis involves two inter-related tasks, whose objectives are to:

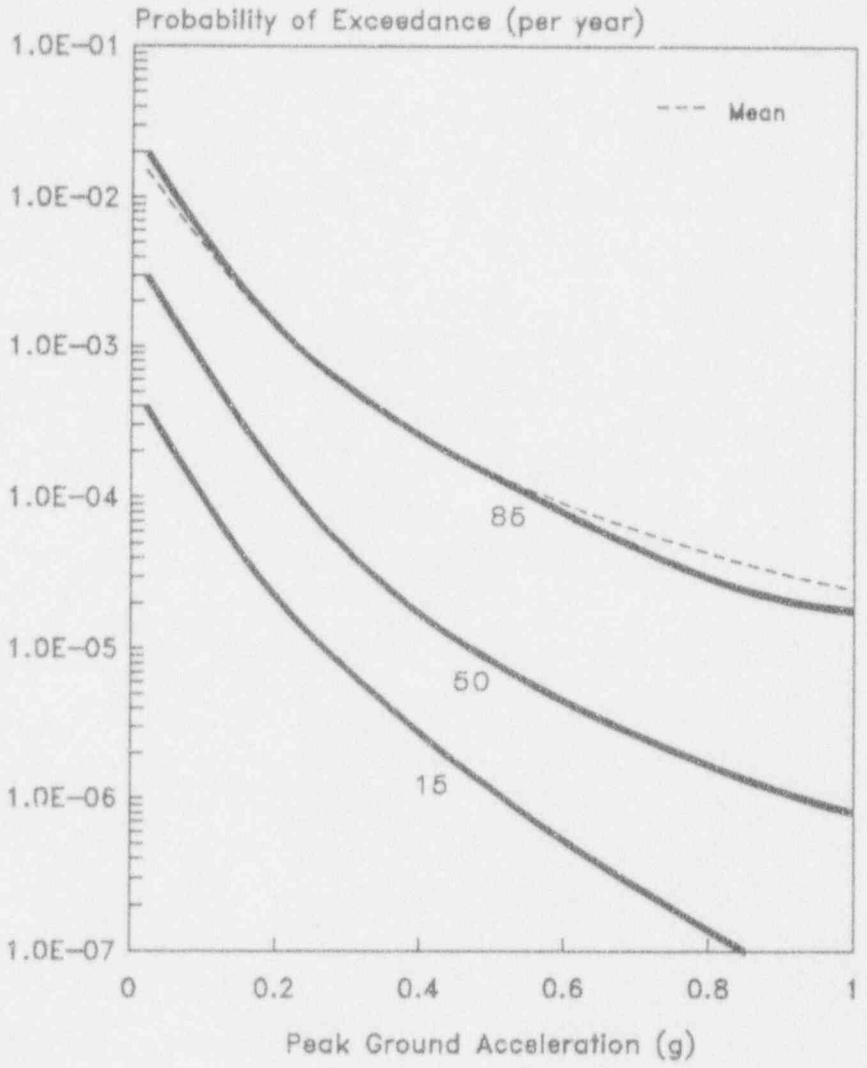

Figure A-19 Peach Bottom LLNL Hazard Curves: Mean, Median, 85th and 15th Percentile Curves

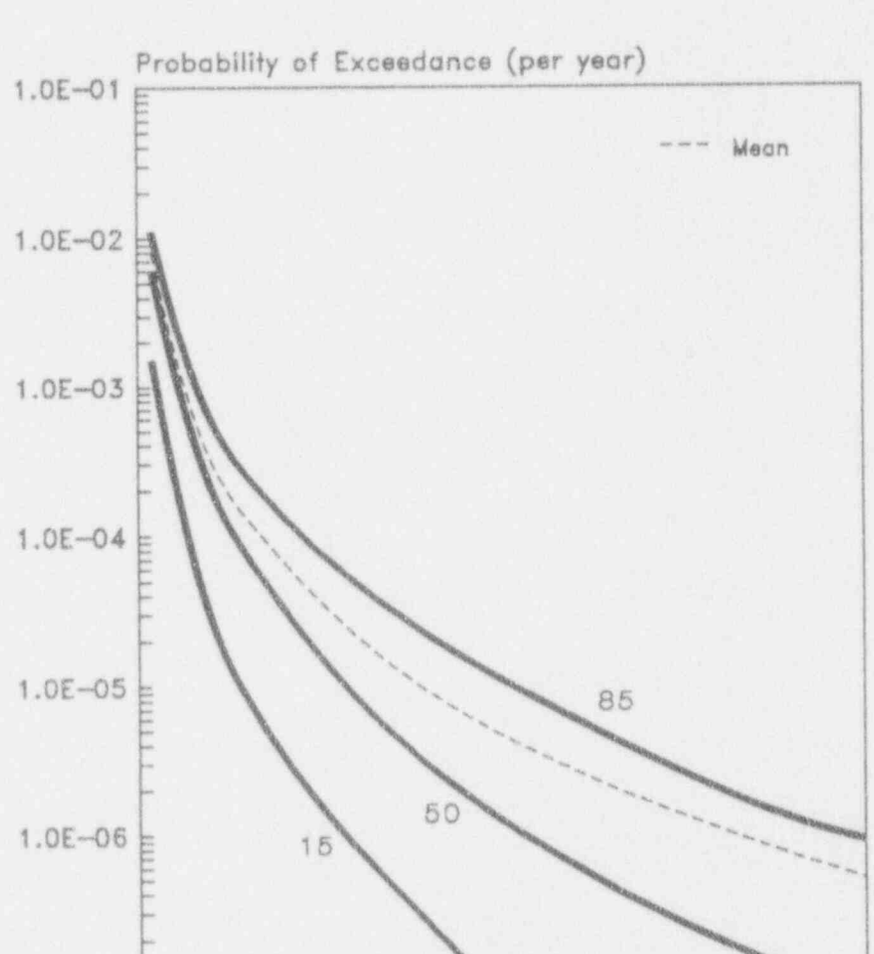

Figure A-20 Peach Bottom EPRI Hazard Curves: Mean, Median, 85th and 15th Percentile Curves

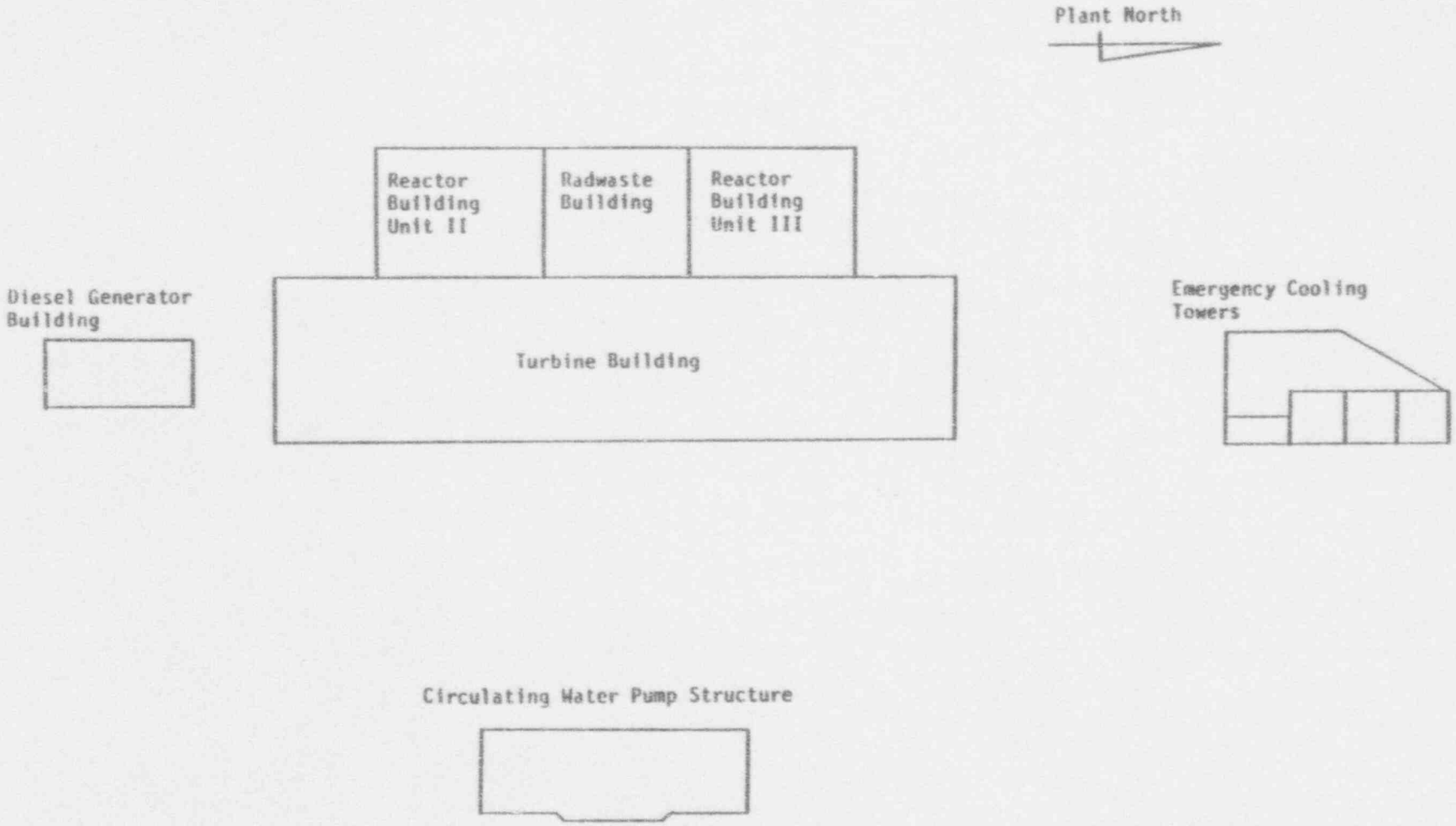

Figure A-21 Peach Bottom Power Station General Arrangement

- define soil properties as a function of excitation level over the range of earthquakes to be considered, ie., as defined by the seismic hazard curve.

- define the input motion for the determination of seismic responses of structures and components for this range of earthquakes.

Due to the rock nature of the Peach Bottom site, all structural analysis were performed using fixed base structural dynamic models for all five of the important structures (RB, RWTB, CWP, DG, and ECT). Therefore, no soil properties such as shear strength or damping will be accounted for in the dynamic analysis of the structures.

Six seismic excitation levels were considered depending on the particular structure being analyzed and were defined by their peak ground acceleration (PGA) in the horizontal direction. A single set of ten earthquakes were chosen and scaled corresponding to the percentage of the safe shutdown earthquake (SSE) desired. One SSE corresponds to a PGA of 0.12 g's. Multiples of 1, 2, 3, 6 and 7 times the SSE were used for the DG, RWTB, and CWP structures, whereas 1, 3, 5, and 7 times the SSE were used for the RB and ECT structures. Ten earthquake acceleration time histories were considered for each component direction of the 3-D models. Each time history is a recorded motion of an actual earthquake from similar rock sites. A total of five earthquakes which are listed in Table A-1 were chosen as the first set of five input motions. For the purpose of analysis, five additional earthquakes were created by rotation of the two horizontal components for those listed in Table A-1. The median acceleration response spectrum of the ten horizontal components is shown in Figure A-22 at 5% damping for comparison to median responses of similar rock sites (from Ref. [A-5]). The comparison shows frequency content and amplification for the median response of the ten horizontal components adequately represent expected motion at the Peach Bottom Site.

A.3.3 Structural Models

Five independent building models were generated: the Reactor/Containment Building, the Radwaste-Turbine Building, the Circulating Water Pump House, the Diesel Generator Building, and the Emergency Cooling Tower structure. These were analyzed in order to determine the final degraded models for each applicable SSE level and to determine maximum probabilistic structure responses of both original and degraded models.

The reduction in stiffnesses for the structural models' beam elements was performed in such a way that only the shear deformation contribution to each element stiffness was reduced, and the bending deformation contribution was unchanged. That is, the term GA_s was reduced (where G is the shear modulus and A_s is the shear area) but EI (where E is Young's Modulus and I is the cross-section area moment of inertia) was unchanged.

The Reactor Building houses the NSSS (nuclear steam supply system), primary containment, and auxiliary systems. It is founded on rock at

Table A-1

Free-Field Acceleration Time History for
Probabilistic Response Analysis

Site	Date
Pacoima Dam	2-9-71
Castaic	2-9-71
Temblor	6-27-66
Helena	10-31-35
Taft (Lincoln School Tunnel)	7-21-52

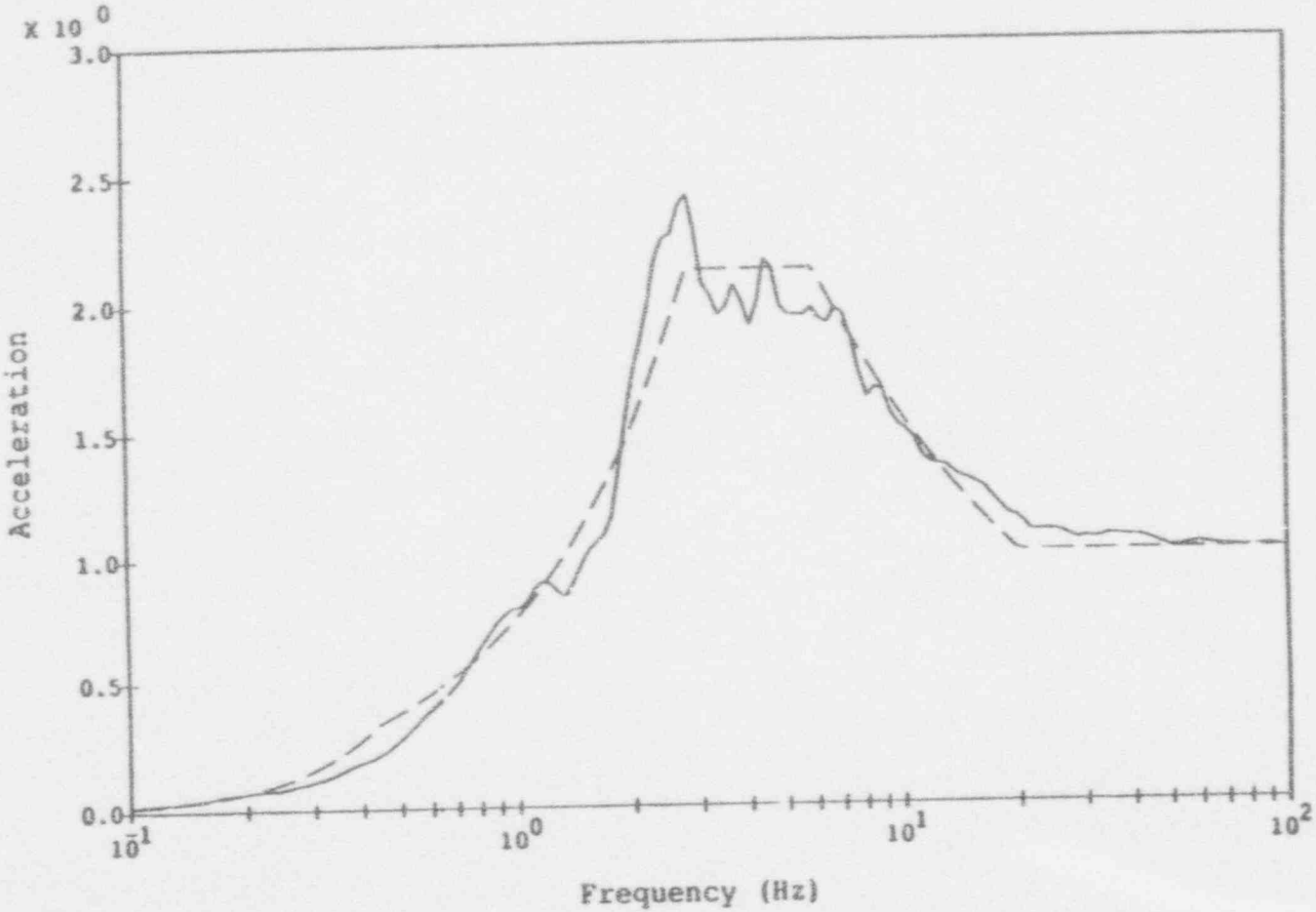

Legend:

Median of 10 Comp. ——————

Rock 50% — — — — —

Notes:

All spectra calculated at 5% damping

Acceleration in units of g

Figure A-22 Peach Bottom Median Free-Field Input Motion Compared to Median Rock Spectra from WASH-1255

elevation 91'-6". It is isolated from adjacent structures by a 0.5 inch gaps. The seismic load-resisting system consists of reinforced concrete walls and slabs up to the refueling floor at elevation 234'. Above this floor is a superstructure of steel framing, siding, and roof decking. The concrete shield wall that encloses the drywell is integral with the reactor building structure. The reactor pedestal and sacrificial shield wall are founded on concrete fill within the drywell. The stabilizer truss connected to the top of the sacrificial shield wall provides lateral support for the internal structures. The structural model of the Reactor/Containment Building consists of two single sticks of collinear equivalent beam elements and lumped floor masses stemming from the same foundation. One stick models containment while the other represents the reactor building internals. Fifteen modes were calculated up to 26 Hz for this simplified stick model which is shown schematically in Figure A-23.

The Radwaste Building and immediately adjacent portion of the Turbine Building were constructed integrally with each other and were thus considered a single structure. The radwaste portion is located between the Reactor Buildings for Units 2 and 3 and houses various components of the radwaste system, the standby gas treatment system, and associated equipment. The turbine portion houses the control room, cable spreading room, switchgear rooms, and battery rooms. The seismic load-resisting system of this building consists of reinforced concrete shear walls and slabs. It is separated from adjacent structures by 0.5 inch gaps. The Radwaste-Turbine Building model consisted of four vertical beam elements located at the center of rigidity connecting each of the five main floor elevations. Lumped floor masses were then rigidly linked to the beam elements at each of the floor elevations. Ten modes were calculated up to 33 Hz for this simplified stick model which is shown schematically in Figure A-24.

The Circulating Water Pump structure houses the Seismic Class I emergency and high-pressure service water systems, and the circulating water systems. The seismic load-resisting system of this building consists of reinforced concrete shear walls and slabs. The Circulating Water Pump House was modeled with six vertical beam elements located at the center of rigidity connecting each of the five main floor elevations. Lumped floor masses were rigidly linked to the beam elements at each of the floor elevations. Fifteen modes were calculated up to 71 Hz for this simplified stick model which is shown schematically in Figure A-25.

The Diesel Generator Building houses the emergency diesel generators and associated components. The seismic load-resisting system of this building consists of reinforced concrete shear walls and slabs. The Diesel Generator Building was modeled with two vertical beam elements located at the center of rigidity between each of the three main floor elevations. Lumped floor masses were rigidly linked to the beam elements at each of the floor elevations. Seven modes were calculated up to 89 Hz for this simplified stick model which is shown schematically in Figure A-26.

The Emergency Cooling Tower structure contains the fans and associated components for the emergency heat sink. The water reservoir below

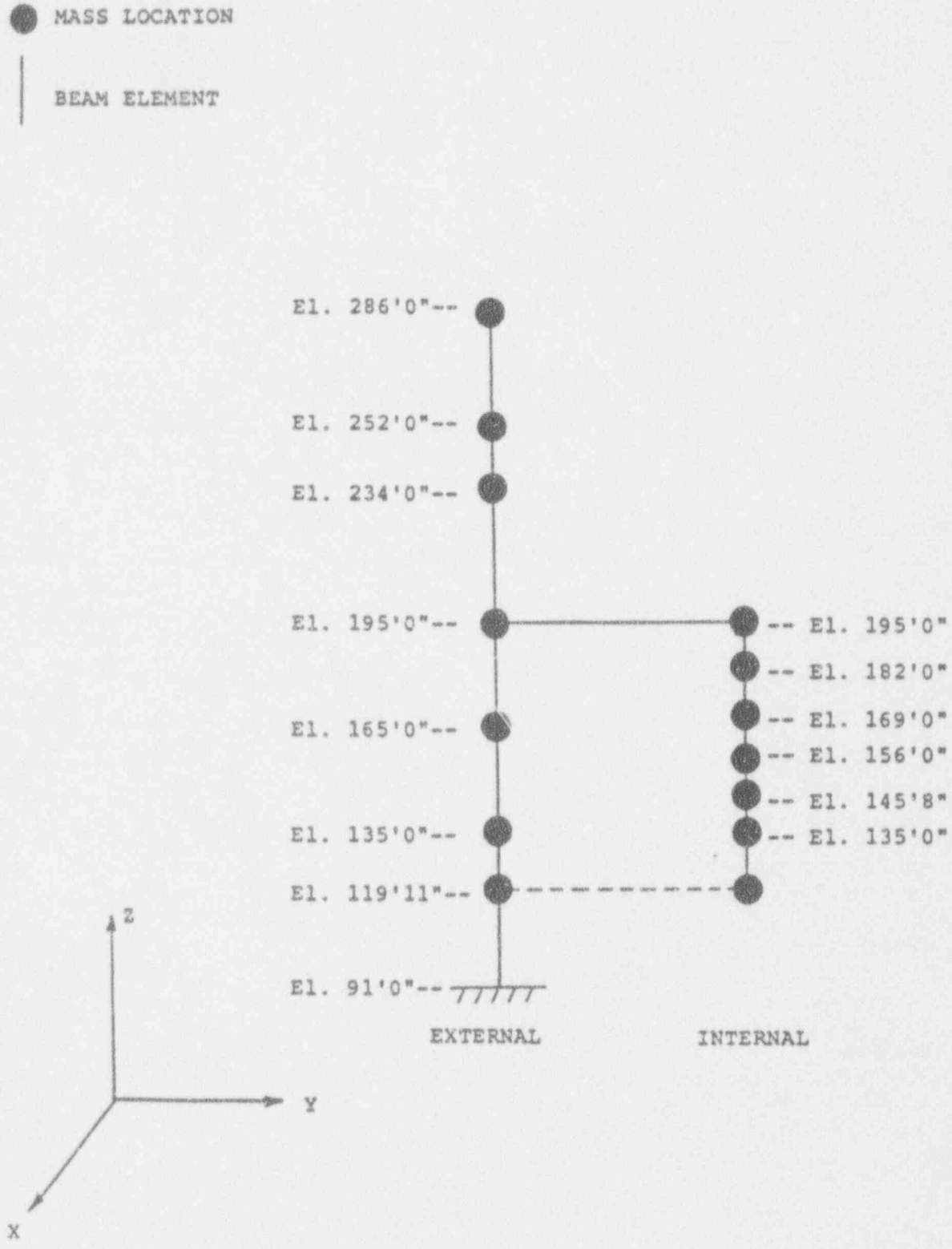

Figure A-23 Peach Bottom Reactor Building Structural Model

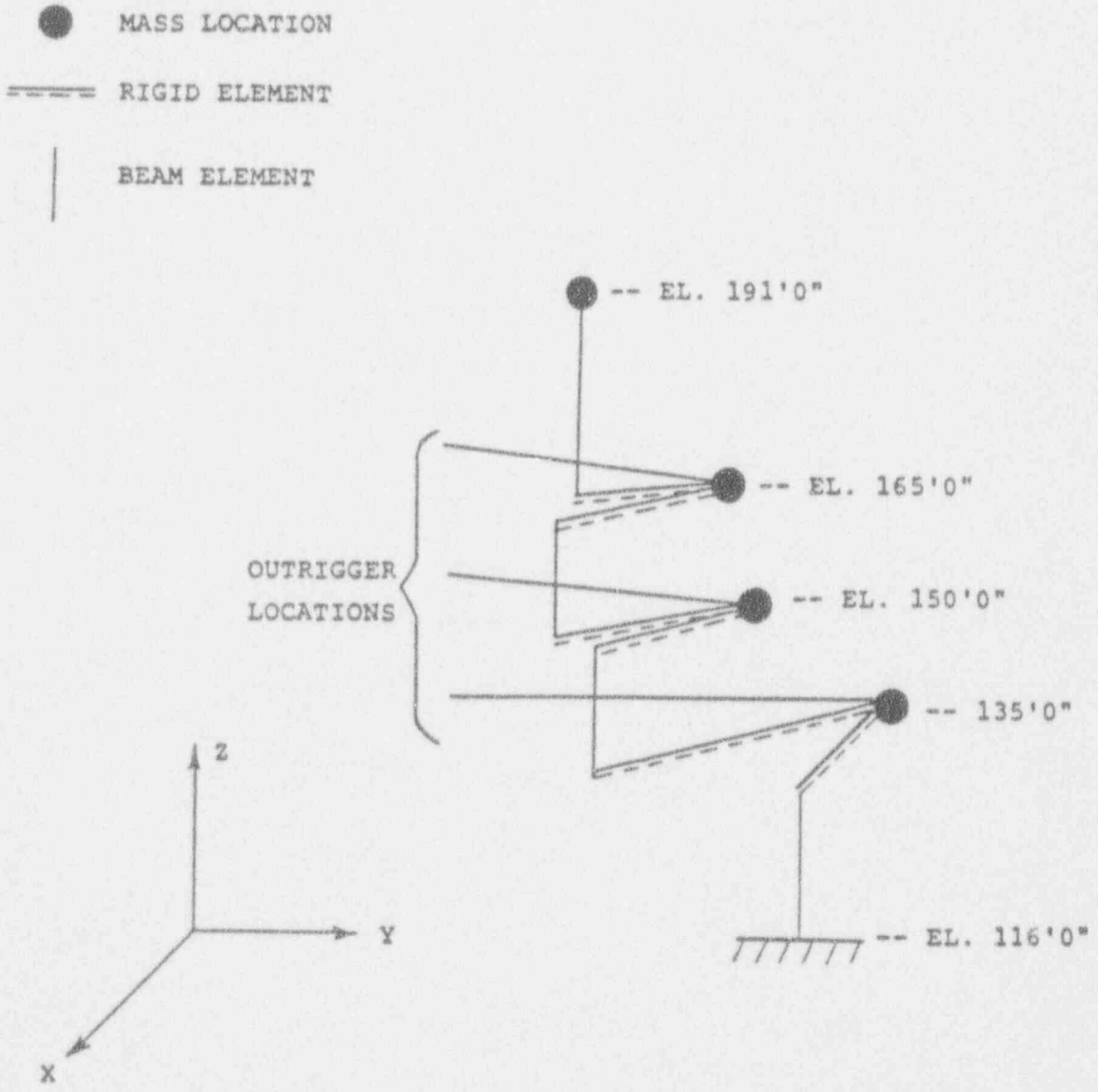

Figure A-24 Peach Bottom Radwaste/Turbine Building Structural Model

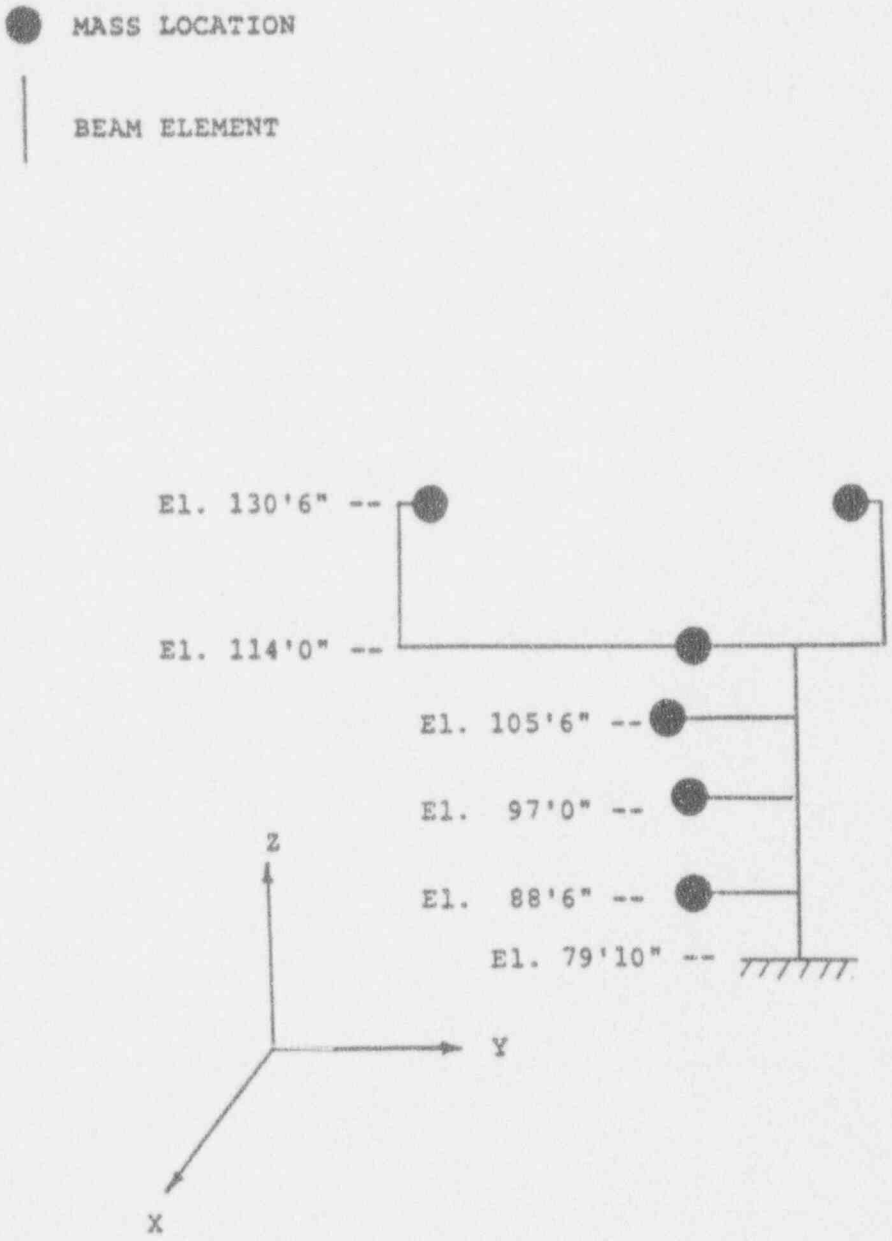

Figure A-25 Peach Bottom Circulating Water Pump Building Structural Model

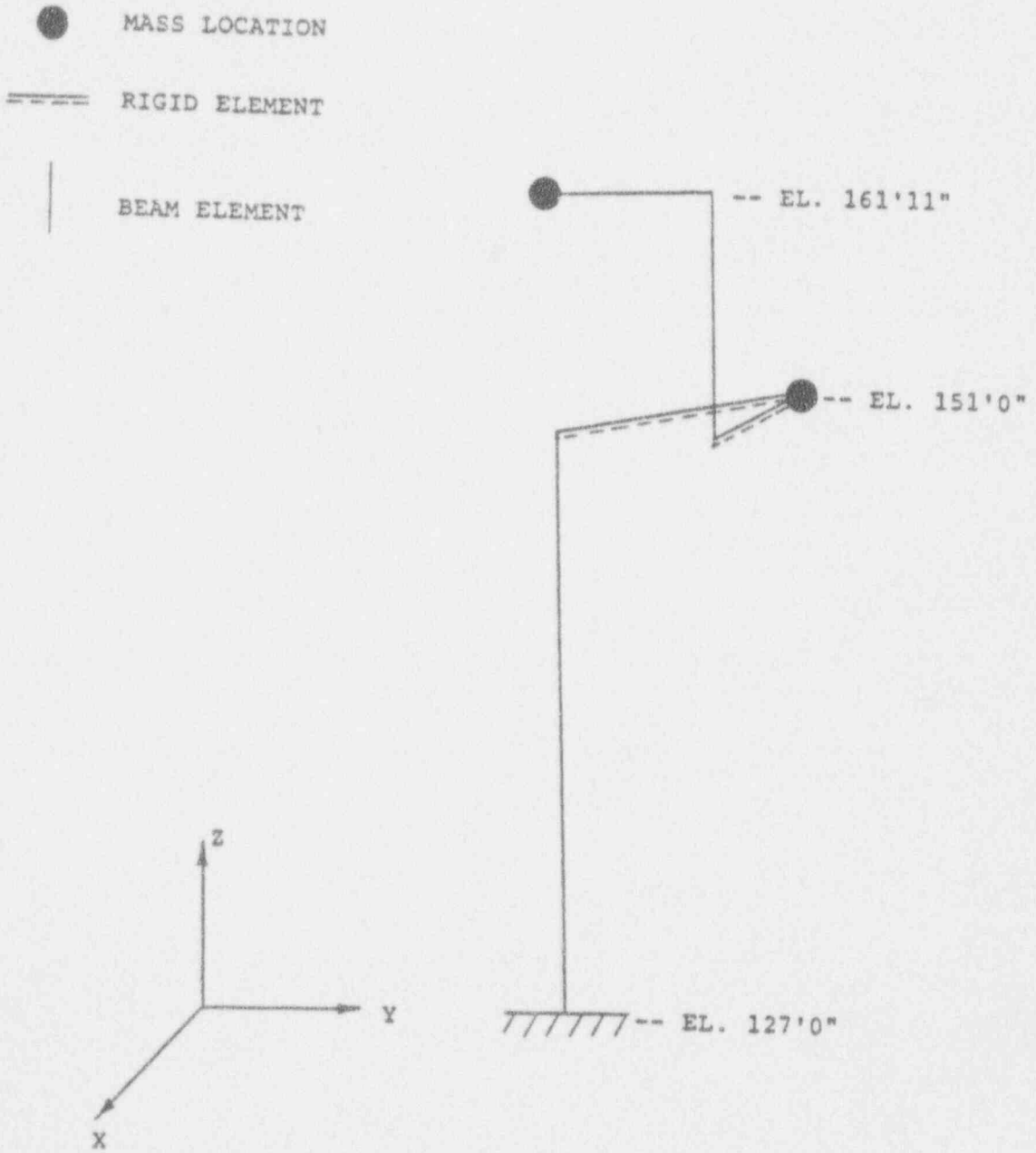

Figure A-26 Peach Bottom Diesel Generator Building Structural Model

elevation 153' is enclosed by the bottom slab, exterior walls, and precast roof panel with concrete fill. The three cells containing fans are enclosed by concrete walls. The Emergency Cooling Tower was modeled with five vertical beam elements located at the center of rigidity connecting each of the six main floor elevations. Lumped floor masses were rigidly linked to the beam elements at each of the floor elevations. Seven modes were calculated up to 30 Hz for this simplified stick model which is shown schematically in Figure A-27.

The models mentioned above are referred to herein as the original models since the element stiffnesses are those of the undegraded buildings. For the shear wall degradation study, at each of the applicable SSE levels (1, 2, 3, 5, 6, and 7 depending on the structure) the shear area of the beams representing the concrete walls was reduced according to the shear stiffness degradation curve defined in Section 3.2 of the main report. In this way stiffnesses associated with bending and axial deformations were not affected. The calculation of the degraded properties for each SSE level was an iterative process. In this process, response spectrum analysis were performed until convergence was reached for the new shear wall stresses. Three distinct sets of mean response spectra were used for these iterative analysis: the mean spectrum of the ten time histories per component discussed previously generated at 7% spectral damping for 1 SSE, 8.5% spectral damping for 2 SSE, and 10% spectral damping for 3 SSE and greater. Figures A-28 thru A-30 compare both horizontal and vertical mean spectra scaled to 1.0 g's for each of the ranges mentioned above. See Table A-2 for the dominant modes of the original and degraded model frequencies for each building analyzed based on the percent of mass participating per mode.

In addition to the original models, models whose shear stiffnesses were reduced to 75% of their original values were also analyzed. These models were used as the starting point for the degraded models and also for a deterministic analysis of the plant structures using the Taft earthquake. A comparison of all dominant modal frequencies for the original and 75% degraded models are shown in Table A-3.

A.3.4 Probabilistic Response Analysis

The general procedure is to perform a series of deterministic analyses, each simulating an earthquake occurrence, including variability in seismic input, soil-structure interaction, and instructure representation. Since Peach Bottom is considered a rock site, no soil-structure interaction analyses were performed, and no variability in the rock properties was needed.

Thus for seismic response at Peach Bottom, the most significant sources of random uncertainty originates from modeling the nodal frequencies and damping of the structures. These two independent random variables were assumed to be lognormally distributed and were varied by multiplying a nominal value, e.g. the nominal material damping and calculated frequencies, by a value selected from a lognormal distribution with median 1.0 and coefficients of variation listed below:

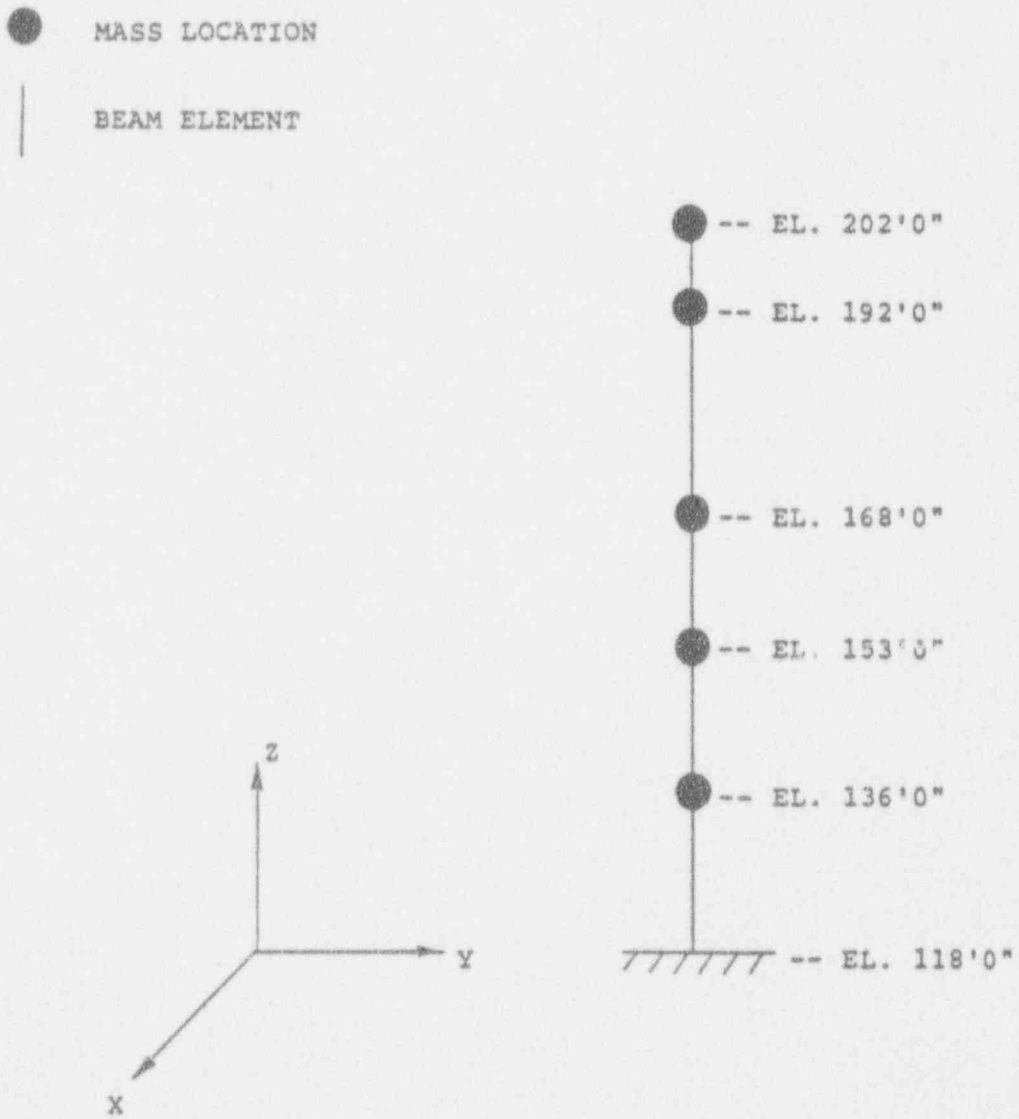

Figure A-27 Peach Bottom Emergency Cooling Towers Structural Model

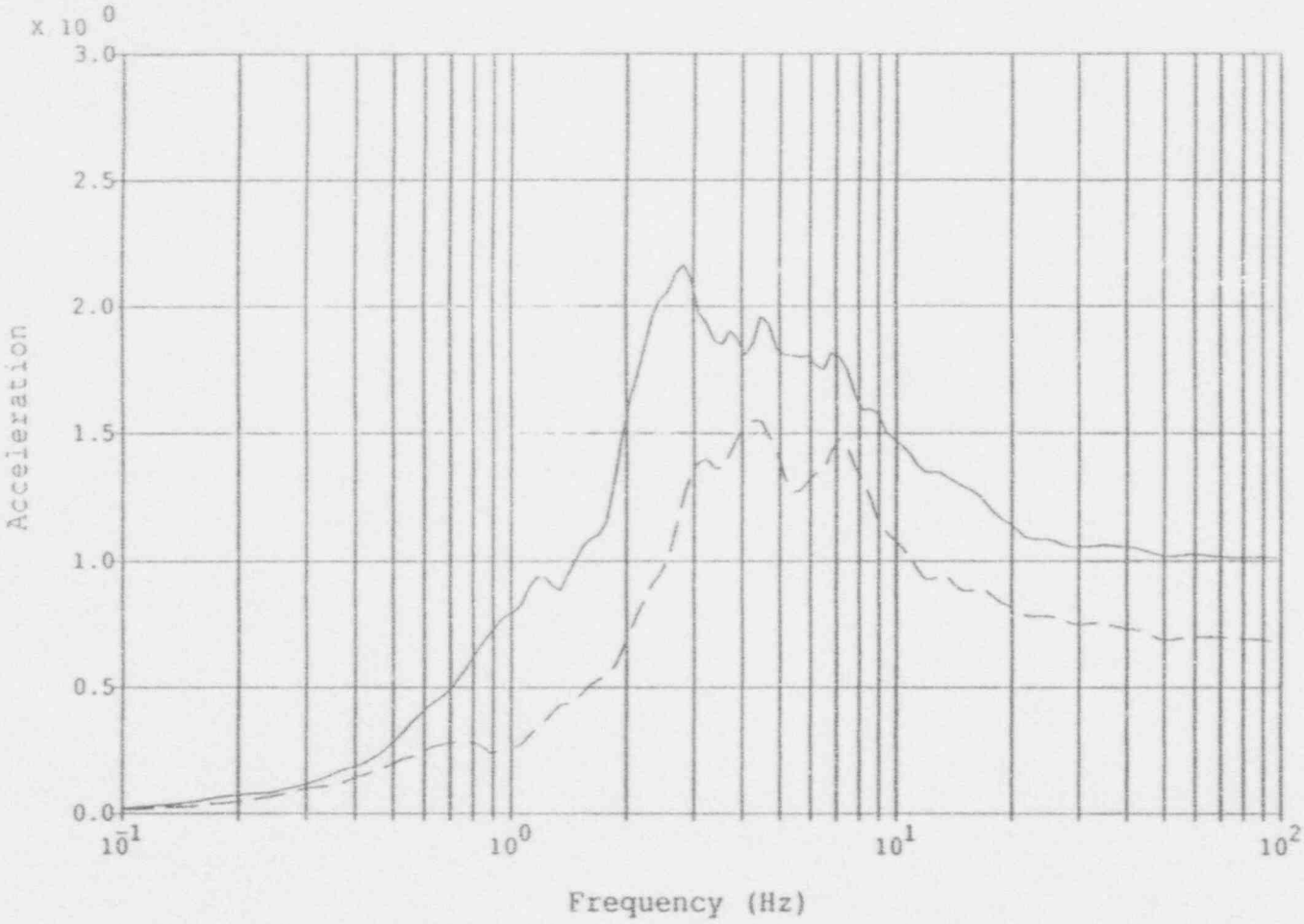

Legend:

Horizontal Spectrum _____

Vertical Spectrum _ _ _ _ _

Notes:

Accelerations in (g)
Horizontal scaled to 1g PGA
Vertical scaled to 0.667g PGA
7% Spectral Damping

Figure A-28 Peach Bottom Mean Input Spectra: 7% Spectral Damping

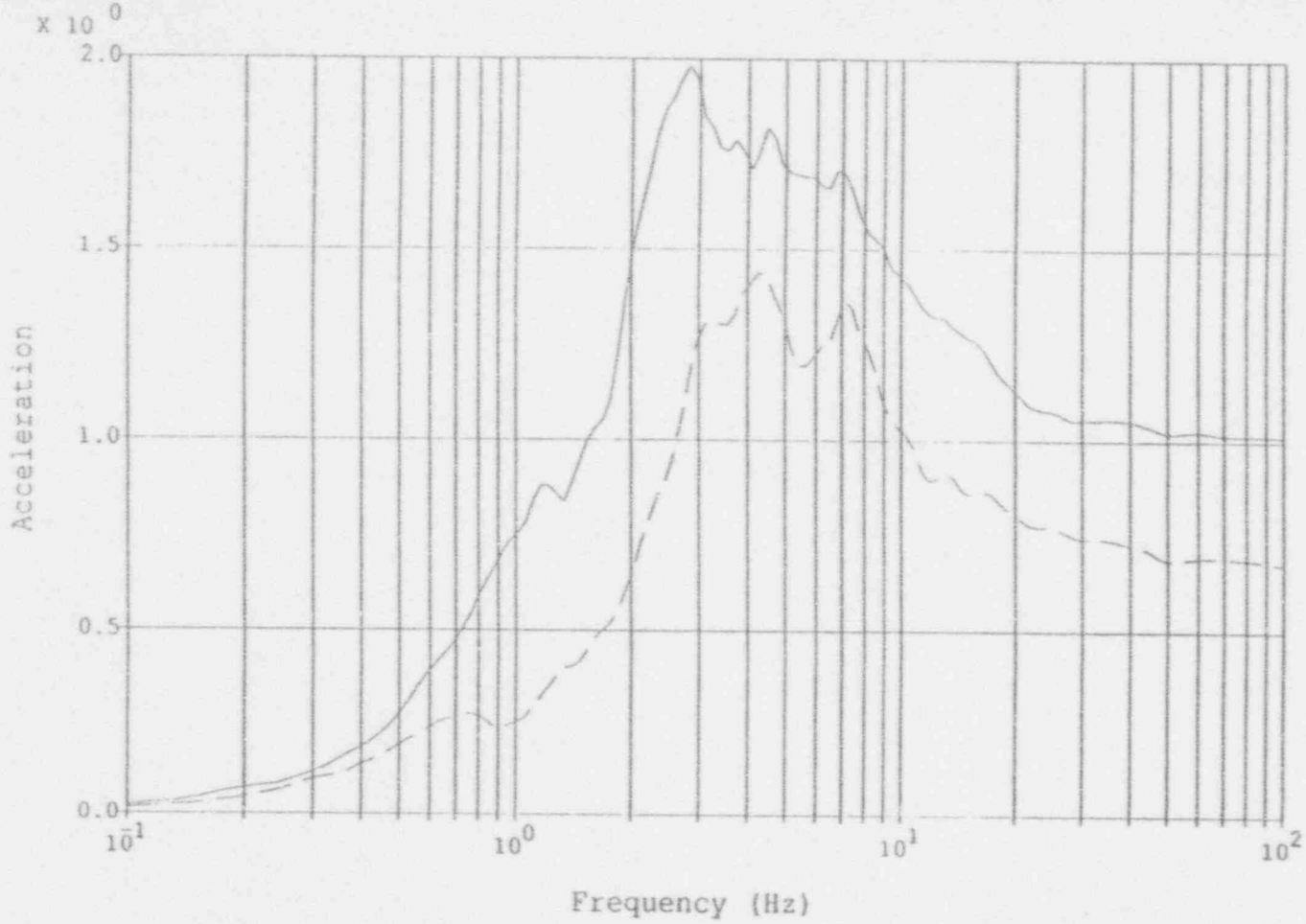

Legend:

Horizontal Spectrum _____

Vertical Spectrum _ _ _ _ _ _

Notes:

Accelerations in (g)
Horizontal scaled to 1g PGA
Vertical scaled to 0.667g PGA
8.5% Spectral Damping

Figure A-29 Peach Bottom Mean Input Spectra: 8.5% Spectral Damping

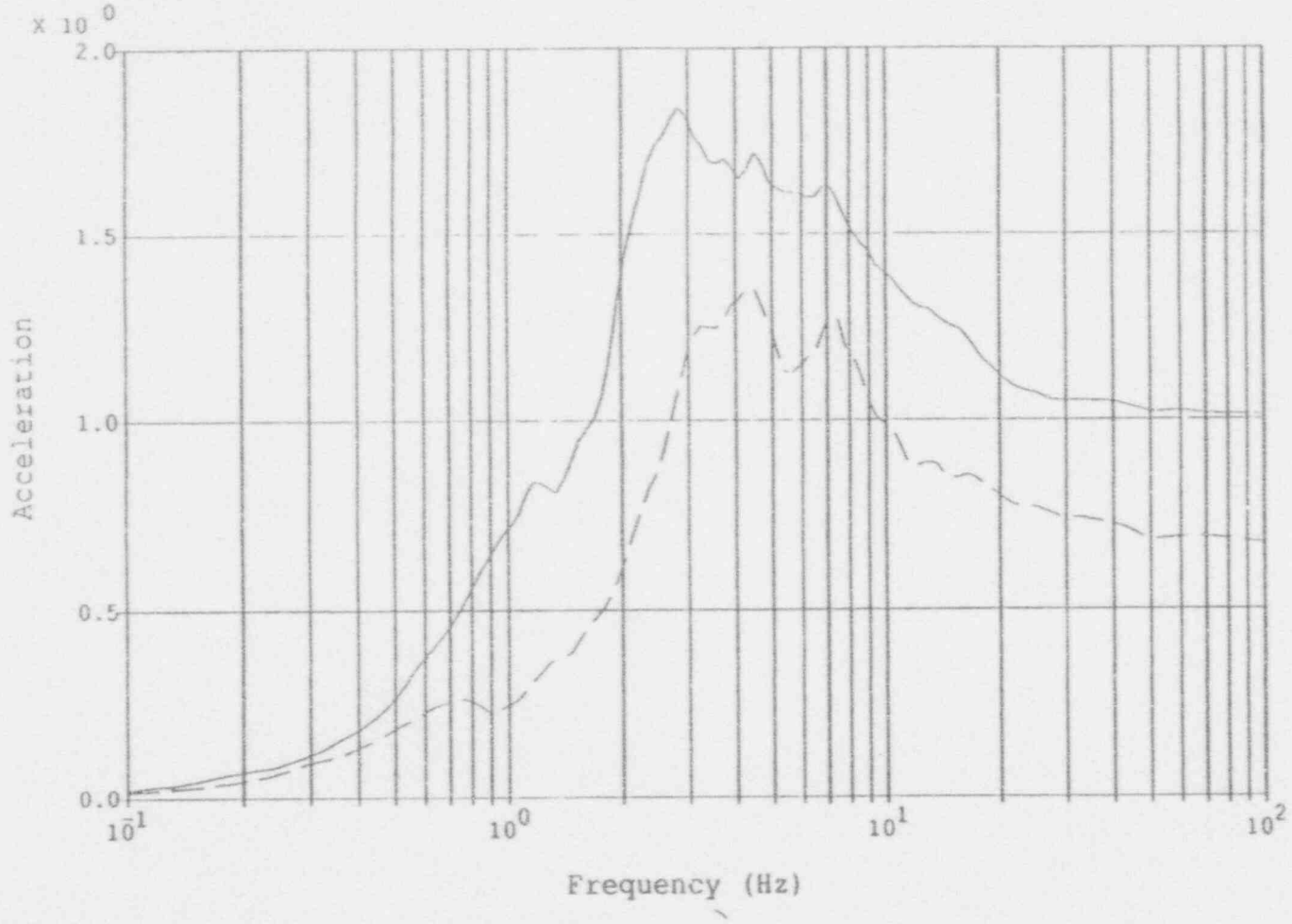

Legend:

Horizontal Spectrum _____

Vertical Spectrum _ _ _ _ _

Notes:

Accelerations in (g)
Horizontal scaled to 1g PGA
Vertical scaled to 0.667g PGA
10% Spectral Damping

Figure A-30 Peach Bottom Mean Input Spectra: 10% Spectral Damping

Table A-2

Peach Bottom Nuclear Power Plant Significant Modes

Blgd	Dir	Original Hz/%mass	1 SSE Hz/%mass	3 SSE Hz/%mass	6 SSE Hz/%mass	7 SSE Hz/%mass
DG	NS (X)	18.3/99.2	15.9/99.3	15.9/99.3	12.7/99.8	12.7/99.8
	EW (Y)	22.8/97.1	20.1/98.0	20.1/98.0	20.1/98.0	20.1/98.0
RWTB	NS (X)	9.38/81.8	8.22/82.6	5.95/89.6	3.43/91.0	3.45/91.2
	EW (Y)	11.5/58.7	10.0/46.5			
	EW (Y)	11.8/15.4	10.2/28.5	8.57/76.7	5.61/81.5	7.00/74.1
	NS (X)	21.6/13.7	19.0/12.8	15.0/8.14	9.42/6.37	9.47/6.13
CWP	NS (X)	14.0/89.4	12.1/89.5	9.95/92.6	6.18/96.4	5.89/96.1
	EW (Y)	20.6/72.1	18.3/74.0	18.3/74.0	16.7/48.1	16.5/45.6

Blgd	Dir	Original Hz/%mass	1 SSE Hz/%mass	3 SSE Hz/%mass	5 SSE Hz/%mass	7 SSE Hz/%mass
RB	NS (X)		6.09/51.2	6.27/38.9	5.70/61.6	5.24/61.6
	EW (Y)		6.41/30.4	5.70/16.2	6.26/25.9	5.41/16.2
	EW (Y)	7.63/71.3	7.21/41.4	7.57/45.3	7.07/37.6	6.37/46.3
	NS (X)	7.06/68.6	7.59/18.5	6.97/27.8	6.68/3.05	
ECT	NS (X)	9.77/36.5	7.26/29.9	4.78/22.1	3.60/21.1	3.59/21.6
	EW (Y)	10.4/79.1	9.16/81.9	7.43/94.4	5.23/97.6	3.90/99.0
	EW (Y)	17.4/18.6	15.6/16.1	14.5/5.05	12.5/2.19	
	NS (X)	19.3/61.7	16.4/68.5	16.0/76.4	13.2/78.3	10.2/77.9

Table A-3

Natural Frequencies for Dominant Modes at Peach Bottom

Building	Mode Number	Original (Hz)	Degraded (0.75) (Hz)
Reactor/ Containment Building	1	7.06	6.41
	2	7.64	6.91
	3	10.71	10.04
	4	10.86	10.44
	5	11.93	10.67
	6	14.41	12.64
	7	17.20	15.65
	8	17.21	15.65
	9	18.45	18.01
Radwaste/ Turbine Building	1	9.39	8.22
	2	11.47	10.01
	3	11.78	10.23
	4	21.62	19.04
	5	24.61	21.93
Circulating Water Pump Structure	1	13.99	12.12
	2	20.64	18.25
	3	29.17	25.26
	4	30.44	26.59
	5	33.41	29.21
Diesel Generator Building	1	18.28	15.88
	2	22.80	20.10
	3	28.07	24.31
Emergency Cooling Towers	1	9.77	8.58
	2	10.41	9.16
	3	17.38	15.58
	4	19.32	16.81

Structure Frequency	COV= 0.30
Structure Damping	COV= 0.30

Each earthquake simulation (10 per SSE level) was for a sampled set of time histories and sampled values of the 2 parameters described above. The values of the input parameters were sampled according to the Latin Hypercube procedure whereby for each parameter ten ranges of equal probability were defined (1/10). Then for each parameter one value was randomly selected from each of these probability ranges. This set of ten values for each parameter represented its possible occurrences and are listed in Table A-4.

A.3.4.1 Response in terms of Peak Ground Acceleration

From the pairs of response spectra (generated with and without stiffness reduction effects) at the various pga levels (0.12g-0.84g) one can construct plots of any particular spectral acceleration response (at any point in the structures being modeled) as a function of pga. The difference between these plots shows the effect of stiffness reduction directly. This was done for the locations of all equipment modeled on the accident sequence expressions (for the spectral acceleration corresponding to the equipment of interest).

A total of ten probabilistic analysis were performed for the DG, CWP, and RWTB structures - five for the original (undegraded) models at 1, 2, 3, 6, and 7 SSE, and five for the degraded models at the same earthquake levels. Eight were performed for the RB and ECT structures - four for the original (undegraded) models at 1, 3, 5, and 7 SSE, and four for the degraded models at the same earthquake levels. The final results of the probabilistic analysis are given in terms of median nodal accelerations for 10 earthquake simulations at all of the aforementioned SSE levels and for various frequency ranges. The median accelerations for the North-South component and East-West component were averaged in order to get a single median acceleration for each floor elevation. The results are shown graphically in the following figures:

RB:	Figures A-31 thru A-34
RWTB:	Figures A-35 thru A-38
CWP:	Figure A-39
DG:	Figure A-40
ECT:	Figure A-41

For the responses in all but the Diesel Generator building, the effect of the modal degradation on the median response is significant (i.e. the difference between the solid and dashed lines). It is also interesting to note that the responses using degraded stiffnesses are not always higher than using original stiffnesses and in some cases are lower. This is because reducing stiffnesses will shift the response spectra into the lower frequencies, and depending on the input spectra, this spectral shift will raise the spectral acceleration for some frequencies and lower others.

Table A-4

Multipliers for Structural Properties Variation

EQ Number	Coefficient	
	Frequencies	Dampings
1	1.06490	1.03230
2	1.00455	1.42363
3	1.17334	0.96900
4	0.98228	1.26656
5	0.87355	1.61678
6	1.32399	0.82709
7	1.77198	0.64389
8	0.74656	1.12330
9	0.74656	0.67147
10	0.92043	0.87502

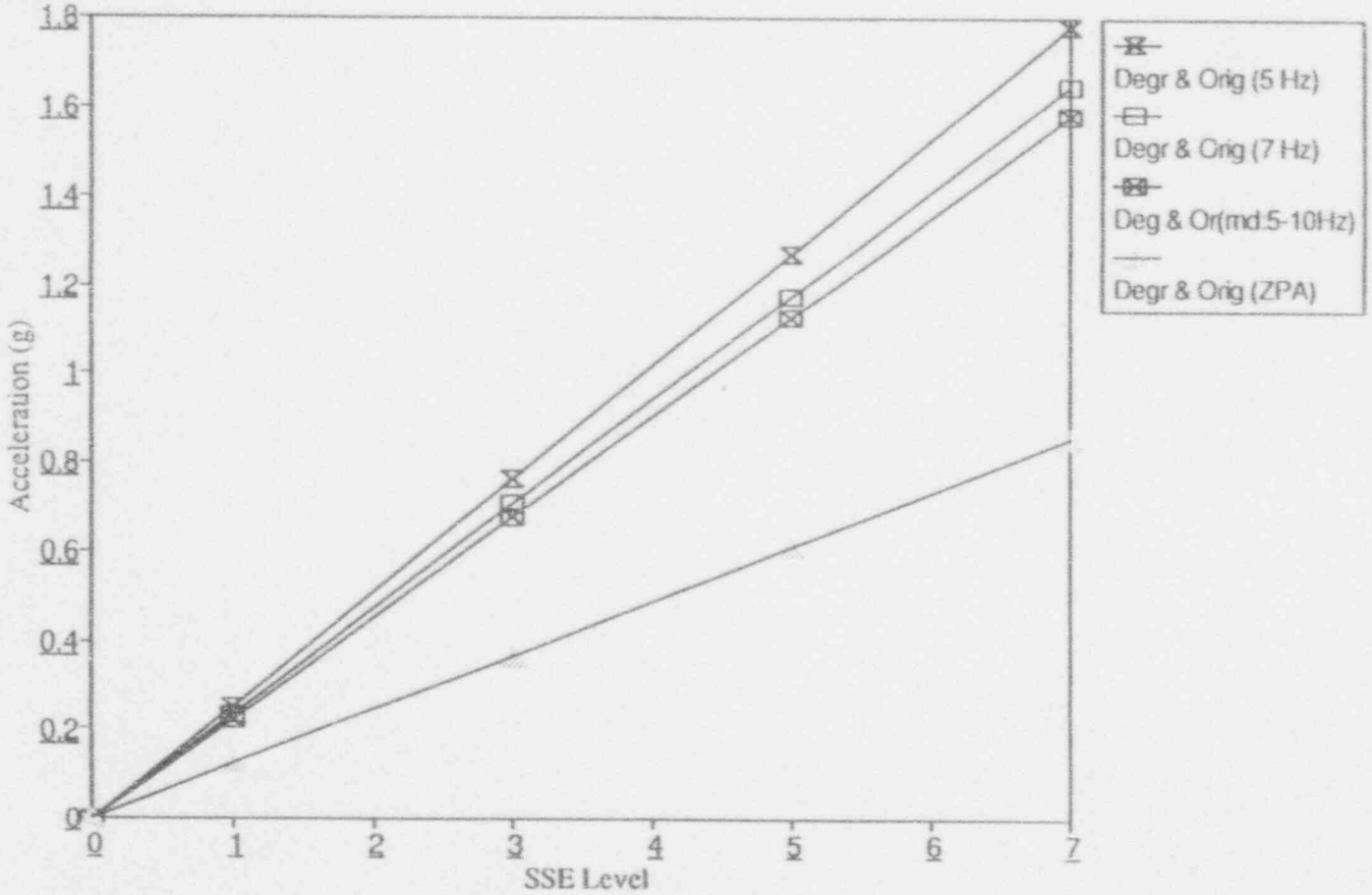

Figure A-31 Median Responses for R/C Building, Foundation, El. 91'

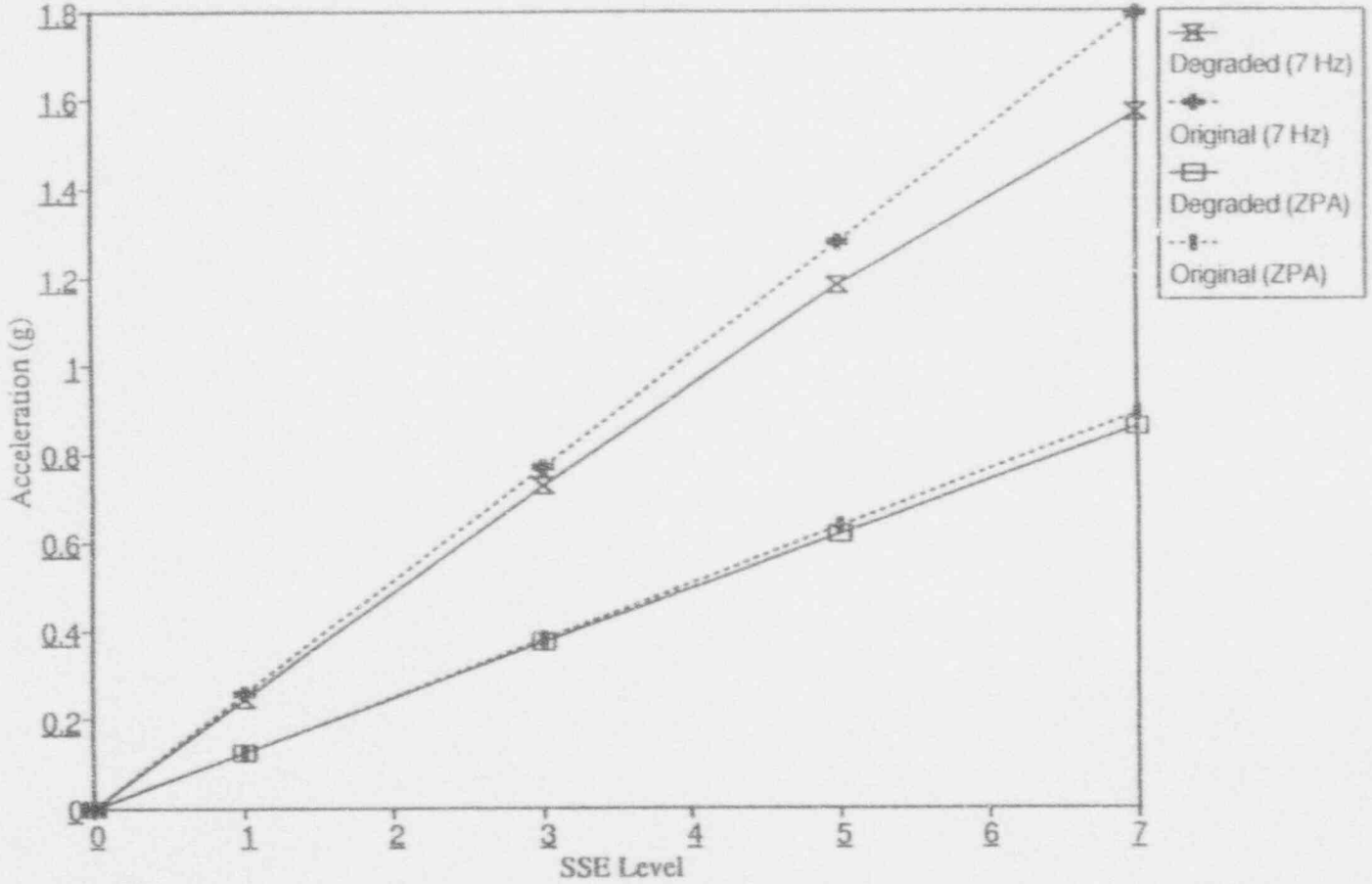

Figure A-32 Median Responses for R/C Building, Node 9, El. 119'

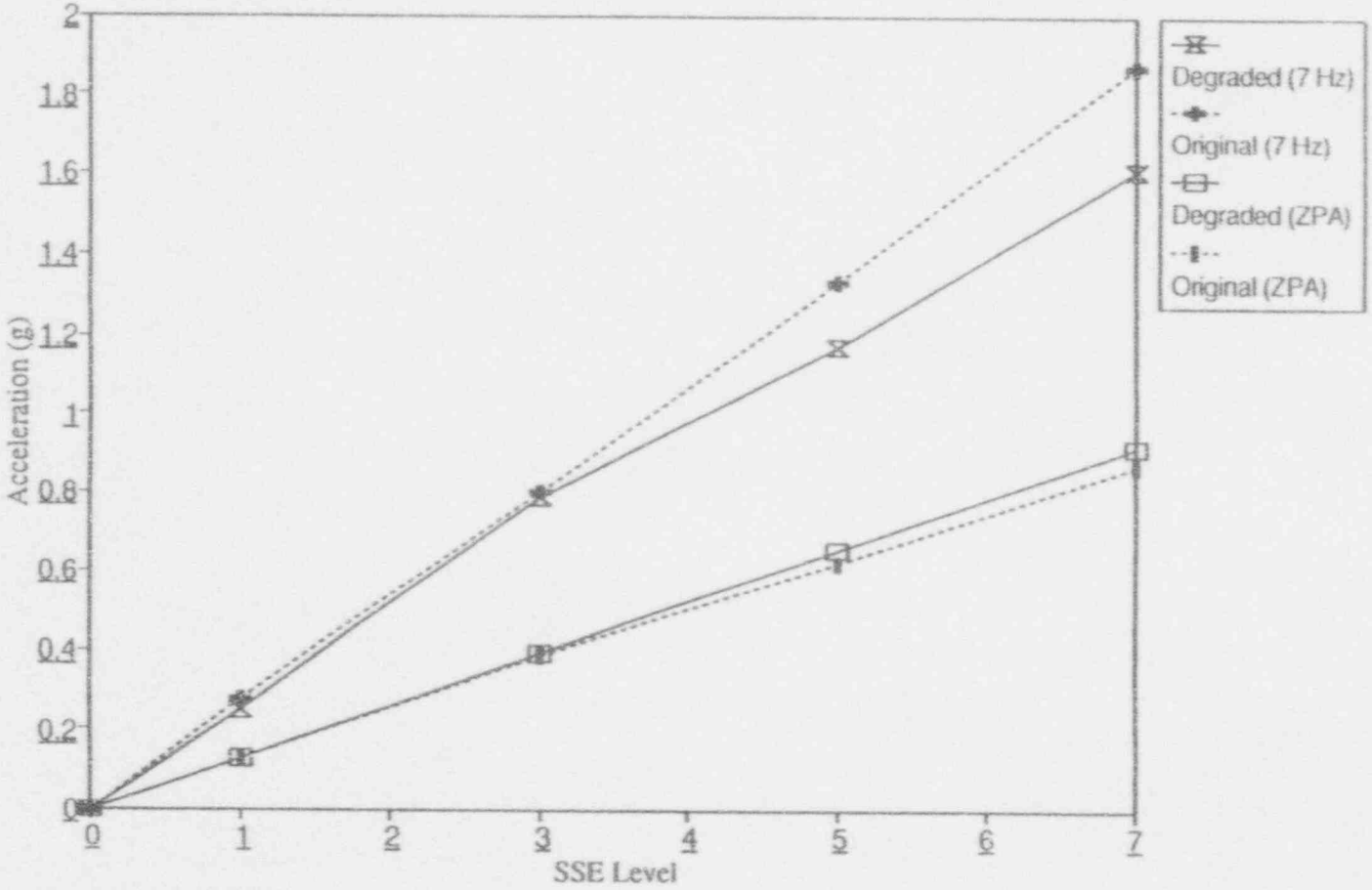

Figure A-33 Median Responses for R/C Building, Node 2, El. 135'

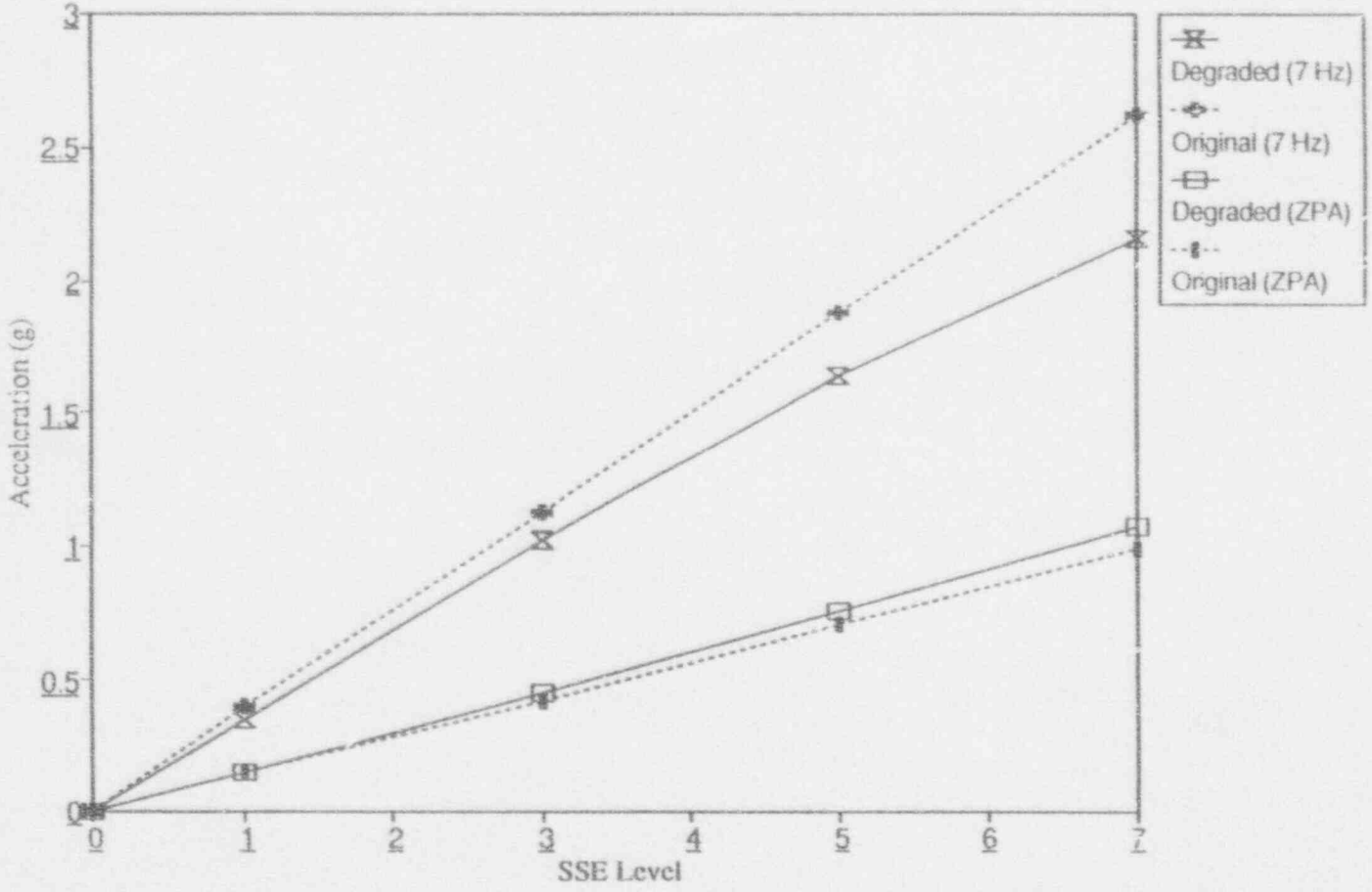

Figure A-34 Median Responses for R/C Building, Node 3, El. 165'

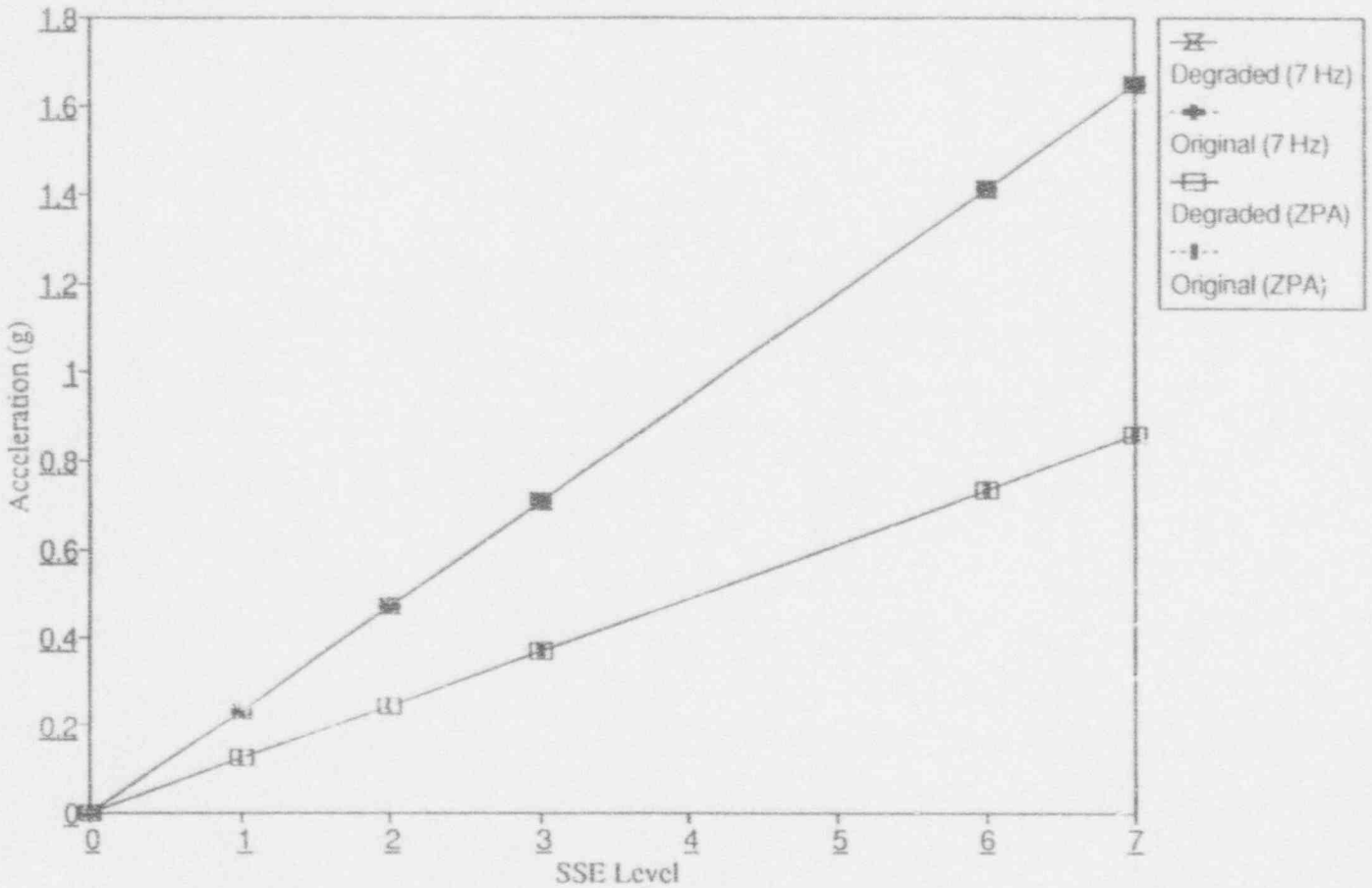

Figure A-35 Median Responses for RWST Building, Foundation, El. 116'

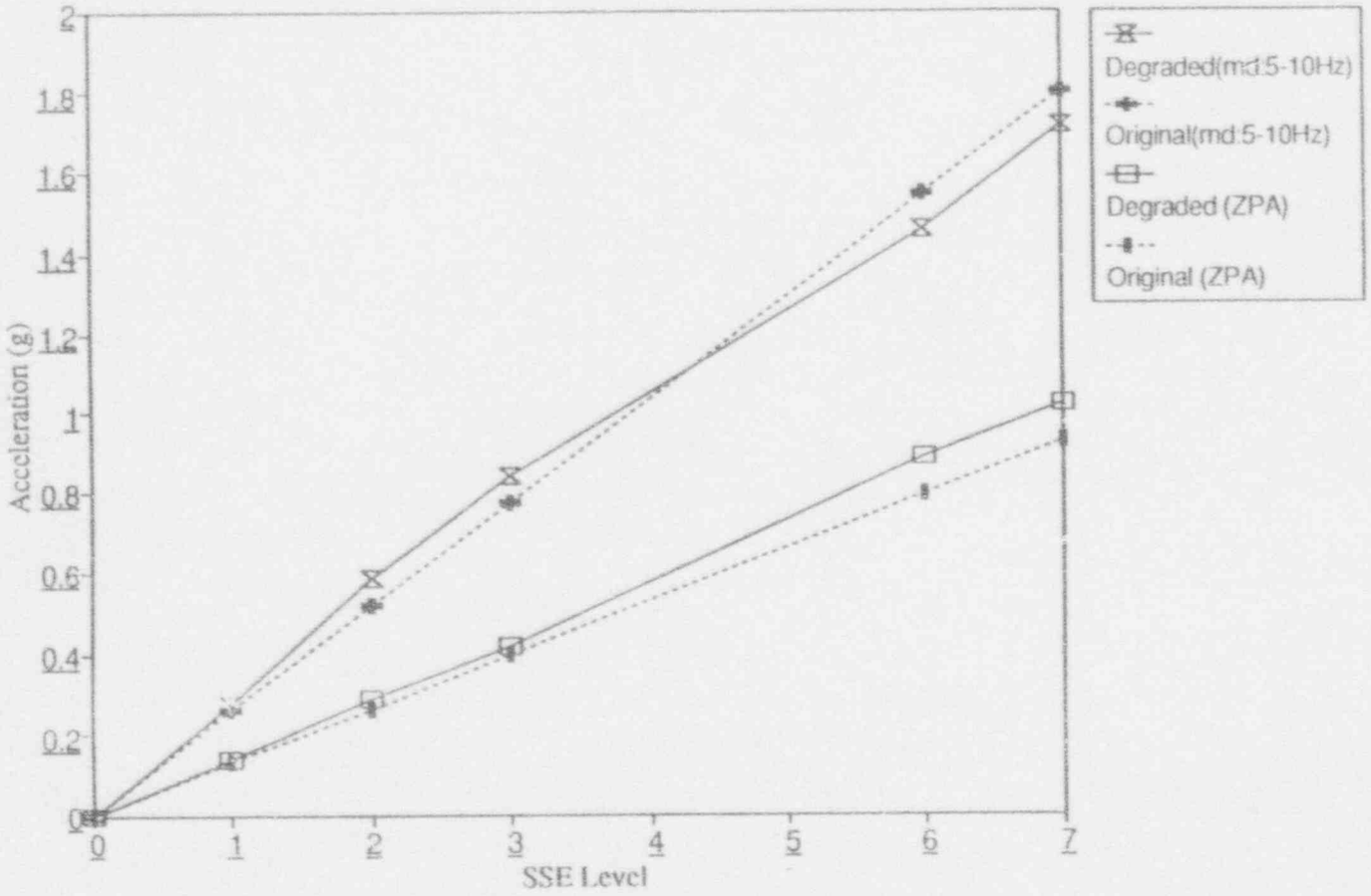

Figure A-36 Median Responses for RWST Building, Node 4, El. 135'

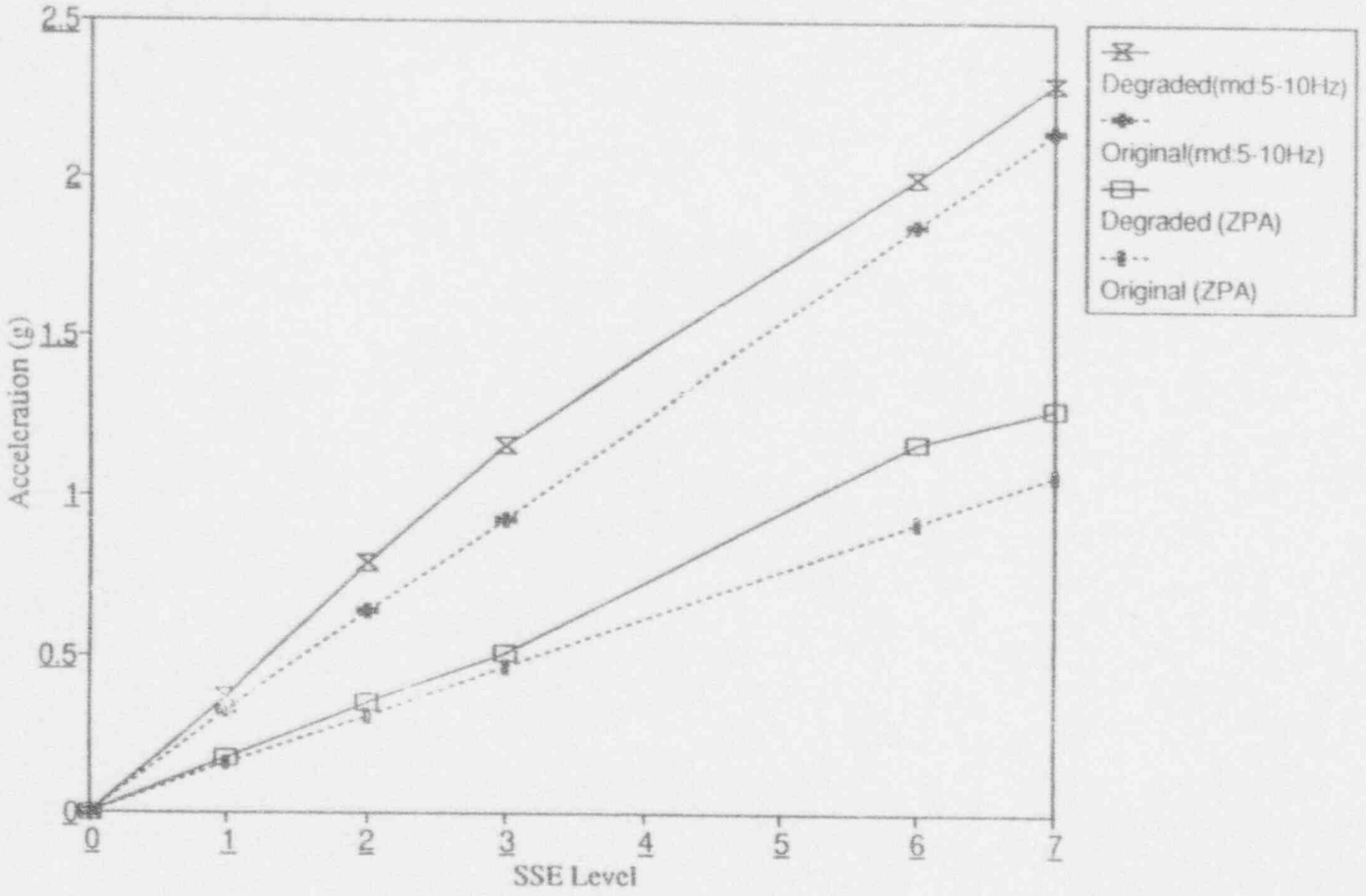

Figure A-37 Median Responses for RWST Building, Node 8, El. 150'

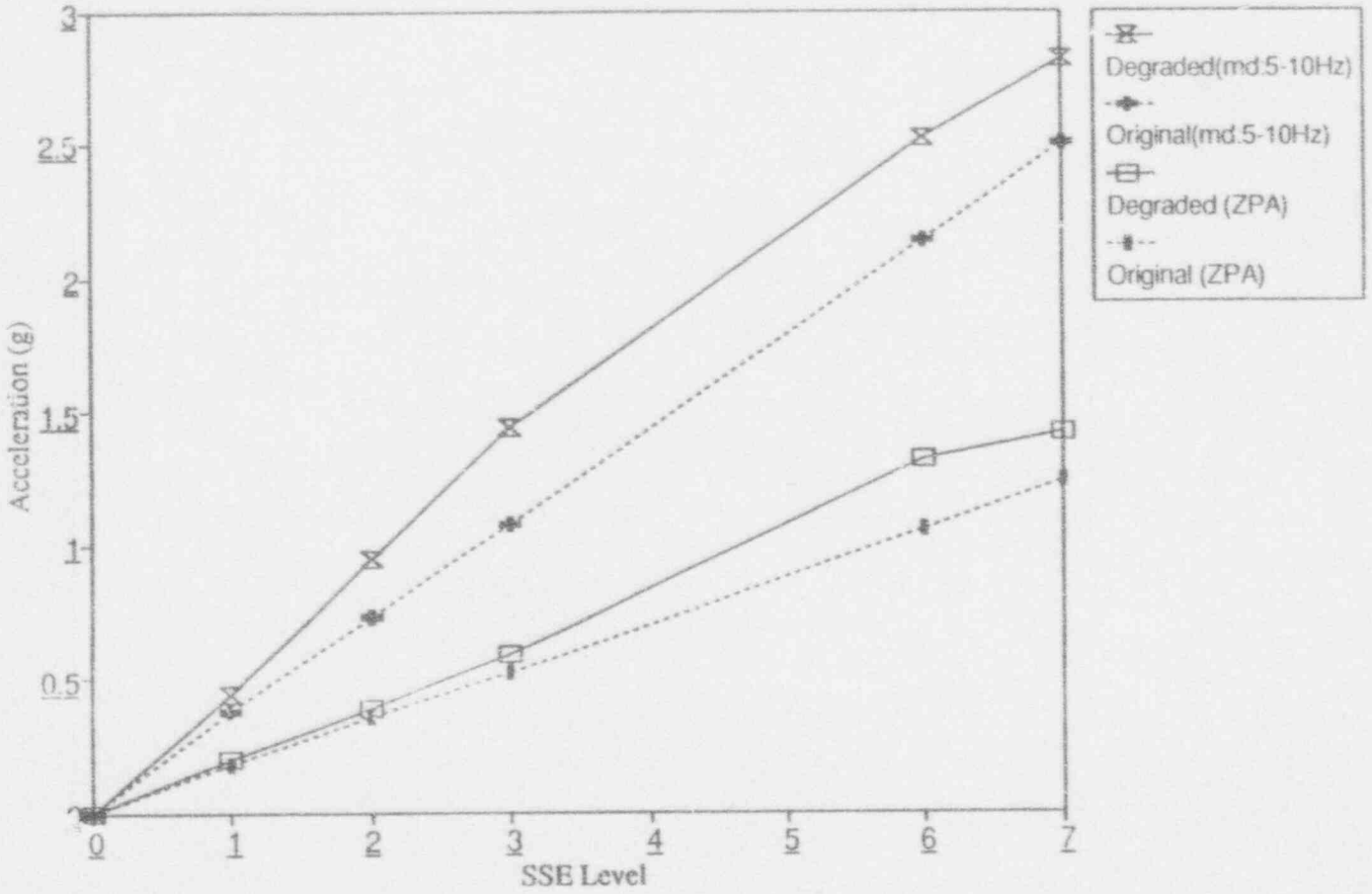

Figure A-38 Median Responses for RWST Building, Node 12, El. 165'

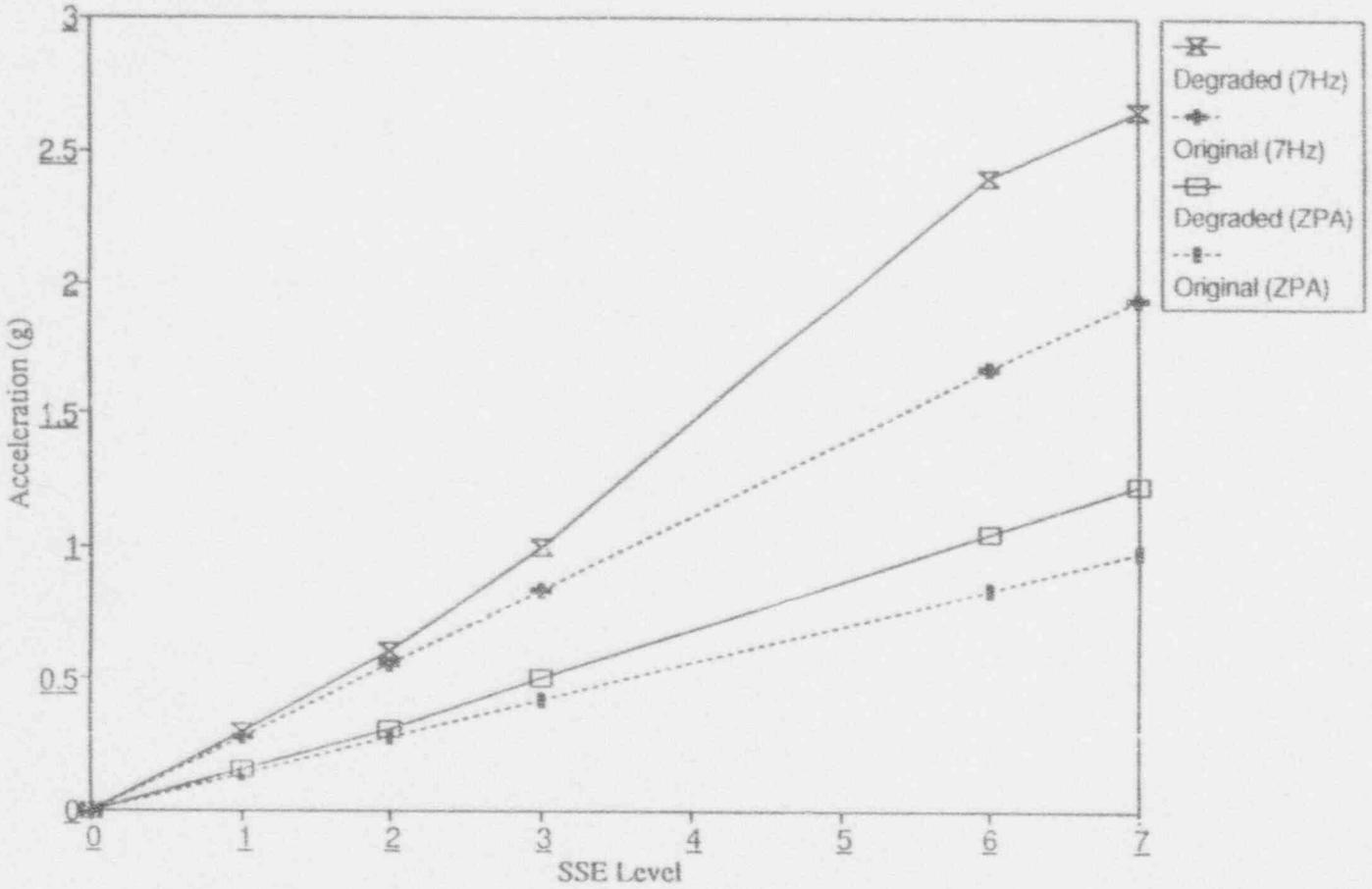

Figure A-39 Median Responses for CWF Structure, Node 13, El. 114'

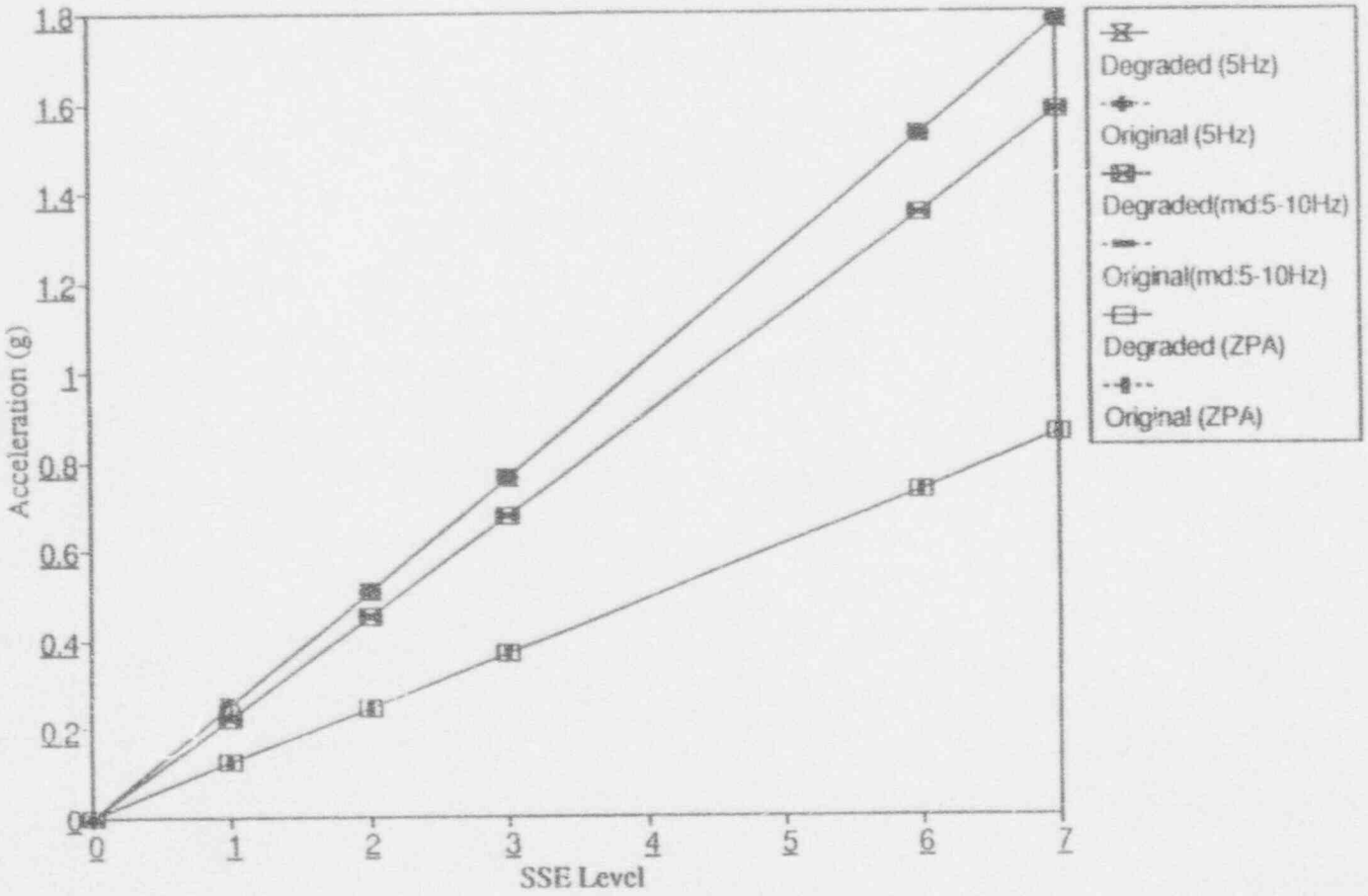

Figure A-40 Median Responses for DG Building, Foundation, El. 127'

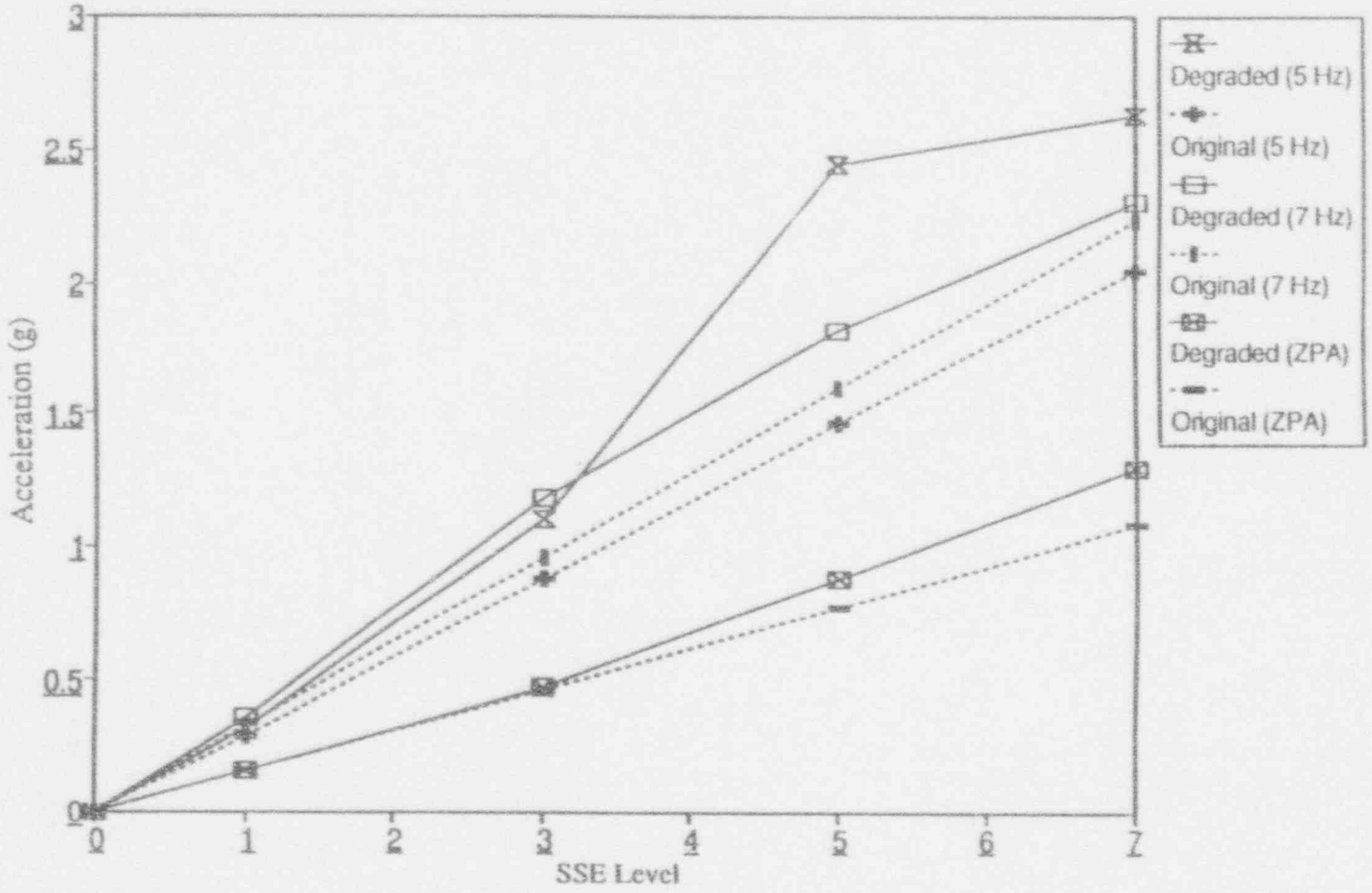

Figure A-41 Median Responses for ECT Structure, Node 3, El. 153'

A.3.4.2 Variability in Response

Variability in responses (floor and spectral accele-a+' is) was assigned based on SSMRP results [A-6]. Confidence bounds w. computed for the final core melt probabilities using both random (irreducible) and systematic (modeling) uncertainties. The uncertainties (expressed as standard deviations of the logarithms of the responses) are shown below:

Quantity	β Random	β Modeling
Peak Ground Acceleration	0.25	See Attachment to
Floor Zero Period Acceleration	0.35	Appendix A -
Floor Spectral Acceleration	0.45	Response Files

where β is the standard deviation of the logarithm of the response.

A.3.4.3 Correlation Between Responses

Correlation in failure probability can exist, in principle, between any two components (like or unlike) which are located at any two locations at the plant. A review of the component responses in conjunction with the fact that fragility correlations were taken as zero allowed determination of those differing components which might be assigned correlation. It was found that only the 4kV busses and the 125 volt busses had any significant correlation. However, a number of identical pairs of components (in the same location) were found to be significantly correlated. These components are listed below.

- 4 kV busses
- 125 volt busses
- diesel generators
- ESW motor driven pumps

Generic rules for estimating the amount of correlation between the various responses was derived from the SSMRP response calculations for the Zion plant [A-6]. These rules are summarized in Table A-5.

A.4 SEISMIC FRAGILITIES

The equipment seismic fragilities used in the NUREG-1150 study were used in the present study. In addition, the building fragilities developed in the NUREG-1150 study were again used in the present study for original stiffnesses. However, in order to include the effects of reduced stiffness, a second set of structural fragilities was developed.

In general, equipment failure is taken as either loss of pressure boundary integrity or loss of operability. Failure (fragility) is characterized by a cumulative distribution function which describes the probability that failure has occurred given a value of loading. Loading may be described by local spectral acceleration or moment, depending on the component

Table A-5

Rules for Assigning Response Correlation $\rho_{R_1 R_2}$

1. Components on the same floor slab, and sensitive to the same spectral frequency range (i.e., ZPA, 5-10 Hz or 5 Hz) will be assigned response correlation = 1.0.

2. Components on different floor slabs, sensitive to different ranges of spectral acceleration will be assigned response correlation = 0.5.

3. Components on different floor slabs (but in the same building) and sensitive to the same spectral frequency range will be assigned response correlation = 0.75.

4. Components on the ground surface (outside tanks, etc.) shall be treated as if they were on the grade floor of an adjacent building.

5. "Ganged" valve configurations (either parallel or series) will have response correlation = 1.0.

6. All other configurations will have response correlation = 0.0.

failure mode. The fragilities are related to the local response to permit an accurate assessment of the effect of earthquake-induced correlation in the evaluation of the accident sequences.

A.4.1 Generic Fragilities

A generic data base of fragility functions for seismically-induced failures was developed in the SSMRP [Ref. A-6]. The generic categories and the corresponding fragility medians and uncertainties used are shown in Tables A-6 and A-7. The NUREG 1150 analyses chose not to include relay chatter as a failure mode for electrical gear but rather to include circuit breaker trip as the lowest functional failure mode.

A.4.2 Site Specific Component Fragilities

Based on the plant walkdown, a number of components were identified as not fitting in the generic fragility data base. These components were later examined for their importance on the system fault trees, and for those playing a role in the systems analysis, site-specific fragilities were derived. The resulting site-specific fragilities are shown on Table A-8. These failure modes are described below.

The 4kV switchgear were found to be anchored with fillet welds into steel imbedded in the floor and a fragility analysis was required to assess the capacity of the welds. The diesel generator day tank is a vertical tank held by 5/8 inch bolts and is critical to the continued operation of the diesel generators in the event of loss of off site power. The HPCI room cooler was found to be anchored to an I beam frame with small welds at its corners. Failure of this cooler would result in long term failure of the HPCI pump (approximately 10 hours). The condensate storage tank plays a role as a suction source for the high pressure injection systems. The tank itself is a vertical water storage tank anchored with six bolts to a mounting pad. Such tanks often have relatively low seismic capacity. However, the tank itself is surrounded by a water tight dike and so credit was given for the possibility that, if the CST failed, water would still be available through the dike. A calculation was made to verify that the level of the water after tank failure was such that suction could still be maintained. Thus, the fragility of the condensate storage tank was based on the fragility of the water tight dike as listed in Table A-9.

A.4.3 Structural Fragilities

The Peach Bottom structural fragilities were expressed in terms of factors which account for structure ultimate strength and inelastic energy absorption capability. The basic techniques used to determine the median values and associated variabilities of the terms were essentially those described in Section 2.5 of the main report.

Table A-6

Generic Component Categories

Fragility Category	Component Class	Typical Components	Frequency (Hz)
1	LOSP	Ceramic Insulators	ZPA
2	Relays		5-10
3	Circuit Breakers		5-10
4	Batteries		ZPA
5	Battery Racks		ZPA
6	Inverters		5-10
7	Transformers	4 kV to 480 V and 480 to 120 V	10
8	Motor Control Centers	Control for ESF Pumps and Valves	5-10
9	Aux. Relay Cabinets		5-10
10	Switchgear (Including Transformers, Buses and Breakers)	416 V and 480 V	5-10
11	Cable Trays		ZPA
12	Control Panels and Racks	RPS Process Control	5-10
13	Local Instruments	Misc. Pressure & Temperature Sensors	5-35
14	Diesel Generators	4160 ac Emergency Power Units	22
15	Horizontal Motors	Motor-Generator Sets	ZPA
16	Motor-Driven Pumps and Compressors	AFWS, RHR, SIS, Charging Pumps, Lube Oil Pumps, Diesel Starting Compressors	7
17	Large Vertical, Centrifugal Pumps (Motor-Drive)	Service Water Pumps	5
18	Large Motor-Operated Valves (10")		ZPA
19	Small Motor-Operated Valves (10")		ZPA
20	Large Pneumatic/Hydraulic Valves	Includes MSIV, ADP, and PORV	ZPA
21	Large Check and Relief Valves		ZPA
22	Miscellaneous Small Valves (8")		ZPA
23	Large Horizontal Vessels & Heat Exchangers	Pressurizer Relief Tank, CCW Heat Exchangers	ZPA
24	Small to Medium Heat Exchangers and Vessels	Boron Injection Tank	20
25	Large Vertical Storage Vessels with Formed Heads	RHR Heat Exchanger, Accumulator Tank	ZPA
26	Large Vertical Flat-Bottomed Storage Tanks	CST, RWST	
27	Air Handling Units	Containment Fan Coolers	5

Table A-7

Generic Component Fragilities, in Units of Gravity (g)

Category	Generic Component	Median*	B_U	B_R
1	Ceramic Insulators	0.25	0.25	0.25
2	Relays	3.00	0.48	0.75
3	Circuit Breakers	7.63	0.48	0.74
4	Batteries	0.80	0.40	0.39
5	Battery Racks	2.29	0.31	0.39
6	Inverters	2.00	0.26	0.35
7	Dry Transformers	8.80	0.28	0.30
8	Motor Control Centers	7.63	0.48	0.74
9	Auxiliary Relay Cabinets	7.63	0.48	0.74
10	Switchgear	6.43	0.29	0.66
11	Cable Trays	2.23	0.34	0.19
12	Control Panels and Racks	11.50	0.48	0.74
13	Local Instruments	7.68	0.20	0.35
14	Diesel Generators	1.00	0.25	0.31
15	Horizontal Motors	12.10	0.27	0.31
16	Motor-Driven Pumps and Compressors	2.80	0.25	0.27
17	Large Vertical Centrifugal Pumps	2.21	0.22	0.32
18	Large Motor-Operated Valves (10 in.)	6.50	0.26	0.60
19	Small Motor-Operated Valves (10 in.)	3.83	0.26	0.35
20	Large Pneumatic/Hydraulic Valves	6.50	0.26	0.35
21	Large Relief, Manual, and Check Valves	8.90	0.20	0.35
22	Miscellaneous Small Valves	12.50	0.33	0.43
23	Large Horizontal Vessels and Heat Exchangers	3.0	0.30	0.53
24	Small to Medium Vessels and Heat Exchangers	1.84	0.25	0.45
25	Large Vertical Vessels With Formed Heads	1.46	0.20	0.35
26	Large Vertical Tanks With Flat Bottoms	0.45	0.25	0.35
27	Air Handling Units	6.90	0.27	0.61

R = Random Uncertainty.

U = Systematic Uncertainty.

*All medians in terms of spectral acceleration at 5% damping.

Table A-8

Peach Bottom Site Specific Fragilities

Component	Failure Mode	M_F	β_R	β_U	Response No.
4KV Switchgear	Anchor weld failure	3.30	0.15	0.25	7 (5-10Hz)
DG Day Tank	Anchorage Failure	0.95	0.15	0.20	22 (ZPA)
HPCI Room Cooler	Weld Failure	3.42	0.15	0.25	13 (5-10HZ)
Condensate Storage Tank	Anchorage/Building	Fragility Based on Dike Table 3.14			
RWST	Unanchored	Not on Fault Trees			

Table A-9

Summary of Structural Fragilities for Peach Bottom

Structure	Element	Original[1] A_m(g)	β_R	β_U	Reduced[2] A_m(g)	β_R	β_U	Effect of Failure
Reactor Building	N-S Shear Walls	1.5	0.16	0.27	1.6	0.17	0.28	Vessel Rupture Initiating Event
Radwaste/Turbine Building	Roof Diaphragm	1.4	0.10	0.23	1.2	0.11	0.24	Cause SBO and loss of all actuation. Modeled as initiating event, and failure event in LOCA sequences.
Radwaste/Turbine Building	N-S Shear Walls	1.5	0.13	0.25	1.6	0.15	0.26	
Diesel Generator Building	E-W Shear Walls	2.3	0.06	0.21	2.3	0.07	0.21	Negligible
Circulating Water Pump Structure	N-S Shear Walls	2.5	0.11	0.28	2.2	0.13	0.29	Negligible
Emergency Cooling Towers	Columns El. 153' to El. 163'	0.55	0.11	0.21	0.55	0.11	0.21	Basic event in ESW system. Screened out due to redundancy.
Turbine Building	-	0.5	0.11	0.21	0.5	0.11	0.21	Fails PCS, ECW pump cables, instrument air, and condensate system. Modeled as a failure event in T1, T3 and LOCA sequences.
Watertight Dike	Surrounds CST	1.0	0.04	0.17	1.0	0.04	0.17	Failure mode of CST. screened out due to redundancy.

1. These fragilities are based on loads from analyses using original stiffnesses.

2. These fragilities are based on loads from analyses including shear wall stiffness degradation.

3. β_R and β_U do not include response variability.

The structures were considered to fail functionally when inelastic deformations of the structure under seismic load are estimated to be sufficient to potentially interfere with the operability of safety-related equipment attached to the structure. The element and system ductility limits chosen for structures were estimated to correspond to the onset of significant structural damage. This was believed to represent a conservative bound on the level of inelastic structural deformation which might interfere with the operability of components housed within the structure.

This approach to determine structural fragilities, which utilizes seismic responses from a single elastic model, is incompatible with the response analyses generated for this reduced stiffness study, which uses multiple models. The following approach described below will be used to resolve this incompatibility, while taking advantage of the structural fragilities calculated for the original NUREG 1150 study, which used no stiffness reduction.

First, we identify bounding ground motion cases for which structural response is essentially linear. The lower bound case will always be the 1*SSE case. The upper bound case will be the one corresponding to the highest ground motion level for which stresses are still "approximately elastic". Based upon the force-deflection curve corresponding to the specified stiffness-NBSS relationship, the structure can be considered "approximately elastic" so long as shear stresses are all less than about 300 psi. Hence the use of linear elastic analysis in this process is valid. This corresponds to a stiffness reduction factor of 0.33 from the model described in Section 3.2 of the main report.

Then, for the lower and upper bound ground motion cases identified above, structural fragilities will be determined using the following guidelines:

1. The strength factor based on the original Peach Bottom fragility evaluation was scaled by the ratio of the median load for the bounding case to the median load from the original stiffness evaluation. (This scaling was performed for the governing shear wall element.)

2. The inelastic energy absorption factor for the bounding case considered was determined using the corresponding frequency for the dominant mode resulting from the reduced stiffness calculation.

3. Median damping values of 7% and 8.5% have been specified for the 1*SSE and 2*SSE cases. Damping factors were included in the fragilities to account for the difference in response associated with a median damping of 10% at structural failure. (Variability associated with damping will not be included in the fragility, since this is included in the response variability.)

The median accelerations at failure for the two bounding cases was compared. So long as they are not significantly different, a single fragility was selected which is thus representative of the range of frequency reduction expected at failure.

The resulting fragilities for both original and reduced stiffnesses of the Peach Bottom structures are listed in Table A-9. In general, several potential failure modes were investigated for each structure. Fragilities for the governing failure modes are reported. These failure modes are typically associated with structural failure which would result in damage to the safety-related equipment located in the building. The failure modes for individual structures are summarized below.

Reactor Building

The reactor building houses the nuclear steam supply system, primary containment, and auxiliary systems. It is founded on rock at Elevation 91 feet-6 inches. The reactor building is isolated from adjacent structures above Elevation 116 feet-0 inches by 0.5-inch-thick gaps. The seismic load-resisting system consists of reinforced concrete walls and slabs up to the refueling floor at Elevation 234 feet-0 inch. The superstructure above the refueling floor consists of structural steel framing, siding, and roof deck. The concrete shield wall that encloses the drywell is integral with the reactor building structure. The reactor pedestal and sacrificial shield wall are founded on fill concrete within the drywell. The stabilizer truss connected to the top of the sacrificial shield wall provides lateral support for these internal structures.

Seismic capacity of the reactor building was found to be governed by failure of the N-S or E-W shear walls. Resistance to lateral seismic loads is provided mainly by the exterior shear walls and the drywell shield wall. Failures of these walls are expected to be initiated at Elevation 135 feet-0 inch. Median pga capacities in both the N-S and E-W directions were determined to be 1.5 g using original stiffnesses and 1.6 g for reduced stiffnesses. Shear wall failure corresponds to gross structural failure and is expected to cause damage to equipment located throughout the entire reactor building, including components housed within the drywell.

Radwaste/Turbine Building

The radwaste building and immediately adjacent portion of the turbine building were constructed integral with each other and are thus considered a single structure. The radwaste building is located between the reactor buildings for Units 2 and 3. It houses various components of the radwaste system, the standby gas treatment system, and associated equipment. The turbine building houses the control room, cable spreading room, switchgear rooms, and battery rooms. The radwaste/turbine building is founded on rock. The seismic load-resisting system consists of reinforced concrete shear walls and slabs. It is separated from adjacent buildings above Elevation 116 feet-0 inch by a 0.5-inch-thick gap.

A number of shear walls and diaphragms were evaluated. The roof diaphragm was found to have the lowest seismic capacity, with a median pga capacity of 1.4 g using original stiffnesses and 1.2 g for reduced stiffnesses. The roof over the radwaste building is either metal deck or 1 foot-6 inches-thick concrete slab. The roof over the control room is a 2 feet-

6 inches-thick concrete slab. This failure mode is localized, and will result in damage to equipment located between Elevation 165 feet-0 inch and the roof, which includes the control room.

Gross structural failure is expected to result from failure of the N-S shear walls. The median pga capacity for this failure mode was calculated to be 1.5 g using original stiffnesses and 1.6 g for reduced stiffnesses. Damage to equipment located throughout the radwaste/turbine building is expected to result.

Diesel Generator Building

The diesel generator building houses the emergency diesel generators and associated components. The lateral load-resisting system consists of reinforced concrete shear walls and slabs. The bottom floor of the diesel generator building is typically at Elevation 127 feet-0 inch, which is approximately at grade. Shear walls below grade were designed to transmit lateral loads down to bedrock. The central portion of the building is supported by piles driven to bedrock. The piles were intended to support gravity loads only.

The seismic capacities of several shear walls and diaphragms above grade were evaluated. Potential seismic-induced failure of the shear walls below grade is not expected to result in a loss of function of equipment components housed within the building. Failure of the diesel generator building was found to be governed by failure of the E-W shear walls. A median pga capacity of 2.3 g was calculated using original stiffnesses and also 2.3 g using reduced stiffnesses. This failure mode is expected to result in gross structural failure with damage to equipment located throughout the building.

Circulating Water Pump Structure

The central portion of the circulating water pump structure (CWPS) houses the Seismic Class I emergency and high-pressure service water systems. The remainder of the structure houses the service and circulating water systems. The CWPS is founded on rock. Lateral load-resisting systems for Class I portions of the building consist of reinforced concrete shear walls and slabs. (The superstructures over the circulating and service water pumps were not evaluated since their failure would not damage Class I equipment.)

Selected shear walls and diaphragms were evaluated. Seismic capacity of the CWPS was found to be governed by failure of the N-S shear walls. A median pga capacity of 2.5 g was calculated using original stiffnesses and 2.2 g for reduced stiffnesses. This failure mode corresponds to gross structural failure and damage to equipment located throughout the building.

Emergency Cooling Tower

The emergency cooling tower contains the fans and associated components for the emergency heat sink. It is founded on rock. The water reservoir below Elevation 153 feet-0 inch is enclosed by the bottom slab, exterior walls, and precast roof panel with concrete fill. The three cells containing the fans are enclosed by concrete walls.

N-S seismic load from the cells above Elevation 163 feet-0 inch is transferred to the structure below Elevation 153 feet-0 inch by a number of reinforced concrete columns. The lateral load capacity of these columns is limited by their bending strength. Column failure was estimated to have a median pga capacity of 0.55 g for both original and reduced stiffnesses, based upon approximate calculations. This capacity is low compared with other Peach Bottom 2 structure capacities for the following reasons:

- The upper elevations of the emergency cooling tower experience significant ground motion amplification.
- The columns have relatively low resistance against lateral loads.

The column failure fragility is assumed to correspond to gross structural failure and damage to equipment located throughout the emergency cooling tower.

Turbine Building

The following components included in the systems analysis are located in Seismic Class II portions of the turbine building:

- Control rod drive water pumps.
- Instrument air compressors.

Design of Seismic Class II structures was based upon the 1967 Uniform Building Code requirements for Seismic Zone I locations. Because the components above are not Class I systems, detailed calculation of turbine building structural fragilities was judged to be unwarranted. The fragilities listed in Table A-9 were estimated and may be conservative.

Both the original and reduced stiffness structural fragilities listed in Table A-9 are typical of fragilities for similar structures at other Nuclear Power Plants. As can be seen, the effect of reduced stiffness was minor. At most, the median capacity was reduced by about 15%. This is expected to have a minor effect on the total core damage frequency due to the already high structural fragilities of vital structures (ie > 1.2g).

A.5 CORE DAMAGE AND RISK COMPUTATIONS

A.5.1 Initiating Events

The seismic analysis performed for Peach Bottom is based on the same set of event trees developed for the internal event analyses of the plant. The initiating events considered were:

- Reactor Vessel Rupture (ECCS ineffective)
- Large LOCA
- Medium LOCA
- Small LOCA
- Radwaste/Turbine Building (RWT) Failure
- Transient Type 1 (LOSP)
- Transient Type 3 (PCS initially available)

The reactor vessel rupture event was computed based on the probability of failure of the supports of the reactor vessel itself. The frequency for the large LOCA event was computed based on the failure of the supports of the recirculation pumps. Failures of the piping (steam outlet, feedwater inlet or recirculation lines) were not included as a review of their capacity showed that they were significantly higher than the pump support failures and hence, would make negligible contribution to the initiating event frequency.

The small and medium LOCA initiating events were computed based on the failure of piping in the reactor coolant loop. The fragility for the pipe failures was generated from the calculations of piping failures for pipes considered in the SSMRP Zion analysis. (In addition, transfers from the transient tree based on stuck open relief valves are considered. Two stuck open relief valves are equivalent to a medium LOCA whereas one stuck open relief valve is equivalent to a small LOCA.)

The Type 1 transient initiating event was based on the probability of loss of offsite power (LOSP). This was modeled by the fragility for the ceramic insulators in the switchyard.

The Type 3 initiating event probability is computed from the condition that the sum of the initiating event probabilities considered must be unity. The hypothesis is that, given an earthquake of reasonable size, at least one the initiating events will occur.

A.5.2 Event Trees

The event trees developed for the NUREG-1150 internal event analyses was used directly. They are repeated here for ease of subsequent discussion as Figures A-42 through A-46

The RWT building failure event identified as causing an initiator does not have a separate event tree. The accident sequences which result from this building failure were identified from the existing LOSP event tree. The failure of the RWT structure causes both loss of off-site power, loss of the control room, and failure of the cabling to the ESW and ECW pumps, which results in station blackout. In addition, loss of all actuation fails HPCI and RCIC. In this case, since both on site AC power as well as HPCI (U_1) and RCIC (U_2) are failed, four essentially identical sequences result.

$$\text{RWT-1} = T_1 CMPBU_1U_2 = \text{RWT} \quad CMP$$

$$\text{RWT-2} = T_1 CMP_1BU_1U_2 = \text{RWT} \quad CMP_1$$

$$\text{RWT-3} = T_1 CMP_2BU_1U_2 = \text{RWT} \quad CMP_2$$

$$\text{RWT-4} = T_1 CMP_3BU_1U_2 = \text{RWT} \quad CMP_3$$

These sequences differ only by the fraction of safety relief valves which fail to close (zero, one, two, or three or more), and all have early failure of HPCI and RCIC and station blackout, leading to early core damage and vulnerable containment. Although all four sequences result in early core damage with the containment being vulnerable, they were kept separate for the purposes of the containment and consequence analysis.

A.5.3 Accident Sequences

A total of 22 accident sequences survived the seismic screening process. These 22 sequences are presented in Table A-10 along with identification of the Boolean sequences that were solved for each accident sequence. (The number of Booleans solved using the SETS code is less than the number of accident sequences because several accident sequences may utilize the same Boolean expression even though the initiating event may be different.) Also identified on this table are the complement expressions which must be included in the numerical sequence quantification at high PGA levels at which success probabilities may be significantly less than unity. The multiplier expression column lists those events specified by algebraic equations rather than by Boolean logical expressions. Table A-11 describes the abbreviations used for the accident sequences in Table A-10.

The dominant accident sequences can be understood after reviewing the basic dependencies at Peach Bottom. Peach Bottom has three systems of high pressure injection (HPCI, RCIC, and CRD). Both HPCI and RCIC are steam driven and dependent only on DC battery power for actuation and control. Given failure of the high pressure injection systems, there are

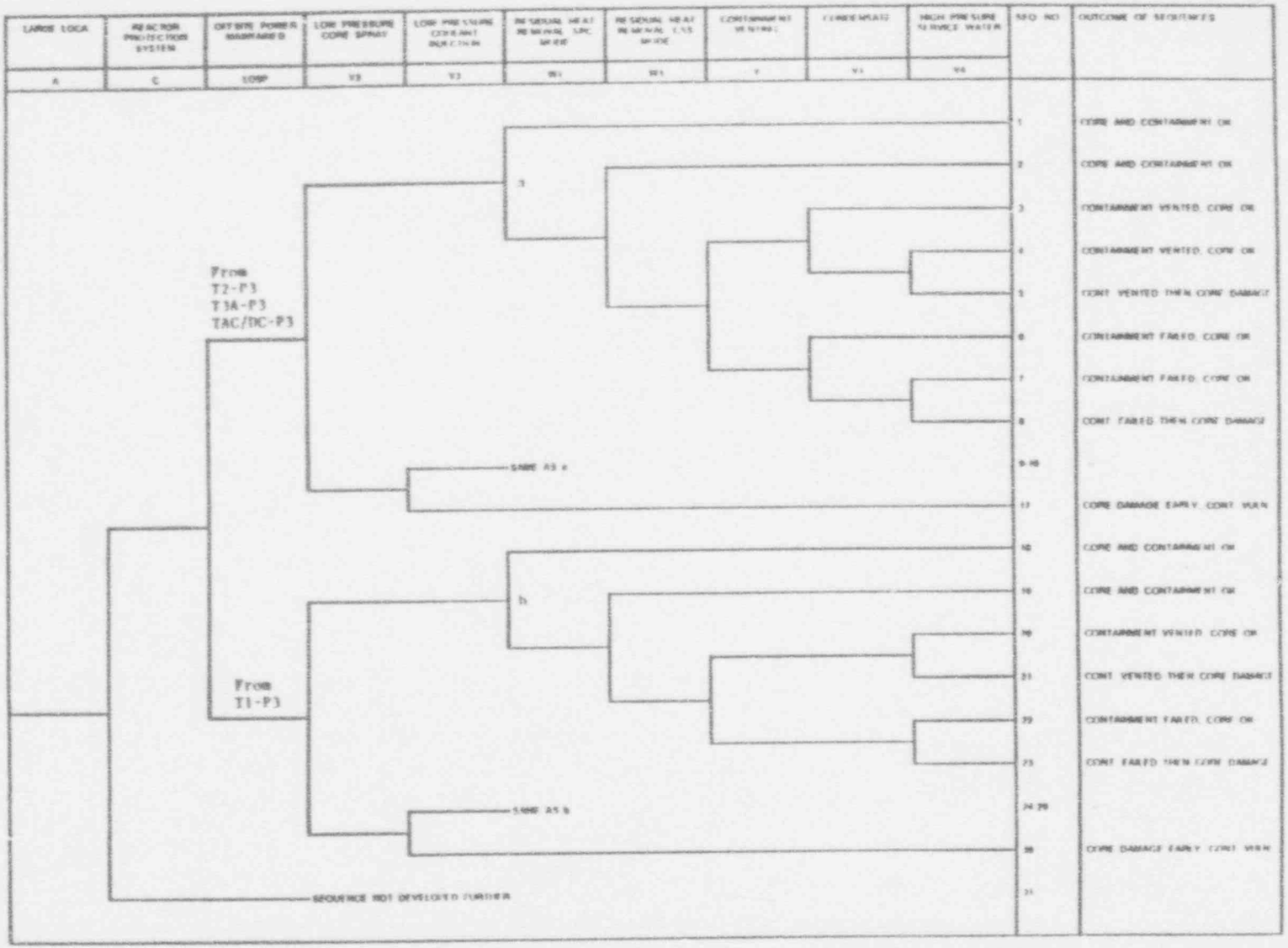

Figure A-42 Large LOCA Event Tree

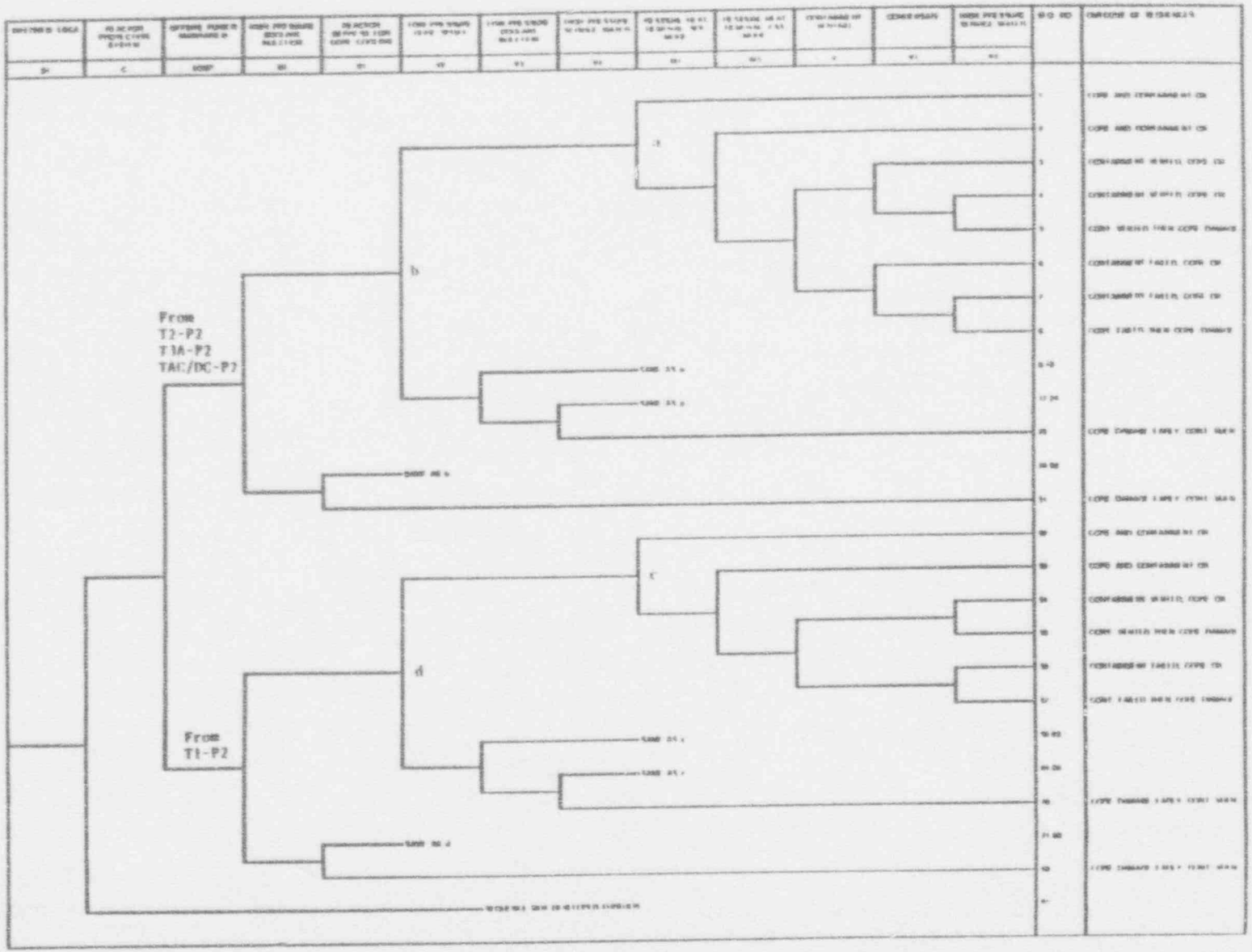

Figure A-43 Medium LOCA Event Tree

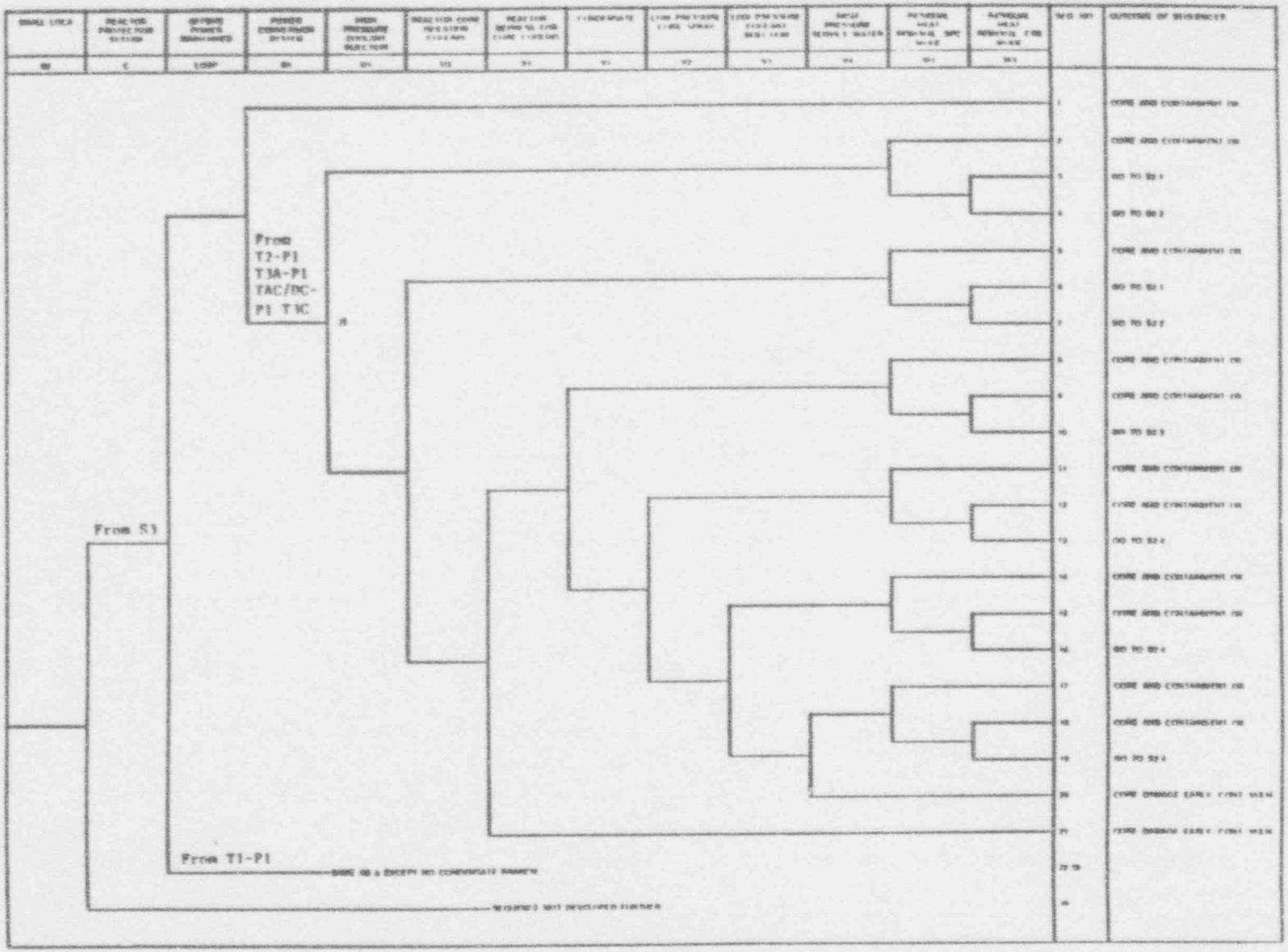

Figure A-44a Small LOCA Event Tree

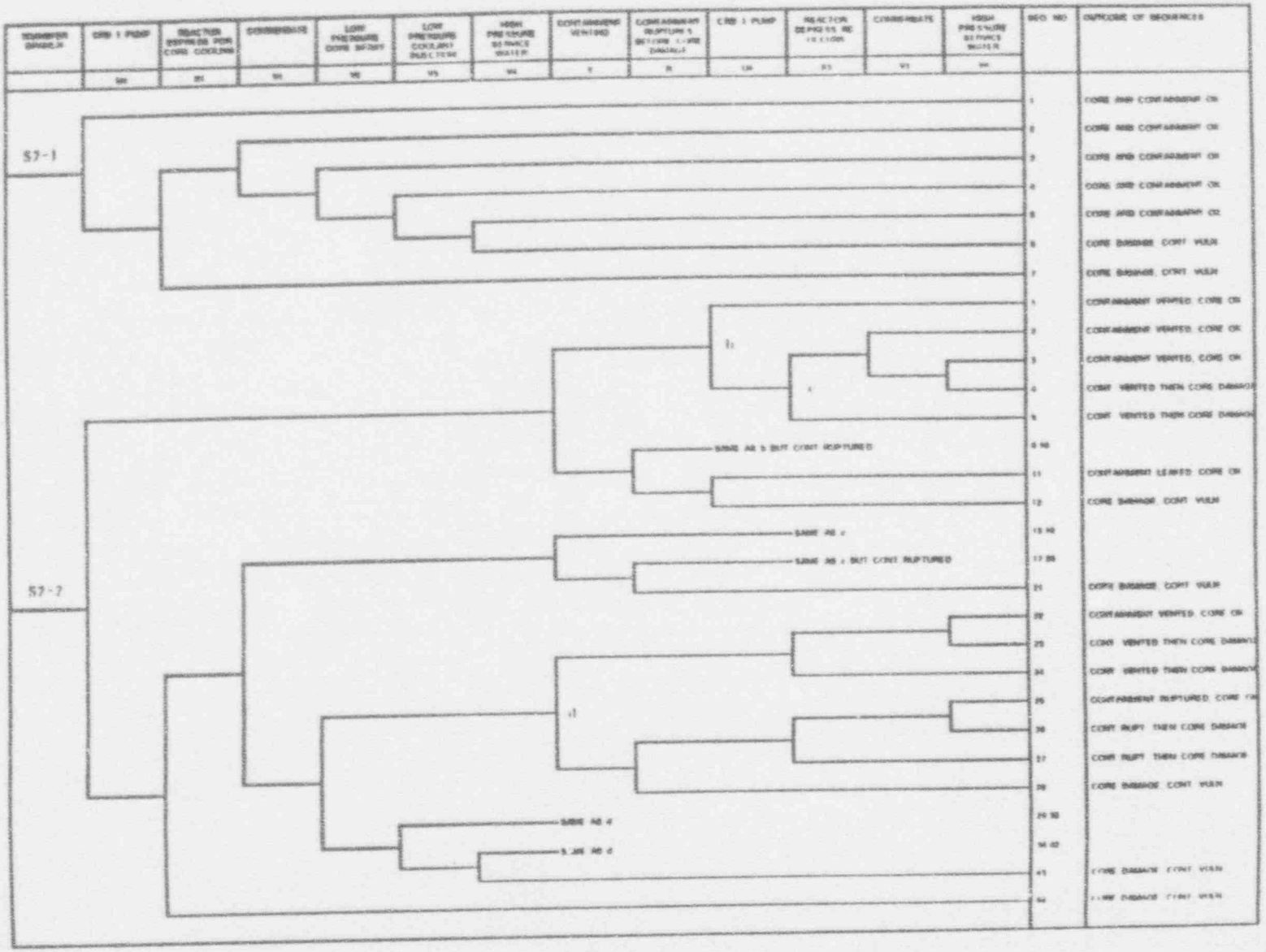

Figure A-44b Small LOCA Event Tree (cont'd)

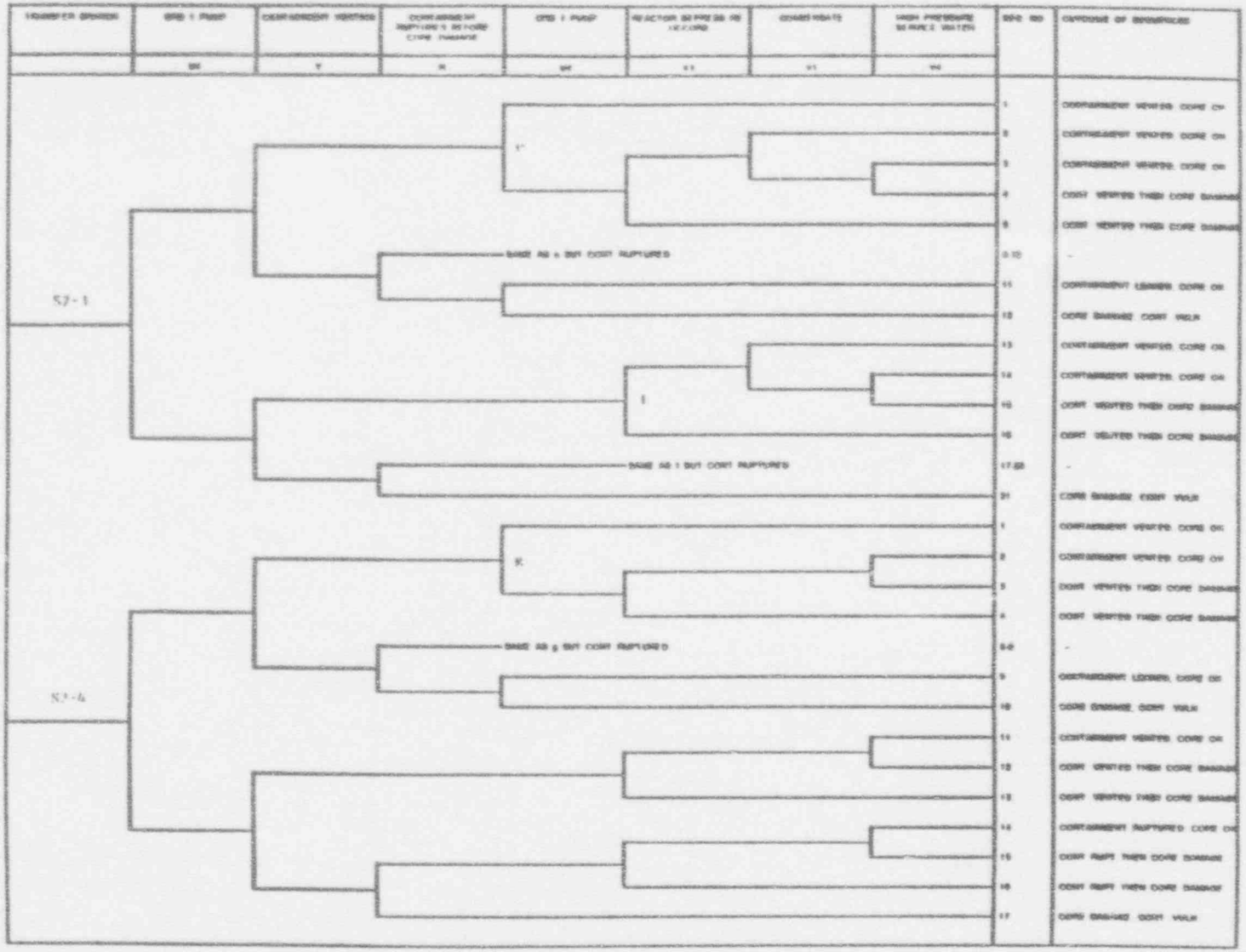

Figure A-44c Small LOCA Event Tree (cont'd)

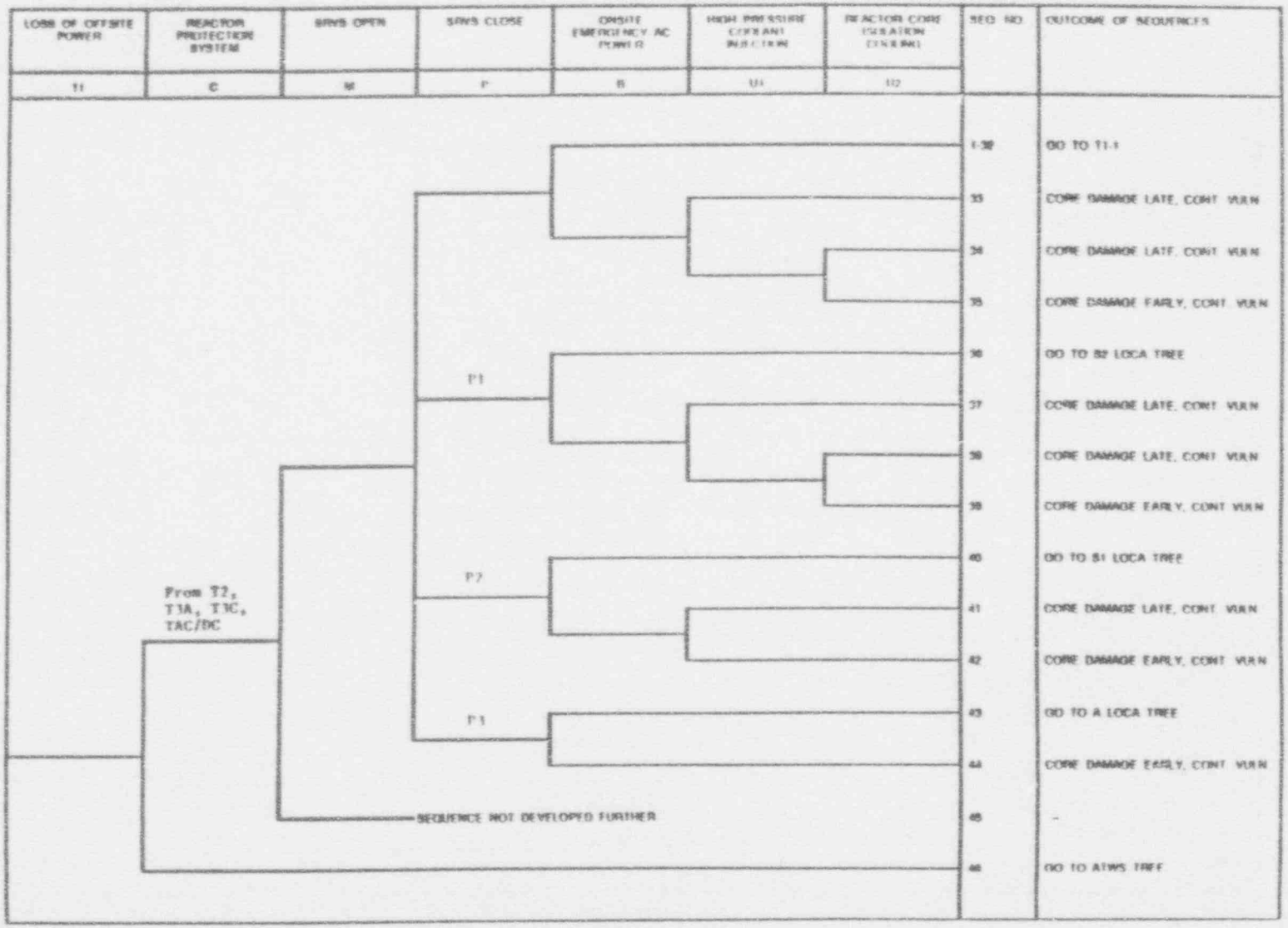

Figure A-45a T_1 (Loss of Offsite Power) Event Tree

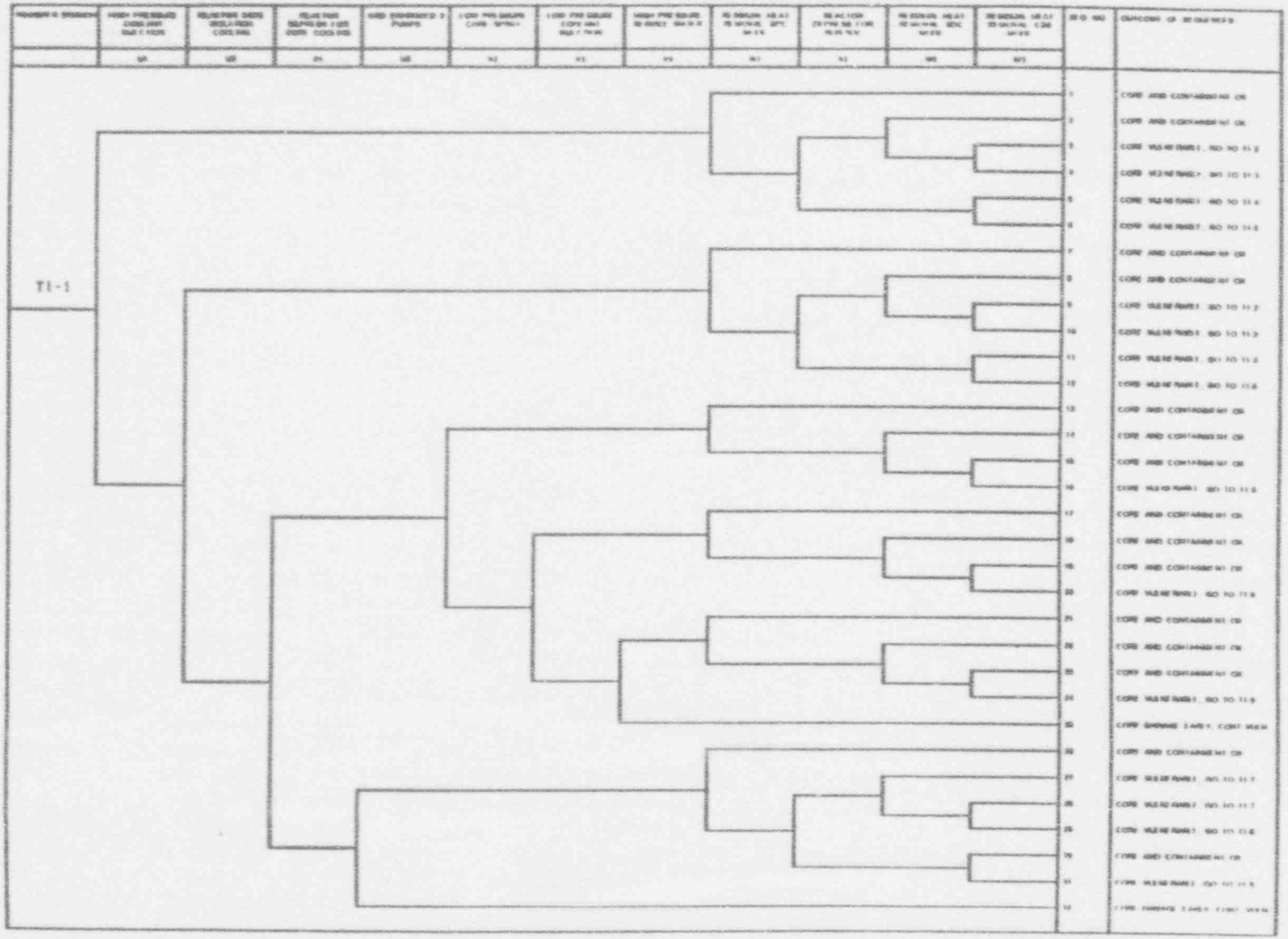

Figure A-45b T_1 (Loss of Offsite Power) Event Tree (cont'd)

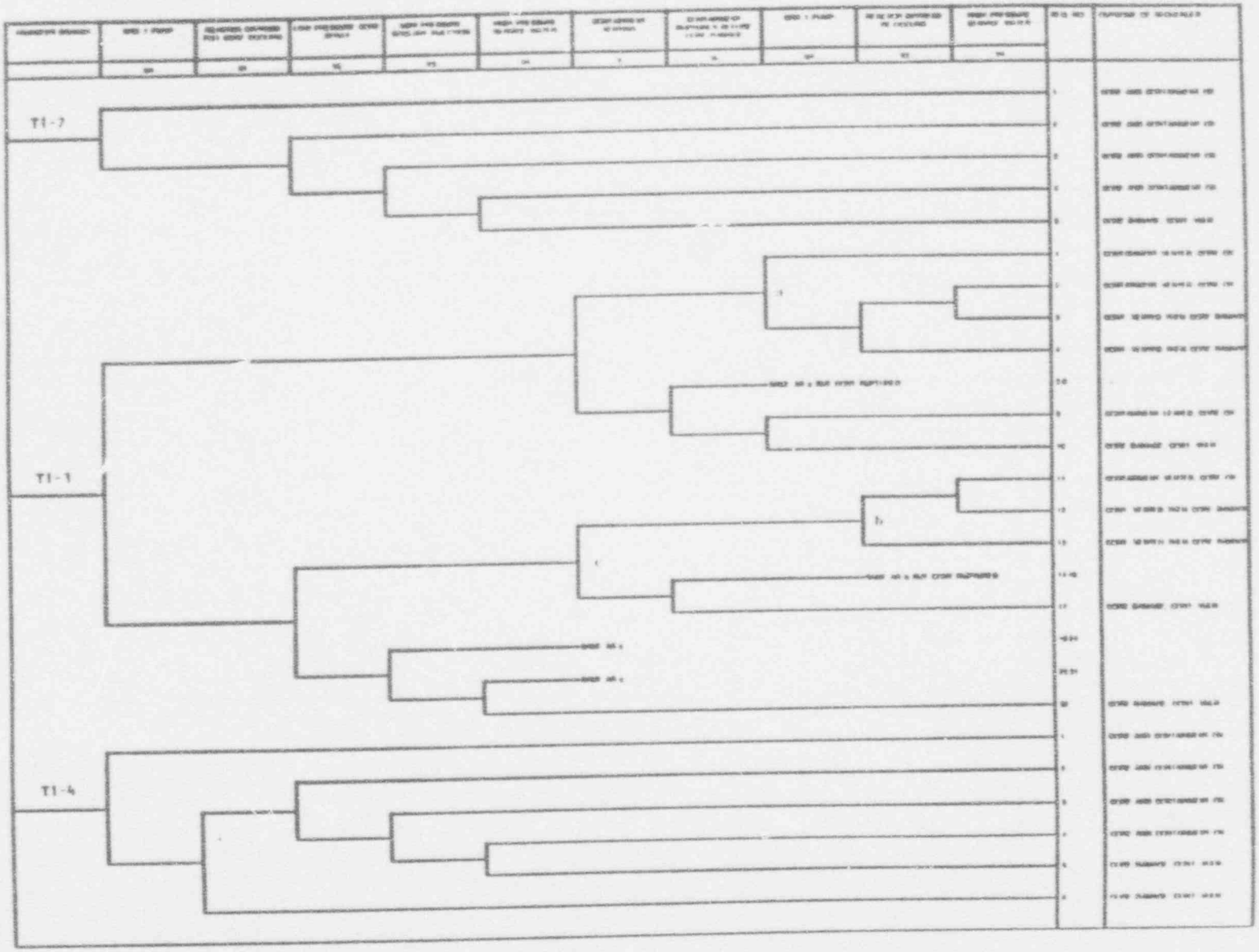

Figure A-45c T_1 (Loss of Offsite Power) Event Tree (cont'd)

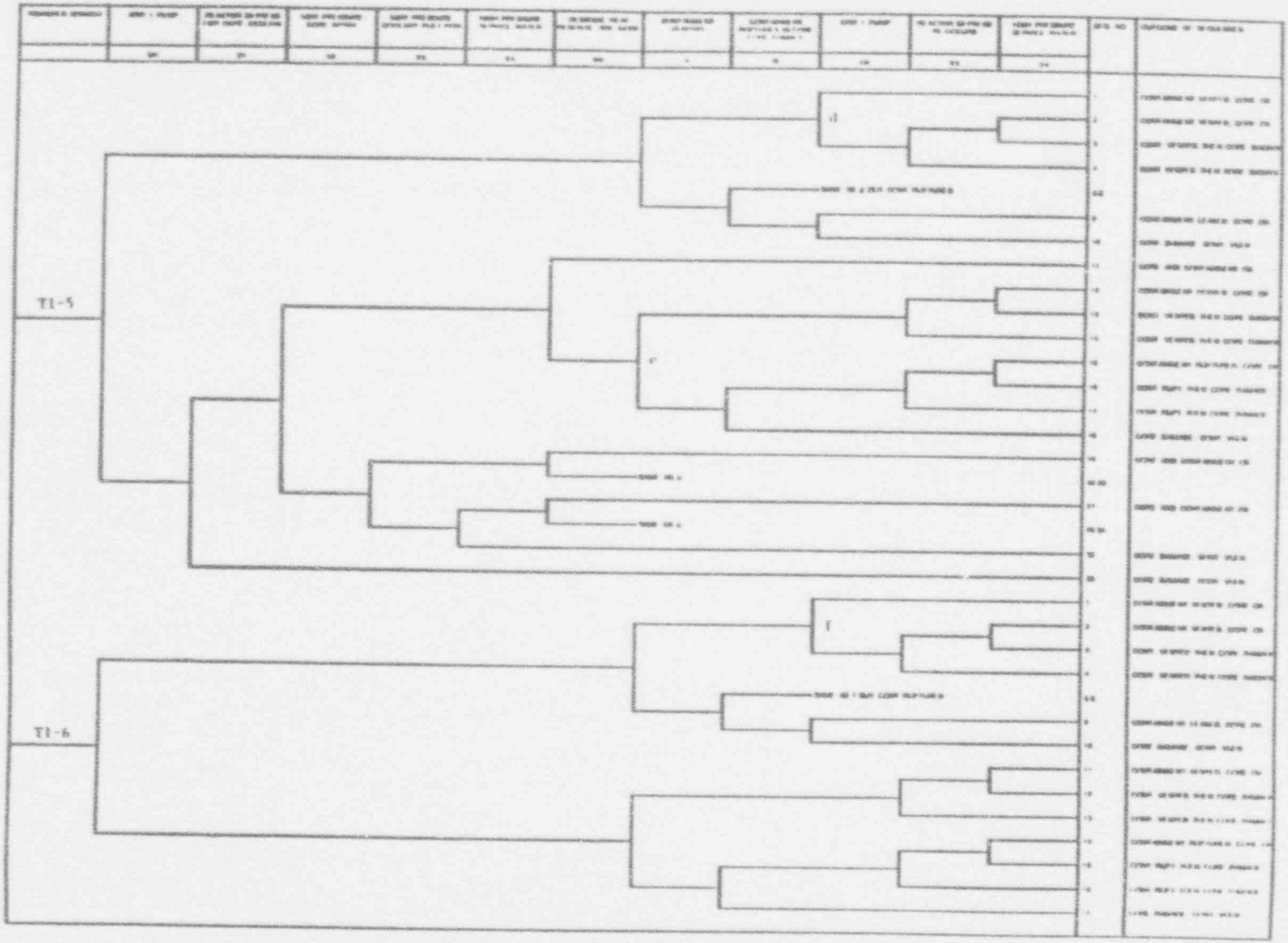

Figure A-45d T_1 (Loss of Offsite Power) Event Tree (cont'd)

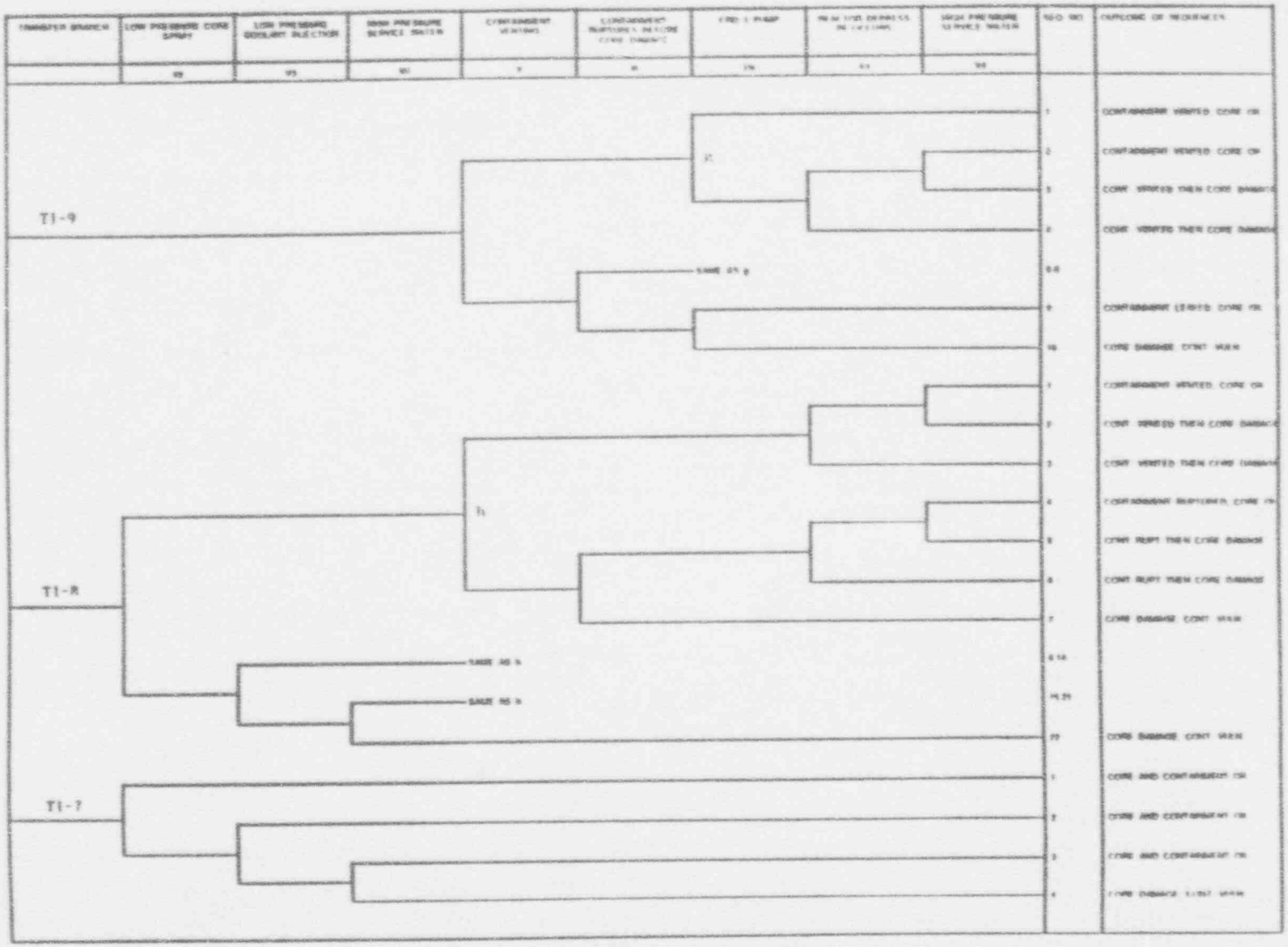

Figure A-45e T_1 (Loss of Offsite Power) Event Tree (cont'd)

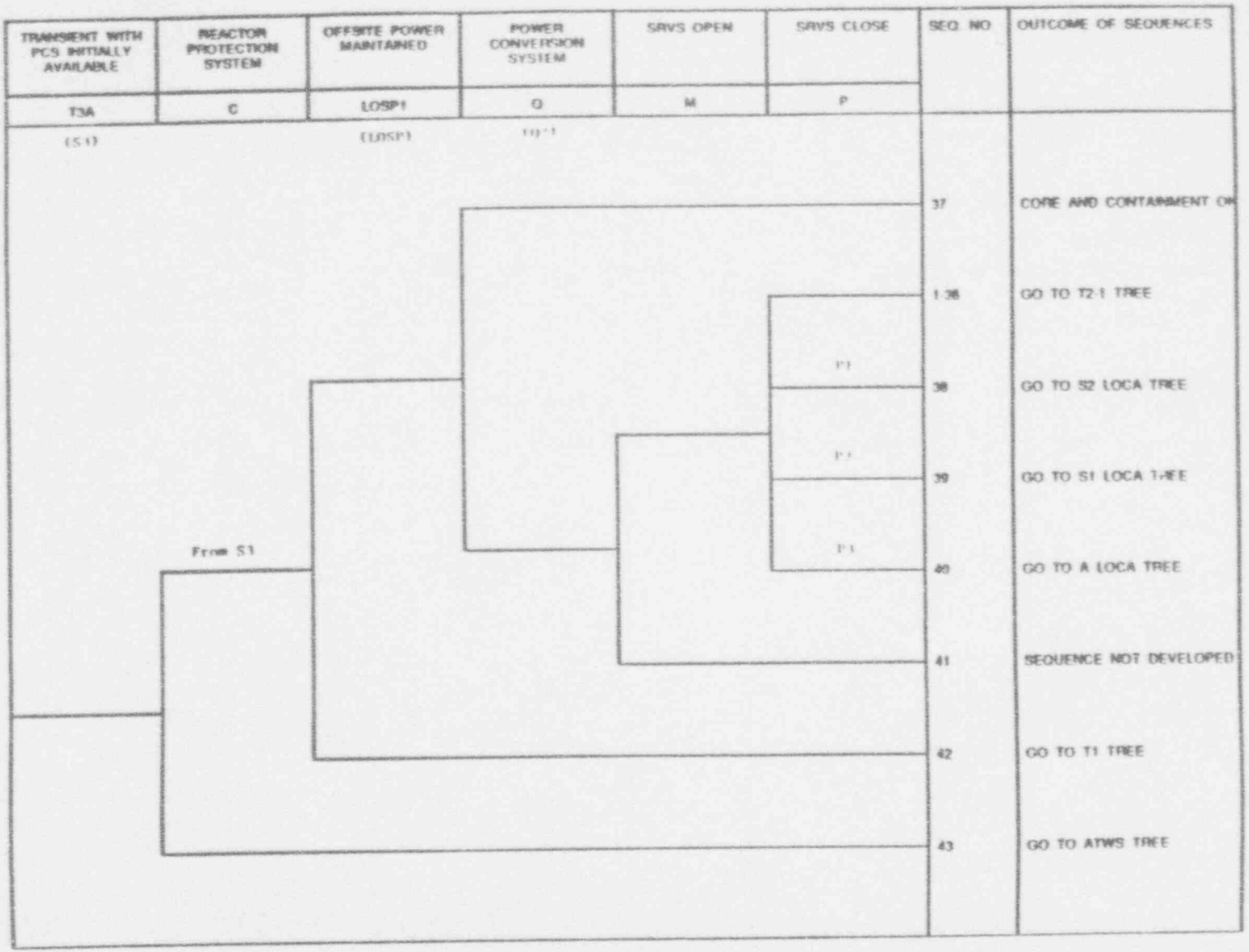

Figure A-46 T_3 (Transient - PCS initially available) Event Tree

Table A-10

Seismic Accident Sequences for Peach Bottom

	Accident Sequence		Multiplier Expression	Boolean Expression	Complement Factor
	Vessel Rupture				
1.	RVR-1		1	1	1
	Large LOCA				
2.	ALOCA-17	$A\ \bar{C}\ \overline{LOSP}\ V_2V_3$	1	BOOL 5	$\bar{C}\ \overline{LOSP}$
3.	ALOCA-30	$A\ \bar{C}\ LOSP\ V_2V_3$	1	POOL 4 + RWT	$\bar{C}$
	Intermediate LOCA				
4.	S1-LOCA-25	$S_1\ \bar{C}\ \overline{LOSP}\ \bar{U}_1\ V_2V_3V_4$	1	BOOL 6	$\bar{C}\ \bar{U}_1\ \overline{LOSP}$
5.	S1-LOCA-70	$S_1\ \bar{C}\ LOSP\ \bar{U}_1\ V_2V_3V_4$	1	BOOL 4	$\bar{C}\ \bar{U}_1$
6.	S1-LOCA-80	$S_1\ \bar{C}\ LOSP\ U_1\ X_1$	1	RWT	$\bar{C}$
	Small LOCA				
7.	S2-LOCA-2-44	$S_2\ \bar{C}\ \overline{LOSP}\ Q_1\bar{U}_1W_1W_3U_4X_1$	1	BOOL 7	$\bar{C}\ \bar{U}_1\ \overline{LOSP}$
8.	S2-LOCA-42	$S_2\ \bar{C}\ LOSP\ U_1U_2X_1$	1	RWT	$\bar{C}$
	Radwaste/Turbine Building				
9.	RWT-1	$RWT\ \overline{CMP}\ B\ U_1U_2$	1	1	$\overline{CMP}$
10.	RWT-2	$RWT\ \overline{CMP}_1\ B\ U_1U_2$	1	1	$\overline{CMP}_1$
11.	RWT-3	$RWT\ \overline{CMP}_2\ B\ U_1U_2$	1	1	$\overline{CMP}_2$
12.	RWT-4	$RWT\ \overline{CMP}_3\ B\ U_1U_2$	1	1	$\overline{CMP}_3$
	LOSP Transient				
13.	T1-25	$T_1\overline{CMPB}\ U_1U_2\bar{X}_1V_2V_3V_4$	1	$\bar{B}U_1U_2X_1V_2V_3V_4$	$\overline{CMPB}\ \bar{X}_1$
14.	T1-25	$T_1\overline{CMPB}\ U_1U_2X_1U_3$	1	$\bar{B}U_1U_2X_1U_3$	$\overline{CMBP}$
15.	T1-33	$T_1\overline{CMPB}\ \bar{U}_1$	1	$B\bar{U}_1$ = BOOL 4	$\overline{CMP}\ \bar{U}_1$
16.	T1-36 to S2-41	$T_1\overline{CMP}_1\bar{B}\ U_1U_2\bar{X}_1V_2V_3V_4$	P_1	$\bar{B}U_1U_2X_1V_2V_2V_3$	$\overline{CM}\ \bar{B}\ \bar{X}_1$
17.	T1-36 to S2-42	$T_1\overline{CMP}_1\bar{B}\ U_1U_2X_1$	P_1	$\bar{B}U_1U_2X_1$	$\overline{CM}\ \bar{B}$
18.	T1-40 to S1-70	$T_1\overline{CMP}_2\bar{B}\ \bar{U}_1\bar{X}_1V_2V_3V_4$	P_2	$\bar{B}\bar{U}_1\bar{X}_1V_2V_3V_4$	$\overline{CM}\ \bar{B}\ \bar{U}_1\ \bar{X}_1$
19.	T1-40 to S1-80	$T_1\overline{CMP}_2\bar{B}\ U_1X_1$	P_2	$\bar{B}U_1X_1$	$\overline{CM}\ \bar{B}$
20.	T1-43 to ALOCA-30	$T_1\overline{CMP}_3\bar{B}\ V_2V_3$	P_3	$\bar{B}V_2V_3$	$\overline{CM}\ \bar{B}$
	Transient with PCS Initially Available				
21.	T3A-1 TO T2-1-29	$T_{3A}\ \bar{C}\ \overline{LOSP}\ Q_R\ \overline{MP}\ U_1U_2X_1U_3$	Q_R	$U_1U_2X_1U_3$	$\bar{C}\ \overline{LOSP}\ \overline{MP}$
22.	T3A-1 to T2-1-36	$T_{3A}\ \bar{C}\ \overline{LOSP}\ Q_R\ \overline{MP}\ U_1U_2\bar{X}_1V_1V_2V_3V_4$	Q_R	$U_1U_2X_1V_1V_2V_3V_4$	$\bar{C}\ \overline{LOSP}\ \overline{MP}\ \bar{X}_1$

Table A-11

Safety Systems Nomenclature

ARI	-	Failure of the Alternate Rod Insertion Systems
B	-	Failure of all AC power (station blackout)
C	-	Failure of the Reactor Protection System (RPS)
C1	-	Failure of the RPS ans manual scram
I	-	Failure to inhibit the ADS system
L	-	Failure of operator to isolate S3 "leak"
LOSP, LOSP1	-	Failure to maintain offsite power; Different Designations for this Event are for different frequencies
M	-	Failure of Safety Relief Valves (SRVs) to open
P	-	Failure of SRVs to close
P1, P2, P3	-	Failure of one, two of three SRVs to reclose
Q, Q1, Q2	-	Failure of the Power Conversion System (PSC), different designations for this event are for different frequencies
R	-	Rupture of the containment
ROD	-	Failure to manually insert control rods
RPSM	-	Failure of the mechanical RPS
RPSE	-	Failure of the electrical RPS
RPT	-	Failure to trip the recirculation pumps
SCRM	-	Failure to manually scram the reactor
SLC	-	Failure of the Standby Liquid Control System
U1	-	Failure of the High Pressure Coolant Injection (HPCI) system
U1'	-	Failure of the HPCI without ventilation
U2	-	Failure of the Reactor Core Isolation Cooling (RCIC) system
U2'	-	Failure of the RCIC without recirculation
U3	-	Failure of the Control Rod Drive (CRD) system (2 pump mode)
U4	-	Failure of the CRD system (1 pump mode)
U4'	-	Failure of the CRD to survive containment venting
V1	-	Failure of the Condensate system
V1'	-	Failure of the Condensate system to to survive containment venting
V2	-	Failure of the Low Pressure Core Spray (LPCS) system
V3	-	Failure of the Low Pressure Coolant Injection (LPCI) system
V4	-	Failure of the High Pressure Service Water (HPSW) system as an injection source to the reactor
V4'	-	Failure of HPSW (injection source) to survive containment venting
W1	-	Failure of the Suppression Pool Cooling (SPC) mode of RHR
W2	-	Failure of the Shutdown Cooling (SDC) mode of the RHR
W3	-	Failure of the Containment Spray (CS) mode of RHR
X1	-	Failure to depressurize the primary system via SRVs of the Automatic Depressurization System (ADS)
X2	-	Failure to depressurize the primary system to allow SDC to operate
X3	-	Failure to depressurize the primary system subsequent to an initial primary system depressurization
Y	-	Failure of Primary Containment Venting System (including makeup to the pool as required)

both manual and automatic means of depressurizing the system. There are then four potential means of cooling the core at low pressure (condensate, LPCS, LPCI, and via the HPSW systems). The low pressure systems all require AC motive power.

Peach Bottom has four diesel generators (shared) and four station batteries (per unit) and thus, a high degree of redundancy is available in the on site AC power system. The diesel generators, however, are dependent on the emergency service water system for cooling. Loss of this cooling is assumed to result in early failure of the diesel generators.

Successful operation of any one of the three pumps (two ESW and one ECW) will provide the necessary cooling to all four diesel generators as well as all emergency room cooling and all emergency pump cooling. Thus, failure of these three pumps together would result in loss of all diesels as well as loss of all room and emergency pump cooling. ESW pump A takes power from diesel generator B while ESW pump B takes power from diesel generator C. Lastly, the ECW pump takes AC power from diesel generator D. Thus, any appropriate combination of electrical bus failure, diesel generator failure, and emergency cooling water pump failure will result in loss of all three diesels and in conjunction with loss of offsite power, will result in station blackout. In addition, failure of the turbine building is assumed to fail the power and control cables to the ECW pump and thus constitutes a means of failing one of the three pumps. These dependencies result in the vast majority of the cutsets computed in the dominant sequences for Peach Bottom as described below.

Sequence T_1-33 is a LOSP transient in which onsite power (B) fails but the HPCI system (U1) succeeds. Thus, the high pressure injection system succeeds initially and will continue functioning until battery depletion occurs or until the HPCI and RCIC pumps fail due to loss of room cooling. Thus the sequence involves station blackout (SBO) and late core damage with the containment being vulnerable. The dominant cutsets are given in Bool(4) and all cutsets constitute the failure of the ESW system. Note that the failure of the ESW system also fails the low pressure systems LPCI and LPCS.

Sequence ALOCA-30 is a large loss of coolant break in conjunction with LOSP and loss of the low pressure LPCI and LPCS systems. The surviving cutsets in this sequence are again due to Bool(4) each of which causes a failure of the emergency service water cooling which fails the diesels. Hence, this is a large LOCA in conjunction with station blackout. Note that the Radwaste-Turbine Building also makes a contribution to this sequence. Dominant cutsets are all failures of the ESW system, which with LOSP, results in station blackout. Hence, the low pressure injection systems are without power. The result is SBO, early core damage with a vulnerable containment.

Sequence S1 LOCA-80 is an intermediate break LOCA in conjunction with loss of offsite power, failure of HPCI, and failure to depressurize the system (X_1). The logical cutset causing immediate failure of HPCI and X_1 is the Radwaste/Turbine Building failure. Failure to depressurize results from

the station blackout situation. The result is SBO, early core damage and a vulnerable containment.

Sequence S2 LOCA-42 is a small break LOCA in conjunction with loss of offsite power and immediate failures of both HPCI and RCIC high pressure systems as well as failure to depressurize due to the RWT failure. The result is SBO, early core damage and containment vulnerability.

Sequence RWT-1 is a transient sequence brought about by the failure of the Radwaste/Turbine Building as an initiator. Both HPCI and RCIC high pressure injection systems fail due to the loss of actuation and control. The result is a station blackout with no high pressure injection leading to early core damage and vulnerable containment.

Sequence S1 LOCA-70 is an intermediate break LOCA with loss of offsite power. In this case, HPCI succeeds long enough until the system is depressurized to the point where low pressure injection could be utilized. However, since a station blackout situation exists there is no motive power for any of the low pressure injection systems. The result is station blackout, early core damage, and a vulnerable containment.

Sequence S1 LOCA-25 is an intermediate break LOCA but with offsite power available. The high pressure coolant injection system (HPCI) succeeds until the system depressurizes. All cutsets result in failures to the ESW system which fail the pump cooling to the LPCS and LPCI systems. The high pressure service water system (V_4) fails due to failure of the 4Kv Bus C which results in inability to open injection valves 176 and 173. The result is early core damage and a vulnerable containment.

Sequence S2 LOCA-2-44 is a small LOCA break for which offsite power is maintained. All cutsets in this sequence involve failure of the ESW system and failure of the turbine building. Failure of the Turbine Building results in failure of PCS, the instrument air system and the emergency cooling water pump. Systems W1, W3, and U4 fail due to loss of the ESW system which results in loss of pump cooling. Both automatic and manual depressurization fails. The manual depressurization system fails due to loss of instrument air caused by the Turbine Building failure. The automatic depressurization fails because the LPCI and LPCS pumps have failed due to lack of cooling. Thus, the reactor is at high pressure and cannot be depressurized, and the situation continues until the HPCI pump fails due to lack of room cooling. The CRD pump (U_4) failed shortly after demand due to lack of pump cooling. Heat removal from the suppression pool (W_1) and heat removal from the containment (W_3) are not available due to pump failures resulting from lack of pump cooling. The result is a delayed core damage situation in which the reactor remains at high pressure and cannot be depressurized and for which the containment is vulnerable due to lack of containment and suppression pool cooling.

A.5.4 Accident Sequence Quantification

To evaluate the effect of including degraded shear wall stiffnesses in the seismic PRA of Peach Bottom, the accident sequences described above were quantified both with and without the stiffness reduction. In each case a complete uncertainty analysis was performed on the dominant accident sequences (and on the dominant cut sets in each accident sequence) as determined in the point estimate evaluations. Thus, the expression for the unconditional accident sequence frequencies (and for core damage frequency), shown as below:

$$ACC_j = \int P(ACC_j, PGA) f_{eq}(PGA) d(PGA)$$

where

$P(ACC_j, PGA)$ is the conditional accident sequence frequency as a function of PGA, and

$f_{eq}(PGA)$ is the probability distribution function for the hazard curve,

was randomly sampled varying the hazard curve parameters, the random failure frequencies, and the seismic response and fragility parameters. From the accumulated values of accident sequence frequency and core damage frequency, exact statistics on their distributions are directly obtainable. The result is an estimate of the mean annual frequency of each accident sequence as well as of the total core damage plus a description of the distributions associated with these estimates.

In addition, a mean point estimate quantification (for which all random parameters were set to their mean values and a single quantification) was made for each case. This allows for an efficient evaluation of each individual component's importance to the total core damage frequency and a determination of the relative contribution of different earthquake levels to the total. (Experience has shown that such mean point estimate calculations yield results which are very close to the actual mean results obtained from the full uncertainty analysis.)

A.5.4.1 Core Damage Frequency Results Without Stiffness Reduction

The 22 accident sequences shown above, were fully quantified using component random failures and the seismic fragilities and responses plus associated random and systematic variabilities. Based on this final quantification, five dominant sequences were identified. These dominant sequences are (in order of importance):

	LLNL	EPRI
T1-33	51%	53%
ALOCA-30	23%	22%
RVR-1	16%	14%
S1LOCA-70	6%	6%
RWT-1	2%	3%

The percentage contributions were taken from the Monte Carlo uncertainty results. The total mean core damage frequency for the Peach Bottom base case was computed to be 6.71E-5 per year using the LLNL seismic hazard curves and 2.77E-6 per year using the EPRI hazard curves. The relative contributions of the accident sequences are shown in Table A-12. Table A-13 shows the various percentiles of distribution from the Monte Carlo analysis for both sets of hazard curves. Relative importance of the basic events to these results are presented in the point estimate results presented below.

Mean Point Estimate

The mean point estimate is based on using the mean values for all variables. Table A-14 presents the mean core damage contributions at seven intervals over the LLNL hazard curve for each accident sequence. Table A-15 presents the mean core damage contributions for the EPRI hazard curve. The right hand column presents the total contribution of each accident sequence to the total core damage frequency of 7.90E-5 for the LLNL hazard curves and 2.67E-6 for the EPRI hazard curves. As can be seen, the incremental contributions from the LOCA events do not become significant until the higher acceleration levels. The reactor vessel rupture sequence does not make a significant contribution until the highest PGA increment.

An important thing to note from Table A-14 is the sum of the accident sequence contributions at each earthquake level, as shown at the bottom of each column on the table. The contributions are seen to be small at the first increment, increasing to a maximum at the forth earthquake increment, and then decreasing at higher earthquake levels. This indicates that the bulk of the risk is occurring in the range of 0.45 g to 0.90 g which roughly corresponds to the range of 4-7 SSE. Further, this shows that the bulk of the risk has been captured by integrating over the range 0.15 g to 1.20 g.

Basic Event Importance

The importance of the basic seismic failure events was evaluated by setting the seismic failure probability to zero in the mean point estimate calculation, which gives a measure of the net reduction in core damage frequency that would occur if that component could never fail due to seismic shaking.

Results of these calculations for both sets of hazard curves are shown in Table A-16. It can be seen that the largest reduction occurs for ceramic insulators. This occurs, of course, because the ceramic insulators are the basis for the loss of off site power and all the T_1 transient sequences. The ESW and ECW pumps have a risk reduction potential of about 30 percent. This reduction potential is large because these pumps provide all the emergency service water cooling to the diesel generators, to all the room cooling (except the diesel generator enclosures) and all emergency pump cooling. The Turbine Building has a significant risk

Table A-12

Accident Sequence and Total Core Damage Mean Frequencies
for Peach Bottom with Original Stiffnesses
(Monte Carlo Uncertainty Analysis)

		Mean Frequency (per year)	
Accident Sequence		LLNL Hazard	EPRI Hazard
1	RVR-1	1.05E-5	3.90E-7
2	ALOCA-17	1.28E-7	5.83E-9
3	ALOCA-30	1.57E-5	5.97E-7
4	S1LOCA-25	5.03E-9	3.01E-10
5	S1LOCA-70	4.29E-6	1.70E-7
6	S1LOCA-80	2.71E-7	1.19E-8
7	S2LOCA-21	9.29E-8	5.29E-9
8	S2LOCA-42	5.05E-7	2.43E-8
9	RWT-1	1.28E-6	7.70E-8
10	RWT-2	1.36E-7	8.20E-9
11	RWT-3	2.84E-9	1.71E-10
12	RWT-4	2.84E-10	1.71E-11
13	T1-25	5.30E-8	2.69E-9
14	T1-32	3.53E-11	1.82E-12
15	T1-33	3.40E-5	1.47E-6
16	T1-36 to S2-41	5.09E-9	2.58E-10
17	T1-36 to S2-42	3.38E-12	1.73E-13
18	T1-40 to S1-70	6.02E-11	2.77E-12
19	T1-40 to S1-80	1.46E-13	8.17E-15
20	T1-43 to ALOCA-30	2.69E-7	9.09E-9
21	T3A-1 to T2-1-29	1.67E-10	1.25E-11
22	[illegible] to [illegible]-1-36	6.03E-11	4.00E-12
	TOTAL	6.71E-5	2.77E-6

Table A-13

Accident Sequence Frequency Distribution Percentiles
for Peach Bottom with Original Stiffnesses
(Monte Carlo Uncertainty Analysis)

	LLNL Hazard	EPRI Hazard
Mean	6.71E-5	2.77E-6
Var	1.20E-7	6.63E-11
5%	4.15E-8	1.82E-8
50%	3.91E-6	6.12E-7
95%	2.46E-4	1.11E-5

Table A-14

Total Accident Sequence Frequency Increments
LLNL Seismic Hazard Curves for Peach Bottom with Original Stiffnesses
(Mean Point Estimate Calculation)

	0.15-0.30g	0.30-0.45g	0.45-0.60g	0.60-0.75g	0.75-0.90g	0.90-1.05g	1.05-1.20g	TOTAL
1	7.2E-08	6.9E-07	1.7E-06	2.5E-06	2.8E-06	2.7E-06	2.4E-06	1.3E-05
2	6.4E-10	3.7E-08	1.0E-07	8.2E-08	3.6E-08	1.1E-08	2.9E-09	2.7E-07
3	9.0E-10	2.7E-07	3.1E-06	6.9E-06	6.0E-06	3.8E-06	2.3E-06	2.2E-05
4	1.5E-12	5.0E-10	3.6E-09	5.3E-09	3.5E-09	1.4E-09	4.7E-10	1.5E-08
5	1.2E-10	5.4E-08	7.7E-07	1.8E-06	1.6E-06	9.7E-07	5.4E-07	5.7E-06
6	7.4E-12	2.9E-09	3.6E-08	1.1E-07	1.8E-07	2.0E-07	1.6E-07	7.0E-07
7	6.9E-10	3.5E-08	7.6E-08	4.8E-08	1.6E-08	3.9E-09	8.1E-10	1.8E-07
8	8.8E-11	1.7E-08	1.4E-07	3.1E-07	3.8E-07	3.1E-07	2.1E-07	1.4E-06
9	1.7E-08	2.6E-07	6.4E-07	7.1E-07	5.0E-07	2.7E-07	1.3E-07	2.5E-06
10	1.8E-09	2.8E-08	6.8E-08	7.6E-08	5.4E-08	2.9E-08	1.3E-08	2.7E-07
11	3.7E-11	5.8E-10	1.4E-09	1.6E-09	1.1E-09	6.1E-10	2.8E-10	5.6E-09
12	3.7E-12	5.8E-11	1.4E-10	1.6E-10	1.1E-10	6.1E-11	2.8E-11	5.6E-10
13	1.2E-11	7.3E-10	3.8E-09	6.9E-09	7.0E-09	4.9E-09	2.7E-09	2.6E-08
14	1.2E-12	8.1E-12	1.7E-11	1.9E-11	1.3E-11	7.1E-12	3.1E-12	6.9E-11
15	1.1E-07	3.8E-06	1.3E-05	1.1E-05	3.9E-06	1.1E-06	2.9E-07	3.2E-05
16	1.1E-12	7.0E-11	3.6E-10	6.6E-10	6.7E-10	4.7E-10	2.6E-10	2.5E-09
17	1.0E-13	7.3E-13	1.6E-12	1.8E-12	1.3E-12	7.1E-13	3.1E-13	6.6E-12
18	7.1E-15	1.8E-13	2.5E-12	1.0E-11	1.8E-11	1.8E-11	1.3E-11	6.3E-11
19	1.5E-14	7.0E-14	9.2E-14	7.2E-14	4.1E-14	1.8E-14	7.2E-15	3.1E-13
20	1.8E-13	2.1E-11	8.7E-10	9.3E-09	3.8E-08	8.7E-08	1.4E-07	2.7E-07
21	4.7E-12	1.1E-10	2.4E-10	1.5E-10	5.1E-11	1.1E-11	1.9E-12	5.7E-10
22	1.1E-12	3.6E-11	8.9E-11	6.8E-11	2.7E-11	7.1E-12	1.4E-12	2.3E-10
	2.0E-07	5.2E-06	1.9E-05	2.3E-05	1.6E-05	9.5E-06	6.2E-06	7.90E-05

Table A-15

Total Accident Sequence Frequency Increments
EPRI Seismic Hazard Curves for Peach Bottom with Original Stiffnesses
(Mean Point Estimate Calculation)

	0.15-0.30g	0.30-0.45g	0.45-0.60g	0.60-0.75g	0.75-0.90g	0.90-1.05g	1.05-1.20g	TOTAL
1	4.8E-09	3.3E-08	6.7E-08	8.6E-08	8.8E-08	6.1E-08	6.7E-08	4.1E-07
2	4.3E-11	1.8E-09	3.9E-09	2.8E-09	1.1E-09	2.5E-10	8.2E-11	1.0E-08
3	6.0E-11	1.3E-08	1.2E-07	2.3E-07	1.9E-07	8.6E-08	6.4E-08	7.1E-07
4	9.8E-14	2.4E-11	1.4E-10	1.8E-10	1.1E-10	3.3E-11	1.3E-11	5.0E-10
5	7.9E-12	2.6E-09	3.0E-08	6.2E-08	5.0E-08	2.2E-08	1.5E-08	1.8E-07
6	5.0E-13	1.4E-10	1.4E-09	3.9E-09	5.7E-09	4.4E-09	4.6E-09	2.0E-08
7	4.6E-11	1.7E-09	3.0E-09	1.6E-09	5.0E-10	8.8E-11	2.3E-11	6.9E-09
8	5.9E-12	8.2E-10	5.3E-09	1.1E-08	1.2E-08	7.1E-09	5.9E-09	4.2E-08
9	1.1E-09	1.2E-08	2.5E-08	2.4E-08	1.6E-08	6.2E-09	3.5E-09	8.8E-08
10	1.2E-10	1.3E-09	2.7E-09	2.6E-09	1.7E-09	6.6E-10	3.8E-10	9.4E-09
11	2.5E-12	2.8E-11	5.5E-11	5.4E-11	3.5E-11	1.4E-11	7.9E-12	2.0E-10
12	2.5E-13	2.8E-12	5.5E-12	5.4E-12	3.5E-12	1.4E-12	7.9E-13	2.0E-11
13	7.8E-13	3.5E-11	1.5E-10	2.3E-10	2.2E-10	1.1E-10	7.6E-11	8.2E-10
14	7.9E-14	3.9E-13	6.6E-13	6.4E-13	4.2E-13	1.6E-13	8.7E-14	2.4E-12
15	7.4E-09	1.8E-07	4.9E-07	3.6E-07	1.2E-07	2.4E-08	8.0E-09	1.2E-06
16	7.5E-14	3.3E-12	1.4E-11	2.2E-11	2.1E-11	1.1E-11	7.3E-12	7.9E-11
17	6.8E-15	3.5E-14	6.3E-14	6.3E-14	4.1E-14	1.6E-14	8.7E-15	2.3E-13
18	4.7E-16	8.6E-15	9.6E-14	3.6E-13	5.7E-13	4.1E-13	3.6E-13	1.8E-12
19	9.8E-16	3.3E-15	3.6E-15	2.4E-15	1.3E-15	4.1E-16	2.0E-16	1.2E-14
20	1.2E-14	9.8E-13	3.4E-11	3.2E-10	1.2E-09	2.0E-09	3.8E-09	7.3E-09
21	3.1E-13	5.2E-12	9.4E-12	5.3E-12	1.6E-12	2.5E-13	5.3E-14	2.2E-11
22	7.2E-14	1.7E-12	3.5E-12	2.3E-12	8.5E-13	1.6E-13	4.0E-14	8.6E-12
	1.4E-08	2.5E-07	7.5E-07	7.9E-07	4.8E-07	2.1E-07	1.7E-07	2.67E-06

Table A-16

Dominant Component Contributions to Mean Core Damage at Peach Bottom Frequency Ranked by Risk Reduction Potential

Component	Percent Reduction if not Failed	
	LLNL Hazard	EPRI Hazard
Ceramic Insulators	48%	52%
ESW/ECW Pumps	31%	34%
Diesel Generator	24%	26%
Turbine Building	14%	16%
4kV Busses	12%	13%
Radwaste/Turbine Building	8%	8%
RV Recirculation Pumps	7%	7%
RV Skirt Support	1%	1%

reduction potential because its failure would serve to fail the cables to the ECW pump. The importance of the Turbine Building may be overestimated due to the conservative estimate of its median failure capacity. The 4kV buses have a significant risk reduction potential inasmuch as all off site power and on site emergency power is fed through these buses. The Radwaste/Turbine Building failure, as noted earlier, is both an initiator and houses the control room and all the emergency switchgear rooms. Thus, its failure would have a significant impact on the overall core damage frequency. The reactor vessel recirculation pumps and the reactor vessel supports have significant reduction potential due to the fact that they are used to model the reactor vessel rupture initiating event and the large LOCA initiating event. All other components and structures had risk reduction potentials of less than 2 percent.

A.5.4.2 Core Damage Frequency Results With Stiffness Reduction

The seismic risk at the Peach Bottom Plant using reduced stiffnesses was recalculated in exactly the same fashion as above using original stiffnesses. The same initiating events, component fragilities, and accident sequence definitions were used. The same interval of integration over the hazard curve (0.15g to 1.20g) was used. The only difference was the floor responses were different based on the reduced shear wall stiffness as discussed in section A.3.4 and structural fragilities also changed as discussed in section A.4.3

The results of this requantification using Monte Carlo uncertainty estimates are summarized in Tables A-17 and A-18. The same dominant accident sequences were identified, although the percentage contributions were slightly different:

	LLNL	EPRI
T1-33	55%	56%
ALOCA-30	22%	20%
RVR-1	10%	9%
S1LOCA-70	6%	6%
RWT-1	3%	5%

Based on the complete uncertainty analysis, the mean core damage frequency was computed to be 8.44E-5 using the LLNL hazard curves and 3.58E-6 for the EPRI hazard curves. This is a 26% and 29% increase over the case with no frequency reduction (6.71E-5 for LLNL and 2.77E-6 for EPRI). The mean frequencies of the original accident sequences are shown in Table A-12. The same dominant accident sequences were found in both cases.

Mean Point Estimate

A point estimate calculation with all values set equal to their mean values was also made. Tables A-19 and A-20 present the total accident sequence frequencies at 7 different intervals over the LLNL and EPRI hazard curves respectively, again for the mean point estimate case. These

Table A-17

Accident Sequence and Total Core Damage Mean Frequencies
for Peach Bottom with Reduced Stiffnesses
(Monte Carlo Uncertainty Analysis)

		Mean Frequency (per year)	
Accident Sequence		LLNL Hazard	EPRI Hazard
1	RVR-1	8.86E-6	3.27E-7
2	ALOCA-17	2.15E-7	1.01E-8
3	ALOCA-30	1.88E-5	7.28E-7
4	S1LOCA-25	5.88E-9	3.53E-10
5	S1LOCA-70	5.20E-6	2.04E-7
6	S1LOCA-80	5.35E-7	2.27E-8
7	S2LOCA-21	1.62E-7	9.19E-9
8	S2LOCA-42	1.05E-6	4.90E-8
9	RWT-1	2.91E-6	1.75E-7
10	RWT-2	3.10E-7	1.86E-8
11	RWT-3	6.45E-9	3.87E-10
12	RWT-4	6.45E-10	3.87E-11
13	T1-25	5.81E-8	3.01E-9
14	T1-32	3.24E-11	1.71E-12
15	T1-33	4.61E-5	2.02E-6
16	T1-36 to S2-41	5.57E-9	2.89E-10
17	T1-36 to S2-42	3.09E-12	1.62E-13
18	T1-40 to S1-70	4.77E-11	2.26E-12
19	T1-40 to S1-80	1.40E-13	8.05E-15
20	T1-43 to ALOCA-30	2.31E-7	7.85E-9
21	T3A-1 to T2-1-29	1.86E-10	1.43E-11
22	T3A-1 to T2-1-36	6.90E-11	4.63E-12
	TOTAL	8.44E-5	3.58E-6

Table A-18

Accident Sequence Frequency Distribution Percentiles
for Peach Bottom with Reduced Stiffnesses
(Monte Carlo Uncertainty Analysis)

	LLNL Hazard	EPRI Hazard
Mean	8.44E-5	3.58E-6
Var	1.78E-7	1.04E-10
5%	6.16E-8	2.66E-8
50%	5.11E-6	8.08E-7
95%	3.09E-4	1.51E-5

Table A-19

Total Accident Sequence Frequency Increments
LLNL Seismic Hazard Curves for Peach Bottom with Reduced Stiffnesses
(Mean Point Estimate Calculation)

	0.15-0.30g	0.30-0.45g	0.45-0.60g	0.60-0.75g	0.75-0.90g	0.90-1.05g	1.05-1.20g	TOTAL
1	5.1E-08	5.2E-07	1.4E-06	2.1E-06	2.4E-06	2.4E-06	2.2E-06	1.1E-05
2	1.8E-09	8.5E-08	1.9E-07	1.3E-07	4.6E-08	1.2E-08	3.2E-09	4.7E-07
3	2.0E-09	5.3E-07	4.8E-06	8.1E-06	6.3E-06	4.0E-06	2.4E-06	2.6E-05
4	2.5E-12	7.7E-10	4.8E-09	6.4E-09	3.9E-09	1.5E-09	4.9E-10	1.8E-08
5	2.5E-10	1.0E-07	1.1E-06	2.2E-06	1.7E-06	1.0E-06	5.7E-07	6.7E-06
6	3.4E-11	8.8E-09	8.6E-08	2.3E-07	3.3E-07	3.2E-07	2.5E-07	1.2E-06
7	1.7E-09	7.8E-08	1.5E-07	7.7E-08	2.2E-08	4.8E-09	9.3E-10	3.3E-07
8	4.0E-10	5.2E-08	3.3E-07	6.3E-07	6.8E-07	5.1E-07	3.2E-07	2.5E-06
9	7.6E-08	8.0E-07	1.5E-06	1.4E-06	9.0E-07	4.4E-07	1.9E-07	5.4E-06
10	8.1E-09	8.5E-08	1.6E-07	1.5E-07	9.6E-08	4.7E-08	2.0E-08	5.7E-07
11	1.7E-10	1.8E-09	3.4E-09	3.2E-09	2.0E-09	9.9E-10	4.3E-10	1.2E-08
12	1.7E-11	1.8E-10	3.4E-10	3.2E-10	2.0E-10	9.9E-11	4.3E-11	1.2E-09
13	3.2E-11	1.4E-09	5.8E-09	8.6E-09	7.4E-09	4.4E-09	2.1E-09	3.0E-08
14	1.5E-12	8.8E-12	1.7E-11	1.7E-11	1.1E-11	5.4E-12	2.2E-12	6.3E-11
15	2.3E-07	7.2E-06	1.9E-05	1.2E-05	3.7E-06	9.6E-07	2.4E-07	4.3E-05
16	3.1E-12	1.4E-10	5.5E-10	8.3E-10	7.1E-10	4.3E-10	2.1E-10	2.9E-09
17	1.3E-13	8.0E-13	1.6E-12	1.6E-12	1.1E-12	5.4E-13	2.2E-13	6.0E-12
18	9.0E-15	2.0E-13	2.4E-12	9.1E-12	1.4E-11	1.3E-11	8.5E-12	4.8E-11
19	1.8E-14	7.6E-14	9.0E-14	6.4E-14	3.4E-14	1.4E-14	5.1E-15	3.0E-13
20	2.2E-13	2.3E-11	8.6E-10	8.5E-09	3.3E-08	7.3E-08	1.1E-07	2.3E-07
21	5.8E-12	1.4E-10	2.9E-10	1.7E-10	4.8E-11	9.5E-12	1.5E-12	6.6E-10
22	1.7E-12	5.2E-11	1.1E-10	7.5E-11	2.7E-11	6.3E-12	1.2E-12	2.8E-10
	3.7E-07	9.5E-06	2.8E-05	2.7E-05	1.6E-05	9.7E-06	6.3E-06	9.73E-05

Table A-20

Total Accident Sequence Frequency Increments
EPRI Seismic Hazard Curves for Peach Bottom with Reduced Stiffnesses
(Mean Point Estimate Calculation)

	0.15-0.30g	0.30-0.45g	0.45-0.60g	0.60-0.75g	0.75-0.90g	0.90-1.05g	1.05-1.20g	TOTAL
1	3.4E-09	2.5E-08	5.3E-08	7.1E-08	7.5E-08	5.4E-08	6.1E-08	3.4E-07
2	1.2E-10	4.1E-09	7.6E-09	4.4E-09	1.4E-09	2.8E-10	8.9E-11	1.8E-08
3	1.3E-10	2.5E-08	1.9E-07	2.8E-07	1.9E-07	8.9E-08	6.8E-08	8.4E-07
4	1.7E-13	3.7E-11	1.9E-10	2.2E-10	1.2E-10	3.5E-11	1.4E-11	6.1E-10
5	1.6E-11	4.8E-09	4.5E-08	7.4E-08	5.2E-08	2.3E-08	1.6E-08	2.1E-07
6	2.3E-12	4.2E-10	3.3E-09	7.9E-09	1.0E-08	7.2E-09	7.0E-09	3.6E-08
7	1.1E-10	3.7E-09	5.7E-09	2.6E-09	6.9E-10	1.1E-10	2.6E-11	1.3E-08
8	2.7E-11	2.5E-09	1.3E-08	2.2E-08	2.1E-08	1.2E-08	8.9E-09	7.9E-08
9	5.1E-09	3.8E-08	6.0E-08	4.9E-08	2.8E-08	1.0E-08	5.4E-09	2.0E-07
10	5.4E-10	4.1E-09	6.4E-09	5.2E-09	3.0E-09	1.1E-09	5.7E-10	2.1E-08
11	1.1E-11	8.5E-11	1.3E-10	1.1E-10	6.2E-11	2.2E-11	1.2E-11	4.3E-10
12	1.1E-12	8.5E-12	1.3E-11	1.1E-11	6.2E-12	2.2E-12	1.2E-12	4.3E-11
13	2.2E-12	6.8E-11	2.2E-10	2.9E-10	2.3E-10	1.0E-10	6.0E-11	9.8E-10
14	9.7E-14	4.2E-13	6.5E-13	5.8E-13	3.5E-13	1.2E-13	6.2E-14	2.3E-12
15	1.6E-08	3.4E-07	7.2E-07	4.0E-07	1.1E-07	2.2E-08	6.8E-09	1.6E-06
16	2.1E-13	6.5E-12	2.2E-11	2.8E-11	2.2E-11	9.6E-12	5.8E-12	9.4E-11
17	8.4E-15	3.8E-14	6.2E-14	5.6E-14	3.4E-14	1.2E-14	6.2E-15	2.2E-13
18	6.0E-16	9.6E-15	9.4E-14	3.1E-13	4.5E-13	3.0E-13	2.4E-13	1.4E-12
19	1.2E-15	3.6E-15	3.5E-15	2.2E-15	1.0E-15	3.2E-16	1.4E-16	1.2E-14
20	1.5E-14	1.1E-12	3.4E-11	2.9E-10	1.0E-09	1.7E-09	3.2E-09	6.2E-09
21	3.9E-13	6.8E-12	1.1E-11	5.6E-12	1.5E-12	2.2E-13	4.2E-14	2.6E-11
22	1.1E-13	2.5E-12	4.4E-12	2.6E-12	8.3E-13	1.4E-13	3.2E-14	1.1E-11
	2.5E-08	4.5E-07	1.1E-06	9.2E-07	5.0E-07	2.2E-07	1.8E-07	3.40E-06

tables may be compared directly to Table A-14 and A-15 for the base cases using original stiffnesses.

The incremental contributions from each of the accident sequences remained about the same when using reduced stiffnesses. Similarly, the contribution and ranking of each earthquake level also was not affected. The bulk of the risk occurred in the 4-7 SSE range, assuring that by integrating from 0.15g to 1.20g we have again captured the bulk of the risk at Peach Bottom.

Basic Event Importance

The importance of the basic seismic failure events was not re-evaluated using reduced stiffnesses. It was assumed they would not be greatly affected by this. The ceramic insulators should again dominate the risk reduction potential since they were not affected by stiffness reductions. The ESW/ECW pumps may contribute slightly more since the responses they get increased. No new contributors are expected to have risk reduction potentials of more than 1%.

A.5.4.3 Summary of Results

The increase in core damage frequency is due primarily to the increased values of the responses for 7 Hz in the Circulating Water Pump Structure and the Emergency Cooling Water Towers. Both these responses have been increased over the case with no stiffness reduction. These responses are related to the fragilities of the Emergency Service Water pumps located in the Circulating Water Pump Structure and the Emergency Cooling Water pump located in the Emergency Cooling Water Tower. These three pumps play a critical role in providing cooling to the diesel generators in the event of loss of off-site power. Further, as seen in Table A-16, they had a very significant risk reduction potential. That is, they were very significant contributors to the base case core damage frequency. In the recalculation of risk, their responses increased due to the frequency reduction as discussed in the last section. Thus, their failure probabilities at all earthquake levels were increased. Hence, the inclusion of reductions in the stiffness of the structural models for the CWPS and the ECW Tower have increased the computed total core damage frequency for Peach Bottom.

A.6 DETERMINISTIC IMPACTS

A.6.1 Deterministic Response Analysis

To assess the impact of the frequency reduction model on the deterministic design calculations for Peach Bottom, a set of "design-like" structural response calculations was performed. These calculations are as close to the original design calculation methods as could be determined from the Peach Bottom Final Safety Analysis Report [A-2]. However, we did not seek

to obtain the original design calculational results themselves. Instead, we performed two sets of calculations using the FSAR guidance. The first set of calculations utilized the "design-like" models with as-calculated stiffnesses. The second set of calculations used the same structural models but incorporated a frequency reduction appropriate to the design level earthquake (0.12g).

A deterministic time history analysis was performed both on the original models and the reduced stiffness models using the 1952 Taft earthquake record scaled to 1 SSE (0.12g). Structural damping was 5% for both sets of calculations. Figure A-47 shows response spectra for the three components of this motion calculated at 5% spectral damping.

A.6.2 Deterministic Results for Peach Bottom

Acceleration response spectra at various nodal locations throughout all five structures comparing the undegraded response to the reduced stiffness response are plotted in the following figures:

RB:	Figs. A-48 thru A-60
RWTB:	Figs. A-61 thru A-67
CWP:	Figs. A-68 thru A-73
DG:	Figs. A-74 thru A-75
ECT:	Figs. A-76 thru A-80

These responses appear much more jagged and have sharper peaks, since these were based on a single time history, as compared to the median spectras generated in the probabilistic responses. It can be seen from these spectra that some very significant shifts in peak values and frequencies are present. Most notably the Radwaste/Turbine Building experienced a significant increase in the 7-8 Hz range in the North-South direction at all floor elevations. In addition, the Emergency Cooling Towers experienced a significant increase in the 7-9 Hz range in both directions for the upper floor elevations.

Tables A-21 thru A-25 show a comparison of story shear and moment loads listed by floor elevation for the same original and reduced stiffness models described above when subjected to the Taft earthquake at 1 SSE. Note that the values listed are net forces and moments for that elevation and have not yet been distributed to the individual walls at that elevation.

In general, it can be seen that there is a maximum increase in loads of about 20% due to the stiffness reduction. Since there is very little assumed torsion in any of these structures, the same increase would apply to loads in the individual walls. Thus, from a design viewpoint, the stiffness reduction does result in a significant increase in net loads, but this increase (20%) is probably well within the range of conservatism implicit in the original design calculations.

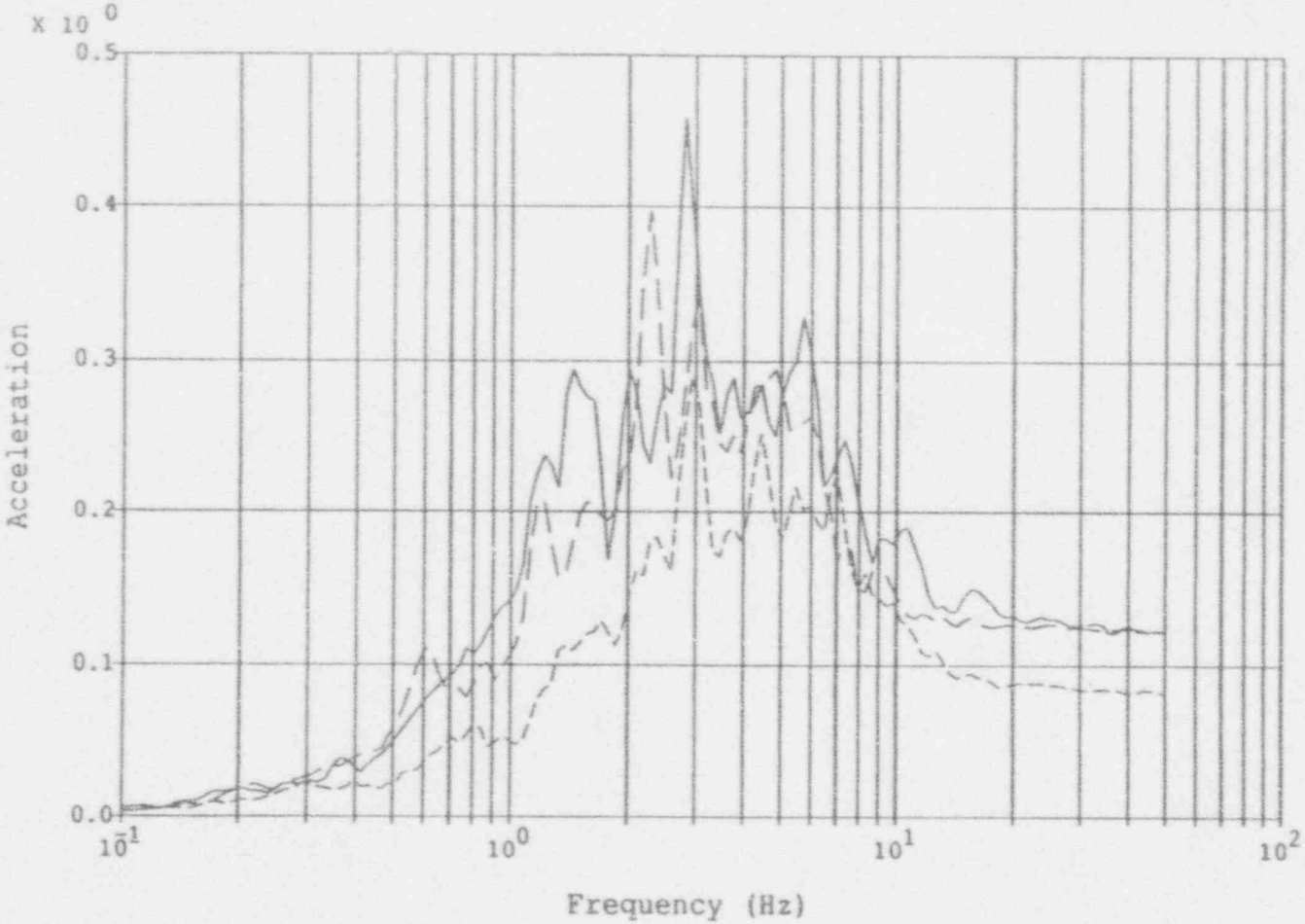

Legend:

N21E Horizontal Comp _____

S69E Horizontal Comp _ _ _ _ _

Vertical Component _ _ _ _ _ _ _ _

Notes:

1SSE Level:
.12g Horiz. PGA
.08g Vert. PGA
Accelerations in g's
5% Spectral Damping

Figure A-47 Taft 1952 Scaled Ground Motion Input Spectra

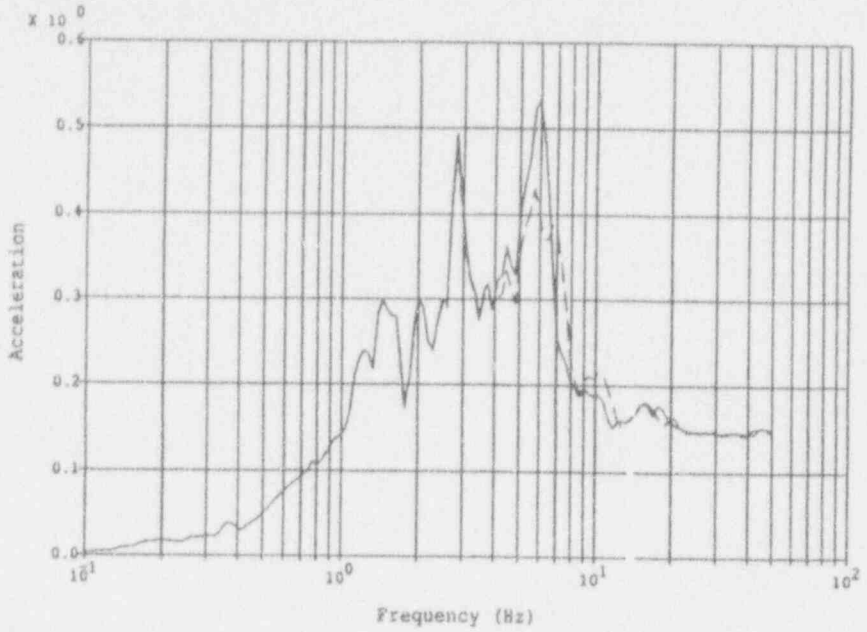

Legend:

Degraded Model
Factor = 0.75 ————————

Original Model — — — — — —

Notes:

1SSE Level, .12g PGA
Accelerations in g's
5% Spectral Damping
5% Struct. Damping

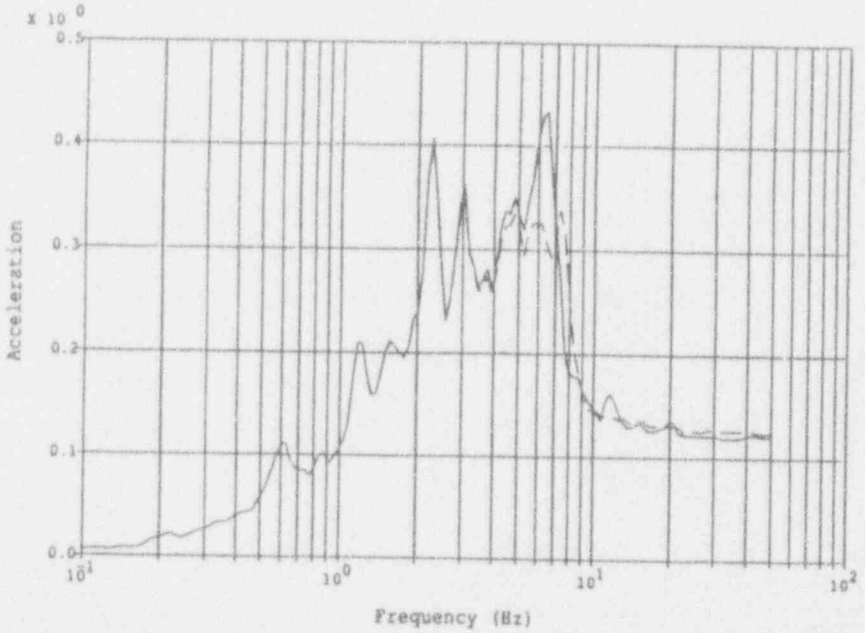

Legend:

Degraded Model
Factor = 0.75 ————————

Original Model — — — — — —

Notes:

1SSE Level, .12g PGA
Accelerations in g's
5% Spectral Damping
5% Struct. Damping

Figure A-48 Peach Bottom Deterministic Analysis, R/C Building Node 2, Elev. 135', N-S dir. (top), E-W dir. (bottom)

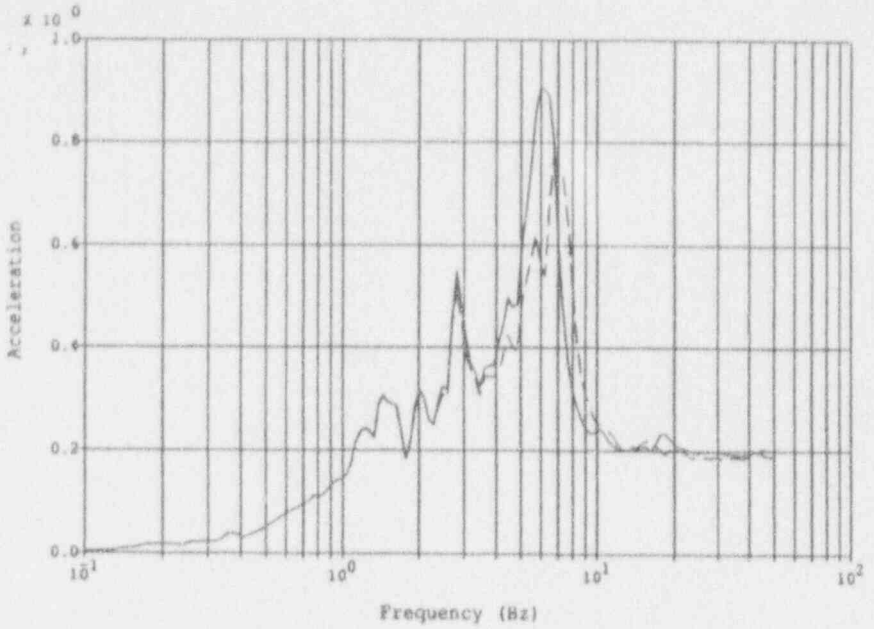

Legend:
Degraded Model
Factor = 0.75
Original Model

Notes:
1SSE Level, .12g PGA
Accelerations in g's
5% Spectral Damping
5% Struct. Damping

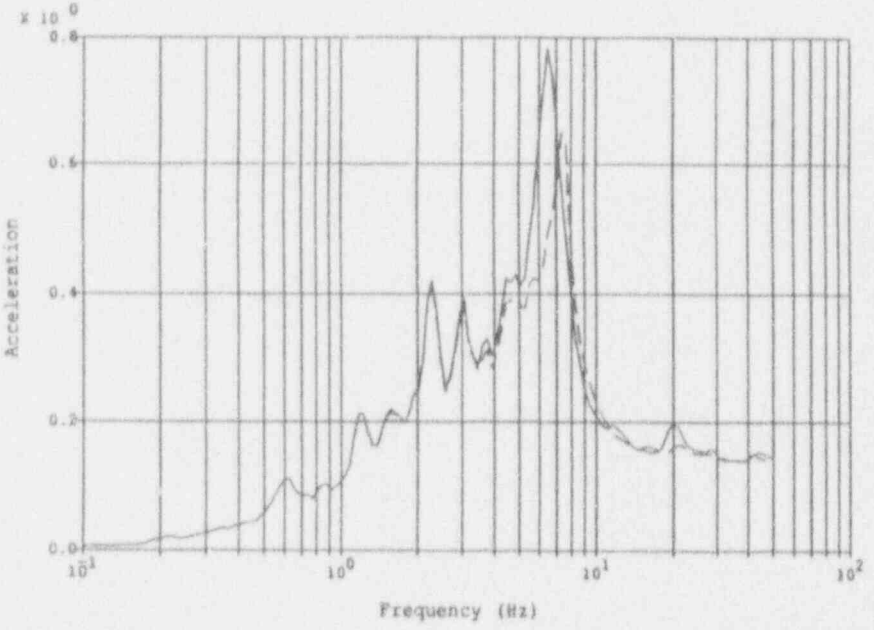

Legend:
Degraded Model
Factor = 0.75
Original Model

Notes:
1SSE Level, .12g PGA
Accelerations in g's
5% Spectral Damping
5% Struct. Damping

Figure A-49 Peach Bottom Deterministic Analysis, R/C Building Node 3, Elev. 165', N-S dir. (top), E-W dir. (bottom)

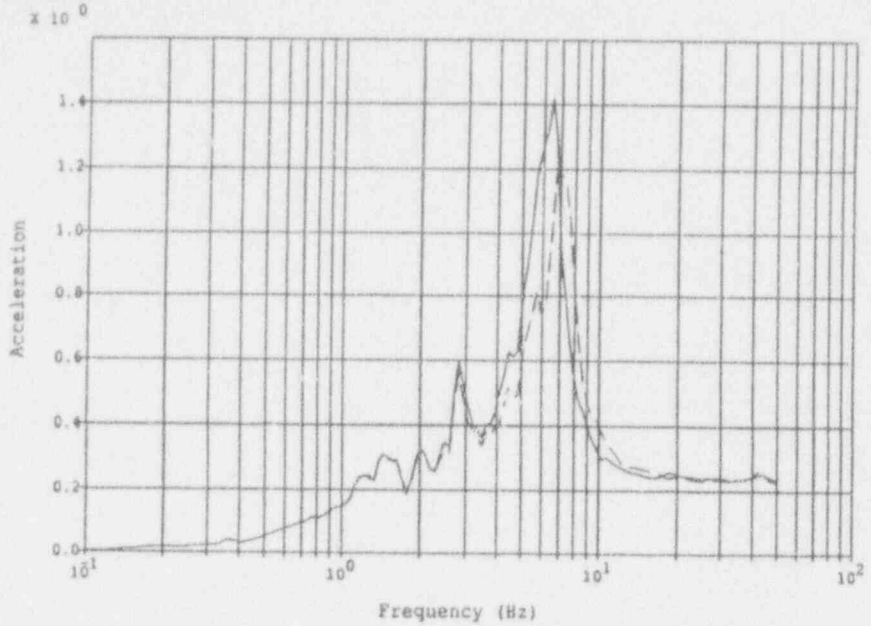

Legend:
Degraded Model
Factor = 0.75
Original Model

Notes:
1SSE Level, .12g PGA
Accelerations in g's
5% Spectral Damping
5% Struct. Damping

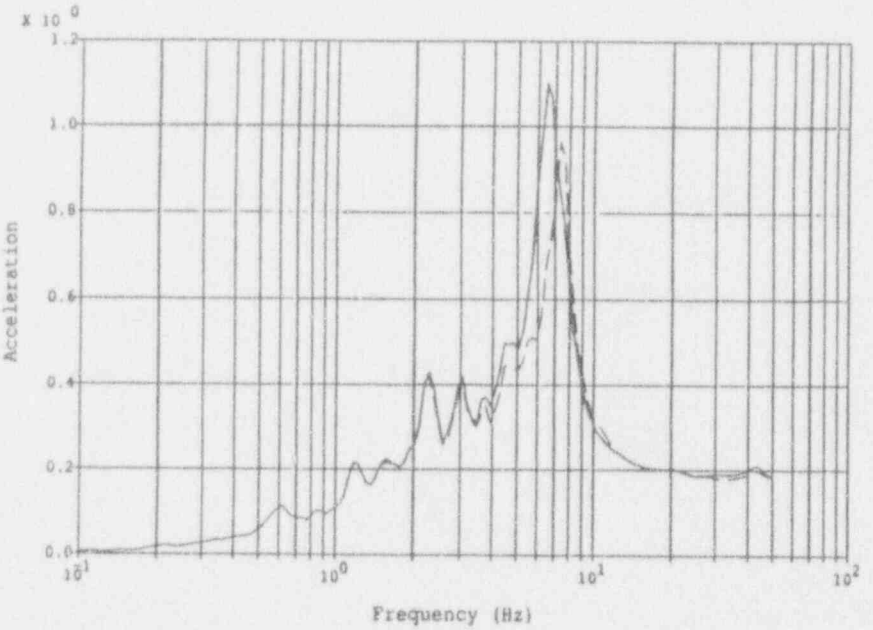

Legend:
Degraded Model
Factor = 0.75
Original Model

Notes:
1SSE Level, .12g PGA
Accelerations in g's
5% Spectral Damping
5% Struct. Damping

Figure A-50 Peach Bottom Deterministic Analysis, R/C Building Node 4, Elev. 195', N-S dir. (top), E-W dir. (bottom)

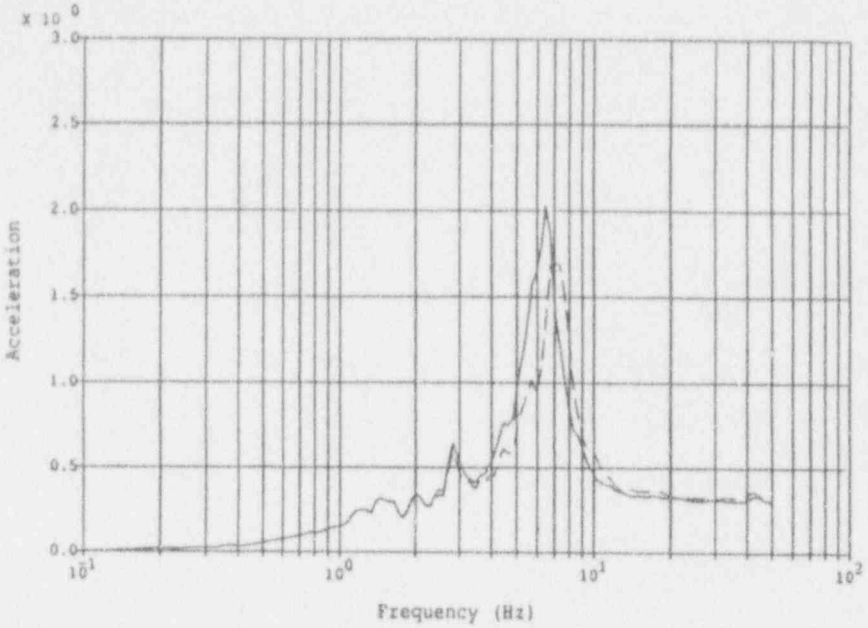

Legend:
Degraded Model Factor = 0.75 ————————
Original Model — — — — —

Notes:
1SSE Level, .12g PGA
Accelerations in g's
5% Spectral Damping
5% Struct. Damping

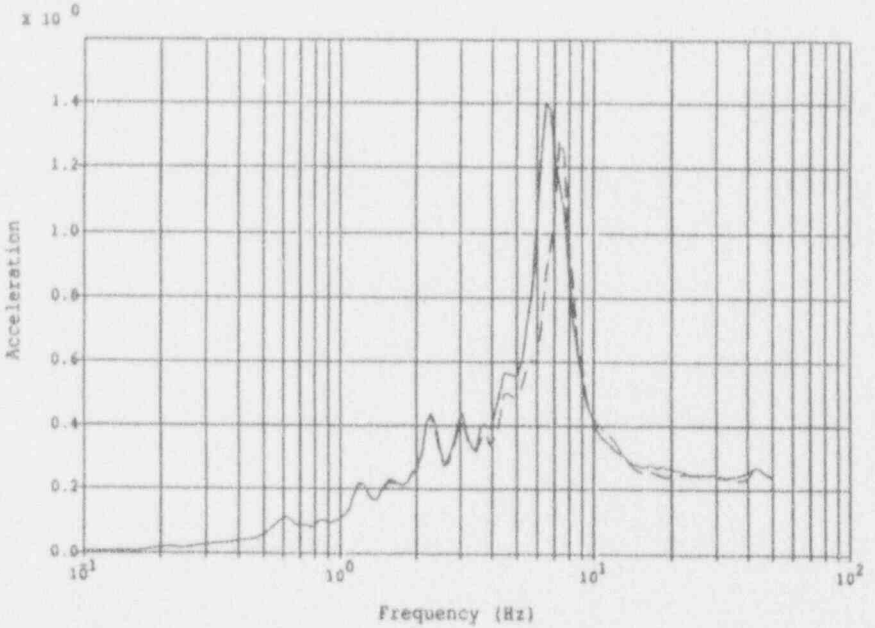

Legend:
Degraded Model Factor = 0.75 ————————
Original Model — — — — —

Notes:
1SSE Level, .12g PGA
Accelerations in g's
5% Spectral Damping
5% Struct. Damping

Figure A-51 Peach Bottom Deterministic Analysis, R/C Building Node 5, Elev. 234', N-S dir. (top), E-W dir. (bottom)

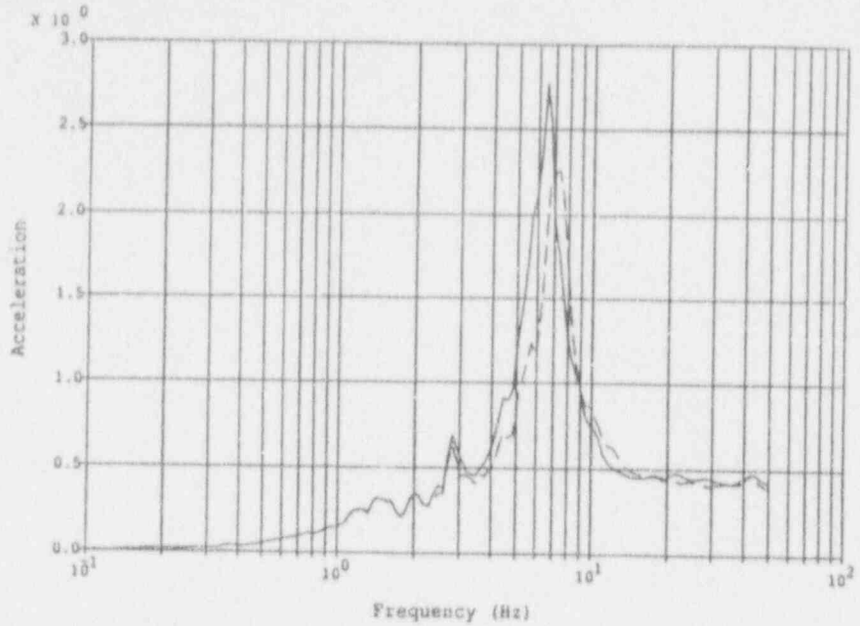

Legend:
Degraded Model
Factor = 0.75
Original Model

Notes:
1SSE Level, .12g PGA
Accelerations in g's
5% Spectral Damping
5% Struct. Damping

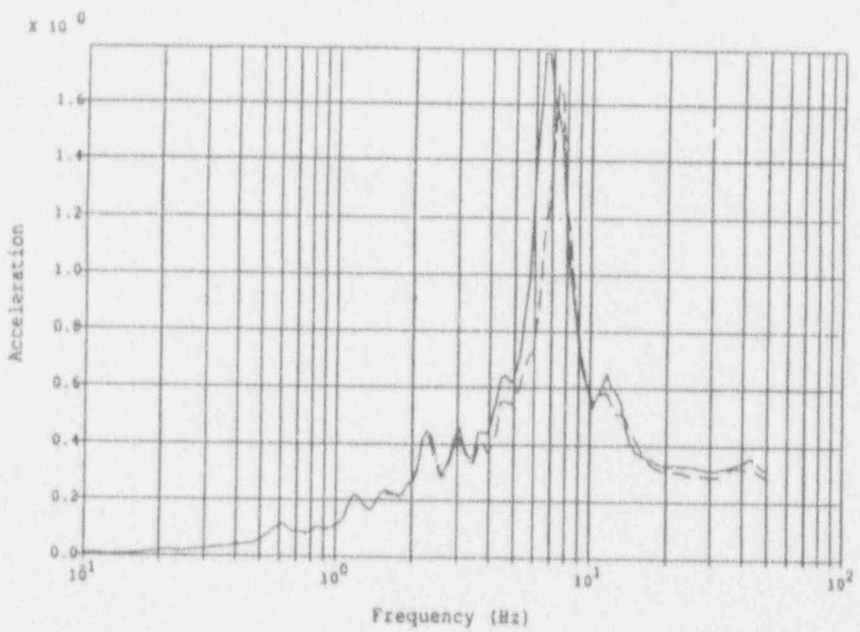

Legend:
Degraded Model
Factor = 0.75
Original Model

Notes:
1SSE Level, .12g PGA
Accelerations in g's
5% Spectral Damping
5% Struct. Damping

Figure A-52 Peach Bottom Deterministic Analysis, R/C Building Node 6, Elev. 252', N-S dir. (top), E-W dir. (bottom)

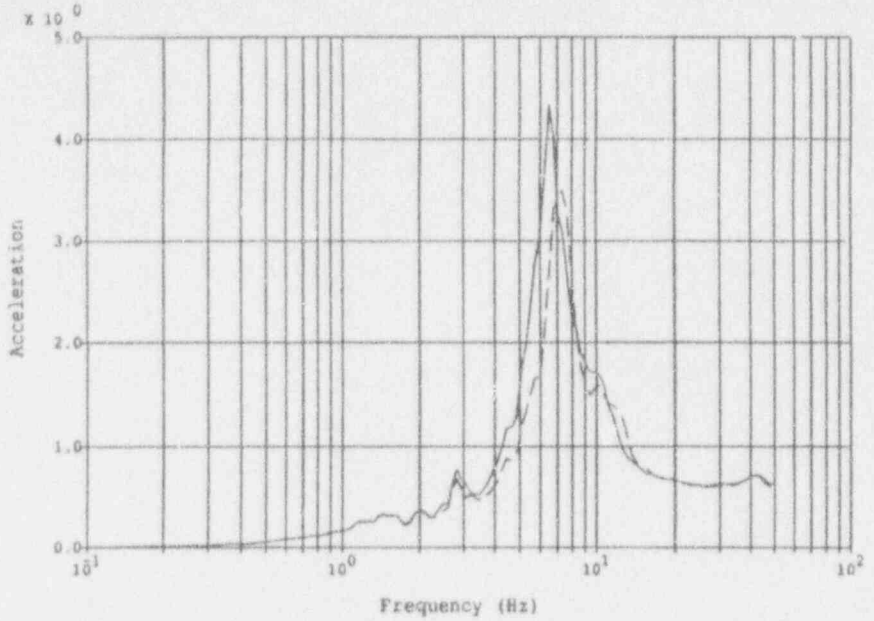

Legend:

Degraded Model Factor = 0.75 ————————

Original Model — — — — —

Notes:

1SSE Level, .12g PGA
Accelerations in g's
5% Spectral Damping
5% Struct. Damping

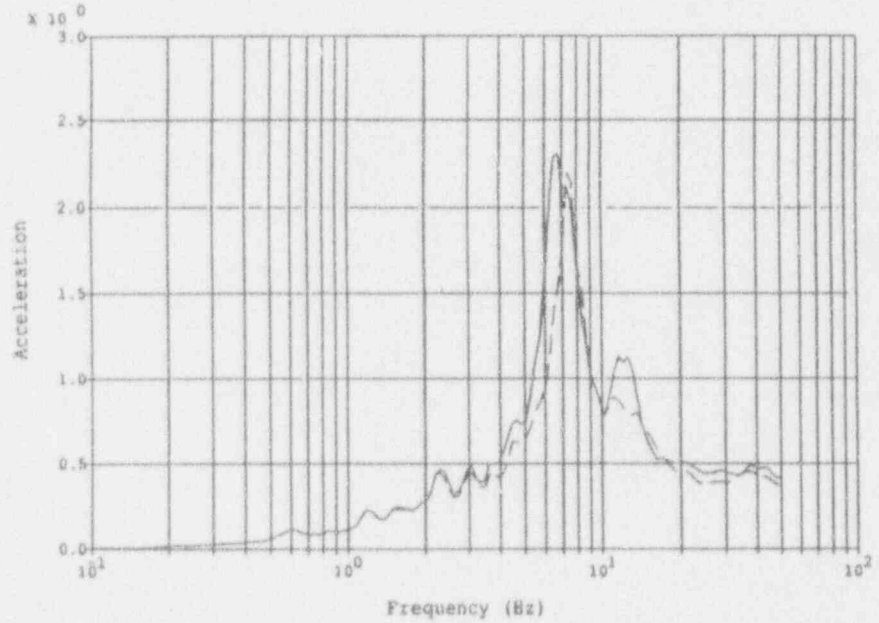

Legend:

Degraded Model Factor = 0.75 ————————

Original Model — — — — —

Notes:

1SSE Level, .12g PGA
Accelerations in g's
5% Spectral Damping
5% Struct. Damping

Figure A-53 Peach Bottom Deterministic Analysis, R/C Building Node 7, Elev. 286', N-S dir. (top), E-W dir. (bottom)

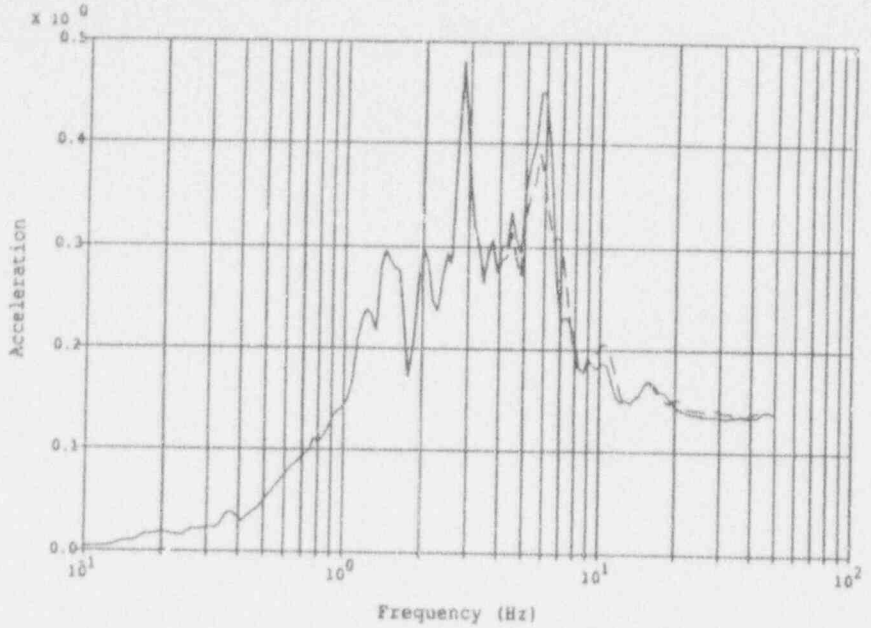

Legend:
Degraded Model
Factor = 0.75
Original Model

Notes:
1SSE Level, .12g PGA
Accelerations in g's
5% Spectral Damping
5% Struct. Damping

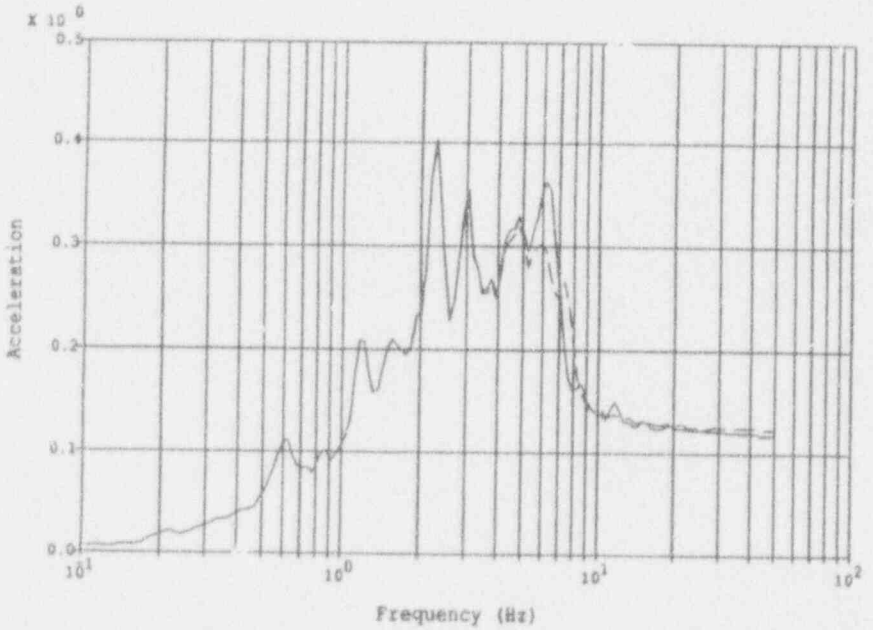

Degraded Model
Factor = 0.75
Original Model

Notes:
1SSE Level, .12g PGA
Accelerations in g's
5% Spectral Damping
5% Struct. Damping

Figure A-54 Peach Bottom Deterministic Analysis, R/C Building Node 9, Elev. 119', N-S dir. (top), E-W dir. (bottom)

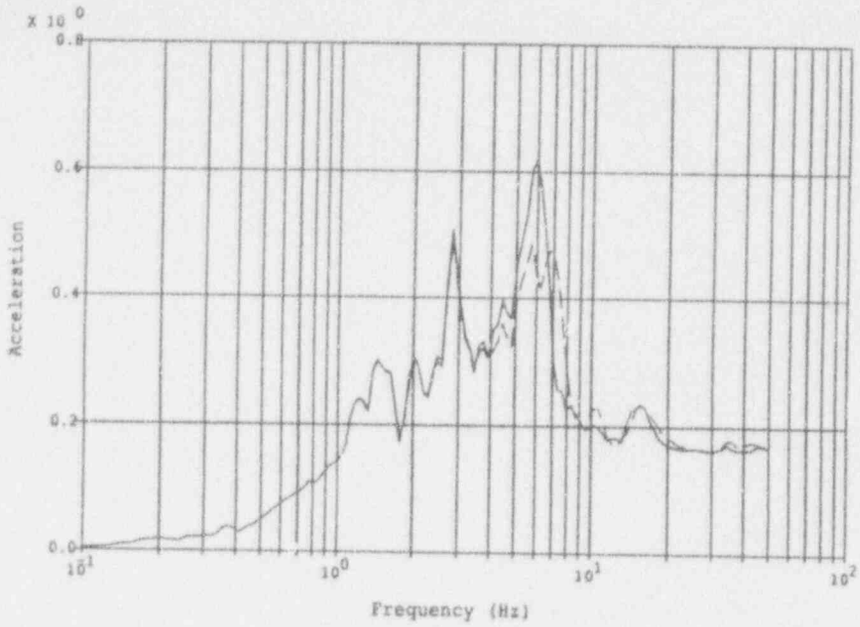

Legend:

Degraded Model
Factor = 0.75 ————————

Original Model — — — — —

Notes:

1SSE Level, .12g PGA
Accelerations in g's
5% Spectral Damping
5% Struct. Damping

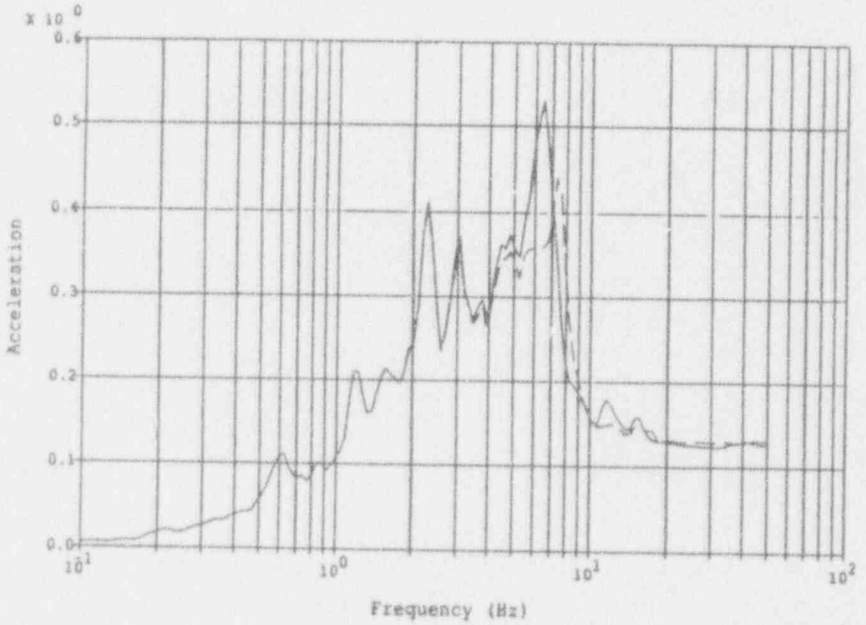

Legend:

Degraded Model
Factor = 0.75 ————————

Original Model — — — — —

Notes:

1SSE Level, .12g PGA
Accelerations in g's
5% Spectral Damping
5% Struct. Damping

Figure A-55 Peach Bottom Deterministic Analysis, R/C Building Node 10, Elev. 135', N-S dir. (top), E-W dir. (bottom)

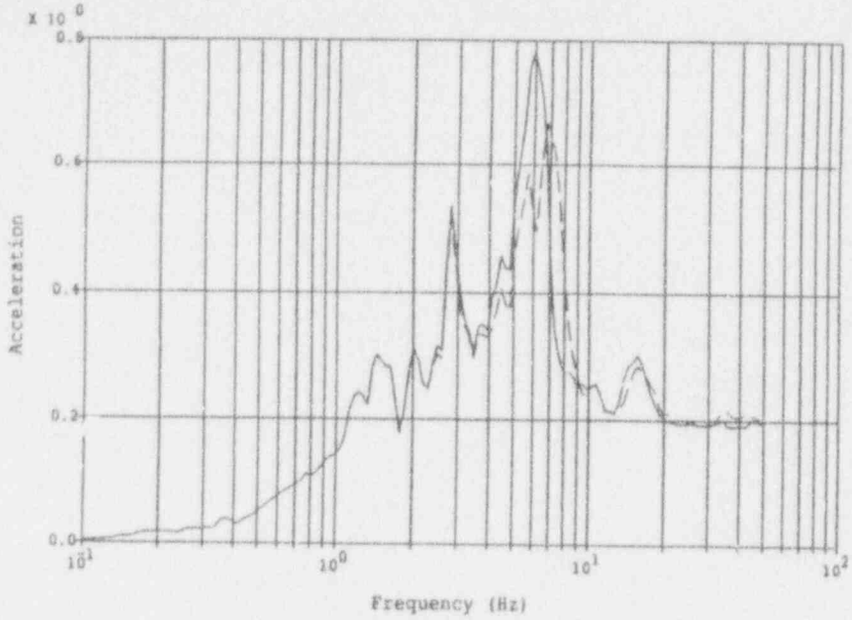

Legend:

Degraded Model
Factor = 0.75

Original Model

Notes:

1SSE Level, .12g PGA
Accelerations in g's
5% Spectral Damping
5% Struct. Damping

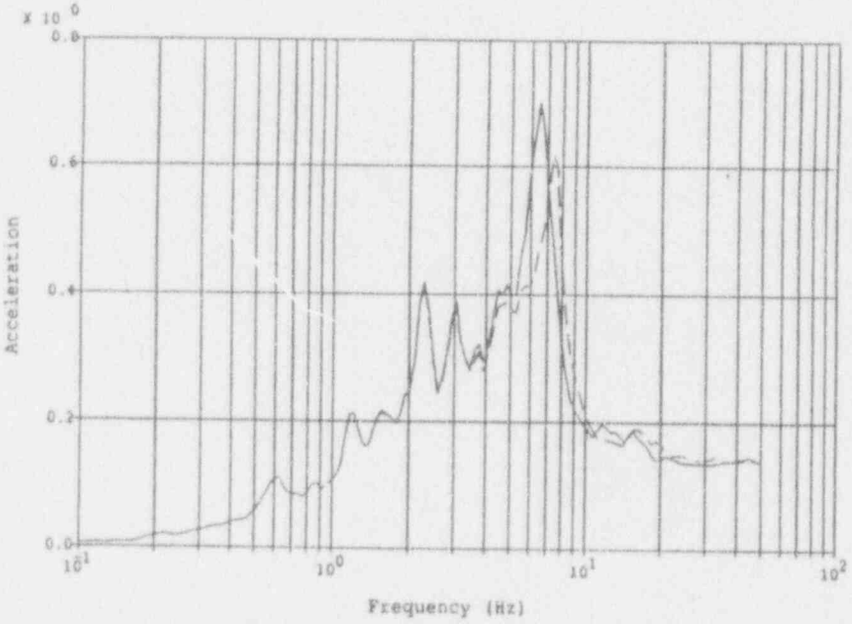

Legend:

Degraded Model
Factor = 0.75

Original Model

Notes:

1SSE Level, .12g PGA
Accelerations in g's
5% Spectral Damping
5% Struct. Damping

Figure A-56 Peach Bottom Deterministic Analysis, R/C Building Node 11, Elev. 145', N-S dir. (top), E-W dir. (bottom)

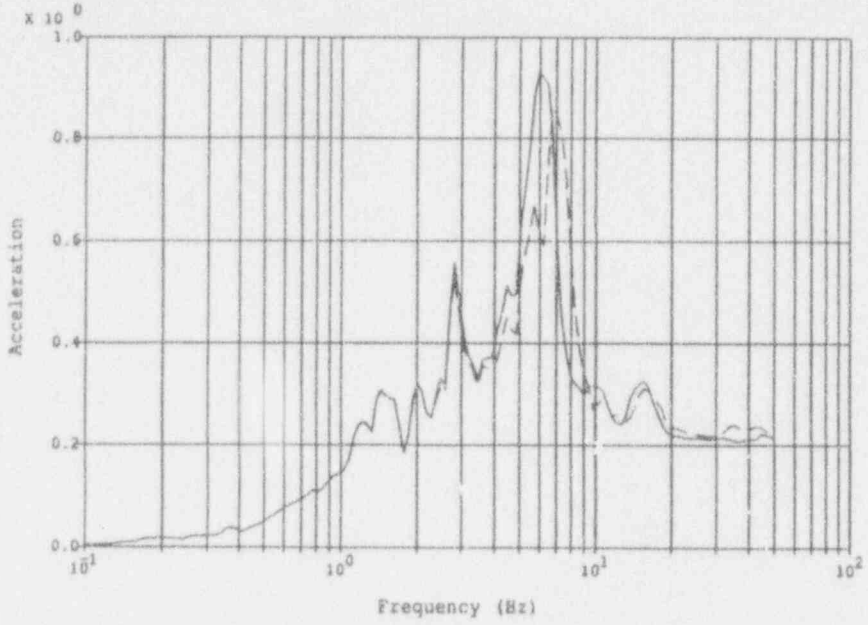

Legend:

Degraded Model
Factor = 0.75 ———————

Original Model — — — — —

Notes:

1SSE Level, .12g PGA
Accelerations in g's
5% Spectral Damping
5% Struct. Damping

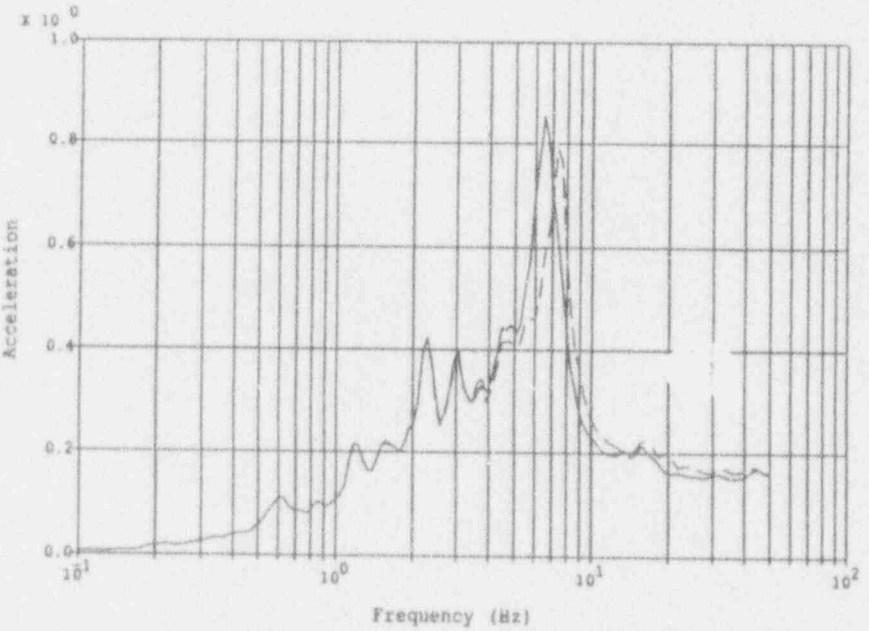

Legend:

Degraded Model
Factor = 0.75 ———————

Original Model — — — — —

Notes:

1SSE Level, .12g PGA
Accelerations in g's
5% Spectral Damping
5% Struct. Damping

Figure A-57 Peach Bottom Deterministic Analysis, R/C Building Node 12, Elev. 156', N-S dir. (top), E-W dir. (bottom)

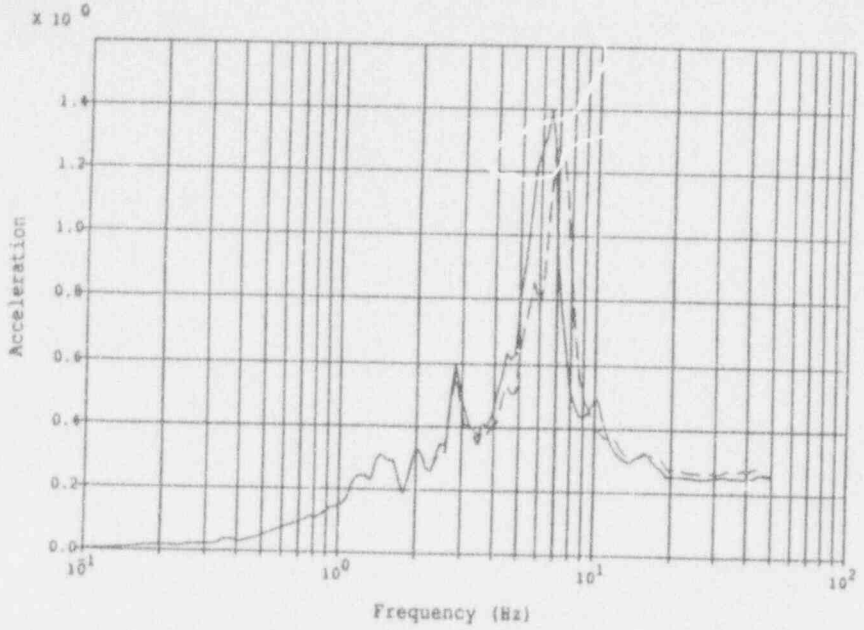

Legend:
Degraded Model
Factor = 0.75
Original Model

Notes:
1SSE Level, .12g PGA
Accelerations in g's
5% Spectral Damping
5% Struct. Damping

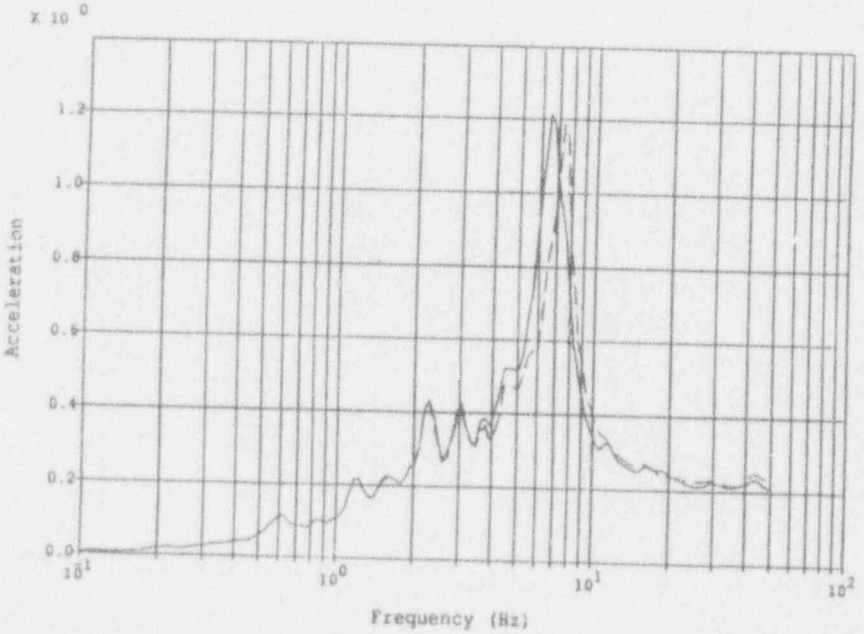

Legend:
Degraded Model
Factor = 0.75
Original Model

Notes:
1SSE Level, .12g PGA
Accelerations in g's
5% Spectral Damping
5% Struct. Damping

Figure A-58 Peach Bottom Deterministic Analysis, R/C Building Node 13, Elev. 169', N-S dir. (top), E-W dir. (bottom)

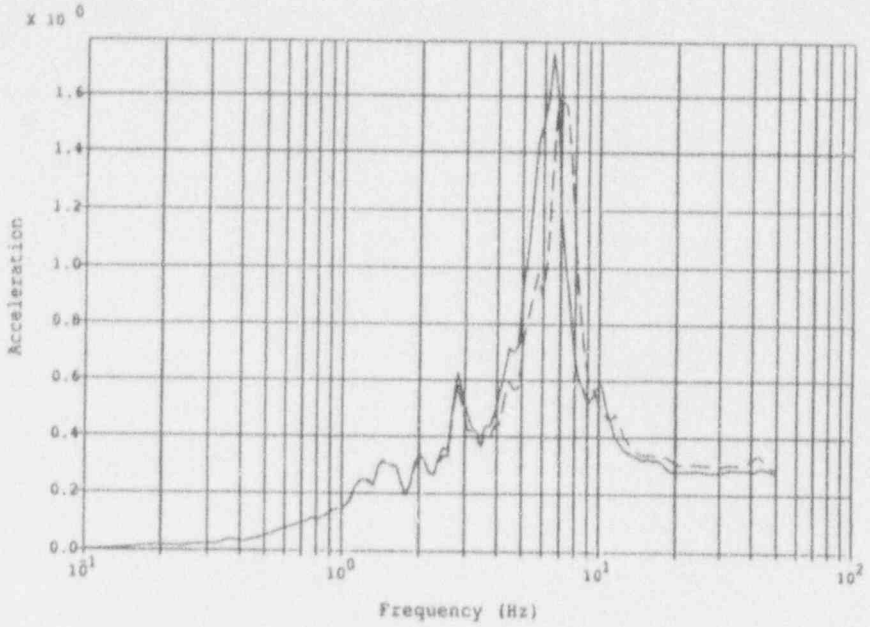

Legend:
Degraded Model
Factor = 0.75
Original Model

Notes:
1SSE Level, .12g PGA
Accelerations in g's
5% Spectral Damping
5% Struct. Damping

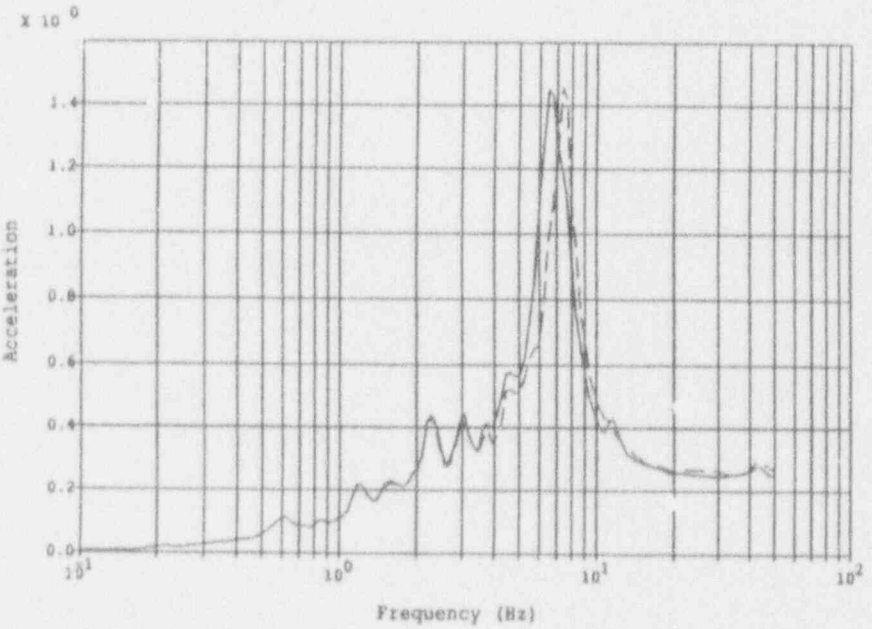

Legend:
Degraded Model
Factor = 0.75
Original Model

Notes:
1SSE Level, .12g PGA
Accelerations in g's
5% Spectral Damping
5% Struct. Damping

Figure A-59 Peach Bottom Deterministic Analysis, R/C Building Node 14, Elev. 182', N-S dir. (top), E-W dir. (bottom)

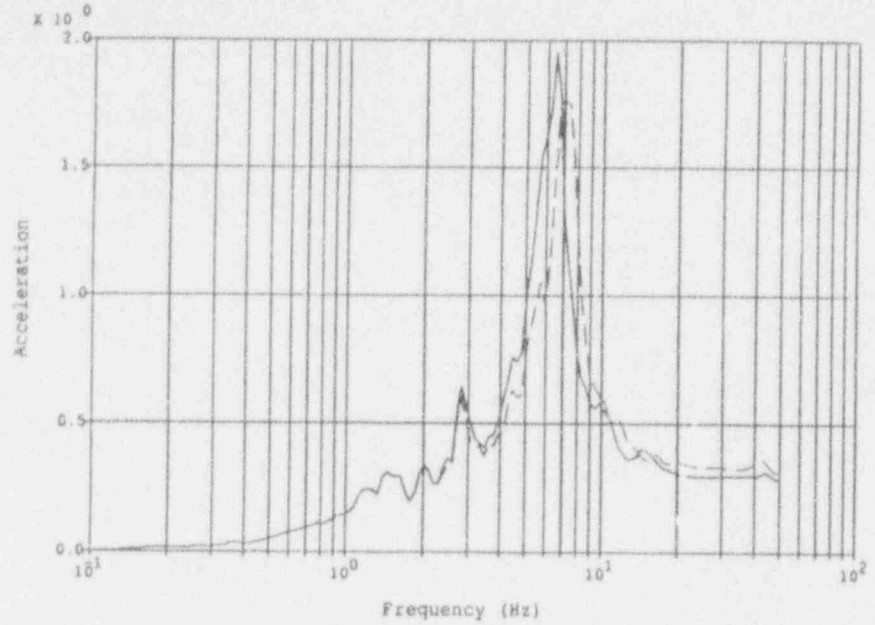

Legend:
Degraded Model
Factor = 0.75 ————————
Original Model — — — — —

Notes:
ISSE Level, .12g PGA
Accelerations in g's
5% Spectral Damping
5% Struct. Damping

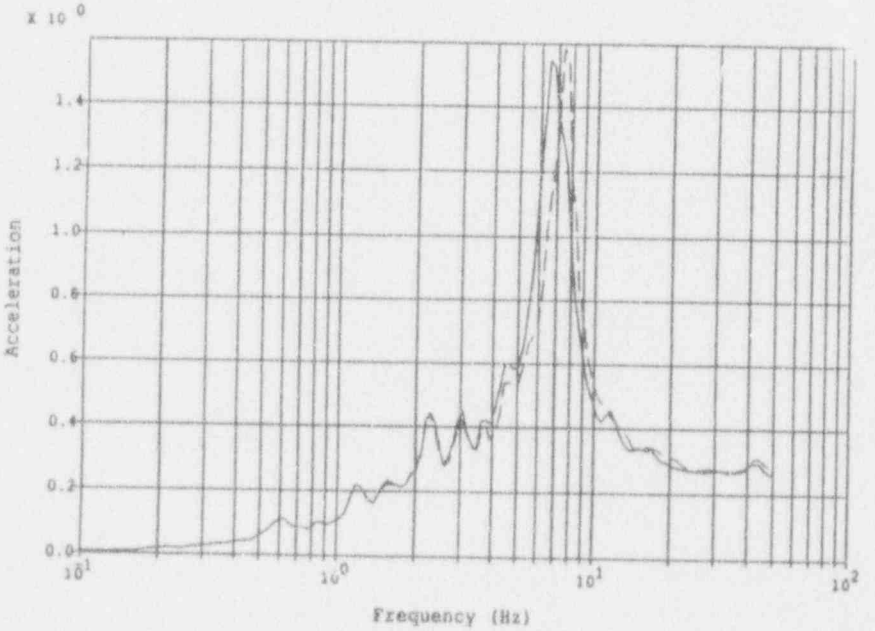

Legend:
Degraded Model
Factor = 0.75 ————————
Original Model — — — — —

Notes:
ISSE Level, .12g FGA
Accelerations in g's
5% Spectral Damping
5% Struct. Damping

Figure A-60 Peach Bottom Deterministic Analysis, R/C Building Node 15, Elev. 195', N-S dir. (top), E-W dir. (bottom)

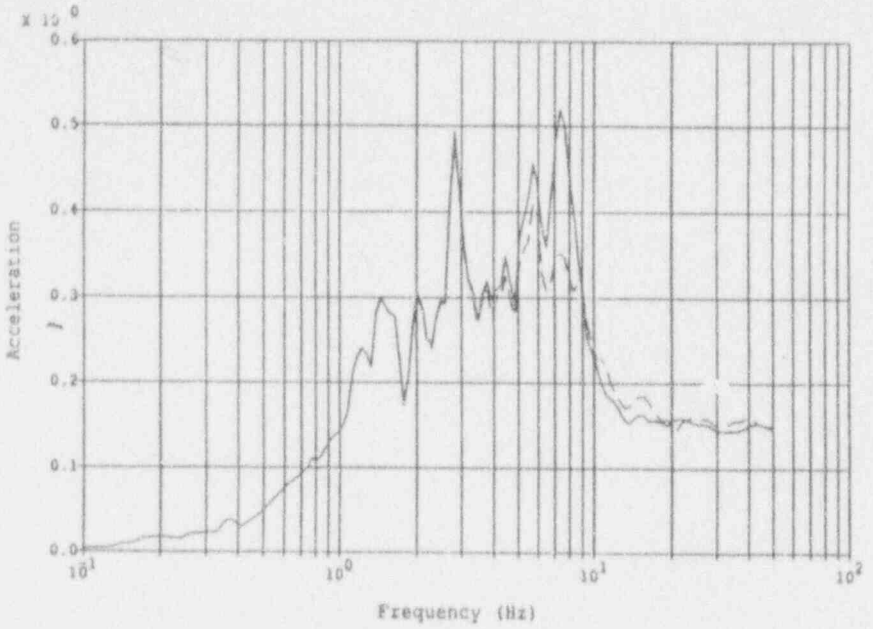

Legend:

Degraded Model
Factor = 0.75 ————————

Original Model — — — — — —

Notes:

1SSE Level, .12g PGA
Accelerations in g's
5% Spectral Damping
5% Struct. Damping

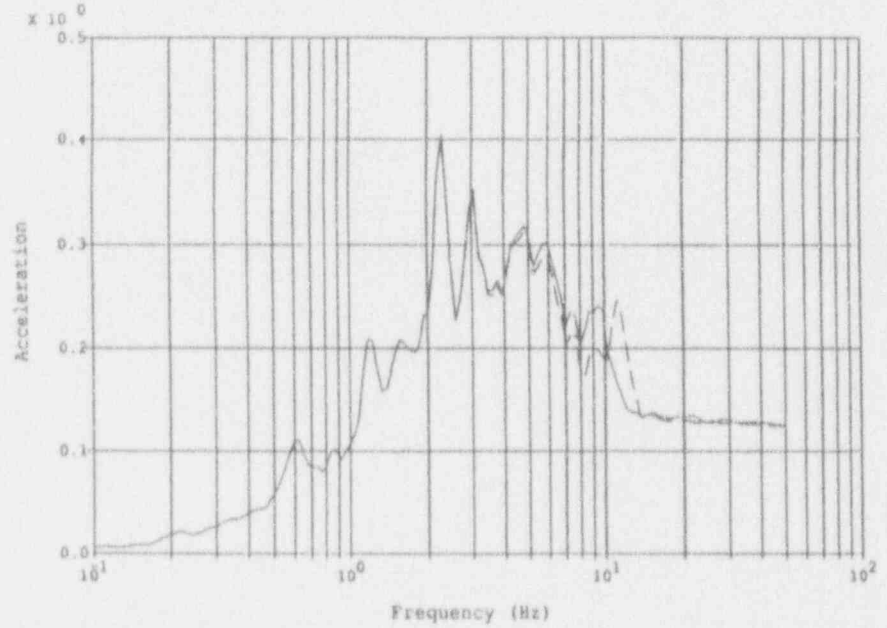

Legend:

Degraded Model
Factor = 0.75 ————————

Original Model — — — — — —

Notes:

1SSE Level, .12g PGA
Accelerations in g's
5% Spectral Damping
5% Struct. Damping

Figure A-61 Peach Bottom Deterministic Analysis, RWST Building Node 4, Elev. 135', N-S dir. (top), E-W dir. (bottom)

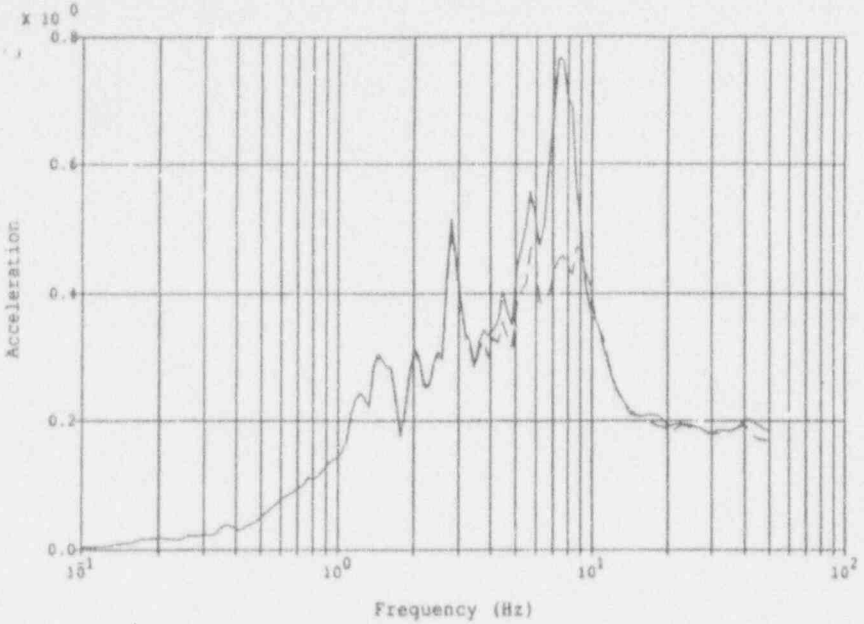

Legend:

Degraded Model
Factor = 0.75 ————————

Original Model — — — — —

Notes:

1SSE Level, .12g PGA
Accelerations in g's
5% Spectral Damping
5% Struct. Damping

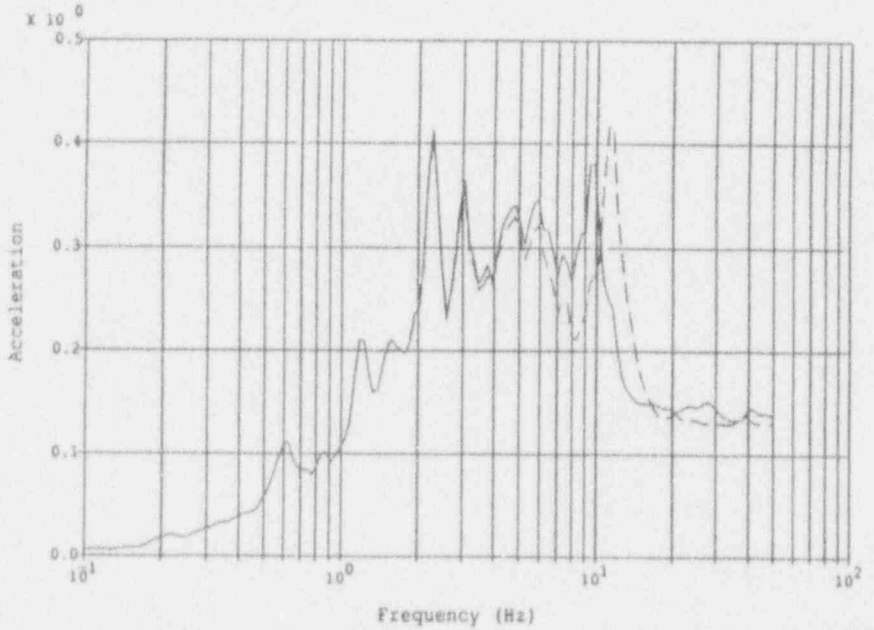

Legend:

Degraded Model
Factor = 0.75 ————————

Original Model — — — — —

Notes:

1SSE Level, .12g PGA
Accelerations in g's
5% Spectral Damping
5% Struct. Damping

Figure A-62 Peach Bottom Deterministic Analysis, RWST Building Node 8, Elev. 150', N-S dir. (top), E-W dir. (bottom)

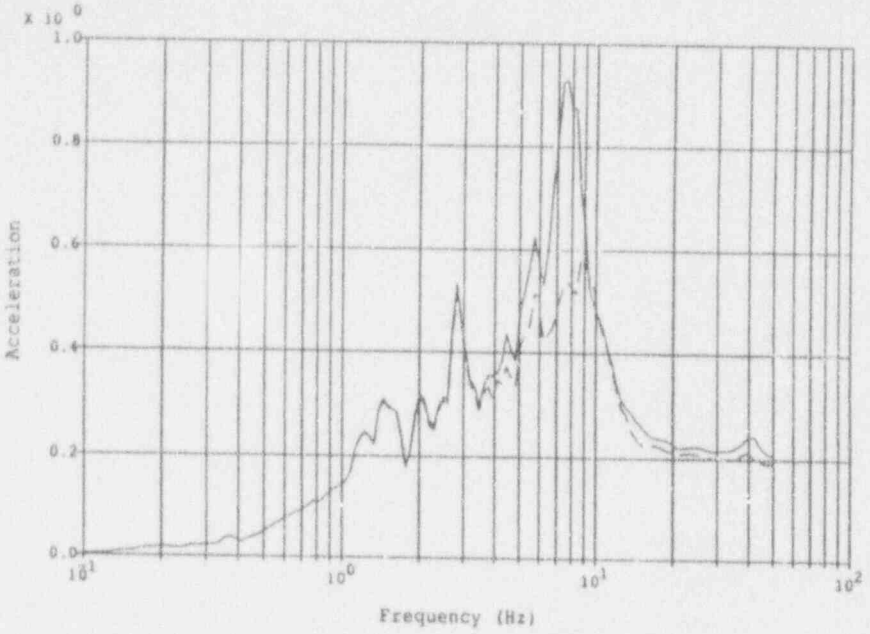

Legend:

Degraded Model
Factor = 0.75 ————————

Original Model — — — — —

Notes:

1SSE Level, .12g PGA
Accelerations in g's
5% Spectral Damping
5% Struct. Damping

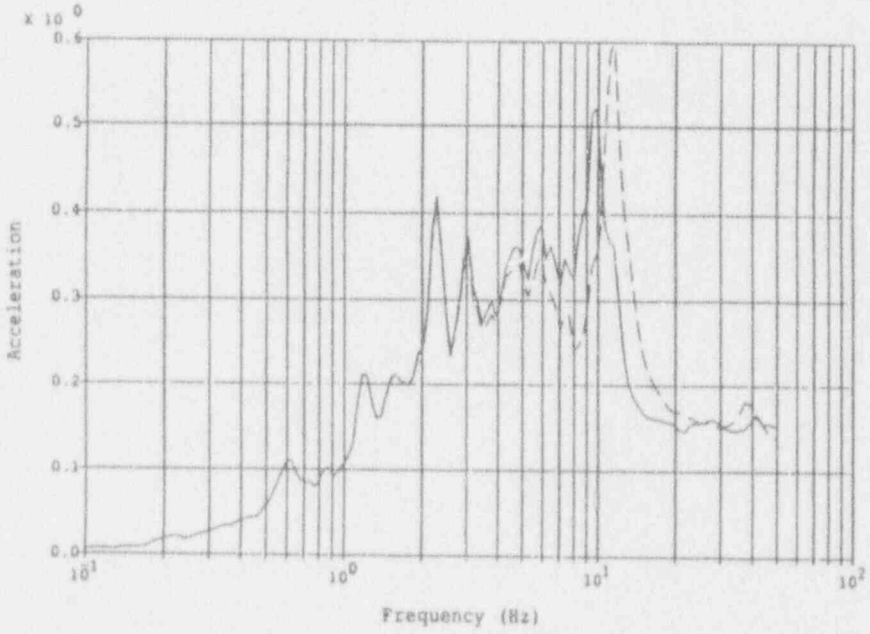

Legend:

Degraded Model
Factor = 0.75 ————————

Original Model — — — — —

Notes:

1SSE Level, .12g PGA
Accelerations in g's
5% Spectral Damping
5% Struct. Damping

Figure A-63 Peach Bottom Deterministic Analysis, RWST Building Node 12, Elev. 165', N-S dir. (top), E-W dir. (bottom)

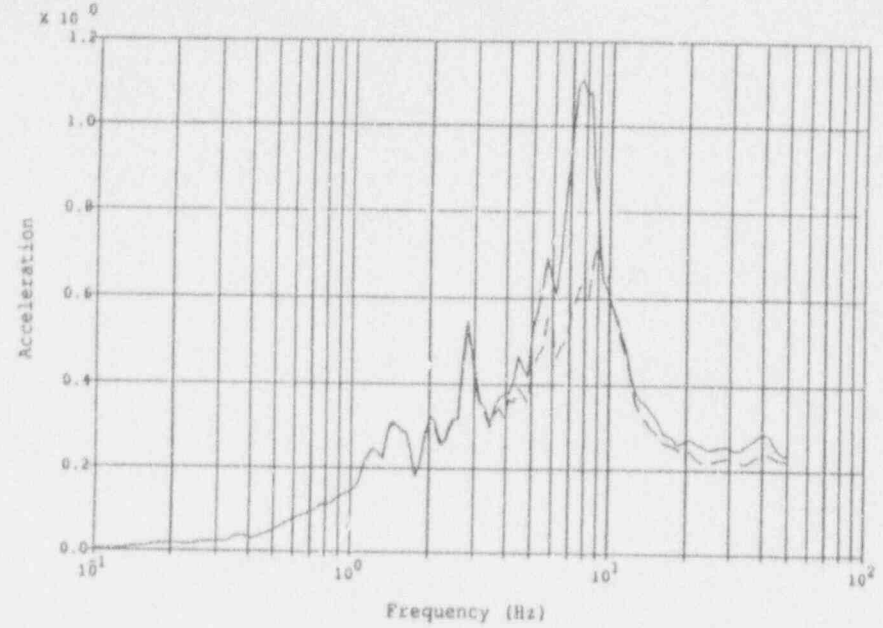

Legend:
Degraded Model
Factor = 0.75
Original Model

Notes:
1SSE Level, .12g PGA
Accelerations in g's
5% Spectral Damping
5% Struct. Damping

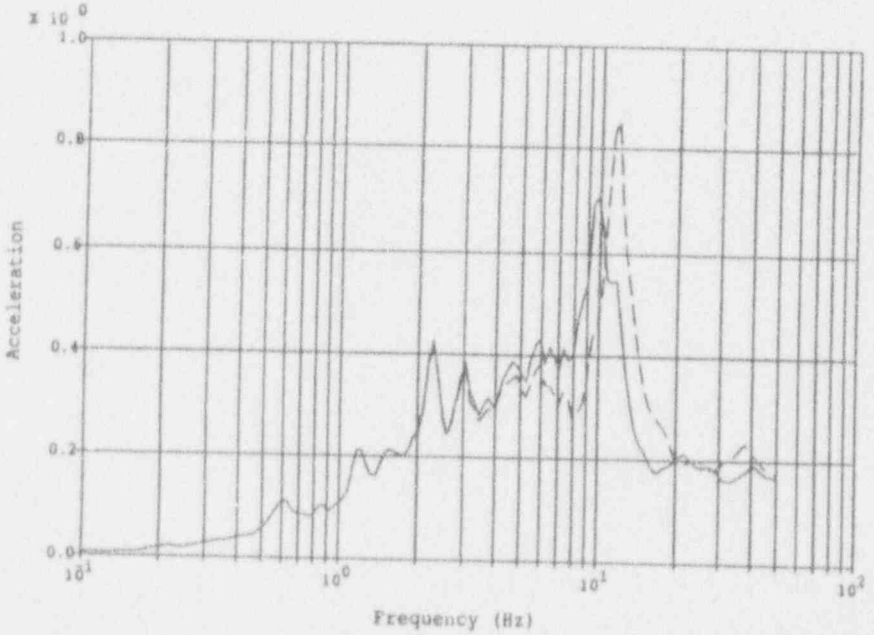

Legend:
Degraded Model
Factor = 0.75
Original Model

Notes:
1SSE Level, .12g PGA
Accelerations in g's
5% Spectral Damping
5% Struct. Damping

Figure A-64 Peach Bottom Deterministic Analysis, RWST Building Node 16, Elev. 191', N-S dir. (top), E-W dir. (bottom)

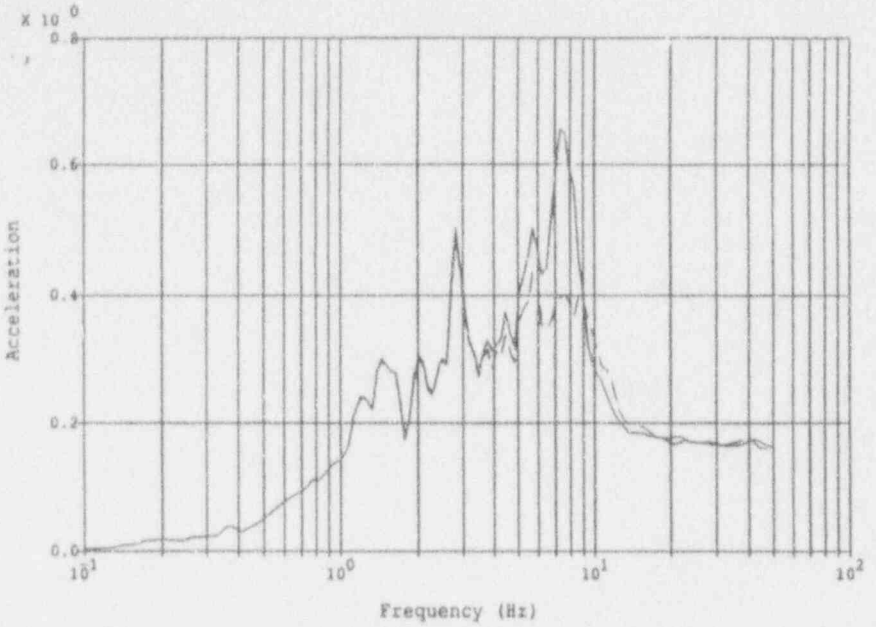

Legend:

Degraded Model
Factor = 0.75 ——————
Original Model — — — — —

Notes:

1SSE Level, .12g PGA
Accelerations in g's
5% Spectral Damping
5% Struct. Damping

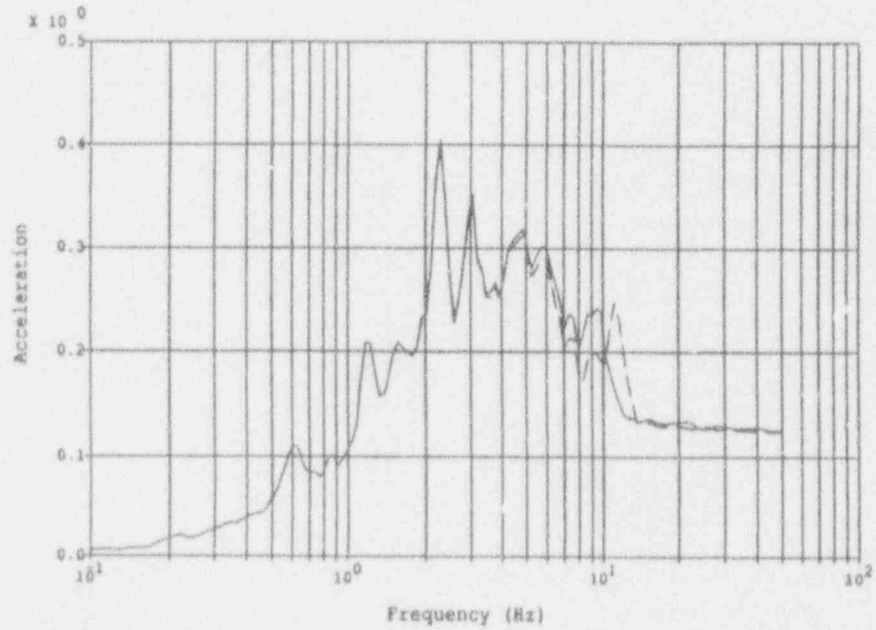

Legend:

Degraded Model
Factor = 0.75 ——————
Original Model — — — — —

Notes:

1SSE Level, .12g PGA
Accelerations in g's
5% Spectral Damping
5% Struct. Damping

Figure A-65 Peach Bottom Deterministic Analysis, RWST Building Node 17, Elev. 135', N-S dir. (top), E-W dir. (bottom)

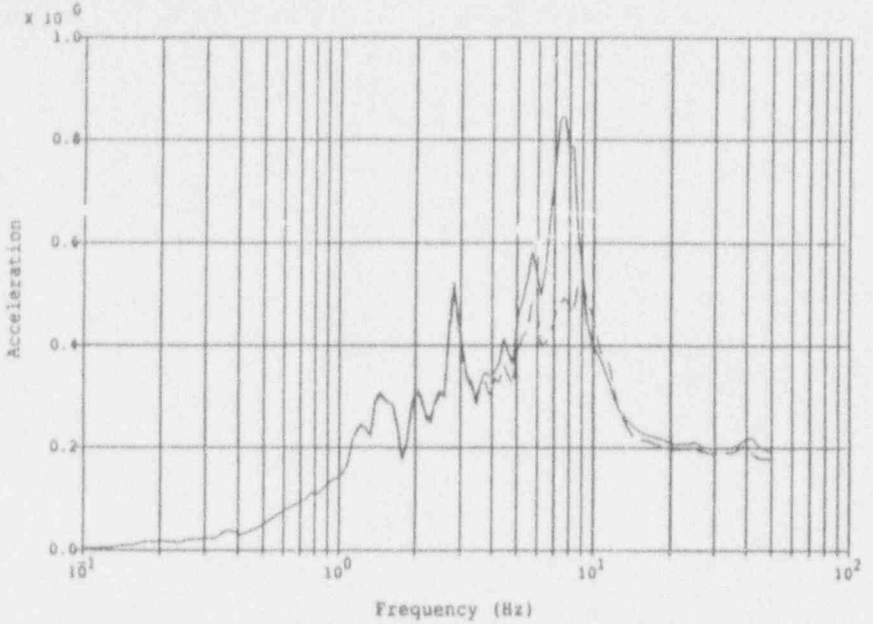

Legend:

Degraded Model
Factor = 0.75 ————————

Original Model – – – – – –

Notes:

1SSE Level, .12g PGA
Accelerations in g's
5% Spectral Damping
5% Struct. Damping

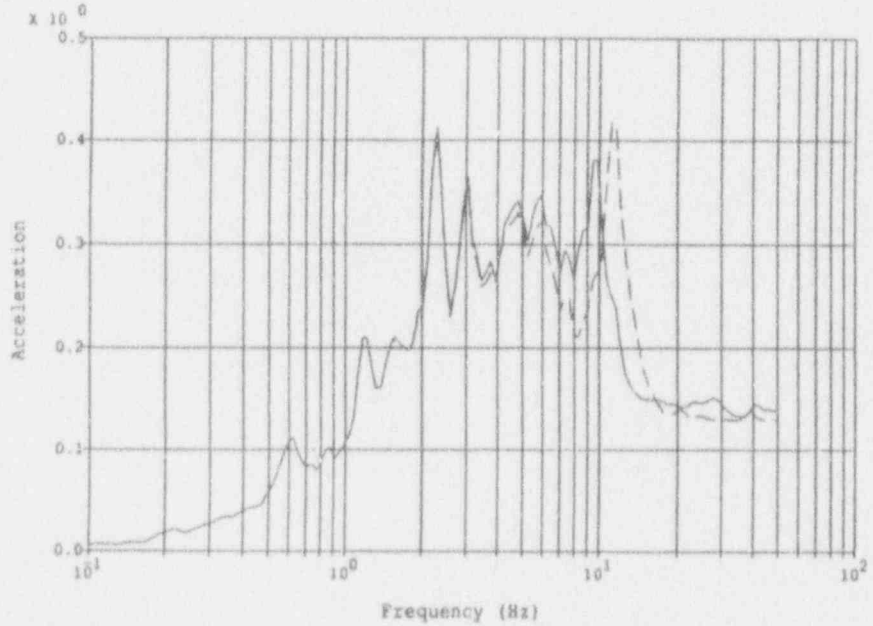

Legend:

Degraded Model
Factor = 0.75 ————————

Original Model – – – – – –

Notes:

1SSE Level, .12g PGA
Accelerations in g's
5% Spectral Damping
5% Struct. Damping

Figure A-66 Peach Bottom Deterministic Analysis, RWST Building Node 18, Elev. 150', N-S dir. (top), E-W dir. (bottom)

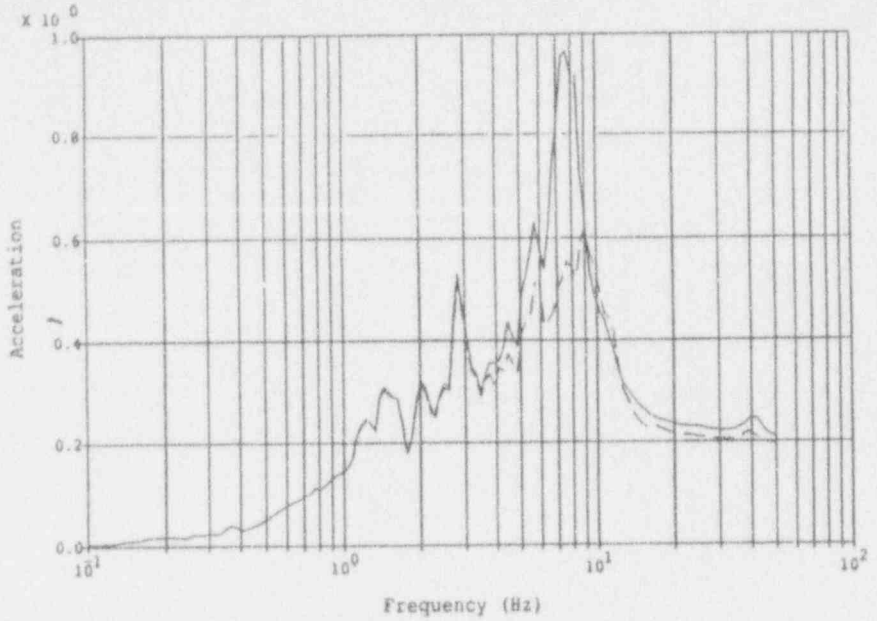

Legend:

Degraded Model
Factor = 0.75

Original Model

Notes:

1SSE Level, .12g PGA
Accelerations in g's
5% Spectral Damping
5% Struct. Damping

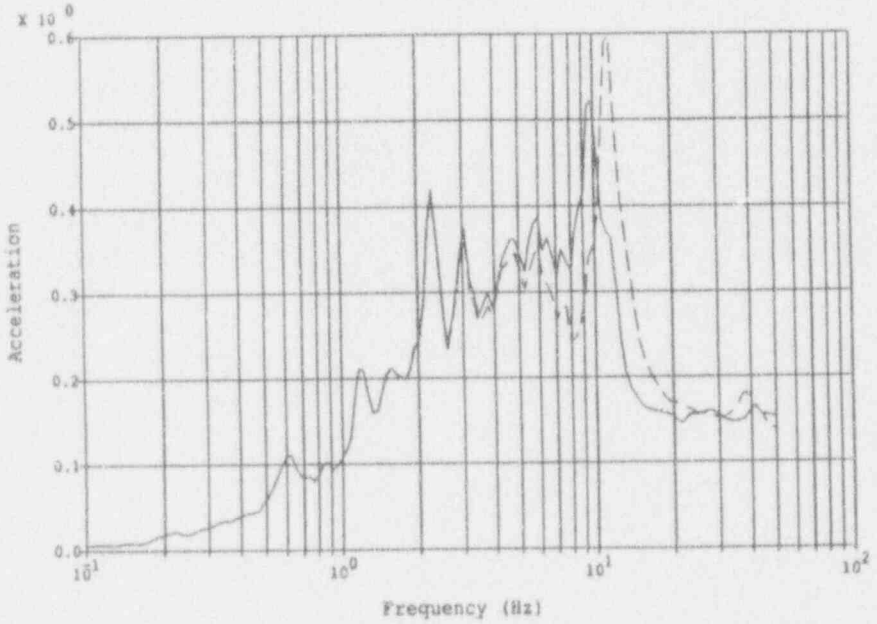

Legend:

Degraded Model
Factor = 0.75

Original Model

Notes:

1SSE Level, .12g PGA
Accelerations in g's
5% Spectral Damping
5% Struct. Damping

Figure A-67 Peach Bottom Deterministic Analysis, RWST Building Node 19, Elev. 165', N-S dir. (top), E-W dir. (bottom)

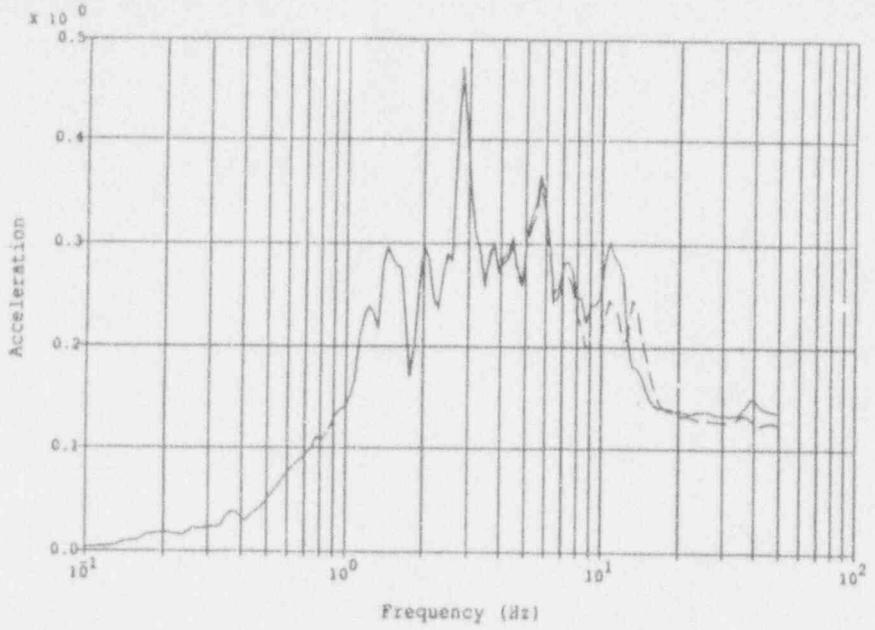

Legend:
Degraded Model
Factor = 0.75
Original Model

Notes:
1SSE Level, .12g PGA
Accelerations in g's
5% Spectral Damping
5% Struct. Damping

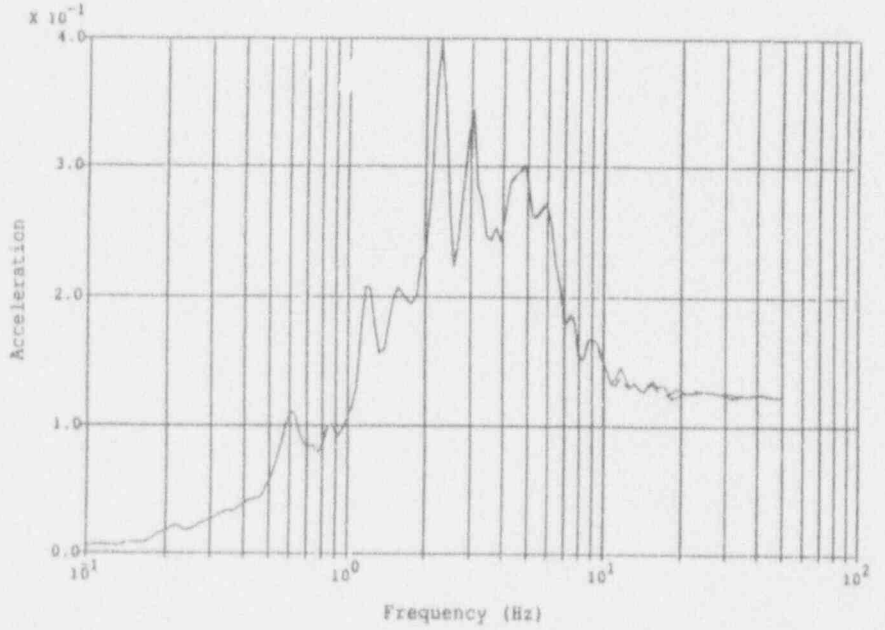

Legend:
Degraded Model
Factor = 0.75
Original Model

Notes:
1SSE Level, .12g PGA
Accelerations in g's
5% Spectral Damping
5% Struct. Damping

Figure A-68 Peach Bottom Deterministic Analysis, CWP Building Node 4, Elev. 88', N-S dir. (top), E-W dir. (bottom)

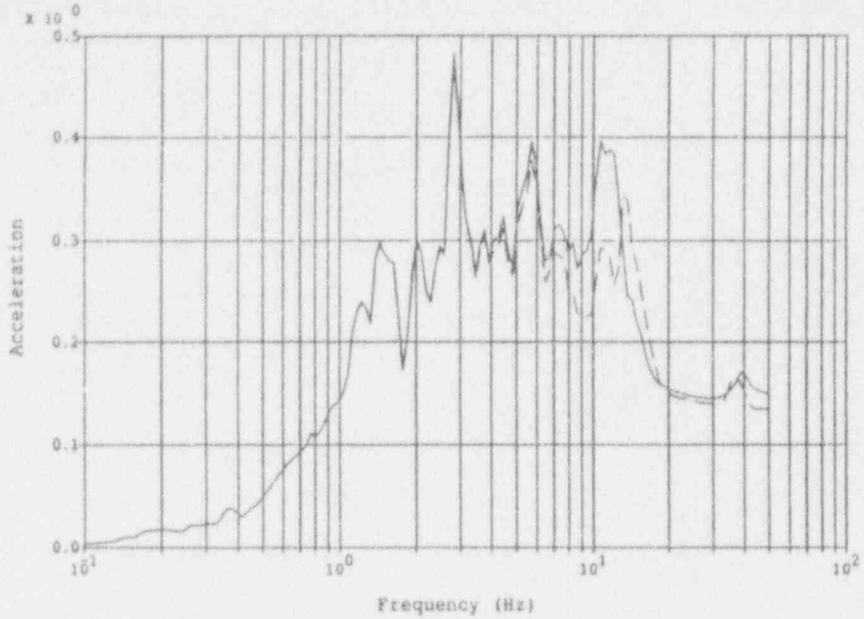

Legend:
Degraded Model Factor = 0.75 ———————
Original Model — — — — — —

Notes:
1SSE Level, .12g PGA
Accelerations in g's
5% Spectral Damping
5% Struct. Damping

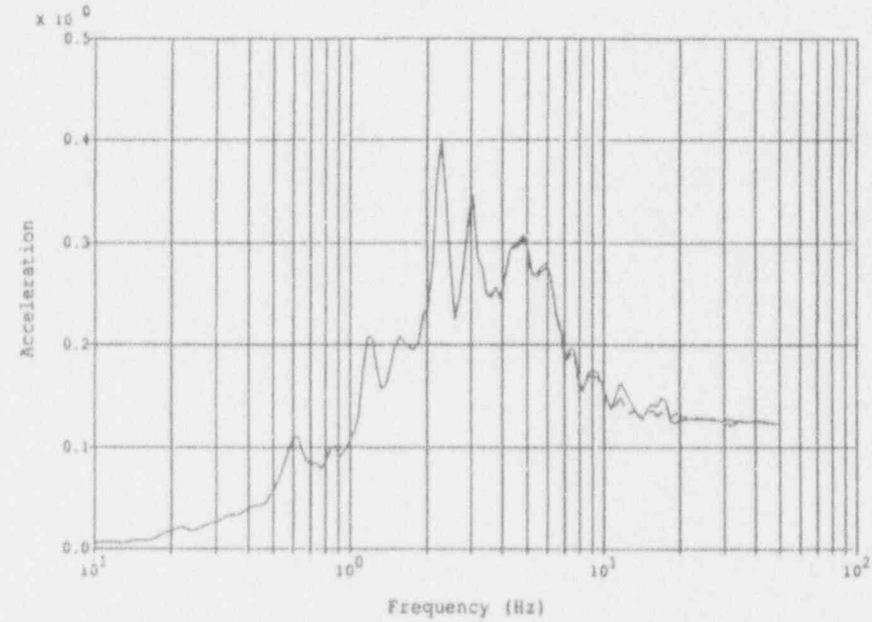

Legend:
Degraded Model Factor = 0.75 ———————
Original Model — — — — — —

Notes:
1SSE Level, .12g PGA
Accelerations in g's
5% Spectral Damping
5% Struct. Damping

Figure A-69 Peach Bottom Deterministic Analysis, CWP Building Node 7, Elev. 97', N-S dir. (top), E-W dir. (bottom)

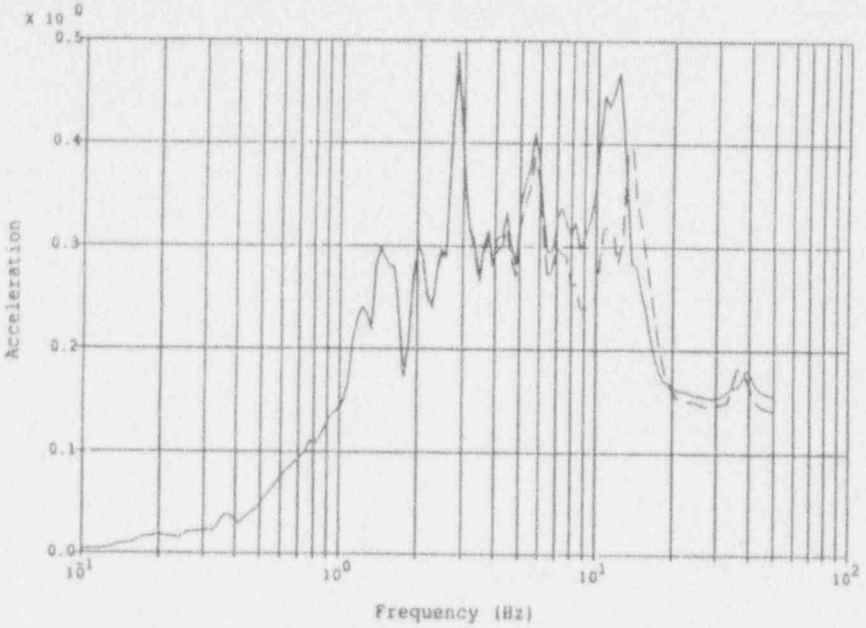

Legend:

Degraded Model
Factor = 0.75

Original Model

Notes:

1SSE Level, .12g PGA
Accelerations in g's
5% Spectral Damping
5% Struct. Damping

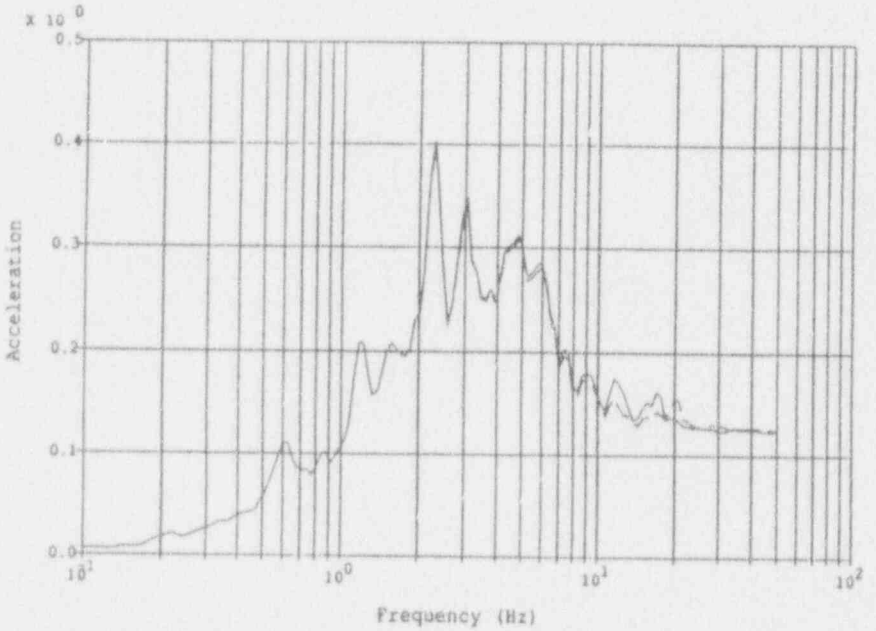

Legend:

Degraded Model
Factor = 0.75

Original Model

Notes:

1SSE Level, .12g PGA
Accelerations in g's
5% Spectral Damping
5% Struct. Damping

Figure A-70 Peach Bottom Deterministic Analysis, CWP Building Node 10, Elev. 105', N-S dir. (top), E-W dir. (bottom)

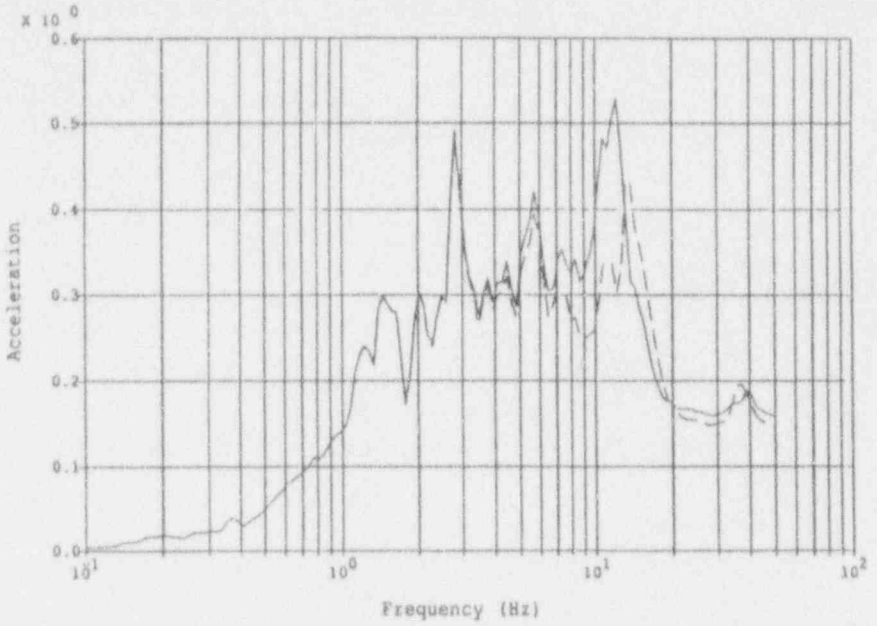

Legend:

Degraded Model
Factor = 0.75 ———————

Original Model — — — — — —

Notes:

1SSE Level, .12g PGA
Accelerations in g's
5% Spectral Damping
5% Struct. Damping

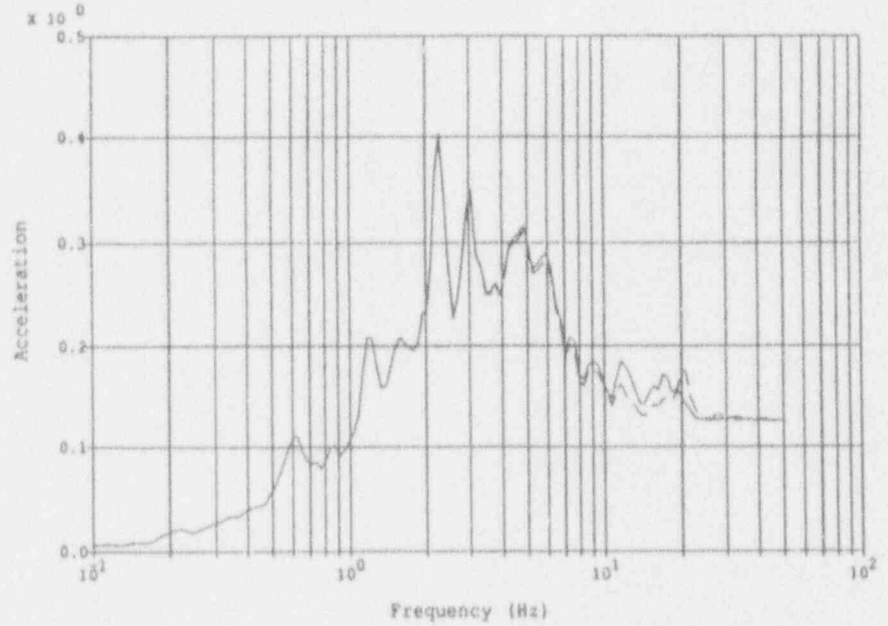

Legend:

Degraded Model
Factor = 0.75 ———————

Original Model — — — — — —

Notes:

1SSE Level, .12g PGA
Accelerations in g's
5% Spectral Damping
5% Struct. Damping

Figure A-71 Peach Bottom Deterministic Analysis, CWP Building Node 13, Elev. 114', N-S dir. (top), E-W dir. (bottom)

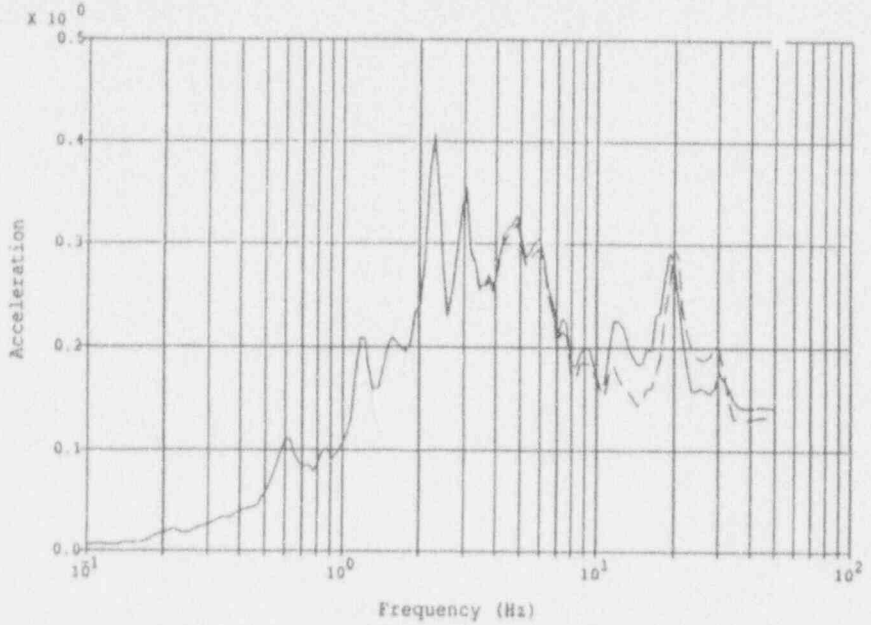

Legend:
Degraded Model
Factor = 0.75
Original Model

Notes:
1SSE Level, .12g PGA
Accelerations in g's
5% Spectral Damping
5% Struct. Damping

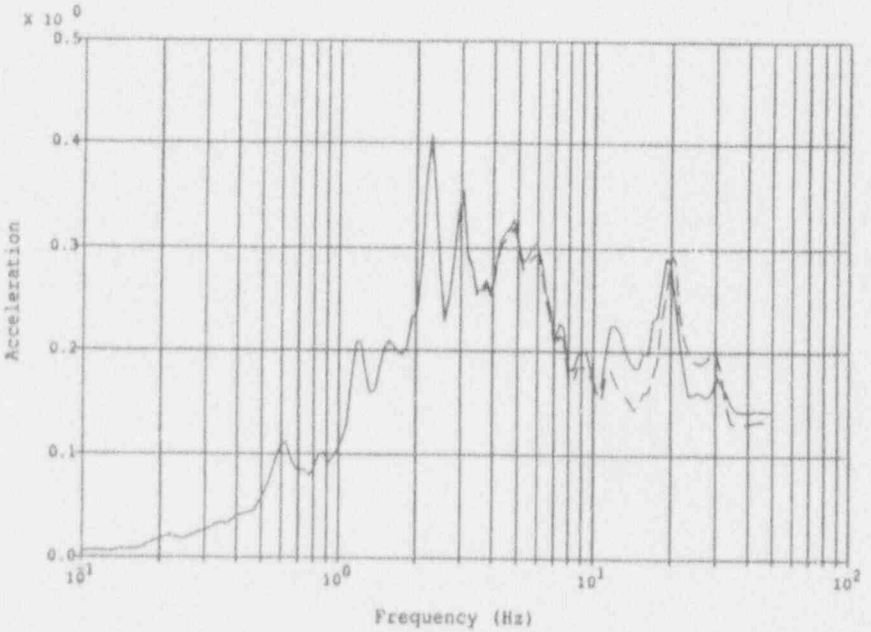

Legend:
Degraded Model
Factor = 0.75
Original Model

Notes:
1SSE Level, .12g PGA
Accelerations in g's
5% Spectral Damping
5% Struct. Damping

Figure A-72 Peach Bottom Deterministic Analysis, CWP Building Node 17, Elev. 130', N-S dir. (top), E-W dir. (bottom)

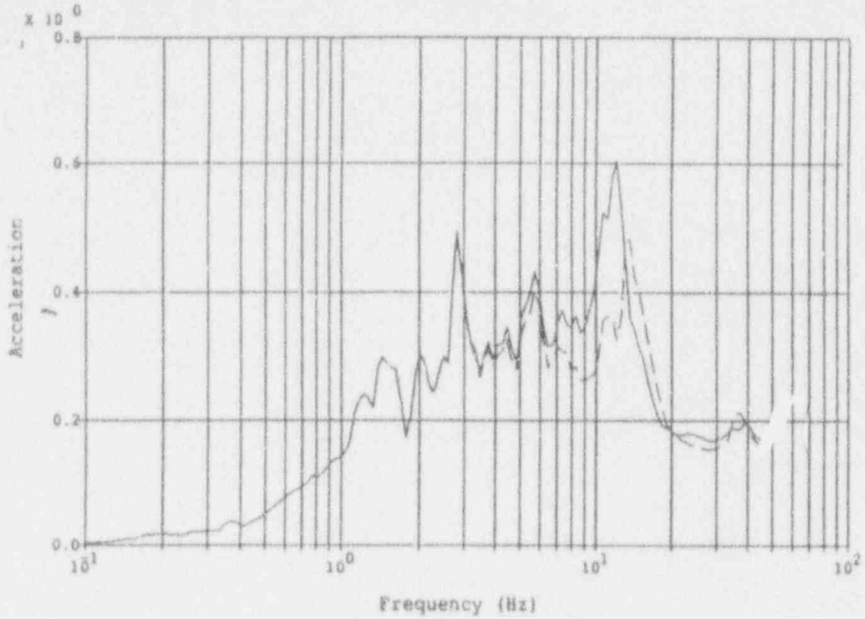

Legend:

Degraded Model
Factor = 0.75 ————————

Original Model — — — — —

Notes:

1SSE Level, .12g PGA
Accelerations in g's
5% Spectral Damping
5% Struct. Damping

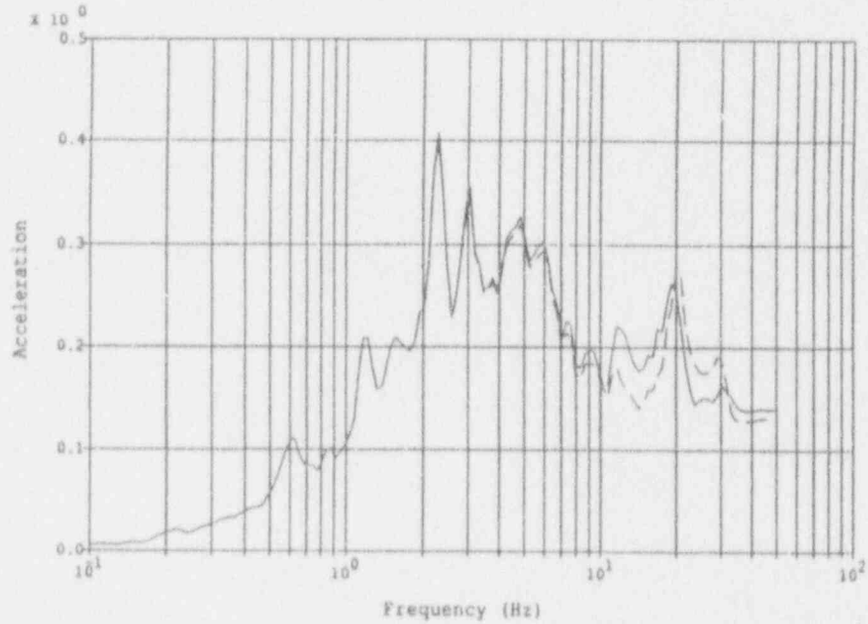

Legend:

Degraded Model
Factor = 0.75 ————————

Original Model — — — — —

Notes:

1SSE Level, .12g PGA
Accelerations in g's
5% Spectral Damping
5% Struct. Damping

Figure A-73 Peach Bottom Deterministic Analysis, CWP Building Node 20, Elev. 130', N-S dir. (top), E-W dir. (bottom)

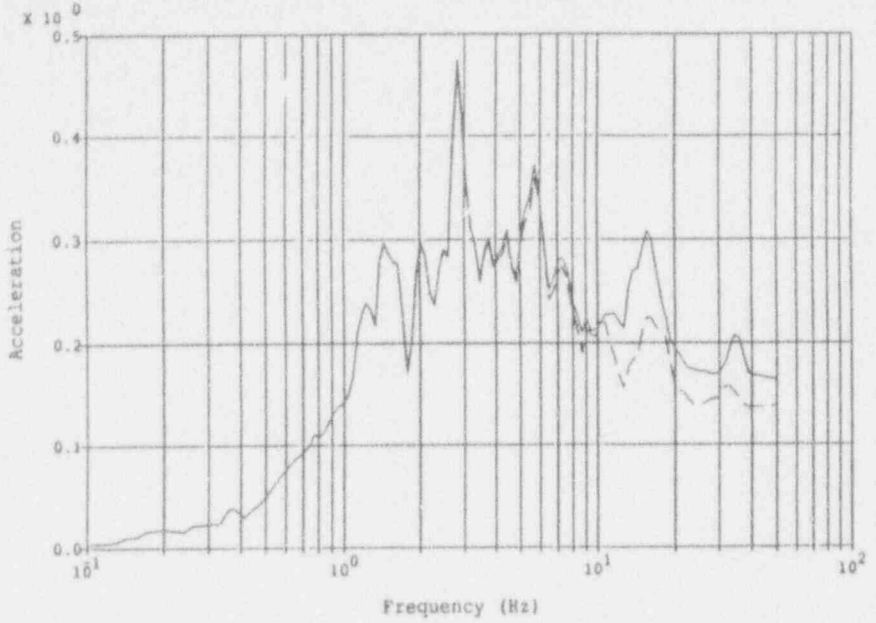

Legend:

Degraded Model
Factor = 0.75 ————————

Original Model — — — — —

Notes:

1SSE Level, .12g PGA
Accelerations in g's
5% Spectral Damping
5% Struct. Damping

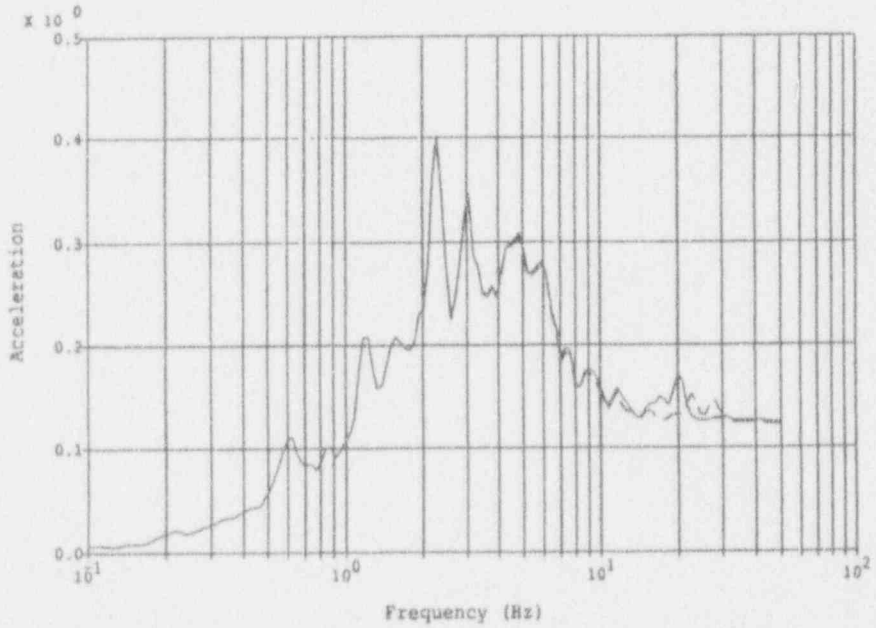

Legend:

Degraded Model
Factor = 0.75 ————————

Original Model — — — — —

Notes:

1SSE Level, .12g PGA
Accelerations in g's
5% Spectral Damping
5% Struct. Damping

Figure A-74 Peach Bottom Deterministic Analysis, DG Building Node 4, Elev. 151', N-S dir. (top), E-W dir. (bottom)

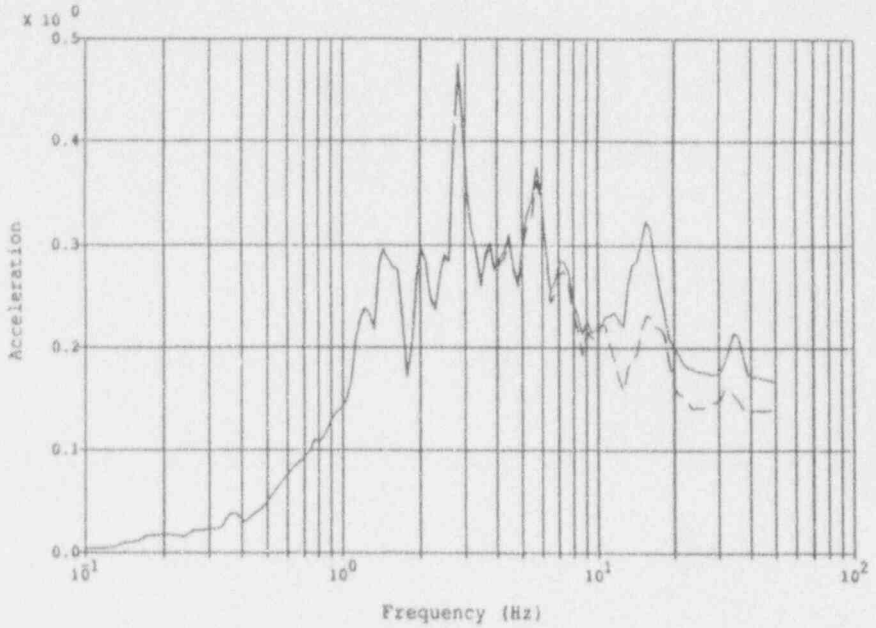

Legend:

Degraded Model
Factor = 0.75 ———————

Original Model — — — — —

Notes:

1SSE Level, .12g PGA
Accelerations in g's
5% Spectral Damping
5% Struct. Damping

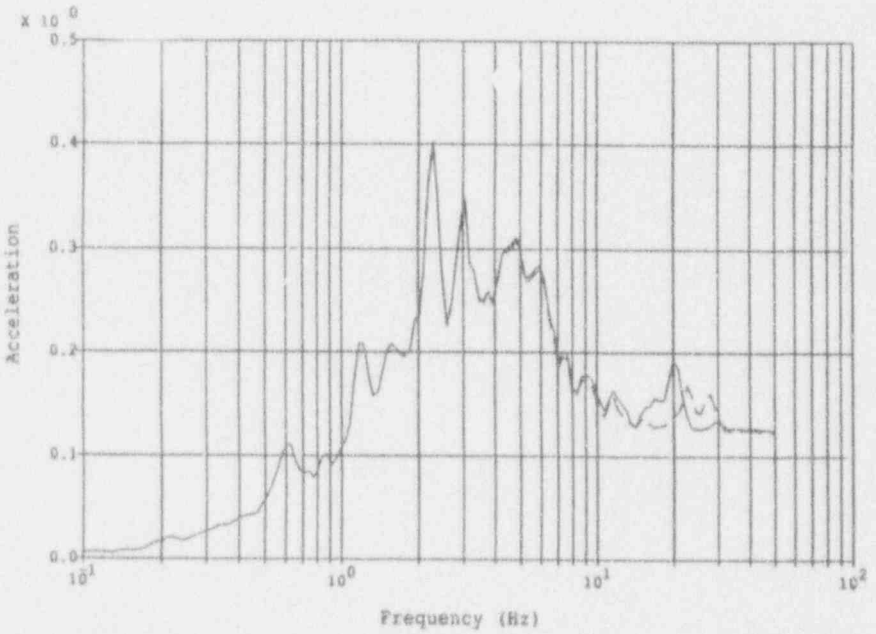

Legend:

Degraded Model
Factor = 0.75 ———————

Original Model — — — — —

Notes:

1SSE Level, .12g PGA
Accelerations in g's
5% Spectral Damping
5% Struct. Damping

Figure A-75 Peach Bottom Deterministic Analysis, DG Building Node 6, Elev. 161', N-S dir. (top), E-W dir. (bottom)

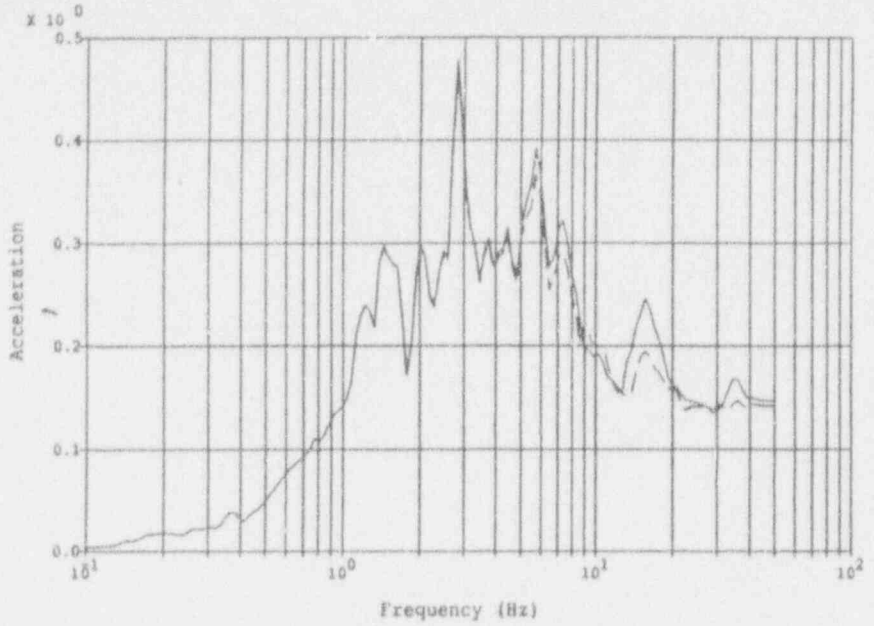

Legend:

Degraded Model
Factor = 0.75 ———————

Original Model — — — — —

Notes:

1SSE Level, .12g PGA
Accelerations in g's
5% Spectral Damping
5% Struct. Damping

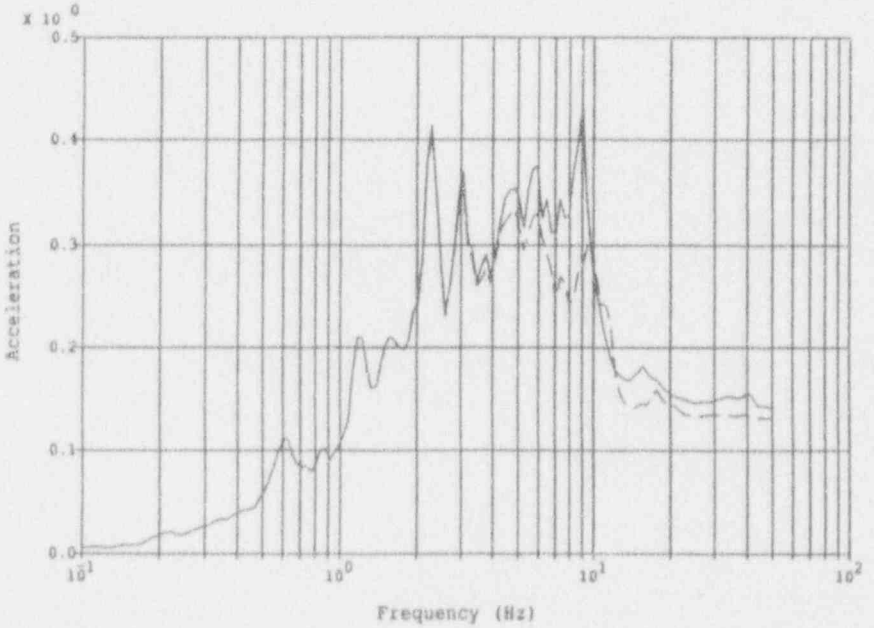

Legend:

Degraded Model
Factor = 0.75 ———————

Original Model — — — — —

Notes:

1SSE Level, .12g PGA
Accelerations in g's
5% Spectral Damping
5% Struct. Damping

Figure A-76 Peach Bottom Deterministic Analysis, EC Towers Node 2, Elev. 136', N-S dir. (top), E-W dir. (bottom)

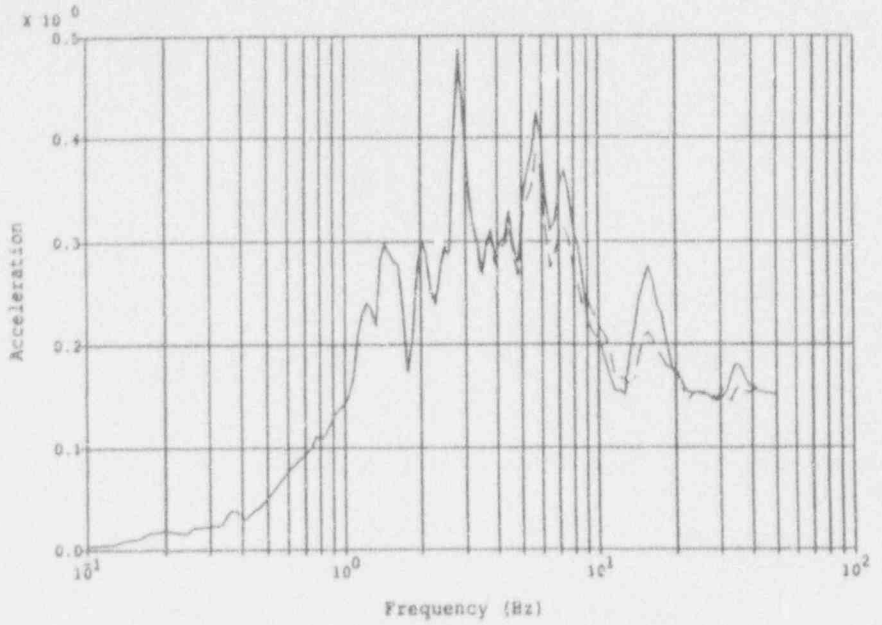

Legend:

Degraded Model
Factor = 0.75 ——————

Original Model — — — — —

Notes:

1SSE Level, .12g PGA
Accelerations in g's
5% Spectral Damping
5% Struct. Damping

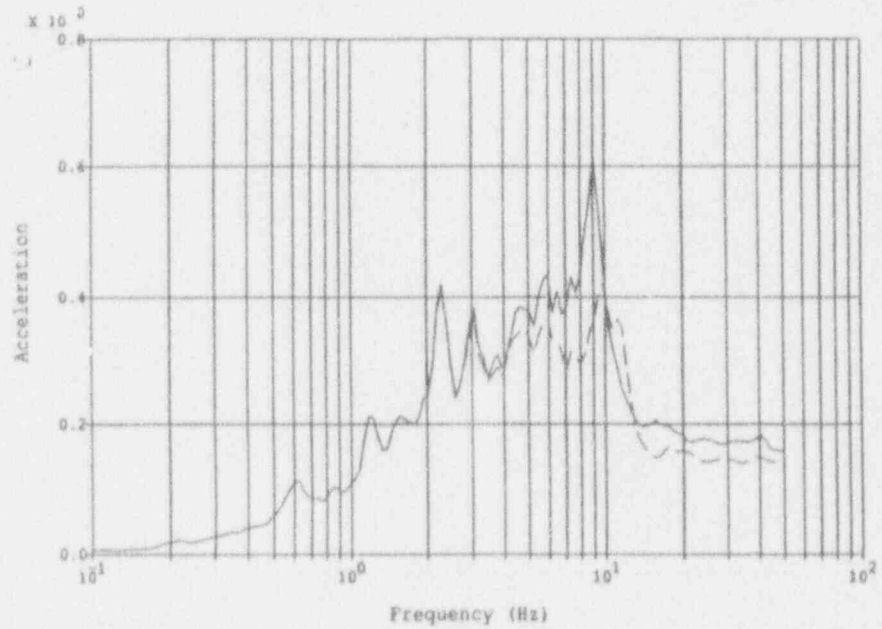

Legend:

Degraded Model
Factor = 0.75 ——————

Original Model — — — — —

Notes:

1SSE Level, .12g PGA
Accelerations in g's
5% Spectral Damping
5% Struct. Damping

Figure A-77 Peach Bottom Deterministic Analysis, EC Towers Node 3, Elev. 153', N-S dir. (top), E-W dir. (bottom)

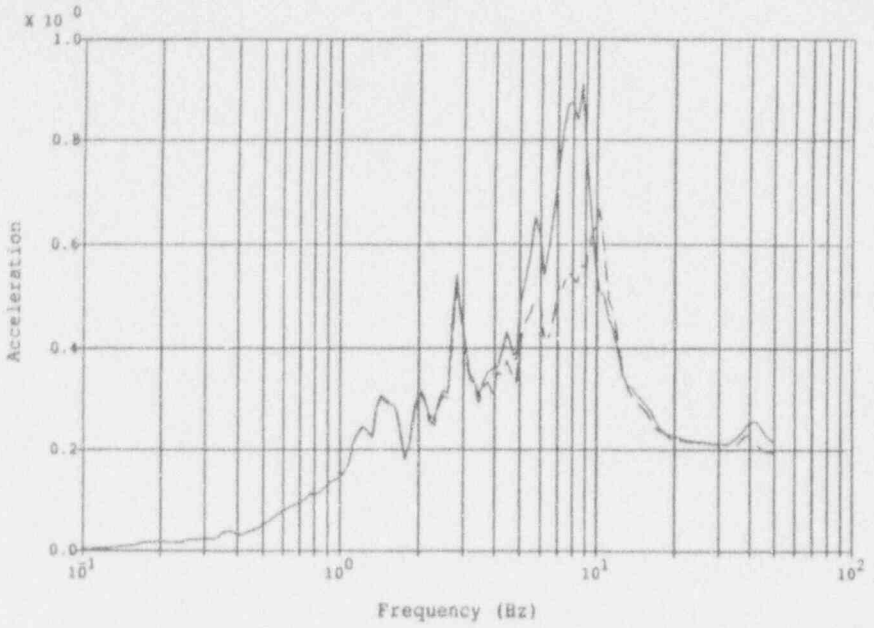

Legend:
Degraded Model
Factor = 0.75
Original Model

Notes:
1SSE Level, .12g PGA
Accelerations in g's
5% Spectral Damping
5% Struct. Damping

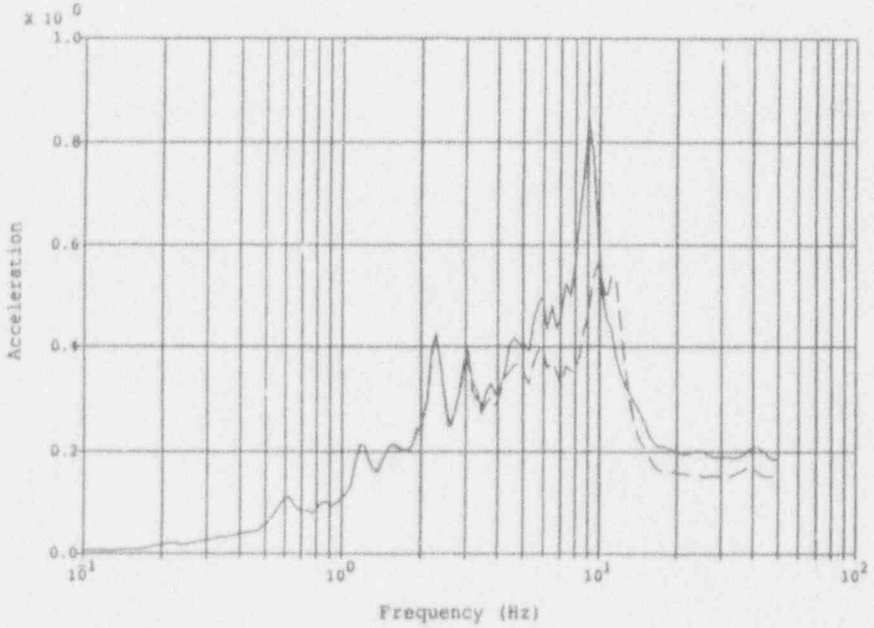

Legend:
Degraded Model
Factor = 0.75
Original Model

Notes:
1SSE Level, .12g PGA
Accelerations in g's
5% Spectral Damping
5% Struct. Damping

Figure A-78 Peach Bottom Deterministic Analysis, EC Towers Node 4, Elev. 168' N-S dir. (top), E-W dir. (bottom)

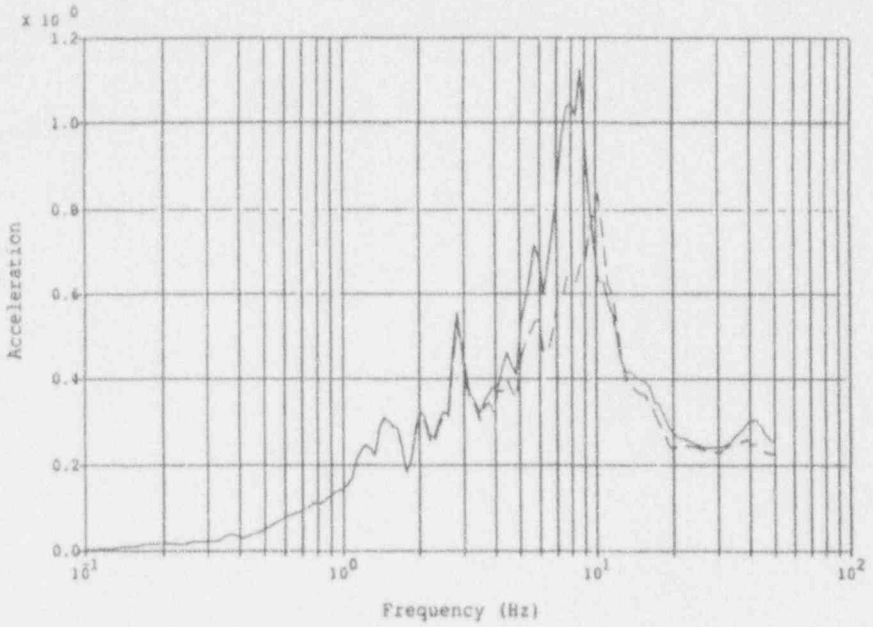

Legend:

Degraded Model
Factor = 0.75 ——————

Original Model — — — — —

Notes:

1SSE Level, .12g PGA
Accelerations in g's
5% Spectral Damping
5% Struct. Damping

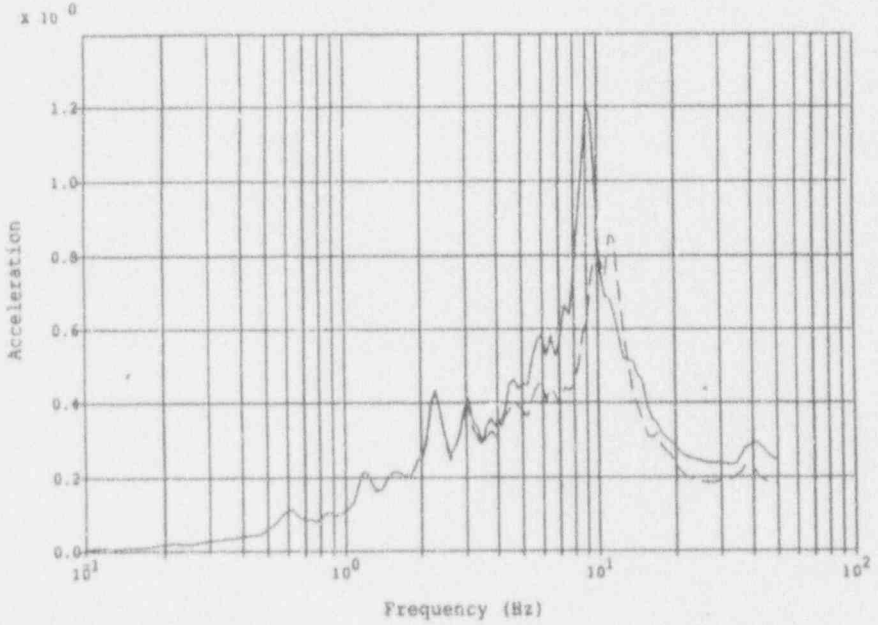

Legend:

Degraded Model
Factor = 0.75 ——————

Original Model — — — — —

Notes:

1SSE Level, .12g PGA
Accelerations in g's
5% Spectral Damping
5% Struct. Damping

Figure A-79 Peach Bottom Deterministic Analysis, EC Towers Node 5, Elev. 192', N-S dir. (top), E-W dir. (bottom)

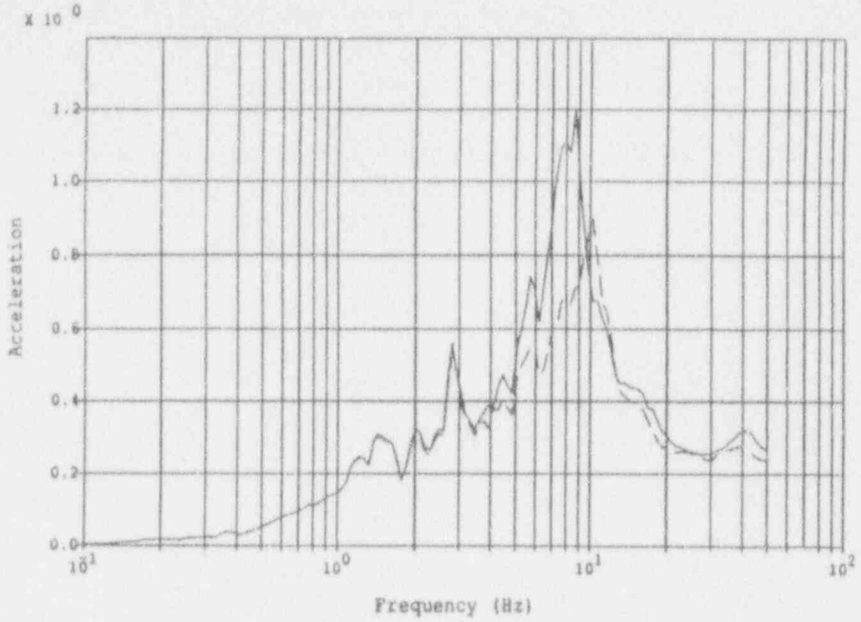

Legend:

Degraded Model
Factor = 0.75

Original Model

Notes:

1SSE Level, .12g PGA
Accelerations in g's
5% Spectral Damping
5% Struct. Damping

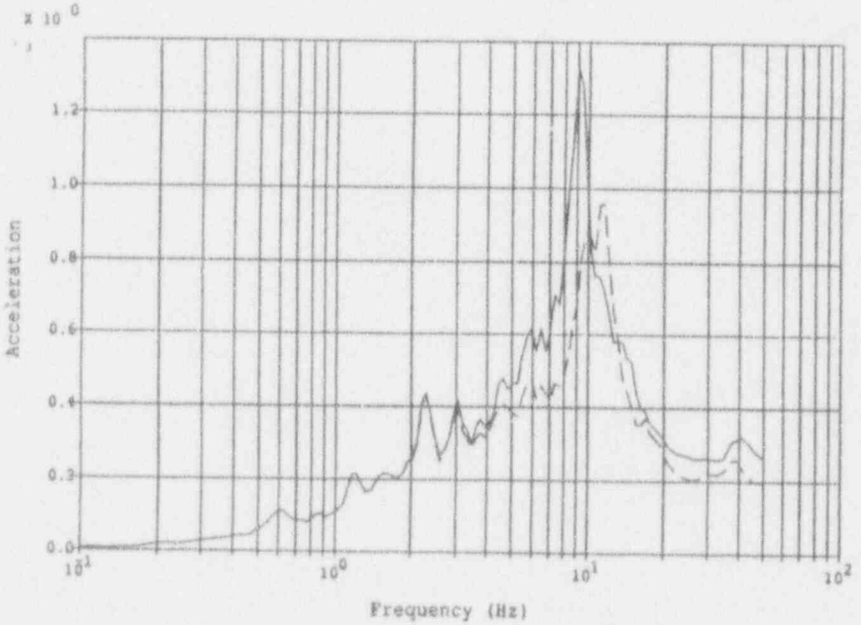

Legend:

Degraded Model
Factor = 0.75

Original Model

Notes:

1SSE Level, .12g PGA
Accelerations in g's
5% Spectral Damping
5% Struct. Damping

Figure A-80 Peach Bottom Deterministic Analysis, EC Towers Node 6, Elev. 202', N-S dir. (top), E-W dir. (bottom)

Table A-21

Forces between Floor Levels of Peach Bottom Reactor/Containment Building

Original Stiffnesses

Elev.	$Shear_X$(kip)	$Shear_Y$(kip)	$Moment_X$(kip-ft)	$Moment_Y$(kip-ft)
Externals:				
91'	16,710	13,100	1,338,000	1,642,000
119'	16,030	12,550	940,900	1,160,000
135'	13,240	10,760	751,600	928,500
165'	10,430	8,494	429,000	532,800
195'	5,224	4,179	174,100	219,800
234'	500	342	11,660	17,300
252'	248	162	5,518	8,444
Internals:				
119'	735	544	18,770	23,280
135'	670	505	10,570	12,550
145'	298	264	5,151	6,688
156'	228	197	2,488	3,631
169'	96	67	545	922
182'	81	74	963	1,056

Reduced Stiffnesses

Elev.	$Shear_X$(kip)	$Shear_Y$(kip)	$Moment_X$(kip-ft)	$Moment_Y$(kip-ft)
Externals:				
91'	17,860	13,450	1,316,000	1,715,000
119'	17,090	12,900	909,000	1,174,000
135'	13,940	10,620	724,400	915,700
165'	10,320	8,151	417,600	509,000
195'	5,130	4,109	173,000	218,300
234'	533	374	12,700	18,310
252'	265	175	5,966	9,018
Internals:				
119'	748	539	18,050	24,690
135'	684	494	9,916	13,390
145'	311	244	5,136	6,322
156'	217	188	2,759	3,699
169'	100	74	737	1,361
182'	69	59	770	902

Table A-22

Forces between Floor Levels of Peach Bottom Radwaste/Turbine Building

Original Stiffnesses

Elev.	$Shear_X$(kip)	$Shear_Y$(kip)	$Moment_X$(kip-ft)	$Moment_Y$(kip-ft)
116′	8,490	6,176	332,800	391,500
135′	6,106	4,619	161,100	223,900
150′	4,388	3,292	92,260	128,800
165′	2,032	1,598	40,100	57,310

Reduced Stiffnesses

Elev.	$Shear_X$(kip)	$Shear_Y$(kip)	$Moment_X$(kip-ft)	$Moment_Y$(kip-ft)
116′	9,154	6,568	322,700	403,900
135′	6,456	4,977	164,100	235,100
150′	4,637	3,559	87,520	137,100
165′	2,183	1,453	35,340	61,600

Table A-23

Forces between Floor Levels of Peach Bottom
Circulating Water Pump Structure

Original Stiffnesses

Elev.	$Shear_X$(kip)	$Shear_Y$(kip)	$Moment_X$(kip-ft)	$Moment_Y$(kip-ft)
79'	6,527	5,746	151,500	159,200
88'	5,079	4,560	99,970	102,400
97'	3,564	2,996	55,760	58,840
105'	2,377	1,873	28,390	28,110
114'	267	234	4,047	4,429
114'	162	139	2,311	2,685

Reduced Stiffnesses

Elev.	$Shear_X$(kip)	$Shear_Y$(kip)	$Moment_X$(kip-ft)	$Moment_Y$(kip-ft)
79'	7,047	5,785	155,800	169,600
88'	5,437	4,646	103,200	108,300
97'	3,793	3,100	57,880	61,820
105'	2,520	1,949	29,510	29,340
114'	281	248	4,299	4,649
114'	170	146	2,437	2,809

Table A-24

Forces between Floor Levels of Peach Bottom
Diesel Generator Building

Original Stiffnesses

Elev.	$Shear_X$(kip)	$Shear_Y$(kip)	$Moment_X$(kip-ft)	$Moment_Y$(kip-ft)
127'	1,256	1,111	30,510	36,080
151'	514	477	5,672	5,677

Reduced Stiffnesses

Elev.	$Shear_X$(kip)	$Shear_Y$(kip)	$Moment_X$(kip-ft)	$Moment_Y$(kip-ft)
127'	1,476	1,129	30,890	42,590
151'	606	480	5,688	6,793

Table A-25

Forces between Floor Levels of Peach Bottom
Emergency Cooling Towers

Original Stiffnesses

Elev.	$Shear_X$(kip)	$Shear_Y$(kip)	$Moment_X$(kip-ft)	$Moment_Y$(kip-ft)
118'	6,205	5,758	173,900	197,000
136'	3,065	2,573	71,510	85,340
153'	1,539	1,141	29,380	38,500
168'	595	472	12,260	15,420
192'	113	91	914	1,134

Reduced Stiffnesses

Elev.	$Shear_X$(kip)	$Shear_Y$(kip)	$Moment_X$(kip-ft)	$Moment_Y$(kip-ft)
118'	5,583	6,440	206,600	184,600
136'	2,895	3,110	90,660	85,260
153'	1,615	1,481	38,530	40,510
168'	628	629	16,320	16,280
192'	119	122	1,220	1,198

A.7 REFERENCES

A-1. J.A. Lambright, et. al., Analysis of Core Damage Frequency: Peach Bottom Unit 2 External Events, NUREG/CR-4550, SAND86-2084, Vol.4, Rev.1, Part 3. December, 1990.

A-2. Peach Bottom Atomic Power Station Updated Final Safety Analysis Report Section 2.0, June 1983.

A-3. D.L. Bernreuter, et. al., Seismic Hazard Characterization of 69 Nuclear Plant Sites East of the Rocky Mountains, NUREG/CR-5250, October, 1988.

A-4. Electric Power Research Institute, Seismic Hazard Methodology for the Central and Eastern United States, EPRI NP-4726, Vols 1-10, July, 1986.

A-5. H.B. Seed, et. al., Site Dependent Spectra for Earthquake Resistant Design, Earthquake Engineering Research Center, University of California, Berkeley, CA, EERC 74-12m, 1974.

A-6. M.P. Bohn, et al., Application of the SSMRP Methodology to the Seismic Risk at the Zion Nuclear Power Plant, Lawrence Livermore National Laboratory, Livermore, CA, UCRL-53483, NUREG/CR-3428, 1983.

ATTACHMENT TO APPENDIX A

FILES FOR PEACH BOTTOM SEISMIC ANALYSIS

Fragility Files

Response Files

Accident Sequence Expressions

Cross-Reference File

PEACH BOTTOM FRAGILITIES FILE (ORIGINAL STIFFNESS CASE)

No.	M_F	β_{tr}	β_{tu}	Category
1	0.25	0.25	.25	CERAMIC INSULATORS
2	4.00	0.48	.75	RELAY CHATTER
3	7.63	0.48	.74	CIRCUIT BREAKER TRIP
4	2.50	0.40	.39	BATTERIES
5	2.29	0.31	.39	BATTERY RACKS
6	2.00	0.26	.35	INVERTORS
7	8.80	0.28	.30	TRANSFORMERS
8	7.63	0.48	.74	MOTOR CONTROL CENTER
9	7.63	0.48	.66	AUX RELAY CABINET
10	6.43	0.29	.66	SWITCHGEAR
11	2.23	0.34	.19	CABLE TRAYS
12	11.50	0.46	.74	CONTROL PANELS AND RACKS
13	7.68	0.20	.35	LOCAL INSTRUMENTS
14	1.00	0.25	.31	DIESEL GENERATOR
15	12.10	0.27	.31	MOTORS-HORIZONTAL
16	2.80	0.25	.27	MOTOR-DRIVEN PUMPS & COMPRESSORS
17	2.21	0.22	.32	LG. VERT. M-D. CENTRIF PUMP
18	6.50	0.26	.60	LMOV
19	4.83	0.26	.60	SMALL MOV & AOVs
20	6.50	0.26	.34	LG. PNEUM/HYD VALVE
21	8.90	0.20	.35	LG. MANUAL,CHECK,RELIEF VALVE
22	12.50	0.33	.43	MISC. SMALL VALVES
23	3.00	0.30	.53	LG. HORIZ. VESSELS
24	1.84	0.25	.45	SM-MED HEAT EXCHANGERS & VESSELS
25	1.46	0.20	.35	LG. VERT VESSELS w/ FORMED HEADS
26	0.45	0.35	.29	LG. VERT. FLAT BOTTOMED TANKS
27	6.90	0.27	.31	AIR HANDLING UNITS
28	1.95	0.26	.28	BWR REACTOR SKIRT (GENERIC)
29	0.95892	0.50	.3	SLOCA FIT (SSMRP)
30	1.4967	0.4681	.3	MLOCA FIT (SSMRP)
31	1.26	0.35	.40	BWR RECIRC PUMP SUPPORT (GENERIC)
32	1.00	0.04	.17	DIKE AROUND CST AND RWST
33	0.55	0.11	.21	EMERGENCY COOLING TOWER (PEACH)
34	1.5	0.16	.27	REACTOR BLDG. SHEAR WALLS
35	1.4	0.10	.23	RADWASTE/TURBINE ROOF DIAPHRAGM
36	1.5	0.13	.25	RADWASTE/TURBINE SHEAR WALLS
37	0.5	0.11	.21	TURBINE BLDG.
38	1.5	0.13	.24	BLOCK WALLS-VARIOUS
39	99.0	0.3	.3	DUMMY EVENT-CAUSES NO SEISMIC FAILURE
40	0.01	0.3	.3	DUMMY EVENT-CAUSES FAILURE PF=1
41	3.30	0.15	.25	4KV BUSSES (PEACH BOTTOM)
42	0.95	0.15	.20	DG DAY TANKS
43	4.42	0.15	.25	HPCI ROOM COOLER

PEACH BOTTOM FRAGILITIES FILE (REDUCED STIFFNESS CASE)

No.	M_F	β_{fr}	β_{fu}	Category
1	0.25	0.25	.25	CERAMIC INSULATORS
2	4.00	0.48	.75	RELAY CHATTER
3	7.63	0.48	.74	CIRCUIT BREAKER TRIP
4	2.50	0.40	.39	BATTERIES
5	2.29	0.31	.39	BATTERY RACKS
6	2.00	0.26	.35	INVERTORS
7	8.80	0.28	.30	TRANSFORMERS
8	7.63	0.48	.74	MOTOR CONTROL CENTER
9	7.63	0.48	.66	AUX RELAY CABINET
10	6.43	0.29	.66	SWITCHGEAR
11	2.23	0.34	.19	CABLE TRAYS
12	11.50	0.46	.74	CONTROL PANELS AND kACKS
13	7.68	0.20	.35	LOCAL INSTRUMENTS
14	1.00	0.25	.31	DIESEL GENERATOR
15	12.10	0.27	.31	MOTORS-HORIZONTAL
16	2.80	0.25	.27	MOTOR-DRIVEN PUMPS & COMPRESSORS
17	2.21	0.22	.32	LG. VERT. M-D. CENTRIF PUMP
18	6.50	0.26	.60	LMOV
19	4.83	0.26	.60	SMALL MOV & AOVs
20	6.50	0.26	.34	LG. PNEUM/HYD VALVE
21	8.90	0.20	.35	LG. MANUAL,CHECK,RELIEF VALVE
22	12.50	0.33	.43	MISC. SMALL VALVES
23	3.00	0.30	.53	LG. HORIZ. VESSELS
24	1.84	0.25	.45	SM-MED HEAT EXCHANGERS & VESSELS
25	1.46	0.20	.35	LG. VERT VESSELS w/ FORMED HEADS
26	0.45	0.35	.29	LG. VERT. FLAT BOTTOMED TANKS
27	6.90	0.27	.31	AIR HANDLING UNITS
28	1.95	0.26	.28	BWR REACTOR SKIRT (GENERIC)
29	0.95892	0.50	.3	SLOCA FIT (SSMRP)
30	1.4967	0.4681	.3	MLOCA FIT (SSMRP)
31	1.26	0.35	.40	BWR RECIRC PUMP SUPPORT (GENERIC)
32	1.00	0.04	.17	DIKE AROUND CST AND RWST
33	0.55	0.11	.21	EMERGENCY COOLING TOWER (PEACH)
34	1.6	0.16	.27	REACTOR BLDG. SHEAR WALLS
35	1.2	0.10	.23	RADWASTE/TURBINE ROOF DIAPHRAGM
36	1.6	0.13	.25	RADWASTE/TURBINE SHEAR WALLS
37	0.5	0.11	.21	TURBINE BLDG.
38	1.5	0.13	.24	BLOCK WALLS-VARIOUS
39	99.0	0.3	.3	DUMMY EVENT-CAUSES NO SEISMIC FAILURE
40	0.01	0.3	.3	DUMMY EVENT-CAUSES FAILURE PF=1
41	3.30	0.15	.25	4KV BUSSES (PEACH BOTTOM)
42	0.95	0.15	.20	DG DAY TANKS
43	4.42	0.15	.25	HPCI ROOM COOLER

PEACH BOTTOM RESPONSE MULTIPLE FILE (ORIGINAL STIFFNESS CASE)

No.	F_1	F_2	β_{rr}	β_{ru}	Response	
1	1.00		0.25	.25	FREE-FIELD	ZPA
2	2.08		0.45	.25		2-5 HZ
3	1.90		0.45	.25		5 (USED 7 HZ)
4	1.78		0.35	.25		5-10
5	1.90		0.35	.25		7
6	1.10		0.35	.25	CS 135	ZPA
7	2.14		0.45	.25		5-10 HZ
8	1.26		0.35	.25	150	ZPA
9	2.56		0.45	.25		5-10
10	1.47		0.35	.25	165	ZPA
11	2.98		0.45	.25		5-10
12	1.00		0.35	.25	RB 91	ZPA
13	1.87		0.45	.25		5-10
14	1.96		0.45	.25		7
15	2.12		0.45	.25		5
16	1.05		0.35	.25	116	ZPA
17	2.13		0.45	.25		7
18	1.09		0.35	.25	135	ZPA
19	2.22		0.45	.25		7
20	1.27		0.35	.25	165	ZPA
21	3.12		0.45	.25		7
22	1.00		0.35	.25	DG 127	ZPA
23	1.88		0.45	.25		5-10
24	2.12		0.45	.25		5
25	1.00		0.35	.25	TB 116	ZPA
26	1.96		0.45	.25		7
27	1.16		0.35	.25	CWPS 114	ZPA
28	2.30		0.45	.25		7
29	1.28		0.35	.25	ECT 153	ZPA
30	2.66		0.45	.25		7
31	2.43		0.45	.25		5
32	1.00		0.00	.25	DUMMY RESPONSE FOR M-LOCA & S-LOCA IE	

PEACH BOTTOM RESPONSE MULTIPLE FILE (REDUCED STIFFNESS CASE)

No.	F_1	F_2	β_{rr}	β_{ru}	Response	
1	1.00		0.25	.25	FREE-FIELD	ZPA
2	2.08		0.47	.25		2-5 HZ
3	1.90		0.45	.25		5 (USED 7 HZ)
4	1.78		0.35	.25		5-10
5	1.90		0.35	.25		7
6	1.11	0.06	0.35	.25	CS 135	ZPA
7	2.28	-0.12	0.45	.25		5-10 HZ
8	1.41	0.09	0.35	.25	150	ZPA
9	3.05	-0.12	0.45	.25		5-10
10	1.65	0.04	0.35	.25	165	ZPA
11	3.71	-0.11	0.45	.25		5-10
12	1.00	0.0	0.35	.25	RB 91	ZPA
13	1.87	0.0	0.45	.25		5-10
14	1.96	0.0	0.45	.25		7
15	2.12	0.0	0.45	.25		5
16	1.04	-0.02	0.35	.25	116	ZPA
17	2.06	-0.11	0.45	.25		7
18	1.07	-0.05	0.35	.25	135	ZPA
19	2.07	-0.09	0.45	.25		7
20	1.26	0.01	0.35	.25	165	ZPA
21	2.87	-0.13	0.45	.25		7
22	1.00	0.0	0.35	.25	DG 127	ZPA
23	1.88	0.0	0.45	.25		5-10
24	2.12	0.0	0.45	.25		5
25	1.00	0.0	0.35	.25	TB 116	ZPA
26	1.96	0.0	0.45	.25		7
27	1.31	0.14	0.35	.25	CWPS 114	ZPA
28	2.54	0.29	0.45	.25		7
29	1.34	0.17	0.35	.25	ECT 153	ZPA
30	3.03	-0.11	0.45	.25		7
31	2.71	0.18	0.45	.25		5
32	1.00		0.00	.25	DUMMY RESPONSE FOR M-LOCA & S-LOCA IE	

PEACH BOTTOM ACCIDENT SEQUENCES

BOOLEAN 4 FAILS ALL ESW AND GIVEN LOSP, CAUSES SBO

BOOL(4) =
ACP-CCF-2-4KV * TURBINE-BLDG +
ACP-CCF-2-4KV * EMER COOL-TOWER +
ACP-DGN-LP-EDGB * ACP-CCF-2-4KV +
ACP-DGN-LP-EDGD * ACP-CCF-2-4KV +
ACP-DGN-LP-EDGC * ACP-CCF-2-4KV +
ESW-MDP-FS-MDPA * ACP-BAC-LP-416C * TURBINE-BLDG +
ESW-MDP-FS-MDPB * ACP-BAC-LP-416B * TURBINE-BLDG +
ACP-BAC-LP-416D * ESW-CCF-PF-MDPS +
ACP-DGN-LP-EDGB * ACP-BAC-LP-416C * TURBINE-BLDG +
ACP-DGN-LP-EDGC * ACP-BAC-LP-416B * TURBINE-BLDG +
ESW-MDP-FS-MDPA * ACP-BAC-LP-416C * EMER-COOL-TOWER +
ESW-MDP-FS-MDPB * ACP-BAC-LP-416B * EMER-COOL-TOWER +
ACP-DGN-LP-EDGB * ACP-BAC-LP-416C * EMER-COOL-TOWER +
ACP-DGN-LP-EDGC * ACP-BAC-LP-416B * EMER-COOL-TOWER +
ESW-MDP-FS-MDPA * ESW-MDP-FS-ECW * ACP-BAC-LP-416C +
ESW-MDP-FS-MDPB * ESW-MDP-FS-ECW * ACP-BAC-LP-416B +
ACP-DGN-LP-EDGC * ESW-MDP-FS-ECW * ACP-BAC-LP-416B +
ACP-DGN-LP-EDGB * ESW-MDP-FS-ECW * ACP-BAC-LP-416C +
ACP-DGN-LP-EDGB * ESW-MDP-FS-MDPB * ACP-BAC-LP-416D +
ACP-DGN-LP-EDGD * ESW-MDP-FS-MDPB * ACP-BAC-LP-416B +
ACP-DGN-LP-EDGC * ESW-MDP-FS-MDPA * ACP-BAC-LP-416D +
ACP-DGN-LP-EDGD * ESW-MDP-FS-MDPA * ACP-BAC-LP-416C +
ESW-MDP-FS-ECW * ESW-CCF-PF-MDPS +
ESW-CCF-2-MDPS * TURBINE-BLDG +
ESW-CCF-2-MDPS * EMER-COOL-TOWER +
ACP-CCF-LP-DGS +
ACP-DGN-FR-EDGD * ACP-CCF-2-4KV +
ACP-DGN-FR-EDGB * ACP-CCF-2-4KV +
ACP-DGN-FR-EDGC * ACP-CCF-2-4KV +
ACP-CCF-2-DGS * ACP-BAC-LP-416D +
ACP-CCF-2-DGS * ACP-BAC-LP-416B +
ACP-CCF-2-DGS * ACP-BAC-LP-416C +
ACP-DGN-LP-EDGC * ESW-MDP-FS-MDPA * TURBINE-BLDG +
ACP-DGN-LP-EDGB * ESW-MDP-FS-MDPB * TURBINE-BLDG +
ACP-DGN-LP-EDGD * ESW-CCF-PF-MDPS +
ACP-DGN-FR-EDGC * ACP-BAC-LP-416B * TURBINE-BLDG +
ACP-DGN-FR-EDGB * ACP-BAC-LP-416C * TURBINE-BLDG +
ACP-CCF-2-DGS * TURBINE-BLDG +
ACP-BAC-LP-416B * DCP-BDC-LP-125C * TURBINE-BLDG +
DCP-BDC-LP-125B * ACP-BAC-LP-416C * TURBINE-BLDG +
ACP-DGN-LP-EDGC * ESW-MDP-FS-MDPA * EMER-COOL-TOWER +
ACP-DGN-LP-EDGB * ESW-MDP-FS-MDPB * EMER-COOL-TOWER +
ACP-DGN-FR-EDGC * ACP-BAC-LP-416B * EMER-COOL-TOWER +
ACP-DGN-FR-EDGB * ACP-BAC-LP-416C * EMER-COOL-TOWER +
ACP-CCF-2-DGS * EMER-COOL-TOWER +
ACP-BAC-LP-416B * DCP-BDC-LP-125C * EMER-COOL-TOWER +
DCP-BDC-LP-125B * ACP-BAC-LP-416C * EMER-COOL-TOWER +

```
ACP-DGN-LP-EDGC * ESW-MDP-FS-MDPA * ESW-MDP-FS-ECW +
ACP-DGN-LP-EDGB * ESW-MDP-FS-MDPB * ESW-MDP-FS-ECW +
ACP-DGN-MA-EDGC * ACP-CCF-2-4KV +
ACP-DGN-MA-EDGD * ACP-CCF-2-4KV +
DCP-BAT-LP-B2 * ACP-BAC-LP-416C * TURBINE-BLDG +
ACP-BAC-LP-416B * DCP-BAT-LP-C3 * TURBINE-BLDG +
DCP-BAT-LP-B2 * ACP-BAC-LP-416C * EMER-COOL-TOWER +
ACP-BAC-LP-416B * DCP-BAT-LP-C3 * EMER-COOL-TOWER +
ACP-CCF-2-4KV * ESW-TNK-LL-PS13 +
ACP-DGN-FR-EDGC * ESW-MDP-FS-ECW * ACP-BAC-LP-416B +
ACP-DGN-FR-EDGB * ESW-MDP-FS-ECW * ACP-BAC-LP-416C +
ACP-CCF-2-DGS * ESW-MDP-FS-ECW +
ACP-DGN-FR-EDGB * ESW-MDP-FS-MDPB * ACP-BAC-LP-416D +
ACP-DGN-FR-EDGC * ESW-MDP-FS-MDPA * ACP-BAC-LP-416D +
ACP-DGN-FR-EDGD * ESW-MDP-FS-MDPA * ACP-BAC-LP-416C +
ACP-DGN-FR-EDGD * ESW-MDP-FS-MDPB * ACP-BAC-LP-416B +
ACP-CCF-2-DGS * ESW-MDP-FS-MDPA +
ACP-CCF-2-DGS * ESW-MDP-FS-MDPB +
ACP-DGN-MA-EDGB * ACP-BAC-LP-416C * TURBINE-BLDG +
ACP-DGN-MA-EDGC * ACP-BAC-LP-416B * TURBINE-BLDG +
ACP-DGN-MA-EDGB * ACP-BAC-LP-416C * EMER-COOL-TOWER +
ACP-DGN-MA-EDGC * ACP-BAC-LP-416B * EMER-COOL-TOWER
```

BOOL 5 = BOOL 4 BUT NO DG'S

```
        BOOL(5) =
ACP-CCF-2-4KV * TURBINE-BLDG +
ACP-CCF-2-4KV * EMER-COOL-TOWER +
ESW-MDP-FS-MDPA * ACP-BAC-LP-416C * TURBINE-BLDG +
ESW-MDP-FS-MDPB * ACP-BAC-LP-416B * TURBINE-BLDG +
ESW-MDP-FS-MDPA * ACP-BAC-LP-416C * EMER-COOL-TOWER +
ESW-MDP-FS-MDPB * ACP-BAC-LP-416B * EMER-COOL-TOWER +
ACP-BAC-LP-416D * ESW-CCF-PF-MDPS +
ESW-MDP-FS-MDPA * ESW-MDP-FS-ECW * ACP-BAC-LP-416C +
ESW-MDP-FS-MDPB * ESW-MDP-FS-ECW * ACP-BAC-LP-416B +
ESW-CCF-PF-MDPS * TURBINE-BLDG +
ESW-MDP-FS-ECW * ESW-CCF-PF-MDPS +
ACP-BAC-LP-416B * DCP-BDC-LP-125C * TURBINE-BLDG +
DCP-BDC-LP-125B * ACP-BAC-LP-416C * TURBINE-BLDG +
DCP-BAT-LP-B2 * ACP-BAC-LP-416C * TURBINE-BLDG +
ACP-BAC-LP-416B * DCP-BAT-LP-C3 * TURBINE-BLDG +
ACP-BAC-LP-416B * DCP-BDC-LP-125C * EMER-COOL-TOWER +
DCP-BDC-LP-125B * ACP-BAC-LP-416C * EMER-COOL-TOWER +
DCP-BAT-LP-B2 * ACP-BAC-LP-416C * EMER-COOL-TOWER +
ACP-BAC-LP-416B * DCP-BAT-LP-C3 * EMER-COOL-TOWER +
ACP-CCF-2-4KV * ESW-TNK-LL-PS13
```

BOOL 6 = BOOL 4 WITH 4KV-C BUT NO DG'S

```
        BOOL(6) =
ACP-CCF-2-4KV * TURBINE-BLDG +
ACP-CCF-2-4KV * EMER-COOL-TOWER +
ESW-MDP-FS-MDPA * ACP-BAC-LP-416C * TURBINE-BLDG +
ESW-MDP-FS-MDPA * ACP-BAC-LP-416C * EMER-COOL-TOWER +
ESW-MDP-FS-MDPA * ESW-MDP-FS-ECW * ACP-BAC-LP-416C +
DCP-BDC-LP-125B * ACP-BAC-LP-416C * TURBINE-BLDG +
DCP-BAT-LP-B2 * ACP-BAC-LP-416C * TURBINE-BLDG +
DCP-BDC-LP-125B * ACP-BAC-LP-416C * EMER-COOL-TOWER +
DCP-BAT-LP-B2 * ACP-BAC-LP-416C * EMER-COOL-TOWER +
ACP-CCF-2-4KV * ESW-TNK-LL-PS13
```

BOOL 7 = BOOL 4 with TURBINE BLDG BUT NO DG'S

```
        BOOL(7) =
ACP-CCF-2-4KV * TURBINE-BLDG +
ESW-MDP-FS-MDPA * ACP-BAC-LP-416C * TURBINE-BLDG +
ESW-MDP-FS-MDPB * ACP-BAC-LP-416B * TURBINE-BLDG +
ESW-CCF-2-MDPS * TURBINE-BLDG +
ACP-CCF-2-4KV * EMER-COOL-TOWER +
ESW-MDP-FS-MDPA * ACP-BAC-LP-416C * EMER-COOL-TOWER +
ESW-MDP-FS-MDPB * ACP-BAC-LP-416B * EMER-COOL-TOWER +
ESW-CCF-2-MDPS * EMER-COOL-TOWER
```

```
      NLOSP = 1.0 - LOSP
      CBAR = 1.0
      Q = 0.01
      MBAR = 1.0
      P1 = 0.096
      P2 = 0.002
      P3 = 0.0002
      PBAR = 1.0-(P1+P2+P3)
      BBAR = 1.0
      X1BAR = 1.0

SEQUENCE 1 RVR-1
    ACC(1) = IE(1)

SEQUENCE 2 ALOCA-17
    ACC(2) = IE(2)*CBAR*NLOSP*BOOL(5)

SEQUENCE 3 ALOCA-30
    ACC(3) = IE(2)*CBAR*LOSP*BOOL(4)*RADWASTE/TB-ROOF

SEQUENCE 4 S1LOCA-25
    ACC(4) = IE(3)*CBAR*NLOSP*BOOL(6)

SEQUENCE 5  S1LOCA-70
    ACC(5) = IE(3)*CBAR*LOSP*BOOL(4)

SEQUENCE 6 S1LOCA-80
    ACC(6) = IE(3)*CBAR*LOSP*RADWASTE/TB-ROOF

SEQUENCE 7 S2LOCA-2-44
    ACC(7) = IE(4)*CBAR*NLOSP*BOOL(7)

SEQUENCE 8 S2LOCA-42
    ACC(8) = IE(4)*CBAR*LOSP*RADWASTE/TB-ROOF

SEQUENCE 9 RWT-1
    ACC(9) = IE(5)*CBAR*MBAR*PBAR

SEQUENCE 10 RWT-2
    ACC(10) = IE(5)*CBAR*MBAR*P1

SEQUENCE 11 RWT-3
    ACC(11) = IE(5)*CBAR*MBAR*P2

SEQUENCE 12 RWT-4
    ACC(12) = IE(5)*CBAR*MBAR*P3
```

```
   SEQUENCE 13  LOSP-SEQ5P
      ACC(13) = ACP-BAC-LP-416C * DCP-BDC-LP-125C * DCP-BDC-LP-125D

      ACC(13) = IE(6)*BBAR*X1BAR*ACC(13)


   SEQUENCE #  14 LOSP-SEQ2P
      ACC(14) =
ACP-CCF-2-4KV * ADS-LOG-HW-INHIB +
ACP-DGN-LP-EDGA * ACP-BAC-LP-416B * ADS-LOG-HW-INHIB +
ACP-DGN-LP-EDGB * ACP-BAC-LP-416A * ADS-LOG-HW-INHIB +
ACP-BAC-LP-416A * CRD-XHE-FO-BRKRS * ADS-LOG-HW-INHIB * HCI-TDP-FS-20S37 +
ACP-BAC-LP-416A * RBC-XHE-FO-SWCH * ADS-LOG-HW-INHIB * HCI-TDP-FS-20S37 +
ACP-BAC-LP-416A * ESF-XHE-FO-DEPRE * ADS-LOG-HW-INHIB * HCI-TDP-FS-20S37 +
ACP-BAC-LP-416B * CRD-XHE-FO-BRKRS * ADS-LOG-HW-INHIB * RCI-TDP-FS-20S38 +
ACP-BAC-LP-416B * RBC-XHE-FO-SWCH * ADS-LOG-HW-INHIB * RCI-TDP-FS-20S38 +
RBC-XHE-FO-LCVAL * ACP-BAC-LP-416B * ADS-LOG-HW-INHIB * RCI-TDP-FS-20S38 +
RBC-XHE-FO-LCVAL * ACP-BAC-LP-416A * ADS-LOG-HW-INHIB * HCI-TDP-FS-20S37 +
ACP-BAC-LP-416A * CRD-XHE-FO-BRKRS * ADS-LOG-HW-INHIB * HCI-TDP-FR-20S37 +
ACP-BAC-LP-416A * RBC-XHE-FO-SWCH * ADS-LOG-HW-INHIB * HCI-TDP-FR-20S37 +
RBC-XHE-FO-LCVAL * ACP-BAC-LP-416A * ADS-LOG-HW-INHIB * HCI-TDP-FR-20S37 +
ACP-BAC-LP-416A * ESF-XHE-FO-DEPRE * ADS-LOG-HW-INHIB * HCI-TDP-FR-20S37 +
ACP-BAC-LP-416B * CRD-XHE-FO-BRKRS * ADS-LOG-HW-INHIB * RCI-TDP-FR-20S38 +
ACP-BAC-LP-416B * RBC-XHE-FO-SWCH * ADS-LOG-HW-INHIB * RCI-TDP-FR-20S38 +
RBC-XHE-FO-LCVAL * ACP-BAC-LP-416B * ADS-LOG-HW-INHIB * RCI-TDP-FR-20S38 +

      ACC(14) = IE(6)*BBAR*ACC(14)


   SEQUENCE #  15 LOSP-SEQ1P
      ACC(15) = IE(6)*CBAR*MBAR*PBAR*BOOL(4)


   SEQUENCE # 16 T1S2-SEQ2P
      ACC(16) = ACP-BAC-LP-416C * DCP-BDC-LP-125C * DCP-BDC-LP-125D

      ACC(16) = IE(6)*P1*BBAR*X1BAR*ACC(16)


   SEQUENCE # 17 T1S2-SEQ1P
      ACC(17) =
ACP-CCF-2-4KV * ADS-LOG-HW-INHIB +
ACP-DGN-LP-EDGA * ACP-BAC-LP-416B * ADS-LOG-HW-INHIB +
ACP-DGN-LP-EDGB * ACP-BAC-LP-416A * ADS-LOG-HW-INHIB +
ACP-BAC-LP-416A * ESF-XHE-FO-DEPRE * ADS-LOG-HW-INHIB * HCI-TDP-FS-20S37 +
ACP-BAC-LP-416A * CRD-XHE-FO-BRKRS * ADS-LOG-HW-INHIB * HCI-TDP-FS-20S37 +
ACP-BAC-LP-416B * ESF-XHE-FO-DEPRE * ADS-LOG-HW-INHIB * RCI-TDP-FS-20S38 +
ACP-BAC-LP-416A * RBC-XHE-FO-SWCH * ADS-LOG-HW-INHIB * HCI-TDP-FS-20S37 +
RBC-XHE-FO-LCVAL * ACP-BAC-LP-416A * ADS-LOG-HW-INHIB * HCI-TDP-FS-20S37 +
ACP-BAC-LP-416B * CRD-XHE-FO-BRKRS * ADS-LOG-HW-INHIB * RCI-TDP-FS-20S38 +
ACP-BAC-LP-416B * RBC-XHE-FO-SWCH * ADS-LOG-HW-INHIB * RCI-TDP-FS-20S38 +
RBC-XHE-FO-LCVAL * ACP-BAC-LP-416B * ADS-LOG-HW-INHIB * RCI-TDP-FS-20S38 +
```

```
RBC-XHE-FO-LCVAL * ACP-BAC-LP-416A * ADS-LOG-HW-INHIB * HCI-TDP-FR-20S37 +
ACP-BAC-LP-416B * CRD-XHE-FO-BRKRS * ADS-LOG-HW-INHIB * RCI-TDP-FR-20S38 +
ACP-BAC-LP-416B * RBC-XHE-FO-SWCH * ADS-LOG-HW-INHIB * RCI-TDP-FR-20S38 +
ACP-BAC-LP-416A * ESF-XHE-FO-DEPRE * ADS-LOG-HW-INHIB * HCI-TDP-FR-20S37 +
ACP-BAC-LP-416A * CRD-XHE-FO-BRKRS * ADS-LOG-HW-INHIB * HCI-TDP-FR-20S37 +

      ACC(17) = IE(6)*P1*BBAR*ACC(17)


   SEQUENCE # 18 T1S1-SEQ2P
      ACC(18) = RHR-CCF-PF-MDPS * ACP-CCF-2-4KV

      ACC(18) = IE(6)*P2*BBAR*X1BAR*ACC(18)


    SEQUENCE # 19 T1S1-SEQ1P
      ACC(19) =
ACP-CCF-2-4KV * ADS-LOG-HW-INHIB +
ACP-BAC-LP-416B * RBC-XHE-FO-SWCH * ADS-LOG-HW-INHIB +
RBC-XHE-FO-LCVAL * ACP-BAC-LP-416B * ADS-LOG-HW-INHIB +
ACP-BAC-LP-416B * CRD-XHE-FO-BRKRS * ADS-LOG-HW-INHIB +
ACP-BAC-LP-416B * ESF-XHE-FO-DEPRE * ADS-LOG-HW-INHIB +
ACP-DGN-LP-EDGA * ACP-BAC-LP-416B * ADS-LOG-HW-INHIB +
ACP-DGN-LP-EDGB * ACP-BAC-LP-416A * ADS-LOG-HW-INHIB +

      ACC(19) = IE(6)*P2*BBAR*ACC(19)


    SEQUENCE #  20 A-SEQ1P
      ACC(20) =
RHR-CCF-PF-MDPS * ACP-CCF-2-4KV +
RHR-CCF-PF-MDPS * ACP-CCF-2-4KV +
RHR-CCF-PF-MDPS * ACP-CCF-2-4KV +

      ACC(20) = IE(2)*BBAR*ACC(20)


    SEQUENCE # 21   T3A-SEQ1P
      ACC(21) =
ACP-CCF-2-4KV * ESF-XHE-FO-DEPRE * ADS-LOG-HW-INHIB +
ACP-CCF-3-4KV * TURBINE-BLDG * ESF-XHE-FO-DEPRE +
ACP-CCF-3-4KV * TURBINE-BLDG * ESF-XHE-FO-DEPRE +
ACP-CCF-2-4KV * TURBINE-BLDG * ESF-XHE-FO-DEPRE * CRD-XHE-FO-CRD +
ESW-MDP-FS-MDPB * ACP-CCF-2-4KV * TURBINE-BLDG * ESF-XHE-FO-DEPRE +
ESW-MDP-FS-MDPA * ACP-CCF-2-4KV * TURBINE-BLDG * ESF-XHE-FO-DEPRE +
ESW-MDP-FS-MDPA * ACP-CCF-2-4KV * TURBINE-BLDG * ESF-XHE-FO-DEPRE +
ESW-MDP-FS-MDPB * ACP-CCF-2-4KV * TURBINE-BLDG * ESF-XHE-FO-DEPRE +
ACP-CCF-3-4KV * EMER-COOL-TOWER * ESF-XHE-FO-DEPRE +
ACP-CCF-3-4KV * EMER-COOL-TOWER * ESF-XHE-FO-DEPRE +
ACP-CCF-2-4KV * EMER-COOL-TOWER * ESF-XHE-FO-DEPRE * CRD-XHE-FO-CRD +
ESW-MDP-FS-MDPB * ACP-CCF-2-4KV * EMER-COOL-TOWER * ESF-XHE-FO-DEPRE +
ESW-MDP-FS-MDPA * ACP-CCF-2-4KV * EMER-COOL-TOWER * ESF-XHE-FO-DEPRE +
```

```
ESW-MDP-FS-MDPA * ACP-CCF-2-4KV * EMER-COOL-TOWER * ESF-XHE-FO-DEPRE +
ESW-MDP-FS-MDPB * ACP-CCF-2-4KV * EMER-COOL-TOWER * ESF-XHE-FO-DEPRE +

       ACC(21) = IE(7)*CBAR*Q*MBAR*PBAR*ACC(21)


     SEQUENCE #  22  T3A-SEQ2P
       ACC(22) =
ACP-CCF-2-4KV * TURBINE-BLDG * CDS-SYS-FC-COND +
ACP-CCF-2-4KV * TURBINE-BLDG * IAS-PTF-HW-IAS +
ESW-MDP-FS-MDPA * ACP-BAC-LP-416C * TURBINE-BLDG * CDS-SYS-FC-COND +
ESW-MDP-FS-MDPB * ACP-CCF-2-4KV * TURBINE-BLDG * CDS-SYS-FC-COND +
ACP-CCF-2-4KV * EMER-COOL-TOWER * CDS-SYS-FC-COND +
ACP-CCF-2-4KV * EMER-COOL-TOWER * IAS-PTF-HW-IAS +
ESW-MDP-FS-MDPA * ACP-BAC-LP-416C * EMER-COOL-TOWER * CDS-SYS-FC-COND +
ESW-MDP-FS-MDPB * ACP-CCF-2-4KV * EMER-COOL-TOWER * CDS-SYS-FC-COND +

       ACC(22) = IE(7)*CBAR*Q*MBAR*PBAR*X1BAR*ACC(22)
```

PEACH BOTTOM CROSS REFRENCE FILE

P_{random}	Basic Event	EF	N_{frag}	N_{resp}	N_{corr}	No.
2.000E-04	$ LOSP	$ 3.0	1	1		1
1.610E-03	$ DGACTA	$	3	23		2
1.610E-03	$ DGACTB	$				3
1.610E-03	$ DGACTC	$				4
1.610E-03	$ DGACTD	$				5
1.000E-03	$ ESF-ACS-FC-MDPA	$	3	11		6
1.000E-03	$ ESF-ACS-FC-MDPB	$				7
1.610E-03	$ ADS-ACT-HW-DIV1	$				8
1.610E-03	$ ADS-ACT-HW-DIV2	$				9
1.610E-03	$ HCI-ACT-HW-HPCI	$				10
1.610E-03	$ HCI-ACT-HW-LOCST	$				11
1.610E-03	$ LCI-ACT-HW-DIV1	$				12
1.610E-03	$ LCI-ACT-HW-DIV2	$				13
1.610E-03	$ LCS-ACT-HW-LOOPA	$				14
1.610E-03	$ LCS-ACT-HW-LOOPB	$				15
1.000E-03	$ RCI-ACT-HW-LOCST	$				16
1.610E-03	$ RCI-ACT-HW-RCIC	$				17
5.000E-05	$ ESW-ACX-FC-HX1	$	24	12		18
5.000E-05	$ ESW-ACX-FC-HX10	$				19
5.000E-05	$ ESW-ACX-FC-HX12	$				20
5.000E-05	$ ESW-ACX-FC-HX13	$				21
5.000E-05	$ ESW-ACX-FC-HX15	$				22
5.000E-05	$ ESW-ACX-FC-HX16	$				23
5.000E-05	$ ESW-ACX-FC-HX18	$				24
5.000E-05	$ ESW-ACX-FC-HX19	$				25
5.000E-05	$ ESW-ACX-FC-HX2	$				26
5.000E-05	$ ESW-ACX-FC-HX21	$				27
5.000E-05	$ ESW-ACX-FC-HX22	$				28
5.000E-05	$ ESW-ACX-FC-HX24	$				29
5.000E-05	$ ESW-ACX-FC-HX25	$				30
5.000E-05	$ ESW-ACX-FC-HX27	$				31
5.000E-05	$ ESW-ACX-FC-HX28	$				32
5.000E-05	$ ESW-ACX-FC-HX3	$				33
5.000E-05	$ ESW-ACX-FC-HX4	$				34
5.000E-05	$ ESW-ACX-FC-HX6	$				35
5.000E-05	$ ESW-ACX-FC-HX7	$				36
5.000E-05	$ ESW-ACX-FC-HX9	$				37
3.750E-04	$ ESF-ADS-FC-LI13A	$	3	13		38
3.750E-04	$ ESF-ADS-FC-LI13B	$				39
3.750E-04	$ ESF-ADS-FC-LI13C	$				40
3.750E-04	$ ESF-ADS-FC-LI13D	$				41
1.000E-03	$ EHV-AOV-CC-AV25	$	19	22		42
1.000E-03	$ EHV-AOV-CC-AV27	$				43
1.000E-03	$ EHV-AOV-CC-AV28	$				44
1.000E-03	$ EHV-AOV-CC-AV30	$				45
1.000E-03	$ EHV-AOV-CC-AV31	$				46

P_{random}	Basic Event	EF	N_{frag}	N_{resp}	N_{corr}	No.
1.000E-03	$ EHV-AOV-CC-AV33	$				47
1.000E-03	$ EHV-AOV-CC-AV34	$				48
1.000E-03	$ EHV-AOV-CC-AV36	$				49
1.000E-03	$ ESW-AOV-CC-0241A	$	19	12		50
1.000E-03	$ ESW-AOV-CC-0241B	$				51
1.000E-03	$ ESW-AOV-CC-0241C	$				52
1.000E-03	$ ESW-AOV-CC-0241D	$				53
1.000E-03	$ ESW-AOV-CC-AV1	$				54
1.000E-03	$ ESW-AOV-CC-AV10	$				55
1.000E-03	$ ESW-AOV-CC-AV11	$				56
1.000E-03	$ ESW-AOV-CC-AV12	$				57
1.000E-03	$ ESW-AOV-CC-AV13	$				58
1.000E-03	$ ESW-AOV-CC-AV14	$				59
1.000E-03	$ ESW-AOV-CC-AV15	$				60
1.000E-03	$ ESW-AOV-CC-AV16	$				61
1.000E-03	$ ESW-AOV-CC-AV17	$				62
1.000E-03	$ ESW-AOV-CC-AV18	$				63
1.000E-03	$ ESW-AOV-CC-AV19	$				64
1.000E-03	$ ESW-AOV-CC-AV2	$				65
1.000E-03	$ ESW-AOV-CC-AV20	$				66
1.000E-03	$ ESW-AOV-CC-AV3	$				67
1.000E-03	$ ESW-AOV-CC-AV4	$				68
1.000E-03	$ ESW-AOV-CC-AV5	$				69
1.000E-03	$ ESW-AOV-CC-AV6	$				70
1.000E-03	$ ESW-AOV-CC-AV7	$				71
1.000E-03	$ ESW-AOV-CC-AV8	$				72
1.000E-03	$ ESW-AOV-CC-AV9	$				73
2.000E-04	$ ESW-AOV-MA-0241A	$	0	0		74
2.000E-04	$ ESW-AOV-MA-0241B	$				75
2.000E-04	$ ESW-AOV-MA-0241C	$				76
2.000E-04	$ ESW-AOV-MA-0241D	$				77
2.000E-04	$ ESW-AOV-MA-AV1	$				78
2.000E-04	$ ESW-AOV-MA-AV10	$				79
2.000E-04	$ ESW-AOV-MA-AV11	$				80
2.000E-04	$ ESW-AOV-MA-AV12	$				81
2.000E-04	$ ESW-AOV-MA-AV13	$				82
2.000E-04	$ ESW-AOV-MA-AV14	$				83
2.000E-04	$ ESW-AOV-MA-AV15	$				84
2.000E-04	$ ESW-AOV-MA-AV16	$				85
2.000E-04	$ ESW-AOV-MA-AV17	$				86
2.000E-04	$ ESW-AOV-MA-AV18	$				87
2.000E-04	$ ESW-AOV-MA-AV19	$				88
2.000E-04	$ ESW-AOV-MA-AV2	$				89
2.000E-04	$ ESW-AOV-MA-AV20	$				90
2.000E-04	$ ESW-AOV-MA-AV3	$				91
2.000E-04	$ ESW-AOV-MA-AV4	$				92
2.000E-04	$ ESW-AOV-MA-AV5	$				93
2.000E-04	$ ESW-AOV-MA-AV6	$				94
2.000E-04	$ ESW-AOV-MA-AV7	$				95
2.000E-04	$ ESW-AOV-MA-AV8	$				96

P_{random}	Basic Event	EF	N_{frag}	N_{resp}	N_{corr}	No.
2.000E-04	$ ESW-AOV-MA-AV9	$				97
1.000E-03	$ RBC-AOV-FT-A2352	$	19	16		98
1.000E-03	$ RBC-AOV-FT-A2354	$				99
1.000E-03	$ RBC-AOV-FT-A8154	$				100
1.000E-03	$ RBC-AOV-FT-A8156	$				101
2.000E-04	$ RBC-AOV-MA-A2352	$	0	0		102
2.000E-04	$ RBC-AOV-MA-A2354	$				103
2.000E-04	$ RBC-AOV-MA-A8154	$				104
2.000E-04	$ RBC-AOV-MA-A8156	$				105
3.000E-03	$ RBC-AOV-OO-2253	$	19	16		106
2.000E-04	$ RCI-AOV-MA-PCV23	$	0	0		107
3.000E-04	$ RCI-AOV-VF-PCV23	$	19	12		108
3.750E-04	$ ESF-ASD-FC-SC15A	$	13	13		109
3.750E-04	$ ESF-ASD-FC-SC15B	$				110
3.750E-04	$ ESF-ASD-FC-SC15C	$				111
3.750E-04	$ ESF-ASD-FC-SC15D	$				112
3.750E-04	$ ESF-ASD-FC-SDC17	$	13	11		113
3.750E-04	$ ESF-ASD-FC-SDC18	$				114
5.400E-04	$ ESF-ASL-FC-LT72A	$	13	21		115
5.400E-04	$ ESF-ASL-FC-LT72B	$				116
5.400E-04	$ ESF-ASL-FC-LT72C	$				117
5.400E-04	$ ESF-ASL-FC-LT72D	$				118
1.000E-03	$ ESF-ASL-FC-P101A	$				119
1.000E-03	$ ESF-ASL-FC-P101B	$				120
1.000E-03	$ ESF-ASL-FC-P101C	$				121
1.000E-03	$ ESF-ASL-FC-P101D	$				122
1.000E-03	$ ESF-ASL-HW-CSTL1	$	13	4		123
1.000E-03	$ ESF-ASL-HW-CSTL2	$				124
1.000E-03	$ ESF-ASL-HW-CSTL3	$				125
1.000E-03	$ ESF-ASL-HW-CSTL4	$				126
1.000E+00	$ ESF-ASL-LRXLEVEL	$	13	11		127
1.000E-03	$ ESF-ASL-NO-RSXDA	$	13	11		128
1.000E-03	$ ESF-ASL-NO-RSXDB	$				129
1.000E-03	$ ESF-ASP-FC-LH12A	$	13	11		130
1.000E-03	$ ESF-ASP-FC-LH12B	$				131
1.000E-03	$ ESF-ASP-FC-LH12C	$				132
1.000E-03	$ ESF-ASP-FC-LH12D	$				133
1.000E-03	$ ESF-ASP-FC-LSPHC	$	13	11		134
1.000E-03	$ ESF-ASP-FC-LSPRC	$				135
5.000E-04	$ ESF-ASP-FC-P100A	$				136
5.000E-04	$ ESF-ASP-FC-P100B	$				137
5.000E-04	$ ESF-ASP-FC-P100C	$				138
5.000E-04	$ ESF-ASP-FC-P100D	$				139
1.000E-03	$ ESF-ASP-FC-P101A	$				140
1.000E-03	$ ESF-ASP-FC-P101B	$				141
1.000E-03	$ ESF-ASP-FC-P101C	$				142
1.000E-03	$ ESF-ASP-FC-P101D	$				143
1.000E-03	$ ESF-ASP-FC-P128C	$				144
1.000E-03	$ ESF-ASP-FC-P128D	$				145
1.000E-03	$ ESF-ASP-FC-PL52A	$				146

P_{random}	Basic Event	EF	N_{frag}	N_{resp}	N_{corr}	No.
1.000E-03	ESF-ASP-FC-PL52B					147
1.000E-03	ESF-ASP-FC-PL52C					148
1.000E-03	ESF-ASP-FC-PL52D					149
1.000E+00	ESF-ASP-HIDWPRES		13	11		150
1.000E-03	ESF-ASP-HW-EX72A		13	13		151
1.000E-03	ESF-ASP-HW-EX72B					152
1.000E+00	ESF-ASP-NOHDPEL		0	0		153
1.000E+00	ESF-ASP-NOHDPLT					154
5.000E-06	ACP-BAC-LP-416A		41	7		155
5.000E-06	ACP-BAC-LP-416B					156
5.000E-06	ACP-BAC-LP-416C					157
5.000E-06	ACP-BAC-LP-416D					158
1.080E-03	DCP-BAT-LP-A2	3.0	4	6		159
1.080E-03	DCP-BAT-LP-B2					160
1.080E-03	DCP-BAT-LP-C2					161
1.080E-03	DCP-BAT-LP-C3					162
1.080E-03	DCP-BAT-LP-D2					163
1.080E-03	DCP-BAT-LP-D3					164
5.000E-06	DCP-BDC-LP-125A	3.0	3	9		165
5.000E-06	DCP-BDC-LP-125B					166
5.000E-06	DCP-BDC-LP-125C					167
5.000E-06	DCP-BDC-LP-125D					168
3.900E-05	ACP-CCF-LP-DGS	3.0	42	22	3	169
1.500E-04	ADS-CCF-CC-ADSRV		20	20	4	170
1.200E-04	ADS-CCF-CC-NADSV		21	20	4	171
1.000E-04	ADS-CCF-LK-ACC					172
1.470E-04	CSS-CCF-LF-MOVS		19	12	4	173
2.500E-06	DCP-CCF-LP-BAT		4	6	3	174
3.600E-05	EHV-CCF-LF-AOVS		19	22	3	175
5.500E-05	ESW-CCF-LF-AOVS		19	12	2	176
9.000E-09	ESW-CCF-MC-ECT		33	1		177
7.800E-05	ESW-CCF-PF-MDPS		17	28	2	178
2.880E-05	HSW-CCF-LF-MDPS					179
9.600E-05	HSW-CCF-LF-MOVS		19	27	4	180
1.470E-04	LCI-CCF-LF-MOVS		19	27	2	181
1.470E-04	LCS-CCF-LF-MOVS		19	12	4	182
3.000E-04	LCS-CCF-PF-MDPS		16	14	4	183
3.000E-04	RHR-CCF-PF-MDPS		16	14	4	184
6.300E-04	SLC-CCF-PF-MDPS	3.	0	0		185
1.470E-04	SPC-CCF-LF-MOVS		19	12	2	186
3.000E-03	ESW-CKV-CB-C515A		0	0		187
3.000E-03	ESW-CKV-CB-C515B					188
1.500E-02	ESW-CKV-CB-CV514					189
1.000E-04	ESW-CKV-HW-C515A		21	12		190
1.000E-04	ESW-CKV-HW-C515B					191
1.000E-04	ESW-CKV-HW-CV506					192
1.000E-04	ESW-CKV-HW-CV513					193
1.000E-04	ESW-CKV-HW-CV516					194
1.000E-04	HCI-CKV-HW-CV32					195
1.000E-04	HCI-CKV-HW-CV61					196

P_{random}	Basic Event	EF	N_{frag}	N_{resp}	N_{corr}	No.
1.000E-04	$ HCI-CKV-HW-CV65 $					197
1.000E-04	$ HSW-CKV-HW-C502A $		21	27		198
1.000E-04	$ HSW-CKV-HW-C502B $					199
1.000E-04	$ HSW-CKV-HW-C502C $					200
1.000E-04	$ HSW-CKV-HW-C502D $					201
1.000E-04	$ HSW-CKV-HW-CV5 $					202
1.000E-04	$ LCI-CKV-HW-CV19A $		21	12		203
1.000E-04	$ LCI-CKV-HW-CV19B $					204
1.000E-04	$ LCI-CKV-HW-CV19C $					205
1.000E-04	$ LCI-CKV-HW-CV19D $					206
1.000E-04	$ LCI-CKV-HW-CV46A $					207
1.000E-04	$ LCI-CKV-HW-CV46B $					208
1.000E-04	$ LCI-CKV-HW-CV48A $					209
1.000E-04	$ LCI-CKV-HW-CV48B $					210
1.000E-04	$ LCI-CKV-HW-CV48C $					211
1.000E-04	$ LCI-CKV-HW-CV48D $					212
1.000E-04	$ LCS-CKV-HW-CV10A $					213
1.000E-04	$ LCS-CKV-HW-CV10B $					214
1.000E-04	$ LCS-CKV-HW-CV10C $					215
1.000E-04	$ LCS-CKV-HW-CV10D $					216
1.000E-04	$ LCS-CKV-HW-CV66A $					217
1.000E-04	$ LCS-CKV-HW-CV66B $					218
1.000E-04	$ LCS-CKV-HW-CV66C $					219
1.000E-04	$ LCS-CKV-HW-CV66D $					220
1.000E-04	$ RCI-CKV-HW-CV19 $					221
1.000E-04	$ RCI-CKV-HW-CV40 $					222
1.000E-04	$ RCI-CKV-HW-CV50 $					223
1.000E-04	$ SLC-CKV-HW-CV16 $		0	0		224
1.000E-04	$ SLC-CKV-HW-CV17 $					225
1.000E-04	$ SLC-CKV-HW-CV43A $					226
1.000E-04	$ SLC-CKV-HW-CV43B $					227
1.600E-02	$ ACP-DGN-FR-EDGA $		0	0		228
1.600E-02	$ ACP-DGN-FR-EDGB $					229
1.600E-02	$ ACP-DGN-FR-EDGC $					230
1.600E-02	$ ACP-DGN-FR-EDGD $					231
3.000E-03	$ ACP-DGN-LP-EDGA $	3.0	42	22		232
3.000E-03	$ ACP-DGN-LP-EDGB $					233
3.000E-03	$ ACP-DGN-LP-EDGC $					234
3.000E-03	$ ACP-DGN-LP-EDGD $					235
6.000E-03	$ ACP-DGN-MA-EDGA $		0	0		236
6.000E-03	$ ACP-DGN-MA-EDGB $					237
6.000E-03	$ ACP-DGN-MA-EDGC $					238
6.000E-03	$ ACP-DGN-MA-EDGD $					239
3.000E-04	$ ACP-DGN-RE-EDGA $	3.0	0			240
3.000E-04	$ ACP-DGN-RE-EDGB $					241
3.000E-04	$ ACP-DGN-RE-EDGC $					242
3.000E-04	$ ACP-DGN-RE-EDGD $					243
2.300E-03	$ ACP-DGN-TE-EDGA $					244
2.300E-03	$ ACP-DGN-TE-EDGB $					245
2.300E-03	$ ACP-DGN-TE-EDGC $					246

P_{random}	Basic Event	EF	N_{frag}	N_{resp}	N_{corr}	No.
2.300E-03	$ ACP-DGN-TE-EDGD	$				247
3.000E-03	$ SLC-EPV-HW-EV14A	$				248
3.000E-03	$ SLC-EPV-HW-EV14B	$				249
2.000E-04	$ SLC-EPV-MA-EV14A	$				250
2.000E-04	$ SLC-EPV-MA-EV14B	$				251
5.000E-04	$ EHV-FAN-FR-OAV64	$				252
5.000E-04	$ EHV-FAN-FR-OAV91	$				253
5.000E-04	$ EHV-FAN-FR-OBV64	$				254
5.000E-04	$ EHV-FAN-FR-OBV91	$				255
5.000E-04	$ EHV-FAN-FR-OCV64	$				256
5.000E-04	$ EHV-FAN-FR-OCV91	$				257
5.000E-04	$ EHV-FAN-FR-ODV64	$				258
5.000E-04	$ EHV-FAN-FR-ODV91	$				259
3.750E-04	$ EHV-FAN-FS-OAV64	$	27	24		260
3.750E-04	$ EHV-FAN-FS-OAV91	$				261
3.750E-04	$ EHV-FAN-FS-OBV64	$				262
3.750E-04	$ EHV-FAN-FS-OBV91	$				263
3.750E-04	$ EHV-FAN-FS-OCV64	$				264
3.750E-04	$ EHV-FAN-FS-OCV91	$				265
3.750E-04	$ EHV-FAN-FS-ODV64	$				266
3.750E-04	$ EHV-FAN-FS-ODV91	$				267
5.000E-04	$ ESW-FAN-FR-HX1	$	0	0		268
5.000E-04	$ ESW-FAN-FR-HX10	$				269
5.000E-04	$ ESW-FAN-FR-HX12	$				270
5.000E-04	$ ESW-FAN-FR-HX13	$				271
5.000E-04	$ ESW-FAN-FR-HX15	$				272
5.000E-04	$ ESW-FAN-FR-HX16	$				273
5.000E-04	$ ESW-FAN-FR-HX18	$				274
5.000E-04	$ ESW-FAN-FR-HX19	$				275
5.000E-04	$ ESW-FAN-FR-HX2	$				276
5.000E-04	$ ESW-FAN-FR-HX21	$				277
5.000E-04	$ ESW-FAN-FR-HX22	$				278
5.000E-04	$ ESW-FAN-FR-HX24	$				279
5.000E-04	$ ESW-FAN-FR-HX25	$				280
5.000E-04	$ ESW-FAN-FR-HX27	$				281
5.000E-04	$ ESW-FAN-FR-HX28	$				282
5.000E-04	$ ESW-FAN-FR-HX3	$				283
5.000E-04	$ ESW-FAN-FR-HX4	$				284
5.000E-05	$ ESW-FAN-FR-HX6	$				285
5.000E-04	$ ESW-FAN-FR-HX7	$				286
5.000E-04	$ ESW-FAN-FR-HX9	$				287
3.750E-04	$ ESW-FAN-FS-HX1	$	27	15		288
3.750E-04	$ ESW-FAN-FS-HX10	$				289
3.750E-04	$ ESW-FAN-FS-HX12	$				290
3.750E-04	$ ESW-FAN-FS-HX13	$				291
3.750E-04	$ ESW-FAN-FS-HX15	$				292
3.750E-04	$ ESW-FAN-FS-HX16	$				293
3.750E-04	$ ESW-FAN-FS-HX18	$				294
3.750E-04	$ ESW-FAN-FS-HX19	$				295
3.750E-04	$ ESW-FAN-FS-HX2	$				296

P_{random}	Basic Event	EF	N_{frag}	N_{resp}	N_{corr}	No.
3.750E-04	$ ESW-FAN-FS-HX21	$				297
3.750E-04	$ ESW-FAN-FS-HX22	$				298
3.750E-04	$ ESW-FAN-FS-HX24	$				299
3.750E-04	$ ESW-FAN-FS-HX25	$				300
3.750E-05	$ ESW-FAN-FS-HX27	$				301
3.750E-04	$ ESW-FAN-FS-HX28	$				302
3.750E-04	$ ESW-FAN-FS-HX3	$				303
3.750E-04	$ ESW-FAN-FS-HX4	$				304
3.750E-04	$ ESW-FAN-FS-HX6	$				305
3.750E-04	$ ESW-FAN-FS-HX7	$				306
3.750E-04	$ ESW-FAN-FS-HX9	$				307
1.860E-03	$ ESW-FAN-MA-HX1	$	0	0		308
1.860E-03	$ ESW-FAN-MA-HX10	$				309
1.860E-03	$ ESW-FAN-MA-HX12	$				310
1.860E-03	$ ESW-FAN-MA-HX13	$				311
1.860E-03	$ ESW-FAN-MA-HX15	$				312
1.860E-03	$ ESW-FAN-MA-HX16	$				313
1.860E-03	$ ESW-FAN-MA-HX18	$				314
1.860E-03	$ ESW-FAN-MA-HX19	$				315
1.860E-03	$ ESW-FAN-MA-HX2	$				316
1.860E-03	$ ESW-FAN-MA-HX21	$				317
1.860E-03	$ ESW-FAN-MA-HX22	$				318
1.860E-03	$ ESW-FAN-MA-HX24	$				319
1.860E-03	$ ESW-FAN-MA-HX25	$				320
1.860E-03	$ ESW-FAN-MA-HX27	$				321
1.860E-03	$ ESW-FAN-MA-HX28	$				322
1.860E-03	$ ESW-FAN-MA-HX3	$				323
1.860E-03	$ ESW-FAN-MA-HX4	$				324
1.860E-03	$ ESW-FAN-MA-HX6	$				325
1.860E-03	$ ESW-FAN-MA-HX7	$				326
1.860E-03	$ ESW-FAN-MA-HX9	$				327
2.660E-04	$ HSW-FAN-FR-ECTFA	$				328
2.660E-04	$ HSW-FAN-FR-ECTFB	$				329
2.660E-04	$ HSW-FAN-FR-ECTFC	$				330
3.500E-03	$ HSW-FAN-FS-ECTFA	$	27	31		331
3.500E-03	$ HSW-FAN-FS-ECTFB	$				332
3.500E-03	$ HSW-FAN-FS-ECTFC	$				333
1.860E-03	$ HSW-FAN-MA-ECTFA	$	0	0		334
1.860E-03	$ HSW-FAN-MA-ECTFB	$				335
1.860E-03	$ HSW-FAN-MA-ECTFC	$				336
2.280E-04	$ HSW-HTX-PG-HXA	$				337
2.280E-04	$ HSW-HTX-PG-HXB	$				338
2.280E-04	$ HSW-HTX-PG-HXC	$				339
2.280E-04	$ HSW-HTX-PG-HXD	$				340
1.200E-04	$ HSW-HTX-RP-HXA	$	25	27		341
1.200E-04	$ HSW-HTX-RP-HXB	$				342
1.200E-04	$ HSW-HTX-RP-HXC	$				343
1.200E-04	$ HSW-HTX-RP-HXD	$				344
1.250E-04	$ HCI-ICC-HW-FC108	$	3	9		345
1.250E-04	$ RCI-ICC-HW-FIC91	$	3	11		346

P_{random}		Basic Event		EF	N_{frag}	N_{resp}	N_{corr}	No.
4.000E-03	$	DCP-INV-LP-24C	$	3.0	6	9		347
4.000E-03	$	DCP-INV-LP-24D	$					348
1.000E-05	$	ADS-LOG-HW-INHIB	$		0			349
1.610E-03	$	ESF-LOG-HW-RHRA	$					350
1.610E-03	$	ESF-LOG-HW-RHRB	$					351
7.200E-04	$	CRD-MDP-FR-PA	$		0	0		352
7.200E-04	$	CRD-MDP-FR-PB	$					353
3.000E-03	$	CRD-MDP-FS-PA	$		16	26		354
3.000E-03	$	CRD-MDP-FS-PB	$					355
1.200E-03	$	ESW-MDP-FR-ECW	$		0	0		356
1.200E-03	$	ESW-MDP-FR-MDPA	$					357
1.200E-03	$	ESW-MDP-FR-MDPB	$					358
3.000E-03	$	ESW-MDP-FS-ECW	$		17	30		359
3.000E-03	$	ESW-MDP-FS-MDPA	$		17	28		360
3.000E-03	$	ESW-MDP-FS-MDPB	$					361
2.000E-03	$	ESW-MDP-MA-ECW	$		0	0		362
2.000E-03	$	ESW-MDP-MA-MDPA	$					363
2.000E-03	$	ESW-MDP-MA-MDPB	$					364
1.200E-03	$	HSW-MDP-FR-MDPA	$					365
1.200E-03	$	HSW-MDP-FR-MDPB	$					366
1.200E-03	$	HSW-MDP-FR-MDPC	$					367
1.200E-03	$	HSW-MDP-FR-MDPD	$					368
3.000E-03	$	HSW-MDP-FS-MDPA	$		17	28		369
3.000E-03	$	HSW-MDP-FS-MDPB	$					370
3.000E-03	$	HSW-MDP-FS-MDPC	$					371
3.000E-03	$	HSW-MDP-FS-MDPD	$					372
2.000E-03	$	HSW-MDP-MA-MDPA	$	3.0	0	0		373
2.000E-03	$	HSW-MDP-MA-MDPB	$					374
2.000E-03	$	HSW-MDP-MA-MDPC	$					375
2.000E-03	$	HSW-MDP-MA-MDPD	$					376
1.200E-03	$	LCI-MDP-FR-2AP35	$					377
1.200E-03	$	LCI-MDP-FR-2BP35	$					378
1.200E-03	$	LCI-MDP-FR-2CP35	$					379
1.200E-03	$	LCI-MDP-FR-2DP35	$					380
3.000E-03	$	LCI-MDP-FS-2AP35	$		16	14		381
3.000E-03	$	LCI-MDP-FS-2BP35	$					382
3.000E-03	$	LCI-MDP-FS-2CP35	$					383
3.000E-03	$	LCI-MDP-FS-2DP35	$					384
2.000E-03	$	LCI-MDP-MA-2AP35	$		0	0		385
2.000E-03	$	LCI-MDP-MA-2BP35	$					386
2.000E-03	$	LCI-MDP-MA-2CP35	$					387
2.000E-03	$	LCI-MDP-MA-2DP35	$					388
1.200E-03	$	LCS-MDP-FR-2AP37	$					389
1.200E-03	$	LCS-MDP-FR-2BP37	$					390
1.200E-03	$	LCS-MDP-FR-2CP37	$					391
1.200E-03	$	LCS-MDP-FR-2DP37	$					392
3.000E-03	$	LCS-MDP-FS-2AP37	$		16	14		393
3.000E-03	$	LCS-MDP-FS-2BP37	$					394
3.000E-03	$	LCS-MDP-FS-2CP37	$					395
3.000E-03	$	LCS-MDP-FS-2DP37	$					396

P_{random}	Basic Event	EF	N_{frag}	N_{resp}	N_{corr}	No.
2.000E-03	LCS-MDP-MA-2AP37		0	0		397
2.000E-03	LCS-MDP-MA-2BP37					398
2.000E-03	LCS-MDP-MA-2CP37					399
2.000E-03	LCS-MDP-MA-2DP37					400
1.200E-03	RBC-MDP-FR-PA					401
1.200E-03	RBC-MDP-FR-PB					402
3.000E-03	RBC-MDP-FS-PA		16	17		403
3.000E-03	RBC-MDP-FS-PB					404
1.500E-05	SLC-MDP-FR-MDPA		0	0		405
1.500E-05	SLC-MDP-FR-MDPB					406
3.000E-03	SLC-MDP-FS-MDPA					407
3.000E-03	SLC-MDP-FS-MDPB					408
2.000E-03	SLC-MDP-MA-MDPA					409
1.200E-03	TBC-MDP-FR-PUMPA					410
1.200E-03	TBC-MDP-FR-PUMPB					411
3.000E-03	CSS-MOV-CC-MV26A		19	12		412
3.000E-03	CSS-MOV-CC-MV26B					413
3.000E-03	CSS-MOV-CC-MV31A					414
3.000E-03	CSS-MOV-CC-MV31B					415
2.000E-04	CSS-MOV-MA-MV26A		0	0		416
2.000E-04	CSS-MOV-MA-MV26B					417
3.000E-03	ESW-MOV-CC-M0841		19	22		418
2.000E-04	ESW-MOV-MA-M0841		0	0		419
2.000E-04	ESW-MOV-MA-MV1					420
4.000E-05	ESW-MOV-PG-M2972		19	22		421
3.000E-04	ESW-MOV-RE-M2972		0	0		422
3.000E-03	HCI-MOV-CC-MV14		19	12		423
3.000E-03	HCI-MOV-CC-MV19		19	18		424
3.000E-03	HCI-MOV-CC-MV57		19	12		425
3.000E-03	HCI-MOV-CC-MV58					426
4.000E-05	HCI-MOV-HW-MV15		19	16		427
4.000E-05	HCI-MOV-HW-MV20					428
2.000E-04	HCI-MOV-MA-MV14		0	0		429
2.000E-04	HCI-MOV-MA-MV17					430
2.000E-04	HCI-MOV-MA-MV20					431
2.000E-04	HCI-MOV-MA-MV57					432
2.000E-04	HCI-MOV-MA-PCV50					433
4.000E-05	HCI-MOV-PG-MV16		19	12		434
4.000E-05	HCI-MOV-PG-MV17					435
3.000E-03	HSW-MOV-CC-2344		19	27		436
3.000E-03	HSW-MOV-CC-2804A		19	29		437
3.000E-03	HSW-MOV-CC-2804B					438
3.000E-03	HSW-MOV-CC-M2803		19	22		439
3.000E-03	HSW-MOV-CC-M502C		19	29		440
3.000E-03	HSW-MOV-CC-MV174					441
3.000E-03	HSW-MOV-CC-MV176					442
3.000E-03	HSW-MOV-CC-MV89A		19	27		443
3.000E-03	HSW-MOV-CC-MV89B					444
3.000E-03	HSW-MOV-CC-MV89C					445
3.000E-03	HSW-MOV-CC-MV89D					446

P_{random}		Basic Event	EF	N_{frag}	N_{resp}	N_{corr}	No.
2.000E-04	$	HSW-MOV-MA-2344	$	0	0		447
2.000E-04	$	HSW-MOV-MA-2804A	$				448
2.000E-04	$	HSW-MOV-MA-2804B	$				449
2.000E-04	$	HSW-MOV-MA-M2486	$				450
2.000E-04	$	HSW-MOV-MA-M2803	$				451
2.000E-04	$	HSW-MOV-MA-M502A	$				452
2.000E-04	$	HSW-MOV-MA-M502B	$				453
2.000E-04	$	HSW-MOV-MA-M502C	$				454
2.000E-04	$	HSW-MOV-MA-MV174	$				455
2.000E-04	$	HSW-MOV-MA-MV176	$				456
2.000E-04	$	HSW-MOV-MA-MV89A	$				457
2.000E-04	$	HSW-MOV-MA-MV89B	$				458
2.000E-04	$	HSW-MOV-MA-MV89C	$				459
2.000E-04	$	HSW-MOV-MA-MV89D	$				460
4.000E-05	$	HSW-MOV-PG-M2486	$	19	22		461
4.000E-05	$	HSW-MOV-PG-M502A	$	19	29		462
4.000E-05	$	HSW-MOV-PG-M502B	$				463
3.000E-04	$	HSW-MOV-RE-2344	$	0	0		464
3.000E-04	$	HSW-MOV-RE-M2803	$				465
3.000E-03	$	LCI-MOV-CC-MV25A	$	19	18		466
3.000E-03	$	LCI-MOV-CC-MV25B	$				467
4.000E-05	$	LCI-MOV-HW-MV13A	$	19	12		468
4.000E-05	$	LCI-MOV-HW-MV13B	$				469
4.000E-05	$	LCI-MOV-HW-MV13C	$				470
4.000E-05	$	LCI-MOV-HW-MV13D	$				471
2.000E-04	$	LCI-MOV-MA-154A	$	0	0		472
2.000E-04	$	LCI-MOV-MA-154B	$				473
2.000E-04	$	LCI-MOV-MA-2677A	$				474
2.000E-04	$	LCI-MOV-MA-2677D	$				475
2.000E-04	$	LCI-MOV-MA-M154A	$				476
2.000E-04	$	LCI-MOV-MA-M154B	$				477
2.000E-04	$	LCI-MOV-MA-MV16A	$				478
2.000E-04	$	LCI-MOV-MA-MV16B	$				479
2.000E-04	$	LCI-MOV-MA-MV16C	$				480
2.000E-04	$	LCI-MOV-MA-MV16D	$				481
4.000E-05	$	LCI-MOV-PG-154A	$	19	18		482
4.000E-05	$	LCI-MOV-PG-154B	$				483
4.000E-05	$	LCI-MOV-PG-2677A	$				484
4.000E-05	$	LCI-MOV-PG-2677D	$				485
4.000E-05	$	LCI-MOV-PG-MV16A	$	19	12		486
4.000E-05	$	LCI-MOV-PG-MV16B	$				487
4.000E-05	$	LCI-MOV-PG-MV16C	$				488
4.000E-05	$	LCI-MOV-PG-MV16D	$				489
1.200E-03	$	LCI-MOV-RE-154A	$	0	0		490
1.200E-03	$	LCI-MOV-RE-154B	$				491
3.000E-03	$	LCS-MOV-CC-MV12A	$	19	18		492
3.000E-03	$	LCS-MOV-CC-MV12B	$				493
1.800E-04	$	LCS-MOV-CO-MV26A	$	19	12		494
1.800E-04	$	LCS-MOV-CO-MV26B	$				495
4.500E-05	$	LCS-MOV-HW-MV7A	$				496

P_{random}	Basic Event	EF	N_{frag}	N_{resp}	N_{corr}	No.
4.500E-05	$ LCS-MOV-HW-MV7B	$				497
4.500E-05	$ LCS-MOV-HW-MV7C	$				498
4.500E-05	$ LCS-MOV-HW-MV7D	$				499
2.000E-04	$ LCS-MOV-MA-MV11A	$	0	0		500
2.000E-04	$ LCS-MOV-MA-MV11B	$				501
2.000E-04	$ LCS-MOV-MA-MV5A	$				502
2.000E-04	$ LCS-MOV-MA-MV5B	$				503
2.000E-04	$ LCS-MOV-MA-MV5C	$				504
2.000E-04	$ LCS-MOV-MA-MV5D	$				505
4.000E-05	$ LCS-MOV-PG-MV11A	$	19	12		506
4.000E-05	$ LCS-MOV-PG-MV11B	$				507
4.000E-05	$ LCS-MOV-PG-MV5A	$				508
4.000E-05	$ LCS-MOV-PG-MV5B	$				509
4.000E-05	$ LCS-MOV-PG-MV5C	$				510
4.000E-05	$ LCS-MOV-PG-MV5D	$				511
1.500E-03	$ LCS-MOV-RE-MV11A	$	0	0		512
1.500E-03	$ LCS-MOV-RE-MV11B	$				513
3.000E-03	$ RCI-MOV-CC-MV131	$	19	12		514
3.000E-03	$ RCI-MOV-CC-MV132	$				515
3.000E-03	$ RCI-MOV-CC-MV21	$	19	18		516
3.000E-03	$ RCI-MOV-CC-MV39	$	19	12		517
3.000E-03	$ RCI-MOV-CC-MV41	$				518
4.000E-05	$ RCI-MOV-HW-MV20	$	19	20		519
2.000E-04	$ RCI-MOV-MA-MV131	$	0	0		520
2.000E-04	$ RCI-MOV-MA-MV132	$				521
2.000E-04	$ RCI-MOV-MA-MV18	$				522
2.000E-04	$ RCI-MOV-MA-MV20	$				523
2.000E-04	$ RCI-MOV-MA-MV39	$				524
4.000E-05	$ RCI-MOV-PG-MV15	$	19	20		525
4.000E-05	$ RCI-MOV-PG-MV16	$				526
4.000E-05	$ RCI-MOV-PG-MV18	$				527
3.000E-03	$ RHR-MOV-CC-MV34A	$	19	12		528
3.000E-03	$ RHR-MOV-CC-MV34B	$				529
3.000E-03	$ RHR-MOV-CC-MV39A	$				530
3.000E-03	$ RHR-MOV-CC-MV39B	$				531
2.000E-04	$ RHR-MOV-MA-MV39A	$	0	0		532
2.000E-04	$ RHR-MOV-MA-MV39B	$				533
3.000E-03	$ SDC-MOV-CC-MV15A	$	19	12		534
3.000E-03	$ SDC-MOV-CC-MV15B	$				535
3.000E-03	$ SDC-MOV-CC-MV15C	$				536
3.000E-03	$ SDC-MOV-CC-MV15D	$				537
3.000E-03	$ SDC-MOV-CC-MV17	$				538
3.000E-03	$ SDC-MOV-CC-MV18	$				539
2.000E-04	$ SDC-MOV-MA-MV15A	$	0	0		540
2.000E-04	$ SDC-MOV-MA-MV15B	$				541
2.000E-04	$ SDC-MOV-MA-MV15C	$				542
2.000E-04	$ SDC-MOV-MA-MV15D	$				543
3.000E-03	$ SDC-MOV-OO-MV13A	$	19	12		544
3.000E-03	$ SDC-MOV-OO-MV13B	$				545
3.000E-03	$ SDC-MOV-OO-MV13C	$				546

P_{random}	Basic Event	EF	N_{frag}	N_{resp}	N_{corr}	No.
3.000E-03	SDC-MOV-OO-MV13D					547
3.000E-03	SLC-MOV-OO-MV15					548
3.000E-03	SLC-MOV-OO-MV18					549
1.000E-03	ESF-PER-LC13ACT		3	11		550
5.000E-04	ESF-PER-LC13ACT2					551
1.000E+00	ESF-PER-LIA3TEST		0	0		552
1.000E+00	ESF-PER-LIB3TEST					553
1.000E+00	ESF-PER-LIC3TEST					554
1.000E+00	ESF-PER-LID3TEST					555
1.000E+00	ESF-PER-RXLNTMET					556
7.000E-04	HSW-PFT-RE-MDPB					557
1.000E-05	CST-PSF-CSTLOST		0			558
000E+00	CST-PSF-DEPLETED		0	0		559
4..00E-05	HCI-PSF-HW-COL13					560
2.000E-03	SLC-PSF-MA-MDPE					561
1.000E-06	ADS-PTF-VF-ADSRV		20	20		562
1.000E-06	ADS-PTF-VF-NADSV		21	20		563
2.000E-03	CRD-PTF-MA-PB		0	0		564
2.000E-03	EHV-PTF-MA-OAV64					565
2.000E-03	EHV-PTF-MA-OAV91					566
2.000E-03	EHV-PTF-MA-OBV64					567
2.000E-03	EHV-PTF-MA-OBV91					568
2.000E-03	EHV-PTF-MA-OCV64					569
2.000E-03	EHV-PTF-MA-OCV91					570
2.000E-03	EHV-PTF-MA-ODV64					571
2.000E-03	EHV-PTF-MA-ODV91					572
9.000E-04	EHV-PTF-RE-OAV64					573
6.000E-04	EHV-PTF-RE-OAV91					574
9.000E-04	EHV-PTF-RE-OBV64					575
6.000E-04	EHV-PTF-RE-OBV91					576
9.000E-04	EHV-PTF-RE-OCV64					577
6.000E-04	EHV-PTF-RE-OCV91					578
9.000E-04	EHV-PTF-RE-ODV64					579
6.000E-04	EHV-PTF-RE-ODV91					580
1.000E-03	ESW-PTF-RE-DGA					581
1.000E-03	ESW-PTF-RE-DGB					582
1.000E-03	ESW-PTF-RE-DGC					583
1.000E-03	ESW-PTF-RE-DGD					584
7.000E-04	ESW-PTF-RE-ECW					585
7.000E-04	ESW-PTF-RE-HX1					586
7.000E-04	ESW-PTF-RE-HX10					587
7.000E-04	ESW-PTF-RE-HX12					588
7.000E-04	ESW-PTF-RE-HX13					589
7.000E-04	ESW-PTF-RE-HX15					590
7.000E-04	ESW-PTF-RE-HX16					591
7.000E-04	ESW-PTF-RE-HX18					592
7.000E-04	ESW-PTF-RE-HX19					593
7.000E-04	ESW-PTF-RE-HX2					594
7.000E-04	ESW-PTF-RE-HX21					595
7.000E-04	ESW-PTF-RE-HX22					596

P_{random}		Basic Event		EF	N_{frag}	N_{resp}	N_{corr}	No.
7.000E-04	$	ESW-PTF-RE-HX24	$					597
7.000E-04	$	ESW-PTF-RE-HX25	$					598
7.000E-04	$	ESW-PTF-RE-HX27	$					599
7.000E-04	$	ESW-PTF-RE-HX28	$					600
7.000E-04	$	ESW-PTF-RE-HX3	$					601
7.000E-04	$	ESW-PTF-RE-HX4	$					602
0.000E-01	$	ESW-PTF-RE-HX5	$					603
7.000E-04	$	ESW-PTF-RE-HX6	$					604
7.000E-04	$	ESW-PTF-RE-HX7	$					605
7.000E-04	$	ESW-PTF-RE-HX9	$					606
7.000E-04	$	ESW-PTF-RE-MDPA	$					607
7.000E-04	$	ESW-PTF-RE-MDPB	$					608
1.000E-03	$	HCI-PTF-VF-NOSUC	$		19	12		609
1.200E-03	$	HSW-PTF-RE-ECTFA	$		0	0		610
1.200E-03	$	HSW-PTF-RE-ECTFB	$					611
1.200E-03	$	HSW-PTF-RE-ECTFC	$					612
1.200E-03	$	HSW-PTF-RE-HXA	$					613
1.200E-03	$	HSW-PTF-RE-HXB	$					614
1.200E-03	$	HSW-PTF-RE-HXC	$					615
1.200E-03	$	HSW-PTF-RE-HXD	$					616
7.000E-04	$	HSW-PTF-RE-MDPA	$					617
7.000E-04	$	HSW-PTF-RE-MDPB	$					618
7.000E-04	$	HSW-PTF-RE-MDPC	$					619
7.000E-04	$	HSW-PTF-RE-MDPD	$					620
6.000E-04	$	HSW-PTF-RE-PS10	$					621
9.000E-04	$	HSW-PTF-RE-PS18	$					622
9.000E-04	$	HSW-PTF-RE-PS20	$					623
1.000E-04	$	IAS-PTF-HW-IAS	$		16	26		624
1.500E-03	$	LCI-PTF-RE-2AP35	$		0	0		625
1.500E-03	$	LCI-PTF-RE-2BP35	$					626
1.500E-03	$	LCI-PTF-RE-2CP35	$					627
1.500E-03	$	LCI-PTF-RE-2DP35	$					628
1.200E-03	$	LCI-PTF-RE-LOOPA	$					629
1.200E-03	$	LCI-PTF-RE-LOOPB	$					630
1.500E-03	$	LCS-PTF-RE-2AP37	$					631
1.500E-03	$	LCS-PTF-RE-2BP37	$					632
1.500E-03	$	LCS-PTF-RE-2CP37	$					633
1.500E-03	$	LCS-PTF-RE-2DP37	$					634
2.000E-03	$	RBC-PTF-MA-PB	$					635
9.000E-04	$	RBC-PTF-RE-2352	$					636
9.000E-04	$	RBC-PTF-RE-2354	$					637
1.200E-03	$	RBC-PTF-RE-PB	$					638
3.000E-03	$	TBC-PTF-FS-PUMPB	$		16	26		639
2.000E-03	$	TBC-PTF-MA-PUMPB	$		0	0		640
1.200E-03	$	TBC-PTF-RE-PUMPB	$					641
1.000E-03	$	ESF-PWR-FC-4160A	$		2	7		642
1.000E-03	$	ESF-PWR-FC-4160B	$					643
1.000E-03	$	ESF-PWR-FC-4160C	$					644
1.000E-03	$	ESF-PWR-FC-4160D	$					645
8.000E-06	$	DCP-REC-LP-1	$		6	7		646

P_{random}	Basic Event	EF	N_{frag}	N_{resp}	N_{corr}	No.
8.000E-06	$ DCP-REC-LP-2	$				647
8.000E-06	$ DCP-REC-LP-3	$				648
8.000E-06	$ DCP-REC-LP-4	$				649
1.000E-03	$ RBC-SOV-FT-S2352	$	20	16		650
1.000E-03	$ RBC-SOV-FT-S2354	$				651
2.000E-04	$ RBC-SOV-MA-S2352	$	0	0		652
2.000E-04	$ RBC-SOV-MA-S2354	$				653
3.000E-04	$ EHV-SRV-CC-RV1	$	21	6		654
3.000E-04	$ EHV-SRV-CC-RV2	$				655
3.000E-04	$ EHV-SRV-CC-RV3	$				656
3.000E-04	$ EHV-SRV-CC-RV4	$				657
3.000E-04	$ SLC-SRV-CC-RV39A	$	0	0		658
3.000E-04	$ SLC-SRV-CC-RV39B	$				659
1.000E-01	$ CDS-SYS-FC-COND	$	16	26		660
1.000E-01	$ NSW-SYS-FO-NSW	$				661
1.000E-04	$ PCV-SYS-HW-SYSTM	$	19	20		662
3.400E-03	$ SLC-SYS-TE-SLC	$	0	0		663
1.000E-04	$ HCI-TCV-HW-TCV18	$	19	12		664
1.000E-04	$ LCS-TCV-HW-TV13A	$				665
1.000E-04	$ LCS-TCV-HW-TV13B	$				666
1.000E-04	$ RCI-TCV-HW-TCV22	$				667
5.000E-02	$ HCI-TDP-FR-20S37	$	0	0		668
3.000E-02	$ HCI-TDP-FS-20S37	$	16	14		669
1.000E-02	$ HCI-TDP-MA-20S37	$	0	0		670
5.000E-02	$ RCI-TDP-FR-20S38	$				671
3.000E-02	$ RCI-TDP-FS-20S38	$	16	14		672
1.000E-02	$ RCI-TDP-MA-20S38	$	0	0		673
1.000E-05	$ ESW-TNK-LL-PS13	$	24	22		674
1.000E-05	$ HSW-TNK-LF-RESVR	$	0			675
1.000E-06	$ ADS-TSW-FT-DC125	$	13	11		676
1.250E-03	$ LCI-TSW-FT-ATOC	$	3	11		677
1.250E-03	$ LCI-TSW-FT-BTOD	$				678
1.000E-05	$ HSW-VFC-LF-PPBAY	$	0	0		679
5.000E-01	$ CRD-XHE-FO-BRKRS	$				680
5.000E-01	$ CRD-XHE-FO-CRD	$				681
4.000E-04	$ CRD-XHE-RE-PB	$				682
5.000E-01	$ ESF-XHE-FO-ADSBT	$				683
5.000E-01	$ ESF-XHE-FO-DEPRE	$				684
5.000E-01	$ ESF-XHE-FO-DEPSD	$				685
5.000E-01	$ ESF-XHE-FO-HCICL	$				686
5.000E-01	$ ESF-XHE-FO-HCIRL	$				687
5.000E-01	$ ESF-XHE-FO-HPSAT	$				688
5.000E-01	$ ESF-XHE-FO-HPSRL	$				689
1.000E-01	$ ESF-XHE-FO-HSWIN	$				690
5.000E-01	$ ESF-XHE-FO-LPSAT	$				691
5.000E-01	$ ESF-XHE-FO-OVRID	$				692
5.000E-01	$ ESF-XHE-FO-RCICL	$				693
5.000E-01	$ ESF-XHE-FO-RCICO	$				694
5.000E-01	$ ESF-XHE-FO-RCIRL	$				695
5.000E-01	$ ESF-XHE-FO-RHRAT	$				696

P_{random}	Basic Event	EF	N_{frag}	N_{resp}	N_{corr}	No.
2.500E-05	ESF-XHE-MC-CSTLV					697
1.000E-04	ESF-XHE-MC-HDPRS					698
2.000E-04	ESF-XHE-MC-PRES					699
5.000E-05	ESF-XHE-MC-VSLVL					700
9.000E-01	ESW-XHE-FO-EHS					701
5.000E-01	HSW-XHE-FO-PS9					702
5.000E-01	PCV-XHE-FO-PCV					703
5.000E-01	RBC-XHE-FO-LCVAL					704
5.000E-01	RBC-XHE-FO-SWCH					705
5.000E-01	SLC-XHE-FO-SLC					706
1.200E-02	SLC-XHE-RE-DIVER					707
3.000E-03	SLC-XHE-RE-EV14A					708
3.000E-03	SLC-XHE-RE-EV14B					709
1.000E-03	SLC-XHE-RE-MDPA					710
1.000E-03	SLC-XHE-RE-MDPB					711
2.000E-04	ESW-XVM-MA-XV517					712
4.000E-05	ESW-XVM-PG-D504A					713
4.000E-05	ESW-XVM-PG-D504B					714
4.000E-05	ESW-XVM-PG-D504C					715
4.000E-05	ESW-XVM-PG-D504D					716
4.000E-05	ESW-XVM-PG-D505A					717
4.000E-05	ESW-XVM-PG-D505B					718
4.000E-05	ESW-XVM-PG-D505C					719
4.000E-05	ESW-XVM-PG-D505D					720
4.000E-05	ESW-XVM-PG-D519A					721
4.000E-05	ESW-XVM-PG-D519B					722
4.000E-05	ESW-XVM-PG-D519C					723
4.000E-05	ESW-XVM-PG-D519D					724
4.000E-05	ESW-XVM-PG-X507A					725
4.000E-05	ESW-XVM-PG-X507B					726
4.000E-05	ESW-XVM-PG-XV13					727
4.000E-05	ESW-XVM-PG-XV15					728
4.000E-05	ESW-XVM-PG-XV16					729
4.000E-05	ESW-XVM-PG-XV17					730
4.000E-05	ESW-XVM-PG-XV18					731
4.000E-05	ESW-XVM-PG-XV19					732
4.000E-05	ESW-XVM-PG-XV20					733
4.000E-05	ESW-XVM-PG-XV21					734
4.000E-05	ESW-XVM-PG-XV22					735
4.000E-05	ESW-XVM-PG-XV23					736
4.000E-05	ESW-XVM-PG-XV24					737
4.000E-05	ESW-XVM-PG-XV25					738
4.000E-05	ESW-XVM-PG-XV26					739
4.000E-05	ESW-XVM-PG-XV27					740
4.000E-05	ESW-XVM-PG-XV28					741
4.000E-05	ESW-XVM-PG-XV29					742
4.000E-05	ESW-XVM-PG-XV30					743
4.000E-05	ESW-XVM-PG-XV31					744
4.000E-05	ESW-XVM-PG-XV32					745
4.000E-05	ESW-XVM-PG-XV33					746

P_{random}	Basic Event	EF	N_{frag}	N_{resp}	N_{corr}	No.
4.000E-05	ESW-XVM-PG-XV34					747
4.000E-05	ESW-XVM-PG-XV35					748
4.000E-05	ESW-XVM-PG-XV36					749
4.000E-05	ESW-XVM-PG-XV37					750
4.000E-05	ESW-XVM-PG-XV38					751
4.000E-05	ESW-XVM-PG-XV39					752
4.000E-05	ESW-XVM-PG-XV40					753
4.000E-05	ESW-XVM-PG-XV41					754
4.000E-05	ESW-XVM-PG-XV42					755
4.000E-05	ESW-XVM-PG-XV43					756
4.000E-05	ESW-XVM-PG-XV44					757
4.000E-05	ESW-XVM-PG-XV45					758
4.000E-05	ESW-XVM-PG-XV46					759
4.000E-05	ESW-XVM-PG-XV47					760
4.000E-05	ESW-XVM-PG-XV48					761
4.000E-05	ESW-XVM-PG-XV49					762
4.000E-05	ESW-XVM-PG-XV50					763
4.000E-05	ESW-XVM-PG-XV502					764
4.000E-05	ESW-XVM-PG-XV506					765
4.000E-05	ESW-XVM-PG-XV509					766
4.000E-05	ESW-XVM-PG-XV51					767
4.000E-05	ESW-XVM-PG-XV510					768
4.000E-05	ESW-XVM-PG-XV517					769
4.000E-05	ESW-XVM-PG-XV52					770
4.000E-05	ESW-XVM-PG-XV53					771
4.000E-05	ESW-XVM-PG-XV54					772
4.000E-05	ESW-XVM-PG-XV55					773
4.000E-05	ESW-XVM-PG-XV56					774
4.000E-05	ESW-XVM-PG-XV57					775
4.000E-05	ESW-XVM-PG-XV58					776
4.000E-05	ESW-XVM-PG-XV59					777
4.000E-05	ESW-XVM-PG-XV60					778
4.000E-05	ESW-XVM-PG-XV61					779
4.000E-05	ESW-XVM-PG-XV62					780
4.000E-05	ESW-XVM-PG-XV63					781
4.000E-05	ESW-XVM-PG-XV64					782
4.000E-05	ESW-XVM-PG-XV65					783
4.000E-05	ESW-XVM-PG-XV66					784
4.000E-05	ESW-XVM-PG-XV67					785
4.000E-05	ESW-XVM-PG-XV68					786
4.000E-05	ESW-XVM-PG-XVA					787
4.000E-05	ESW-XVM-PG-XVB					788
4.000E-05	ESW-XVM-PG-XVC					789
4.000E-05	ESW-XVM-PG-XVD					790
4.000E-05	ESW-XVM-PG-XVE					791
4.000E-05	ESW-XVM-PG-XVF					792
4.000E-05	ESW-XVM-PG-XVG					793
4.000E-05	ESW-XVM-PG-XVH					794
4.000E-05	ESW-XVM-PG-XVI					795
4.000E-05	ESW-XVM-PG-XVJ					796

P_{random}	Basic Event	EF	N_{frag}	N_{resp}	N_{corr}	No.
4.000E-05	ESW-XVM-PG-XVK					797
4.000E-05	ESW-XVM-PG-XVL					798
4.000E-05	ESW-XVM-PG-XVM					799
4.000E-05	ESW-XVM-PG-XVN					800
4.000E-05	ESW-XVM-PG-XVO					801
4.000E-05	ESW-XVM-PG-XVP					802
4.000E-05	ESW-XVM-PG-XVQ					803
4.000E-05	ESW-XVM-PG-XVR					804
4.000E-05	ESW-XVM-PG-XVS					805
4.000E-05	ESW-XVM-PG-XVT					806
3.000E-04	ESW-XVM-RE-XV517					807
0.000E-01	ESW-XVM-RE-XVA					808
9.000E-04	ESW-XVM-RE-XVAB					809
9.000E-04	ESW-XVM-RE-XVCD					810
9.000E-04	ESW-XVM-RE-XVEF					811
9.000E-04	ESW-XVM-RE-XVGH					812
9.000E-04	ESW-XVM-RE-XVIJ					813
9.000E-04	ESW-XVM-RE-XVKL					814
9.000E-04	ESW-XVM-RE-XVMN					815
9.000E-04	ESW-XVM-RE-XVOP					816
9.000E-04	ESW-XVM-RE-XVQR					817
9.000E-04	ESW-XVM-RE-XVST					818
4.000E-05	HCI-XVM-HW-CST01					819
4.000E-05	HCI-XVM-PG-XV12					820
4.000E-05	HCI-XVM-PG-XV23					821
1.250E-04	HSW-XVM-OO-516A					822
4.000E-05	HSW-XVM-PG-X501A					823
4.000E-05	HSW-XVM-PG-X501B					824
4.000E-05	HSW-XVM-PG-X501C					825
4.000E-05	HSW-XVM-PG-X501D					826
4.000E-05	HSW-XVM-PG-X515B					827
4.000E-05	HSW-XVM-PG-XV11					828
4.000E-05	HSW-XVM-PG-XV5					829
4.000E-05	HSW-XVM-PG-XV6					830
4.000E-05	HSW-XVM-PG-XV7					831
4.000E-05	HSW-XVM-PG-XV8					832
4.000E-05	HSW-XVM-PG-XV9					833
4.000E-05	LCI-XVM-PG-XV81A					834
4.000E-05	LCI-XVM-PG-XV81B					835
4.000E-05	LCS-XVM-PG-XV14A					836
4.000E-05	LCS-XVM-PG-XV14B					837
4.000E-05	LCS-XVM-PG-XV63A					838
4.000E-05	LCS-XVM-PG-XV63B					839
4.000E-05	LCS-XVM-PG-XV63C					840
4.000E-05	LCS-XVM-PG-XV63D					841
4.000E-05	RCI-XVM-PG-XV17					842
4.000E-05	RCI-XVM-PG-XV9					843
4.000E-05	SDC-XVM-PG-XV1					844
4.000E-05	SLC-XVM-PG-XV11					845
4.000E-05	SLC-XVM-PG-XV12A					846

P_{random}		Basic Event		EF	N_{frag}	N_{resp}	N_{corr}	No.
4.000E-05	$	SLC-XVM-PG-XV12B	$					847
4.000E-05	$	SLC-XVM-PG-XV13A	$					848
4.000E-05	$	SLC-XVM-PG-XV13B	$					849
4.000E-05	$	SLC-XVM-PG-XV15	$					850
4.000E-05	$	SLC-XVM-PG-XV18	$					851
0.000E-00	$	SLOCA-FIT	$	3.0	29	32		852
0.000E-00	$	MLOCA-FIT	$	3.0	30	32		853
0.000E-00	$	RECIRC-PUMP	$	3.0	31	1		854
0.000E-00	$	VESSEL-SKIRT	$	3.0	28	1		855
5.000E-06	$	ACP-CCF-2-4KV	$		41	7	2	856
7.800E-05	$	ESW-CCF-2-MDPS	$		17	28	2	857
3.900E-05	$	ACP-CCF-2-DGS	$	3.0	42	22	2	858
0.000E-00	$	DIKE-CST-RWST	$	3.0	32	1		859
0.000E-00	$	EMER-COOL-TOWER	$	3.0	33	1		860
0.000E-00	$	REACTOR-BLDG	$	3.0	34	1		861
0.000E-00	$	RADWASTE/TB-ROOF	$	3.0	35	1		862
0.000E-00	$	RADWASTE/TB-WALL	$	3.0	36	1		863
0.000E-00	$	TURBINE-BLDG	$	3.0	37	1		864
0.000E-00	$	BLOCK-WALLS-VAR	$	3.0	38	1		865
0.000E+00	$	RECIRC-PUMP-2CCF	$	3.0	31	1	2	866
5.000E-06	$	ACP-CCF-3-4KV	$		41	7	3	867

APPENDIX B

ZION ANALYSIS

CONTENTS

B.1 INTRODUCTION

The Zion plant was selected for analyzing the potential impact of degraded shear wall stiffness on plant seismic design loads and plant seismic risk because systems models and data had been developed in the earlier NRC-sponsored Seismic Safety Margins Research Program (SSMRP), as described in Reference B-1. (In addition, the Zion plant was the subject of a PRA sponsored by the utility, Commonwealth Edison, Inc., as described in Reference B-2. However, the present study was based entirely on the results from the SSMRP.)

In the SSMRP, a seismic PRA based on five different loss of coolant accident (LOCA) break sizes and two types of transient initiators was performed, and dynamic structural models of the buildings important to safety were developed. In addition, piping models were developed for the dynamic response analysis of critical piping segments associated with five systems important to safety. Thus the models developed in the SSMRP allowed the evaluation of the impact of degraded shear wall stiffnesses on the response of important safety related piping systems.

In this study, the same LOCA and transient event accident sequence Boolean expressions developed in the SSMRP program were used. In addition, the seismic hazard curves for the site were updated, and were based on the results developed in the NRC-sponsored Seismic Hazard Characterization of the Central and Eastern United States program as reported in Reference B-3. (These results were not available at the time the SSMRP was completed.) Of course, a full set of new structural and piping responses was computed--both with and without degraded shear wall stiffnesses, as described in this Appendix.

B.1.1 Plant Description

The Zion nuclear power plant is a 1040 MWe pressurized water reactor (PWR) located on the shore of Lake Michigan north of Chicago, Illinois. Commonwealth Edison, Inc. owns and operates the facility. Zion entered commercial operation on April, 1973.

The reactor vendor for Zion was Westinghouse (W). The architect/engineer was Sargent and Lundy. The design of the reactor coolant system is typical of other W plants currently in commercial operation; there are four steam generators and four reactor coolant loops. Most of the major safety system designs are also fairly typical of other W plants.

The plant is founded on a site characterized by 110 feet of soil overlying bedrock. The top layer of soil, about 35 ft thick, consists of granular lake deposits of dense, fine-to medium sands, together with variable amounts of coarse sand and gravel. The second layer, 30 ft thick, is a cohesive, firm-to-hard glacial till The remaining 45-ft layer of soil is a cohesionless glacial deposit of dense sands and gravel. Based on the Final Safety Analysis Report (Reference B-4), a horizontal peak ground accceleration of 0.17g was defined for the SSE.

B.1.2 Description of Plant Systems

In this section, the plant systems important to safety are briefly discussed, along with the functional interactions which cause the dominant seismic failure modes highlighted. The systems descriptions were taken directly from Reference B-5.

B.1.2.1 Emergengy Core Cooling System (ECCS) Description

In response to a LOCA, the ECCS is called upon to reflood the core if necessary and keep it covered. The ECCS success criteria are shown in Table B-1. As shown in this table, the ECCS is made up of three pumping

Table B-1 Definition of ECCS Success Requirements for LOCA Events at Zion Unit 1

LOCA size (equivalent diam.)	Injection Mode (ECI)	Recirculation Mode (ECR)
Large Breaks > 6"	1/2 LPIS[a] + 3/4 ACC	1/2 LPIS
Medium 6" ≥ Breaks 3"	1/2 CP + 1/2 SIP + 3/4 ACC or 2/2 SIP + 3/4 ACC	1/2 CP + 1/2 SIP or 2/2 SIP or 1/2 LPIS
Small 3" ≥ Breaks > 1.5"	1/2 CP + 1/2 SIP or 2/2 SIP	1/2 CP + 1/2 SIP or 2/2 SIP
Small-small 1.5" ≥ Breaks > 0.5"	1/2 CP + 1/2 SIP or 2/2 SIP or 2/2 CP	1/2 CP + 1/2 SIP or 2/2 SIP or 2/2 CP

[a]The RHR pumps are used for LPIS because there are no separate LPIS pumps.

systems and four accumulators. Different combinations of these systems can be used in responding to different break sizes. The following components are part of the ECCS:

1. Two centrifugal charging pumps (CP)
2. Two high head safety injection pumps (SIP)
3. Two residual heat removal pumps (RHR)
4. Two residual heat exchangers
5. Four accumulator tanks (one on each loop)
6. One boron injection tank (BIT)
7. Refueling water storage tank (RWST)
8. All related valves and piping

Figure B-1 shows the major components of the ECCS.

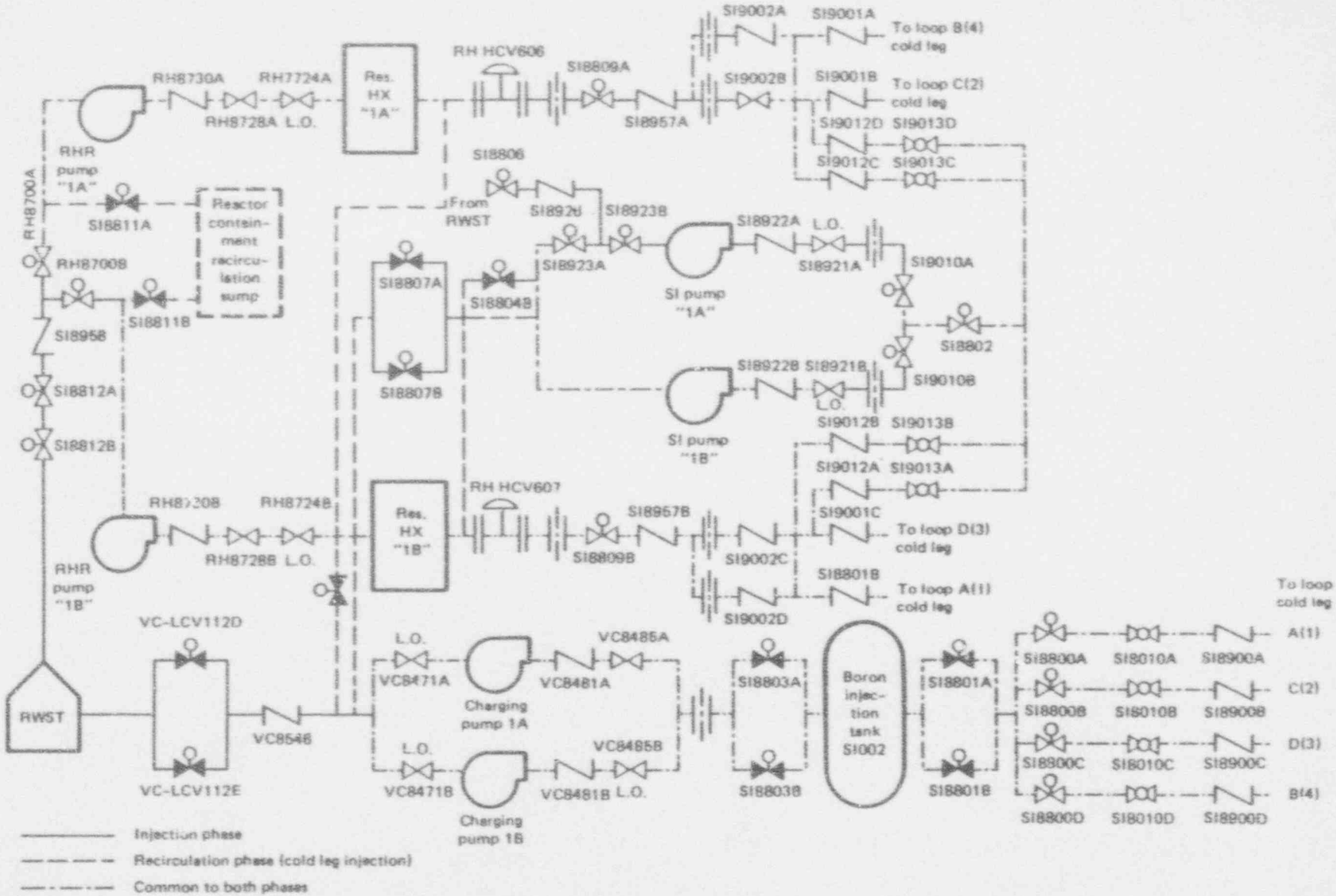

Figure B-1 Description of ECCS

Accumulators

There are four accumulator tanks, one for each cold leg of the primary coolant system. In the event of a large or medium LOCA, the borated water in the accumulators is injected into the primary system as soon as the pressure of the primary system drops below that of the accumulators (650 psig normal pressure). (It should be noted that in a less than medium size break the primary system pressure will not drop below 650 psig as a result of the blow-down.)

Centrifugal Charging Pumps

Two high pressure centrifugal charging pumps are provided. These two pumps serve as part of the Chemical and Volume Control System (CVCS) during normal plant operation. In an accident, these pumps supply high pressure borated water to the primary system at a rate of 150 gpm each. During the injection phase operation of ECCS, these pumps take water from the refueling water storage tank (RWST) and inject the water into the primary coolant system via the boron injection tank.

The discharge pressure of 2670 psig for these pumps enables them to inject high boron concentrated water into the primary coolant in the event of a transient or small-small LOCA. The charging pumps can pump water into the primary system at normal or above normal operating pressures. [This feature differentiates the charging pumps from the safety injection (SI) and residual heat removal (RHR) pumps.]

During the recirculation phase of operation, the charging pumps take water from the containment sump via RHR Pump 1A. If this pump fails, but the crosstie valves between the SI and charging pumps are opened, the charging pumps can take water from RHR Pump 1B.

Safety Injection Pumps

Two high pressure safety injection pumps are part of the ECCS and these provide water to the primary coolant system at the rate of 400 gpm each when the primary system pressure drops below 1520 psig. (Above a pressure of 1520 psig, the SI pumps recirculate the water back to the RWST.) During the injection phase, the SI pumps take water from the RWST to supply borated water to the four primary coolant cold legs. During recirculation, these pumps take water from the containment sump via RHR Pump 1B. If this pump fails, but the crosstie valves between the SI and charging pumps are opened, the SI pumps can also take water from RHR Pump 1A.

Residual Heat Removal Pumps

Two low pressure RHR pumps deliver high quantities of borated water (3000 gpm for each pump) when the primary system pressure drops below 170 psig. Before the primary system pressure drops below 170 psig, these pumps take water from the RWST during the injection phase and recirculate the water back to the RSWT. During the recirculation phase, the RHR pumps take

water from the containment sump and recirculate the water back to the four cold legs through residual heat exchangers.

B.1.2.2 Auxiliary Feedwater System (AFWS) Description

If the power conversion system (PCS) is not available, the AFWS is required to provide adequate coolant to the steam generators. The design of the AFWS specifies that one of the three auxiliary feedwater pumps delivers water to two of the four steam generators at or below the pressure of the secondary steam relief safety valve set points. The system is composed of:

- Five secondary steam relief safety valves and one power-operated relief valve for each steam generator, any one of which will sufficiently pressurize the steam generator.
- Two motor-driven pumps requiring power from the 4160 KV emergency AC buses.
- One turbine-driven pump at twice the required rated capacity, requiring steam from either the main steam line A or D.
- Two headers connected by normally locked-closed manual isolation valves, each of which can deliver water to all four steam generators through normally open valves.
- Eight normally open, air-operated throttling valves requiring instrument air, but failing open.
- One connection from each of the two headers to each main feedwater line leading to each of the steam generators.
- The preferred source of cooling water is the secondary condensate storage tank, located outside the auxiliary building. An alternate (secondary) source of auxiliary feedwater is from the service water system.

A line diagram of the AFWS is shown in Fig. B-2.

The AFWS naturally interfaces with the instrumentation and control system. The motor-driven pumps are activated by the following signals:

- Low water level in any steam generator.
- Safety injection control signal.
- Loss of offsite AC electric power.

The steam turbine-driven pump is activated by eitner of two signals -- low water level in any two steam generators or complete loss of AC power (offsite plus emergency AC). In addition, the cooling water supply from

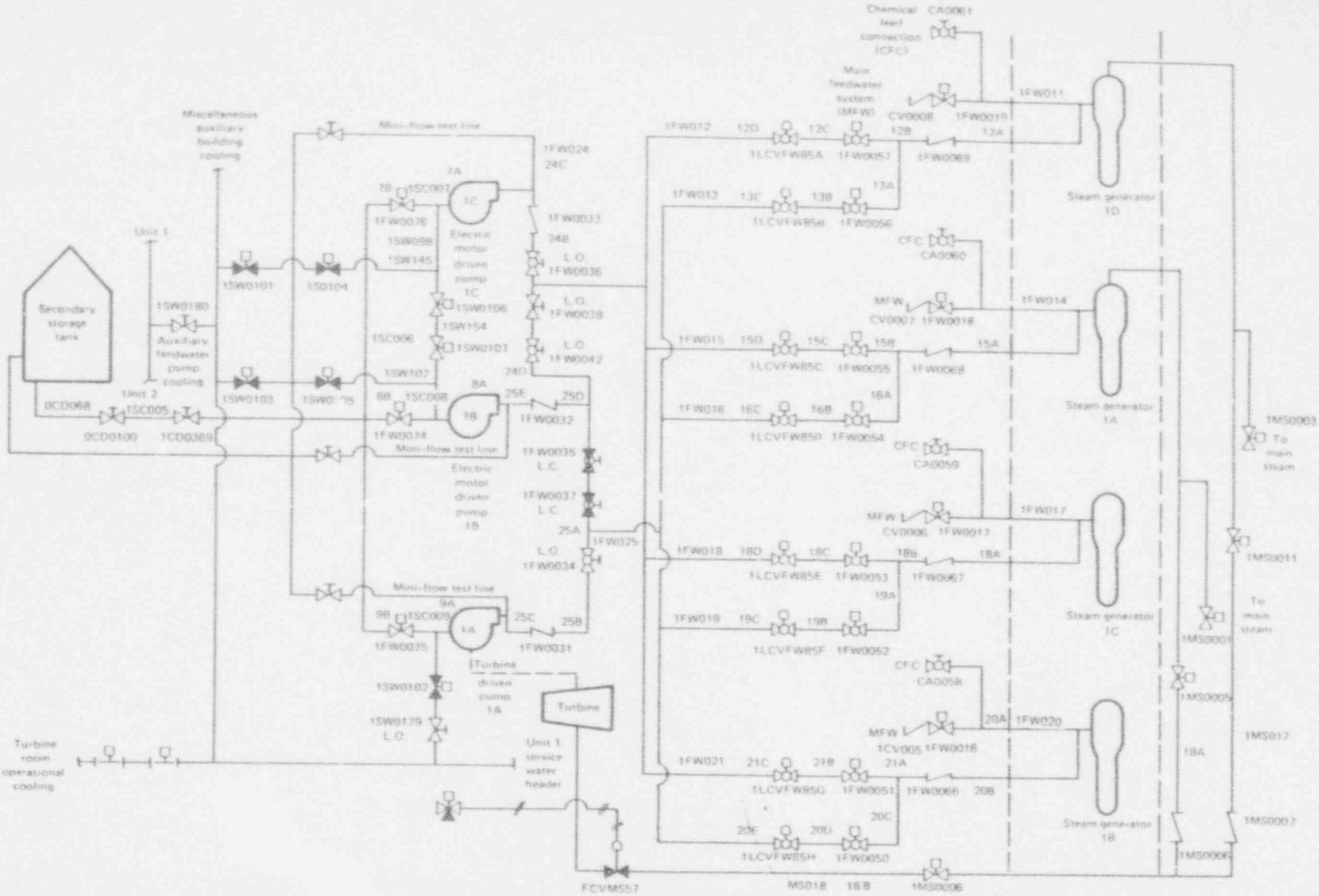

Figure B-2 Description of AFWS

the service water system is activated automatically on low suction pressure to the pumps. Manual activation of the pumps and valves is possible if automatic signals do not initiate operation of the system.

B.1.2.3 Service Water System (SWS) Description

The function of the service water system is to provide the cooling water necessary for all plant equipment. The service water system differs from the other important plant systems in two respects: it is interconnected with Zion Unit 2, and it is required for both normal and emergency operation. The design requirements for both LOCA and transient-initiated events are that one out of three SWS pumps per unit must be operational. (In normal operation, two out of three service water pumps per unit are required.) It has been assumed that the one-out-of-three requirement will satisfy all emergency requirements only if the system can be brought from the normal configuration to emergency configuration. In addition, the water delivered from the crib house on Lake Michigan by the pump sets of both Unit 1 and Unit 2 must reach the equipment it is designed to service.

The following equipment cooling functions were analyzed:

- Containment fan cooling system fan motors and heat exchangers
- Component cooling-water heat exchangers
- Diesel-generator-cooling heat exchangers
- Auxiliary feedwater pump cooling

The following emergency cooling functions were assumed to be less important to the systems analysis task and were not modeled:

- Auxiliary building HVAC
- Emergency pump room coolers: RHR, SIS, etc.
- Penetration pressurizers for the containment
- Computer room and control room HVAC

The following assumptions were made for the analysis: The HVAC and pump room coolers are not crucial for bringing the plant to hot shutdown, the penetration pressurizers do not have a critical effect on containment leakage paths, and equipment could run without room-cooling under emergency conditions. This may be modeled more accurately if one assumes that the equipment failure rates would be dependent on the temperature in the room.

The service water system has four main safety-related functions. These functions (and the supply configuration) are shown in the following figures:

- Main Service water supply headers and pumps for Unit 1 and Unit 2 (Figure B-3)
- Cooling for diesel generator 0A, 1A, and 1B (Figure B-4)
- Cooling for the containment fan coolers and motors 1A through 1E (Figure B-5)
- Cooling for AFWS pumps 1A, 1B, and 1C (Figure B-6)
- Cooling for the component cooling water heat exchangers for Unit 1, Unit 2, and the shared heat exchanger

Each of these figures shows the configurations which results in the system bringing cooling water from Lake Michigan to the equipment in question.

B.1.2.4 Electric Power (EP) System Description

Unit 1 of the Zion plant has three major electrical divisions--17, 18, and 19. A division consists of a 4160 VAC engineered safety feature bus, a 480 V engineered safety feature bus, a 480 VAC motor control center, a 120 VAC instrumentation bus, and a 125 VDC control bus. Each division can be fed from a 4160 VAC bus supplied by the system auxiliary transformer. In Unit 1, Divisions 18 and 19 have a diesel generator dedicated to supplying them power in the event of loss of offsite power. Division 17 has a swing diesel attached to it. The swing diesel can feed either Division 17 for Unit 1 or the equivalent division for Unit 2--it aligns to the division first requiring power. Single-line diagrams for the three divisions are shown of Figures B-7 through B-9. These diagrams show the interrelationships of the buses and motor control centers (MCCs) within a division.

B.2 HAZARD CURVES USED FOR ZION

The Zion Nuclear Power Plant is located in Zion, Illinois approximately 40 miles north of Chicago. The Zion site is characterized by 111 ft of soil consisting of three distinct layers overlying bedrock of Niagara Dolomite. The seismicity of the area is affected by a nearby structure known as the Wisconsin Arch on which a number of small earthquakes have occurred. The SSE for the site is 0.17g horizontal peak ground acceleration.

One set of hazard curves used for this study was taken from the NRC-sponsored Eastern and Central United States Seismic Characterization Program (Reference B-3) and are shown in Figure B-10. On these plots are shown the 15%, 50%, 85%, and the mean hazard curves. The median curve and the mean curve were input, and random realizations for the Monte Carlo study were generated assuming a lognormal distribution for any given peak ground acceleration.

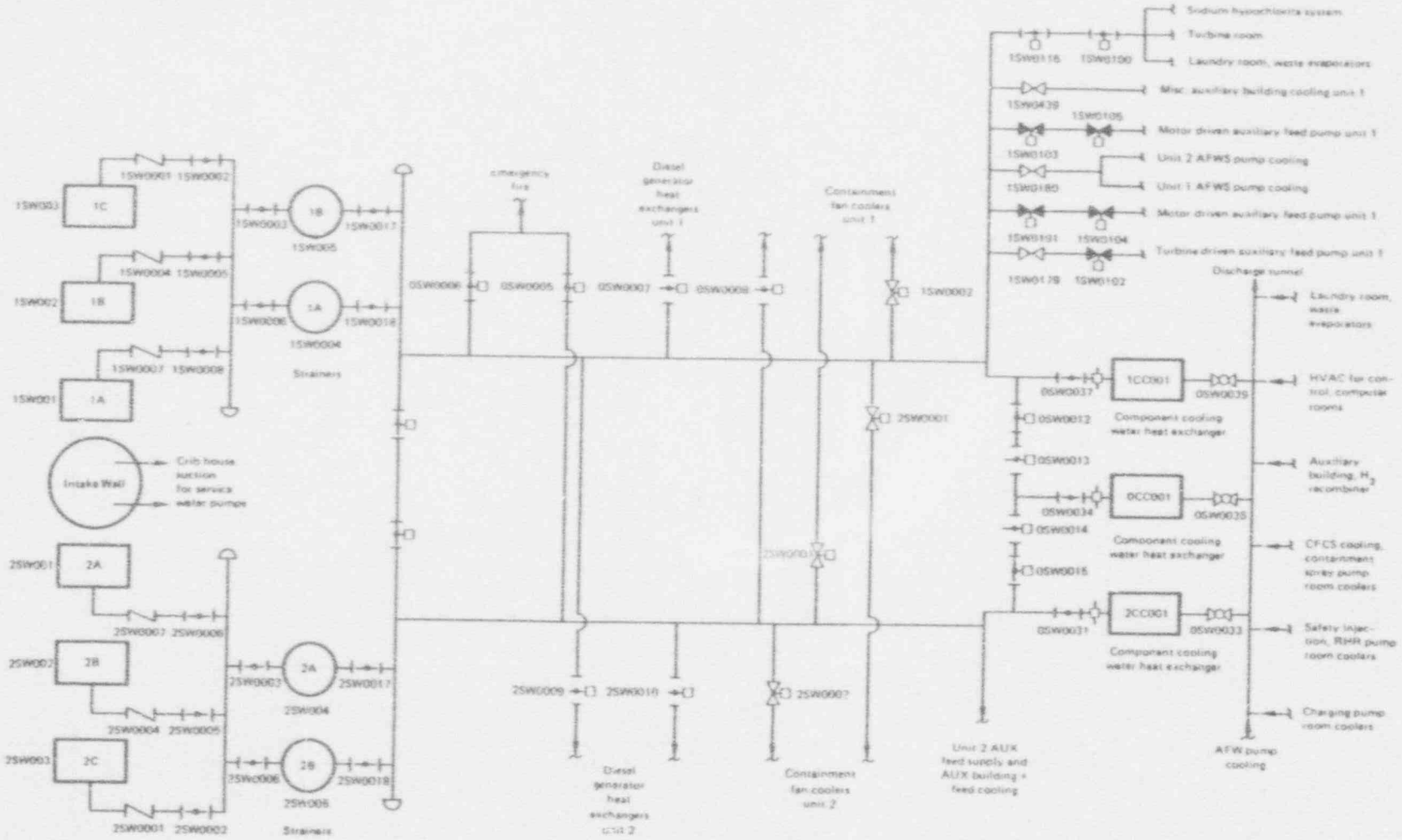

Figure B-3 Service Water Pumps and Supply

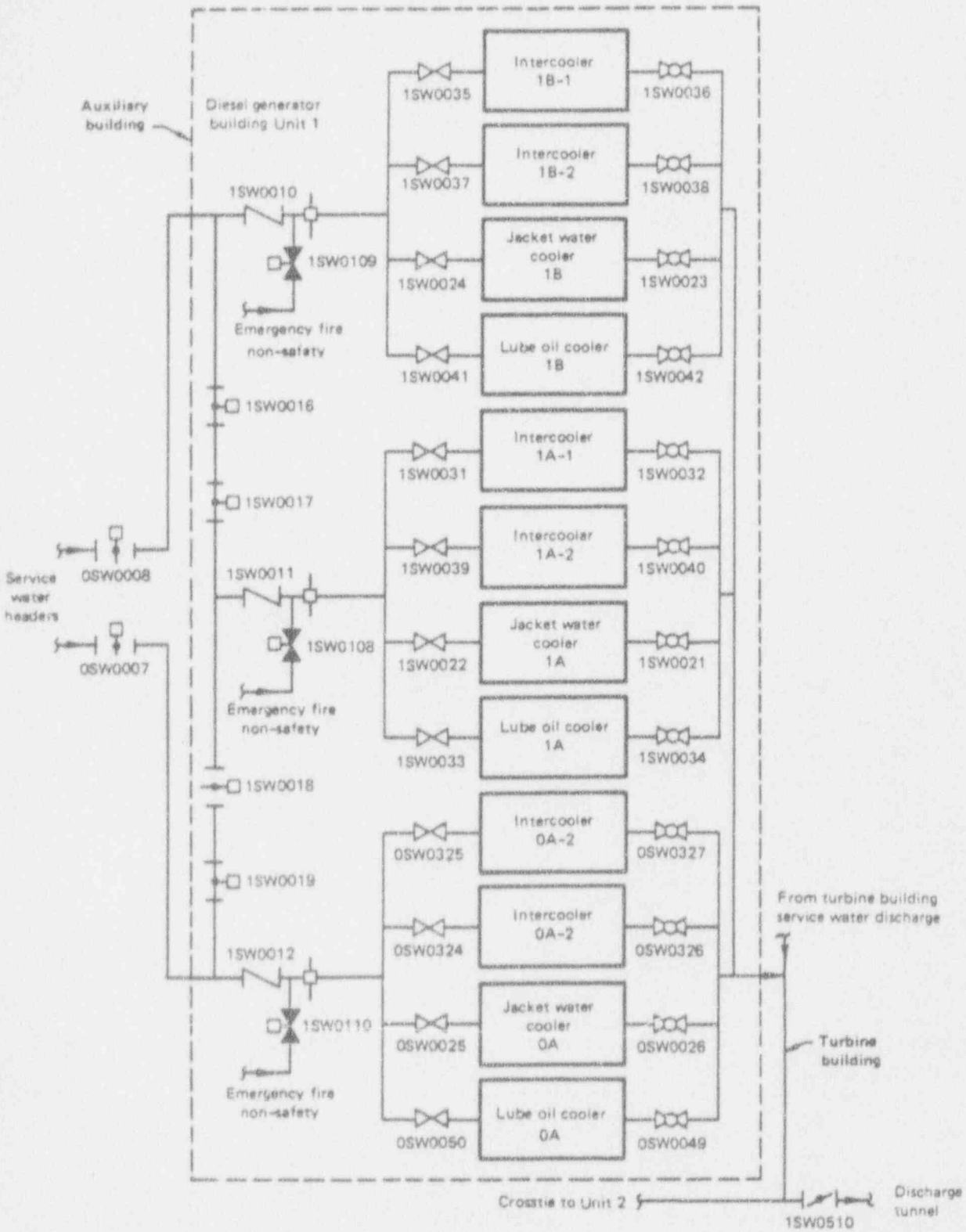

Figure B-4 Diesel Generator Cooling Portion of the SWS

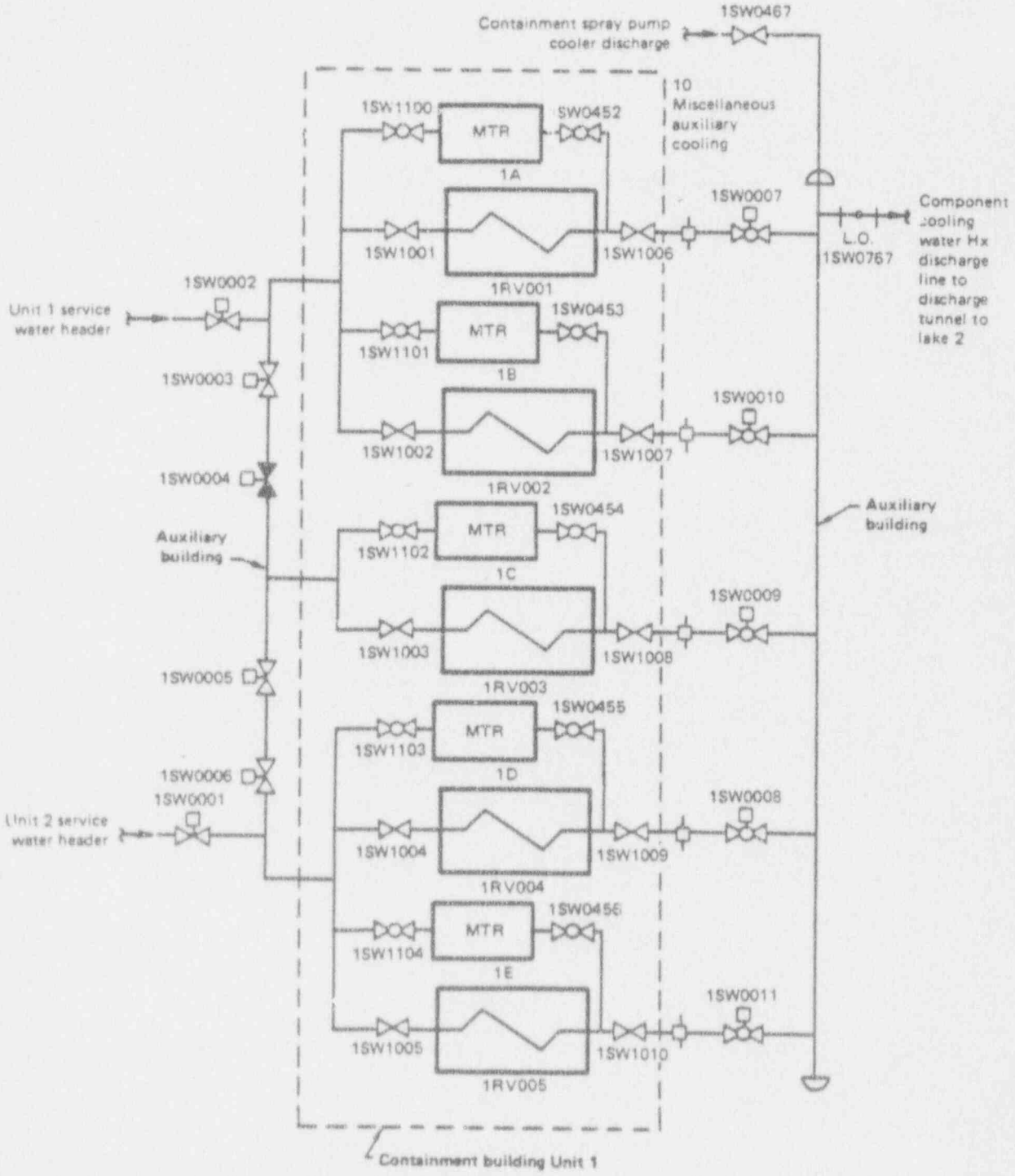

Figure B-5 Containment Fan Coolers Portion of the SWS

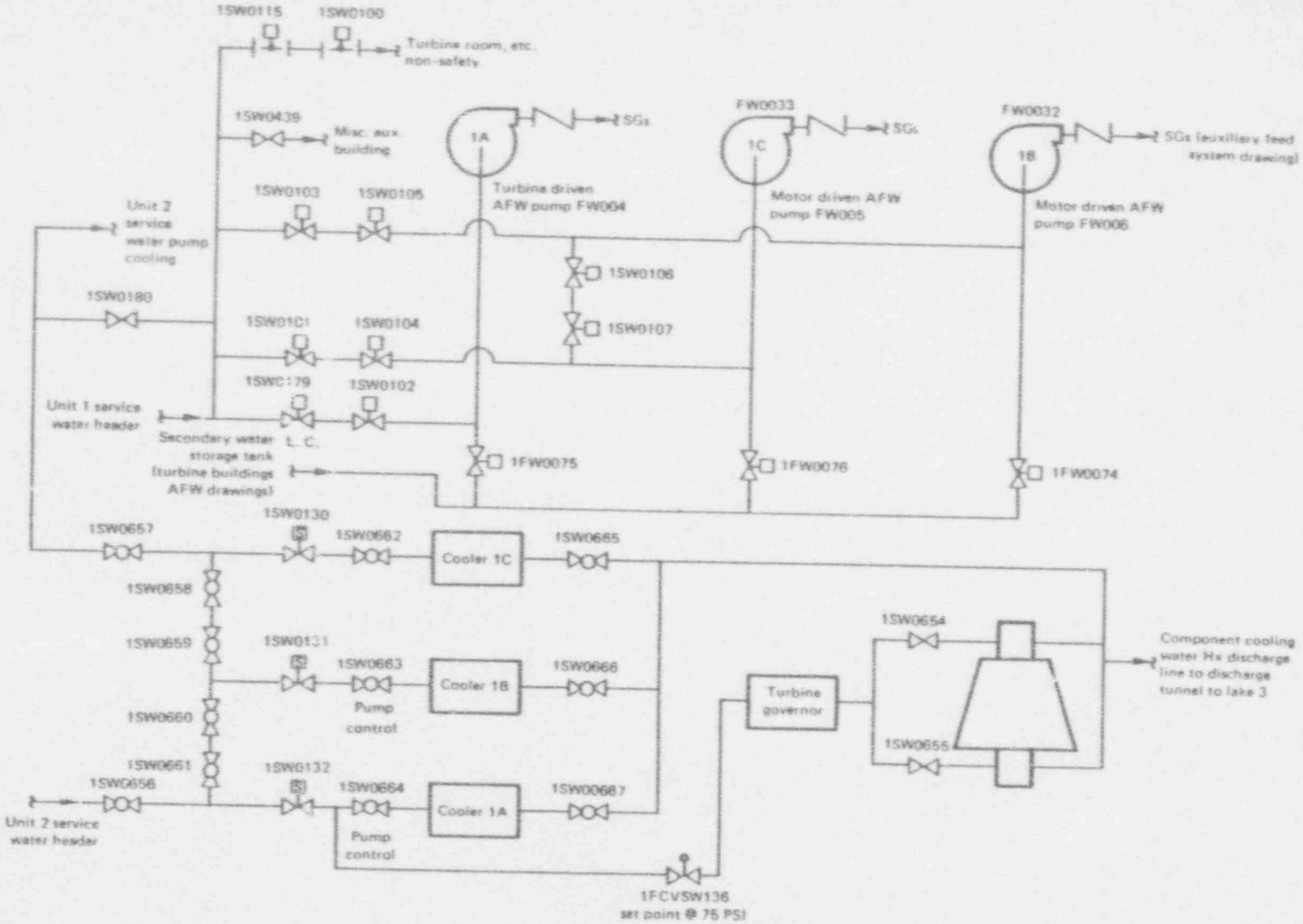

Figure B-6 Auxiliary Feedwater Supply and Cooling Portion of the SWS

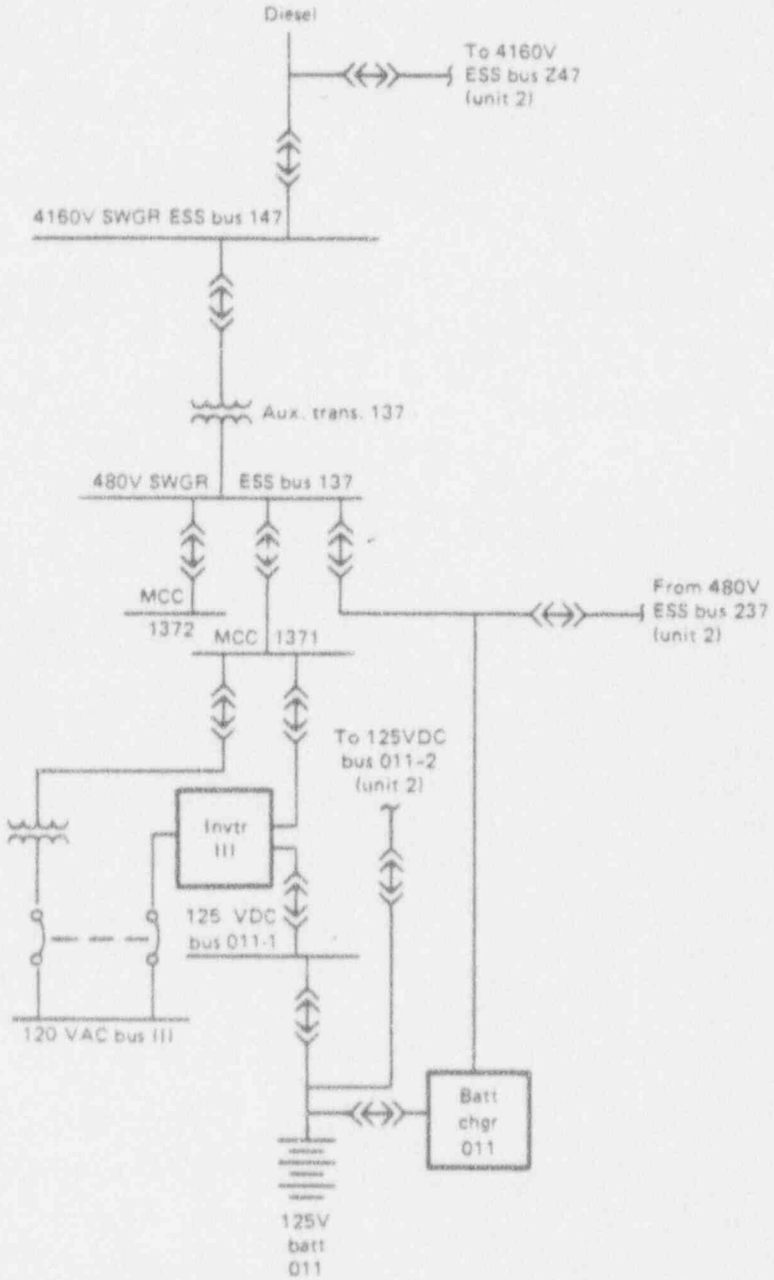

Figure B-7 Electrical Power - Division 17

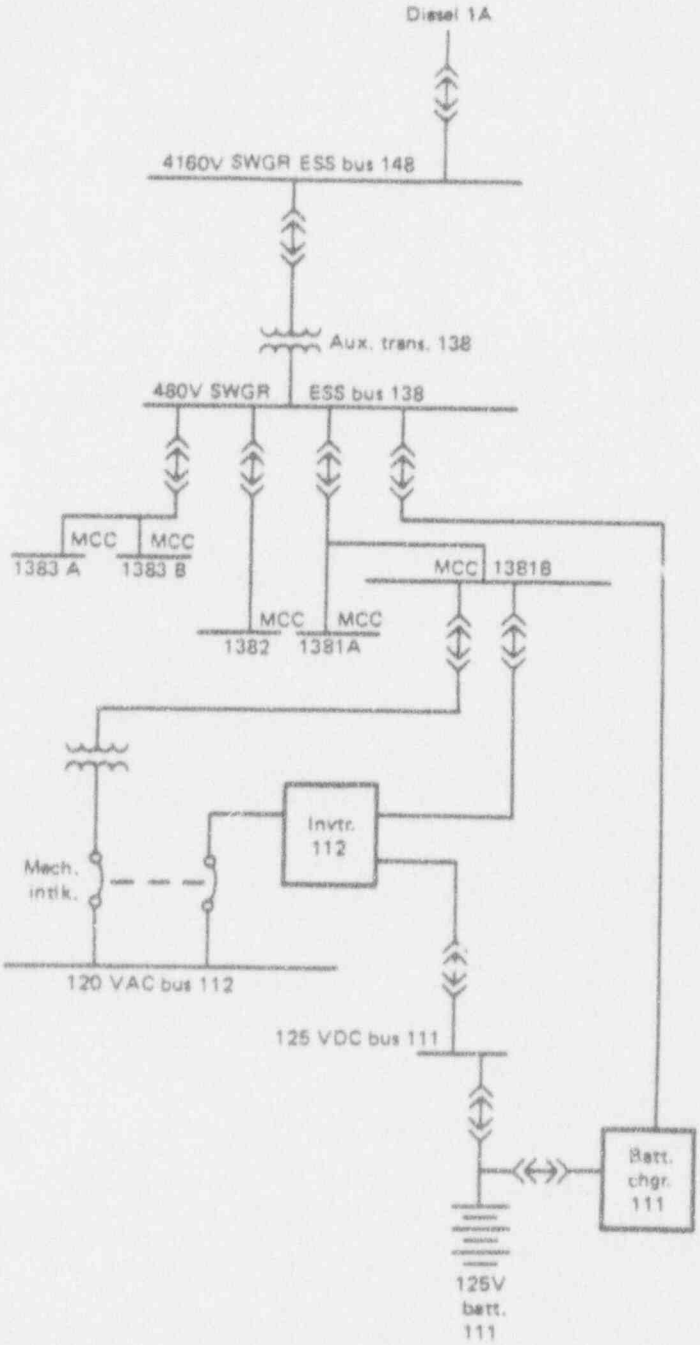

Figure B-8 Electrical Power - Division 18

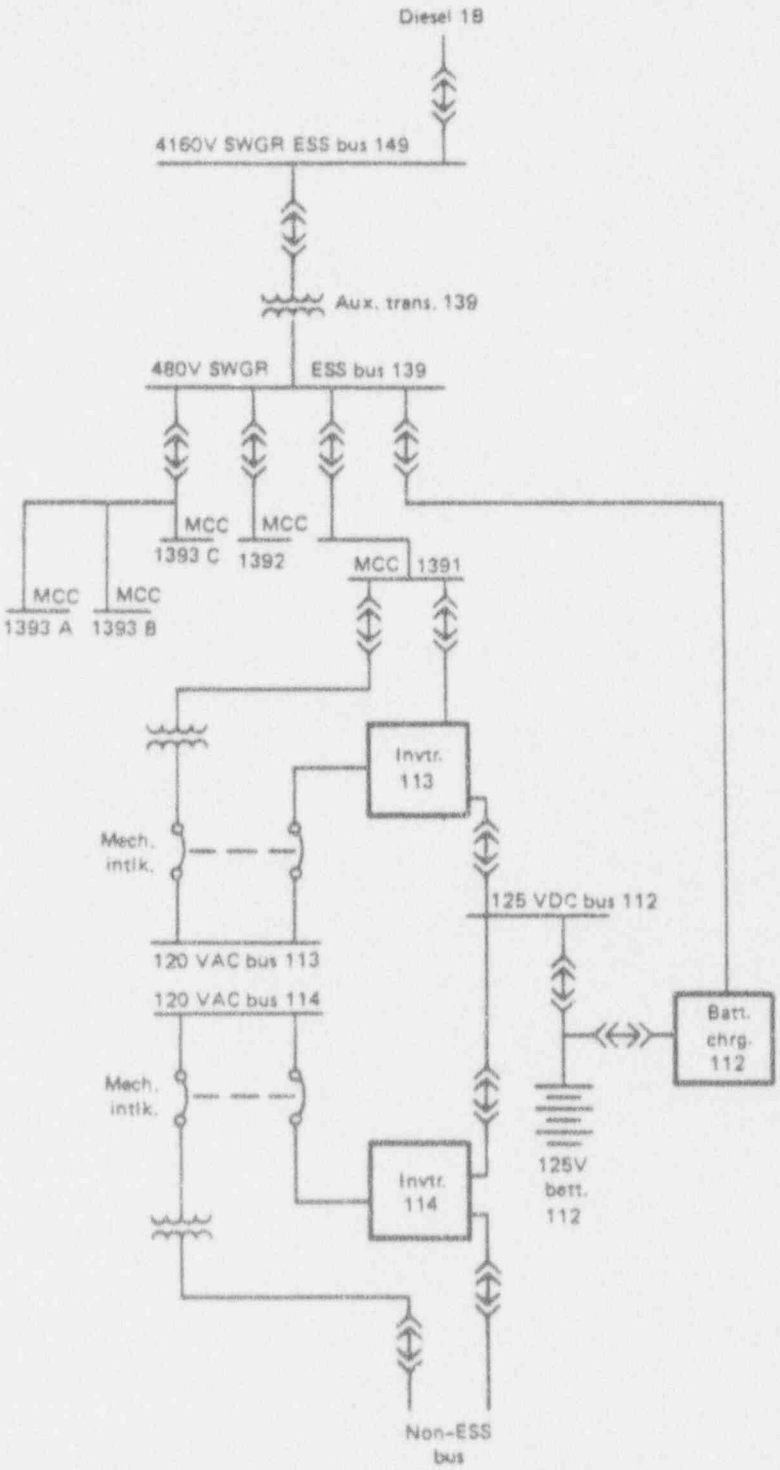

Figure B-9 Electrical Power - Division 19

1

IMAGE EVALUATION
TEST TARGET (MT-3)

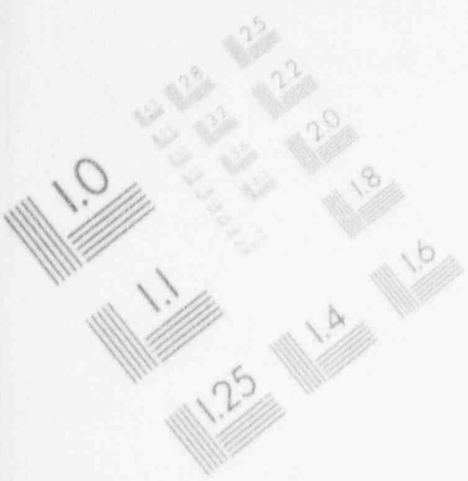

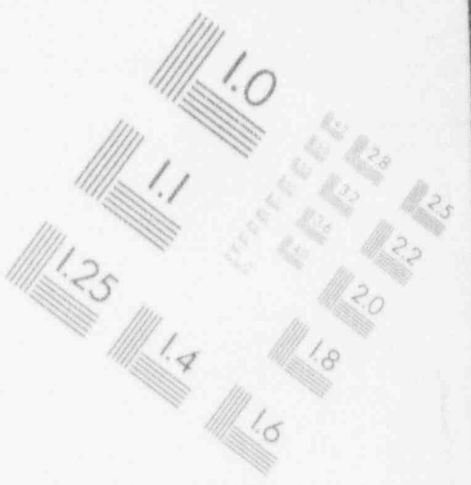

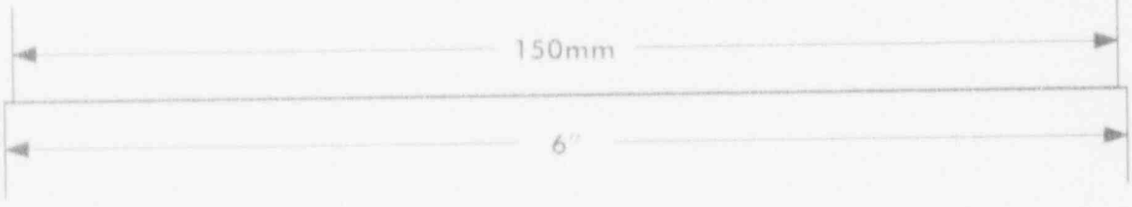

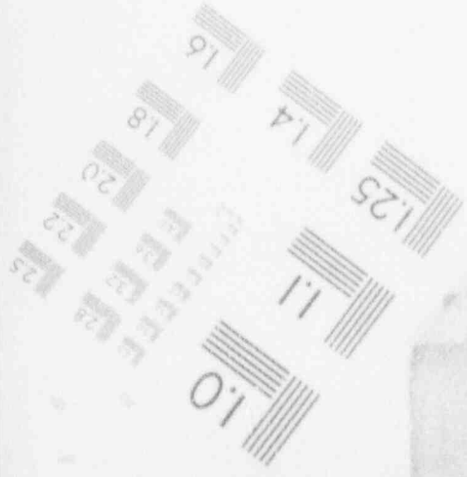

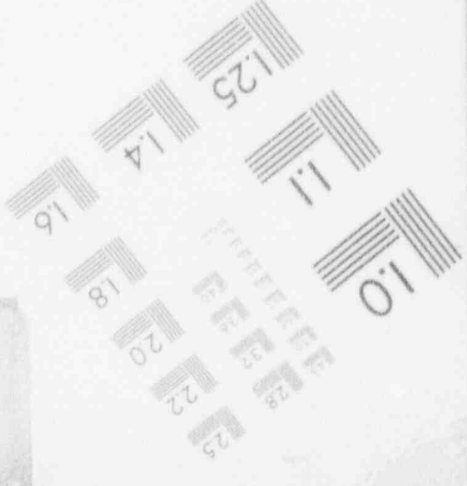

1

IMAGE EVALUATION
TEST TARGET (MT-3)

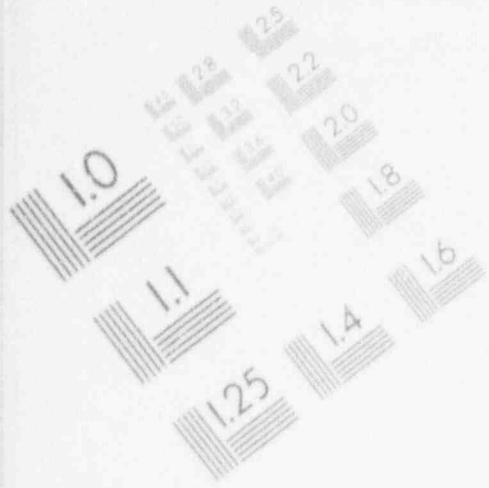

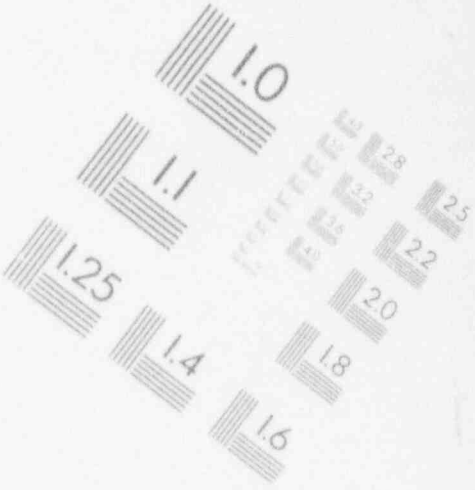

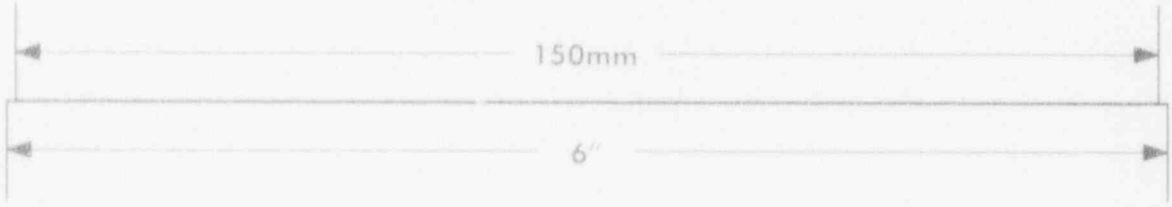

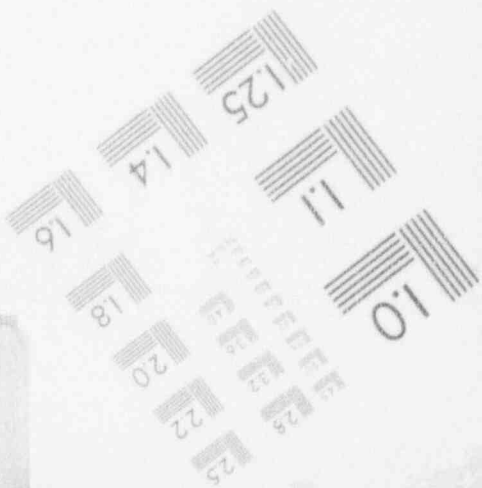

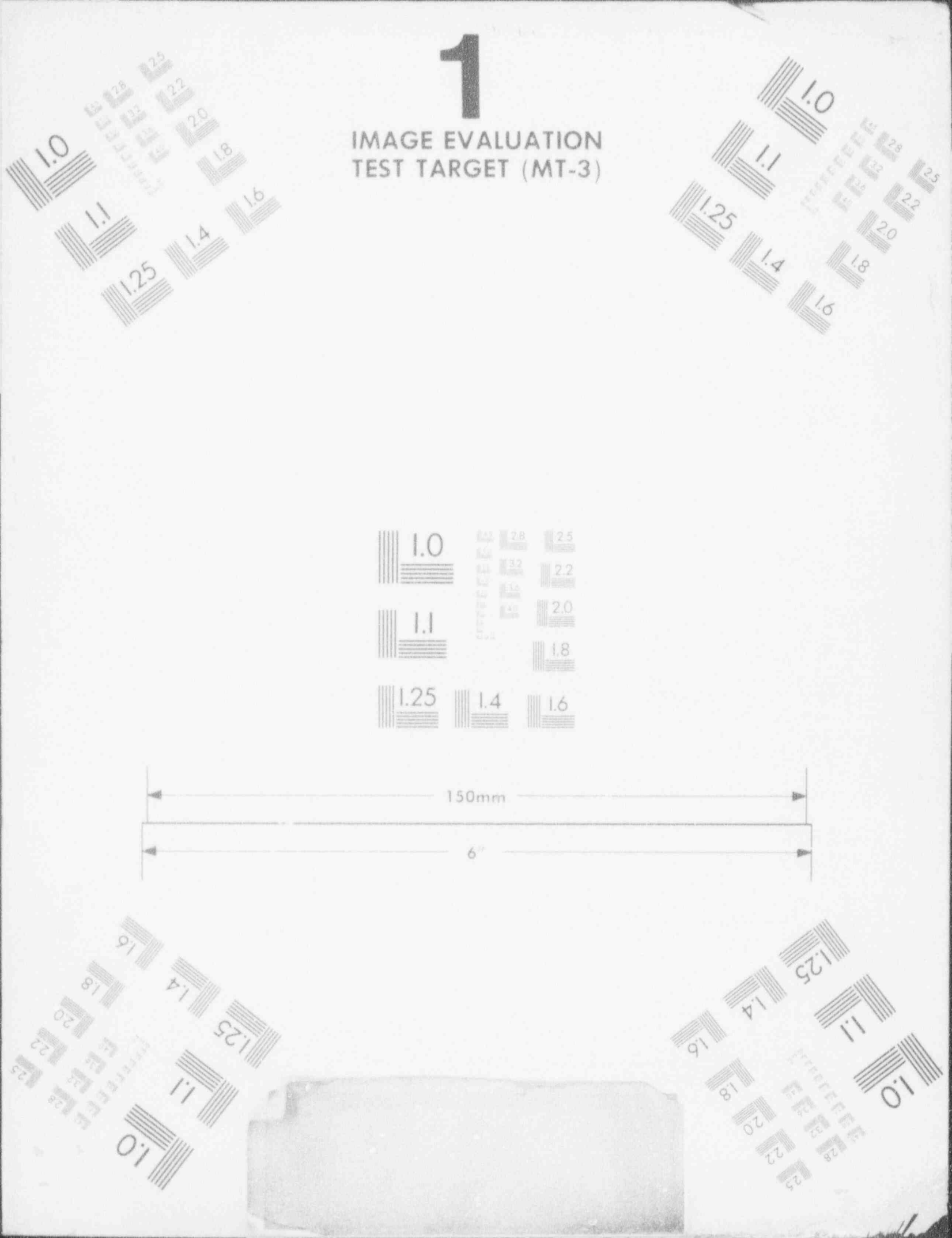
1
IMAGE EVALUATION
TEST TARGET (MT-3)
1.0
1.1
1.25
1.4
1.6
1.8
2.0
2.2
2.5
2.8
3.2
3.5
4.0
4.5
150mm
6"

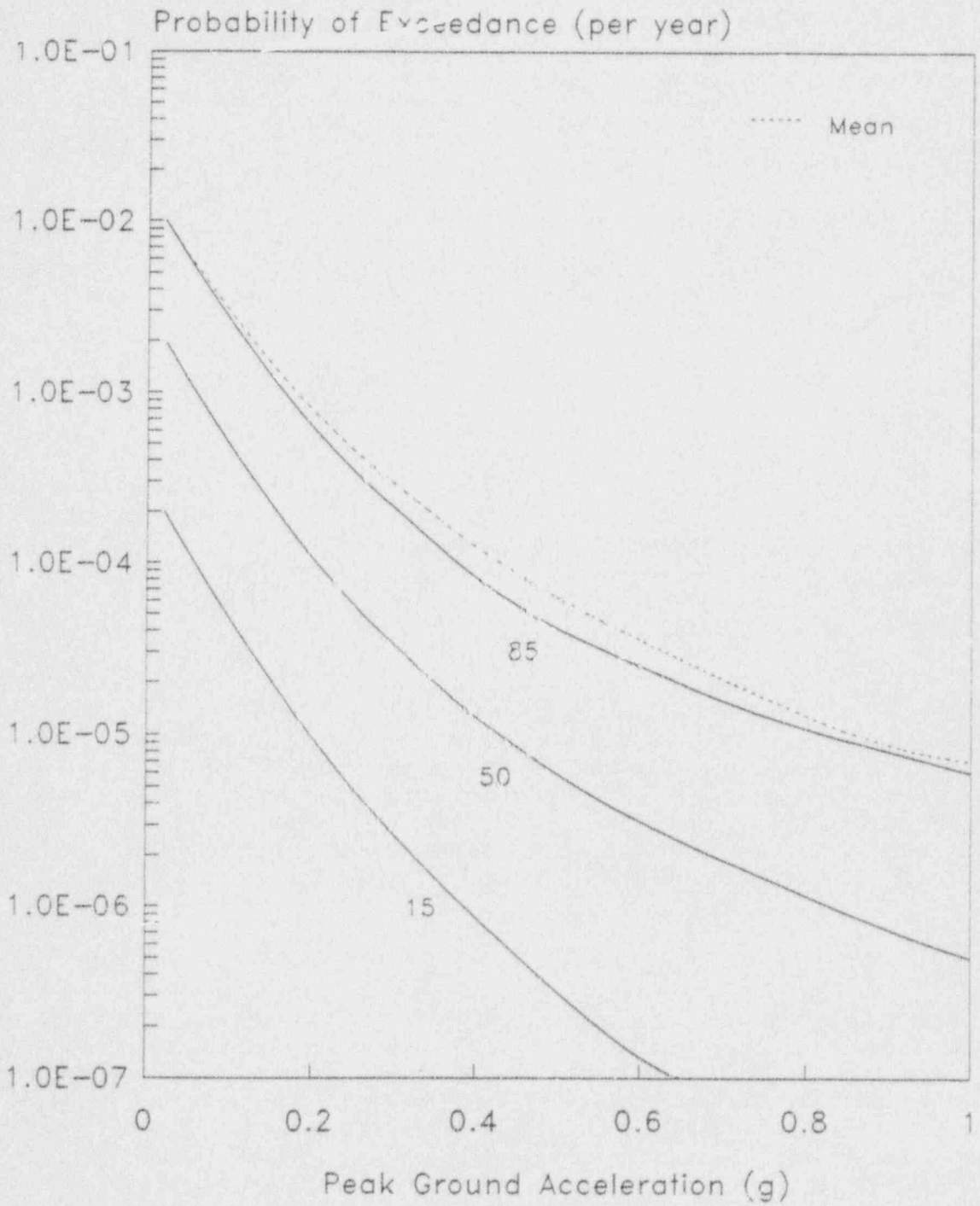

Figure B-10 Zion LLNL Hazard Curves: Mean Median 85th and 15th Percentile Curves

A second set of hazard curves was obtained from the seismic PRA performed by the plant owner (Commonwealth Edison) as reported in Reference B-2. These hazard curves are shown in Figure B-11. This discrete family of curves (with associated confidence levels for each curve expressed as a split fraction) was used directly. That is, for each realization in the Monte Carlo uncertainty analysis, one of the discrete curves was selected by random sampling. The percentage of samples corresponding to any given hazard curve corresponds to its associated confidence level split fraction.

B.3 RESPONSE CALCULATIONS

This chapter will describe and summarize:

- the site and earthquake characteristics that provide the starting point in the best-estimate soil-structure analysis of the ANO structures,
- the probabilistic dynamic response analysis of the reactor building and the auxiliary building with and without degraded shear wall stiffnesses, and
- the in-structure responses that define the response of components identified on the Boolean expressions for the LOCA and transient accident sequences analyzed.

B.3.1 Site Description

The Zion Nuclear Power Plant is located in Zion, Illinois approximately 40 miles north of Chicago. The Zion site is characterized by 111 ft of soil consisting of three distinct layers overlying a bedrock of Niagara Dolomite. The low strain soil profile from surface to bedrock consists of a very soft 6 ft layer and a somewhat stiffer 30 ft layer (both comprised of lake deposits), and a medium stiffness 75 ft layer comprised of glacial deposits. See Ref [B-1] for characteristic soil properties by layer. The general layout of the plant is shown in Figure B-12.

B.3.2 Earthquake Definition

Ref [B-1] describes the formulation of the seismic hazard curve developed for the Zion site which formed the basis for generating a set of 30 earthquakes - 30 time histories per component direction - for each of six distinct peak ground acceleration ranges - as developed in the SSMRP. These were all initially generated at an assumed rock outcrop, i.e. not accounting for the effect of the 111 ft soil deposit. To perform the probabilistic response analysis in this shear wall degradation study, three sets of these rock time histories were chosen corresponding to multiples of the safe shutdown earthquake (SSE) desired at the soil surface (1, 3 and 5 times the safe shutdown earthquake were used). Of the

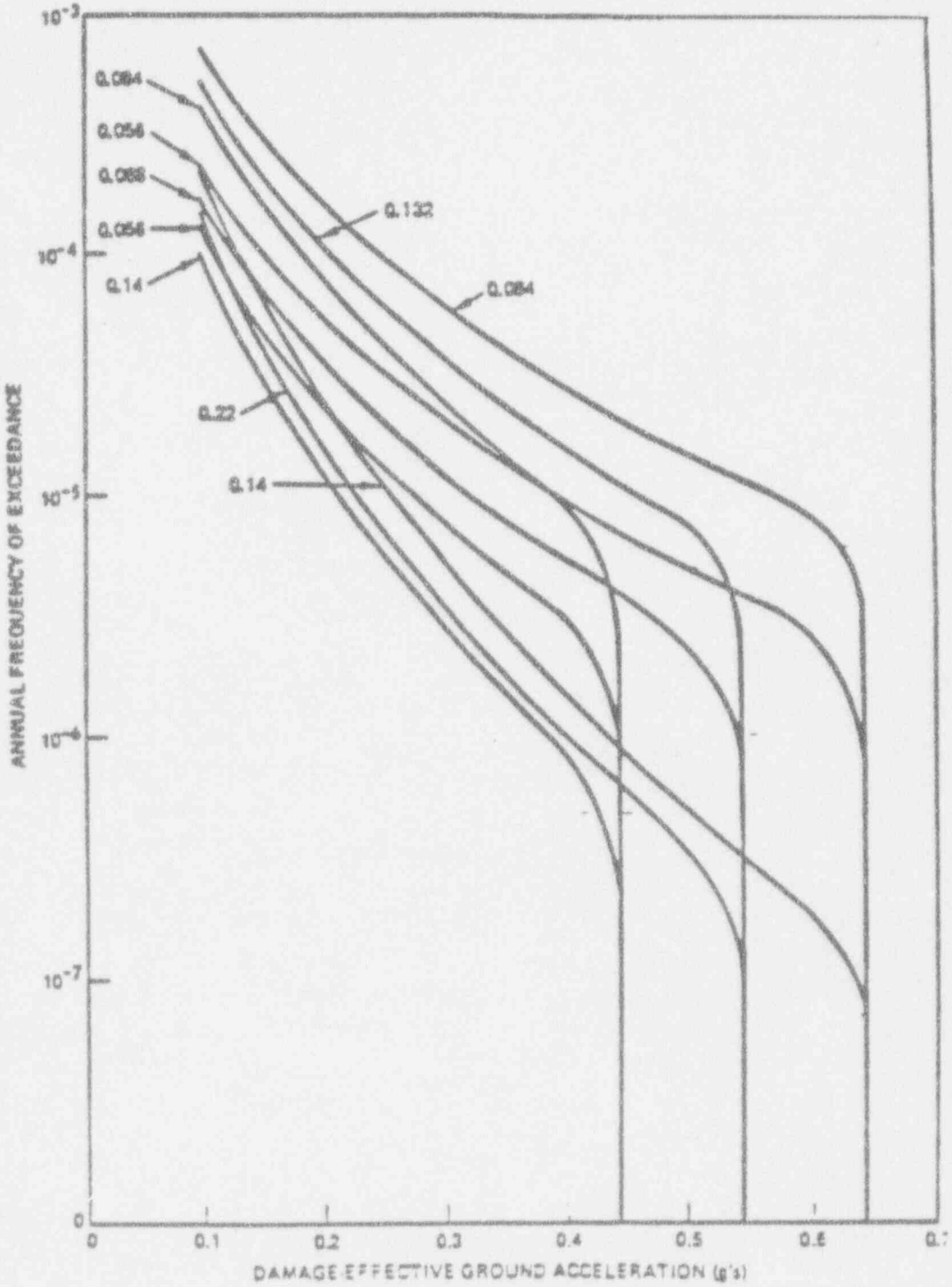

Figure B-11 Zion Family of Hazard Curves from Zion PRA (weighting values shown)

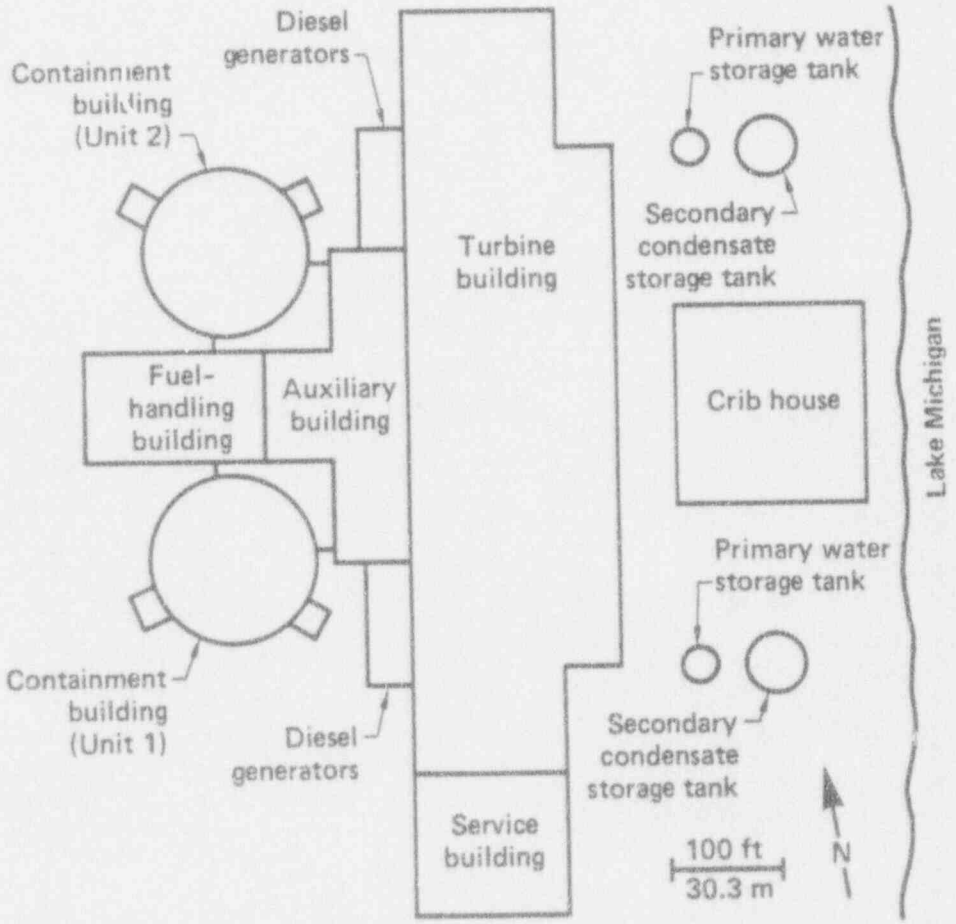

Figure B-12 General Arrangement of the Zion Nuclear Power Station

original 30 earthquakes, only ten earthquakes were used for the probabilistic analysis. These ten were modified such that the mean and standard deviation spectra of the original 30 were maintained. The high strain soil properties calculated in Ref [B-1] consistent with the original set of 30 earthquakes at the rock outcrop for each range were used to generate a new set of ten earthquakes at the soil surface for each range. See Figures B-13 to B-21 for a comparison of the mean spectra both at the rock outcrop and at the soil surface for each component and acceleration range. Note the large amplifying effect of the soil at the Zion site. Figures B-22 to B-24 compare only the final median spectra at the soil surface for all three acceleration ranges per component direction.

B.3.3 Impedances and Scattering

The five major buildings at the Zion site were considered for this shear wall degradation study. These included two reactor containment shells (denoted RCB), two reactor internal buildings (denoted INT), and one auxiliary/fuel/turbine complex serving both units 1 and 2 (denoted AFT). The containment shell and internal building for each unit are essentially independent of one another except that both are supported on the same circular embedded foundation. The AFT complex lies on its own embedded foundation between the two reactor foundations. See Figure B-25 for the shape and embedment of each foundation.

The frequency-dependent impedances and scattering matrices required for a dynamic building response analysis including soil-structure interaction (SSI) are governed by the characteristics of the soil deposit (configuration and material behavior) and the geometry and stiffness of the structures' foundations. The impedances included the effect of structure-to-structure interaction and therefore three foundations were considered. Impedance and scattering matrices were generated for the containment building foundation modeled as a circular cylindrical foundation 157 ft in diameter and embedded 36 ft. For the AFT foundation, impedances were generated for a flat surface foundation identical in shape to the AFT complex resting on a soil layer of depth equal to the average soil depth under the real foundation. This representation maintained the general characteristics of the foundation's dynamic behavior, i.e. differing translational and rocking impedances in each direction and appropriate coupling terms. To account for embedment, an equivalent cylindrical shape with dimensions obtained by matching the total volume and the area of the deepest portions of the foundation. Scattering matrices were generated using this equivalent cylinder. To correct the AFT impedances for the effect of embedment, a correction term was obtained by comparing impedances for the equivalent cylinder with those for an assumed circular disk resting on the same soil layer as the AFT complex. In modeling foundation-to-foundation interaction, scattering matrices were assumed to be unaltered; whereas, the impedances were modified to account for this phenomenon. Impedances and scattering were calculated for the set of low strain material properties previously mentioned and then factored such that the reference shear modulus, shear wave velocity and

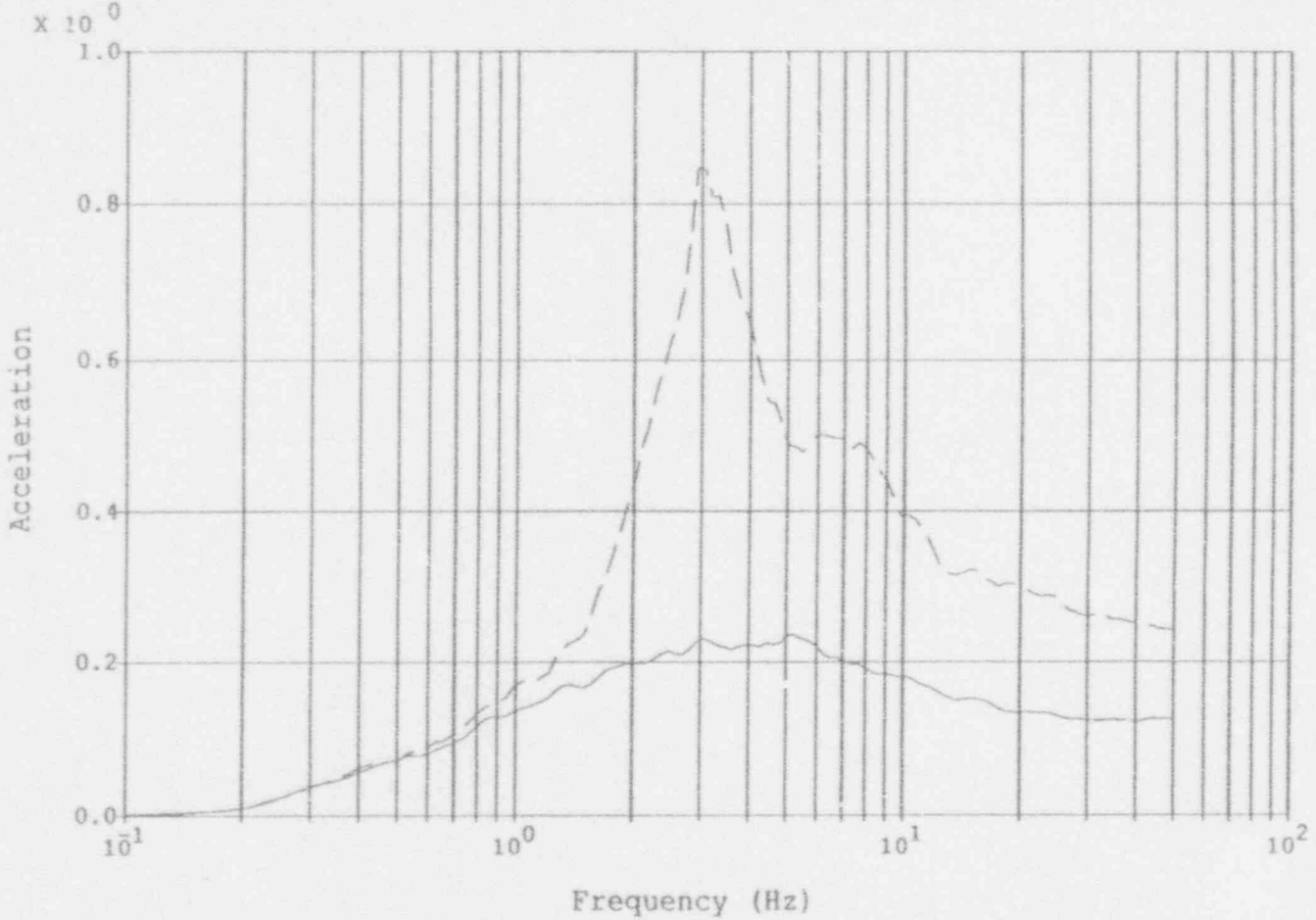

Legend:

Mean Spectrum on Rock (30 EQ's) ————————

Mean Spectrum on Soil (10 EQ's) — — — — — —

Notes:

Range 1 - 1SSE
Accelerations in g's
5% Spectral Damping

Figure B-13 Comparison Spectra for 1 SSE, Horizontal X Component

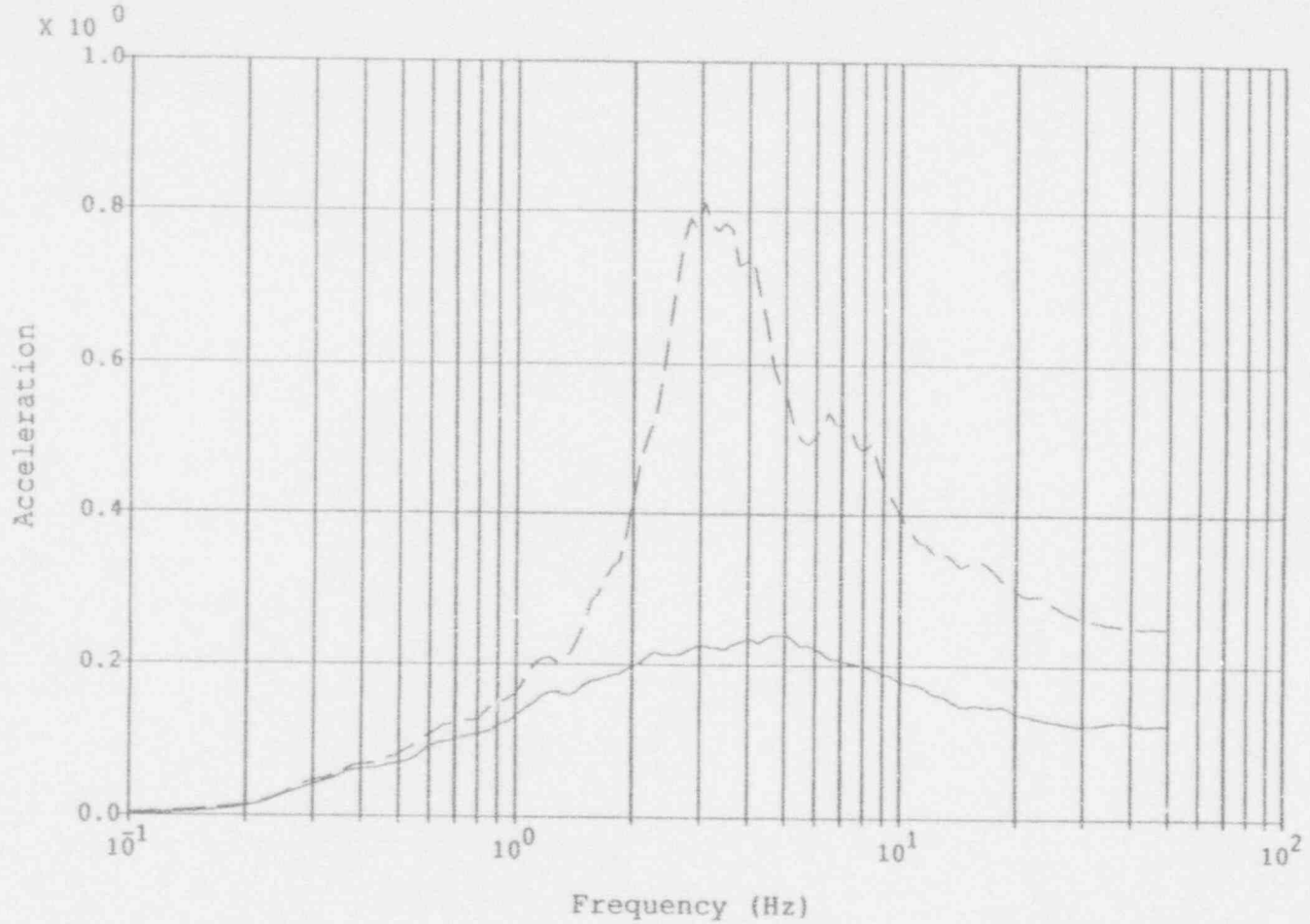

Legend:

Mean Spectrum on Rock (30 EQ's) ————————

Mean Spectrum on Soil (10 EQ's) — — — — —

Notes:

Range 1 - 1SSE
Accelerations in g's
5% Spectral Damping

Figure B-14 Comparison Spectra for 1 SSE, Horizontal Y Component

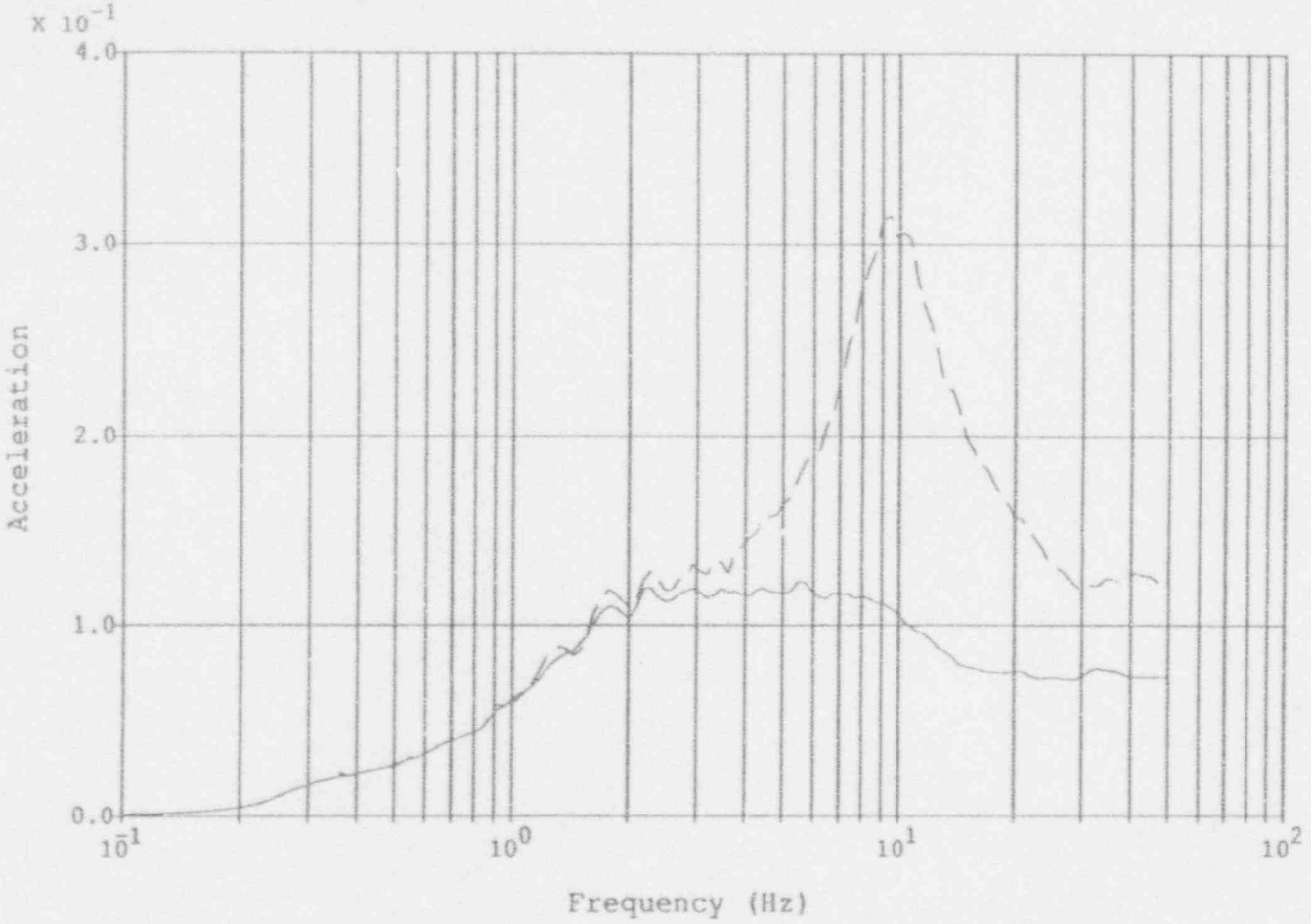

Legend:

Mean Spectrum on Rock (30 EQ's) ————————

Mean Spectrum on Soil (10 EQ's) — — — — —

Notes:

Range 1 - 1SSE
Accelerations in g's
5% Spectral Damping

Figure B-15 Comparison Spectra for 1 SSE, Vertical Component

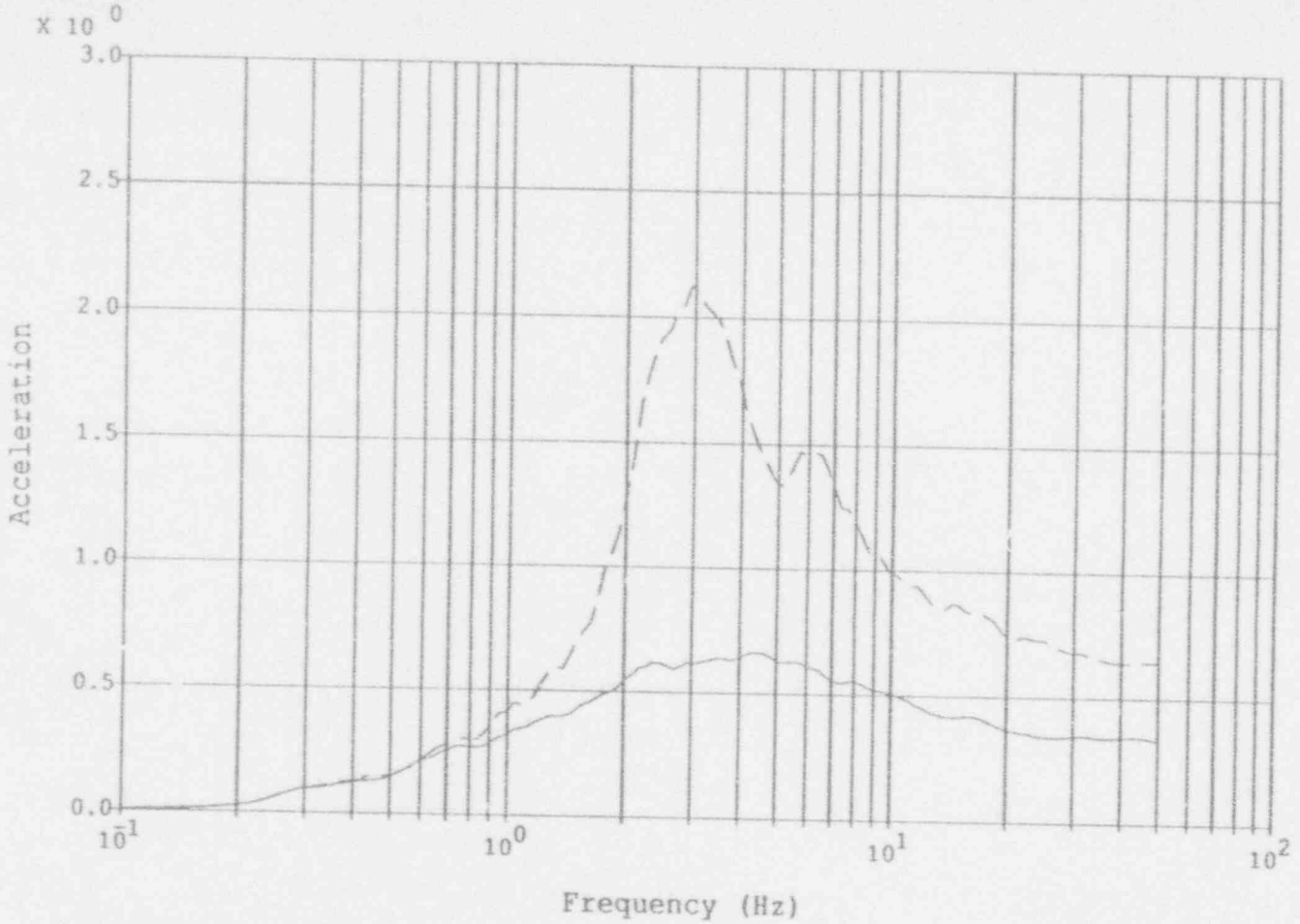

Legend:

Mean Spectrum on Rock (30 EQ's) ———————

Mean Spectrum on Soil (10 EQ's) — — — — —

Notes:

Range 3 - 3SSE
Accelerations in g's
5% Spectral Damping

Figure B-16 Comparison Spectra for 3 SSE, Horizontal X Component

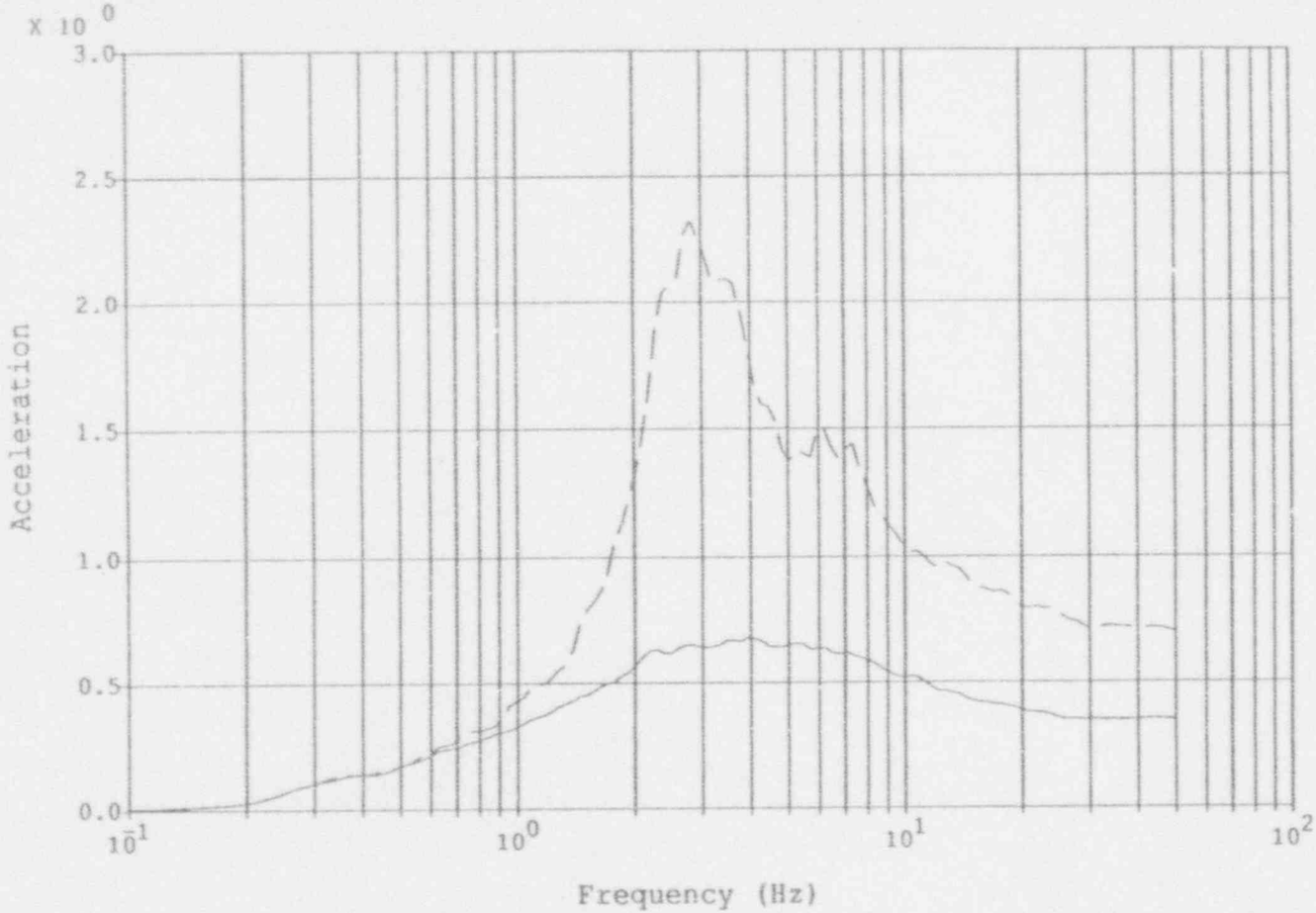

Legend:

Mean Spectrum on Rock (30 EQ's) ————————

Mean Spectrum on Soil (10 EQ's) — — — — — —

Notes:

Range 3 - 3SSE
Accelerations in g's
5% Spectral Damping

Figure B-17 Comparison Spectra for 3 SSE, Horizontal Y Component

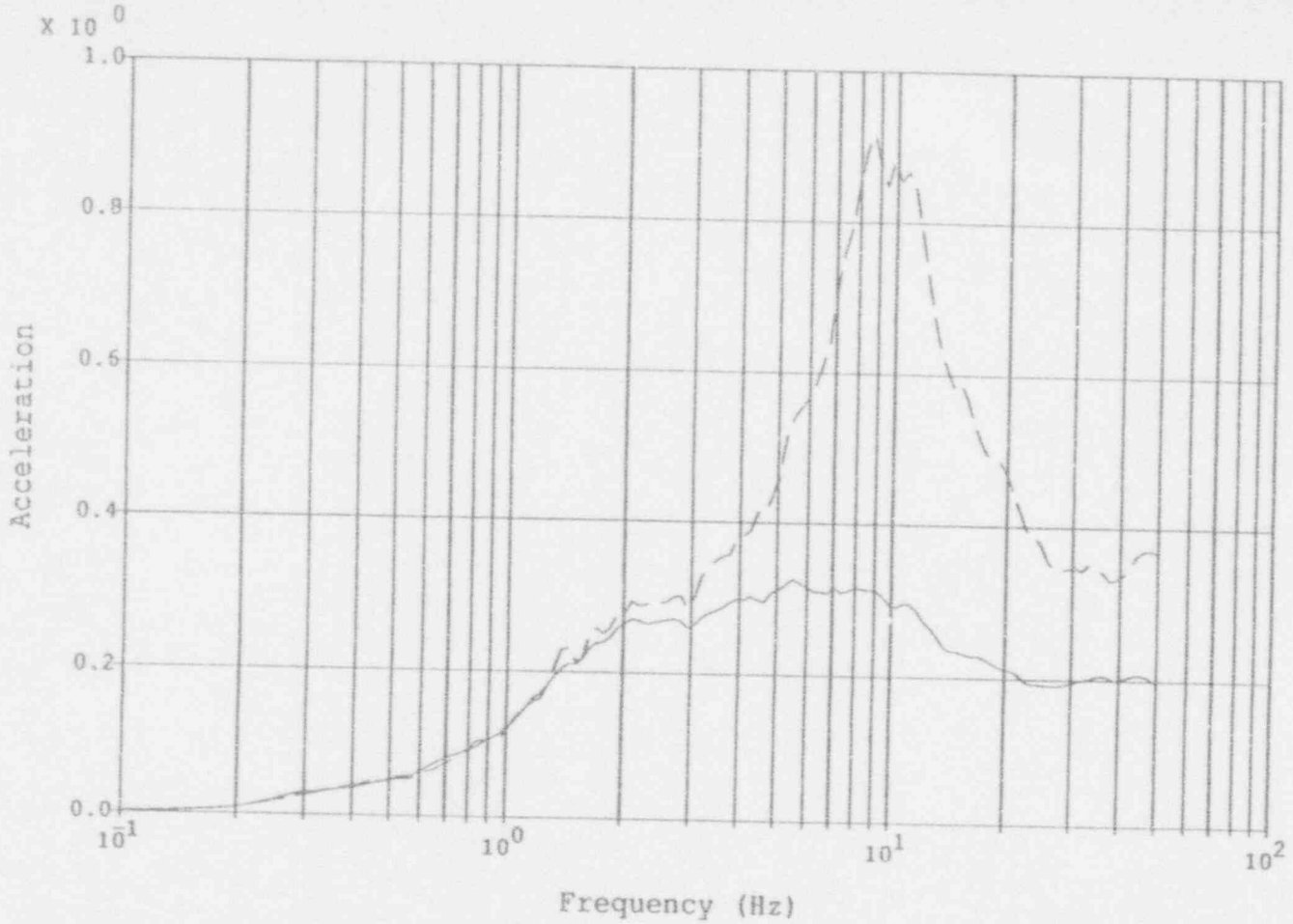

Legend:

Mean Spectrum on Rock (30 EQ's) _____

Mean Spectrum on Soil (10 EQ's) _ _ _ _ _ _

Notes:

Range 3 - 3SSE
Accelerations in g's
5% Spectral Damping

Figure B-18 Comparison Spectra for 3 SSE, Vertical Component

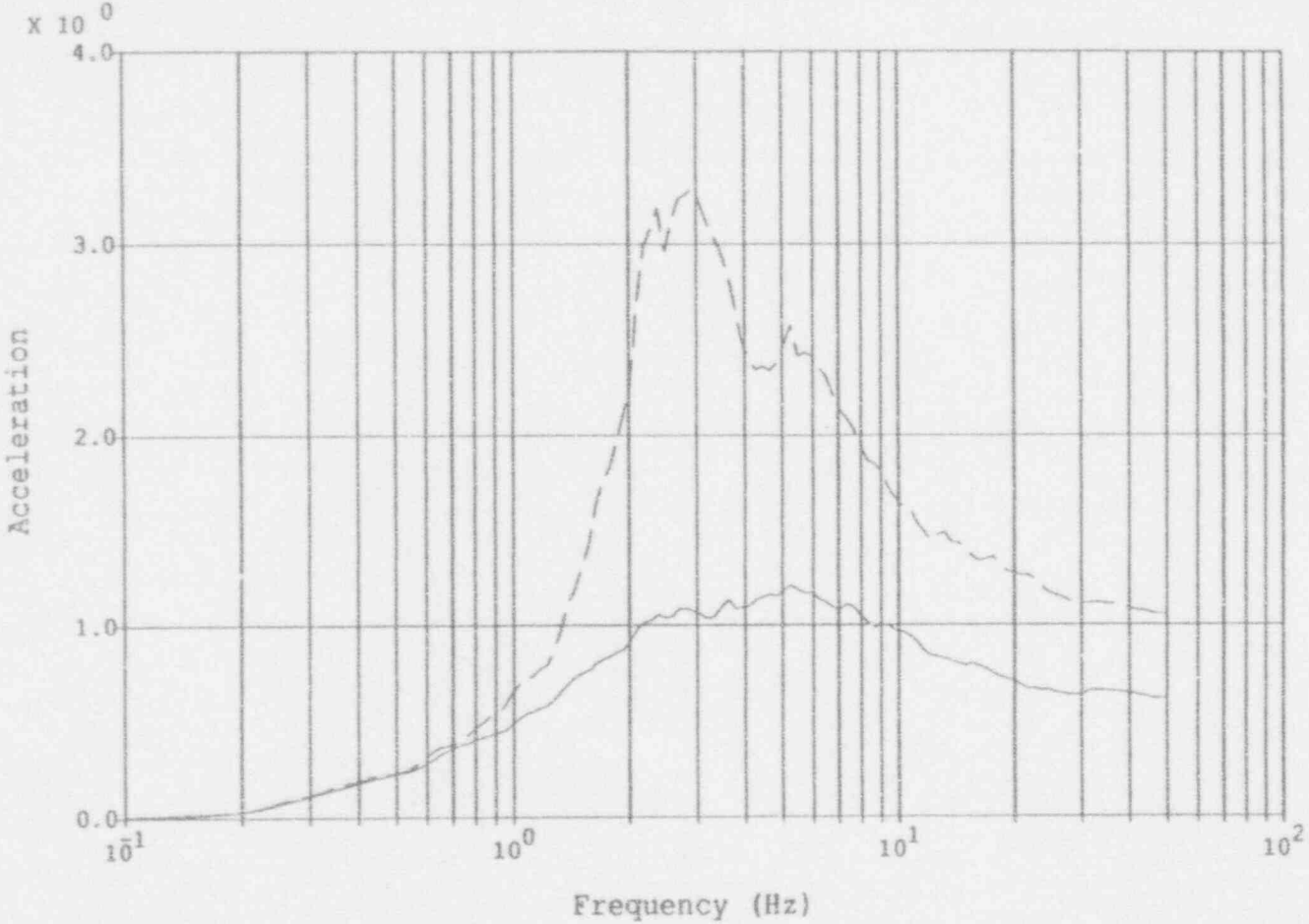

Legend:

Mean Spectrum on Rock (30 EQ's) ————————

Mean Spectrum on Soil (10 EQ's) — — — — — —

Notes:

Range 5 - 5SSE
Accelerations in g's
5% Spectral Damping

Figure B-19 Comparison Spectra for 5 SSE, Horizontal X Component

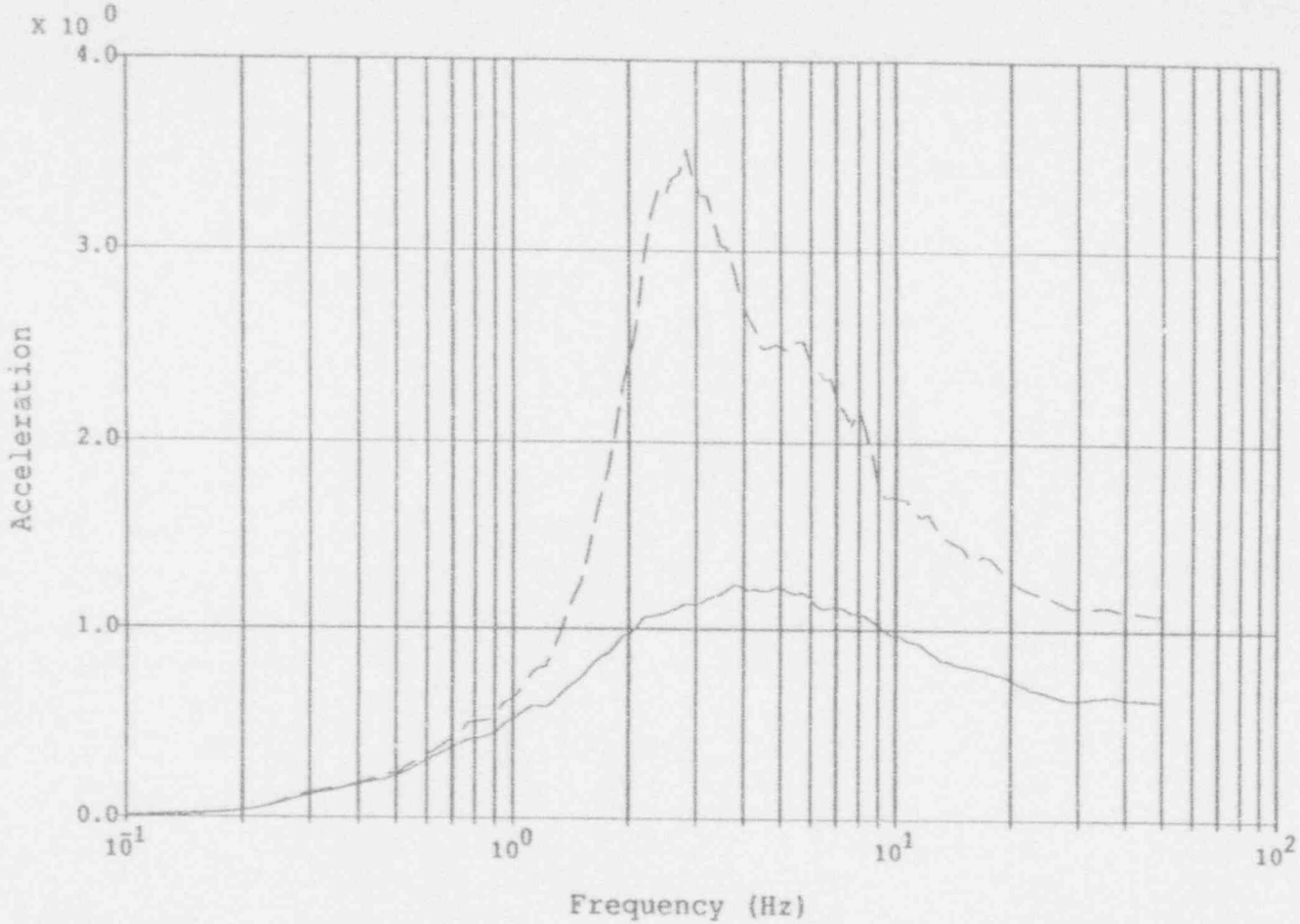

Legend:

Mean Spectrum on Rock (30 EQ's) ————————

Mean Spectrum on Soil (10 EQ's) — — — — —

Notes:

Range 5 - 5SSE
Accelerations in g's
5% Spectral Damping

Figure B-20 Comparison Spectra for 5 SSE, Horizontal Y Component

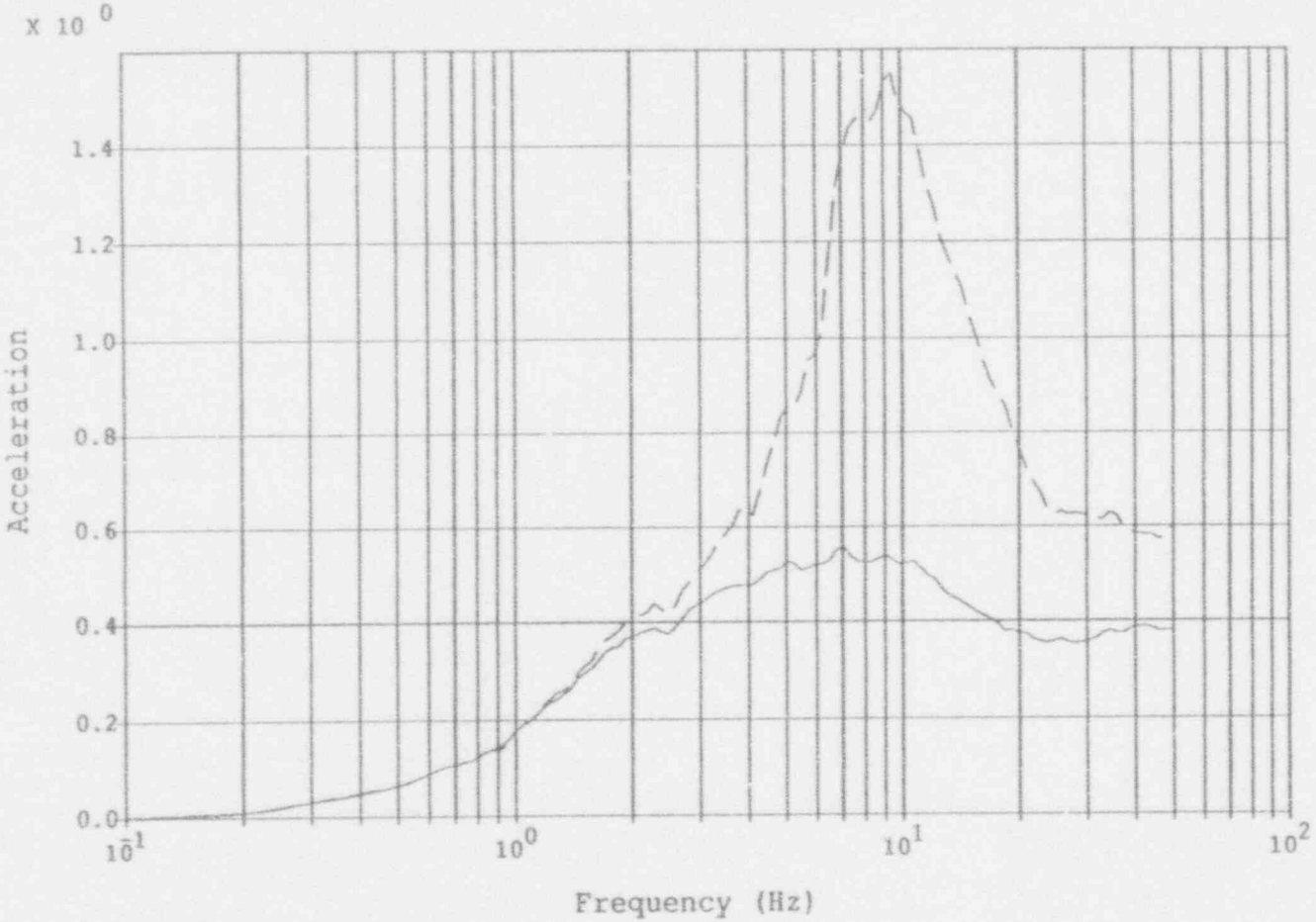

Legend:

Mean Spectrum on Rock (30 EQ's) ————————

Mean Spectrum on Soil (10 EQ's) — — — — —

Notes:

Range 5 - 5SSE
Accelerations in g's
5% Spectral Damping

Figure B-21 Comparison Spectra for 5 SSE, Vertical Component

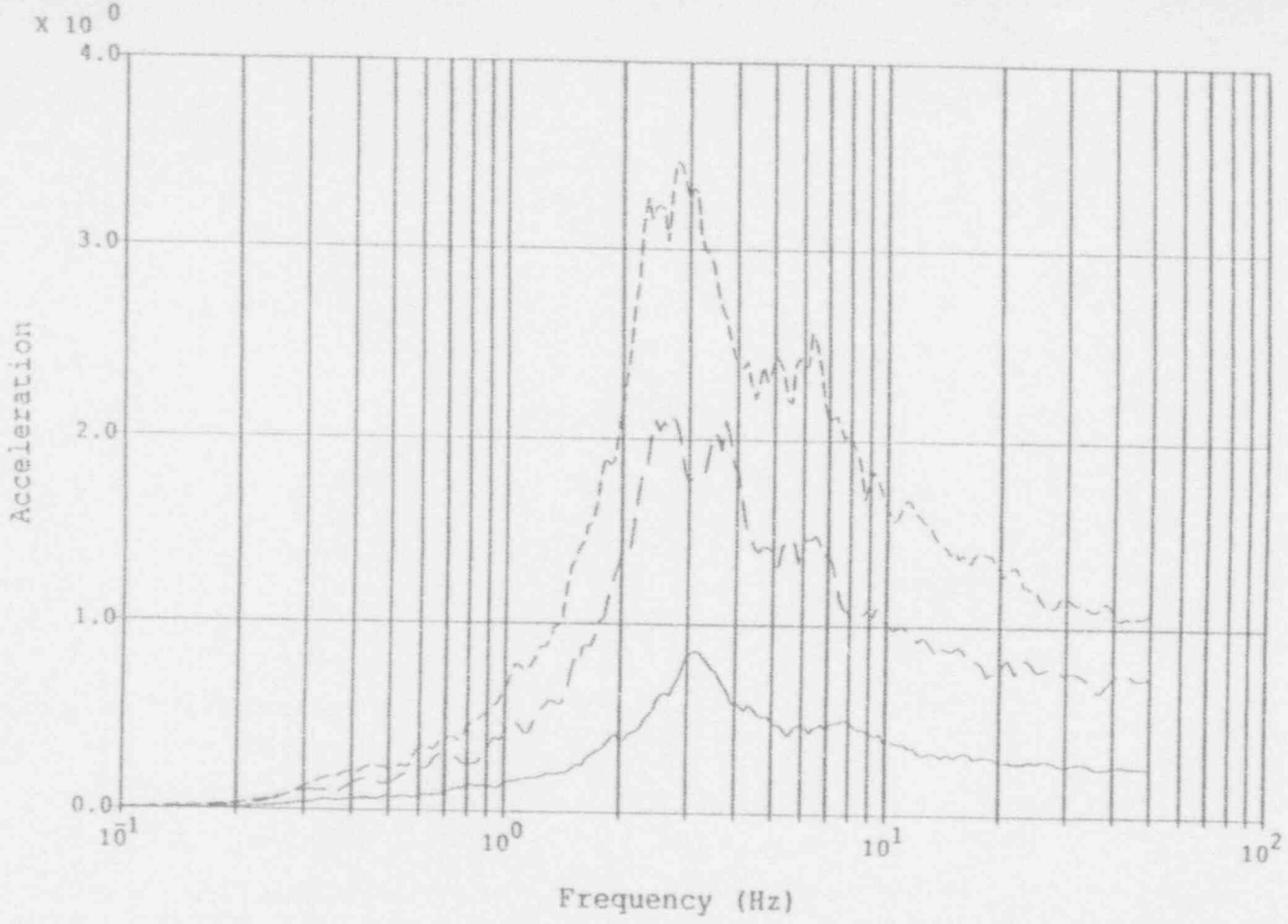

Legend:

10th Iteration, 1SSE _____

10th Iteration, 3SSE _ _ _ _ _

10th Iteration, 5SSE _ _ _ _ _ _

Notes:

accelerations in g's

5% spectral Damping

Component 1

Figure B-22 Final Spectra Fit, Horizontal X Component (Median of 10 Soil T/H's)

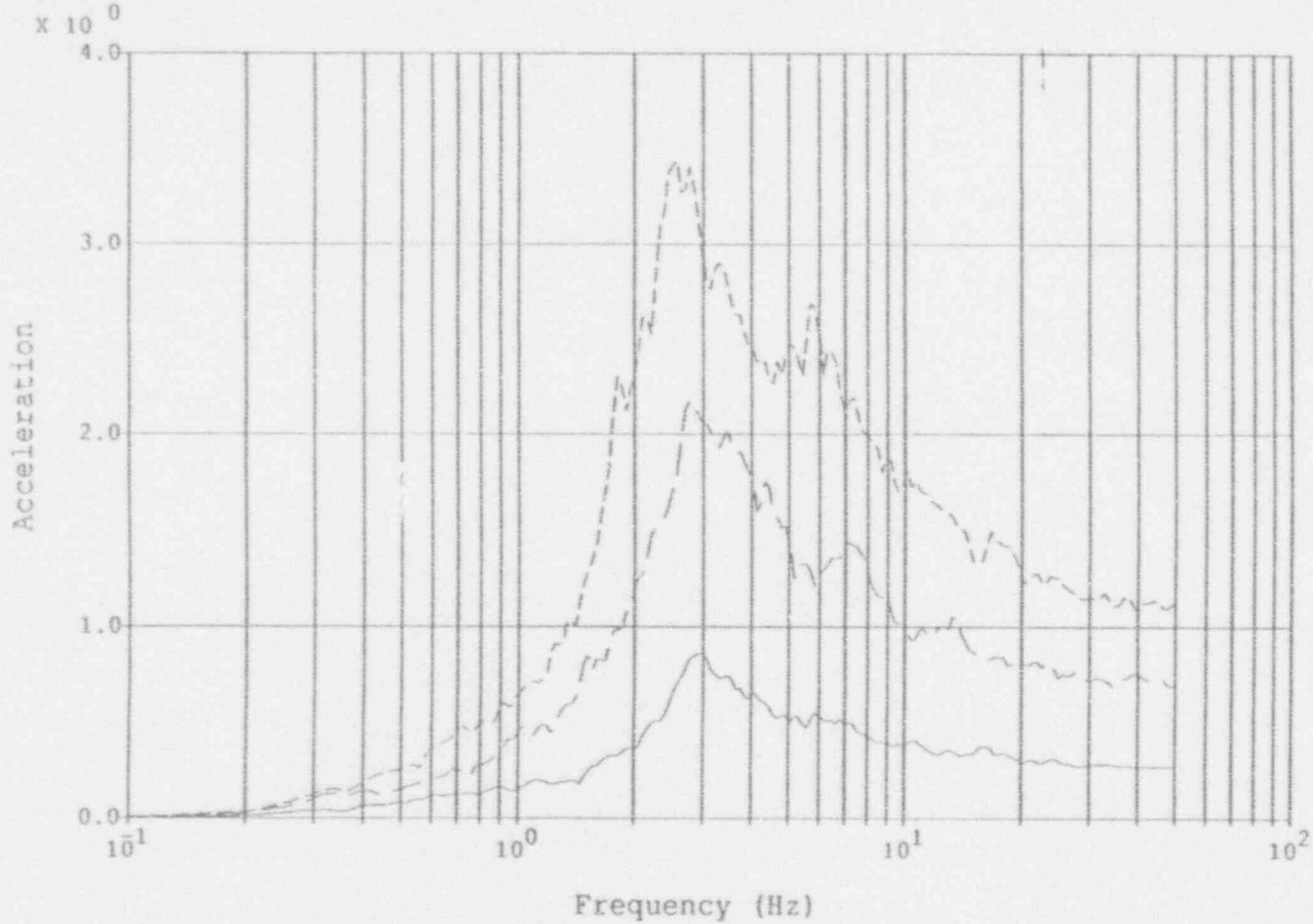

Legend:

10th Iteration, 1SSE _____

10th Iteration, 3SSE _ _ _ _ _

10th Iteration, 5SSE _ _ _ _ _ _

Notes:

accelerations in g's

5% spectral Damping

Component 2

Figure B-23 Final Spectra Fit, Horizontal Y Component (Median of 10 Soil T/H's)

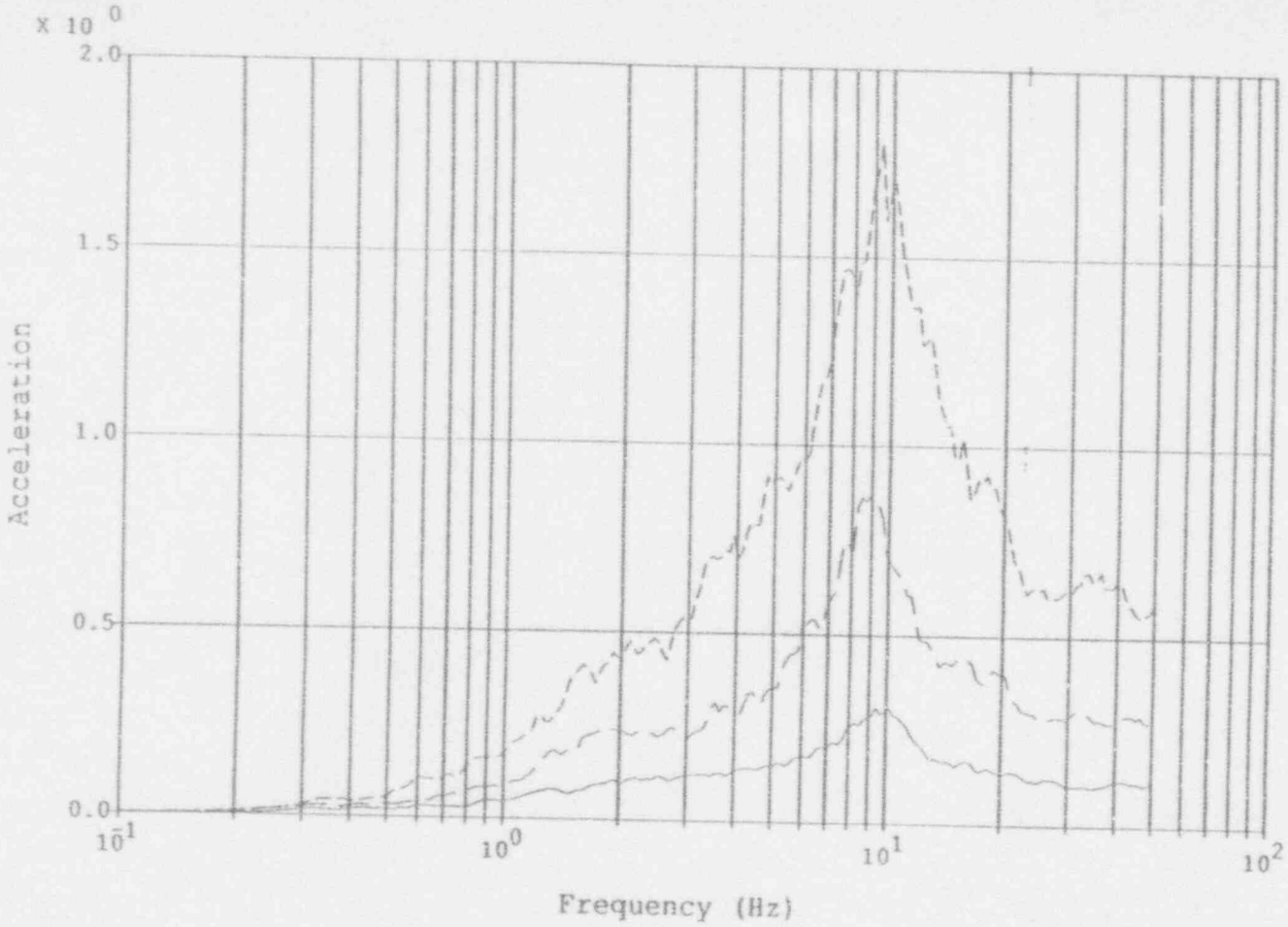

Legend:

10th Iteration, 1SSE _____

10th Iteration, 3SSE — — — — —

10th Iteration, 5SSE - - - - - - - - -

Notes:

accelerations in g's

5% spectral Damping

Component 3

Figure B-24 Final Spectra Fit, Vertical Component (Median of 10 Soil T/H's)

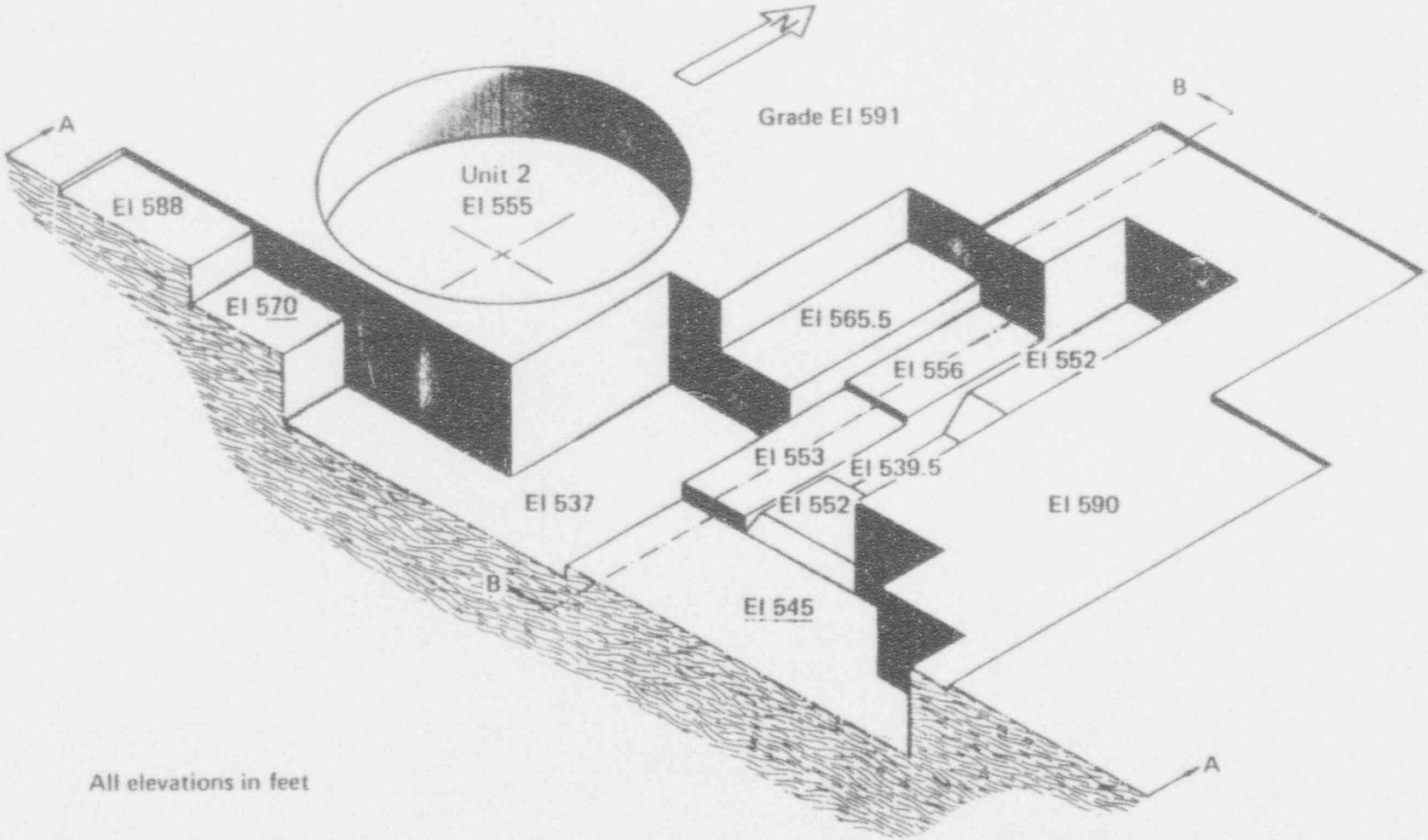

Figure B-25 Simplified Diagram of a Portion of the Foundation Excavation for Zion

damping ratio for each SSE level were equal to the high strain soil properties shown in Table B-2.

B.3.4 Structural Models

Fixed-base finite element models of the three critical structures at Zion were developed: Reactor containment building, Reactor building internal structure, and the Auxiliary/Fuel Handling/Turbine (AFT) building complex.

B.3.4.1 Building Models

Three distinct building models were generated: a reactor containment model, a reactor internal building model, and an AFT model. Ultimately, there were five structures supported on three foundations which were coupled through the soil impedances that were analyzed in order to determine the final degraded models for each SSE level and to determine maximum probabilistic structure/piping subsystem responses of both original and degraded models.

The structural model of the containment shell consisted of a single stick of collinear beam elements and lumped masses at the floor elevations. In addition, six rigid links were added from the single stick out to various pipe support locations on the shell itself. This simplified model contained 18 nodes and 15 fixed base natural frequency modes were calculated up to 39 Hz.

The reactor internal building model was modeled in far more detail. The walls and floors were modeled using concrete plate elements and the NSSS (nuclear steam supply system) was modeled with steel pipe elements. There were also some steel truss elements used in this model. A total of 1559 nodes were required to accommodate these elements. Since this building consists of both concrete and steel, mass proportional composite modal damping ratios were calculated for each of the 61 modes necessary to define the dynamic behavior of the building up to 33 Hz. Material damping ratios of 2% for steel and 5% for concrete were used for all SSE levels [B-6].

The AFT complex is a combination of a concrete shear wall building (auxiliary and fuel) and a connected steel turbine building all on the same T-shaped foundation. It was divided into symmetric and antisymmetric halves due to the extreme size of the model. The AFT models consisted of concrete plate elements for walls and floors and steel beam elements for beams and columns. Mass proportional composite modal damping was calculated for the AFT complex as it was for the internal building. A total of 4065 nodes were required for each half model and a total of 113 modes were calculated for the AFT complex - 56 antisymmetric modes and 57 symmetric modes up to 36 Hz.

The models mentioned above are referred to herein as the original models since the element stiffnesses were those of the undegraded buildings. For

Table B-2

Nominal vs. High Strain Soil Properties

Level	G (psi)	V (ft/s)	Damping (%)	Range of Peak Rock Outcrop Accelerations (g) (Median Surface Acceleration)
Nominal (layer 3)	8.57E+6	1390	2.5	
1 SSE (layer 3)	8.70E+6	1405	4.3	0.071-0.104 (0.1782)
3 SSE (layer 3)	7.54E+6	1308	6.2	0.211-0.300 (0.5045)
5 SSE (layer 3)	6.51E+6	1215	7.6	0.422-0.513 (0.7858)

the shear wall degradation study, at each SSE level (1, 3, and 5) the shear modulus G of all vertical concrete shear walls was reduced according to the shear stiffness degradation curve defined in Section 3.2. In this way, stiffnesses associated with bending and axial deformations were not affected. The calculation of the degraded properties for each SSE level was an iterative process. In this process, SSI analysis were performed until the change in the new shear wall stresses was less than 3%. A single set of three time histories whose spectra matched the median spectra at the soil surface for each SSE level were used for these iterative SSI analyses to determine the extent of model degradation. No reduction, however was made for the containment shell since it is a prestressed structure and the shear stiffness reduction curve was not applicable. See Tables B-3 through B-5 for frequencies of the original and degraded AFT, INT and RCB structural models respectively. Figure B-26 illustrates the extent of degradation for each structure at all three SSE levels. To reduce the the computational effort, mode shapes and frequencies at each step were calculated from the mode shapes and frequencies calculated in the previous step and from change in stiffness (see Attachment to Appendix B - Description of Methodology).

From the frequency tables for the INT and AFT buildings it is apparent that decreases in shear stiffness to 75% (of original) or greater resulted in only very small decreases in frequency. Considering only shear deformation, a decrease in shear stiffness to 75% of the original value would yield a frequency 86.6% of the original value since frequency varies as the square root of stiffness. This decrease was not seen for the INT and AFT buildings at Zion because it was determined that (1) wall shear contributed less than bending to the building response and (2) the floor slabs contributed about a third to the overall building response (see Attachment to Appendix B - Further Details). Therefore, wall shear stiffness ultimately only contributed about 27% to the overall response of the INT and AFT buildings.

In addition to the original models, models whose shear stiffnesses were reduced to 75% of their original values were also analyzed. These models were used as the starting point for the degraded models and also for a deterministic SSI analysis of the plant using the 1941 El Centro time history records.

B.3.4.2 Piping Models

A representative array of seven piping subsystems were incorporated with the original and degraded building models previously discussed for probabilistic SSI analysis. All piping systems were assumed to be linear elastic. Piping supports, rigid hangers and snubbers were all assumed rigid; constant and variable hangers were not included because their stiffnesses were small compared to the stiffness of other restraints. Pipe whip restraints were not included in the models because gaps between the restraints and the pipes were assumed to be large enough to accommodate seismic movement. The effect of inertial pressure on bend flexibility was included in the stiffness formulation of the elbow/pipe

Table B-3

Modal Frequencies for Zion Auxiliary/Fuel/Turbine Complex

	Frequency (Hz)					
	LLNL	EQE Analyses				
	Original	Original	Degraded Models			
Mode	1,3,5 SSE	1,3,5	75 %	1 SSE	3 SSE	5 SSE
1	1.55 ns	1.55 ns	1.54 ns	1.54 ns	1.54 ns	1.54 ns
2	2.06 ns	2.10 ns	2.10 ns	2.10 ns	2.10 ns	2.09 ns
3	3.68 ns	3.68 ns	3.68 ns	3.68 ns	3.68 ns	3.68 ns
4	3.83 ns	3.83 ns	3.77 ns	3.77 ns	3.72 ns	3.68 ns
5	4.64 ns	4.64 ns	4.62 ns	4.62 ns	4.61 ns	4.61 ns
6	4.79 ns	4.79 ns	4.79 ns	4.79 ns	4.79 ns	4.79 ns
7	5.01 ns	5.01 ns	4.86 ns	4.86 ns	4.86 ns	4.86 ns
8	5.77 ns	5.77 ns	5.74 ns	5.74 ns	5.74 ns	5.73 ns
9	6.34 ns	6.34 ns	6.31 ns	6.31 ns	6.29 ns	6.28 ns
10	6.87 ns	6.87 ns	6.84 ns	6.84 ns	6.83 ns	6.81 ns
11	7.01 ns	7.01 ns	6.98 ns	6.98 ns	6.98 ns	6.96 ns
12	7.48 ns	7.48 ns	7.46 ns	7.46 ns	7.45 ns	7.44 ns
13	8.82 ns	8.82 ns	8.45 ns	8.45 ns	8.45 ns	8.41 ns
14	9.96 ns	8.96 ns	8.95 ns	8.95 ns	8.94 ns	8.93 ns
15	9.84 ns	9.84 ns	9.44 ns	9.44 ns	9.38 ns	9.19 ns
16	10.75 ns	10.75 ns	10.36 ns	10.36 ns	10.34 ns	10.22 ns
17	11.12 ns	11.12 ns	10.58 ns	10.58 ns	10.58 ns	10.36 ns
18	11.46 ns	11.46 ns	11.15 ns	11.15 ns	11.14 ns	11.11 ns
19	12.96 ns	12.96 ns	12.82 ns	12.82 ns	12.81 ns	12.78 ns
20	13.19 ns	13.19 ns	13.18 ns	13.18 ns	13.18 ns	13.18 ns
21	14.04 ns	14.04 ns	13.84 ns	13.84 ns	13.84 ns	13.80 ns
22	14.39 ns	14.39 ns	14.34 ns	14.34 ns	14.34 ns	14.34 ns
23	14.78 ns	14.78 ns	14.78 ns	14.78 ns	14.78 ns	14.78 ns
24	15.97 ns	15.97 ns	15.96 ns	15.96 ns	15.96 ns	15.96 ns
25	15.98 ns	15.98 ns	15.34 ns	15.34 ns	15.34 ns	15.30 ns

Table B-3 (con't)

Modal Frequencies for Zion Auxiliary/Fuel/Turbine Complex

26	16.35 ns	16.35 ns	15.86 ns	15.86 ns	15.86 ns	15.82 ns
27	17.68 ns	17.68 ns	17.11 ns	17.11 ns	17.11 ns	17.03 ns
28	18.44 ns	18.44 ns	17.98 ns	17.98 ns	17.98 ns	17.90 ns
29	18.53 ns	18.53 ns	18.30 ns	18.30 ns	18.30 ns	18.24 ns
30	18.90 ns	18.90 ns	17.71 ns	17.71 ns	17.71 ns	17.62 ns
31	19.01 ns	19.01 ns	17.94 ns	17.94 ns	17.94 ns	17.75 ns
32	19.45 ns	19.45 ns	18.83 ns	18.83 ns	18.81 ns	18.73 ns
33	19.72 ns	19.72 ns	19.26 ns	19.26 ns	19.26 ns	19.16 ns
34	19.93 ns	19.93 ns	19.46 ns	19.46 ns	19.46 ns	19.40 ns
35	20.17 ns	20.17 ns	19.83 ns	19.83 ns	19.83 ns	19.81 ns
36	21.15 ns	21.15 ns	20.24 ns	20.24 ns	20.23 ns	20.23 ns
37	21.56 ns	21.56 ns	20.79 ns	20.79 ns	20.79 ns	20.74 ns
38	21.58 ns	21.58 ns	21.58 ns	21.58 ns	21.58 ns	21.58 ns
39	21.62 ns	21.62 ns	21.09 ns	21.09 ns	21.09 ns	21.07 ns
40	22.00 ns	21.99 ns	21.39 ns	21.39 ns	21.37 ns	21.28 ns
41	22.97 ns	22.97 ns	22.07 ns	22.07 ns	22.07 ns	22.00 ns
42	23.79 ns	23.75 ns	22.49 ns	22.49 ns	22.49 ns	22.47 ns
43	23.90 ns	23.90 ns	23.22 ns	23.22 ns	23.20 ns	23.06 ns
44	24.33 ns	24.33 ns	23.81 ns	23.81 ns	23.81 ns	23.81 ns
45	24.59 ns	24.59 ns	23.71 ns	23.71 ns	23.71 ns	23.52 ns
46	23.48 ns	25.47 ns	24.61 ns	24.61 ns	24.61 ns	24.57 ns
47	27.14 ns	27.14 ns	26.58 ns	26.58 ns	26.58 ns	26.56 ns
48	27.31 ns	27.31 ns	26.47 ns	26.47 ns	26.47 ns	26.47 ns
49	28.13 ns	28.13 ns	26.93 ns	26.93 ns	26.91 ns	26.79 ns
50	28.36 ns	28.36 ns	28.00 ns	28.00 ns	28.00 ns	27.96 ns
51	28.57 ns	28.57 ns	27.53 ns	27.53 ns	27.53 ns	27.52 ns
52	28.80 ns	28.80 ns	27.98 ns	27.98 ns	27.98 ns	27.96 ns
53	29.13 ns	29.13 ns	28.50 ns	28.50 ns	28.50 ns	28.43 ns
54	29.35 ns	29.35 ns	28.65 ns	28.65 ns	28.65 ns	28.62 ns
55	31.18 ns	31.17 ns	29.97 ns	29.97 ns	29.97 ns	29.86 ns
56	32.06 ns	32.06 ns	31.99 ns	31.99 ns	31.99 ns	31.96 ns

Table B-3 (con't)

Modal Frequencies for Zion Auxiliary/Fuel/Turbine Complex

57	1.09 ew	1.09 ew	1.09 ew	1.09 ew	1.09 ew	1.09 ew
58	1.16 ew	1.16 ew	1.16 ew	1.16 ew	1.16 ew	1.16 ew
59	1.85 ew	1.85 ew	1.84 ew	1.84 ew	1.84 ew	1.84 ew
60	3.68 ew	3.68 ew	3.68 ew	3.68 ew	3.68 ew	3.68 ew
61	4.61 ew	4.61 ew	4.59 ew	4.59 ew	4.57 ew	4.55 ew
62	4.81 ew	4.89 ew	4.85 ew	4.85 ew	4.81 ew	4.80 ew
63	6.38 ew	6.38 ew	6.32 ew	6.32 ew	6.30 ew	6.27 ew
64	6.79 ew	6.79 ew	6.77 ew	6.77 ew	6.77 ew	6.76 ew
65	8.49 ew	8.49 ew	8.10 ew	8.10 ew	8.09 ew	7.98 ew
66	10.29 ew	10.29 ew	9.99 ew	9.99 ew	9.99 ew	9.88 ew
67	10.98 ew	10.98 ew	10.76 ew	10.76 ew	10.69 ew	10.59 ew
68	11.05 ew	11.05 ew	11.02 ew	11.02 ew	11.01 ew	11.00 ew
69	11.27 ew	11.27 ew	10.57 ew	10.57 ew	10.57 ew	10.34 ew
70	13.19 ew	13.19 ew	13.18 ew	13.18 ew	13.18 ew	13.18 ew
71	13.54 ew	13.54 ew	12.37 ew	12.37 ew	12.37 ew	12.37 ew
72	14.40 ew	14.40 ew	14.36 ew	14.36 ew	14.36 ew	14.36 ew
73	14.78 ew	14.78 ew	14.78 ew	14.78 ew	14.78 ew	14.78 ew
74	14.95 ew	14.95 ew	14.46 ew	14.46 ew	14.46 ew	14.40 ew
75	15.81 ew	15.81 ew	15.14 ew	15.14 ew	15.14 ew	14.92 ew
76	15.97 ew	15.97 ew	15.96 ew	15.96 ew	15.96 ew	15.96 ew
77	16.31 ew	16.31 ew	15.59 ew	15.59 ew	15.58 ew	15.44 ew
78	17.00 ew	17.00 ew	16.27 ew	16.27 ew	16.27 ew	16.23 ew
79	17.58 ew	17.58 ew	17.00 ew	17.00 ew	17.00 ew	16.58 ew
80	17.77 ew	17.77 ew	17.20 ew	17.20 ew	17.20 ew	17.09 ew
81	18.30 ew	18.30 ew	17.70 ew	17.70 ew	17.70 ew	17.55 ew
82	19.13 ew	19.13 ew	18.30 ew	18.30 ew	18.30 ew	18.16 ew
83	20.04 ew	20.04 ew	19.51 ew	19.51 ew	19.50 ew	19.40 ew
84	20.27 ew	20.27 ew	19.83 ew	19.83 ew	19.83 ew	19.78 ew
85	21.12 ew	21.12 ew	20.37 ew	20.37 ew	20.37 ew	20.36 ew
86	21.47 ew	21.47 ew	20.74 ew	20.74 ew	20.74 ew	20.69 ew
87	21.58 ew	21.58 ew	21.58 ew	21.58 ew	21.58 ew	21.58 ew

Table B-3 (con't)

Modal Frequencies for Zion Auxiliary/Fuel/Turbine Complex

88	22.41 ew	22.41 ew	21.85 ew	21.85 ew	21.85 ew	21.77 ew
89	22.67 ew	22.69 ew	22.07 ew	22.07 ew	22.07 ew	21.98 ew
90	23.09 ew	23.09 ew	22.33 ew	22.33 ew	22.31 ew	22.15 ew
91	23.23 ew	23.23 ew	22.39 ew	22.39 ew	22.39 ew	22.35 ew
92	24.36 ew	24.36 ew	23.67 ew	23.67 ew	23.67 ew	23.57 ew
93	24.44 ew	24.44 ew	23.83 ew	23.83 ew	23.83 ew	23.83 ew
94	24.66 ew	24.65 ew	23.76 ew	23.76 ew	23.76 ew	23.46 ew
95	24.86 ew	24.86 ew	24.37 ew	24.37 ew	24.37 ew	24.29 ew
96	25.41 ew	25.41 ew	24.76 ew	24.76 ew	24.76 ew	24.68 ew
97	25.93 ew	25.93 ew	25.23 ew	25.23 ew	25.21 ew	25.10 ew
98	26.21 ew	26.21 ew	24.86 ew	24.86 ew	24.86 ew	24.84 ew
99	26.47 ew	26.47 ew	25.91 ew	25.91 ew	25.91 ew	25.89 ew
100	27.09 ew	27.09 ew	26.28 ew	26.28 ew	26.28 ew	26.26 ew
101	27.17 ew	27.17 ew	26.55 ew	26.55 ew	26.55 ew	26.53 ew
102	27.24 ew	27.24 ew	26.53 ew	26.53 ew	26.53 ew	26.48 ew
103	27.63 ew	27.63 ew	26.79 ew	26.79 ew	26.79 ew	26.77 ew
104	28.00 ew	28.00 ew	27.04 ew	27.04 ew	27.04 ew	26.94 ew
105	29.18 ew	28.18 ew	27.49 ew	27.49 ew	27.49 ew	27.47 ew
106	28.34 ew	28.34 ew	27.15 ew	27.15 ew	27.14 ew	27.04 ew
107	28.88 ew	28.88 ew	28.19 ew	28.19 ew	28.19 ew	28.17 ew
108	29.29 ew	29.29 ew	28.50 ew	28.50 ew	28.50 ew	28.50 ew
109	30.49 ew	30.49 ew	29.43 ew	29.43 ew	29.43 ew	29.32 ew
110	30.96 ew	30.96 ew	30.30 ew	30.30 ew	30.30 ew	30.27 ew
111	31.06 ew	31.06 ew	30.27 ew	30.27 ew	30.26 ew	30.08 ew
112	31.75 ew	31.75 ew	30.97 ew	30.97 ew	30.97 ew	30.75 ew
113	35.76 ew	35.76 ew	35.51 ew	35.51 ew	35.51 ew	35.38 ew

Table B-4

Modal Frequencies for Zion Reactor Internal Structure

	Frequency (Hz)					
	LLNL	EQE Analyses				
	Original	Original	Degraded Models			
Mode	1,3,5 SSE	1,3,5	75 %	1 SSE	3 SSE	5 SSE
1	6.54 ew	6.54 ew	6.49 ew	6.49 ew	6.49 ew	6.49 ew
2	6.70 ew	6.70 ew	6.68 ew	6.68 ew	6.68 ew	6.68 ew
3	7.11 ns	7.11 ns	7.10 ns	7.10 ns	7.10 ns	7.10 ns
4	7.13 ns	7.13 ns	7.12 ns	7.12 ns	7.12 ns	7.12 ns
5	7.28 ns	7.27 ns	7.25 ns	7.25 ns	7.25 ns	7.25 ns
6	8.11 ns	8.11 ns	8.07 ns	8.07 ns	8.07 ns	8.07 ns
7	8.88 ew	8.87 ew	8.86 ew	8.86 ew	8.86 ew	8.86 ew
8	8.91	8.90	8.89	8.89	8.89	8.89
9	9.20	9.18	9.16	9.16	9.16	9.16
10	9.23	9.21	9.20	9.20	9.20	9.20
11	9.36	9.34	9.33	9.33	9.33	9.33
12	9.38	9.35	9.35	9.35	9.35	9.35
13	9.81 ns	9.79 ns	9.78 ns	9.78 ns	9.78 ns	9.78 ns
14	9.89 ew	9.88 ew	9.87 ew	9.87 ew	9.87 ew	9.87 ew
15	9.96	9.95	9.94	9.94	9.94	9.94
16	9.99	9.98	9.98	9.98	9.98	9.98
17	12.87 ew	12.88 ew	12.45 ew	12.45 ew	12.45 ew	12.45 ew
18	13.78 ew	13.78 ew	13.70 ew	13.70 ew	13.70 ew	13.70 ew
19	13.89 ns	13.88 ns	13.84 ns	13.84 ns	13.84 ns	13.84 ns
20	13.95 v	13.95 v	13.95 v	13.95 v	13.95 v	13.95 v
21	13.96 v	13.95 v	13.95 v	13.95 v	13.95 v	13.95 v
22	14.27 ns	14.27 ns	14.02 ew	14.02 ew	14.02 ew	14.02 ew
23	14.52 ew	14.52 ew	14.29 ew	14.29 ew	14.29 ew	14.29 ew
24	15.39 ns	15.40 ns	15.18 ns	15.18 ns	15.18 ns	15.18 ns

Table B-4 (con't)

Modal Frequencies for Zion Reactor Internal Structure

25	16.18 ew	16.29 ew	15.84 ew	15.84 ew	15.84 ew	15.84 ew
26	17.18 ns	17.18 ns	16.70 ns	16.70 ns	16.70 ns	16.70 ns
27	17.63 ns	17.75 ns	17.40	17.40	17.40	17.40
28	18.35 v	18.35 v	18.33 v	18.33 v	18.33 v	18.33 v
29	19.35 ns	19.47	19.45	19.45	19.45	19.45
30	19.49	19.48	18.73	18.73	18.73	18.73
31	19.53 v	19.53 v	19.50 v	19.50 v	19.50 v	19.50 v
32	19.55 v	19.54 v	19.53 v	19.53 v	19.53 v	19.53 v
33	19.58 v	19.57 v	19.56 v	19.56 v	19.56 v	19.56 v
34	19.96	19.98	19.80	19.80	19.80	19.80
35	20.25 ns	20.26 ns	20.16 ns	20.16 ns	20.16 ns	20.16 ns
36	21.24 ns	21.30 ns	20.93 ns	20.93 ns	20.93 ns	20.93 ns
37	21.51 ns	21.57 ns	21.34 ns	21.34 ns	21.34 ns	21.34 ns
38	22.00 ns	22.01 ns	21.85 ns	21.85 ns	21.85 ns	21.85 ns
39	22.54 ns	22.63 ns	22.19 ns	22.19 ns	22.19 ns	22.19 ns
40	22.87 ew	22.98 ew	22.81 ew	22.81 ew	22.81 ew	22.81 ew
41	23.76 ns	24.51 ew	23.78 ns	23.78 ns	23.78 ns	23.78 ns
42	24.81 ew	25.24 ew	24.16 ns	24.16 ns	24.16 ns	24.16 ns
43	25.31 ew	25.75 ns	25.04	25.04	25.04	25.04
44	25.73 ns	26.05 ns	25.27 ns	25.27 ns	25.27 ns	25.27 ns
45	26.07 ns	26.71	26.07	26.07	26.07	26.07
46	26.74 ew	27.14 ns	26.79	26.79	26.79	26.79
47	27.21	27.41 ew	26.29	26.29	26.29	26.29
48	28.27 ns	28.70	28.27	28.27	28.27	28.27
49	28.79 ns	28.80	28.52	28.52	28.52	28.52
50	28.90	29.63 ew	29.13 ew	29.13 ew	29.13 ew	29.13 ew
51	29.82	30.24 v	29.87 v	29.87 v	29.87 v	29.87 v
52	30.36 v	30.90 ew	30.45 ew	30.45 ew	30.45 ew	30.45 ew
53	31.01 v	31.51 v	30.99 v	30.99 v	30.99 v	30.99 v
54	31.65 v	31.78	31.11 ew	31.11 ew	31.11 ew	31.11 ew
55	31.80 v	32.13 v	31.61 v	31.61 v	31.61 v	31.61 v

Table B-5

Modal Frequencies for Zion Reactor Containment Building

	Frequency (Hz)					
	LLNL	EQE Analyses				
	Original	Original	Degraded Models			
Mode	1,3,5 SSE	1,3,5	75 %	1 SSE	3 SSE	5 SSE
1	4.15 ew	3.98 ew	----	3.98 ew	3.98 ew	3.98 ew
2	4.15 ns	3.98 ns	----	3.98 ns	3.98 ns	3.98 ns
3	8.54	7.85	----	7.85	7.85	7.85
4	11.92 v	11.80 v	----	11.80 v	11.80 v	11.80 v
5	13.32 ew	12.64 ew	----	12.64 ew	12.64 ew	12.64 ew
6	13.32 ns	12.64 ns	----	12.64 ns	12.64 ns	12.64 ns
7	19.29 v	20.55 ns	----	20.55 ns	20.55 ns	20.55 ns
8(7)	22.58 ns	20.55 ew	----	20.55 ew	20.55 ew	20.55 ew
9(8)	22.58 ew	23.21	----	23.21	23.21	23.21
10	26.95	28.37 ew	----	28.37 ew	28.37 ew	28.37 ew
11(10)	30.76 ew	28.37 ns	----	28.37 ns	28.37 ns	28.37 ns
12(11)	30.76 ns	36.63 v	----	36.63 v	36.63 v	36.63 v
13	43.46 ns	38.93 ns	----	38.93 ns	38.93 ns	38.93 ns
14	43.46 ew	38.93 ew	----	38.93 ew	38.93 ew	38.93 ew
15	------	39.83	----	39.83	39.83	39.83

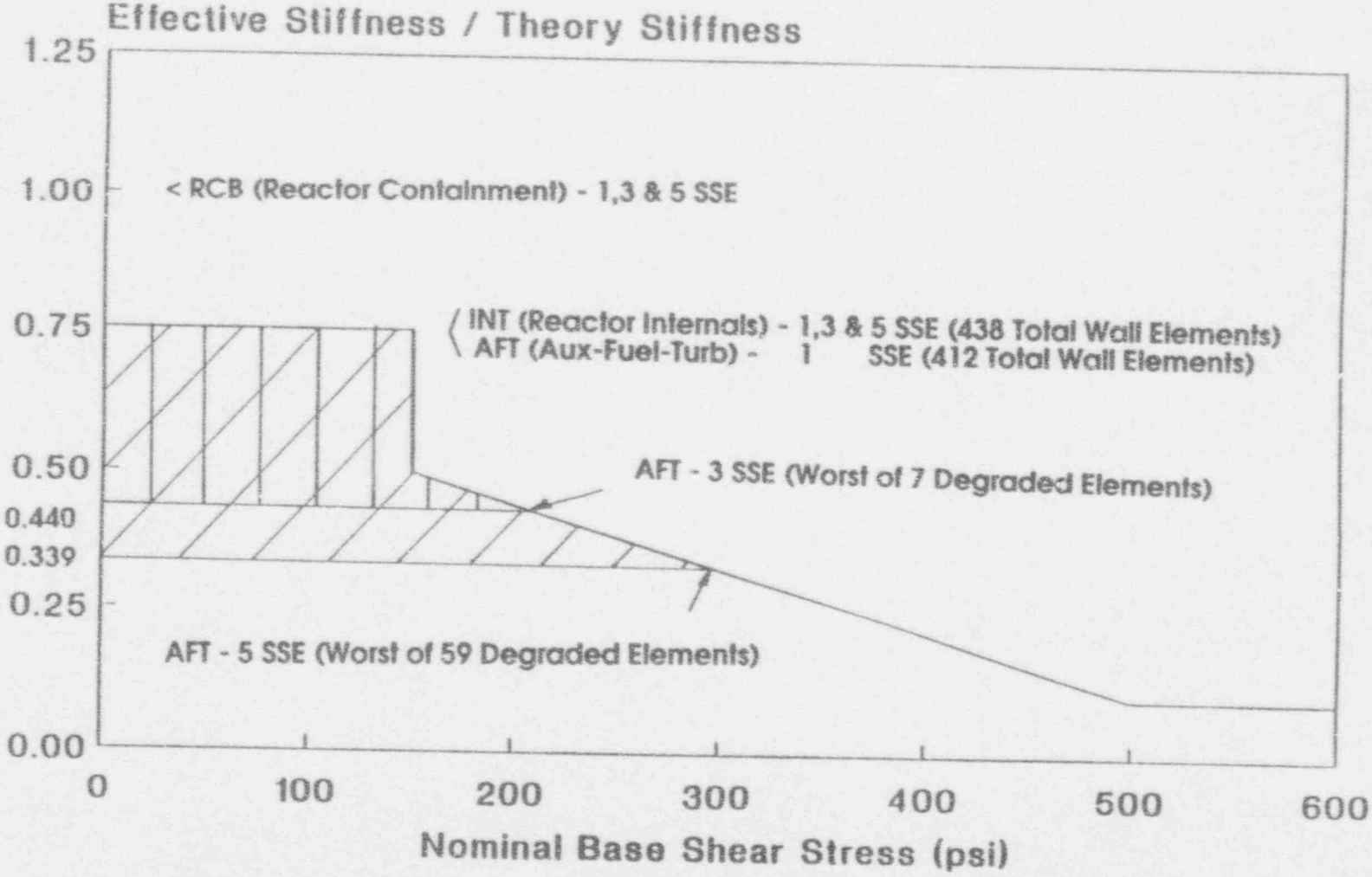

Figure B-26 Levels of Stiffness Reduction Found in each Zion Structural Model

bend elements. The piping system models were developed for best-estimate assumptions and the resulting eigensystems were assumed to be the nominal case. Multi-support time history analyses were performed to calculate piping response. Two parameters were varied to incorporate uncertainty in piping systems - frequency and damping. The nominal modal damping ratio for the piping was assumed to be a uniform 2% for all SSE levels.

The seven subsystems were as follows:

1) Steam Generator 1-A to Containment Penetration P-69 (part of the Aux. Feed Water system inside the reactor building with 2 supports on the containment shell and 13 in the INT building)
   Fundamental Frequency: 2.85 Hz, 36 Modes up to 32 Hz

2) Containment Penetration to Aux Feed Pump (part of the Aux. Feed Water system outside of containment with 4 supports on the containment shell and 17 in the AFT complex)
   Fundamental Frequency: 3.27 Hz, 93 Modes up to 33 Hz

3) Residual Heat Removal Pumps (Suction to Exchangers) (one containment shell support, 3 in the INT building and 9 in the AFT complex)
   Fundamental Frequency: 4.33 Hz, 32 Modes up to 33 Hz

4) Safety Injection and Residual Heat Removal Piping 2 (one containment shell support, and 24 in the AFT complex)
   Fundamental Frequency: 2.65 Hz, 115 Modes up to 33 Hz

5) Charging Pump Discharge to Boron Injection Tank 1 (one containment shell support, and 6 in the AFT complex)

6) Reactor Coolant Loop
   (59 supports in the INT building)
   Fundamental Frequency: 1.43 Hz, 130 Modes up to 33 Hz

7) Reactor Coolant Loop
   (59 supports in the INT building)
   Fundamental Frequency: 1.43 Hz, 130 Modes up to 33 Hz

See Table B-6 for the fixed support frequencies for all seven piping subsystems.

B.3.5 Probabilistic Response Analysis

For seismic response many sources of random uncertainty exist - e.g. the properties of the soil, structures, and subsystems. All sources of random uncertainty were assumed to be represented by a limited number of parameters of the models. For SSI, uncertainty was described by variability in soil shear modulus and material damping; in the structures and subsystems variations in the modal frequencies and damping were the mechanisms to describe uncertainty. The independent random variables numbered 26 i.e., 2 soil parameters, 2 structure parameters in each of

Table B-6

Original Zion Subsystem Frequencies (Hz)

MODE	SUB #1	SUB #2	SUB #3	SUB #4	SUR #5	SUB #6	SUB #7
1	2.85	3.27	4.33	2.65	9.08	1.43	1.43
2	3.76	5.80	6.22	3.03	10.15	2.42	2.42
3	4.48	7.44	6.82	3.11	15.99	3.26	3.26
4	4.89	7.66	7.09	3.59	20.44	3.47	3.47
5	7.28	8.65	7.15	4.01	21.31	4.39	4.39
6	7.56	8.82	7.83	4.18	25.06	4.84	4.84
7	7.86	9.53	8.40	4.49	30.65	5.25	5.25
8	8.01	9.86	9.46	5.01	32.69	5.99	5.99
9	9.05	10.44	10.09	5.34		6.03	6.03
10	9.63	10.81	10.13	5.60		6.40	6.40
11	9.84	11.12	11.31	5.70		6.61	6.61
12	11.29	11.28	12.79	5.94		6.66	6.66
13	12.48	11.71	14.78	6.18		7.03	7.03
14	12.94	12.31	15.18	6.22		7.06	7.06
15	13.95	13.07	15.59	6.52		7.26	7.26
16	14.28	13.42	15.94	6.80		7.29	7.29
17	14.78	13.81	16.11	6.83		7.29	7.29
18	15.28	13.86	19.22	7.13		7.31	7.31
19	15.87	14.38	20.16	7.36		8.23	8.23
20	16.69	15.17	21.03	7.41		8.37	8.37
21	17.24	15.48	21.29	7.63		8.55	8.55
22	17.69	16.27	21.61	7.63		8.60	8.60
23	17.71	16.30	21.72	8.23		8.60	8.60
24	18.66	16.55	22.04	8.38		8.89	8.89
25	19.39	16.83	24.36	8.45		9.10	9.10
26	21.89	17.25	26.27	8.66		9.10	9.10
27	22.31	17.83	27.14	8.98		9.10	9.10
28	22.40	18.41	29.70	9.34		9.11	9.11
29	23.70	18.60	29.90	9.62		9.11	9.11
30	24.20	19.00	32.47	9.67		9.14	9.14
31	26.13	19.27	32.67	9.77		9.31	9.31
32	26.87	19.98	33.54	10.04		9.49	9.49
33	27.21	14.37		10.70		9.51	9.51
34	28.12	14.45		11.04		9.51	9.51
35	28.38	15.06		11.15		9.52	9.52
36	32.02	15.33		11.58		9.56	9.56
37		15.86		12.00		9.92	9.92
38		16.28		12.05		9.95	9.95
39		16.80		12.07		9.98	9.98
40		17.27		12.66		10.00	10.00
41		17.64		12.67		10.09	10.09
42		17.67		12.90		10.16	10.16

Table B-6 (con't)

Original Zion Subsystem Frequencies (Hz)

MODE	SUB #1	SUB #2	SUB #3	SUB #4	SUB #5	SUB #6	SUB #7
43		17.86		13.83		10.38	10.38
44		18.09		13.86		10.56	10.56
45		18.44		13.92		11.19	11.19
46		18.70		14.10		11.32	11.32
47		18.83		14.42		11.48	11.48
48		19.23		14.54		11.57	11.57
49		19.33		14.82		11.80	11.81
50		19.59		14.96		12.76	12.76
51		19.99		15.11		13.25	13.25
52		20.10		15.12		13.32	13.32
53		20.16		15.66		13.89	13.89
54		20.70		15.91		13.92	13.92
55		20.94		16.27		13.95	13.95
56		21.39		16.43		13.95	13.95
57		21.51		16.56		14.64	14.64
58		21.80		16.94		14.78	14.78
59		22.29		17.70		14.90	14.90
60		22.76		17.85		14.94	14.94
61		23.39		18.13		15.00	15.00
62		23.43		18.34		15.12	15.12
63		23.72		18.67		15.32	15.32
64		23.94		19.05		15.90	15.90
65		24.21		19.39		15.92	15.92
66		25.00		19.54		16.07	16.07
67		25.34		19.57		16.24	16.24
68		25.39		19.67		17.05	17.05
69		25.65		20.18		17.14	17.14
70		26.05		20.21		17.49	17.49
71		26.09		20.92		17.60	17.60
72		26.34		21.33		17.68	17.68
73		26.46		21.44		18.03	18.03
74		26.81		21.56		18.25	18.25
75		26.91		21.76		18.61	18.61
76		27.49		21.98		18.71	18.71
77		27.53		22.05		18.94	18.94
78		28.13		23.14		18.98	18.98
79		28.69		23.24		19.34	19.34
80		28.88		23.60		19.47	19.47
81		29.00		23.68		19.56	19.56
82		29.28		23.96		19.60	19.60
83		29.40		24.11		19.72	19.72
84		29.88		24.34		19.79	19.79

Table B-6 (con't)

Original Zion Subsystem Frequencies (Hz)

MODE	SUB #1	SUB #2	SUB #3	SUB #4	SUB #5	SUB #6	SUB #7
85		30.20		24.41		20.24	20.24
86		30.24		24.87		20.32	20.32
87		30.45		24.93		20.43	20.42
88		30.88		25.37		20.77	20.77
89		32.04		25.73		20.82	20.82
90		32.42		25.99		20.95	20.95
91		32.97		26.00		20.97	20.97
92		33.01		26.51		21.18	21.18
93		33.25		26.56		21.51	21.51
94				26.76		21.56	21.56
95				27.47		22.01	22.01
96				27.48		22.15	22.15
97				27.54		23.43	23.43
98				27.81		23.93	23.93
99				28.09		24.02	24.02
100				28.19		24.31	24.31
101				28.37		24.37	24.37
102				28.42		24.90	24.90
103				28.50		24.98	24.98
104				28.72		25.95	25.95
105				28.89		26.20	26.20
106				29.38		26.36	26.36
107				29.66		26.44	26.44
108				30.55		26.50	26.50
109				30.87		26.61	26.61
110				31.10		26.67	26.67
111				31.26		27.21	27.21
112				31.46		27.23	27.23
113				32.59		27.62	27.62
114				33.19		28.06	28.06
115				33.52		28.91	28.91
116						29.00	29.00
117						29.11	29.11
118						29.86	29.86
119						30.28	30.28
120						30.63	30.63
121						30.78	30.78
122						31.18	31.18
123						31.23	31.23
124						31.46	31.46
125						32.50	32.50
126						32.78	32.78

the five structures analyzed (Units 1 and 2 containment and internal structures and the AFT complex), and 2 each in the 7 piping subsystems analyzed. These parameters were assumed to be lognormally distributed and were varied by multiplying a nominal value, e.g. the nominal soil shear modulus, by a value selected from a lognormal distribution with median 1.0 and coefficients of variation listed below (from ref [B-6]):

Soil Shear Modulus	COV= 0.35
Soil Damping	COV= 0.50
Structure Frequency	COV= 0.25
Structure Damping	COV= 0.35
Subsystem Frequency	COV= 0.25
Subsystem Damping	COV= 0.35

Each earthquake simulation (that is, each of 10 time histories for each SSE level) incorporated one of the sampled set of time histories and sampled values of the 26 parameters. The values of the input parameters were sampled according to the Latin Hypercube procedure whereby for each parameter ten ranges of equal probability were defined (1/10). Then for each parameter one value was randomly selected from each of these probability ranges. This set of ten values for each parameter represented its possible occurrences.

B.3.5.1 Responses in Terms of Peak Ground Acceleration

A total of six probabilistic dynamic response analyses were performed - three for the original (undegraded) models at 1, 3, and 5 SSE, and three for the degraded models at the same earthquake levels. The final results of the probabilistic analysis are given in terms of the median values of the maximum nodal accelerations or pipe moments for 10 earthquake simulations. The median was calculated for 47 groupings of nodes and pipe elements. Each grouping is referred to by its original (SEISIM code) response number on Table B-7 and are distinguished by the following: type of response requested (acceleration or moment), frequency at which response is calculated (4 Hz, 8 Hz, 16 Hz, and ZPA), and nodes (by building and elevation) or elements (by subsystem) whose responses are considered in the grouping. Comparisons of the original vs. degraded median responses are plotted in Figures B-27 thru B-73 for each response number.

For the building responses, note the very minor effect of the shear stiffness degradation on the median response (i.e. the difference between the solid and dashed lines). Also apparent from these figures is the effect of softening of the soil underlying the buildings over the range from 1 to 5 SSE. Generally, the response was not quite linear from 1 to 5 SSE, but it decreased somewhat indicating the decrease in the soil parameters affected the building response. The piping response, however, was much less predictable. This irregular response was determined to be due to differential pipe support motions. This finding was substantiated from a comparison of deterministic analysis performed for 1 and 3 SSE using time histories whose spectra matched the respective median spectra T

Table B-7

Zion SSMRP Response Numbers

Response Number	Freq(Hz) or Response	Component	Building/Elevation or Subsystem
1	zpa	Many	Free-Field
3	8	CST	Free-Field
7	8		RCB/INT:Foundation, 556'
10	zpa		INT:Operating Floor, 617'
11	4		INT:Operating Floor, 617'
12	8	Accumulators	INT:Operating Floor, 617'
14	4	RCP's	INT:RCS Model, 588'
15	8	Steam Gen.	INT:RCS Model, 615'
16	16	RPV Nozels	INT:RCS Model
18	4	RHR Pumps	AFT:Aux, 542'
22	4	SIS Pumps	AFT:Turb/Aux, 560'
26	4	CHG Pumps	AFT:Turb/AUX, 567'
29	zpa	RHR HTX	AFT:Aux, 592'
86	Valve Acc.	Most Valves	Subsystem 1, Node 110
87	Moment		Subsystem 1 and 2
105	Valve Acc.	2 Valves	MFW/AFW Subsystem 2, Node 248
120	Moment		Subsystem 2
121	"		" 2
122	"		" 2
213	Moment	SIS Pipes	Subsystem 3
215	"	"	" 3
241	"	"	" 4
257	"	"	" 4
259	"	"	" 4
265	Moment		Subsystem 5
284	"		" 6
285	"		" 6
286	"		" 6
287	"		" 6
288	"		" 6
289	"		" 6
290	"		" 6
291	"		" 6
292	"		" 6
293	"		" 6
294	"		" 6
295	"		" 7
296	"	RCS Pipes	" 7
297	"		" 7
298	"		" 7
299	"		" 7
300	"		" 7
301	"	RCS Pipes	" 7
302	zpa	DG's	AFT:Turb/Aux, 591'
308	8	Transformers, Chargers	AFT:Turb/Aux, 617'
310	zpa	RWST	AFT:Turb/Aux, 642'
311	4	Elec. Components	AFT:Turb/Aux, 642'

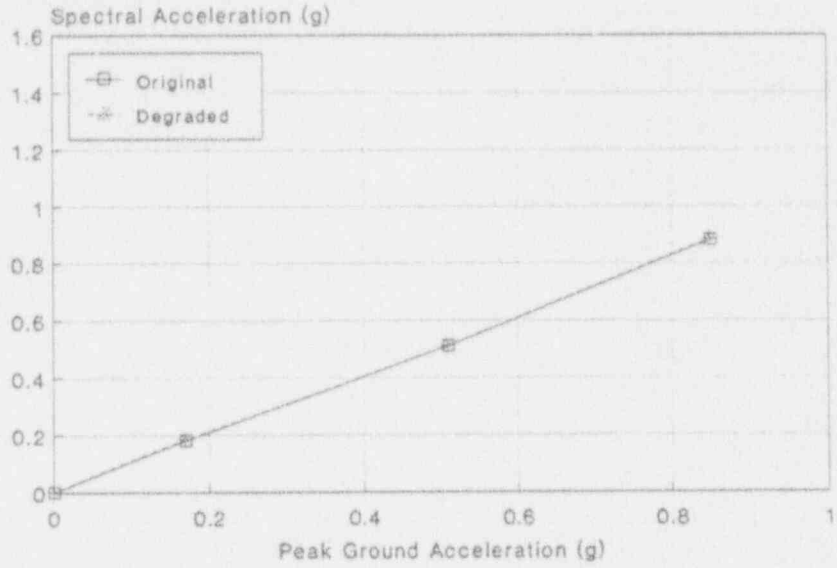

Figure B-27 Median Responses SEISIM #1
Free-Field Motion at zpa

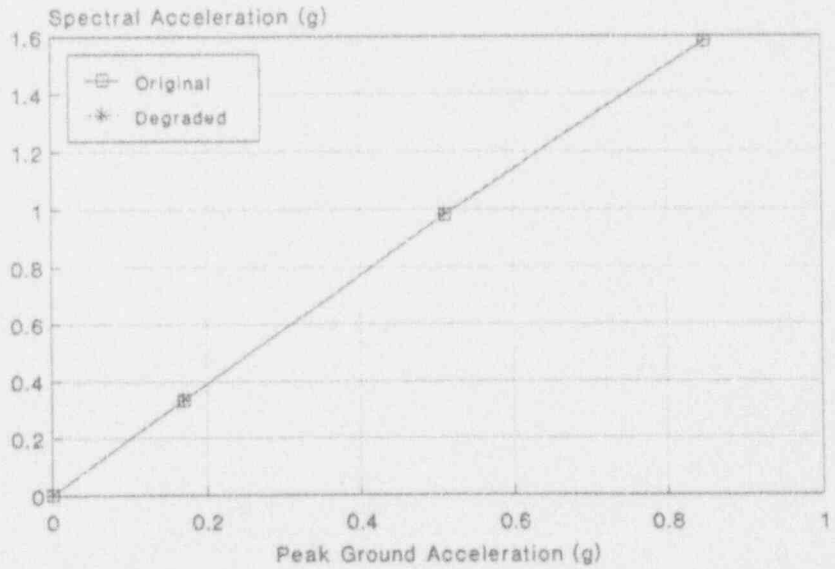

Figure B-28 Median Responses SEISIM #3
Free-Field Motion at 8 Hz

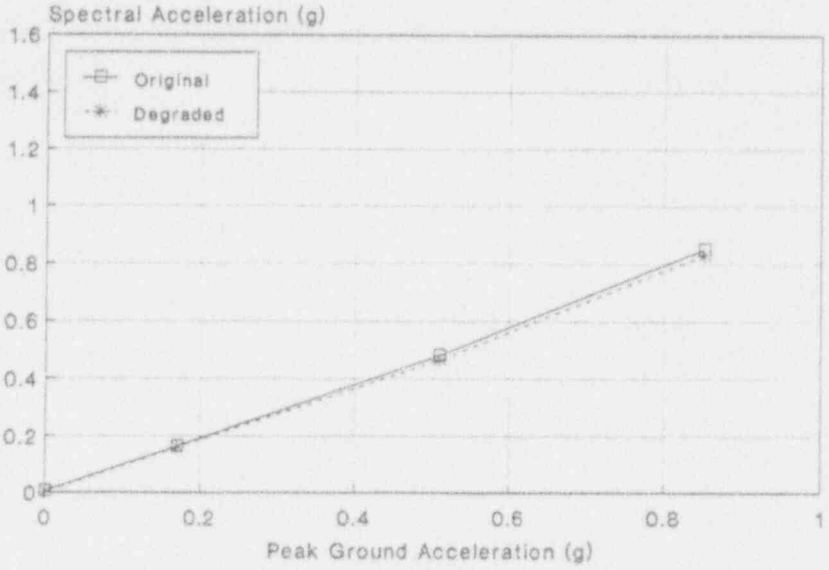

Figure B-29 Median Responses SEISIM #7
Containment Basemat at 8 Hz

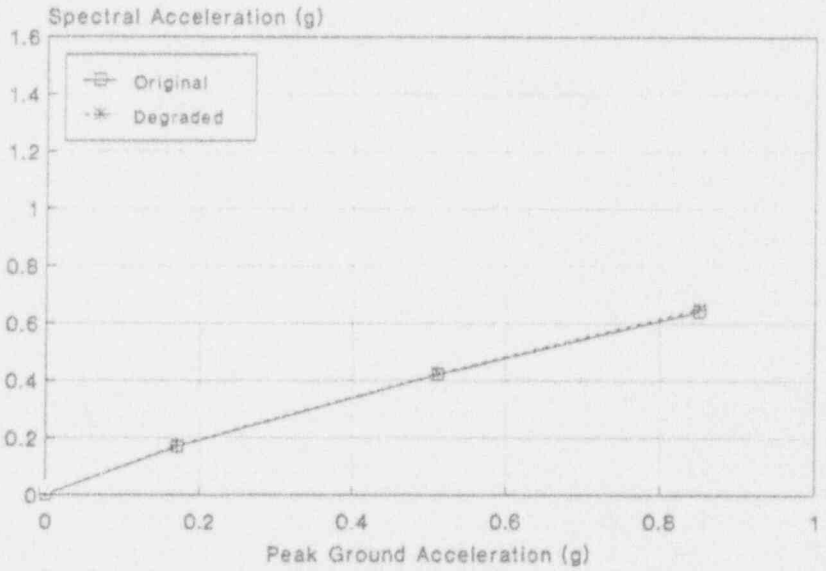

Figure B-30 Median Responses SEISIM #10
Containment Internal Node 936 at zpa

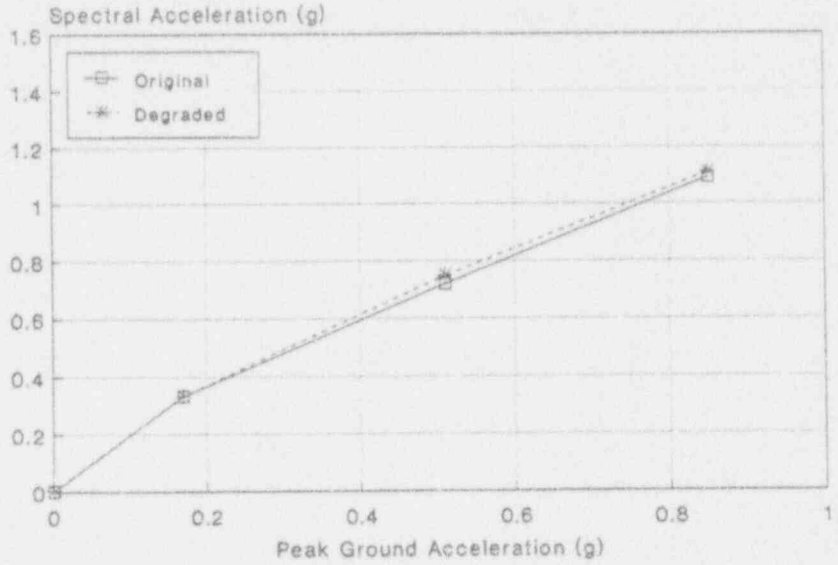

Figure B-31 Median Responses SEISIM #11
Containment Internal Node 936 at 4 Hz

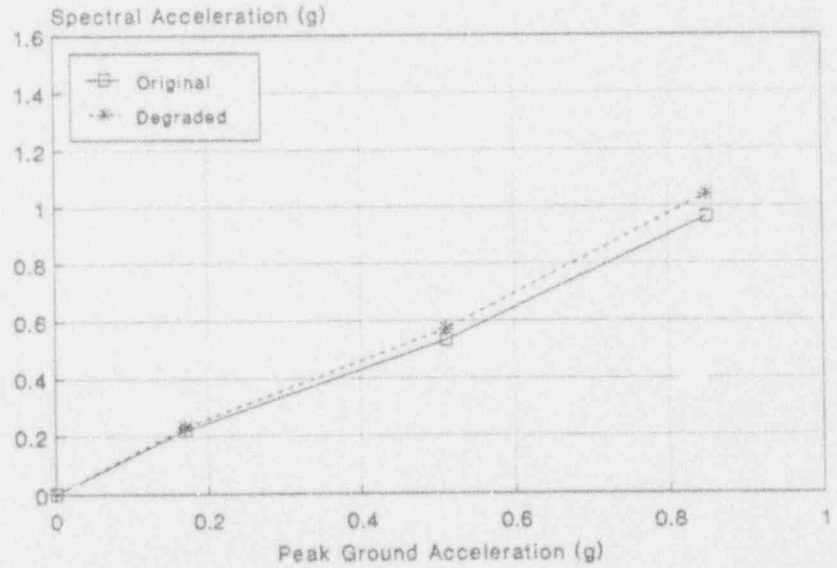

Figure B-32 Median Responses SEISIM #12
Containment Internal Node 936 at 8 Hz

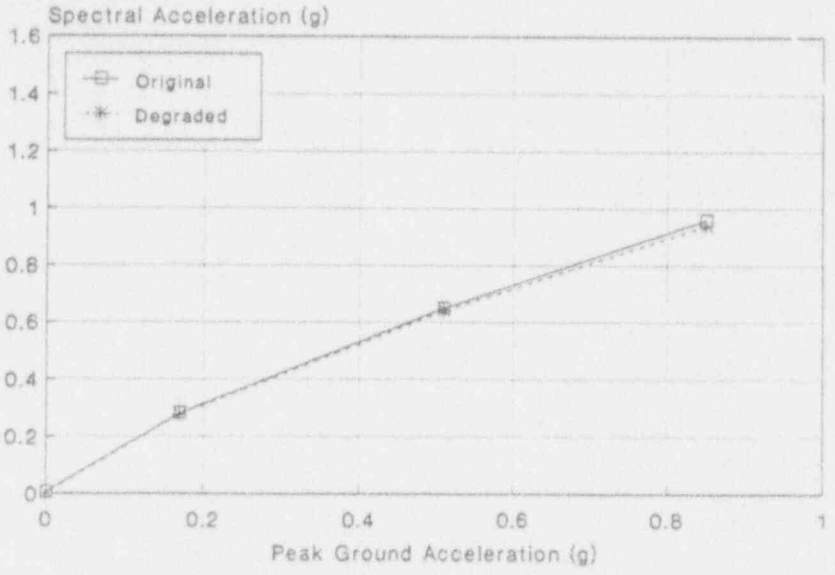

Figure B-33 Median Responses SEISIM #14
Containment Internal Node 1412 at 4 Hz

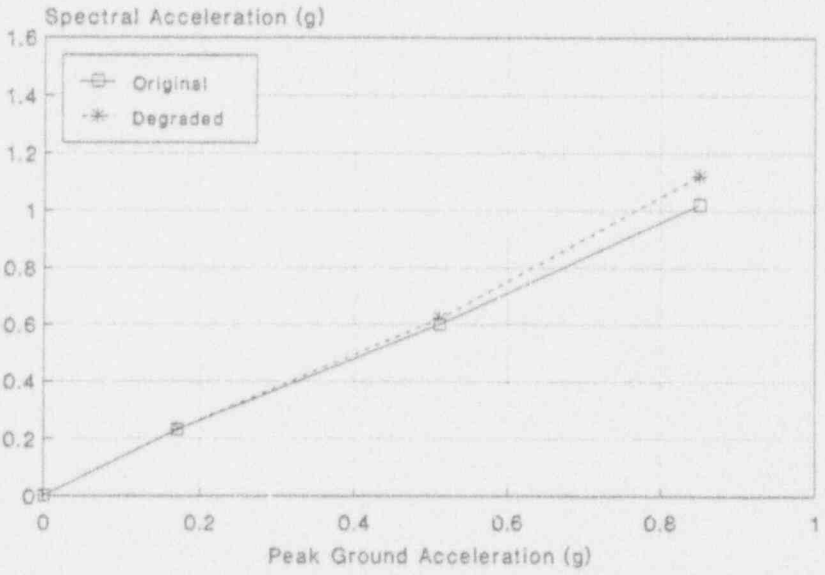

Figure B-34 Median Responses SEISIM #15
Containment Internal Node 1418 at 8 Hz

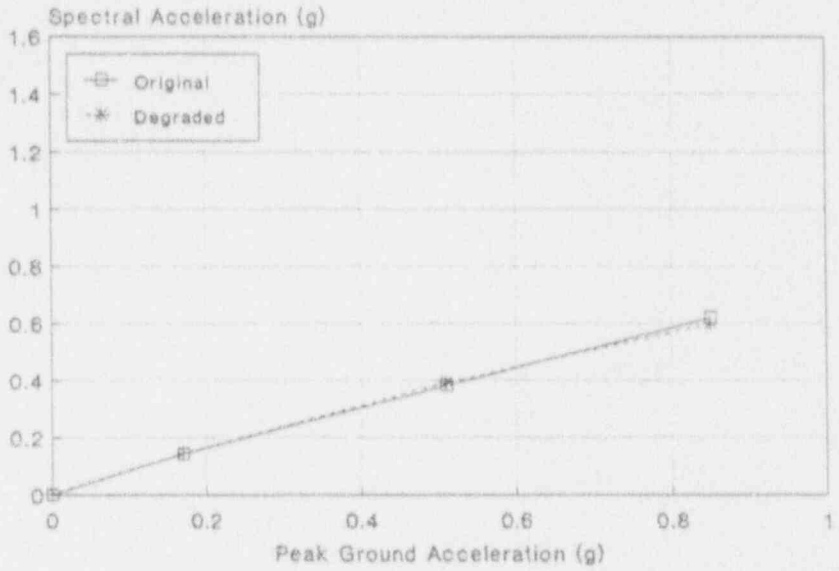

Figure B-35 Median Responses SEISIM #16
Containment Internal Nodes 1462 and 1463 at 16 Hz

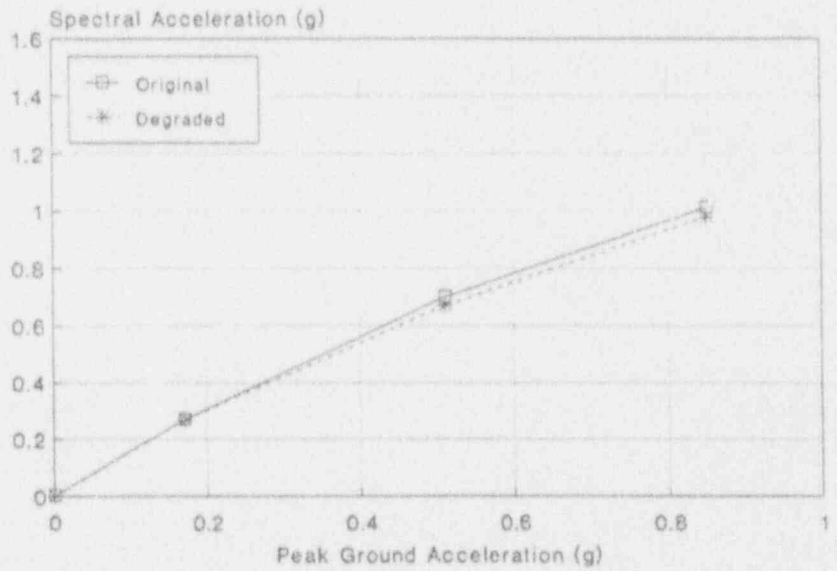

Figure B-36 Median Responses SEISIM #18
AFT Nodes 13 and 21 at 4 Hz

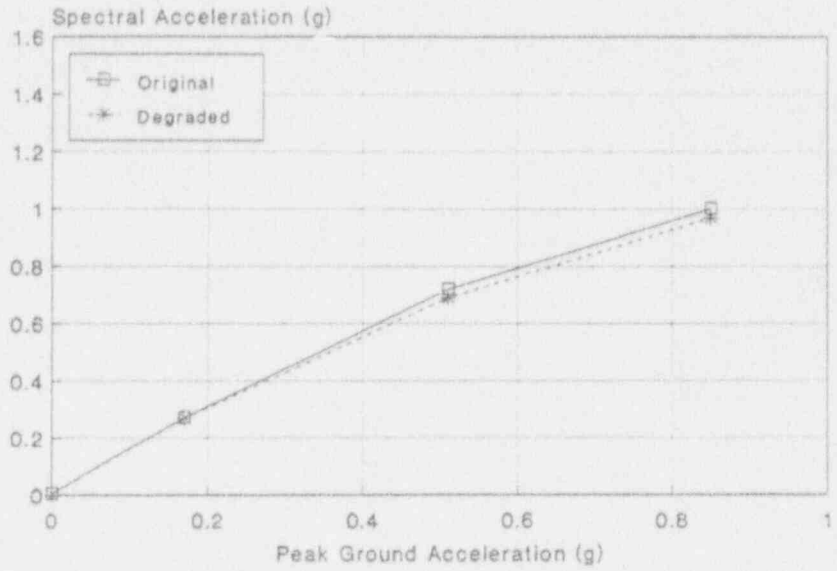

Figure B-37 Median Responses SEISIM #22
AFT Nodes 505 and 530 at 4 Hz

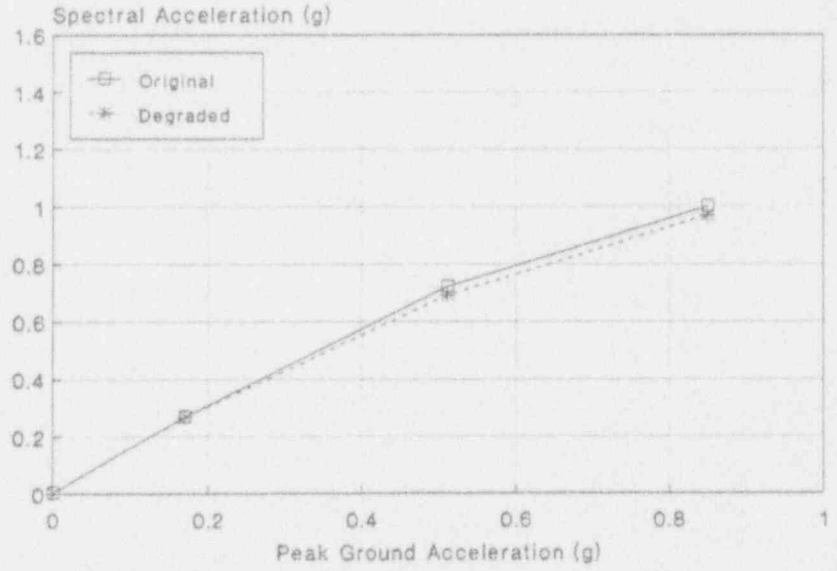

Figure B-38 Median Responses SEISIM #26
AFT Nodes 530 and 544 at 4 Hz

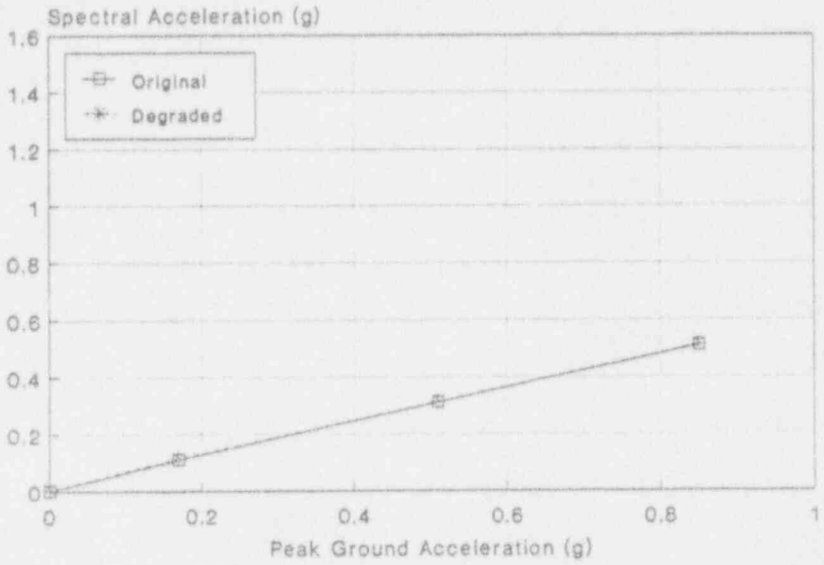

Figure B-39 Median Responses SEISIM #29
AFT Nodes 1511 and 1543 at zpa

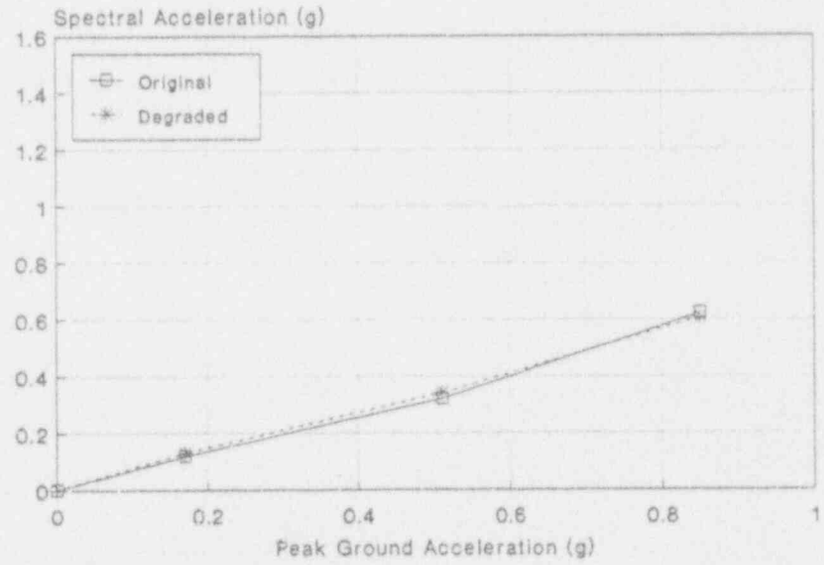

Figure B-40 Median Responses SEISIM #302
AFT Nodes 1543 and 1562 at zpa

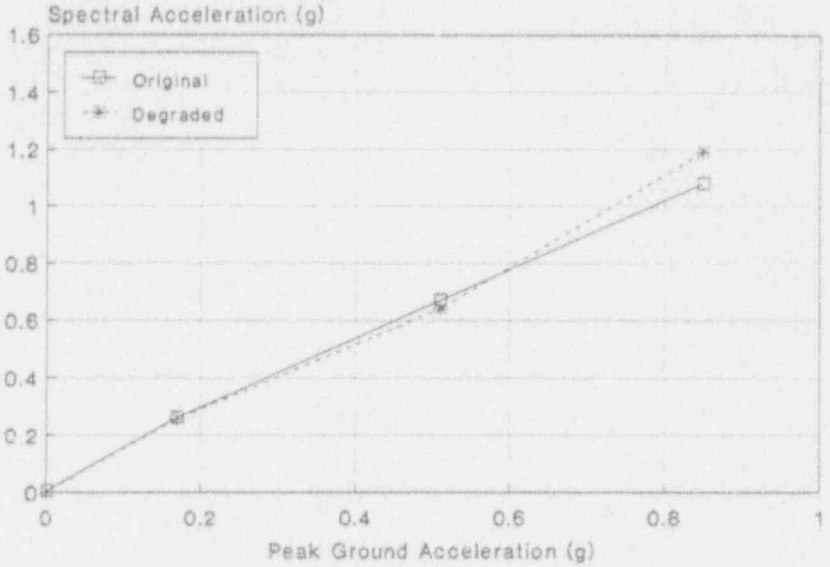

Figure B-41 Median Responses SEISIM #308
AFT Node 2012 at 8 Hz

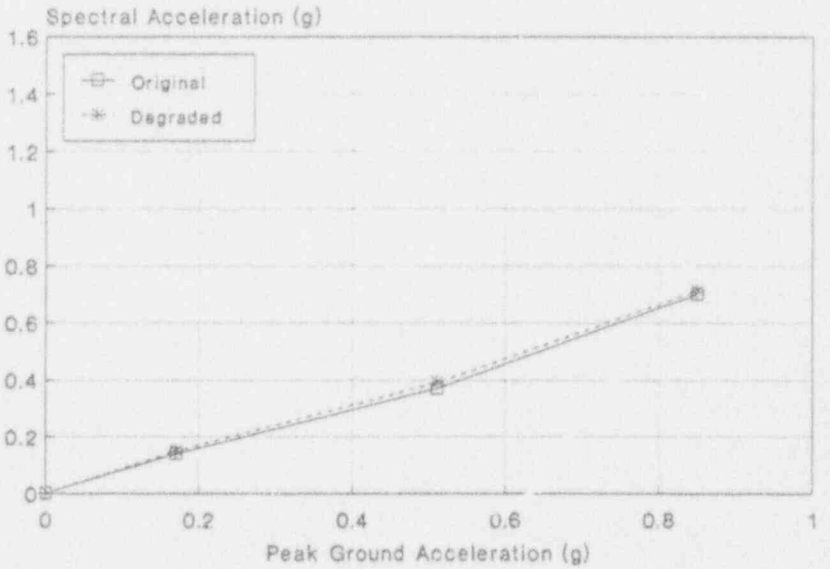

Figure B-42 Median Responses SEISIM #310
AFT Nodes 3005 and 3006 at zpa

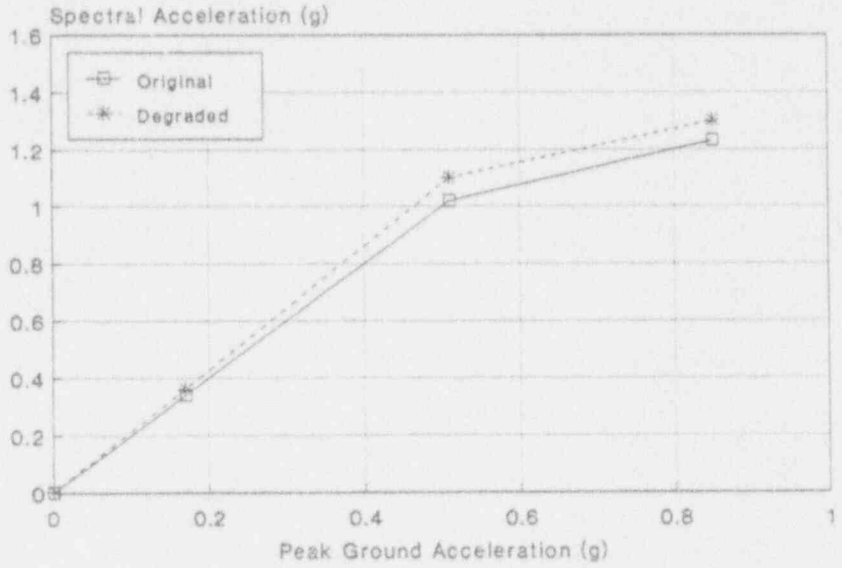

Figure B-43 Median Responses SEISIM #311
AFT Nodes 3005 and 3006 at 4 Hz

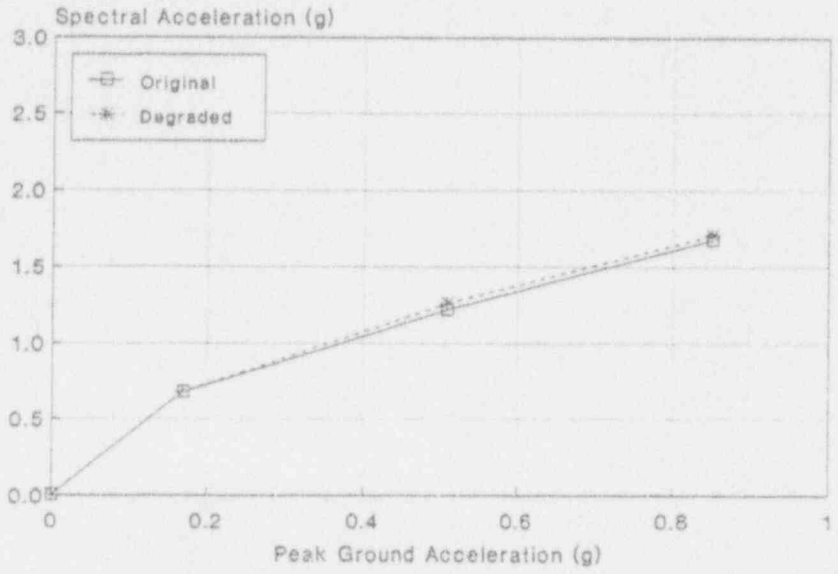

Figure B-44 Median Responses SEISIM #86
Subsystem 1 Node 110, Valve Acceleration

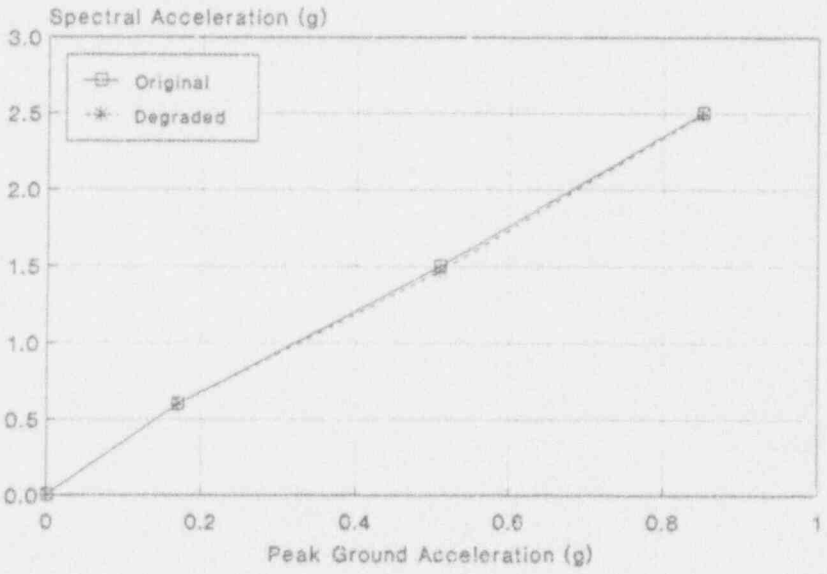

Figure B-45 Median Responses SEISIM #105
Subsystem 2 Node 248, Valve Acceleration

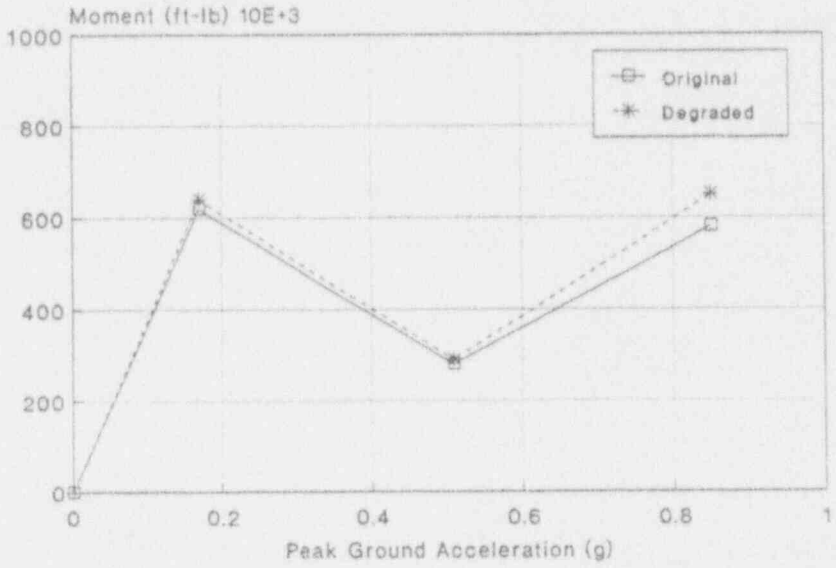

Figure B-46 Median Responses SEISIM #87
Subsystem 1 and 2 Pipe Moments

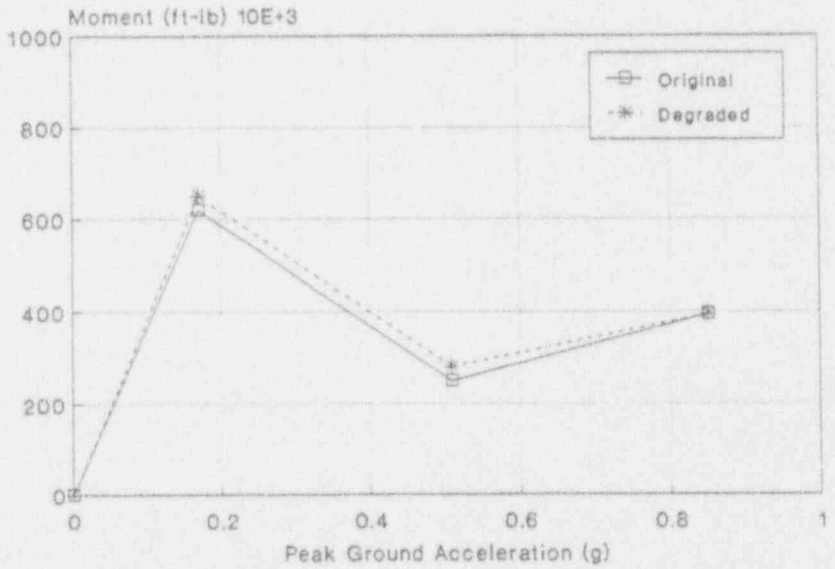

Figure B-47 Median Responses SEISIM #120
Subsystem 2 Pipe Moments

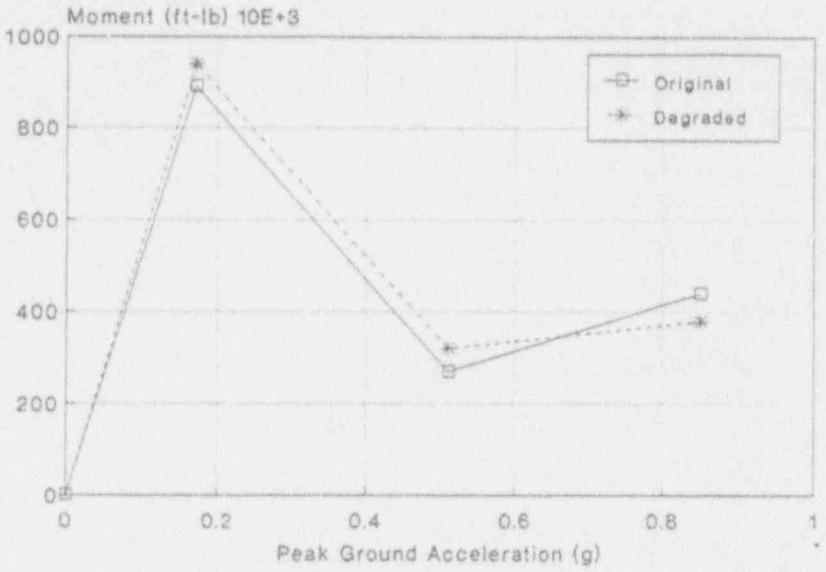

Figure B-48 Median Responses SEISIM #121
Subsystem 2 Pipe Moments

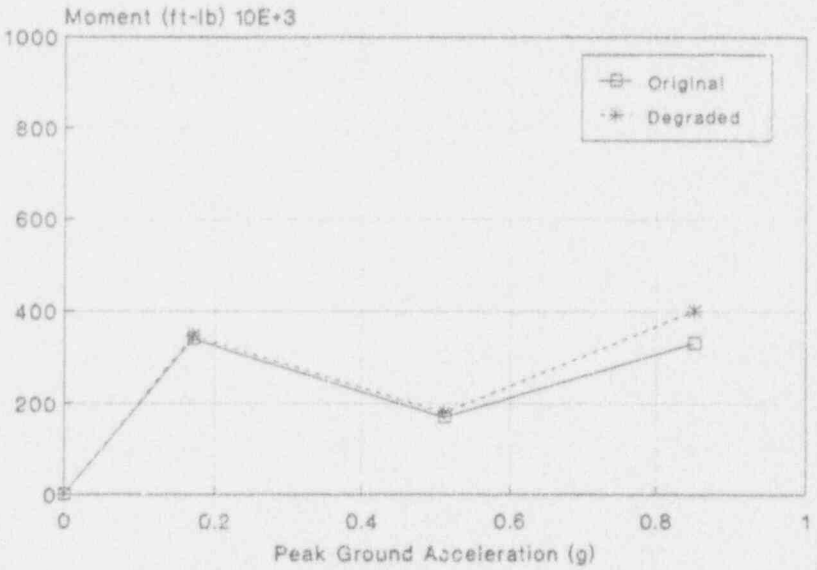

Figure B-49 Median Responses SEISIM #122
Subsystem 2 Pipe Moments

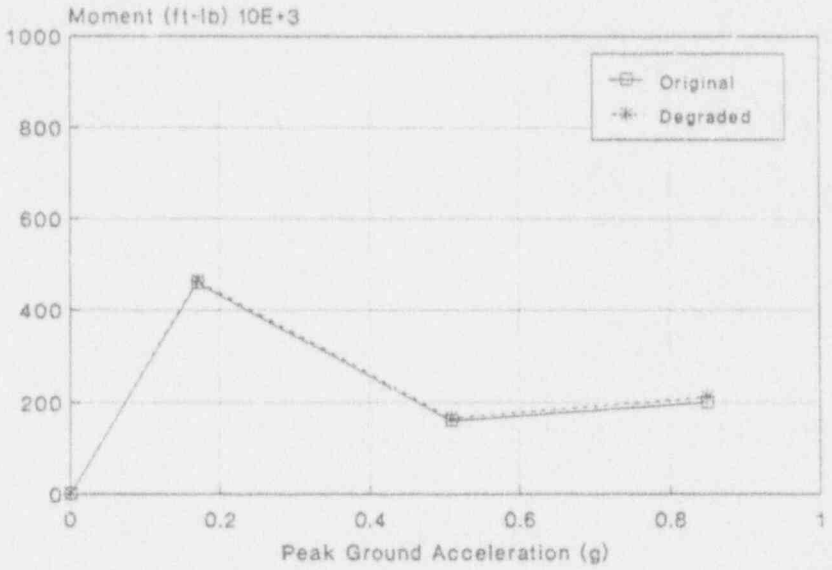

Figure B-50 Median Responses SEISIM #213
Subsystem 3 Pipe Moments

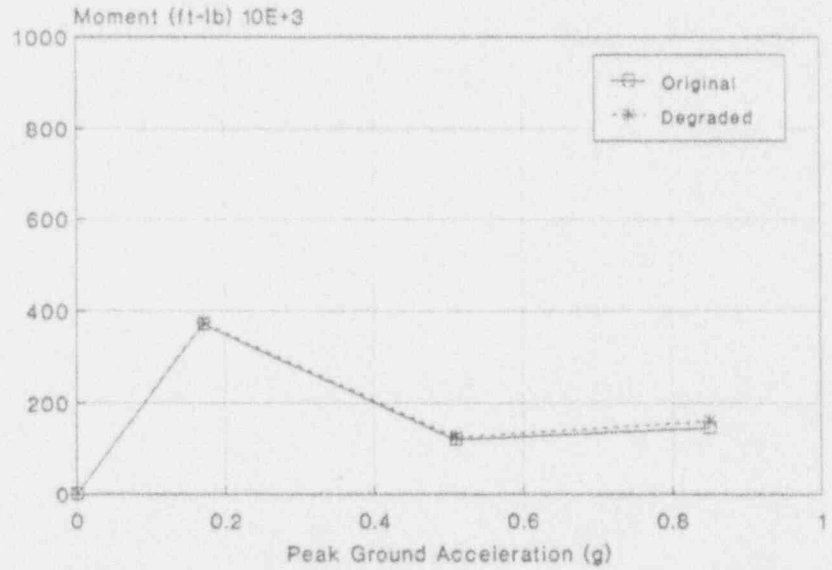

Figure B-51 Median Responses SEISIM #215
Subsystem 3 Pipe Moments

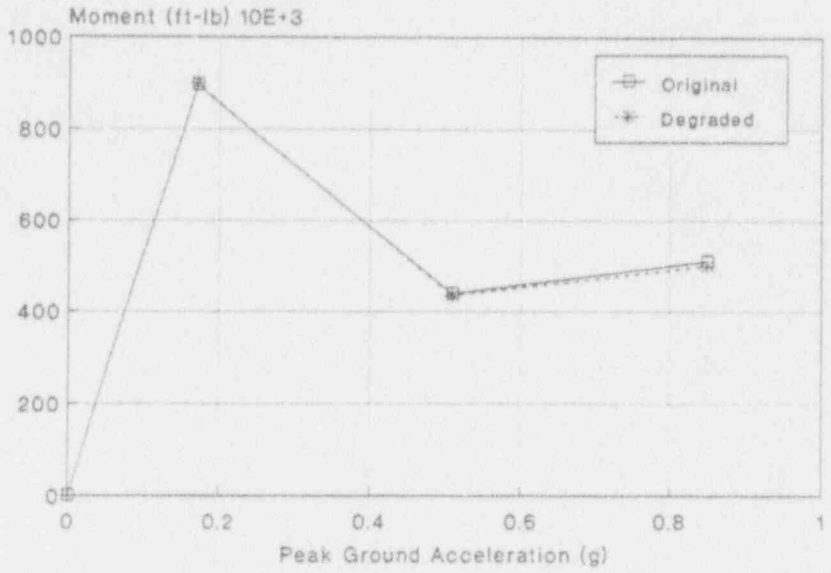

Figure B-52 Median Responses SEISIM #241
Subsystem 4 Pipe Moments

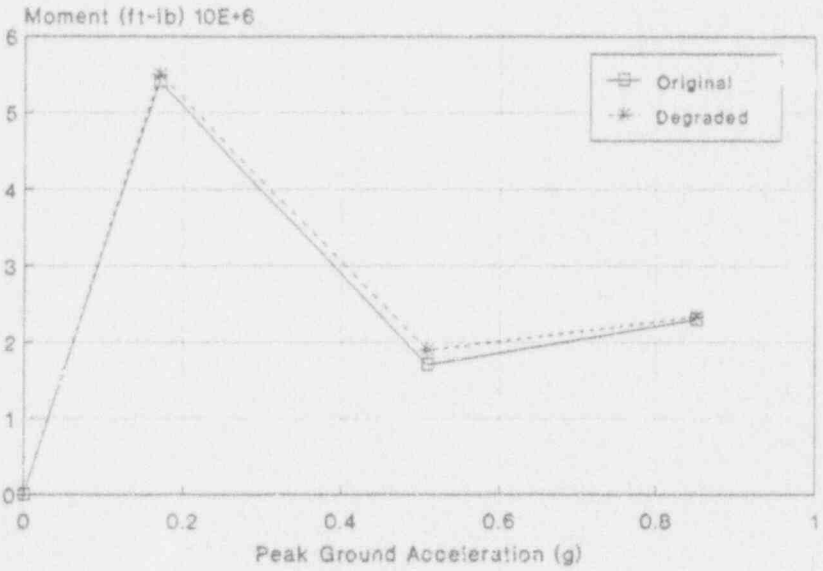

Figure B-53 Median Responses SEISIM #257
Subsystem 4 Pipe Moments

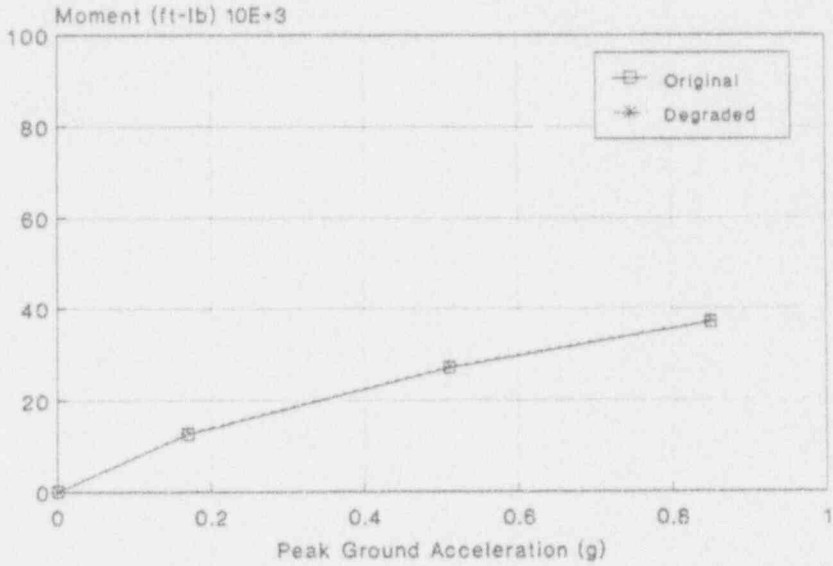

Figure B-54 Median Responses SEISIM #259
Subsystem 4 Pipe Moments

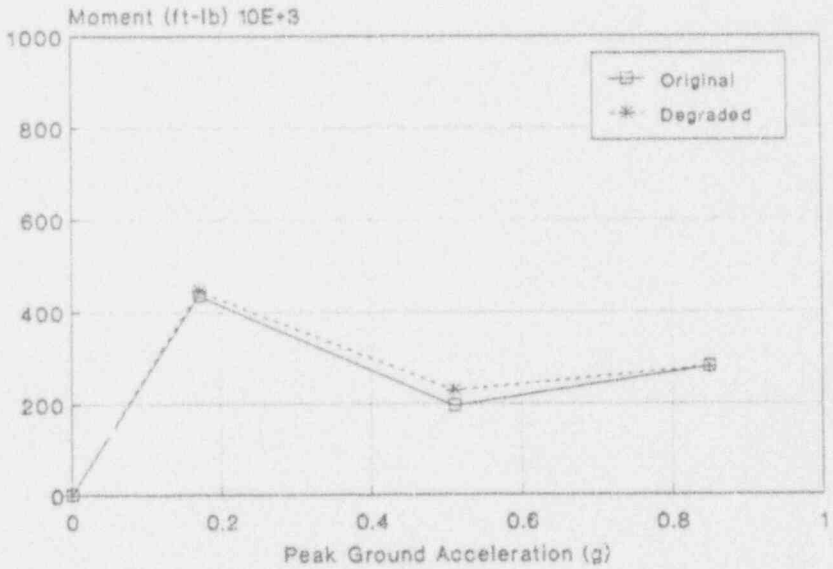

Figure B-55 Median Responses SEISIM #265
Subsystem 5 Pipe Moments

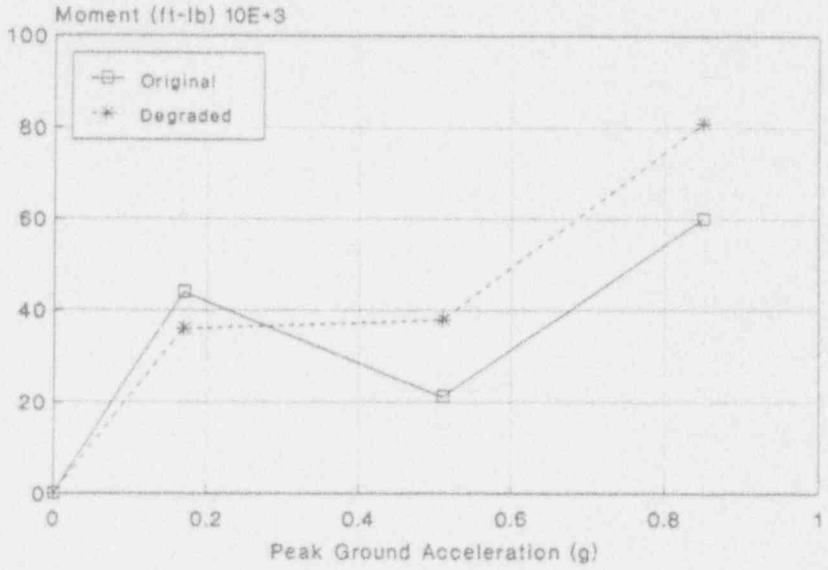

Figure B-56 Median Responses SEISIM #284
Subsystem 6 Pipe Moments

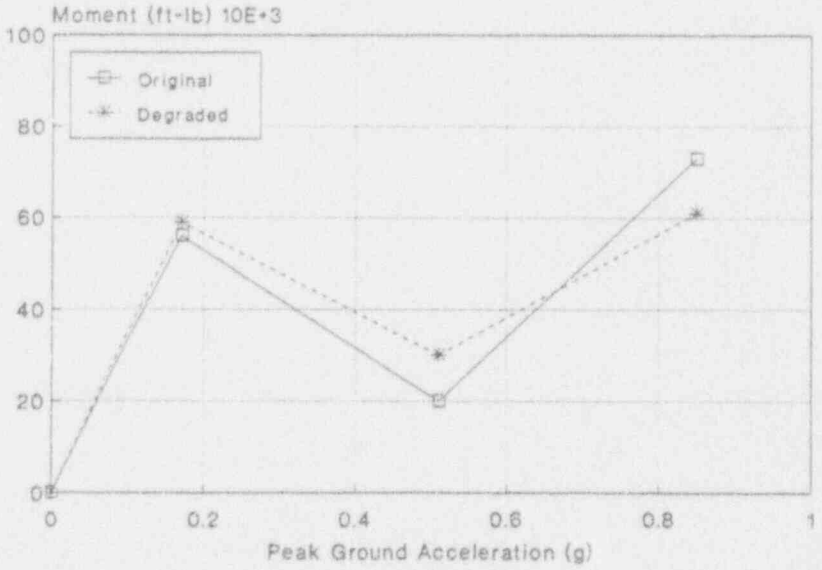

Figure B-57 Median Responses SEISIM #285
Subsystem 6 Pipe Moments

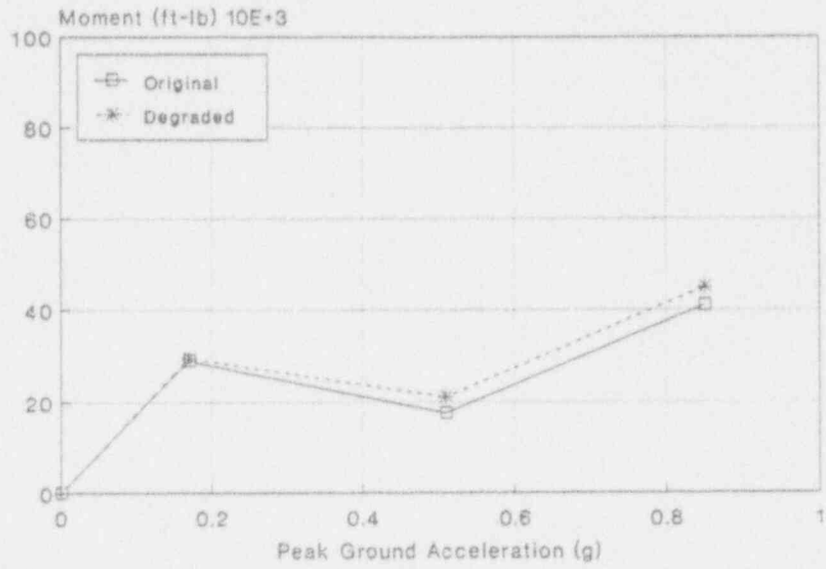

Figure B-58 Median Responses SEISIM #286
Subsystem 6 Pipe Moments

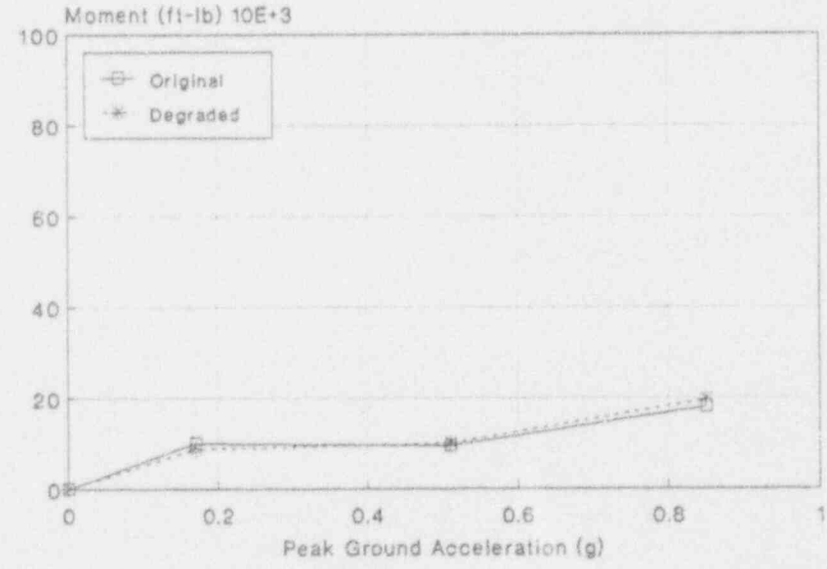

Figure B-59 Median Responses SEISIM #287
Subsystem 6 Pipe Moments

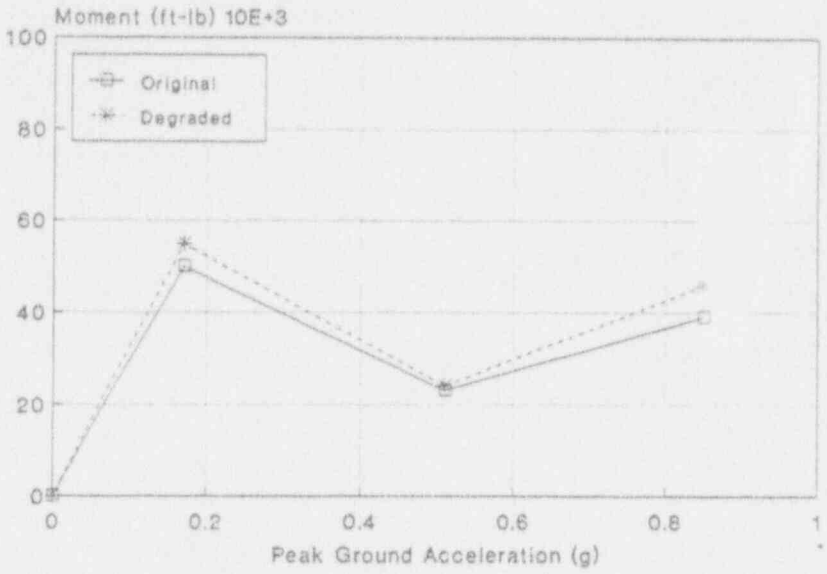

Figure B-60 Median Responses SEISIM #288
Subsystem 6 Pipe Moments

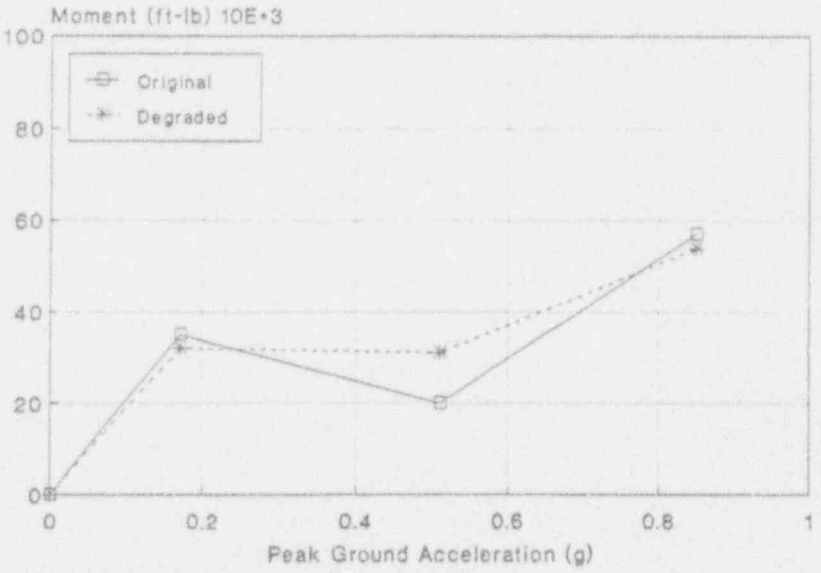

Figure B-61 Median Responses SEISIM #289
Subsystem 6 Pipe Moments

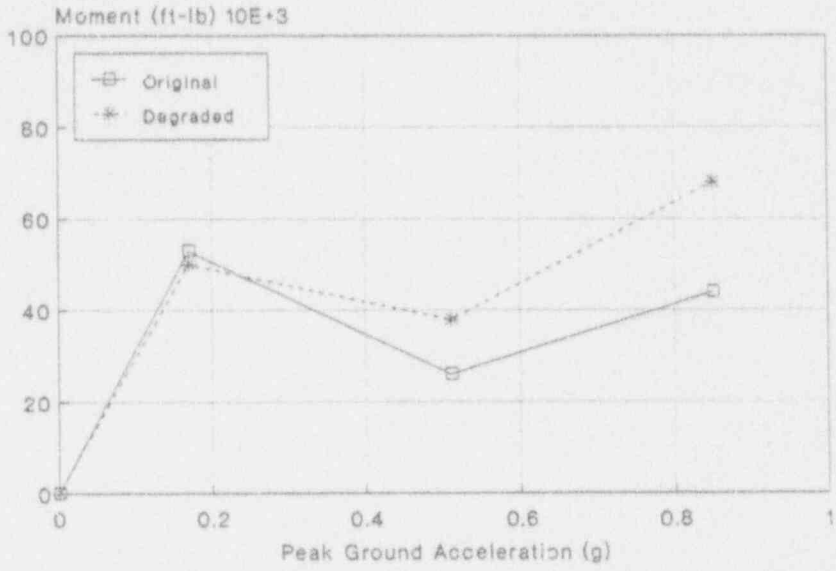

Figure B-62 Median Responses SEISIM #290
Subsystem 6 Pipe Moments

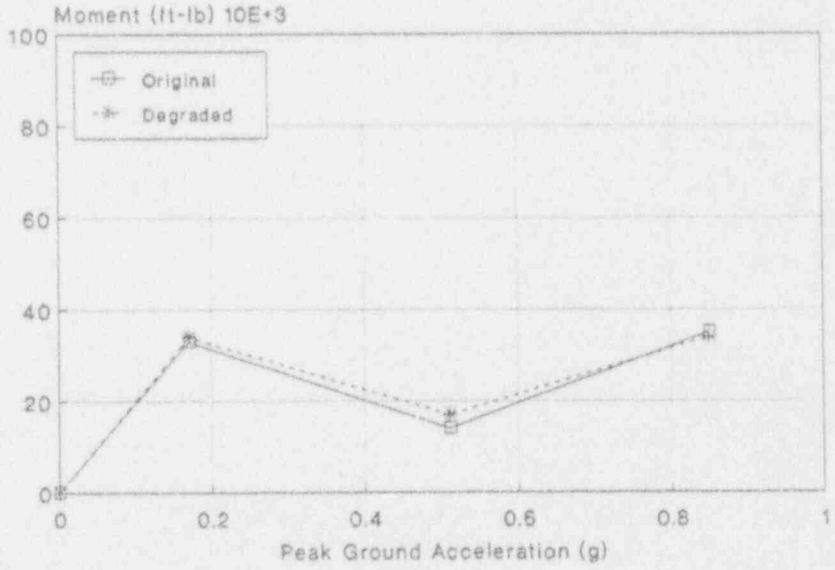

Figure B-63 Median Responses SEISIM #291
Subsystem 6 Pipe Moments

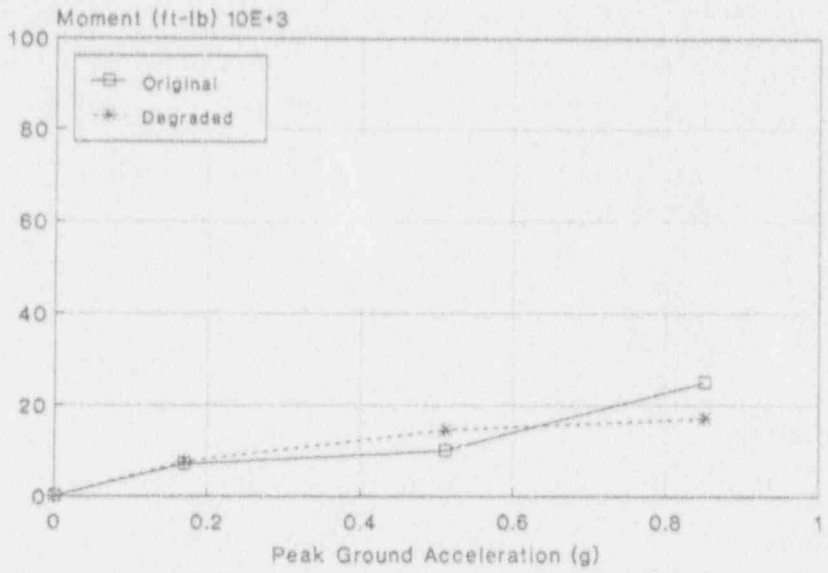

Figure B-64 Median Responses SEISIM #292
Subsystem 6 Pipe Moments

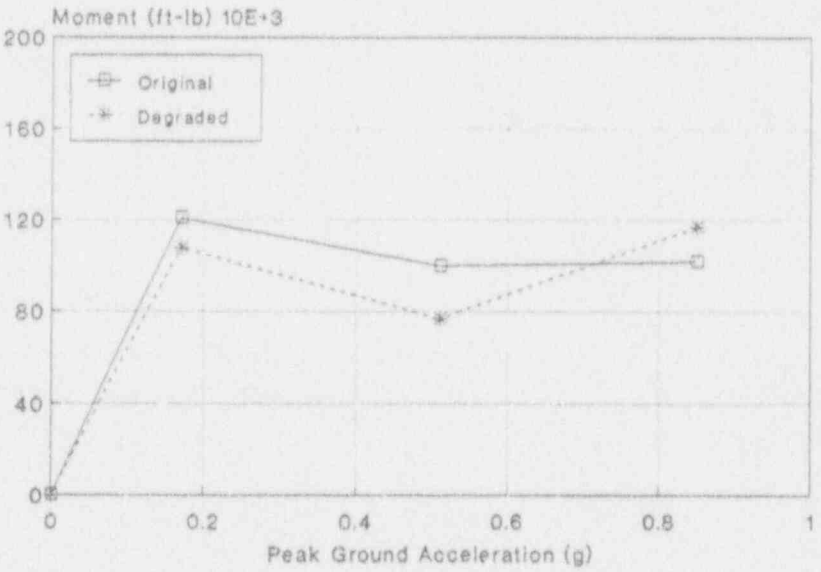

Figure B-65 Median Responses SEISIM #293
Subsystem 6 Pipe Moments

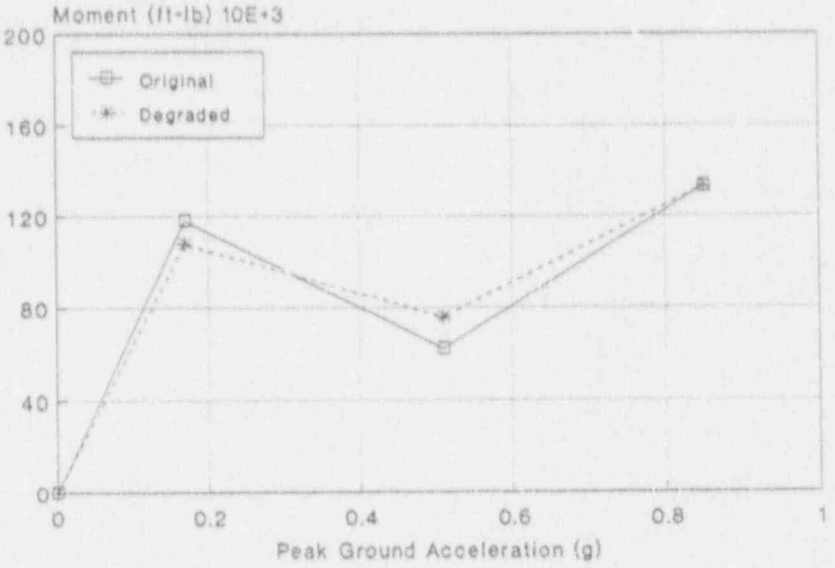

Figure B-66 Median Responses SEISIM #294
Subsystem 6 Pipe Moments

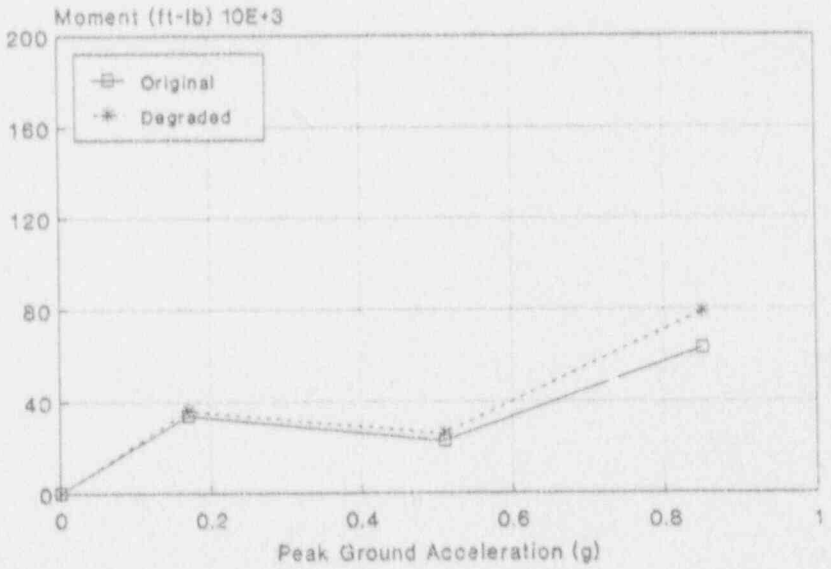

Figure B-67 Median Responses SEISIM #295
Subsystem 7 Pipe Moments

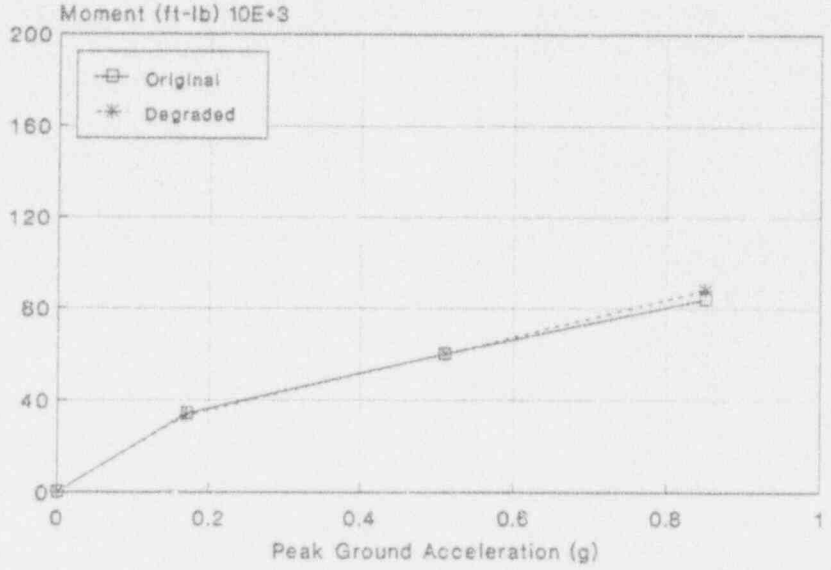

Figure B-68 Median Responses SEISIM #296
Subsystem 7 Pipe Moments

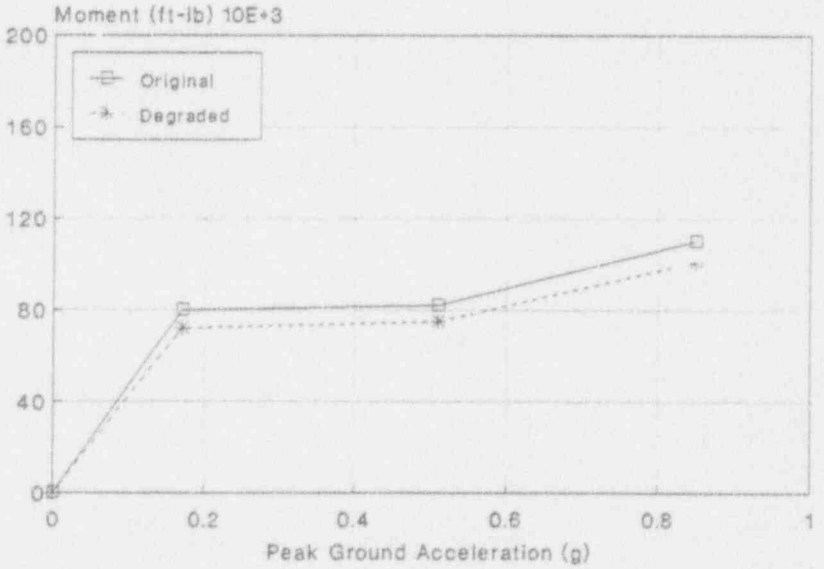

Figure B-69 Median Responses SEISIM #297
Subsystem 7 Pipe Moments

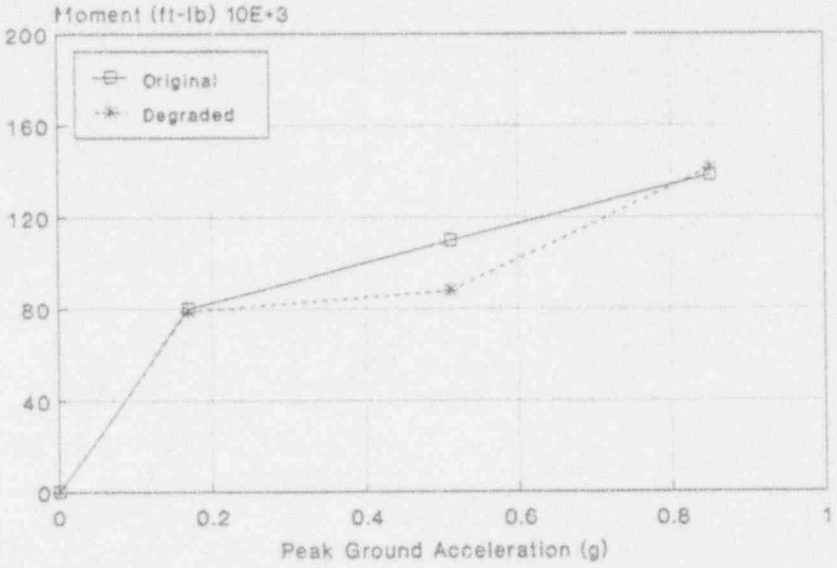

Figure B-70 Median Responses SEISIM #298
Subsystem 7 Pipe Moments

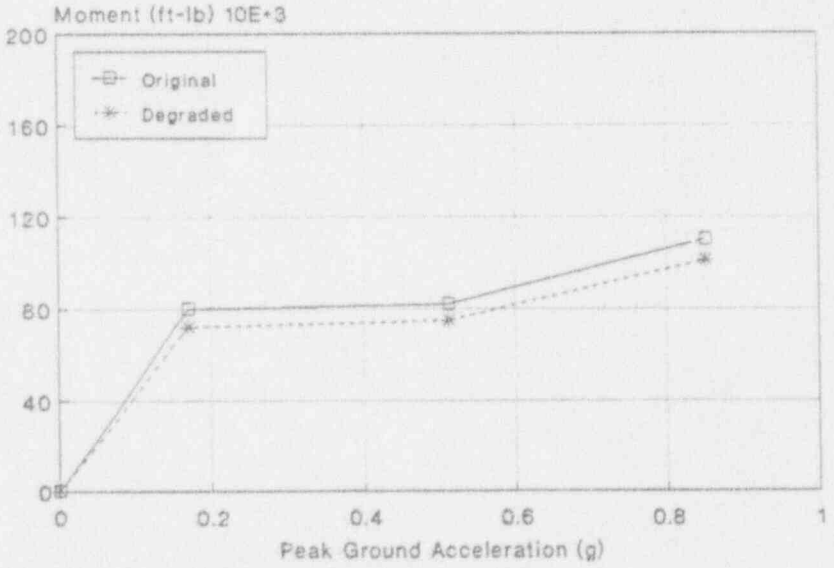

Figure B-71 Median Responses SEISIM #299
Subsystem 7 Pipe Moments

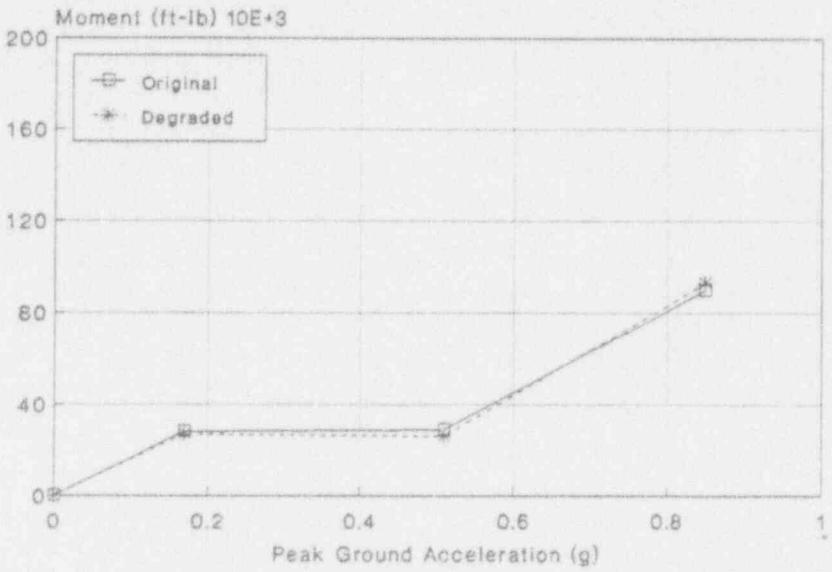

Figure B-72 Median Responses SEISIM #300
Subsystem 7 Pipe Moments

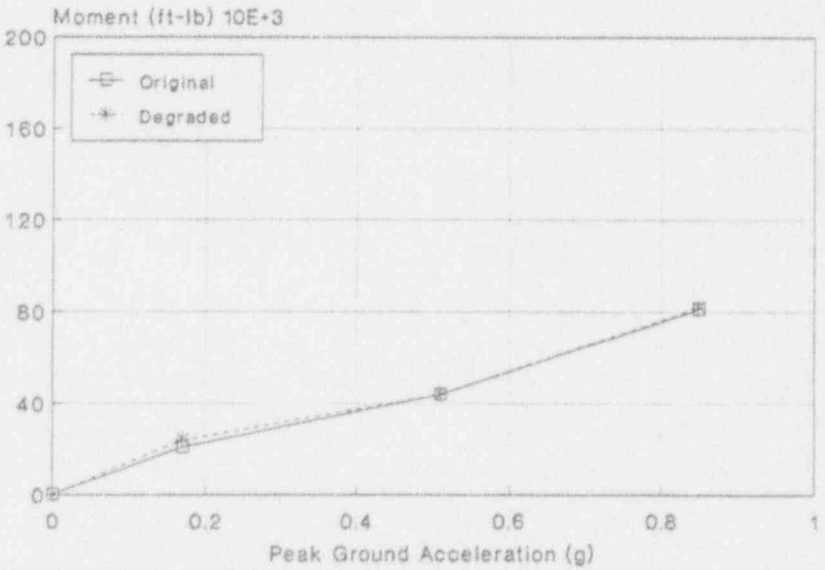

Figure B-73 Median Responses SEISIM #301
Subsystem 7 Pipe Moments

of the 10 previously generated input earthquakes. Acceleration response spectra were calculated at three points located near three pipe supports for subsystem 2 for this comparison. Response spectra of these nodes at 2% spectral damping (the same damping as the piping) were compared at 1 and 3 SSE. Near the fundamental frequency for this subsystem (3.27 Hz) the difference in the response between 1 and 3 SSE was not uniform for all supports indicating that the differential motion between supports will vary for different SSE levels. This, in conjunction with the fact that maximum responses from those in a single group could be from different pipe locations, gives rise to the irregular pipe moment distribution from 1 to 5 SSE.

From these figures of response versus peak ground acceleration, a bilinear representation of each response could be fit. The parameters of these bilinear response models are coded in the RESPONSE file which is listed in the Attachment to Appendix B - Response Files.

B.3.5.2 Variability in Response

Variability in responses (floor slab and spectral accelerations) is assigned using simplified rules derived from the detailed response calculations made for the Zion Nuclear Power Plant in the original SSMRP (Ref. B-6). In that program, an attempt was made to accurately compute the responses of walls and floor slabs in the Zion structures, moments in the important piping systems, accelerations of all important valves, and the spectral accelerations at each safety system component (pump, electrical bus, motor control center, etc.,). With these detailed response calculations, the random variability and correlation between the responses of all components could be computed directly. Detailed summary plots showed that the random uncertainty in the various responses could be reasonably approximated as follows:

Response Type	β-random
Peak Ground Acceleration	0.25
Floor Zero Period Acceleration	0.35
Floor Spectral Acceleration	0.45

where β-random is the standard deviation of the logarithm of the response (denoted β_{RR}). These simplified rules were used to define the random variability in responses for the present study. The modeling (systematic) variability (denoted β_{RU}) is taken as 0.3 for all responses.

B.3.5.3 Correlation

Generic rules for estimating correlations between the various responses were also derived from SSMRP response calculations for the Zion plant. These rules are summarized in Table B-8. By use of this table, the

Table B-8

Rules for Assigning Response Correlation $\rho_{R_1 R_2}$

1. Components on the same floor slab, and sensitive to the same spectral frequency range (i.e., ZPA, 5-10 Hz or 5 Hz) will be assigned response correlation = 1.0.

2. Components on different floor slabs, sensitive to different ranges of spectral acceleration will be assigned response correlation = 0.5.

3. Components on different floor slabs (but in the same building) and sensitive to the same spectral frequency range will be assigned response correlation = 0.75.

4. Components on the ground surface (outside tanks, etc.) shall be treated as if they were on the grade floor of an adjacent building.

5. "Ganged" valve configurations (either parallel or series) will have response correlation = 1.0.

6. All other configurations will have response correlation = 0.0.

correlation between any pair of responses (R_i,R_j) can be determined. The SSMRP assumed no correlation between the fragilities of any two components (F_i,F_j) and this assumption was, in general, used here also. These response and fragility correlations are used in evaluating the probabilities for cut sets involving dependent failures.

These rules were applied to the dominant cutsets in the accident sequences evaluated (as described in Section B.5) and it was found that correlation affected only the following pairs of like components:

Relay pairs

Circuit breaker pairs

Reactor coolant pump supports

Steam generator supports

Pipe segment pairs

Based on the rules above, all of these were given a failure correlation of 0.5 with the exception of piping segments. For piping segments, the fragilities as well as the responses were assumed to be fully correlated, which implies a failure correlation of 1.0 for the piping segment pairs. This last assumption was made because it was not possible to retrieve the correlations between the different piping moment responses calculated in the SSMRP, and this assumption is a conservative one. Note that only pipe segments of the same size and in the same piping subsystem were assumed to be correlated.

B.4 SEISMIC FRAGILITIES

The equipment seismic fragilities developed in the original SSMRP study were used in the present study. The same building structural fragilities were used. These were not modified for the effects of shear wall stiffness reduction as the studies on both Peach Bottom and ANO-1 (Appendices A and C of this report) showed only a minimal effect of shear wall stiffness degradation on the capacity of the structural fragilities.

In general, equipment failure is taken as either loss of pressure boundary integrity or loss of operability. Failure (fragility) is characterized by a cumulative distribution function which describes the probability that failure has occurred given a value of loading. Loading may be described by local spectral acceleration or moment, depending on the component failure mode. The fragilities are related to the local response to permit an accurate assessment of the effect of earthquake-induced correlation in the evaluation of the accident sequences.

B.4.1 Generic Fragilities

A generic data base of fragility functions for seismically-induced failures was developed in the original SSMRP [Ref. B-7]. As a first step, all components were grouped into generic categories. For example, all motor operated valves located on piping with diameters between 2-1/2 and 8 inches were placed into a single generic category, and similarly, all motor control centers were placed into another generic category. The generic categories are shown on Table B-9. The median failure accelerations and both random and systematic uncertainties (expressed as standard deviations of the logarithms of the fragility) are listed in Table B-10.

Fragilities for electrical components were assigned based on either anchorage failure, generic circuit breaker trip, or generic relay chatter. The relay chatter mode assignment may be conservative because (in most cases) circuits are protected by time delay circuits and because (in most cases) chatter of relays would not cause a change in the state of the system being controlled. The circuit breaker trip mode assignment may be conservative (in some cases) if the circuit breakers are easily re-settable from the control room.

B.4.2 Piping Fragilities

A study of the seismic capacity of pipes of different sizes (i.e., schedules), materials (stainless and carbon steels), and temperatures due to inertia-induced stresses was made in the SSMRP. A "Master Piping Fragility" function was developed having a median moment at failure (and corresponding random and modelling variabilities) given by:

$$\hat{M}_{\text{master piping}} = 2.44E{+}6 \text{ inch-lbs}$$

$$\beta_{fr} = 0.18$$

$$\beta_{fu} = 0.33$$

This master fragility applies directly to a Sch. 160 carbon steel (A-106) butt weld of 6 inch inside diameter pipe (at 70° F). For pipes of other sizes, configurations (straight pipe, elbow, tee, etc.), materials and temperatures, scale factors (denoted piping β factors) were determined. The fragility parameters for a pipe of another size (say, pipe i) are determined from the table of these piping β factors given in Ref. B-7. Using the appropriate β factor for the pipe of interest, the applicable median moment at failure for pipe i with an associated piping β factor (say, β_i) is given by:

$$\hat{M}_{\text{pipe i}} = \hat{M}_{\text{master piping}} / \beta_i$$

Table B-9
Generic Component Categories

Fragility Category	Component Class	Typical Components	Frequency (Hz)
1	LOSP	Ceramic Insulators	ZPA
2	Relays		5-10
3	Circuit Breakers		5-10
4	Batteries		ZPA
5	Battery Racks		ZPA
6	Inverters		5-10
7	Transformers	4 kV to 480 V and 480 to 120 V	10
8	Motor Control Centers	Control for ESF Pumps and Valves	5-10
9	Aux. Relay Cabinets		5-10
10	Switchgear (Including Transformers, Buses and Breakers)	416 V and 480 V	5-10
11	Cable Trays		ZPA
12	Control Panels and Racks	RPS Process Control	5-10
13	Local Instruments	Misc. Pressure & Temperature Sensors	5-35
14	Diesel Generators	4160 ac Emergency Power Units	22
15	Horizontal Motors	Motor-Generator Sets	ZPA
16	Motor-Driven Pumps and Compressors	AFWS, RHR, SIS, Charging Pumps, Lube Oil Pumps, Diesel Starting Compressors	7
17	Large Vertical, Centrifugal Pumps (Motor-Drive)	Service Water Pumps	5
18	Large Motor-Operated Valves (10")		ZPA
19	Small Motor-Operated Valves (10")		ZPA
20	Large Pneumatic/Hydraulic Valves	Includes MSIV, ADP, and PORV	ZPA
21	Large Check and Relief Valves		ZPA
22	Miscellaneous Small Valves (8")		ZPA
23	Large Horizontal Vessels & Heat Exchangers	Pressurizer Relief Tank, CCW Heat Exchangers	ZPA
24	Small to Medium Heat Exchangers and Vessels	Boron Injection Tank	20
25	Large Vertical Storage Vessels with Formed Heads	RHR Heat Exchanger, Accumulator Tank	ZPA
26	Large Vertical Flat-Bottomed Storage Tanks	CST, RWST	
27	Air Handling Units	Containment Fan Coolers	5

Table B-10

Generic Component Fragilities, in Units of Gravity (g)

Category	Generic Component	Median*	b_U	b_R
1	Ceramic Insulators	0.25	0.25	0.25
2	Relays	3.00	0.48	0.75
3	Circuit Breakers	7.63	0.48	0.74
4	Batteries	0.80	0.40	0.39
5	Battery Racks	2.29	0.31	0.39
6	Inverters	2.00	0.26	0.35
7	Dry Transformers	8.80	0.28	0.30
8	Motor Control Centers	7.63	0.48	0.74
9	Auxiliary Relay Cabinets	7.63	0.48	0.74
10	Switchgear	6.43	0.29	0.66
11	Cable Trays	2.23	0.34	0.19
12	Control Panels and Racks	11.50	0.48	0.74
13	Local Instruments	7.68	0.20	0.35
14	Diesel Generators	1.00	0.25	0.31
15	Horizontal Motors	12.10	0.27	0.31
16	Motor-Driven Pumps and Compressors	2.80	0.25	0.27
17	Large Vertical Centrifugal Pumps	2.21	0.22	0.32
18	Large Motor-Operated Valves (10 in.)	6.50	0.26	0.60
19	Small Motor-Operated Valves (10 in.)	3.83	0.26	0.35
20	Large Pneumatic/Hydraulic Valves	6.50	0.26	0.35
21	Large Relief, Manual, and Check Valves	8.90	0.20	0.35
22	Miscellaneous Small Valves	12.50	0.33	0.43
23	Large Horizontal Vessels and Heat Exchangers	3.0	0.30	0.53
24	Small to Medium Vessels and Heat Exchangers	1.84	0.25	0.45
25	Large Vertical Vessels With Formed Heads	1.46	0.20	0.35
26	Large Vertical Tanks With Flat Bottoms	0.45	0.25	0.35
27	Air Handling Units	6.90	0.27	0.61

R = Random Uncertainty.

U = Systematic Uncertainty.

*All medians in terms of spectral acceleration at 5% damping.

and the same β_{fr} and β_{fu} values are used. Thus the fragility of any particular piping segment may be determined. This method was used for generating all the piping fragilities needed in this study.

B.4.3 Site Specific Component Fragilities

During the original SSMRP study, the following components were identified as requiring plant-specific fragility derivations:

1) Refuelling water storage tank
2) Condensate storage tank
3) Reactor vessel supports
4) Reactor coolant pump supports
5) Steam generator supports

All other components were assigned fragility values from the generic fragility data base developed in the SSMRP. The site specific component fragilities are listed on Table B-11. (Both the generic fragilities and the site-specific fragilities were originally reported in Ref. B-7.)

B.4.4 Structural Fragilities

The structural fragilities developed in the original SSMRP were used in this study. The Zion structural fragilities were derived in terms of factors which account for structure ultimate strength and inelastic energy absorption capability. The basic techniques used to determine the median values and associated variabilities of the terms were essentially those described in Section 2.5 of the main report.

The structures were considered to fail functionally when inelastic deformations of the structure under seismic load are estimated to be sufficient to potentially interfere with the operability of safety-related equipment attached to the structure. The element and system ductility limits chosen for structures were estimated to correspond to the onset of significant structural damage. This was believed to represent a conservative bound on the level of inelastic structural deformation which might interfere with the operability of components housed within the structure.

In order to determine the structural fragilities at Zion in the original SSMRP analyses, the complete structural model for each structure (including every load-resisting shear wall) was used. After determining maximum floor loads from a time history analysis of each structure, the resulting shear forces in each wall, including any torsional effects, could then be computed. A total shear force and overturning moment was then computed for each elevation. In addition, using the drawings, the ultimate capacity of each wall could be determined. The loads and capacities then provide the necessary factors used to determine the

Table B-11

Summary of Site-Specific Equipment Fragilities for Zion

Equipment	Failure Mode	Median*	β_R	β_U	Effect of Failure
Refuelling Water Storage Tank	Shell Buckling	3.83	0.24	0.32	Fails ECCS and Bleed and Feed Cooling
Condensate Storage Tank	Shell Buckling	0.81	0.28	0.30	Fails AFWS
Reactor Vessel	Support Failure	3.83	0.24	0.32	RVR Initiator
Reactor Coolant Pumps	Support Failure	2.64	0.24	0.37	RVR, LOCA Initiator
Steam Generators	Support Failure	2.45	0.24	0.37	RVR, LOCA Initiator
Pressurizer	Support Failure	2.00	0.21	0.34	LOCA Initiator
Reactor Core Assembly	Support Failure	2.06	0.24	0.32	ECCS Blockage

* Median values in [illegible] spectral acceleration at 5% damping

structural fragility for each structure.

The fragilities for the Zion structures are listed in Table B-12. In general, several potential failure modes were investigated for each structure. Fragilities for the governing failure modes are shown. These failure modes are typically associated with structural failure which would result in damage to the safety-related equipment located in the building.

In addition to the fragilities of the structures, a fragility based on soil failure and uplift of the containment basemat was developed. This was done because the walls of the Auxillary/Turbine building are quite close to the containment building, and a number of important safety piping systems run into the containment at that point. Hence, relative motion between these two structures could impart severe local displacement-induced strains in the pipes. It was assumed in the SSMRP that sufficient uplift would fail all these pipes leading to failure of ECCS and also failure of the AFWS as well as precluding bleed and feed cooling. This "structural" failure mode fragility is also shown on Table B-12.

B.5 CORE DAMAGE AND RISK COMPUTATIONS

B.5.1 Initiating Events

The initiating events considered for the seismic analysis for Zion were:

- Reactor Vessel Rupture [RVR] (ECCS rendered ineffective by single or multiple pipe breaks)
- Large LOCA [ALOCA] (pipe break with ID > 6.0" but ECCS not rendered ineffective)
- Medium LOCA [MLOCA] (pipe break between 3.0" < ID < 6.0")
- Small LOCA [SLOCA] (pipe break between 1.5" < ID < 3.0")
- Small-Small LOCA [SSLOCA] (pipe break with ID < 1.5")
- Type 2 Transient [T2] (PCS failed by the initiator)
- Type 1 Transient [T1] (PCS initially available)

where PCS is the power conversion system (i.e., the secondary heat removal function).

The reactor vessel rupture initiating event was computed based on the probability of failure of the supports of a steam generator and/or a reactor coolant pump in two different reactor coolant loops. The frequency for the large LOCA initiating event was computed based on the

Table B-12

Summary of Structural Fragilities for Zion

Structure	Element	A_m(g)	B_R	B_U	Effect of Failure
Crib House	Roof Diaphragm	0.86	0.24	0.27	Fails all six service water pumps
Containment Building	Uplift	0.70	0.40	0.40	Fails all pipes in ECCS, RHR, AFWS, CSIS, AND CSRS.
Auxiliary Building	E-W Shear Wall	2.79	0.11	0.26	Loss of electrical power and control circuits between the axuiliary building and containment building

1. These fragilities are the same used in the original SSMRP analysis.

2. b_R and b_U do not include response variability.

failure of the supports of either one steam generator or one reactor coolant pump in any reactor coolant loop. Failures of the piping were not included as a review of their seismic capacities showed that they were significantly higher than the pump or steam generator support capacities and hence, would make negligible contribution to the initiating event frequencies.

The small-small, small and medium LOCA initiating events were computed based on failures of piping in the reactor coolant loop. The fragility for the pipe failures was generated from the calculations of piping failures for pipes considered in the SSMRP Zion analysis. (In addition, transfers from the transient tree based on stuck open relief valves are considered. Two stuck open relief valves are equivalent to a medium LOCA whereas one stuck open relief valve is equivalent to a small LOCA.)

The frequency of the Type 2 transient initiating event (in which loss of offsite power is implied) is computed based on the failure of ceramic insulators. These have a relatively low median failure level, and are the dominant cause of seismically-induced loss of offsite power.

Finally, the Type 1 transient initiating event probability is computed from the condition that the sum of the initiating event probabilities considered must be unity. The hypothesis is that, given an earthquake above the Operating Basis Earthquake (OBE), at least one the initiating events will occur. At the least, the operators must manually shut the plant down for inspection following an OBE level earthquake.

B.5.2 Event Trees

The event trees developed for the original SSMRP program are shown in Figures B-74 through B-80. The nomenclature used for the systems shown on these trees is given on Table B-13. It should be noted that these accident sequences each have a "plant damage state" as the end point rather than "onset of core damage". [That is, each sequence involves sucess or failure of the containment safety systems (the containment sprays and fan coolers) as well as pressure relief and core cooling systems]. Based on these event trees, a total of 148 so-called "terminal event sequences" were quantified in the original SSMRP. The terminal event sequences whose contributions dominated the original SSMRP results (as identified on Table 7.4 of the SSMRP final Zion report, Reference B-1) are shown on Table B-14. The contributions (and ranking) of the top 15 dominant are given on this table. As can be seen, these 15 sequences contributed 88.5 % to the total core damage point estimate* frequency (3.53e-6 per year). The rest of the core damage frequency is spread among the remaining 133 terminal event sequences.

---

*The reported SSMRP point estimate frequency was computed using all component failure probabilities set to their median values and a single "best estimate" hazard curve. This point estimate is significantly lower than the true mean value computed in this work using the full set of Zion hazard curves.

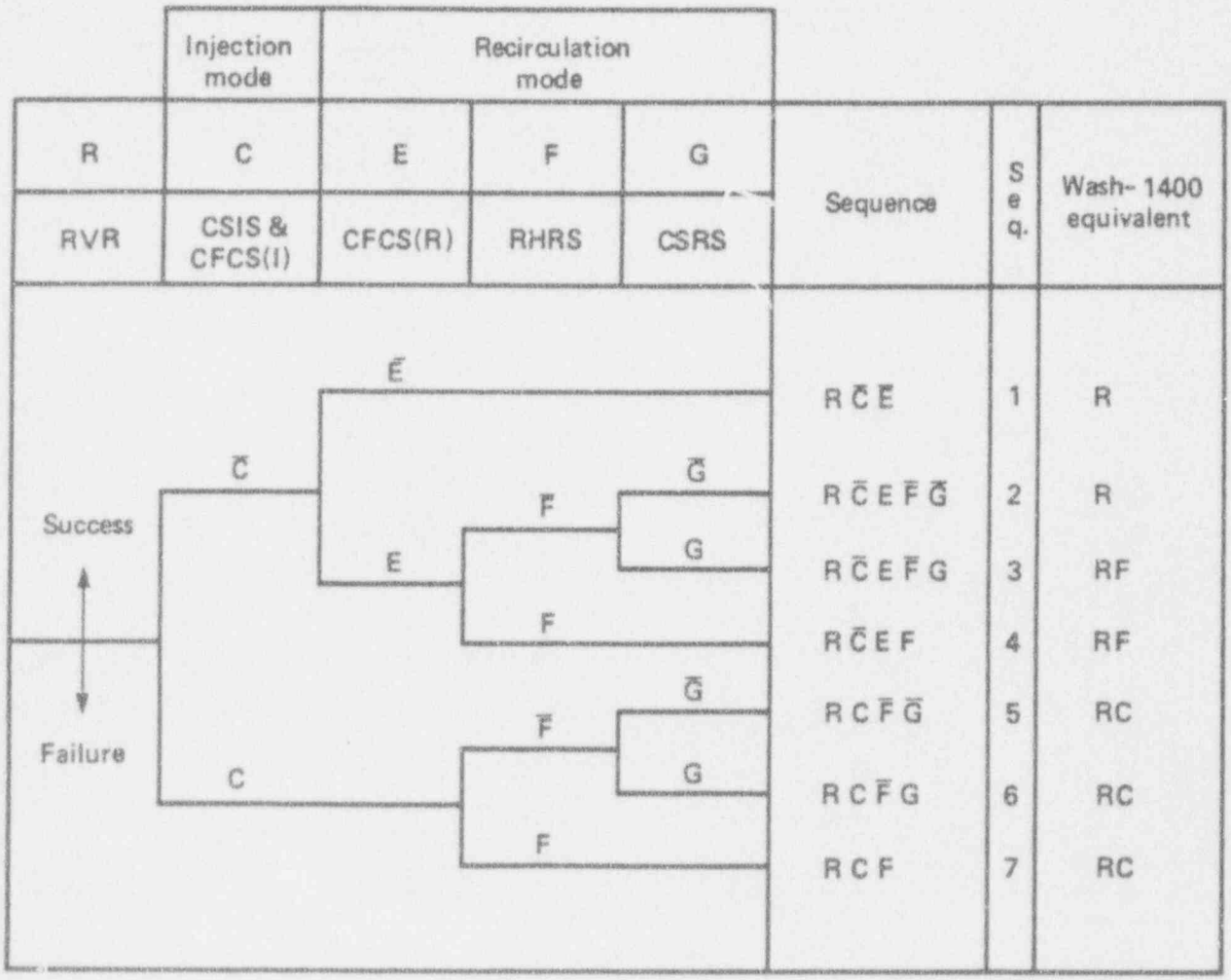

Figure B-74 Reactor Vessel-Rupture (TES) Event Tree

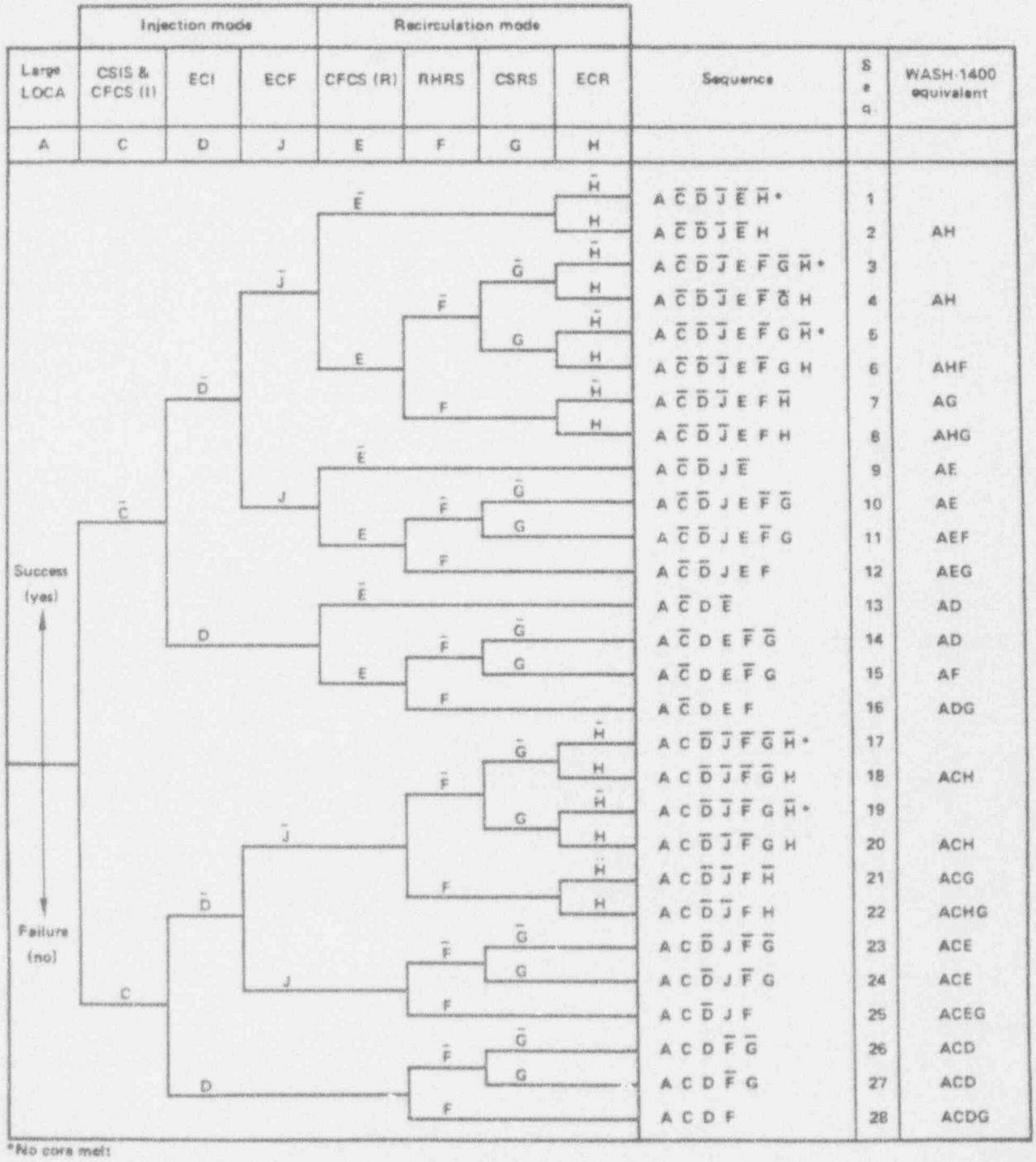

Figure B-75 Large LOCA (TES) Event Tree

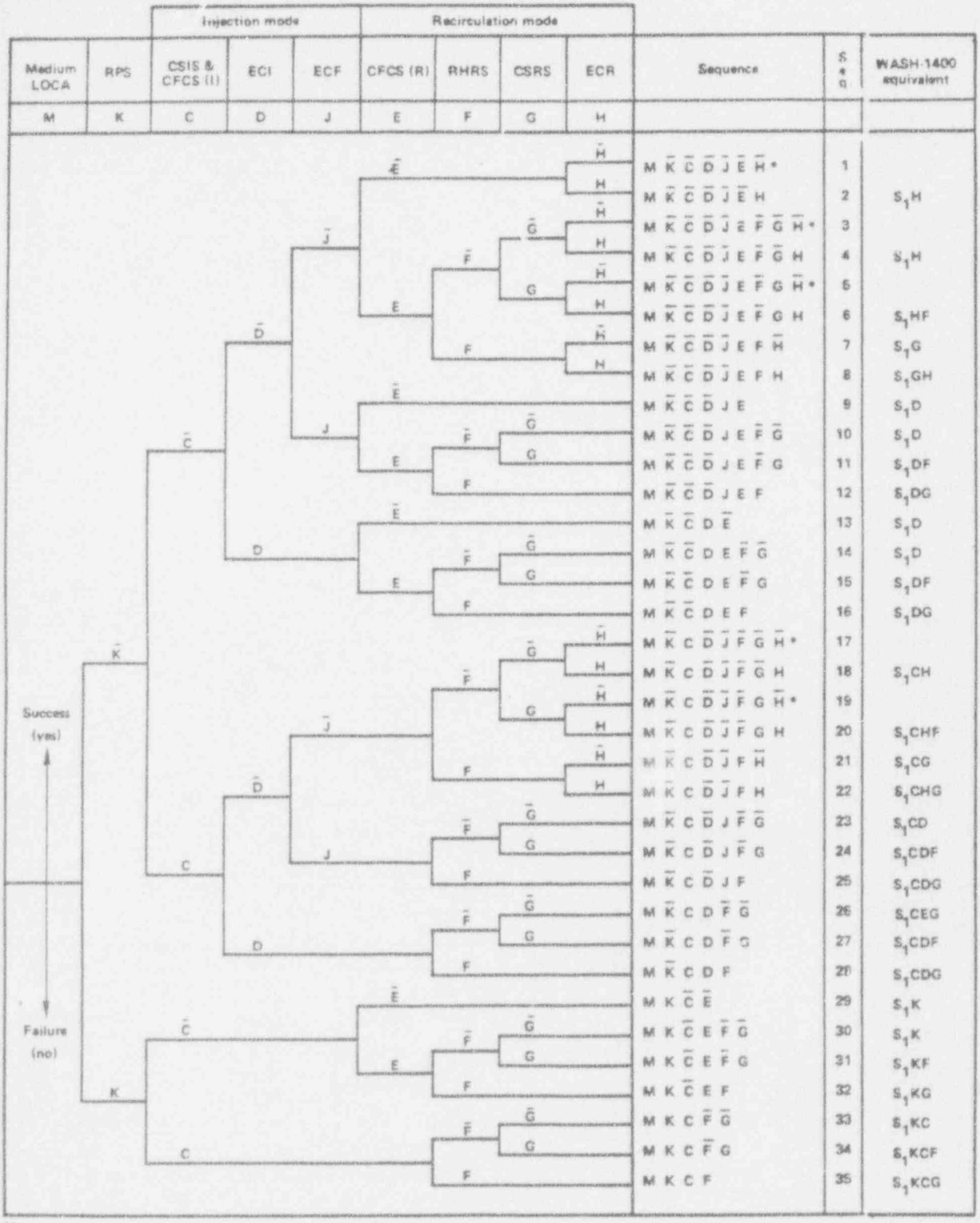

Figure B-76 Medium LOCA (TES) Event Tree

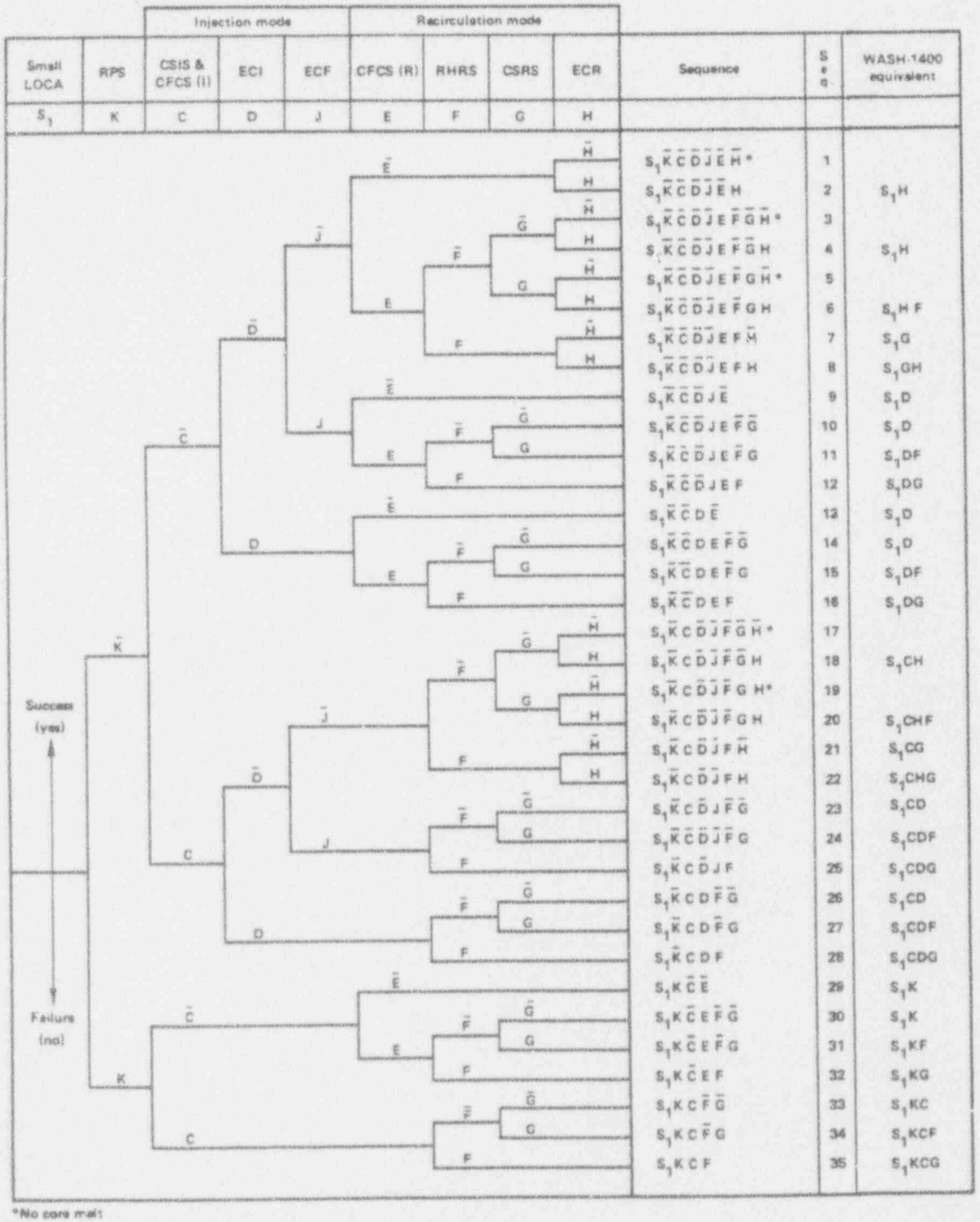

*No core melt

Figure B-77 Small LOCA (TES) Event Tree

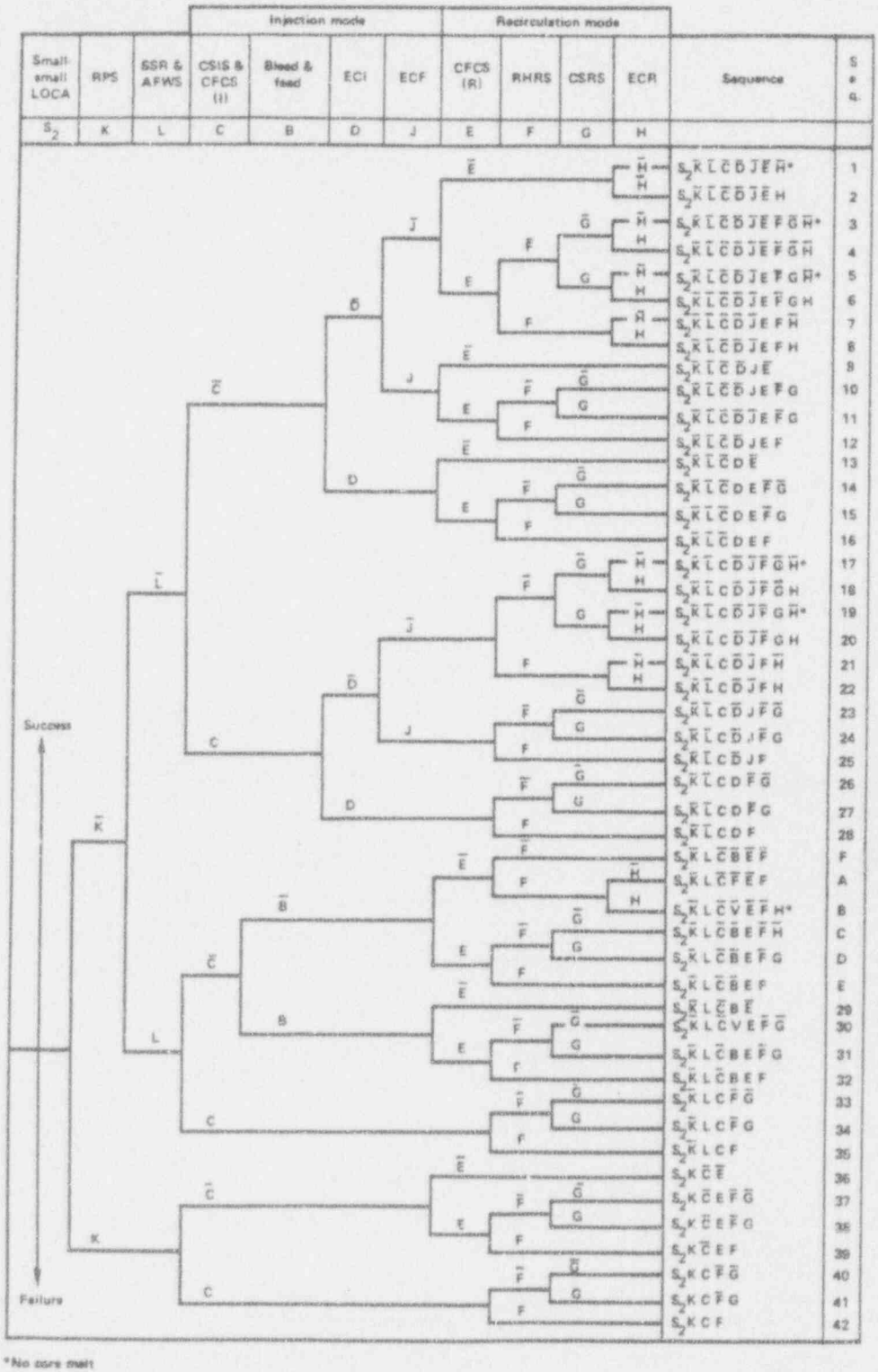

Figure B-78 Small-small LOCA (TES) Event Tree Assuming Feed-and-Bleed Capability

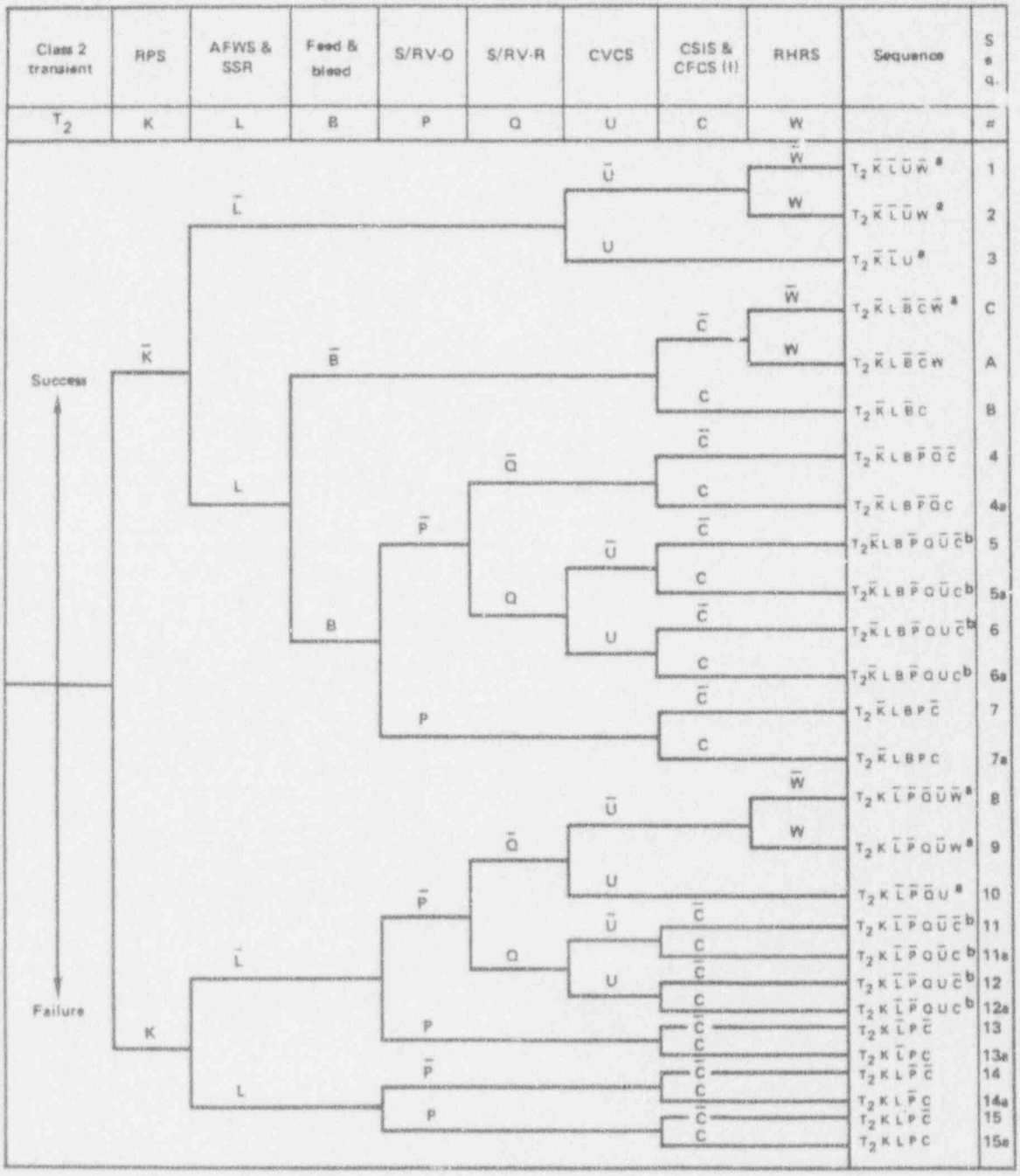

[a] No core melt

[b] These accident sequences include the following events: safety relief valve opens and fails to reclose, which initiates a LOCA. The LOCA event tree is appended to the footnoted sequences.

Figure B-79 Class 2 Transient (TES) Event Tree

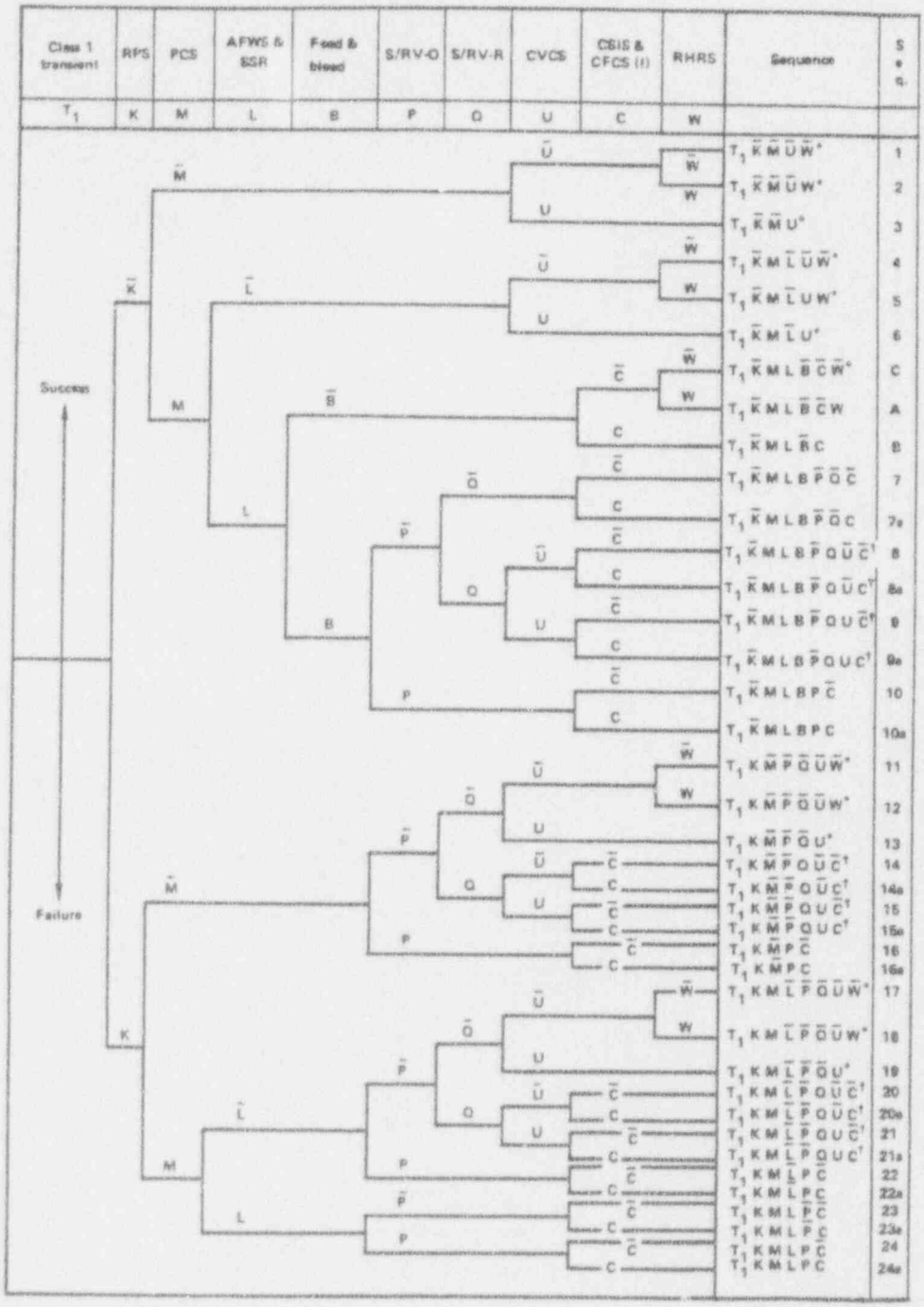

*No core melt

†These accident sequences include the following events: safety relief valve opens and fails to reclose, which initiates a LOCA. The LOCA event tree is appended to the footnoted sequences.

Figure B-80 Class 1 Transient (TES) Event Tree

Table B-13

SSMRP Zion Event Tree Nomenclature

Symbol	System/Function
B	Bleed and Feed Cooling Mode
C	Containment Sprays [CSIS and CFCS(I)]
D	Emergency Core Cooling (Injection) [ECI]
E	Containment Fan Coolers (Recirculation) [CFCS(R)]
F	Residual Heat Removal System [RHRS]
G	Containment Spray Recirculation System [CSRS]
H	Emergency Core Cooling (Recirculation) [ECR]
J	ECCS Function Effectiveness [ECF] (not used, J = 0.0)
K	Reactor Protection System [RPS]
L	Auxillary Feedwater System [AFWS]
M	Power Conversion System [PCS]
P	Safety Relief Valves - Open [SRV-O]
Q	Safety Relief Valves - Close [SRV-R]

Table B-14

Dominant Terminal Event Sequences and Relative Contributions
From Original SSMRP Calculations

Dominant Sequence	Description	Annual Frequency	Fraction	Rank
TES-T2-4	T2*(-K)*L*B*(-P)*(-Q)*(-C)	1.28e-6	36.3%	1
TES-T1-7	T1*(-K)*M*L*B*(-P)*(-Q)*(-C)	7.34e-8	2.1%	9
TES-SSLOCA-35	SSLOCA *(-K)*L*C*F	3.63e-7	10.3%	2
TES-RVR-7	RVR*C*F	1.50e-7	4.2%	7
TES-RVR-6		8.95e-9	0.3%	13
TES-SLOCA-21	SLOCA*(-K)*C*(-D)*(-J)*F*(-H)	3.26e-7	9.2%	3
TES-SSLOCA-21	SSLOCA*(-K)*(-L)*C*(-D)*(-J)*F*(-H)	1.54e-7	4.4%	6
TES-SSLOCA-34		4.25e-8	1.2%	12
TES-LLOCA-27		4.95e-8	1.4%	11
TES-MLOCA-27		5.70e-9	0.2%	14
TES-SSLOCA-D		3.12e-9	0.1%	15
TES-LLOCA-13	LLOCA*(-C)*D*(-E)	2.20e-7	6.2%	5
TES-SLOCA-28	SLOCA*(-K)*C*D*F	3.01e-7	8.5%	4
TES-RVR-1	RVR*(-C)*(-E)	9.40e-8	2.7%	8
TES-MLOCA-13		4.80e-8	1.4%	10
	Total	3.12e-6	88.5%	

Because the 15 dominant terminal event sequences contributed only 88.5% of the total, and because the thrust of this project was to determine the impact of reduced shear wall stiffnesses on core damage frequency, the original SSMRP terminal event sequence trees were "collapsed" down to a corresponding set of core damage event trees. This is done by grouping and combining the individual terminal event tree sequences so that the containment systems (which in the SSMRP did not contribute to core damage but only split the core damage frequency into different plant damage states) drop out. For example, for each sequence associated with success of the containment spray system (CSIS) there is a corresponding accident sequence involving failure of the CSIS, and so forth. There is no loss of generality in collapsing the terminal event sequence trees down to core damage event trees, since the total accident frequency (i.e., the sum of all the accident sequence frequencies) computed from either set of trees will be the same.

The core damage event trees developed from the original SSMRP terminal event sequence trees are shown in Figures B-81 to B-86. (No tree is now needed for the RVR event, since the occurrence of the RVR initiating event implies core damage.) These trees identify 30 core damage accident sequences, which are described on Table B-15. These accident sequences involve the same Boolean and logical component equations as did the original terminal event sequences, except that - for the sequence Booleans - the terms involving the containment systems must be deleted. (This is true since the SSMRP used simple step functions for the fragilities of the containment systems rather than fault trees and logical component equations and thus the containment terms were treated as logically independent of the remainder of the expression).

B.5.3 Accident Sequences

Of the complete set of 30 core damage accident sequences corresponding to the 7 initiating events identified on the core damage event trees, four sequences were screened out in the process of solving the accident sequences for their expressions in terms of component (basic event) failures, and all sequences involving failure of the Reactor Protection System (K) were dropped from further consideration based on the value for random RPS failure frequency used in the SSMRP (3.0E-05 per demand). Thus, a total of 15 accident sequences were evaluated in this study. These 15 sequences are presented in Table B-16, which includes the definitions of the Boolean sequences that were solved for each accident sequence. (The number of Booleans is less than the number of accident sequences because several accident sequences may utilize the same Boolean expression even though the initiating event may be different.) Also identified on this table are the complement expressions which must be included in the sequence quantification, since, at high PGA levels, success probabilities may be significantly less than unity. Table B-17 describes the abbreviations used for the accident sequences in Table B-16.

The Boolean expressions (in terms of component failure basic events) for the terminal event sequences and individual systems developed in the

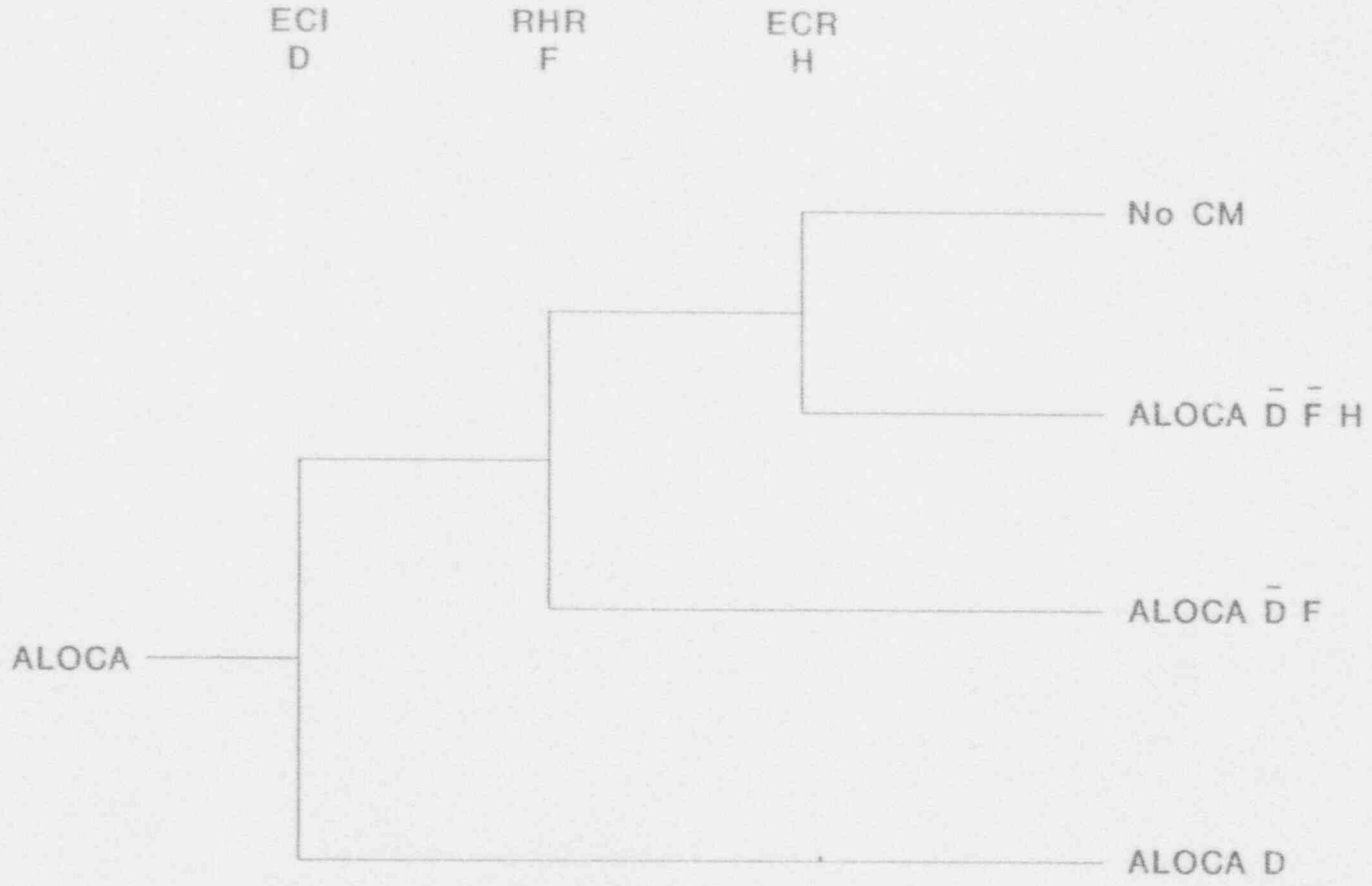

Figure B-81 Large LOCA Core Damage Event Tree

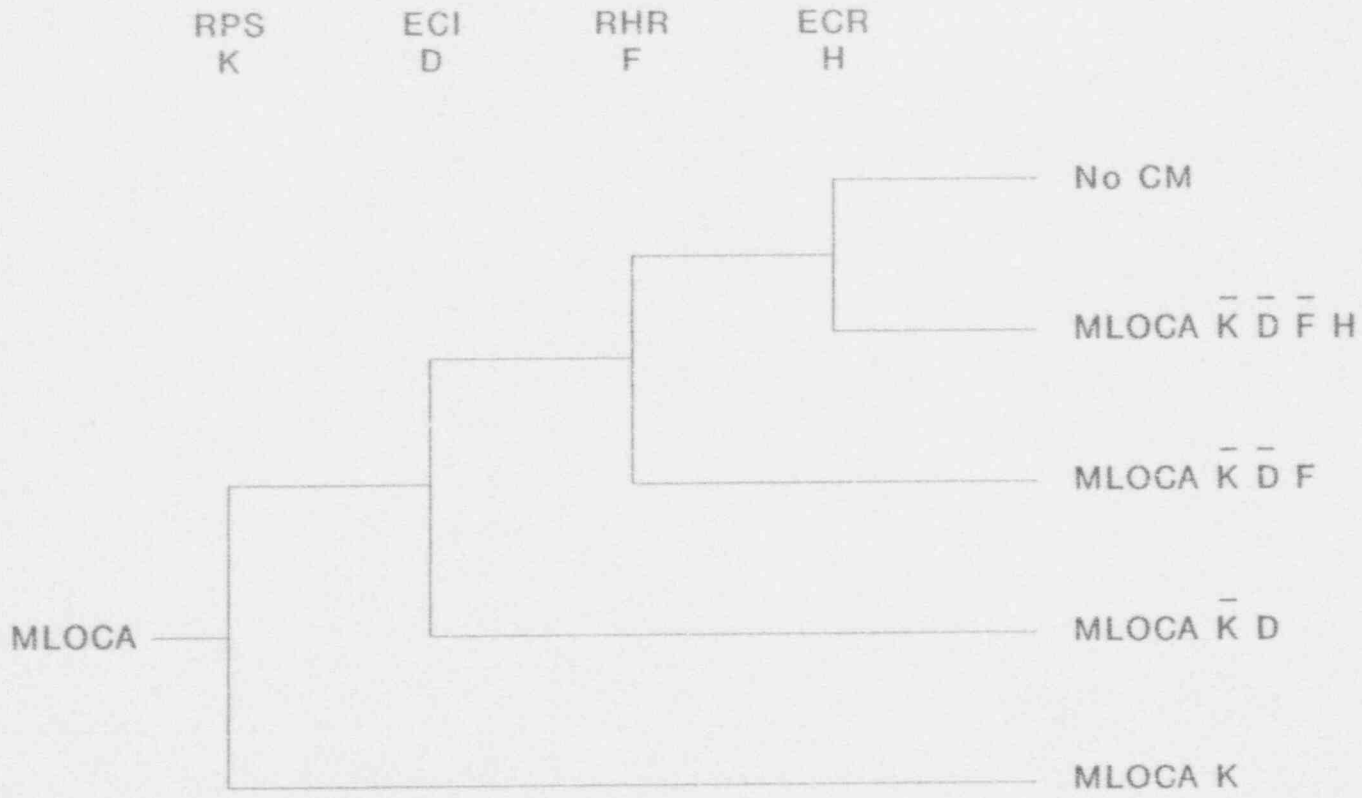

Figure B-82 Medium LOCA Core Damage Event Tree

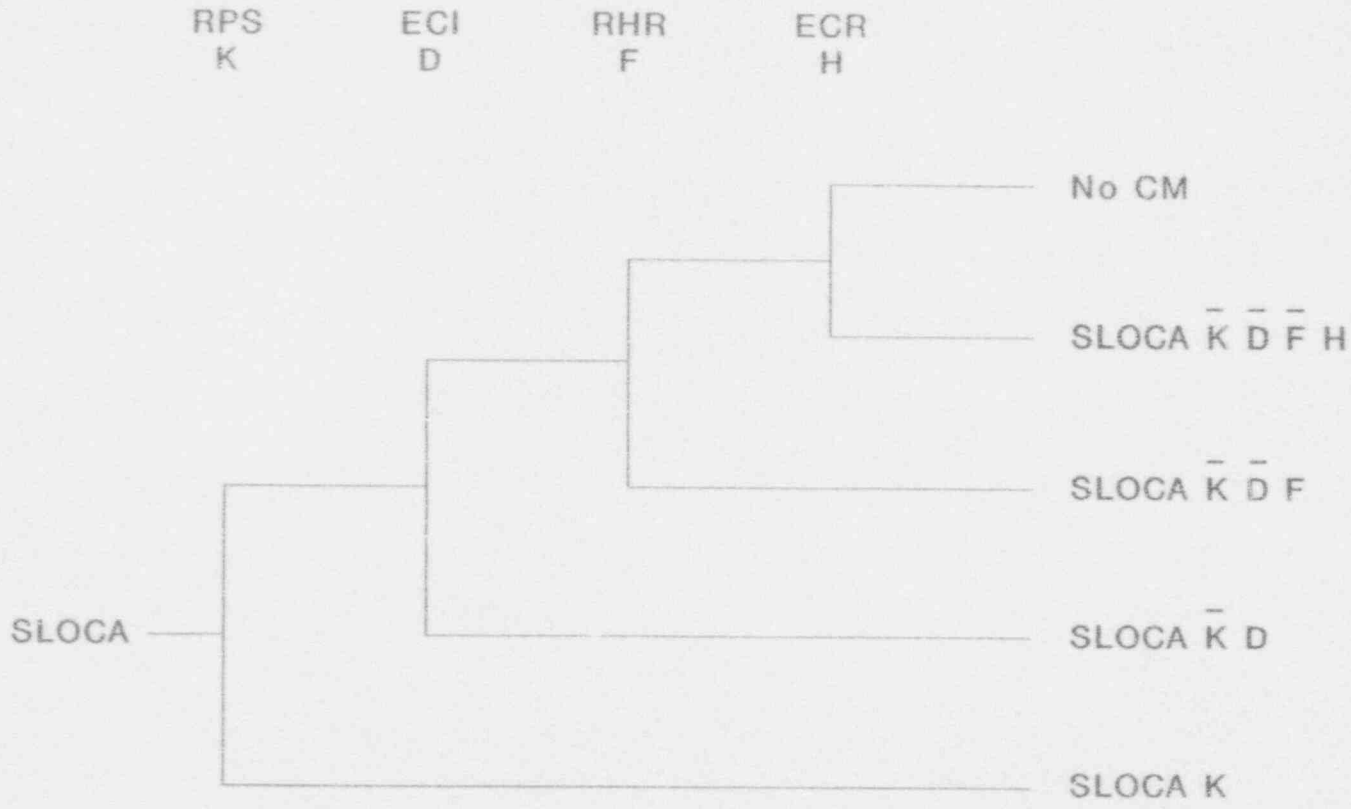

Figure B-83 Small LOCA Core Damage Event Tree

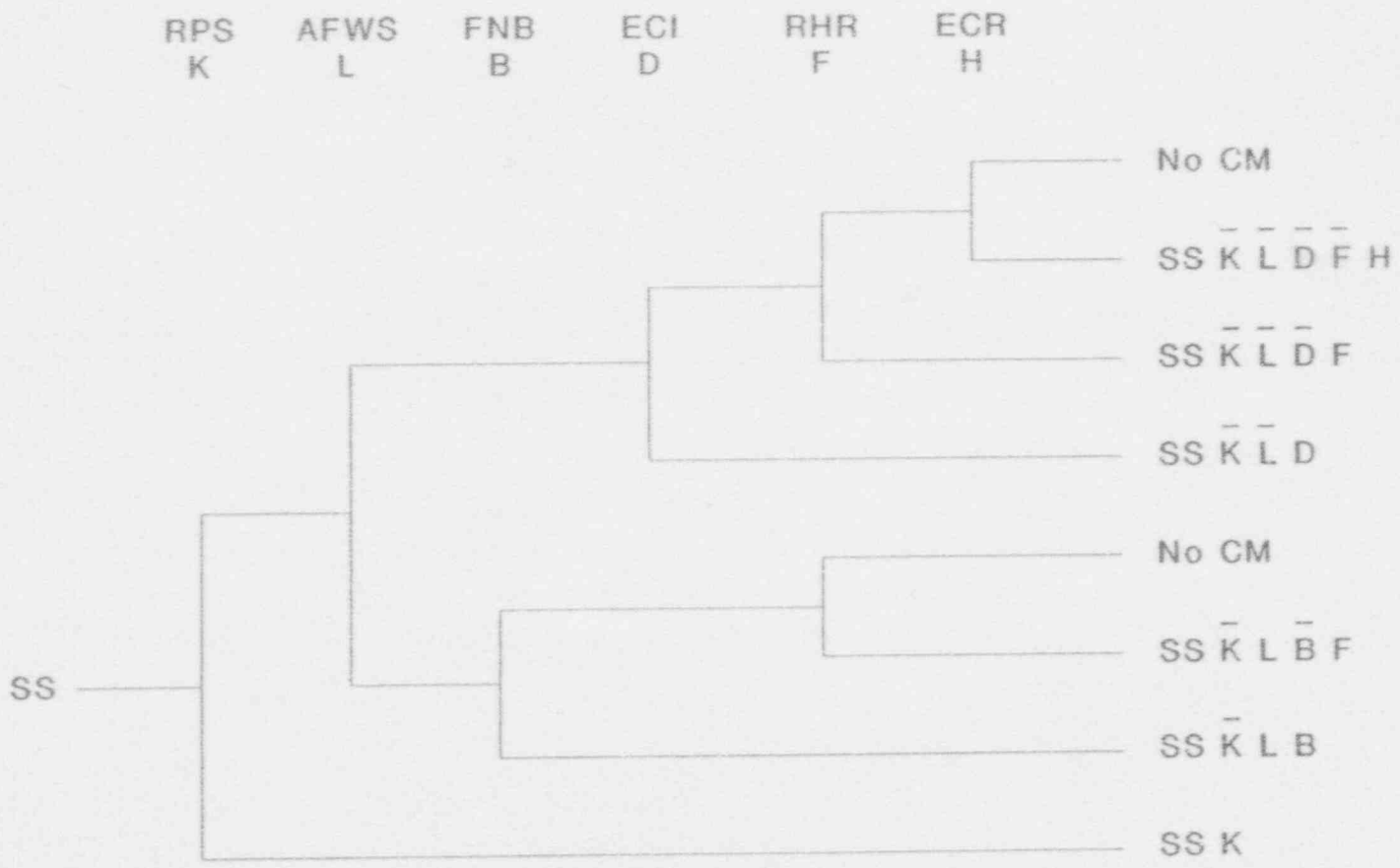

Figure B-84 Small-Small LOCA Core Damage Event Tree

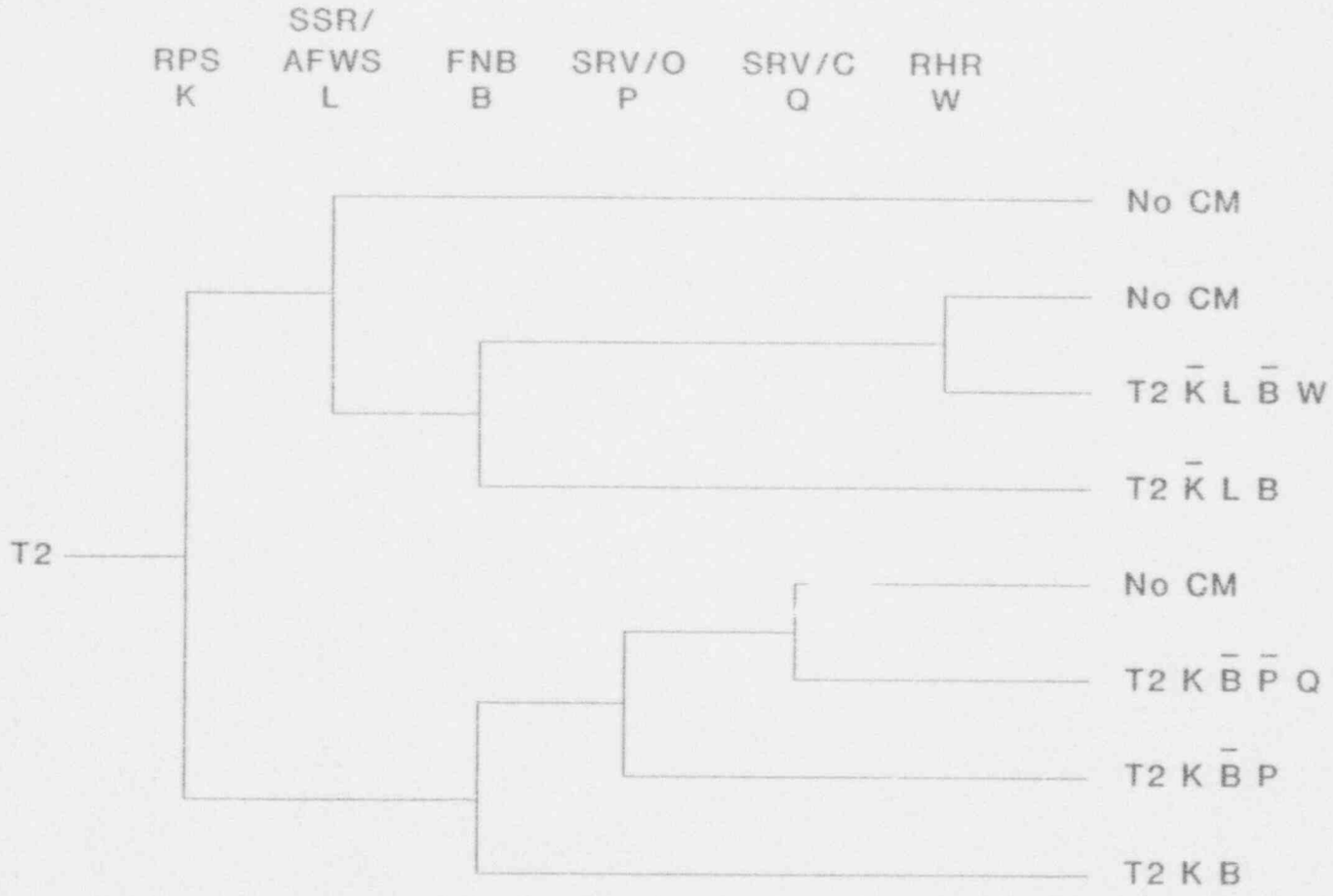

Figure B-85 Class 2 Transient Core Damage Event Tree

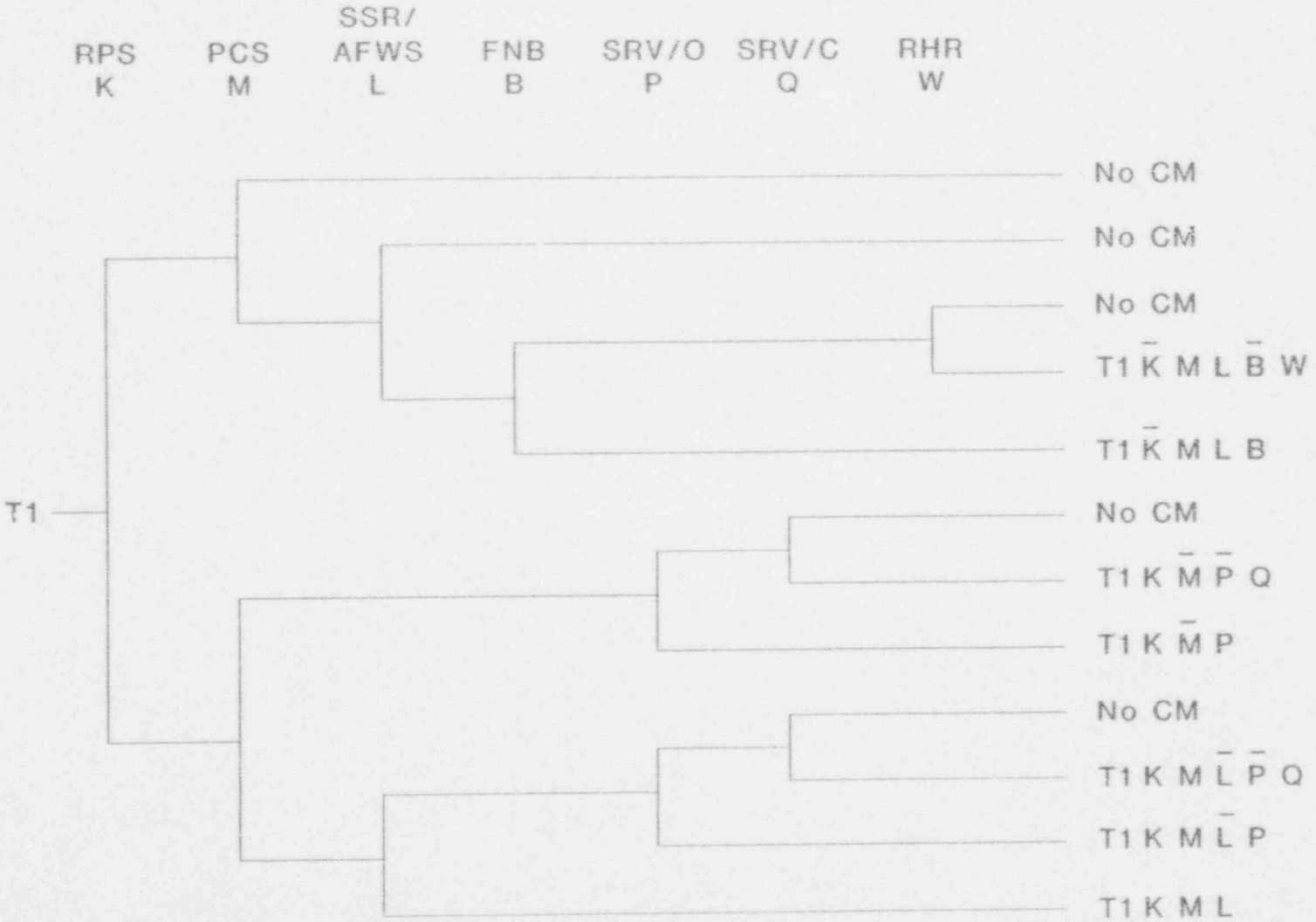

Figure B-86 Class 1 Transient Core Damage Event Tree

Table B-15

Zion Core Damage Accident Sequences

	Sequence	Status	Contributing Dominant TES Sequences
1.	RVR		TES-RVR-7 (#7), TES-RVR 1 (#8), TES-RVR-6 (#13)
2.	ALOCA-1 = ALOCA * $\bar{D}$ $\bar{F}$ H		
3.	ALOCA-2 = ALOCA * $\bar{D}$ F		
4.	ALOCA-3 = ALOCA * D		TES-ALOCA-27 (#5), TES-ALOCA-27 (#10)
5.	MLOCA-1 = MLOCA * $\bar{K}$ $\bar{D}$ $\bar{F}$ H	(0)	
6.	MLOCA-2 = MLOCA * $\bar{K}$ $\bar{D}$ F		
7.	MLOCA-3 = MLOCA * $\bar{K}$ D		TES-MLOCA-13 (#11), TES-MLOCA-27 (#14)
8.	MLOCA-4 = MLOCA * K		
9.	SLOCA-1 = SLOCA * $\bar{K}$ $\bar{D}$ $\bar{F}$ H	(0)	
10.	SLOCA-2 = SLOCA * $\bar{K}$ $\bar{D}$ F		TES-SSLOCA-21 (#3)
11.	SLOCA-3 = SLOCA * $\bar{K}$ D		TES-SLOCA-28 (#4)
12.	SLOCA-4 = SLOCA * K		
13.	SSLOCA-1 = SSLOCA * $\bar{K}$ $\bar{L}$ $\bar{D}$ $\bar{F}$ H	(0)	
14.	SSLOCA-2 = SSLOCA * $\bar{K}$ $\bar{L}$ $\bar{D}$ F		TES-SSLOCA-21 (#6)
15.	SSLOCA-3 = SSLOCA * $\bar{K}$ $\bar{L}$ D		
16.	SSLOCA-4 = SSLOCA * $\bar{K}$ L $\bar{B}$ F		TES-SSLOCA-D (#15)
17.	SSLOCA-5 = SSLOCA * $\bar{K}$ L B		TES-SSLOCA-35 (#2), SSLOCA-34 (#12)
18.	SSLOCA-6 = SSLOCA * K	Negligible	
19.	T2-1 = T2 * $\bar{K}$ L $\bar{B}$ W	(0)	
20.	T2-2 = T2 * $\bar{K}$ L B		TES-T2-4 (#1)
21.	T2-3 = T2 * K $\bar{L}$ $\bar{P}$ Q	Negligible	
22.	T2-4 = T2 * K $\bar{L}$ P	Negligible	
23.	T2-5 = T2 * K $\bar{L}$	Negligible	
24.	T1-1 = T1 * $\bar{K}$ M L $\bar{B}$ W		
25.	T1-2 = T1 * $\bar{K}$ M L B		TES-T1-7 (#9)
26.	T1-3 = T1 * K $\bar{M}$ $\bar{P}$ Q	Negligible	
27.	T1-4 = T1 * K $\bar{M}$ P	Negligible	
28.	T1-5 = T1 * K M $\bar{L}$ $\bar{P}$ Q	Negligible	
29.	T1-6 = T1 * K M $\bar{L}$ P	Negligible	
30.	T1-7 = T1 * K M L	Negligible	

Table B-16

Non-negligible Zion Core Damage Accident Sequences

	Core Damage Sequence	Logical Component Groups	Complements
1.	RVR		
2.	ALOCA-1 = ALOCA * $\bar{D}$ $\bar{F}$ H	ZZ-ECR-LL	(-ZZ-ECI-LL) * (-ZZ-RH-R-L)
3.	ALOCA-2 = ALOCA * $\bar{D}$ F	ZZ-RH-R-L	(-ZZ-ECI-LL)
4.	ALOCA-3 = ALOCA * D	ZZ-ECI-LL	
5.	MLOCA-2 = MLOCA * $\bar{K}$ $\bar{D}$ F	ZZ-RH-R-L	(-K) (-ZZ-ECI-ML)
6.	MLOCA-3 = MLOCA * $\bar{K}$ D	ZZ-ECI-ML	(-K)
7.	SLOCA-2 = SLOCA * $\bar{K}$ $\bar{D}$ F	ZZ-RH-R-L	(-K) (-ZZ-ECI-SL)
8.	SLOCA-3 = SLOCA * $\bar{K}$ D	ZZ-ECI-SL	(-K)
9.	SSLOCA-2 = SSLOCA * $\bar{K}$ $\bar{L}$ $\bar{D}$ F	ZZ-RH-R-L	(-K)(-ZZ-AFWS-L)(-ZZ-ECI-SS)
10.	SSLOCA-3 = SSLOCA * $\bar{K}$ $\bar{L}$ D	ZZ-ECI-SS	(-K)(-ZZ-AFWS-L)
11.	SSLOCA-4 = SSLOCA * $\bar{K}$ L $\bar{B}$ F	SSLOCA-D	(-K)(-FNB-DUMMY)
12.	SSLOCA-5 = SSLOCA * $\bar{K}$ L B	T1-7	(-K)
13.	T2-2 = T2 $\bar{K}$ L B	LB = T2-4	(-K)
14.	T1-1 = T1 $\bar{K}$ M L $\bar{B}$ W	MLW = T1-A	(-K)(-FNB-DUMMY)
15.	T1-2 = T1 $\bar{K}$ M L B	MLB = T1-7	(-K)

Table B-17

SSMRP Zion Boolean Expression Nomenclature

SSLOCA-D*	Boolean expression for L*F in SSLOCA event
T_1-7*	Boolean expression for M*L*B in Type 1 Transient
T_1-A*	Boolean expression for M*L*W in Type 1 Transient
T_2-4*	Boolean expression for L*B in Type 2 Transient
T_2-A*	Boolean expression for L*W in Type 2 Transient
ZZ-ECI-LL	Boolean expression for LLOCA Core Cooling (Injection)
ZZ-ECI-ML	Boolean expression for MLOCA Core Cooling (Injection)
ZZ-ECI-SL	Boolean expression for SLOCA Core Cooling (Injection)
ZZ-ECI-SS	Boolean expression for SSLOCA Core Cooling (Injection)
ZZ-ECR-LL	Boolean expression for LLOCA Core Cooling (Recirculation)
ZZ-ECR-ML	Boolean expression for MLOCA Core Cooling (Recirculation)
ZZ-ECR-SL	Boolean expression for SLOCA Core Cooling (Recirculation)
ZZ-ECR-SS	Boolean expression for SSLOCA Core Cooling (Recirculation)
AFWS-L	Boolean expression for AFWS in SSLOCA event
AFWS-T	Boolean expression for AFWS in Transient events
FNB-DUMMY	Boolean expression for Feed and Bleed cooling mode
ZZ-RH-R-L	Boolean expression for Residual Heat Removal in LOCAs
ZZ-RH-R-T	Boolean expression for Residual Heat Removal in Transients

original SSMRP program (and obtained from computer output for the final results reported in Ref. B-1) were used in this evaluation of the effect of shear wall degradation on seismic risk. There is no approximation in this, since these Booleans apply exactly to the core damage sequences used here.

Further, the same dominant components are involved in these expressions since very conservative screening criteria were used in the SSMRP program in solving the fault trees and event trees for the accident sequences in terms of the basic failure events. That is, in the SSMRP, screening failure probabilities were developed for each component on the fault trees for use in the screening process, and these probabilities were based on very conservative estimates of the seismic response that the components could experience. These screening response estimates were more than adequate to encompass the increases in responses which were found (due to degrading the shear wall stiffnesses) in this program. Thus the Boolean sequence expressions developed in the SSMRP program were directly useable in the context of this shear wall degradation study.

The dominant cutsets in the Boolean expressions were identified from computer printout of all the terminal event sequences and systems sequences computed for the SSMRP Zion seismic PRA. The Level 4 cutset listings (0.32 - 0.42g) were used, and all cutsets whose conditional probability (i.e., without hazard curve probability) was greater than 8e-4 were kept. This assured that no cutsets that could possibly contribute to the total core damage frequency at any level were lost. The actual equations for the sequences, systems and complement events expressions are given at the end of this Appendix (Attachment to Appendix B - Accident Sequence Expressions).

B.5 Accident Sequence Evaluation

A complete uncertainty analysis was performed on the 15 (non-negligible) accident sequences described above. A Monte Carlo analysis was used for the analysis. Thus, the expression for the unconditional accident sequence frequencies (and for core damage frequency), shown as below:

$$ACC_j = \int P(ACC_j, PGA) f_{eq}(PGA) d(PGA)$$

where

$P(ACC_j, PGA)$ is the conditional accident sequence frequency as a function of PGA, and

$f_{eq}(PGA)$ is the probability distribution function for the hazard curve,

was randomly sampled varying the hazard curve parameters, the random failure frequencies, and the seismic response and fragility parameters. From the accumulated values of each accident sequence frequency and the core damage frequency, exact statistics on their distributions are

directly obtainable. The result is an estimate of the mean annual frequency of each accident sequence as well as of the total core damage, plus a description of the probability distributions associated with these estimates.

In addition, a mean point estimate quantification (in which all random parameters were set to their mean values and a single quantification is made) was performed for each case of original or degraded stiffness. This mean point estimate allows for an efficient evaluation of each individual component's importance to the total core damage frequency and a determination of the relative contribution of different earthquake levels to the total. (Experience has shown that such mean point estimate calculations yield results which are very close to the true mean results obtained from the full Monte Carlo uncertainty analysis.)

B.5.4.1 Benchmarking Against Original SSMRP Calculations

The first step in re-computing the risk at Zion was to benchmark our models against the original SSMRP Zion seismic risk assessment results. This was necessary due to the fact that all the original Zion input and output files could could not be retrieved. For example, all the original SSMRP finite element structural models for Zion were located, and thus floor responses as well as piping responses could be re-computed using the same (original) structural concrete stiffnesses. However, the actual response files giving the results of these calculations were not obtainable. Thus, validating the response analyses had to be done using the reported failure probabilities of the different components at different earthquake levels. Similarly, the files of correlations between responses were not available. However, these correlation files had been examined in the past (for another project) and simplified rules for specifying correlations between responses had been developed. These simplified rules were used in this study (see Sect. B.3.4.3).

Further, although fragilities for most of the components were known precisely, the files listing the various individual piping scale factors were not available. (Recall from Section B.4.2 that a master piping fragility is used for all piping, and each piping segment has a different median failure moment based on its size, material, connection type, etc., based on its associated piping scale factor, β_i.) Therefore, it was necessary to estimate this scale factor for each individual pipe segment from the reported piping failure probabilities.

The first step in the benchmarking process was to reproduce the values of the frequencies of the initiating events. Originally, the frequency of LOCAs were determined using anchorage failures of the reactor coolant pumps and steam generators and failures of different combinations of pipes. This could not be reproduced directly since the piping scale factor and correlation files were not available. Therefore, an equivilent fragility for each LOCA initiating event was developed from the table of initiating events given in the SSMRP Final Zion Report (Reference B-1) for each earthquake acceleration level. (This involved removing the hierarchy

assumed in constructing the original table, and then curve-fitting the occurrence frequencies to obtain a median capacity (as a function of pga) and an uncertainty (β_{rr}) for each LOCA initiating event.

The Type 2 transient event was dominated by LOSP (for which the exact fragility was known) and hence in our model, only LOSP was used in modeling this initiator. As in the SSMRP, the remaining Type 1 transient initiator was computed based on the condition that the sum of the initiator frequencies must equal unity at each earthquake level, as described earlier.

Table B-18 compares the original initiating event frequencies and those calculated by our models at four acceleration levels. Good agreement can be seen.

Note that the same initiating event frequencies were used in both the original and reduced shear wall stiffness cases. This is appropriate since the reduction of structural stiffness has little effect on the initiating event frequencies. This follows from the fact that the LOCA producing piping and support failures are keyed to to the operating floor response which was very little changed by reduced concrete stiffness. And the LOSP failure which totally dominated the Type 2 transient initiator depends only on peak ground acceleration.

The next step was to compare the conditional accident sequence probabilities at the different earthquake levels. This comparison allowed us to verify or correct the assumptions that were made as to the piping scale factors for the different piping segments. It also allowed us to verify or correct the response input to each individual component by directly comparing the reported failure probabilities for individual components with our model's calculations. The exact response input was not known exactly because - within a given earthquake acceleration level - the individual component responses were taken to be a probabilistically weighted average of all the computed time history responses in that interval. These exact response values used within each interval were specified in the response files that could not be located. (Knowing the exact response point in an interval is needed only for the benchmark comparison, and does <u>not</u> affect results calculated directly for this study).

The final step in the benchmarking process was to compare the terminal event sequence and core damage frequencies computed with the dominant sequence models extracted and coded for this project and those reported for the original SSMRP results for Zion. The latter, however, were computed as a function of peak ground acceleration based on a hypothetical rock outcrop at the site. By contrast, in this study, we developed the responses in terms of peak ground acceleration based on the soil surface. Thus it was necessary to determine the relationship between rock outcrop acceleration and free-field surface acceleration in order to make the comparison. An estimate of this relation was developed using spectra developed for both rock outcrop and the soil surface. This relation was used to adjust the original (rock outcrop) hazard curve to a soil surface

Table B-18 (a)

Conditional Probabilities of Initiating Events
Original SSMRP Zion Analysis
(Table 7.3 of Reference B-1)

Initiating event	Earthquake acceleration level (pga) 0.258g	0.512g	0.722g	0.943g
RVR	7.4E-07	7.7E-03	9.7E-03	1.7E-01
LLOCA	2.2E-05	1.8E-02	3.8E-02	1.9E-01
MLOCA	6.0E-05	1.1E-02	3.6E-02	5.5E-02
SLOCA	6.5E-04	8.7E-02	2.6E-01	3.0E-01
SSLOCA	1.1E-02	1.5E-01	2.8E-01	1.9E-01
T2	8.1E-01	7.3E-01	3.7E-01	9.2E-02
T1	1.8E-01	6.0E-04	1.1E-06	3.5E-08

Table B-18 (b)

Conditional Probabilities of Initiating Events
Using Fitted Curves for Re-analysis of Zion

Initiating event	Earthquake acceleration level (pga) 0.258g	0.512g	0.722g	0.943g
RVR	3.0E-06	2.0E-03	2.0E-02	7.8E-02
LLOCA	2.2E-05	5.5E-03	3.8E-02	1.1E-01
MLOCA	6.0E-05	6.7E-03	3.5E-02	8.7E-02
SLOCA	6.4E-04	7.2E-02	2.6E-01	4.0E-01
SSLOCA	1.1E-02	1.7E-01	2.8E-01	2.1E-01
T2	7.9E-01	7.4E-01	3.7E-01	1.2E-01
T1	2.0E-01	9.8E-04	6.1E-06	3.7E-08

pga scale. (This adjustment was required only for the benchmarking comparisons, and played no part in the remainder of this study.)

Using this adjusted hazard curve with the terminal event sequence logical models extracted from the SSMRP output produced an overall (comparable point estimate) core damage frequency of 3.0e-6 per year for the top six dominant sequences. This compares well with the final SSMRP Zion results, which reported a total core damage frequency (for all 146 sequences) of 2.6e-6 per year reported for the same six dominant sequences, as shown below:

	SSMRP	This Study
TES-RVR-7	1.5E-7	0.7E-7
TES-SLOCA-21	3.3E-7	4.0E-7
TES-SLOCA-28	3.0E-7	3.9E-7
TES-SSLOCA-21	1.5E-7	0.9E-7
TES-SSLOCA-35	3.6E-7	4.7E-7
TES-T2-4	1.3E-6	1.6E-6
Total	2.6E-6	3.0E-6

This agreement - both in terms of initiating event frequencies, conditional component failure probabilities and core damage frequencies - demonstrated that the responses, fragilities and logical sequence models had been appropriately extracted, modeled and coded. These benchmarked models were then used to perform the study comparing the seismic risk at Zion both with and without reduction in concrete shear wall stiffness.

Note that the benchmark comparisons were made for the terminal event sequences (as described in Section B.5.2). The shear wall stiffness reduction studies presented below are based on the 15 core damage frequency sequences described on Table B-15. This was done since these 15 accident sequences include all the core damage sequences implied by the SSMRP event trees. (By contrast, if we had restricted ourselves to the terminal event sequences, we would have been able to study only the dominant TES sequences which contribute only 80% of the total.) However, the benchmarking described above also validates the core damage sequence expressions since the same Boolean expressions are utilized in both sequence formulations.

B.5.4.2 Core Damage Frequency Results With No Stiffness Reduction

The 15 core damage accident sequences were fully quantified using component random failures and the seismic fragilities and responses plus their associated random and systemic variabilities. Using this benchmarked model of the seismic accident sequences for Zion, and performing a full Monte Carlo uncertainty analysis, a new overall core damage frequency was computed. The total mean core damage frequency for this base case was computed to be 5.23E-5 per year using the LLNL seismic hazard curves and 1.05E-5 per year using the Zion PRA discrete family of hazard curves. The relative contributions of the accident sequences are

shown in Table B-19. Table B-20 shows the percentiles of the distributions from the Monte Carlo analysis for both sets of hazard curves. Relative importance of the basic events to these results are presented in the point estimate results presented below.

Description of Accident Sequences

The dominant accident sequences (based on the LLNL hazard curves) are as shown below:

T2-2	31%
SLOCA-2	20%
SSLOCA-2	16%
SSLOCA-5	7%
SLOCA-3	6%
ALOCA-3	5%
RVR	4%
T1-2	3%

These seven sequences contribute 94 percent of the computed core damage frequency.

The dominant sequence is the loss of offsite power transient T2-2 which involves success of the RPS but failure of both the AFWS and feed and feed cooling. The dominant component failures are uplift of the AFT building basemat, and failure of the crib house roof (which fails all six service water pumps). Failure of the AFT building shear wall also contributes to this sequence but with lower impact.

The second most dominant sequence is SLOCA-2. This is a late core damage sequence involving successful ECI but failure of the RHR ystem. Failure of the RHR system is totally dominated by a single pipe and several pairs of pipes passing between the AFT building and the containment building. The large strains induced in this (interbuilding) piping are due to relative motion between the buildings and are not due to inertia induced stresses. The AFT building and the containment building are less than 2 feet apart at the point where these pipes run between the buildings, and it is differential motions which give rise to the large displacement-induced strains.

The third most important sequence, SSLOCA-2 is essentially the same as the SLOCA-2, and again involves failure of the RHR system and a late core damage scenario. Failure of the RHR results from the same interbuilding pipes described above.

The fourth dominant sequence is SSLOCA-5 which is a small-small LOCA followed by failure of both the AFWS system and failure of bleed and feed cooling. Dominant component failures in this sequence involve the crib house roof, uplift of the AFT basemat and AFT shear wall failures.

Table B-19

Accident Sequence and Total Core Damage Mean Frequencies
for Zion - Original Stiffnesses

	Accident Sequence	Mean Frequency (per year) LLNL Hazard	Zion PRA Hazard
1	RVR-1	2.02E-6	2.19E-7
2	ALOCA-1	7.93E-9	1.29E-9
3	ALOCA-2	2.52E-8	3.53E-9
4	ALOCA-3	2.57E-6	2.76E-7
5	MLOCA-2	1.05E-6	1.59E-7
6	MLOCA-3	1.50E-6	1.84E-7
7	SLOCA-2	1.06E-5	1.65E-6
8	SLOCA-3	3.16E-6	3.62E-7
9	SSLOCA-2	8.43E-6	2.28E-6
10	SSLOCA-3	1.08E-6	1.42E-7
11	SSLOCA-4	5.02E-7	8.48E-8
12	SSLOCA-5	3.48E-6	5.36E-7
13	T2-2	1.61E-5	3.73E-6
14	T1-1	1.72E-9	3.00E-10
15	T1-2	1.81E-6	8.57E-7
	TOTAL	5.23E-5	1.05E-5

Table B-20

Core Damage Frequency Distribution Percentiles
for Zion - Original Stiffness

	LLNL Hazard	Zion PRA Hazard
Mean	5.23E-5	1.04E-5
Var	4.30E-8	1.55E-10
5%	3.38E-7	1.14E-6
50%	8.30E-6	5.81E-6
95%	1.93E-4	3.48E-5

The fifth dominant sequence is SLOCA-3 which is a small LOCA followed by failure of the ECI system. The dominant component contributing to the failure of ECI is failure of the RWST.

Dominant sequence number six is the large LOCA sequence ALOCA-3 which is an early core damage sequence involving failure of ECI. Dominant components contributing to the failure of ECI are the RHR interbuilding pipes (which, if failed, cause a diversion path) and failure of the RWST. The interbuilding RHR pipes are the dominant contributors to this sequence.

Dominant sequence number seven is the reactor vessel rupture sequence RVR. Components contributing to the RVR event are the support failures of the steam generators and the reactor coolant pumps. Occurrence of this event requires simultaneous failure of two or more steam generator or steam generator/reactor coolant pump pairs (in different reactor coolant loops).

Finally, the eight dominant sequence is the transient with offsite initially available, T1-2. This involves failures of the main feedwater system, the AFWS and bleed and feed cooling. The same dominant components give rise to this sequence as for SSLOCA-5, that is, crib house roof failure or basemat uplift of the AFT building or shear wall failure in the AFT building.

Mean Point Estimate

The mean point estimate is based on using the mean values for all random variables and the mean hazard curve. Table B-21 presents the mean core damage contributions at seven intervals over the LLNL hazard curve for each accident sequence. Table B-22 presents the mean core damage contributions using the Zion PRA hazard curves. The right hand column presents the total contribution of each accident sequence to the total core damage frequency of 5.61E-05 for the LLNL hazard curves and 1.21E-5 for the Zion PRA hazard curves. As can be seen, the incremental contributions from the LOCA events do not become significant until the higher acceleration levels.

An important thing to note from Tables B-21 is the sum of the accident sequence contributions at each earthquake level, as shown at the bottom of each column on these tables. The contributions are seen to be small at the first increment, increasing to a maximum, and then decreasing at higher earthquake levels. This indicates that the bulk of the risk has been captured by integrating over the range 0.10 g to 1.15 g.

Basic Event Importance

Table B-23 lists the dominant contributors to the seismic core damage frequency at Zion based on their risk reduction potential. That is, the percent reduction in core damage frequency that would occur if that component were infinitely strong (i.e., would never be failed by an earthquake). These risk reduction potentials are computed using the mean point estimate calculations for each component - one at a time.

Table B-21

Total Accident Sequence Frequency Increments for Zion
LLNL Hazard Curves - Original Stiffness
(Mean Point Estimate Calculation)

	0.10-0.25g	0.25-0.40g	0.40-0.55g	0.55-0.70g	0.70-0.85g	0.85-1.00g	1.00-1.15g	TOTAL
1	5.8E-09	8.7E-08	2.4E-07	3.6E-07	4.2E-07	4.1E-07	3.8E-07	1.9E-06
2	3.6E-13	3.0E-12	5.3E-12	4.9E-12	3.2E-12	1.7E-12	8.2E-13	1.9E-11
3	2.6E-12	2.2E-11	4.0E-11	3.7E-11	2.5E-11	1.3E-11	6.5E-12	1.5E-10
4	2.4E-08	2.1E-07	4.5E-07	5.7E-07	5.7E-07	4.8E-07	3.9E-07	2.7E-06
5	2.6E-08	1.4E-07	2.0E-07	1.7E-07	1.0E-07	5.1E-08	2.2E-08	7.2E-07
6	1.6E-08	9.8E-08	2.1E-07	3.1E-07	3.3E-07	2.9E-07	2.3E-07	1.5E-06
7	4.4E-07	2.1E-06	2.5E-06	1.6E-06	8.2E-07	3.5E-07	1.4E-07	8.0E-06
8	4.9E-09	1.3E-07	6.1E-07	1.0E-06	1.0E-06	7.6E-07	4.9E-07	4.0E-06
9	2.2E-06	2.9E-06	1.3E-06	3.2E-07	5.2E-08	7.8E-09	1.3E-09	6.8E-06
10	3.6E-09	1.5E-07	3.1E-07	1.9E-07	6.4E-08	1.7E-08	4.7E-09	7.4E-07
11	9.0E-10	4.5E-08	1.4E-07	1.4E-07	7.5E-08	2.9E-08	9.0E-09	4.3E-07
12	4.6E-08	5.1E-07	1.3E-06	1.4E-06	9.2E-07	4.7E-07	2.1E-07	4.8E-06
13	4.6E-06	7.0E-06	5.5E-06	2.6E-06	9.7E-07	3.0E-07	8.9E-08	2.1E-05
14	1.4E-15	3.0E-17	9.5E-19	3.3E-10	1.2E-11	4.8E-13	1.9E-14	3.5E-10
15	2.4E-06	8.1E-07	9.6E-08	7.7E-09	5.1E-10	3.2E-11	2.0E-12	3.4E-06
	9.9E-06	1.4E-05	1.3E-05	8.7E-06	5.3E-06	3.2E-06	2.0E-06	5.61E-05

Table B-22

Total Accident Sequence Frequency Increments for Zion
Zion PRA Hazard Curves - Original Stiffness
(Mean Point Estimate Calculation)

	0.10-0.25g	0.25-0.40g	0.40-0.55g	0.55-0.70g	0.70-0.85g	0.85-1.00g	1.00-1.15g	TOTAL
1	2.5E-09	1.7E-08	4.2E-08	6.1E-08	1.1E-07	0.0E+00	0.0E+00	2.3E-07
2	1.5E-13	6.0E-13	9.2E-13	8.2E-13	8.4E-13	0.0E+00	0.0E+00	3.3E-12
3	1.1E-12	4.5E-12	6.9E-12	6.3E-12	6.5E-12	0.0E+00	0.0E+00	2.5E-11
4	1.0E-08	4.3E-08	7.9E-08	9.6E-08	1.5E-07	0.0E+00	0.0E+00	3.8E-07
5	1.1E-08	2.8E-08	3.6E-08	2.9E-08	2.7E-08	0.0E+00	0.0E+00	1.3E-07
6	6.8E-09	2.0E-08	3.7E-08	5.2E-08	8.7E-08	0.0E+00	0.0E+00	2.0E-07
7	1.5E-07	4.3E-07	4.3E-07	2.8E-07	2.2E-07	0.0E+00	0.0E+00	1.5E-06
8	2.1E-09	2.6E-08	1.1E-07	1.7E-07	2.7E-07	0.0E+00	0.0E+00	5.7E-07
9	9.4E-07	5.9E-07	2.3E-07	5.3E-08	1.4E-08	0.0E+00	0.0E+00	1.8E-06
10	1.5E-09	3.0E-08	5.4E-08	3.2E-08	1.7E-08	0.0E+00	0.0E+00	1.3E-07
11	3.8E-10	9.0E-09	2.4E-08	2.3E-08	1.9E-08	0.0E+00	0.0E+00	7.5E-08
12	2.0E-08	1.0E-07	2.2E-07	2.3E-07	2.4E-07	0.0E+00	0.0E+00	8.1E-07
13	2.0E-06	1.4E-06	9.5E-07	4.4E-07	2.5E-07	0.0E+00	0.0E+00	5.0E-06
14	5.9E-16	5.9E-18	1.6E-19	5.6E-11	3.2E-12	0.0E+00	0.0E+00	5.9E-11
15	1.0E-06	1.6E-07	1.7E-08	1.3E-09	1.3E-10	0.0E+00	0.0E+00	1.2E-06
	4.2E-06	2.9E-06	2.2E-06	1.5E-06	1.4E-06	0.0E+00	0.0E+00	1.21E-05

Table B-23

Dominant Component Contributors to Core Damage Frequency
Ranked by Risk Reduction Potential

Component	Percent Reduction if not Failed	
	LLNL Hazard	EPRI Hazard
AFT Uplift	28%	34%
Crib House Roof	26%	24%
6OH1005A Pipe	11%	11%
Ceramic Insulators (LOSP)	5%	10%

All other components and structures less than 1%

The risk at Zion is dominated by soil failure and basemat uplift of the containment (28%), by failure of the crib house roof (26%), by failure of a single pipe in the RHR system (11%), and by failure of the ceramic insulators in the switchyard (causing loss of offsite power). All other components had risk reduction potentials less than 1%.

The soil failure and basemat uplift was calculated to fail all ECCS, AFWS and RHR piping running between the AFT building and the containment, and thus has a very pervasive effect on computed core damage frequency. Failure of the crib house roof was assumed to fail all six service water pumps, resulting in loss of cooling to the component cooling water system which provides pump, equipment and room cooling. Finally, failure of pipe 6OH1005A provides a diversion path for ECCS cooling, and, in conjunction with other failures, fails the RHR system.

B.5.4.3 Core Damage Frequency Results With Stiffness Reduction

The seismic risk at the Zion Plant was then requantified - in exactly the same fashion as in the previous section - using reduced shear wall stiffnesses. The same initiating events, component fragilities, and accident sequence definitions were used. The same interval of integration over the hazard curve (0.10g to 1.15g) was used. The only difference was the floor responses were those based on the reduced shear wall stiffnesses as discussed in section B.3.5. Further, only the shear deformation stiffnesses were reduced, while the bending deformation stiffness was unchanged as explained in Section 3.5 of the main report.

The results of this requantification using Monte Carlo uncertainty analysis are summarized in Tables B-24 and B-25. Based on the complete uncertainty analysis, the mean core damage frequency was computed to be 5.20E-5 using the LLNL hazard curves and 1.05E-5 using the Zion PRA hazard curves. This is only a slight change from the case with no stiffness frequency reduction presented in the last section. The same dominant accident sequences are found in both cases.

Mean Point Estimate

A point estimate calculation with all values set equal to their mean values was also made. Tables B-26 and B-27 present the total accident sequence frequencies at 7 different intervals over the LLNL and Zion PRA hazard curves respectively, for the mean point estimate evaluation. These tables may be compared directly to Tables B-19 and B-20 for the base case. The same dominant contributors to core damage frequency are found in both cases.

B.5.4.4 Summary of Results

There are two main reasons the overall core damage frequencies with and without stiffness reduction did not change much. One, is that responses inside to the containment building and internal structure are not being

Table B-24

Accident Sequence and Total Core Damage Mean Frequencies
for Zion - Reduced Stiffness

	Accident Sequence	Mean Frequency (per year) LLNL Hazard	Zion PRA Hazard
1	RVR-1	2.02E-6	2.19E-7
2	ALOCA-1	7.94E-9	1.29E-9
3	ALOCA-2	2.52E-8	3.54E-9
4	ALOCA-3	2.57E-6	2.76E-7
5	MLOCA-2	1.04E-6	1.58E-7
6	MLOCA-3	1.51E-6	1.86E-7
7	SLOCA-2	1.06E-5	1.65E-6
8	SLOCA-3	3.16E-6	3.62E-7
9	SSLOCA-2	8.12E-6	2.23E-6
10	SSLOCA-3	9.62E-7	1.30E-7
11	SSLOCA-4	5.87E-7	9.84E-8
12	SSLOCA-5	3.48E-6	5.37E-7
13	T2-2	1.61E-5	3.74E-6
14	T1-1	1.73E-9	3.06E-10
15	T1-2	1.81E-6	8.57E-7
	TOTAL	5.20E-5	1.05E-5

Table B-25

Total Core Damage Frequency Distribution Percentiles
for Zion - Reduced Stiffness

	LLNL Hazard	Zion PRA Hazard
Mean	5.20E-5	1.045-5
Var	4.26E-8	1.54E-10
5%	3.38E-7	1.15E-6
50%	8.28E-6	5.767-6
95%	1.93E-4	3.47E-5

Table B-26

Total Accident Sequence Frequency Increments
LLNL Hazard Curves - Reduced Stiffness
(Mean Point Estimate Calculation)

	0.10-0.25g	0.25-0.40g	0.40-0.55g	0.55-0.70g	0.70-0.85g	0.85-1.00g	1.00-1.15g	TOTAL
1	5.8E-09	8.7E-08	2.4E-07	3.6E-07	4.2E-07	4.1E-07	3.8E-07	1.9E-06
2	3.6E-13	3.0E-12	5.2E-12	4.8E-12	3.2E-12	1.7E-12	8.1E-13	1.9E-11
3	2.6E-12	2.2E-11	3.9E-11	3.7E-11	2.5E-11	1.3E-11	6.5E-12	1.5E-10
4	2.4E-08	2.1E-07	4.5E-07	5.7E-07	5.7E-07	4.8E-07	3.9E-07	2.7E-06
5	2.5E-08	1.4E-07	2.0E-07	1.7E-07	1.0E-07	5.0E-08	2.2E-08	7.1E-07
6	1.6E-08	9.9E-08	2.2E-07	3.1E-07	3.4E-07	2.9E-07	2.3E-07	1.5E-06
7	4.4E-07	2.1E-06	2.5E-06	1.6E-06	8.3E-07	3.5E-07	1.4E-07	8.0E-06
8	4.9E-09	1.3E-07	6.1E-07	1.0E-06	1.0E-06	7.6E-07	4.9E-07	4.0E-06
9	2.2E-06	2.9E-06	1.2E-06	2.5E-07	3.3E-08	3.5E-09	3.9E-10	6.6E-06
10	3.6E-09	1.4E-07	2.9E-07	1.5E-07	4.0E-08	7.5E-09	1.4E-09	6.3E-07
11	9.7E-10	5.1E-08	1.6E-07	1.6E-07	9.2E-08	3.6E-08	1.2E-08	5.1E-07
12	4.6E-08	5.1E-07	1.3E-06	1.4E-06	9.2E-07	4.7E-07	2.1E-07	4.8E-06
13	4.7E-06	7.1E-06	5.5E-06	2.6E-06	9.7E-07	3.0E-07	8.9E-08	2.1E-05
14	1.4E-15	3.0E-17	9.7E-19	3.4E-10	1.3E-11	4.9E-13	2.0E-14	3.6E-10
15	2.4E-06	8.1E-07	9.6E-08	7.7E-09	5.1E-10	3.2E-11	2.0E-12	3.4E-06
	9.9E-06	1.4E-05	1.3E-05	8.6E-06	5.3E-06	3.2E-06	2.0E-06	5.59E-05

Table B-27

Total Accident Sequence Frequency Increments
Zion PRA Hazard Curves - Reduced Stiffness
(Mean Point Estimate Calculation)

	0.10-0.25g	0.25-0.40g	0.40-0.55g	0.55-0.70g	0.70-0.85g	0.85-1.00g	1.00-1.15g	TOTAL
1	2.5E-09	1.7E-08	4.2E-08	6.1E-08	1.1E-07	0.0E+00	0.0E+00	2.3E-07
2	1.5E-13	6.0E-13	9.1E-13	8.1E-13	8.3E-13	0.0E+00	0.0E+00	3.3E-12
3	1.1E-12	4.4E-12	6.8E-12	6.2E-12	6.5E-12	0.0E+00	0.0E+00	2.5E-11
4	1.0E-08	4.3E-08	7.9E-08	9.6E-08	1.5E-07	0.0E+00	0.0E+00	3.8E-07
5	1.1E-08	2.8E-08	3.5E-08	2.9E-08	2.7E-08	0.0E+00	0.0E+00	1.3E-07
6	6.8E-09	2.0E-08	3.8E-08	5.2E-08	8.8E-08	0.0E+00	0.0E+00	2.0E-07
7	1.9E-07	4.3E-07	4.3E-07	2.8E-07	2.2E-07	0.0E+00	0.0E+00	1.5E-06
8	2.1E-09	2.6E-08	1.1E-07	1.7E-07	2.7E-07	0.0E+00	0.0E+00	5.7E-07
9	9.3E-07	5.7E-07	2.1E-07	4.2E-08	8.5E-09	0.0E+00	0.0E+00	1.8E-06
10	1.5E-09	2.9E-08	5.0E-08	2.5E-08	1.0E-08	0.0E+00	0.0E+00	1.2E-07
11	4.1E-10	1.0E-08	2.8E-08	2.7E-08	2.4E-08	0.0E+00	0.0E+00	9.0E-08
12	2.0E-08	1.0E-07	2.2E-07	2.3E-07	2.4E-07	0.0E+00	0.0E+00	8.1E-07
13	2.0E-06	1.4E-06	9.5E-07	4.4E-07	2.5E-07	0.0E+00	0.0E+00	5.0E-06
14	6.0E-16	6.0E-18	1.7E-19	5.8E-11	3.3E-12	0.0E+00	0.0E+00	6.1E-11
15	1.0E-06	1.6E-07	1.7E-08	1.3E-09	1.3E-10	0.0E+00	0.0E+00	1.2E-06
	4.2E-06	2.9E-06	2.2E-06	1.5E-06	1.4E-06	0.0E+00	0.0E+00	1.21E-05

effected much by the stiffness reductions. This is because the concrete in the containment building was not reduced at all since that is not in the scope of this project and because the stiffness reductions used for this project were based on concrete shear wall tests and not concrete cylindrical containment structures. Also, the internal structure, although did see an initial stiffness reduction of 25%, saw no further reductions even at the 5*SSE level. This initial reduction only lowered the first structural frequency of the internal structure from 12.88 Hz to 12.45 Hz, which is well above the 2-8 Hz range of most earthquakes energy.

The second reason for the responses showing little change with stiffness reduction is due to the high amount of bending stiffness in the walls and flexibility of the floor slabs. It was determined that for the finite element model of the Internal Structure, 42% of the lateral flexibility came from the bending stiffness of the walls, 27% came from shear stiffness of the walls and the other 31% was coming from the floor slab, which is usually considered rigid. Since only 27% of the stiffness is due to shear and this is the only stiffness that is being reduced, it is apparent why the frequency of the Internals dropped so little. Similarly, the first structural frequency of the AFT building only dropped from 8.49 Hz to 8.10 Hz for an initial reduction of 25%. At higher pga levels, further reductions did occur in some of the walls of the AFT, but at 5*SSE the first structural frequency only dropped to 7.98 Hz. Therefore, since the frequencies are not being degraded enough the push them into the range of higher earthquake energies, the responses are not seeing much of a change.

B.6 DETERMINISTIC IMPACTS

B.6.1 Deterministic Response Analysis

To assess the impact of the frequency reduction model on the deterministic design calculations for Zion, a set of "design-like" structural response calculations was performed. These calculations are as close to the original design calculation methods as could be determined from the Zion Final Safety Analysis Report [B-4]. However, we did not seek to obtain the original design calculational results themselves. Instead, we performed two sets of calculations using the FSAR guidance. The first set of calculations utilized the "design-like" models with as-calculated stiffnesses. In these "design-like" calculations, typical design damping levels were used, i.e.,

Concrete Structures	5%
Steel Structures	2%
Piping	2%

and a single time history dynamic response analysis is made.

The second set of calculations used the same structural models, time history and damping levels, but incorporated a shear wall stiffness reduction appropriate to the design level earthquake.

B.6.2 Deterministic Results for Zion

The deterministic time history analysis was performed both on the original models and the 75% degraded models using the 1941 El Centro earthquake record scaled to 1 SSE (0.17g). (As before, the containment shell stiffness not altered). Acceleration response spectra at various nodal locations throughout all three structures comparing the undegraded response to the 75% degraded response have been plotted in Figures B-87 thru B-96. For the reasons described previously these figures indicate only slight modifications in response in narrow frequency ranges for the degraded models.

Table B-28 shows a comparison of the maximum shear stresses in the outside walls of the AFT building at the basement and grade levels. (These are the maximum shear stresses in the structure.) It can be seen that, at the design earthquake level, only one of the outermost walls experiences any further stiffness degradation (i.e., reaches a shear stress greater than 150 psi). Comparing the shear stresses with and without stiffness reduction effects included shows a slight reduction in shear stresses. This is due to the fact that the stiffness reduction caused a small decrease in dominant natural frequencies, and pushed the response into a local "dip" in the ground motion input spectra. Table B-29 gives similar results for the concrete containment internals. It can be seen that, at the design earthquake level, all the stresses are very low, and no dynamic reduction in shear wall stiffness is to be expected for the concrete internals.

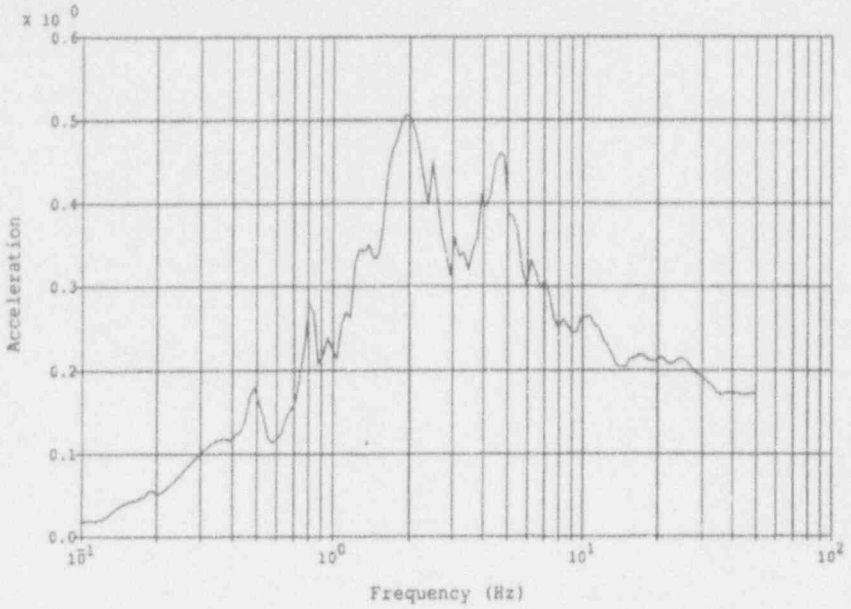

Legend:
Original Model ————————
75% Reduced Model — — — — —

Notes:
East-West Direction
Accelerations in g's
5% Spectral Damping

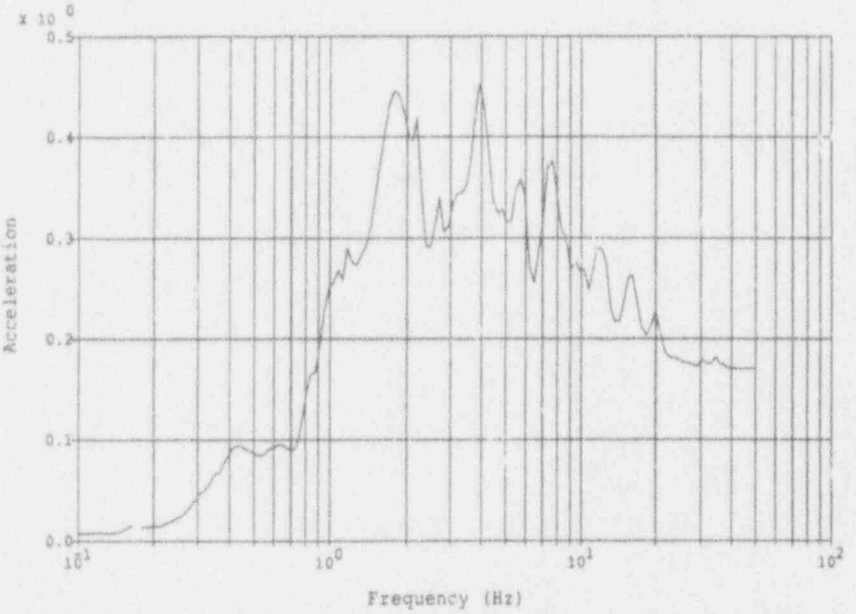

Legend:
Original Model ————————
75% Reduced Model — — — — —

Notes:
Ncr-So. Direction
Accelerations in g's
5% Spectral Damping

Figure B-87 Zion Deterministic Analysis
Free-Field Motion (El Centro 1940)

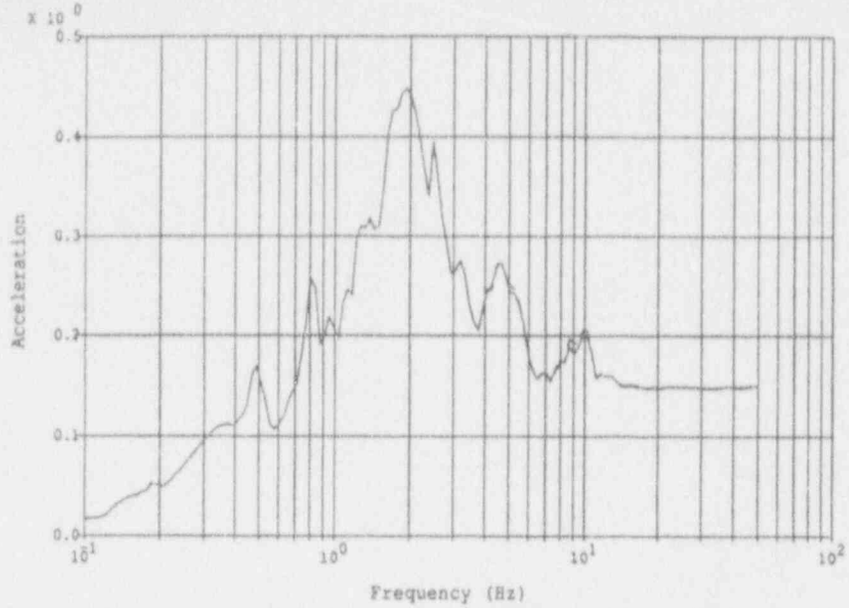

Legend:
Original Model ——————
75% Reduced Model — — — — —

Notes:
East-West Direction
Accelerations in g's
5% Spectral Damping

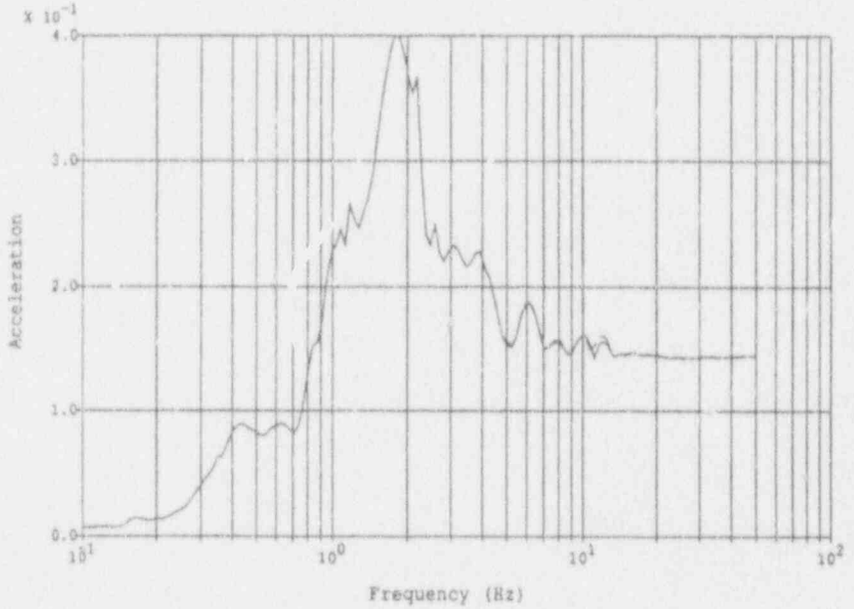

Legend:
Original Model ——————
75% Reduced Model — — — — —

Notes:
Nor-So. Direction
Accelerations in g's
5% Spectral Damping

Figure B-88 Zion Deterministic Analysis
AFT Node 13, El 542'

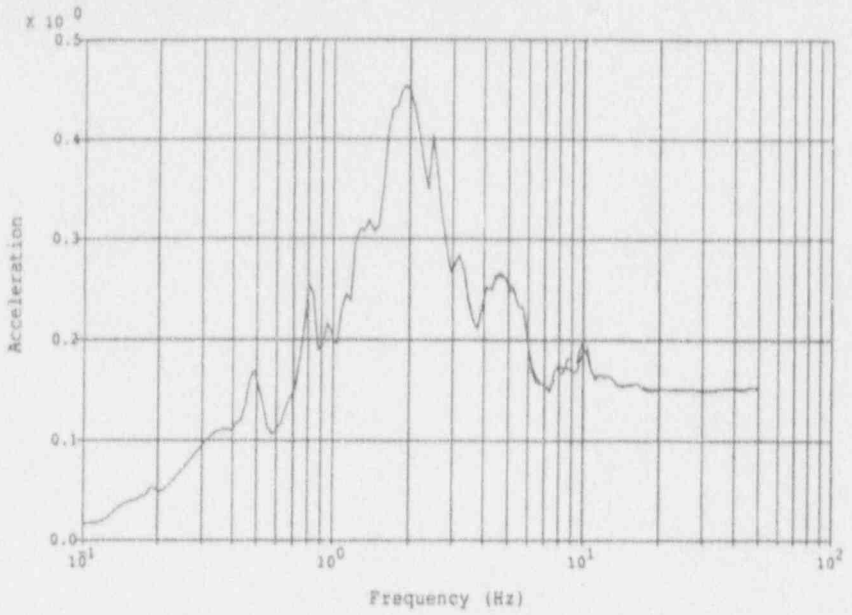

Legend:
Original Model
75% Reduced Model

Notes:
East-West Direction
Accelerations in g's
5% Spectral Damping

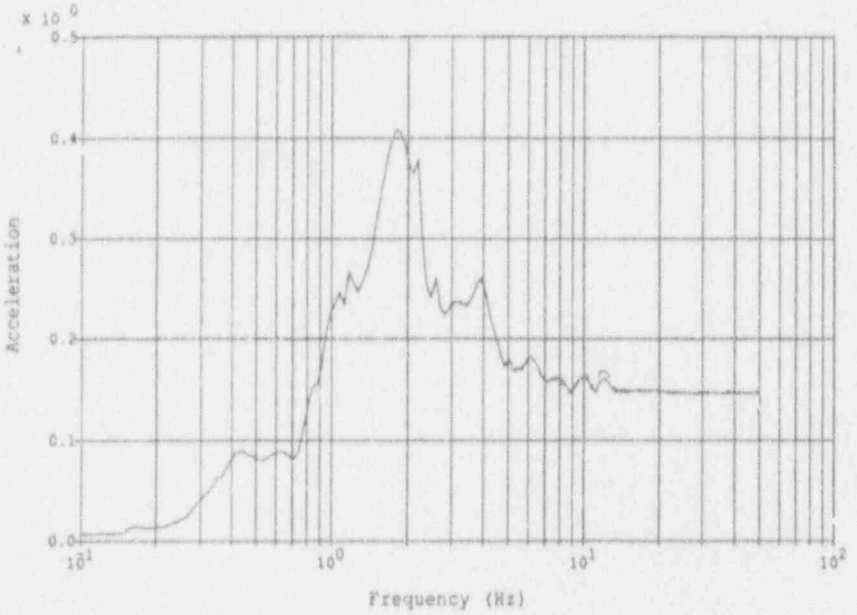

Legend:
Original Model
75% Reduced Model

Notes:
Nor-So. Direction
Accelerations in g's
5% Spectral Damping

Figure B-89 Zion Deterministic Analysis
AFT Node 1537, El 592'

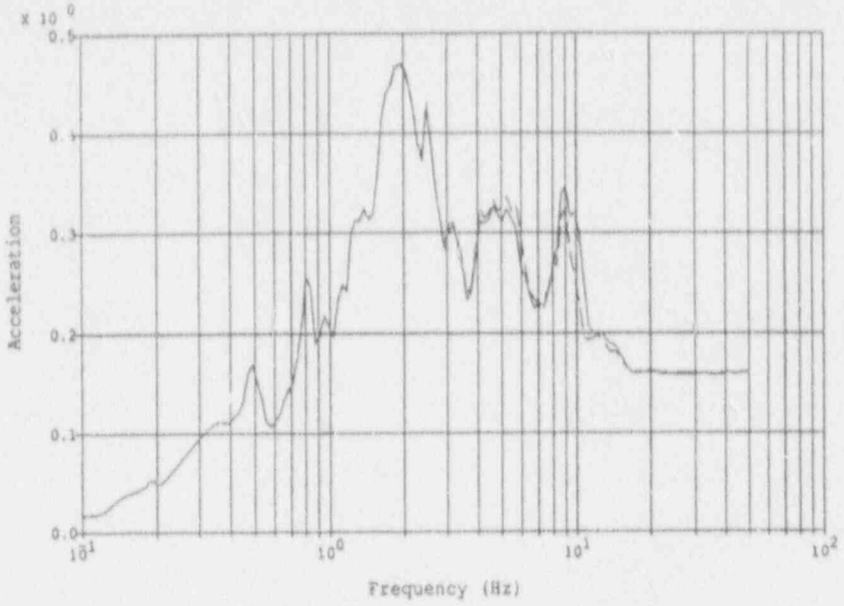

Legend:
Original Model ——————
75% Reduced Model — — — — —

Notes:
East-West Direction
Accelerations in g's
5% Spectral Damping

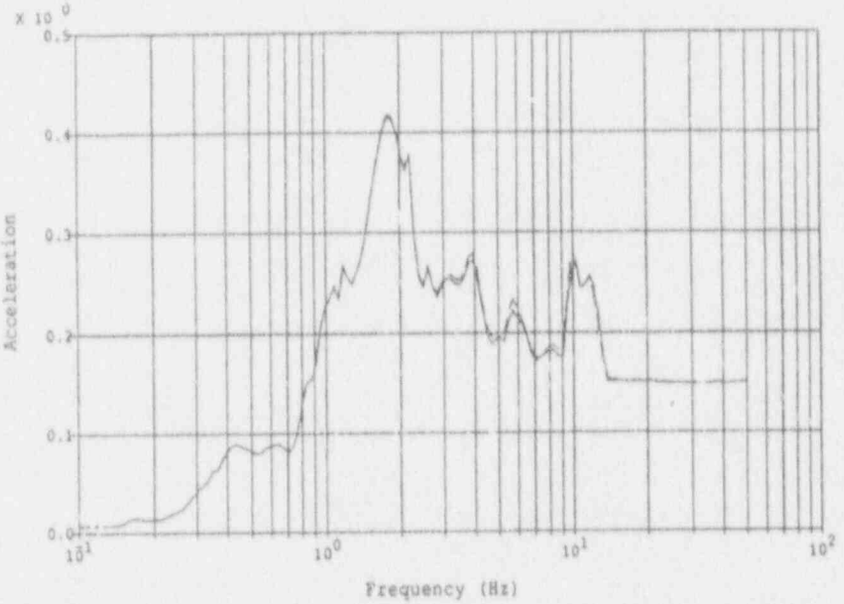

Legend:
Original Model ——————
75% Reduced Model — — — — —

Notes:
Nor-So. Direction
Accelerations in g's
5% Spectral Damping

Figure B-90 Zion Deterministic Analysis
AFT Node 2012, El 617'

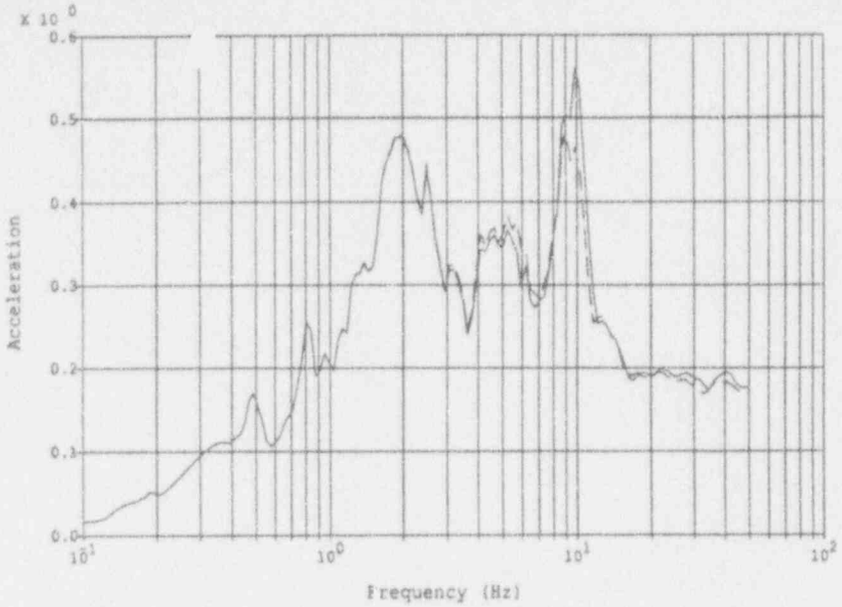

Legend:
Original Model ————————
75% Reduced Model — — — — —

Notes:
East-West Direction
Accelerations in g's
5% Spectral Damping

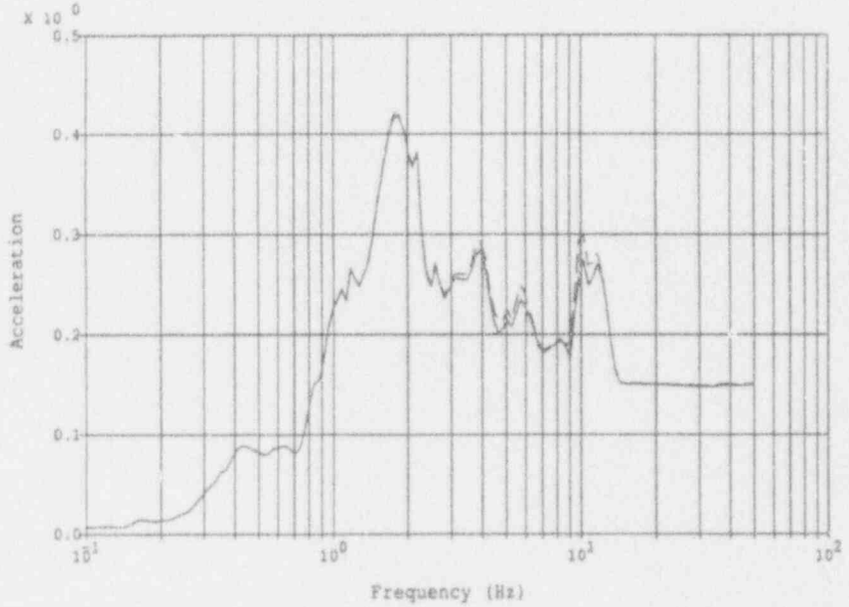

Legend:
Original Model ————————
75% Reduced Model — — — — —

Notes:
Nor-So. Direction
Accelerations in g's
5% Spectral Damping

Figure B-91 Zion Deterministic Analysis
AFT Node 3005, El 642'

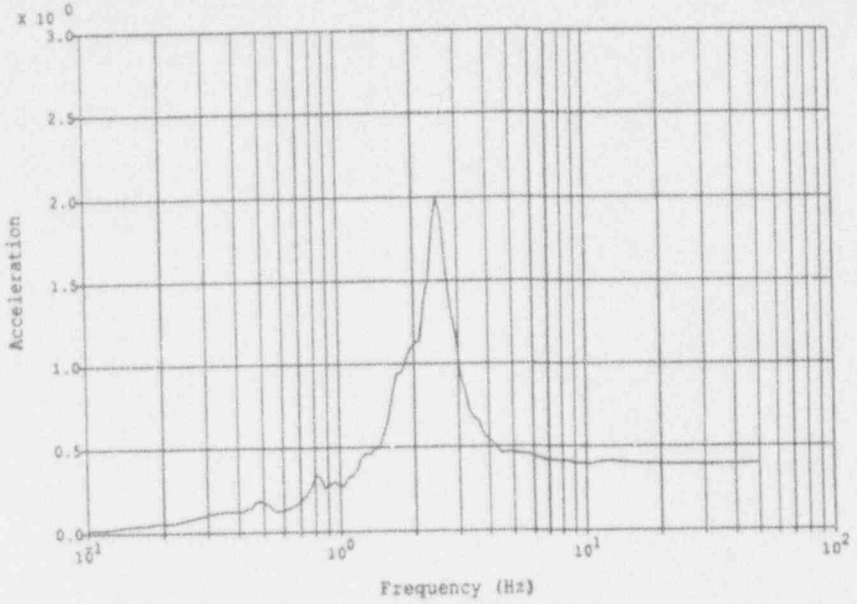

Legend:
Original Model ————————
75% Reduced Model — — — — —

Notes:
East-West Direction
Accelerations in g's
5% Spectral Damping

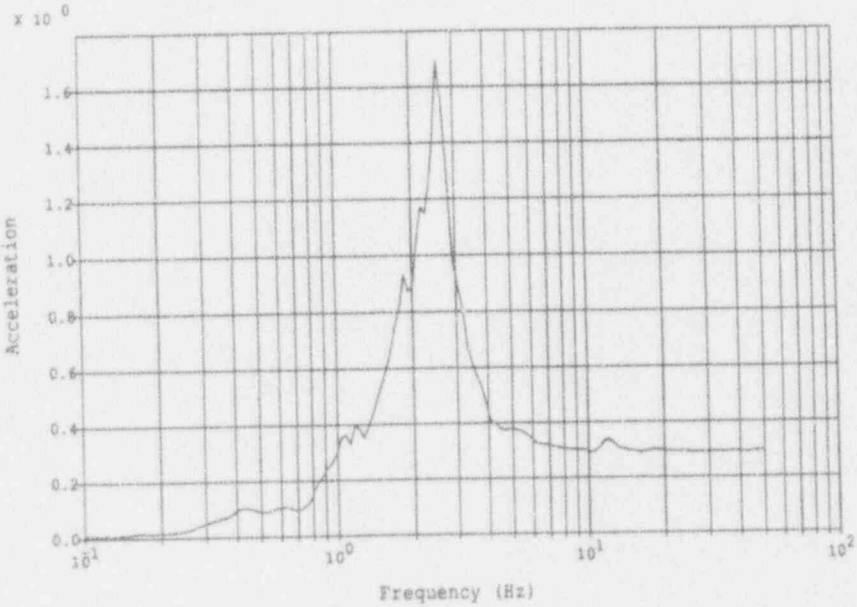

Legend:
Original Model ————————
75% Reduced Model — — — — —

Notes:
Nor-So. Direction
Accelerations in g's
5% Spectral Damping

Figure B-92 Zion Deterministic Analysis
RCB Node 2, El 718'

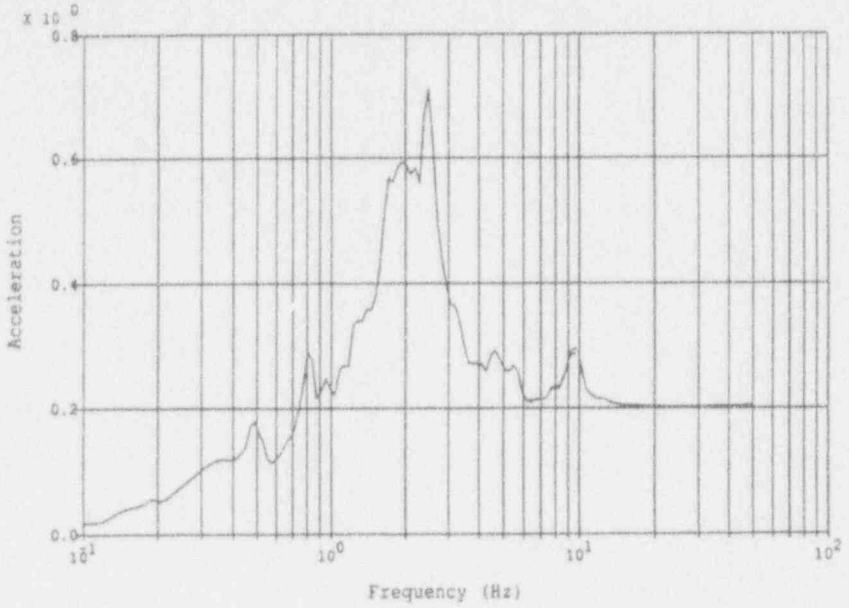

Legend:
Original Model _____
75% Reduced Model _ _ _ _ _ _

Notes:
East-West Direction
Accelerations in g's
5% Spectral Damping

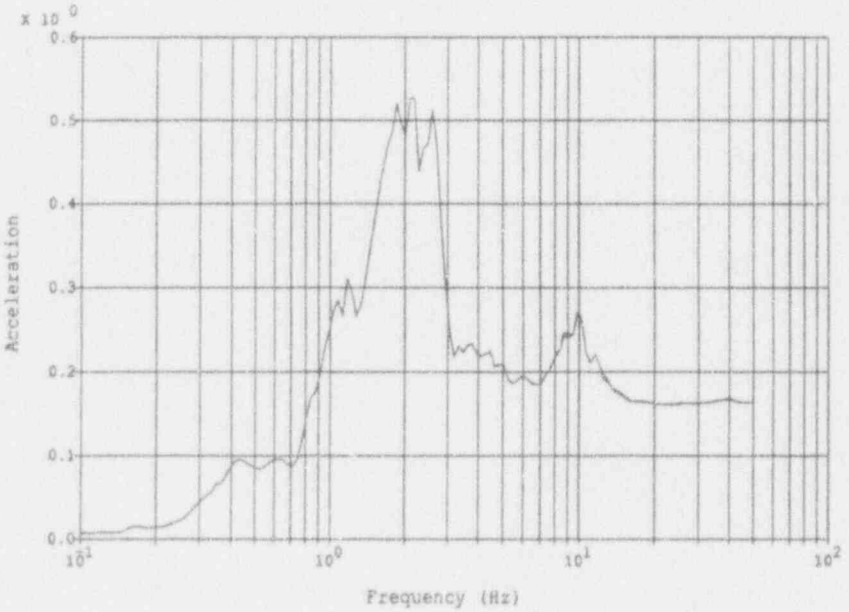

Legend:
Original Model _____
75% Reduced Model _ _ _ _ _ _

Notes:
Nor-So. Direction
Accelerations in g's
5% Spectral Damping

Figure B-93 Zion Deterministic Analysis
RCB Node 9, El 592'

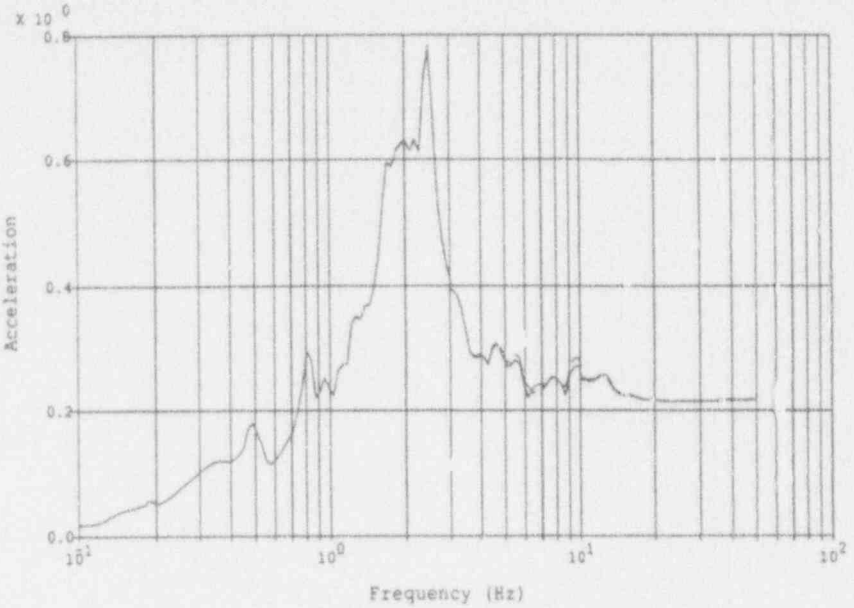

Legend:
Original Model ——————
75% Reduced Model — — — — —

Notes:
East-West Direction
Accelerations in g's
5% Spectral Damping

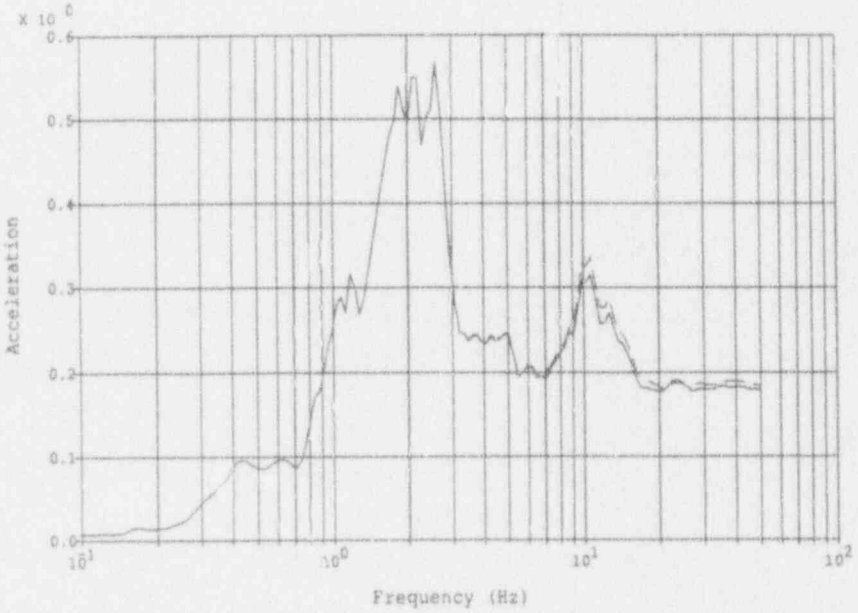

Legend:
Origina' Mode' ——————
75% Reduced Model — — — — —

Notes:
Nor-So. Direction
Accelerations in g's
5% Spectral Damping

Figure B-94 Zion Deterministic Analysis
RCB INT Node 936, El 617'

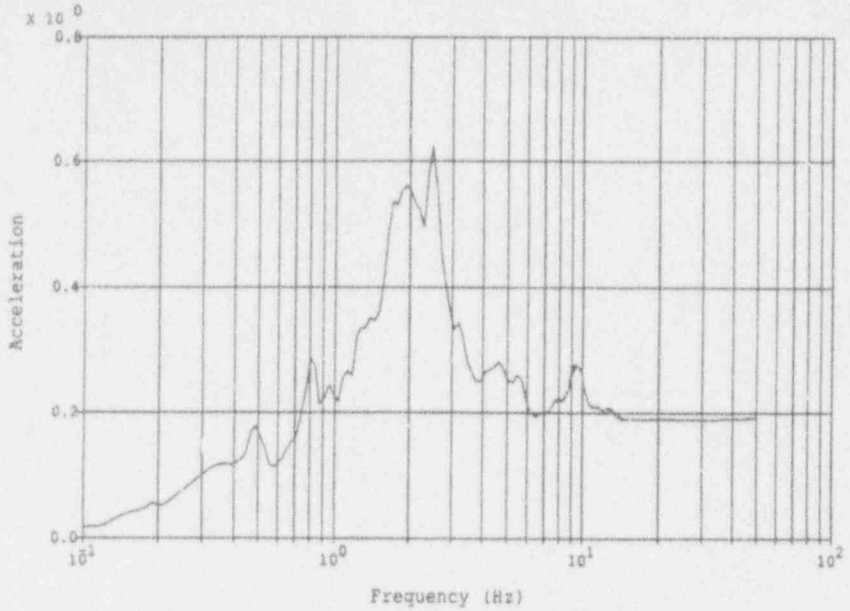

Legend:
Original Model ——————
75% Reduced Model — — — — —

Notes:
East-West Direction
Accelerations in g's
5% Spectral Damping

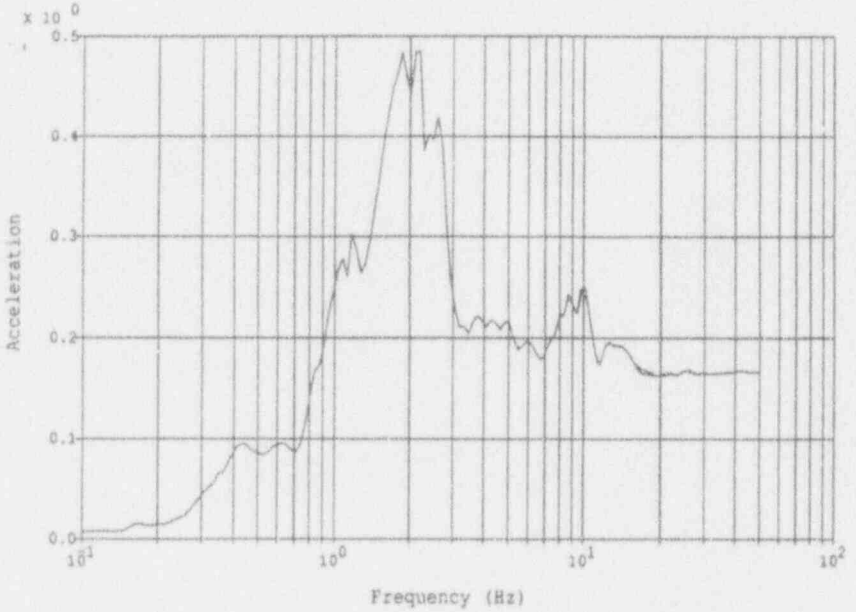

Legend:
Original Model ——————
75% Reduced Model — — — — —

Notes:
Nor-So. Direction
Accelerations in g's
5% Spectral Damping

Figure B-95 Zion Deterministic Analysis
RCB INT Node 1412, El 588'

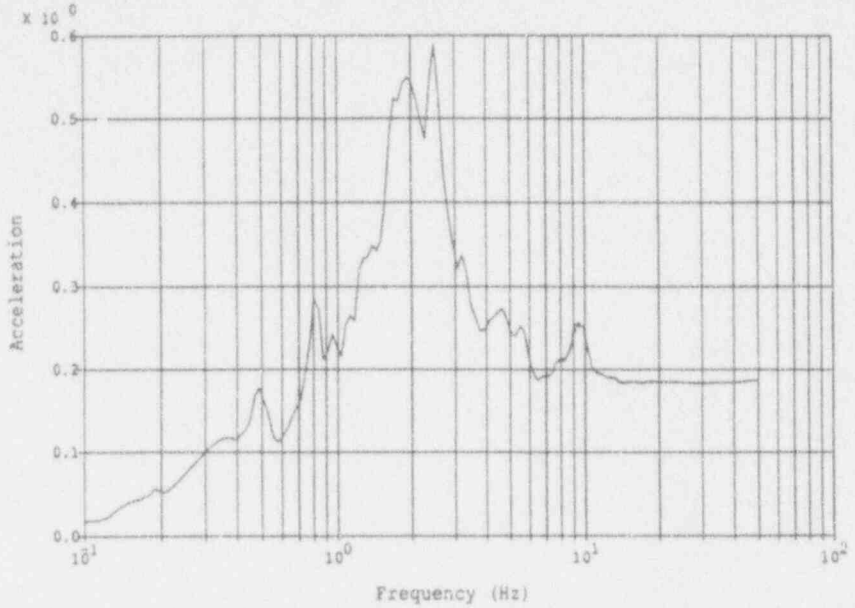

Legend:
Original Model ——————
75% Reduced Model — — — — —

Notes:
East-West Direction
Accelerations in g's
5% Spectral Damping

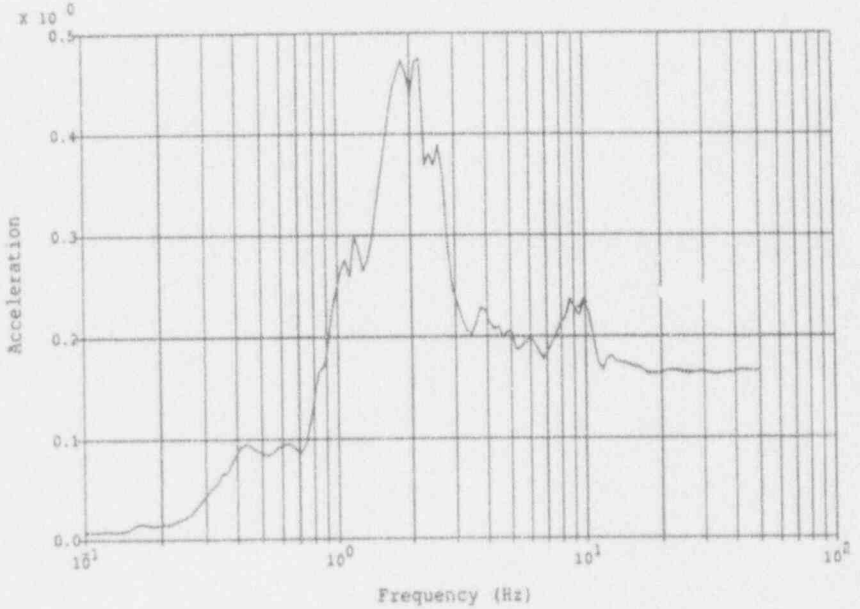

Legend:
Original Model ——————
75% Reduced Model — — — — —

Notes:
Nor-So. Direction
Accelerations in g's
5% Spectral Damping

Figure B-96 Zion Deterministic Analysis
RCB INT Node 1463, El 579'

Table B-28

Maximum Element Stresses at Zion, Deterministic Study
Auxiliary/Fuel/Turbine Building

Original Stiffnesses

Continuous Group #	Direction	Elevation	Element	Max. Stress (psf)
1	N-S	542'-560'	30	885
			40	332
2	E-W	542'-560'	54	670
3	N-S	592'-617'	445	2,725
			452	3,148
4	E-W	592'-617'	519	21,720

Reduced Stiffnesses

Continuous Group #	Direction	Elevation	Element	Max. Stress (psf)
1	N-S	542'-560'	30	718
			40	275
2	E-W	542'-560'	54	526
3	N-S	592'-617'	445	2,393
			452	2,686
4	E-W	592'-617'	519	18,550

Table B-29

Maximum Element Stresses at Zion, Deterministic Study
Reactor Internals Building

Original Stiffnesses

Group #	Elevation	Element	Max. Stress (psf)
1	568'-581'	1	2,463
		7	3,425
		19	3,131
		24	2,724
2	568'-581'	25	2,971
		26	1,906
		27	1,775
		28	2,390
3	568'-581'	32	3,494
		33	2,117
		41	2,513
		42	2,028
		60	3,861
		70	2,867
		80	3,118
		87	3,749
		88	3,806
4	568'-581'	34	3,558
		35	3,309
		37	2,313
		38	653
		39	1,252
		40	2,670

Table B-29 (cont'd)

Maximum Element Stresses at Zion, Deterministic Study
Reactor Internals Building

Reduced Stiffnesses

Group #	Elevation	Element	Max. Stress (psf)
1	568'-581'	1	2,029
		7	2,982
		19	2,708
		24	2,272
2	568'-581'	25	2,652
		26	1,638
		27	1,525
		28	2,086
3	568'-581'	32	3,172
		33	1,947
		41	2,325
		42	1,849
		60	3,272
		70	2,431
		80	2,821
		87	3,388
		88	3,397
4	568'-581'	34	3,245
		35	3,028
		37	2,019
		38	609
		39	1,128
		40	2,410

B.7 REFERENCES

B-1. Application of the SSMRP Methodology to the Seismic Risk at the Zion Nuclear Power Plant, M. P. Bohn, L. C. Shieh, J. E. Wells, L. C. Cover, D. L. Bernreuter, J.C. Chen, J. J. Johnson, S. E. Bumpus, R. W. Mensing, W. J. O'Connell, and D. A. Lappa, NUREG/CR-3428, January 1984

B-2. Zion Probabilistic Safety Study, prepared by Pickard, Lowe and Garrick for Commonwealth Edison, Chicago, Illinois, 1982

B-3 Seismic Hazard Characterization of 69 Nuclear Plant Sites East of the Rocky Mountains, D.L. Bernreuter, et. al., NUREG/CR-5250, October, 1988.

B-4 Zion Station Updated Final Safety Analysis Report, Vol. 1, Commonwealth Edison, Chicago, Illinois

B-5 Phase I Final Report - Systems Analysis (Project VIII), J. E. Wells, L. L. George, and G. E. Cummings, Prepared for U.S. Nuclear Regulatory Commission, NUREG/CR-2015, Vol. 8, July 1981

B-6 Phase I Final Report - SMACS - Seismic Methodology Analysis Chain with Statistics (Project VIII), J. J. Johnson, G. L. Goudreau, S. E. Bumpus, O. R. Maslenikov, Prepared for U.S. Nuclear Regulatory Commission, NUREG/CR-2015, Vol. 9, UCRL-53021, Vol. 9, July 1981

B-7 Handbook of Nuclear Power Plant Seismic Fragilities, L. E. Cover, M. P. Bohn, R. D. Campbell, and D. A. Wesley, NUREG/CR-3558, June 1985.

ATTACHMENT TO APPENDIX P

FILES FOR ZION SEISMIC ANALYSIS

Fragility Files

Response Files

Accident Sequence Expressions

Cross-Reference File

Description of Methodology

Further Details

ZION FRAGILITIES FILE

No.	M_F	β_{fr}	β_{fu}	Category
1	2.06	0.24	.32	Reactor Core
2	3.83	0.23	.39	RPV
3	2.00	0.21	.34	PZR
4	2.45	0.24	.37	SG
5	2.03E+5	0.18	.33	Master Piping (ft-lb)
6	2.03E+5	0.18	.33	Same as above
7	1.46	0.20	.35	Larger Vert vessel w/formed heck
8	2.01	0.25	.29	Large Vert Tank w/flat bottom *
9	3.91	0.30	.53	Large Horiz Vessels
10	1.84	0.25	.45	Small/Med Vessesl w/HTX
11	1.27	0.51	.0	Not Used
12	2.64	0.33	.0	Not Used
13	2.64	0.24	.37	Reactor Coolant Pumps
14	2.21	0.22	.32	Large Vert Pumps
15	3.19	0.21	.27	Motor driven pumps & compressors
16	4.83	0.26	.60	Valves of all sizes
17	4.83	0.26	.60	Same as above
18	4.83	0.26	.60	Same as above
19	12.10	0.27	.31	Horizontal Motors
20	0.65	0.25	.31	Diesel Generators
21	2.29	0.31	.39	Batteries & Racks
22	4.00	0.48	.75	Relays (should be 1.66 and
23	2.87	0.28	.30	Transformers (also used for Batt Charger)
24	2.24	0.27	.31	Air handling units
25	11.5	0.48	.66	Inst Panels & racks
26	0.708	0.833	.0	Not Used
27	3.66	0.82	.0	Not Used
28	0.708	0.833	.0	Same as 26?
29	0.86	0.24	.27	Crib House Roof - Phase II
30	7.68	0.20	.35	Local Instruments
31	7.71	0.730	.0	Not Used
32	0.81	0.28	.30	CST
33	1.54	0.197	.0	Not Used
34	9.9e+10	0.05	.0	No fail
35	15.6	0.26	.35	Inverters
36	2.23	0.34	.19	Cable Trays
37	3.97	0.29	.46	Ducting (?)
38	1.46	0.22	.49	Snubbers
39	1.60	0.158	.3	MLOCA
40	1.35	0.164	.3	SLOCA and LOCA-A thru LOCA-D
41	7.63	0.48	.74	Circuit Breaker
42	1.11	0.17	.3	SSLOCA
43	4.03	0.251	.3	RPS and RVR
44	0.708	0.833	.0	Same as 26 & 28. Dummy?
45	0.761	0.21	.27	RWST

No.	M_F	β_{fr}	β_{fu}	Category
46	13.00	0.15	.18	Cont Basemat Fails b = bT
47	3.00	0.15	.27	OZZ1ROOFMG
48	8.25	0.144	.0	Not Used
49	0.20	0.25	.25	LOSP
50	0.275	0.471	.0	Not Used
51	2.70	0.11	.26	Aux Bldg Shear Wall
52	0.70	0.40	.40	Uplift
53	0.60	0.001	.0	CSIS & CFC & PCS step failure
54	1.29e+3	0.18	.33	OA <1" Pipes
55	2.43e+3	0.18	.33	OB >=1" Pipes
56	1.13e+4	0.18	.33	OC >=2" Pipes
57	1.00e+6	0.18	.33	OD >=3" Pipes
58	1.00e+6	0.18	.33	OE >=4" Pipes
59	2.03e+5	0.18	.33	OF >=6" Pipes
60	3.63e+5	0.18	.33	OG >=8" Pipes
61	1.00e+6	0.18	.33	OH >=10" Pipes
62	1.00e+6	0.18	.33	OI >=12" Pipes
63	2.64e+6	0.18	.33	OJ >=16" Pipes
64	2.70e+6	0.18	.33	OK >=24" Pipes
65	1.70	0.416	.3	RVR
66	1.583	0.4436	.3	LLOCA
67	1.749	0.4971	.3	MLOCA
68	.9009	0.3883	.3	SLOCA
69	.7903	0.4889	.3	SSLOCA
70	0.085	0.3	.3	PSC failure NOT USED (#53 step)

ZION RESPONSE MULTIPLE FILE (ORIGINAL STIFFNESS CASE)

No.	F_1	F_2	β_{rr}	β_{ru}	Response	
1	1.00	0.0	0.25	.25	Free Field - ZPA	1
2	1.91	0.0	0.35	.25	- 8 Hz	3
3	0.96	0.0	0.45	.25	R.Int. 556' - 8 Hz	7
4	1.00	-0.277	0.35	.25	617' - ZPA	10
5	2.00	-0.422	0.45	.25	- 4 Hz	11
6	1.10	0.0	0.45	.25	- 8 Hz	12
7	1.65	-0.378	0.45	.25	588' - 4 Hz	14
8	1.20	0.0	0.45	.25	615' - 8 Hz	15
9	0.82	-0.151	0.45	.25	-16 Hz	16
10	1.59	-0.305	0.45	.25	AFT 542' - 4 Hz	18
11	1.59	-0.305	0.45	.25	560' - 4 Hz	22
12	1.59	-0.305	0.45	.25	567' - 4 Hz	26
13	0.61	0.0	0.35	.25	592' - ZPA	29
14	0.71	0.0	0.35	.25	591' - ZPA	302
15	1.53	-0.199	0.45	.25	617' - 8 Hz	308
16	0.82	0.0	0.35	.25	642' - ZPA	310
17	2.35	-0.412	0.45	.25	- 4 Hz	311
18	4.12	-0.571	0.45	.25	Valve - Subs 1	86
19	3.65e+6	0.0	0.45	.25	Moment - Subs 1&2	87
20	3.05	0.0	0.45	.25	Valve - Subs 2	105
21	3.65e+6	0.0	0.45	.25	Moment - Subs 2	120
22	5.24e+6	0.0	0.45	.25	(ft-lb) 2	121
23	2.00e+6	0.0	0.45	.25	2	122
24	2.70e+6	0.0	0.45	.25	3	213
25	2.18e+6	0.0	0.45	.25	3	215
26	5.24e+6	0.0	0.45	.25	4	241
27	3.12e+7	0.0	0.45	.25	4	257
28	7.35e+4	3.90e+4	0.45	.25	4	259
29	2.59e+6	0.0	0.45	.25	5	265
30	2.53e+5	2.50e+4	0.45	.25	6	284
31	3.29e+5	2.50e+4	0.45	.25	6	285
32	1.70e+5	1.80e+4	0.45	.25	6	286
33	5.90e+4	1.20e+4	0.45	.25	6	287
34	2.94e+5	0.0	0.45	.25	6	288
35	1.94e+5	3.40e+4	0.45	.25	6	289
36	3.06e+5	0.0	0.45	.25	6	290
37	1.94e+5	2.90e+3	0.45	.25	6	291
38	3.80e+4	2.70e+4	0.45	.25	6	292
39	7.06e+5	0.0	0.45	.25	6	293
40	6.94e+5	2.20e+4	0.45	.25	6	294
41	2.00e+5	4.30e+4	0.45	.25	7	295
42	1.94e+5	7.80e+4	0.45	.25	7	296
43	4.70e+5	4.20e+4	0.45	.25	7	297
44	4.70e+5	8.80e+4	0.45	.25	7	298
45	2.76e+5	0.0	0.45	.25	7	299
46	1.65e+5	9.30e+4	0.45	.25	7	300
47	1.29e+5	8.80e+4	0.45	.25	7	301
48	1.0	0.0	0.0	.00	Initiating Events	
49	0.613	0.0	0.27	.25	Containment Basemat	

ZION RESPONSE MULTIPLE FILE (REDUCED STIFFNESS CASE)

No.	F_1	F_2	β_{rr}	β_{ru}	Response	
1	1.00	0.0	0.25	.25	Free Field - ZPA	1
2	1.91	0.0	0.35	.25	- 8 Hz	3
3	0.94	0.0	0.45	.25	R.Int. 556'- 8 Hz	7
4	1.00	-0.277	0.35	.25	617'- ZPA	10
5	2.00	-0.422	0.45	.25	- 4 Hz	11
6	1.20	0.0	0.45	.25	- 8 Hz	12
7	1.65	-0.378	0.45	.25	588'- 4 Hz	14
8	1.29	0.0	0.45	.25	615'- 8 Hz	15
9	0.82	-0.151	0.45	.25	-16 Hz	16
10	1.59	-0.322	0.45	.25	AFT 542'- 4 Hz	18
11	1.59	-0.322	0.45	.25	560'- 4 Hz	22
12	1.59	-0.322	0.45	.25	567'- 4 Hz	26
13	0.61	0.0	0.35	.25	592'- ZPA	29
14	0.71	0.0	0.35	.25	591'- ZPA	302
15	1.53	-0.091	0.45	.25	617'- 8 Hz	308
16	0.82	0.0	0.35	.25	642'- ZPA	310
17	2.35	-0.353	0.45	.25	- 4 Hz	311
18	4.12	-0.571	0.45	.25	Valve - Subs 1	86
19	3.82e+6	0.0	0.45	.25	Moment - Subs 1&2	87
20	3.05	0.0	0.45	.25	Valve - Subs 2	105
21	3.82e+6	0.0	0.45	.25	Moment - Subs 2	120
22	5.53e+6	0.0	0.45	.25	(ft-lb) 2	121
23	2.06e+6	7.40e+4	0.45	.25	2	122
24	2.70e+6	0.0	0.45	.25	3	213
25	2.18e+6	0.0	0.45	.25	3	215
26	5.24e+6	0.0	0.45	.25	4	241
27	3.12e+7	0.0	0.45	.25	4	257
28	7.35e+4	3.90e+4	0.45	.25	4	259
29	2.59e+6	0.0	0.45	.25	5	265
30	2.06e+5	6.90e+4	0.45	.25	6	284
31	3.47e+5	4.40e+3	0.45	.25	6	285
32	1.70e+5	2.40e+4	0.45	.25	6	286
33	5.30e+4	1.60e+4	0.45	.25	6	287
34	3.24e+5	0.0	0.45	.25	6	288
35	1.94e+5	3.40e+4	0.45	.25	6	289
36	3.00e+5	2.50e+4	0.45	.25	6	290
37	1.94e+5	2.90e+3	0.45	.25	6	291
38	4.10e+4	2.20e+4	0.45	.25	6	292
39	6.35e+5	1.17e+4	0.45	.25	6	293
40	6.35e+5	3.70e+4	0.45	.25	6	294
41	2.18e+5	7.60e+4	0.45	.25	7	295
42	1.94e+5	7.80e+4	0.45	.25	7	296
43	4.24e+5	4.30e+4	0.45	.25	7	297
44	4.70e+5	8.80e+4	0.45	.25	7	298
45	3.06e+5	1.60e+4	0.45	.25	7	299
46	1.65e+5	9.30e+4	0.45	.25	7	300
47	1.29e+5	8.80e+4	0.45	.25	7	301
48	1.0	0.0	0.0	.00	Initiating Events	
49	0.613	0.0	0.27	.25	Containment Basemat	

```
ZZPCS = ZZPCS

ZZECISS =
    6TA1001AMJ * INJECTION

ZZECISL =
    6VX1880600 * INJECTION +
    6TA1001AMJ * INJECTION

ZZECIML =
    LOCA-C * LOCA-D +
    LOCA-B * LOCA-D +
    LOCA-B * LOCA-C +
    LOCA-A * LOCA-D +
    LOCA-A * LOCA-C +
    LOCA-A * LOCA-B +
    6VX1880600 * INJECTION +
    6TA1008DMJ * LOCA-C +
    6TA1008DMJ * LOCA-B +
    6TA1008DMJ * LOCA-A +
    6TA1007CMJ * LOCA-D +
    6TA1007CMJ * LOCA-B +
    6TA1007CMJ * LOCA-A +
    6TA1006BMJ * LOCA-D +
    6TA1006BMJ * LOCA-C +
    6TA1006BMJ * LOCA-A +
    6TA1005AMJ * LOCA-D +
    6TA1005AMJ * LOCA-C +
    6TA1005AMJ * LOCA-B +
    6TA1001AMJ * INJECTION +
    6OH1034BMJ * LOCA-D +
    6OH1034BMJ * LOCA-C +
    6OH1034BMJ * LOCA-A

ZZECILL =
    ZOI1006AMJ +
    ZOH1001CMJ * ZOH1002DMJ +
    ZOH1001CMJ * ZOH1002CMJ +
    ZOH1001BMJ * ZOH1002DMJ +
    ZOH1001BMJ * ZOH1002CMJ +
    LOCA-C * LOCA-D +
    LOCA-B * LOCA-D +
    LOCA-B * LOCA-C +
    LOCA-A * LOCA-D +
    LOCA-A * LOCA-C +
    LOCA-A * LOCA-B +
    INJECTION * ZOI1013BMJ +
    INJECTION * ZOG1011AMJ +
    6TA1008DMJ * LOCA-C +
    6TA1008DMJ * LOCA-B +
```

```
      6TA1008DMJ * LOCA-A +
      6TA1007CMJ * LOCA-D +
      6TA1007CMJ * LOCA-B +
      6TA1007CMJ * LOCA-A +
      6TA1006BMJ * LOCA-D +
      6TA1006BMJ * LOCA-C +
      6TA1006BMJ * LOCA-A +
      6TA1005AMJ * LOCA-D +
      6TA1005AMJ * LOCA-C +
      6TA1005AMJ * LOCA-B +
      6TA1001AMJ * INJECTION +
      6OH1034BMJ * LOCA-D +
      6OH1034BMJ * LOCA-C +
      6OH1034BMJ * LOCA-A +
      6OH1005AMJ * ZVG1606-OO +
      6OH1005AMJ * ZOH1001CMJ +
      6OH1005AMJ * ZOH1001BMJ +
      6OH1005AMJ * INJECTION +
      6OH1005AMJ * 6VX1809AOO +
      6OH1004AMJ * ZOH1002DMJ +
      6OH1004AMJ * ZOH1002CMJ +
      6OH1004AMJ * INJECTION +
      6OH1004AMJ * 6OH1005AMJ

ZZECRSS = 0.0

ZZECRSL = 0.0

ZZECRML = 0.0

ZZECRLL =
     ZOI1006AMJ +
     ZOH1001CMJ * ZOH1002DMJ +
     ZOH1001CMJ * ZOH1002CMJ +
     ZOH1001BMJ * ZOH1002DMJ +
     ZOH1001BMJ * ZOH1002CMJ +
     6OH1005AMJ * ZVG1606-OO +
     6OH1005AMJ * ZOH1001CMJ +
     6OH1005AMJ * ZOH1001BMJ +
     6OH1005AMJ * 6VX1809AOO +
     6OH1004AMJ * ZOH1002DMJ +
     6OH1004AMJ * ZOH1002CMJ +
     6OH1004AMJ * 6OH1005AMJ +
     LOCA-B * LOCA-C * ZOH1002CMJ +
     LOCA-B * LOCA-C * ZOG1011AMJ +
     LOCA-A * LOCA-D * ZOH1001CMJ +
     LOCA-A * LOCA-D * ZOH1001BMJ +
     6OH1005AMJ * RECIRC * ZPB1001AOX +
     6OH1005AMJ * LOCA-B * LOCA-C +
     6OH1004AMJ * LOCA-A * LOCA-D +
     LOCA-B * LOCA-C * RECIRC * ZPBR002BMG +
     LOCA-B * LOCA-C * RECIRC * ZPBR002BME +
```

```
    LOCA-B * LOCA-C * REC1383BMJ * RECIRC +
    LOCA-B * LOCA-C * REC1383AMJ * RECIRC +
    LOCA-A * LOCA-D * RECIRC * ZPBR001AMG +
    LOCA-A * LOCA-D * RECIRC * ZPBR001AME +
    LOCA-A * LOCA-D * REC1393CMJ * RECIRC +
    LOCA-A * LOCA-D * REC1393BMJ * RECIRC +
    LOCA-A * LOCA-D * REC1393AMJ * RECIRC +
    LOCA-A * LOCA-B * LOCA-C * LOCA-D +
    60J1008AMJ * LOCA-B * LOCA-C * RECIRC +
    60J1007AMJ * LOCA-A * LOCA-D * RECIRC

ZZAFWSL =
    QOF118B-MJ +
    REC1383BMJ * REC1393CMJ +
    REC1383BMJ * REC1393BMJ +
    REC1383BMJ * REC1393AMJ +
    REC1383AMJ * REC1393CMJ +
    REC1383AMJ * REC1393BMJ +
    REC1383AMJ * REC1393AMJ +
    REC111--MJ * REC1393CMJ +
    REC111--MJ * REC1393BMJ +
    REC111--MJ * REC1393AMJ +
    RCA149D-MJ * REC1383BMJ +
    RCA149D-MJ * REC1383AMJ +
    RCA149D-MJ * REC111--MJ +
    RCA149A-MJ * REC1383BMJ +
    RCA149A-MJ * REC1383AMJ +
    RCA149A-MJ * REC111--MJ +
    RCA148D-MJ * REC1393CMJ +
    RCA148D-MJ * REC1393BMJ +
    RCA148D-MJ * REC1393AMJ +
    RCA148A-MJ * REC1393CMJ +
    RCA148A-MJ * REC1393BMJ +
    RCA148A-MJ * REC1393AMJ +
    RCA1393-MJ * REC1383BMJ +
    RCA1393-MJ * REC1383AMJ +
    RCA1393-MJ * REC111--MJ +
    RCA1393-MC * REC1383BMJ +
    RCA1393-MC * REC1383AMJ +
    RCA1393-MC * REC111--MJ +
    RCA1392-MJ * REC1383BMJ +
    RCA1392-MJ * REC1383AMJ +
    RCA1392-MJ * REC111--MJ +
    RCA1391-MJ * REC1383BMJ +
    RCA1391-MJ * REC1383AMJ +
    RCA1391-MJ * REC111--MJ +
    RCA139--MJ * REC1383BMJ +
    RCA139--MJ * REC1383AMJ +
    RCA139--MJ * REC111--MJ +
    RCA139--MC * REC1383BMJ +
    RCA139--MC * REC1383AMJ +
    RCA139--MC * REC111--MJ +
```

RCA1383-MJ * REC1393CMJ +
RCA1383-MJ * REC1393BMJ +
RCA1383-MJ * REC1393AMJ +
RCA1383-MC * REC1393CMJ +
RCA1383-MC * REC1393BMJ +
RCA1383-MC * REC1393AMJ +
RCA1382-MJ * REC1393CMJ +
RCA1382-MJ * REC1393BMJ +
RCA1382-MJ * REC1393AMJ +
RCA1381-MJ * REC1393CMJ +
RCA1381-MJ * REC1393BMJ +
RCA1381-MJ * REC1393AMJ +
RCA138--MJ * REC1393CMJ +
RCA138--MJ * REC1393BMJ +
RCA138--MJ * REC1393AMJ +
RCA138--MC * REC1393CMJ +
RCA138--MC * REC1393BMJ +
RCA138--MC * REC1393AMJ +
RCA112C-MC * REC1383BMJ +
RCA112C-MC * REC1383AMJ +
RCA112C-MC * REC111--MJ +
RCA111J-MJ * REC1393CMJ +
RCA111J-MJ * REC1393BMJ +
RCA111J-MJ * REC1393AMJ +
RCA111J-MC * REC1393CMJ +
RCA111J-MC * REC1393BMJ +
RCA111J-MC * REC1393AMJ +
RCA111D-MJ * REC1393CMJ +
RCA111D-MJ * REC1393BMJ +
RCA111D-MJ * REC1393AMJ +
RCA111D-MC * REC1393CMJ +
RCA111D-MC * REC1393BMJ +
RCA111D-MC * REC1393AMJ +
RCA111C-MJ * REC1393CMJ +
RCA111C-MJ * REC1393BMJ +
RCA111C-MJ * REC1393AMJ +
RCA111B-MJ * REC1393CMJ +
RCA111B-MJ * REC1393BMJ +
RCA111B-MJ * REC1393AMJ +
MVD1007400 * REC1393CMJ +
MVD1007400 * REC1393BMJ +
MVD1007400 * REC1393AMJ +
MRA1LUBBMG * REC1393CMJ +
MRA1LUBBMG * REC1393BMJ +
MRA1LUBBMG * REC1393AMJ +
MRA1LUBBMG * RCA149D-MJ +
MRA1LUBBMG * RCA149A-MJ +
MRA1LUBBMG * RCA1393-MJ +
MRA1LUBBMG * RCA1393-MC +
MRA1LUBBMG * RCA1392-MJ +
MRA1LUBBMG * RCA1391-MJ +
MRA1LUBBMG * RCA139--MJ +

```
MRA1LUBBMG * RCA139--MC +
MRA1LUBBMG * RCA112C-MC +
MRA11B--MG * REC1393CMJ +
MRA11B--MG * REC1393BMJ +
MRA11B--MG * REC1393AMJ +
MRA11B--MG * RCA149D-MJ +
MRA11B--MG * RCA149A-MJ +
MRA11B--MG * RCA1393-MJ +
MRA11B--MG * RCA1393-MC +
MRA11B--MG * RCA1392-MJ +
MRA11B--MG * RCA1391-MJ +
MRA11B--MG * RCA139--MJ +
MRA11B--MG * RCA139--MC +
MRA11B--MG * RCA112C-MC +
MPX11B--MG * REC1393CMJ +
MPX11B--MG * REC1393BMJ +
MPX11B--MG * REC1393AMJ +
MPB11B--MG * REC1393CMJ +
MPB11B--MG * REC1393BMJ +
MPB11B--MG * REC1393AMJ +
MPB11B--ME * REC1393CMJ +
MPB11B--ME * REC1393BMJ +
MPB11B--ME * REC1393AMJ +
MPB11B--DO * REC1393CMJ +
MPB11B--DO * REC1393BMJ +
MPB11B--DO * REC1393AMJ +
MOD1018DMJ * MOD1019CMJ +
MOD1018CMJ * MVG185E-MB +
MOD1018CMJ * MRA185E-MB +
MOD1018CMJ * MOD1019CMJ +
MOD1016CMJ * MVG185E-MJ +
MOD1016CMJ * MOD1018DMJ +
MOD1016CMJ * MOD1018CMJ +
MOD1016BMJ * MRA185D-MB +
MOD1016BMJ * MOD1018DMJ +
MOD1016BMJ * MOD1018CMJ +
MCE1LUBCMG * REC1383BMJ +
MCE1LUBCMG * REC1383AMJ +
MCE1LUBCMG * REC111--MJ +
MCE1LUBCMG * MRA1LUBBMG +
MCE1LUBCMG * MRA11B--MG +
MCE1LUBBMG * REC1393CMJ +
MCE1LUBBMG * REC1393BMJ +
MCE1LUBBMG * REC1393AMJ +
MCA11B--MD * REC1393CMJ +
MCA11B--MD * REC1393BMJ +
MCA11B--MD * REC1393AMJ +
7VD1----OA * FTA1SCSTMJ

ZZAFWST = ZZAFWSL
```

```
RHRINJ =
    ZOI1006AMJ +
    ZOH1001CMJ * ZOH1002DMJ +
    ZOH1001CMJ * ZOH1002CMJ +
    ZOH1001BMJ * ZOH1002DMJ +
    ZOH1001BMJ * ZOH1002CMJ +
    INJECTION * ZOI1015AMJ +
    INJECTION * ZOI1013BMJ +
    INJECTION * ZOG1011AMJ +
    6OH1005AMJ * ZVG1606-OO +
    6OH1005AMJ * ZOH1001CMJ +
    6OH1005AMJ * ZOH1001BMJ +
    6OH1005AMJ * INJECTION +
    6OH1005AMJ * 6VX1809AOO +
    6OH1004AMJ * ZOH1002DMJ +
    6OH1004AMJ * ZOH1002CMJ +
    6OH1004AMJ * INJECTION +
    6OH1004AMJ * 6OH1005AMJ +
    LOCA-B * LOCA-C * ZOH1002DMJ +
    LOCA-B * LOCA-C * ZOH1002CMJ +
    LOCA-B * LOCA-C * ZOG1011AMJ +
    LOCA-A * LOCA-D * ZOH1001CMJ +
    LOCA-A * LOCA-D * ZOH1001BMJ +
    6OH1005AMJ * LOCA-B * LOCA-C +
    6OH1004AMJ * LOCA-A * LOCA-D +
    LOCA-A * LOCA-B * LOCA-C * LOCA-D +
    INJECTION * LOCA-B * LOCA-C * ZPBI002BMG +
    INJECTION * LOCA-B * LOCA-C * ZPBI002BME +
    INJECTION * LOCA-B * LOCA-C * REC111--MJ +
    INJECTION * LOCA-A * LOCA-D * ZPBI001AMG +
    INJECTION * LOCA-A * LOCA-D * ZPBI001AME +
    INJECTION * LOCA-A * LOCA-D * REC112--MJ

ZZRHRL =
    ZOI1006AMJ +
    ZOH1001CMJ * ZOH1002DMJ +
    ZOH1001CMJ * ZOH1002CMJ +
    ZOH1001BMJ * ZOH1002DMJ +
    ZOH1001BMJ * ZOH1002CMJ +
    6OH1005AMJ * ZVG1606-OO +
    6OH1005AMJ * ZOH1001CMJ +
    6OH1005AMJ * ZOH1001BMJ +
    6OH1005AMJ * 6VX1809AOO +
    6OH1004AMJ * ZOH1002DMJ +
    6OH1004AMJ * ZOH1002CMJ +
    6OH1004AMJ * 6OH1005AMJ +
    LOCA-B * LOCA-C * ZOH1002DMJ +
    LOCA-B * LOCA-C * ZOH1002CMJ +
    LOCA-B * LOCA-C * ZOG1011AMJ
    LOCA-A * LOCA-D * ZOH1001CMJ +
    LOCA-A * LOCA-D * ZOH1001BMJ +
    6OH1005AMJ * RECIRC * ZPB1001AOX +
```

```
    60H1005AMJ * LOCA-B * LOCA-C +
    60H1004AMJ * LOCA-A * LOCA-D +
    LOCA-B * LOCA-C * RECIRC * ZPBR002BMG +
    LOCA-B * LOCA-C * RECIRC * ZPBR002BME +
    LOCA-B * LOCA-C * REC1383BMJ * RECIRC +
    LOCA-B * LOCA-C * REC1383AMJ * RECIRC +
    LOCA-A * LOCA-D * REC1393CMJ * RECIRC +
    LOCA-A * LOCA-D * REC1393BMJ * RECIRC +
    LOCA-A * LOCA-D * REC1393AMJ * RECIRC +
    LOCA-A * LOCA-B * LOCA-C * LOCA-D +
    60J1008AMJ * LOCA-B * LOCA-C * RECIRC +
    60J1007AMJ * LOCA-A * LOCA-D * RECIRC

ZZRHRT =
    ZOI1006AMJ +
    ZOH1001CMJ * ZOH1002DMJ +
    ZOH1001CMJ * ZOH1002CMJ +
    ZOH1001BMJ * ZOH1002DMJ +
    ZOH1001BMJ * ZOH1002CMJ +
    60H1005AMJ * ZVG1606-OO +
    60H1005AMJ * ZOH1001CMJ +
    60H1005AMJ * ZOH1001BMJ +
    60H1005AMJ * 6VX1809AOO +
    60H1004AMJ * ZOH1002DMJ +
    60H1004AMJ * ZOH1002CMJ +
    60H1004AMJ * 60H1005AMJ +
    LOCA-B * LOCA-C * ZOH1002DMJ +
    LOCA-B * LOCA-C * ZOH1002CMJ +
    LOCA-B * LOCA-C * ZOG1011AMJ +
    LOCA-A * LOCA-D * ZOH1001CMJ +
    LOCA-A * LOCA-D * ZOH1001BMJ +
    60H1005AMJ * RECIRC * ZPB1001AOX +
    60H1005AMJ * LOCA-B * LOCA-C +
    60H1004AMJ * LOCA-A * LOCA-D +
    LOCA-B * LOCA-C * RECIRC * ZPBR002BMG +
    LOCA-B * LOCA-C * RECIRC * ZPBR002BME +
    LOCA-B * LOCA-C * REC1383BMJ * RECIRC +
    LOCA-B * LOCA-C * REC1383AMJ * RECIRC +
    LOCA-A * LOCA-D * RECIRC * ZPBR001AMG +
    LOCA-A * LOCA-D * RECIRC * ZPBR001AME +
    LOCA-A * LOCA-D * REC1393CMJ * RECIRC +
    LOCA-A * LOCA-D * REC1393BMJ * RECIRC +
    LOCA-A * LOCA-D * REC1393AMJ * RECIRC +
    LOCA-A * LOCA-B * LOCA-C * LOCA-D +
    60J1008AMJ * LOCA-B * LOCA-C * RECIRC +
    60J1007AMJ * LOCA-A * LOCA-D * RECIRC
```

```
BAFDUMMY =
    B&F-OP-ERR +
    6TA1001AMJ * INJECTION +
    6VX1880600 * 8RD-092-MJ * INJECTION +
    6VX1880600 * 8RD-091-MJ * INJECTION +
    6RD1071-MJ * 6VX1880600 * INJECTION +
    60E1098AMJ * 60E1100AMJ * 8RD-092-MJ * INJECTION +
    60E1098AMJ * 60E1100AMJ * 8RD-091-MJ * INJECTION +
    60E1098AMJ * 60E1100AMJ * 80E1091AMJ * INJECTION +
    60E1098AMJ * 60E1100AMJ * 6RD1071-MJ * INJECTION +
    60D1100AMJ * 60E1098AMJ * 8RD-092-MJ * INJECTION +
    60D1100AMJ * 60E1098AMJ * 8RD-091-MJ * INJECTION +
    60D1100AMJ * 60E1098AMJ * 6RD1071-MJ * INJECTION +
    60E1100AMJ * 8RD-092-MJ * ORA1A---MB * ORA1B---MB * RZZ0LOSPMP +
    60E1100AMJ * 8RD-092-MJ * 9RA1B6--MG * ORA1A---MB * RZZ0LOSPMP +
    60E1100AMJ * 8RD-092-MJ * 9RA1A6--MG * ORA1B---MB * RZZ0LOSPMP +
    60E1100AMJ * 8RD-092-MJ * 9RA1A6--MG * 9RA1B6--MG * RZZ0LOSPMP +
    60E1100AMJ * 8RD-091-MJ * ORA1A---MB * ORA1B---MB * RZZ0LOSPMP +
    60E1100AMJ * 8RD-091-MJ * 9RA1B6--MG * ORA1A---MB * RZZ0LOSPMP +
    60E1100AMJ * 8RD-091-MJ * 9RA1A6--MG * ORA1B---MB * RZZ0LOSPMP +
    60E1100AMJ * 8RD-091-MJ * 9RA1A6--MG * 9RA1B6--MG * RZZ0LOSPMP +
    60D1100AMJ * 8RD-092-MJ * ORA1A---MB * ORA1B---MB * RZZ0LOSPMP +
    60D1100AMJ * 8RD-092-MJ * 9RA1B6--MG * ORA1A---MB * RZZ0LOSPMP +
    60D1100AMJ * 8RD-092-MJ * 9RA1A6--MG * ORA1B---MB * RZZ0LOSPMP +
    60D1100AMJ * 8RD-092-MJ * 9RA1A6--MG * 9RA1B6--MG * RZZ0LOSPMP +
    60D1100AMJ * 8RD-091-MJ * ORA1A---MB * ORA1B---MB * RZZ0LOSPMP +
    60D1100AMJ * 8RD-091-MJ * 9RA1B6--MG * ORA1A---MB * RZZ0LOSPMP +
    60D1100AMJ * 8RD-091-MJ * 9RA1A6--MG * ORA1B---MB * RZZ0LOSPMP +
    60D1100AMJ * 8RD-091-MJ * 9RA1A6--MG * 9RA1B6--MG * RZZ0LOSPMP +
    60E1100AMJ * 6RD1071-MJ * INJECTION * ORA1A---MB * ORA1B---MB *
                                                          RZZ0LOSPMP +
    60E1100AMJ * 6RD1071-MJ * 9RA1B6--MG * INJECTION * ORA1A---MB *
                                                          RZZ0LOSPMP +
    60E1100AMJ * 6RD1071-MJ * 9RA1A6--MG * INJECTION * ORA1B---MB *
                                                          RZZ0LOSPMP +
    60E1100AMJ * 6RD1071-MJ * 9RA1A6--MG * 9RA1B6--MG * INJECTION *
                                                          RZZ0LOSPMP +
    60D1100AMJ * 6RD1071-MJ * 9RA1B6--MG * INJECTION * ORA1A---MB *
                                                          RZZ0LOSPMP +
    60D1100AMJ * 6RD1071-MJ * 9RA1A6--MG * 9RA1B6--MG * INJECTION *
                                                            RZZ0LOSPMP

SSLOCAD =
    MRA1LUBBMG * REC1393CMJ +
    MRA1LUBBMG * REC1393BMJ +
    MRA1LUBBMG * REC1393AMJ +
    MRA11B--MG * REC1393CMJ +
    MRA11B--MG * REC1393BMJ +
    MRA11B--MG * REC1393AMJ +
    MRA1LUBBMG * REC1393CMJ
```

```
T1A =
    MOD1018DMJ * MOD1019CMJ * ZOI1006AMJ +
    MOD1018CMJ * MVG185E-MB * ZOI1006AMJ +
    MOD1018CMJ * MRA185E-MB * ZOI1006AMJ +
    MOD1018CMJ * MOD1019CMJ * ZOI1006AMJ

T17 =
    ZZCH--ROOF * ZZCH-EFFEC +
    ZZ--UPLIFT * ZZUP-EFFEC +
    ZZSHR-WALL * ZZSW-EFFEC +
    B&F-OP-ERR * ZZAFWST * ZZPCS

T17NPCS =
    ZZCH--ROOF * ZZCH-EFFEC +
    ZZ--UPLIFT * ZZUP-EFFEC +
    ZZSHR-WALL * ZZSW-EFFEC +
    B&F-OP-ERR * ZZAFWST


  ACC(1) = IE(1)
  ACC(2) = IE(2) * ZZECRLL * (1-ZZECILL) * (1-ZZRHRL)
  ACC(3) = IE(2) * ZZRHRL  * (1-ZZECILL)
  ACC(4) = IE(2) * ZZECILL
  ACC(5) = IE(3) * ZZRHRL *  (1-ZZECIML) * (1-RPS)
  ACC(6) = IE(3) * ZZECIML * (1-RPS)
  ACC(7) = IE(4) * ZZRHRL *  (1-ZZECISL) * (1-RPS)
  ACC(8) = IE(4) * ZZECISL * (1-RPS)
  ACC(9) = IE(5) * ZZRHRL *  (1-ZZAFWSL) * (1-ZZECISS) * (1.-RPS)
  ACC(10)= IE(5) * ZZECISS * (1-ZZAFWSL) * (1-RPS)
  ACC(11)= IE(5) * SSLOCAD * ZZRHRL * (1.-BAFDUMMY) * (1-RPS)
  ACC(12)= IE(5) * T17NPCS * (1-RPS)
  ACC(13)= IE(6) * T17NPCS * (1-RPS)
  ACC(14)= IE(7) * T1A * ZZPCS * (1-BAFDUMMY) * (1-RPS)
  ACC(15)= IE(7) * T17 * (1-RPS)
```

ZION REFRENCE FILE

P_{random}	Basic Event	EF	N_{frag}	N_{resp}	N_{corr}	No.
0.0	RZZOLOSPMP	3.0	49	1		1
0.0	RVR		65	48		2
0.0	LLOCA		66	48		3
0.0	MLOCA		67	48		4
0.0	SLOCA		68	48		5
0.0	SSLOCA		69	48		6
0.25	LOCA-A		0	0		7
0.25	LOCA-B					8
0.25	LOCA-C					9
0.25	LOCA-D					10
1.0E-2	B&F-OP-ERR		0	0		11
1.0	INJECTION		0	0		12
0.0	ECF		0	0		13
1.0	RECIRC		0	0		14
3.0E-5	RPS		0	0		15
0.010	SRV/O		0	0		16
0.098	SRV/R		0	0		17
0.0	ZZCH--ROOF		29	1		18
0.0	ZZ--UPLIFT		52	49		19
0.0	ZZSHR-WALL		51	16		20
1.0	ZZCH-EFFEC		0	0		21
1.0	ZZUP-EFFEC		0	0		22
1.0	ZZSW-EFFEC		0	0		23
0.0	ZZCSIS-CFC		53	48		24
	MOD1016BMJ		57	24		25
	MOD1016CMJ		57	26		26
	MOD1018CMJ		57	22		27
	MOD1018DMJ		57	22		28
	MOD1019CMJ		57	23		29
	QOF118B-MJ		59	45		30
	XOA10010MJ		54	23		31
	XOA10173MJ		54	23		32
	XOA10174MJ		54	29		33
	XOA10180MJ		54	22		34
	XOB10011MJ		55	47		35
	XOB10079MJ		55	25		36
	XOC10126MJ		56	19		37
	XOC10200MJ		56	21		38
	XOE1141-MJ		58	47		39
	XOE1142-MJ		58	42		40
	XOE10142MJ		58	19		41
	XOG10007MJ		60	38		42
	XOG10008MJ		60	34		43
	XOG10046MJ		60	34		44
	XOG10083MJ		60	38		45
	XOG10090MJ		60	34		46
	XOG10111MJ		60	38		47
	XOG10113MJ		60	34		48

P_{random}	Basic Event	EF	N_{frag}	N_{resp}	N_{corr}	No.
	XOG10125MJ		60	38		49
	XOI10004MJ		62	33		50
	XOI10140MJ		62	46		51
	XOI10141MJ		62	47		52
	XOK10001MJ		64	30		53
	XOK10002MJ		64	31		54
	XOK10003MJ		64	32		55
	XOK10033MJ		64	35		56
	XOK10034MJ		64	36		57
	XOK10035MJ		64	37		58
	XOK10068MJ		64	39		59
	XOK10069MJ		64	40		60
	XOK10070MJ		64	41		61
	XOK10110MJ		64	43		62
	XOK10121MJ		64	44		63
	XOK10122MJ		64	45		64
	ZOD1032AMJ		57	28		65
	ZOG1011AMJ		60	25		66
	ZOH1001BMJ		61	26		67
	ZOH1001CMJ		61	26		68
	ZOH1002CMJ		61	47		69
	ZOH1002DMJ		61	42		70
	ZOI1006AMJ		62	24		71
	ZOI1013BMJ		62	25		72
	6OH1004AMJ		61	26		73
	6OH1005AMJ		61	27		74
	6OH1034BMJ		61	23		75
	6OJ1007AMJ		63	25		76
	6OJ1008AMJ		63	24		77
	FTA1SCSTMJ		32	2		78
	KPX1RCPAMQ		13	7		79
	KPX1RCPBMQ					80
	KPX1RCPCMQ					81
	KPX1RCPDMQ					82
	MCA11B--MD		41	17		83
	MCE1LUBBMG		41	17		84
	MCE1LUBCMG					85
	MHA1SGA-MQ		4	8		86
	MHA1SGB-MQ					87
	MHA1SGC-MQ					88
	MHA1SGD-MQ					89
8.0E-3	MPB11B--DO		0	0		90
	MPB11B--ME		14	12		91
	MPB11B--MG		14	12		92
	MPX11B--MG		14	12		93
	MRA185D-MB		22	17		94
	MRA185E-MB					95
	MRA11B--MG					96
	MRA1LUBBMG					97
	MVA1005-MD		16	18		98

P_{random}	Basic Event	EF	N_{frag}	N_{resp}	N_{corr}	No.
	MVA1006-MD					99
	MVA1007-MD					100
	MVA1008-MD					101
	MVA10045MD					102
	MVD10005MD					103
	MVD10016MD		16	18		104
	MVD10017MD					105
	MVD10018MD		16	18		106
	MVD10019MD					107
	MVD10020MD					108
8.0E-3	MVD1007400		0	0		109
	MVG1510-MD		16	18		110
	MVG1520-MD					111
	MVG1530-MD					112
	MVG1540-MD					113
	MVG185--MP					114
	MVG185E-MB		16	20		115
	MVG185E-MJ		19	20		116
	RCA111B-MJ		41	17		117
	RCA111C-MJ					118
	RCA111D-MC					119
	RCA111D-MJ					120
	RCA111J-MC					121
	RCA111J-MJ					122
	RCA112C-MC					123
	RCA138--MC					124
	RCA138--MJ					125
	RCA1381-MJ					126
	RCA1382-MJ					127
	RCA1383-MC					128
	RCA1383-MJ					129
	RCA139--MC					130
	RCA139--MJ					131
	RCA1391-MJ					132
	RCA1392-MJ					133
	RCA1393-MC					134
	RCA1393-MJ					135
	RCA148A-MJ					136
	RCA148D-MJ					137
	RCA149A-MJ					138
	RCA149D-MJ					139
	REC1383AMJ		36	17		140
	REC1383BMJ					141
	REC1383CMJ					142
	REC1393AMJ					143
	REC1393BMJ					144
	REC1393CMJ					145
	REC111--MJ					146
5.0E-3	ZPB1001AOX		0	0		147
1.0E-3	ZVM1728BOD		0	0		148

P_{random}	Basic Event	EF	N_{frag}	N_{resp}	N_{corr}	No.
8.0E-3	ZVG1606-OO		0	0		149
8.0E-3	ZVG1607-OO					150
	5TA1----MJ		32	2		151
8.0E-3	6VX1809AOO		0	0		152
8.0E-3	6VX1880600					153
	6TA1001AMJ		45	1		154
	6TA1005AMJ		8	3		155
	6TA1006BMJ					156
	6TA1007CMJ					157
	6TA1008DMJ					158
1.0E-3	7VD1----OA		0	0		159
	KPX2RCP-CC		13	7	2	160
	MHA2SG--CC		4	8	2	161
	ZOI1015AMJ		62	25		162
	6OE1098AMJ		58	26		163
	6OE1100AMJ		58	26		164
	6OD1100AMJ		57	26		165
	8OE1091AMJ		58	26		166
	REC112--MJ		36	17		167
3.0E-3	ZPBI001AME	10.0	0	0		168
3.0E-3	ZPBI002BME					169
3.0E-3	ZPBR001AME					170
3.0E-3	ZPBR002BME					171
7.2E-4	ZPBI001AMG					172
7.2E-4	ZPBI002BMG					173
7.2E-4	ZPBR001AMG					174
7.2E-4	ZPBR002BMG					175
	6RD1071-MJ	3.0	41	17		176
	8RD-091-MJ					177
	8RD-092-MJ					178
3.0E-6	ORA1A---MB	10.0	22	17		179
3.0E-6	ORA1B---MB					180
3.0E-6	9RA1A6--MG					181
3.0E-6	9RA1B6--MG					182
0.0	ZZPCS	3.0	53	48		183
	6OE-CM		58	26	1	184
3.0E-6	ORA-CM	10.0	22	17	2	185
3.0E-6	9RA-CM	10.0	22	17	2	186
	REC-CM	3.0	36	17	2	187
	ZOH-CM		61	47	1	188
	6OH-CM		61	26	1	189
	MOD-CM		57	24	1	190

DESCRIPTION OF METHODOLOGY

Approximate Method of calculating New Eigenvalues and Eigenvectors for small Variations in the Stiffness Matrix

Due to the large size of the structural models for the Zion plant, the calculation of the Eigenvalues and Eigenvectors during the iterative analyses performed to determine the final degraded models was carried out using a methodology which approximates the degraded Eigensystem making the iterative process far more efficient and faster than starting with an unapproximated Eigensystem. Since the change in stiffness properties is small at each iteration step, the new Eigenvectors do not vary significantly and can be expressed as a truncated series using the old Eigenvectors as a starting point. In this way, only a reduced new Eigenproblem needs to be solved. The development of this methodology is presented below:

The original Eigenproblem can be expressed by

$$K\phi - \lambda M\phi = 0$$

where K is the stiffness matrix, M the mass matrix, ϕ the Eigenvector, and λ the Eigenvalue.

For the modified stiffness, the new Eigenproblem can be written as

$$K^*\phi^* - \lambda^* M\phi^* = 0$$

If the new Eigenvectors are expressed as a truncated series of the old ones, then,

$$\phi^* = \sum_i c_i\phi_i$$

and if the new stiffness matrix is expressed as

$$K^* = K + \Delta K$$

where ΔK is the change in stiffness, then

$$(K + \Delta K) \sum_i c_i\phi_i - \lambda^* M \sum_i c_i\phi_i = 0$$

Multiplying the above equation by the transpose of ϕ_j and using orthogonality,

$$c_j K_j + \sum_i c_i \Delta K_{ji} - \lambda^* c_j M_j = 0$$

where

$$\Delta K_{ji} = \phi_j{}^T \Delta K \phi_i$$

$$K_j = \phi_j^T K \phi_j$$

$$M_j = \phi_j^T M \phi_j \quad \text{and}$$

$$K_j = \lambda_j M_j$$

Then a new Eigenproblem can be expressed by

$$\begin{vmatrix} \lambda_1 M_1 + \Delta K_{11} & \Delta K_{12} & \cdots & \Delta K_{1n} \\ \Delta K_{21} & \lambda_2 M_2 + \Delta K_{22} & & \Delta K_{2n} \\ \cdot & & & \\ \cdot & & & \\ \cdot & & & \\ \Delta K_{n1} & \Delta K_{n2} & \cdots & \lambda_n M_n + \Delta K_{nn} \end{vmatrix} \begin{vmatrix} c_1 \\ c_2 \\ \\ \\ \\ c_n \end{vmatrix} = \lambda \begin{vmatrix} M_1 & 0 & .. & 0 \\ & M_2 & .. & 0 \\ & & & \\ & & \cdot & \\ 0 & 0 & & M_n \end{vmatrix} \begin{vmatrix} c_1 \\ c_2 \\ \\ \\ \\ c_n \end{vmatrix}$$

The Eigenvalues obtained from the above equation correspond to the new Eigenvalues. Each of the Eigenvectors correspond to the coefficients of the series used to calculate the new Eigenvectors ϕ^*.

Since ΔK has values different then 0 only for those degrees of freedom associated with elements whose stiffness change, the value ΔK_{ij} can be calculated as follows;

$$\Delta K_{ij} = \sum_k \sum_l \phi_i(k) \phi_j(l) \Delta K(k,l)$$

where k and l are the degrees of freedom associated with stiffness matrix changes. It is important to note then that the evaluation ΔK_{ij} can be done at the element level.

This approximate method greatly reduces the computational effort in the calculation of the new Eigenvalues and Eigenvectors at each iteration of the stiffness degradation process.

FURTHER DETAILS

Relative Contribution of Shear vs. Bending Stiffness and Wall vs. Floor Stiffness for Zion.

This appendix describes the relative contributions of shear vs. bending stiffness and wall vs. floor stiffness to the dynamic response of the Reactor Internal Building at the Zion Power Plant. For this study, the first structural mode was chosen for comparison purposes (mode 17). Four different cases were modeled given the parameters listed in the table below and eigenvalues were calculated for each case. Only mode 17 is shown for comparison.

Case A	Case B	Case C	Case D
Original	Reduced Wall (Shear Only)	Reduced Wall (Shear+Bending)	Reduced Wall/Floor (Shear+Bending)
100%E-Walls	100%E-Walls	75%E-Walls	75%E-Walls
100%G-Walls	75%G-Walls	75%G-Walls	75%G-Walls
100%E-Floors	100%E-Floors	100%E-Floors	75%E-Floors
100%G-Floors	100%G-Floors	100%G-Floors	75%G-Floors
1st Structural Mode 17 12.88 Hz	1st Structural Mode 17 12.45 Hz	1st Structural Mode 17 11.77 Hz	1st Structural Mode 17 11.27 Hz
	96.7% of Original delta = 0.43	91.4% of Original delta = 1.11	87.5% of Original delta = 1.61

First the contribution of shear vs. bending stiffness was compared:

Cases A and B: Shear contributes 0.43/1.11 = 39% to the overall frequency.
Cases A and C: Bending contributes (1.11-0.43)/1.11 = 61% to the overall frequency.

Second the contribution of wall vs. floor stiffness was compared:

Cases A and C: Walls contribute 1.11/1.61 = 69% to the overall frequency.
Cases A and D: Floors contribute (1.61-1.11)/1.61 = 31% to the overall frequency.

Assuming motion in the building to be restrained entirely by wall shear deformations, a reduction of stiffness to 75% produced a reduction of frequency to sqrt(75%) which equals 86.6% (consistent with case D above).

However, for the shear wall degradation study the contribution of the walls deforming in shear consisted of 39% * 69% = 27%. This degradation in shear wall stiffness produced only a (100-86.6)*0.27 = 3.62% reduction in frequency (consistent with case B above). In other words, the degraded model in the shear stiffness degradation study should be 100-3.62 = 96.4% of the original model (consistent with Table 4.## for the horizontal structural modes).

APPENDIX C

ANO-1 ANALYSIS

CONTENTS

C.1 INTRODUCTION

The ANO-1 plant was selected for analyzing the potential impacts of degraded shear wall stiffness on plant seismic design loads and plant seismic risk because systems models and data had been developed in two previous NRC-sponsored studies, namely:

a) the Interim Reliability Evaluation Program [IREP, Reference C-1], and

b) the TAP A-45 Evaluation of the Adequacy of Decay Heat Removal Systems program [Reference C-2]

In the TAP-45 program, a seismic PRA based on small LOCAs and two types of transient initiators was performed, and dynamic structural models of the buildings important to safety were developed.

In this study, the same small and small-small LOCA and transient event accident sequence expressions developed in the TAP A-45 program were used, and new sequences based on large and medium LOCAs from the IREP study were incorporated. In addition, the seismic hazard curves for the site were updated, and are now based on the results developed in the NRC-sponsored Seismic Hazard Characterization of the Central and Eastern United States program as reported in Reference C-3. (These results were not available at the time the TAP A-45 program was completed). In addition, the industry-sponsored Electric Power Research Institute's Seismic Hazard Methodology Development program for the Eastern United States [Reference C-4], was also used. Of course, a full set of new structural responses was computed -- both with and without degraded shear wall stiffnesses -- as described in this Appendix.

An important difference between this study and the TAP A-45 study is that, in the TAP A-45 work, only point estimates of core damage frequencies were calculated, whereas in this study, true mean values were calculated and a full uncertainty analysis was performed. Hence the numerical results are expected to differ between the two studies.

C.1.1 Plant Description

The Arkansas Nuclear One Unit-1 (ANO-1) nuclear power plant is an 836 MWe pressurized water reactor (PWR) located on Lake Dardanelle near Russelville, Arkansas. Arkansas Power and Light Company owns and operates the facility. ANO-1 entered commercial operation in December 1974.

The reactor vendor for ANO-1 was Babcock and Wilcox (B&W). The architect/engineer was the Bechtel Power Corporation. The design of the reactor coolant system is typical of other B&W plants currently in commercial operation; there are two once-through steam generators and four reactor coolant loops. Most of the major safety system designs are also fairly typical of other B&W plants.

The plant is on a site where shallow clay and silty clay deposit overlie bedrock consisting of Pennsylvanian McAlester Formation shale. Hard, fine-grained sandstone of the Harthshorne formation underlie the shale and is encountered at depth of 150 ft. The plant foundation was placed on bedrock, so this is considered a rock site. Based on the ANO-1 Final Safety Analysis Report [Reference C-5], a horizontal peak ground acceleration of 0.20g was defined for the SSE.

C.1.2 Description of Plant Systems

In this section, the important plant systems are briefly discussed with the functional interactions which cause the dominant seismic failure modes highlighted.

High Pressure Injection/High Pressure Recirculation

The high pressure (HP) system is utilized during those LOCAs where the reactor coolant pressure remains high (i.e., above about 150 psig). Figures C-1 through C-3 are simplified schematics of the HP system.

The HP system is a two-train, three-pump system which injects water into the reactor pressure vessel via four injection headers (one for each cold leg of the RCS). The injection headers are cross-connected such that each pump has an open flow path to all four reactor coolant system (RCS) cold legs. Suction in the injection mode is from the BWST, while in the recirculation mode it is from the low pressure injection system. Pumps A and B are powered from AC/DC train A and pump C is powered from AC/DC train B.

Low Pressure Injection/Low Pressure Recirculation

The LPI/LPR system serves a number of functions during both accident conditions and normal operations. Along with providing decay heat removal and filling and draining of the fuel transfer canal during plant outages and refueling, the system also provides emergency core cooling (ECC) during a LOCA. Figures C-4 through C-8 are simplified schematics of the LPI/LPR system.

The LPI/LPR system consists of two independent trains which draw water via a common header from the BWST in the injection mode and the reactor building sump in the recirculation mode. Each train of the LP system consists of an LP pump decay heat cooler, piping and valves Water is injected directly into the reactor pressure vessel through the two cross-tied injection headers. LP pumps A and B are powered from AC/DC trains A and B respectively.

Emergency Feedwater System

The emergency feedwater (EFW) system is backup for the main feedwater system (MFWS). Post-shutdown decay heat is removed from the reactor coolant system (RCS) via the steam generators (SGs). Figure C-9 is a simplified schematic of the EFW system.

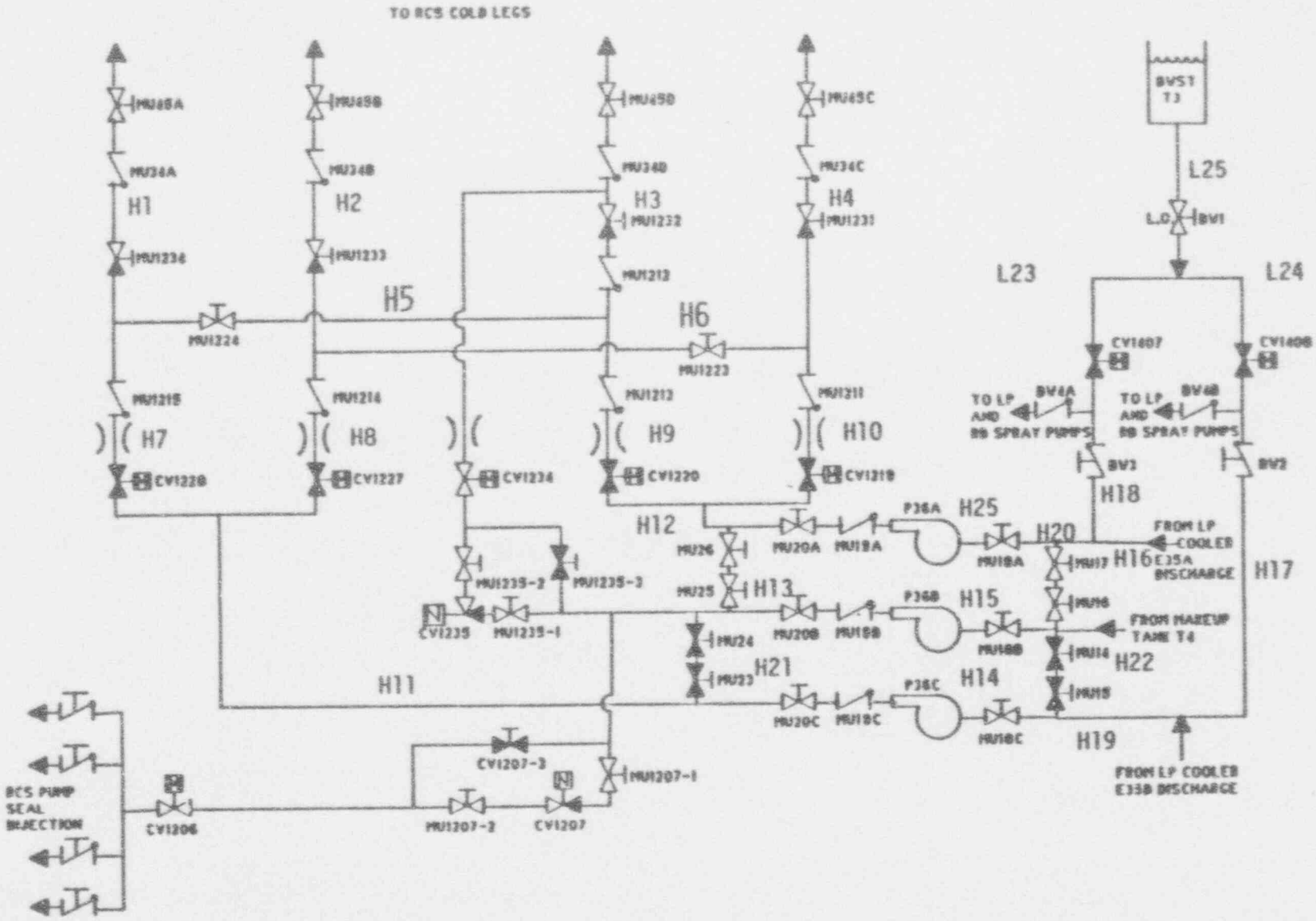

Figure C-1 Pipe Segments of High Pressure Injection System

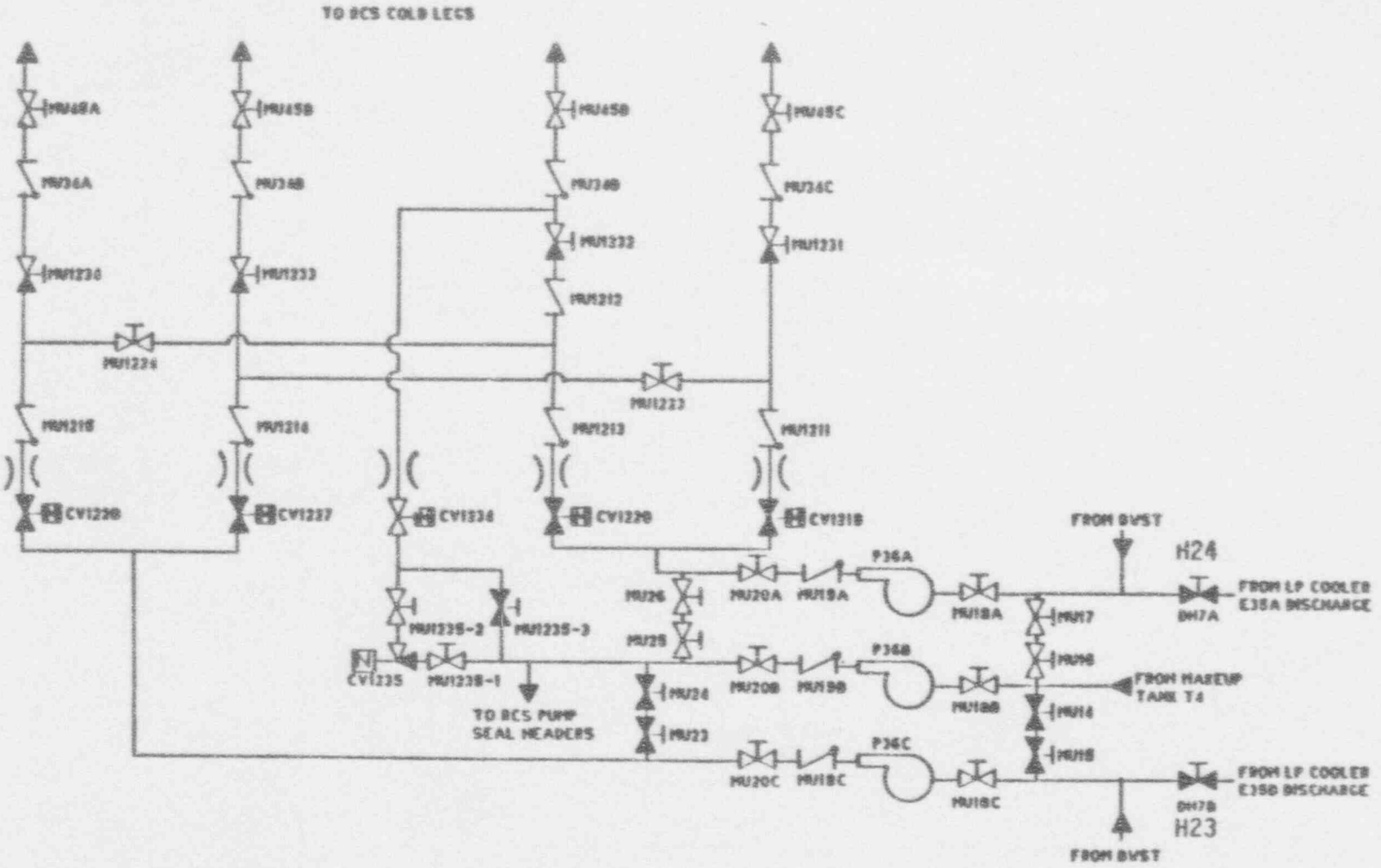

Figure C-2 Pipe Segments for High Pressure Recirculation System

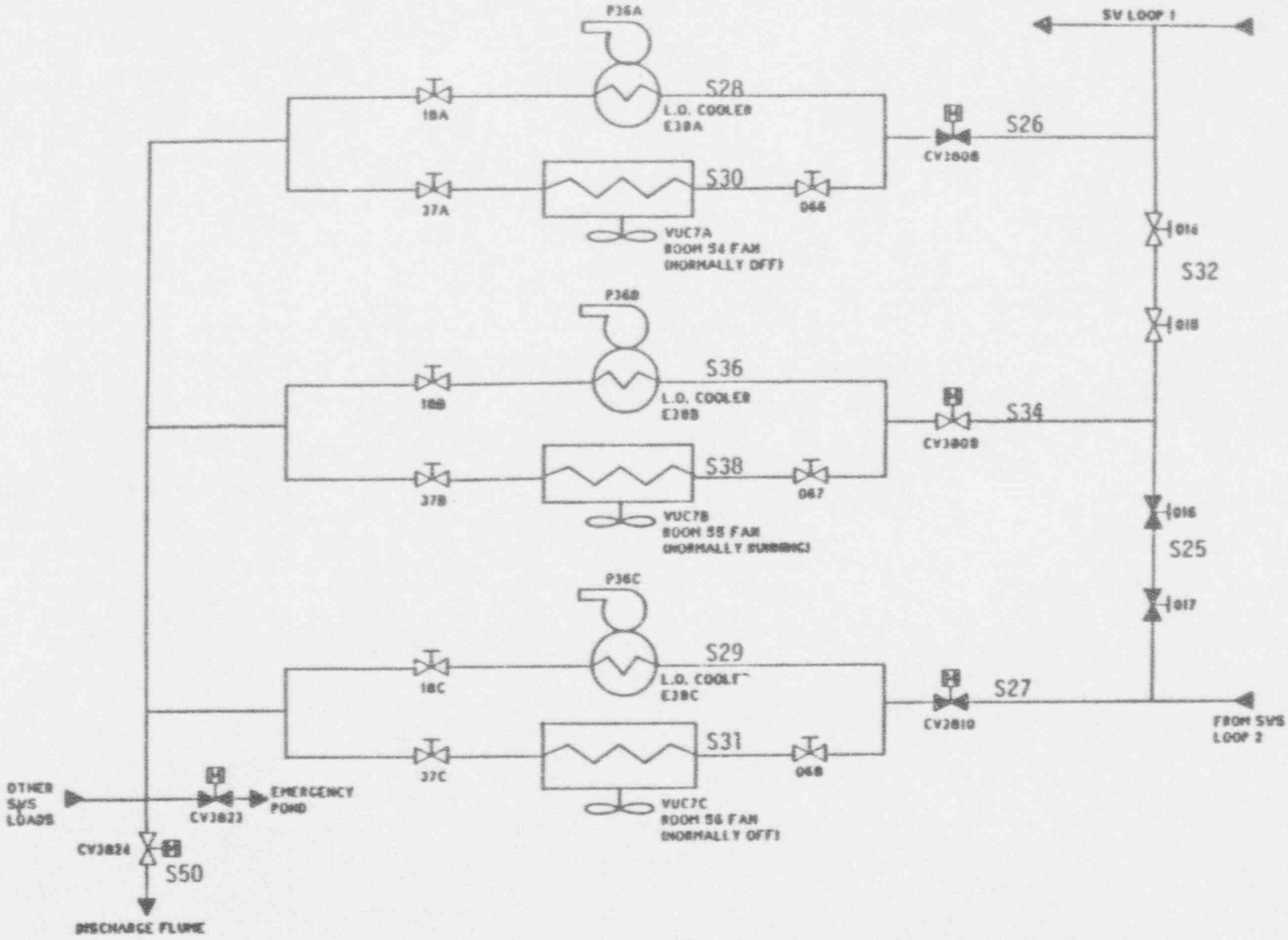

Figure C-3 Pipe Segments for High Pressure Pumps Lube Oil and Room Cooling

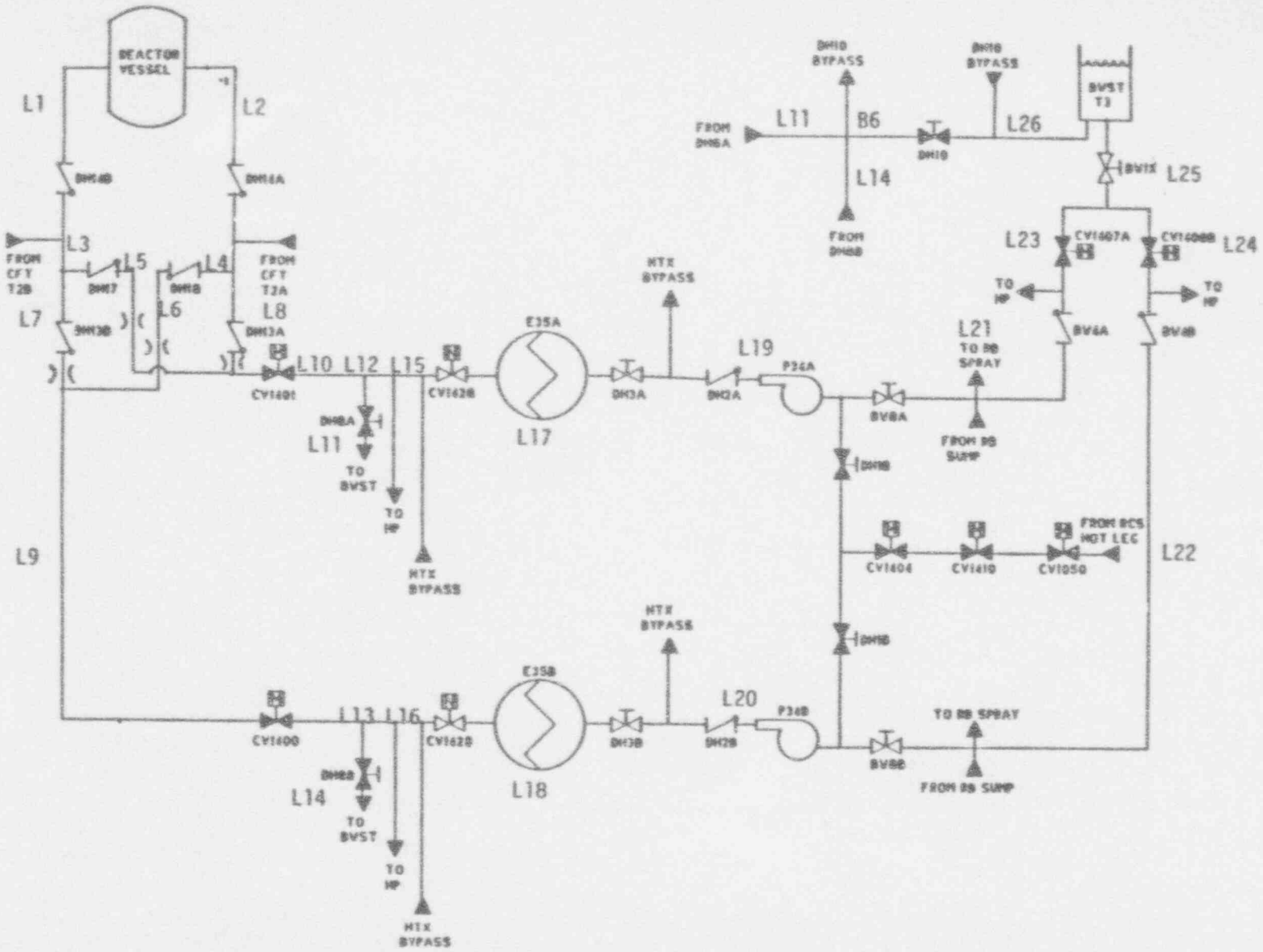

Figure C-4 Pipe Segments for Low Pressure Injection System

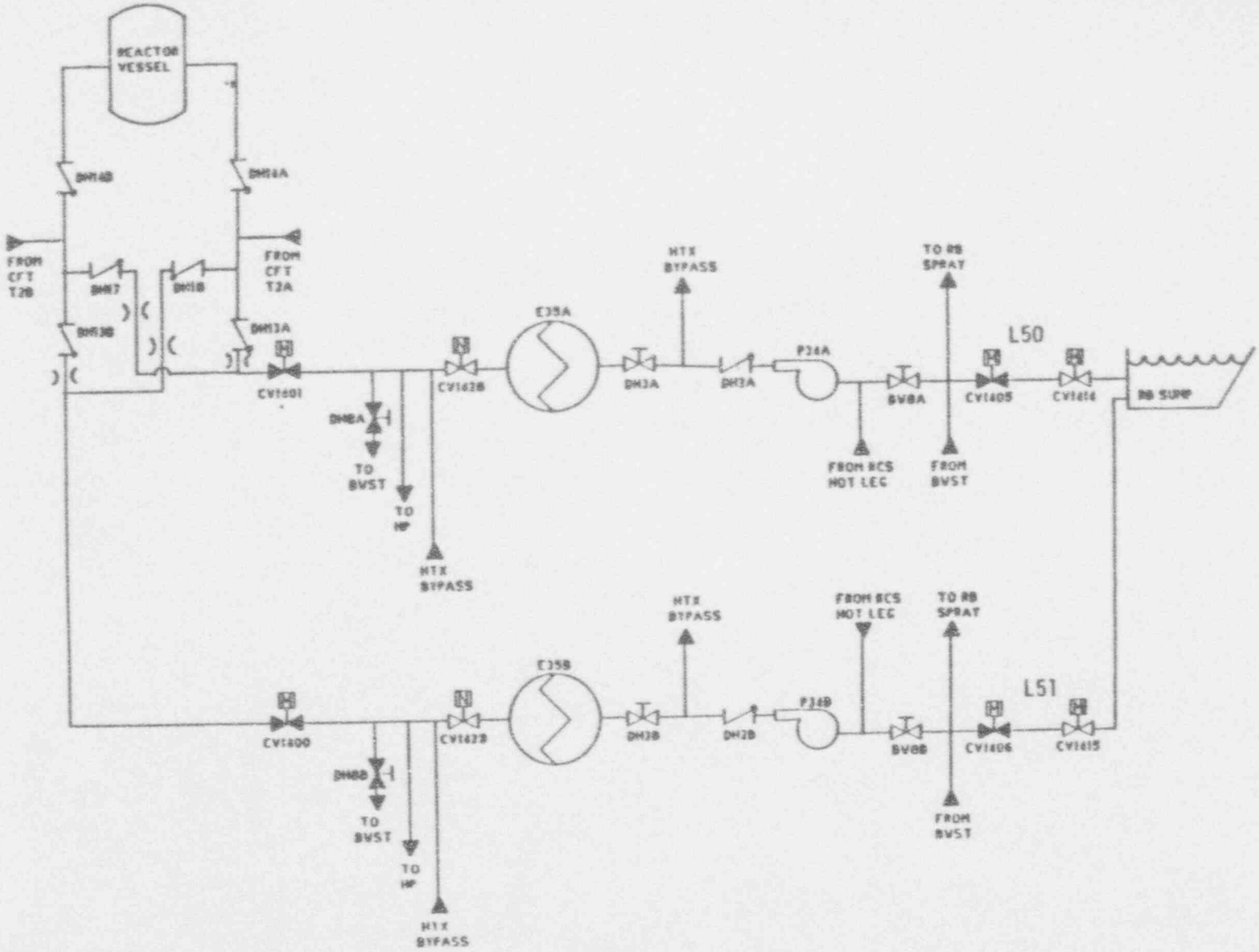

Figure C-5 Pipe Segments for Low Pressure Recirculation System

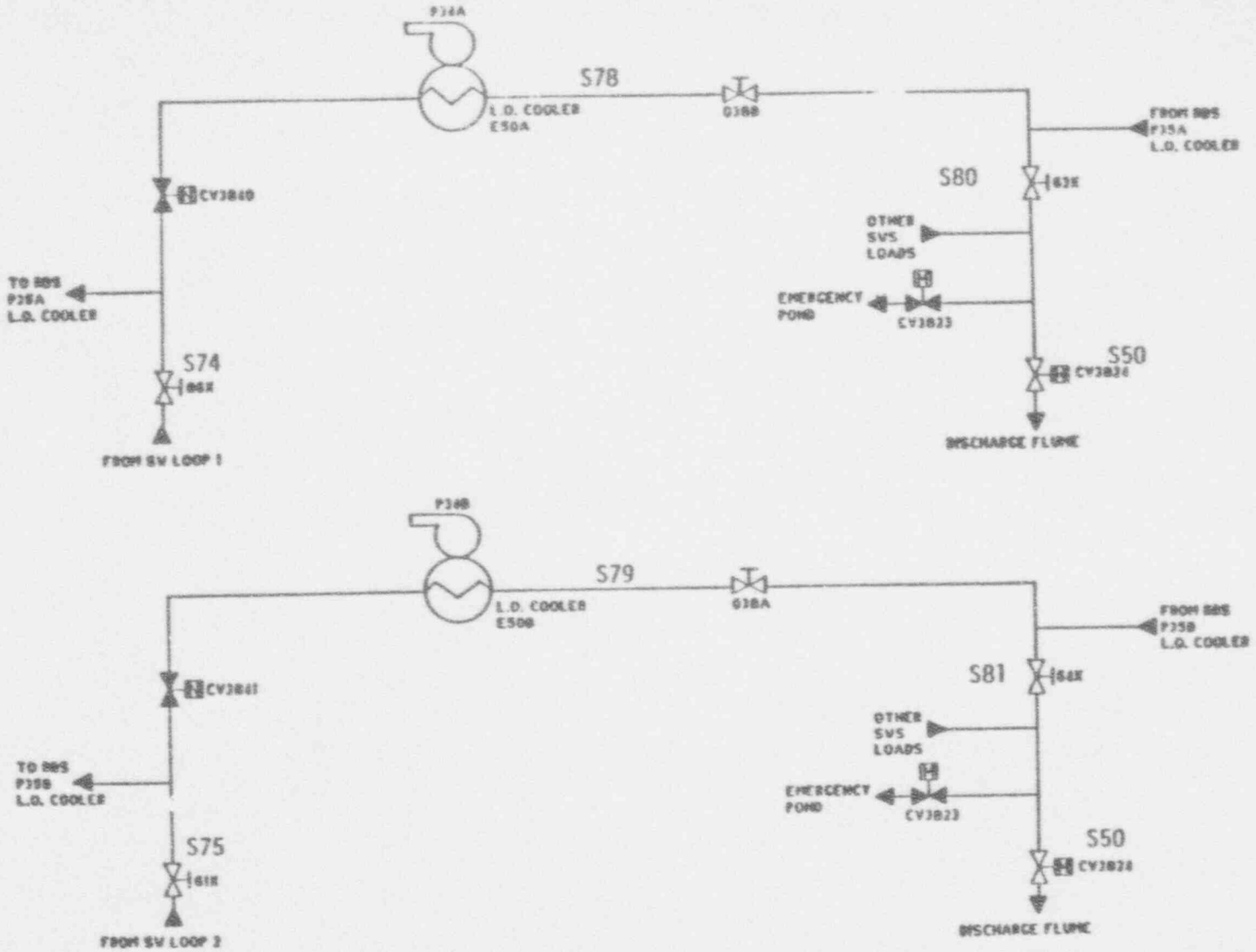

Figure C-6 Pipe Segments for Low Pressure Pump Lube Oil Coolers

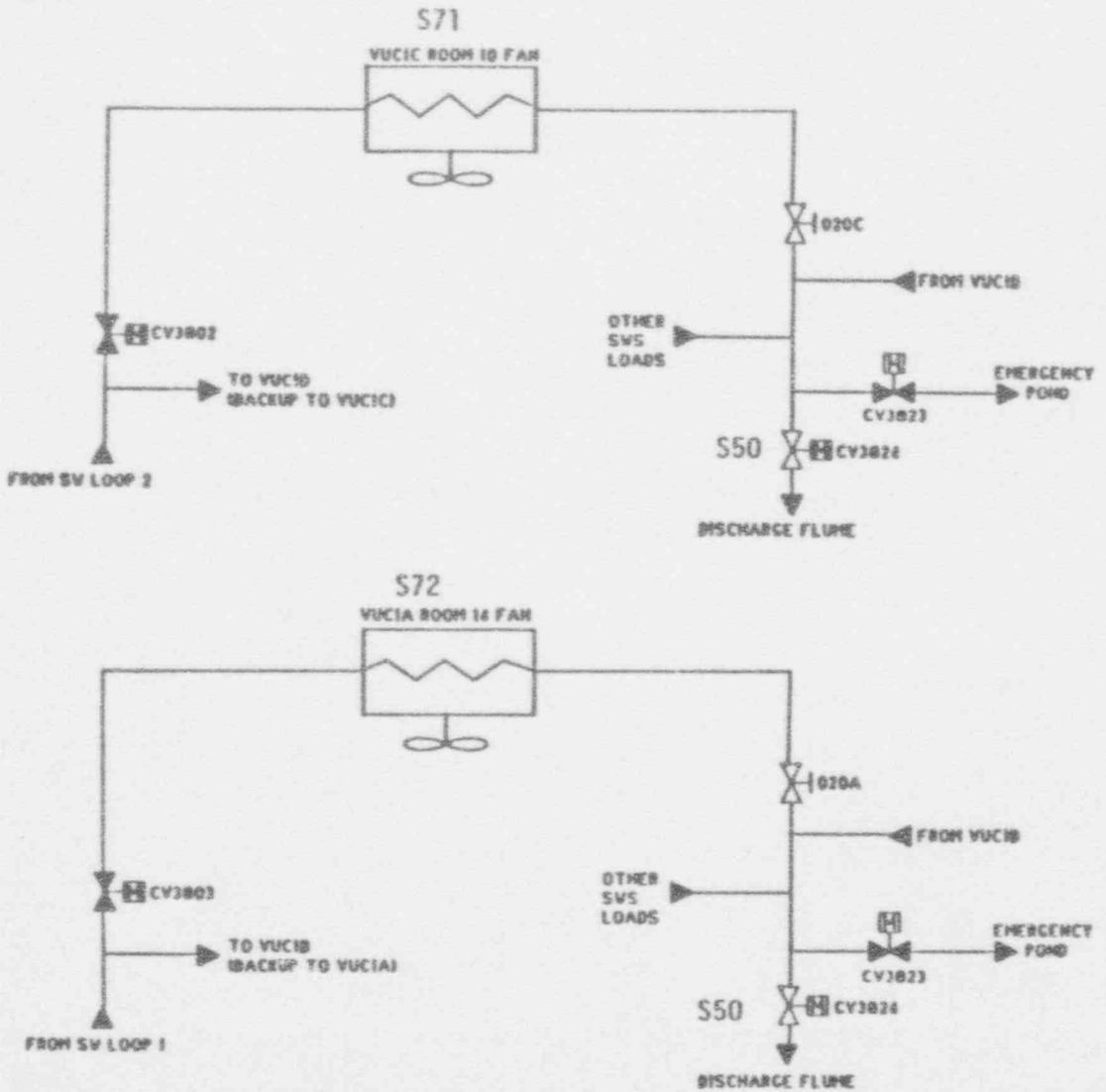

Figure C-7 Pipe Segments for Low Pressure Pump Room Coolers

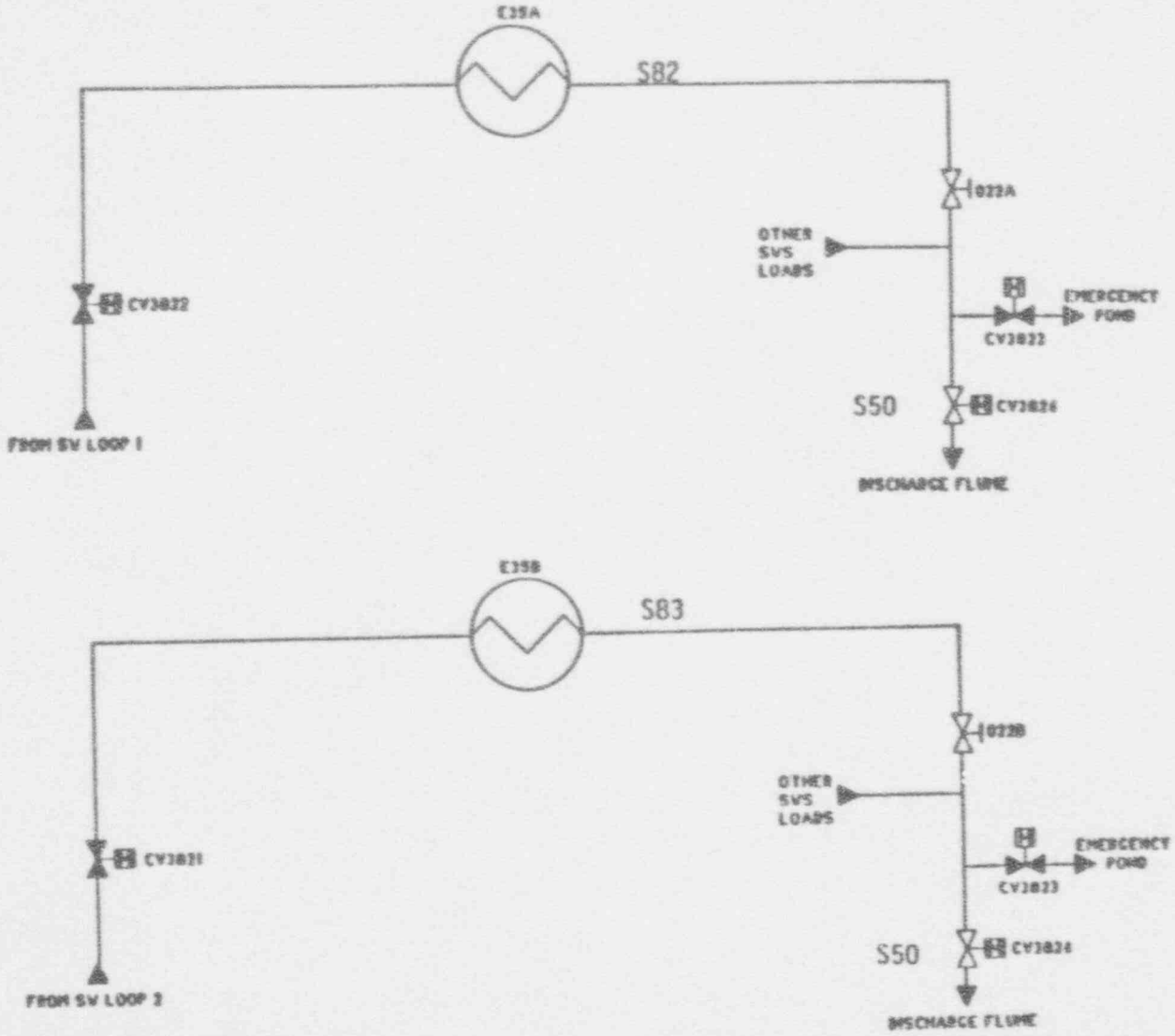

Figure C-8 Pipe Segments for Low Pressure Decay Heat Exchangers Cooling

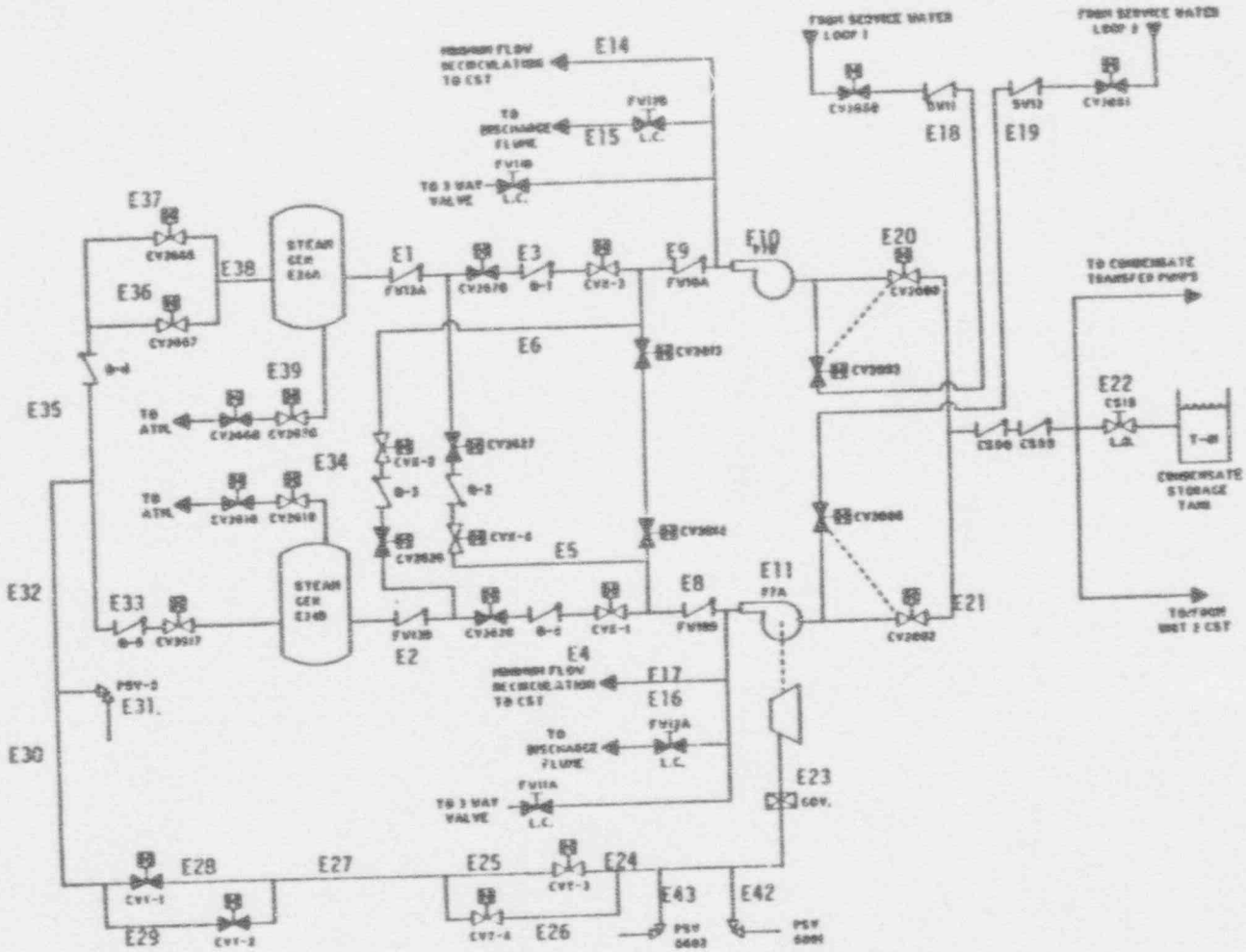

Figure C-9 Pipe Segments for the Emergency Feedwater System

The EFW system consists of two interconnected trains, capable of supplying feedwater to either or both steam generators. Train A contains a motor-driven pump, and the pump of train B is turbine driven. The system pumps take suction from the condensate storage tank (CST). The motor-driven pump is powered from AC/DC train A, while the steam admission valves A and B for the turbine-driven pump are powered from DC trains A and B respectively.

Reactor Building Cooling System

Reactor building cooling system (RBCS) limits post-accident reactor building pressure during steam evolution within the building due to an accident. Figure C-10 is a simplified schematic of the RBCS.

The reactor building atmosphere enters each of the fan coolers at the fan locations. All four fans discharge into a supply air plenum which distributes cooled air throughout the reactor building.

Power Conversion System

The power conversion system (PCS) provides feedwater to the secondary side of the steam generators which in turn, transfers energy to the turbine generator system. Figure C-11 is a simplified schematic of the PCS.

The feedwater portion of the PCS consists of two pump trains. Three low pressure motor-driven condensate pumps feed two high pressure motor-driven auxiliary feedwater pump. These latter three pumps in turn feed both steam generators via two injection lines.

Service Water System

The service water system (SWS) provides cooling water to the following equipment during emergency conditions: (1) reactor building cooling system cooling coils, (2) diesel generator jacket heat exchangers, (3) high pressure pump lube oil coolers, (4) high pressure pump room coolers, (5) circulating water pumps bearing lubrication, (6) low pressure/building spray pump room coolers, (7) low pressure pump(s) bearing coolers, (8) low pressure system heat exchangers, (9) building spray pump(s) bearing lube oil coolers, and (10) emergency feedwater system water sources. Figure C-12 is a simplified schematic of the SWS.

The SWS consists of two redundant loops. Normal cooling is supplied from Lake Dardanelle with an emergency pond available as a backup. There are three SW pumps. During normal operation, two are running with one in standby.

Emergency AC Electrical System

The emergency AC electrical (EAC) system provides electrical power to ESF equipment. The EACS is composed of two trains, each comprised of a diesel generator, 4160V switchgear, 480V load centers and motor control centers, 120V instrumentation panels, and associated transformers and circuit breakers. The normal power supply to the two trains is offsite power.

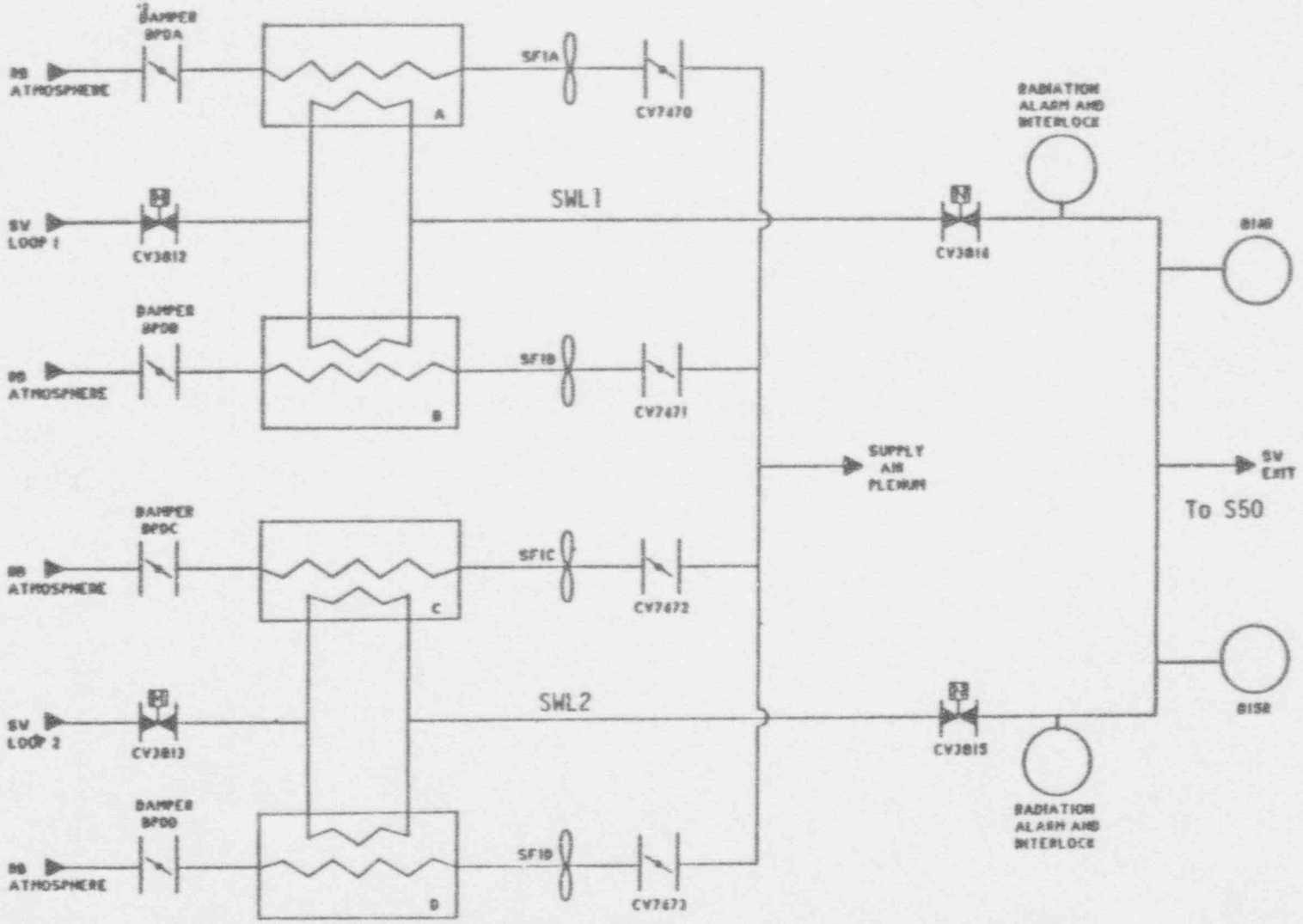

Figure C-10 Pipe Segments for the Reactor Building Cooling System

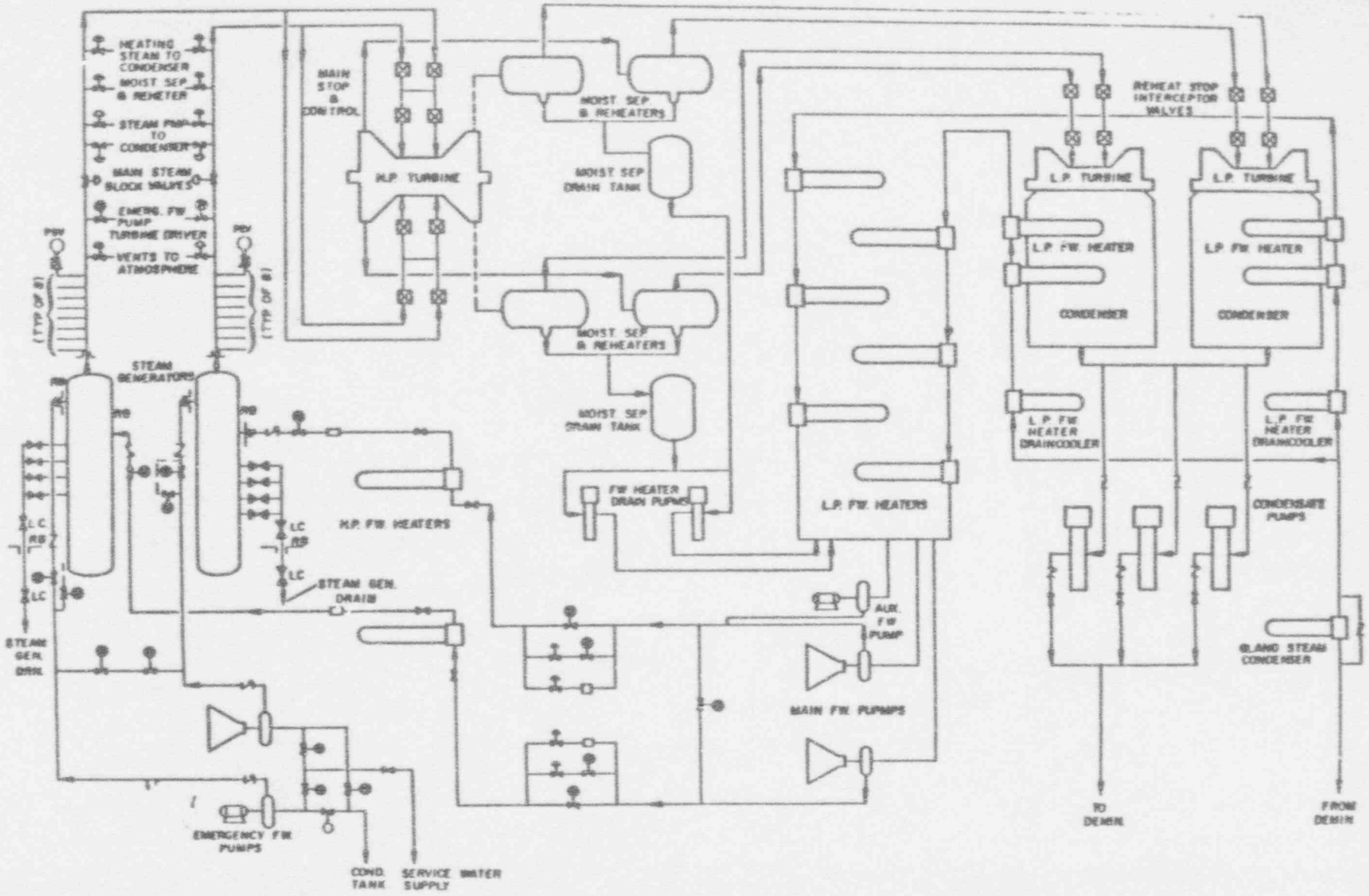

Figure C-11 Schematic of Power Conversion System

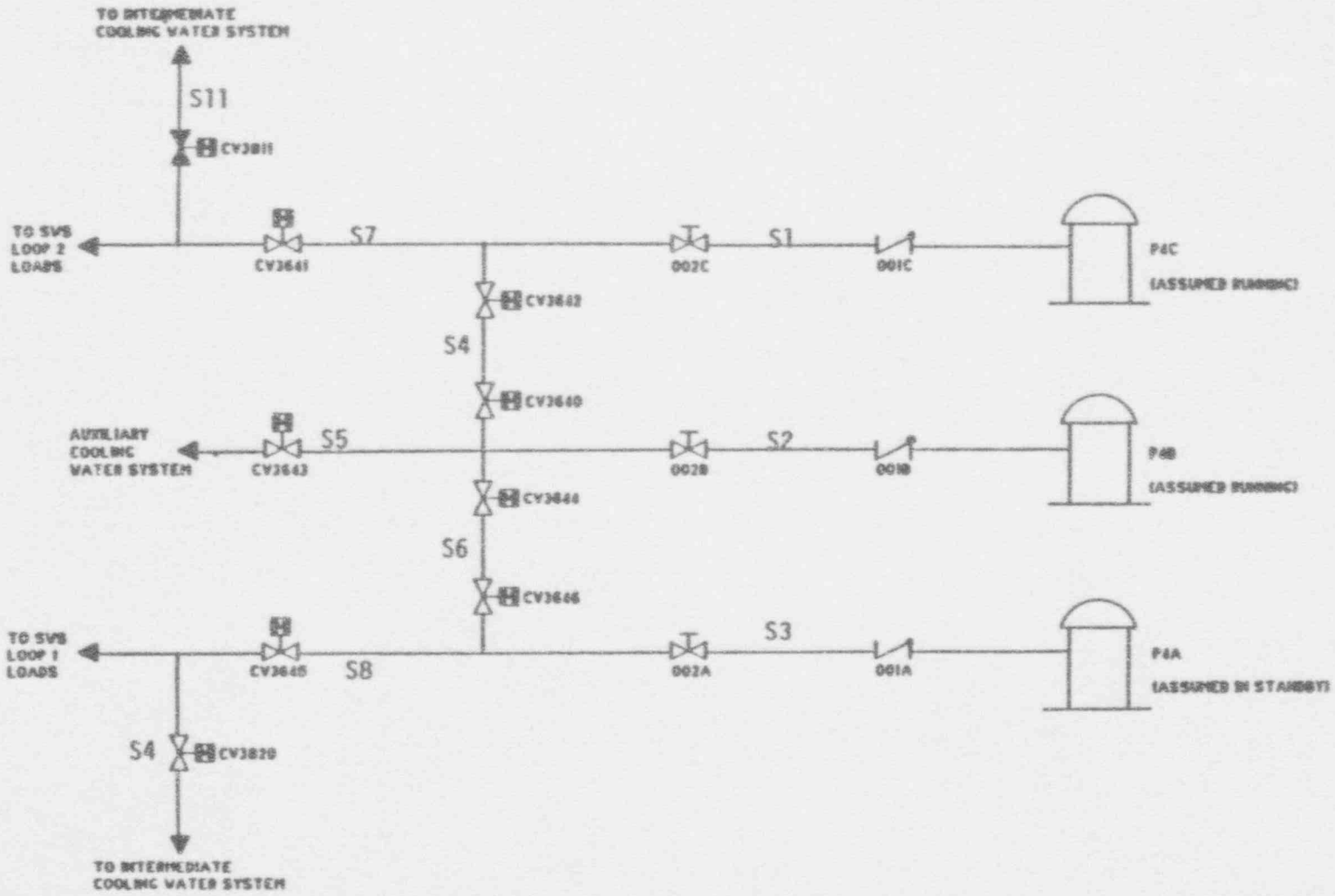

Figure C-12 Pipe Segments for Service Water System Pump Loops

As can be seen from Figure C-13, the two trains are capable of being cross-tied. Normal practice at ANO-1 IS NOT TO CROSS-TIE THE TWO TRAINS. Figure C-14 shows the service water dependency of the diesel generators.

DC Power System

The 125-volt DC system provides continuous power for control, instrumentation, reactor protection and engineered safeguards actuation systems, and emergency safeguard actuation control systems. In addition, it powers the control valves in the emergency feedwater system and provides control power for the diesel generators in the emergency AC electrical system. Figure C-15 is a simplified schematic of the DC system.

The DC system is composed of two separate trains, each comprising a 125-volt battery, bus, and control panels. In addition to the batteries, the DC system is also supplied from the emergency AC electrical system via three battery chargers, with two in service at any given time. The busses cannot be cross-tied.

Reactor Building Spray Injection/Reactor Building Spray Recirculation

The reactor building spray system (RBSS) reduces post-accident pressure to nearly atmospheric pressure, removes heat from the containment during recirculation, and removes radioactivity from the containment atmosphere. Figures C-16 and C-17 are simplified schematics of the RBSS.

The RBSS consists of two independent trains. Suction sources are the borated water storage tank during injection and the reactor building sump during recirculation. Each train contains a pump with its associated piping and valves.

C.2 HAZARD CURVES USED FOR ANO-1

The ANO-1 Nuclear Power Plant is located in northwestern Arkansas and is founded directly on shale rock. The location of the plant is generally considered to be in the Central Stable Zone of seismicity. The proximity to the New Madrid earthquake epicenter results in a relatively high SSE equal to 0.20g.

The hazard curves used for this study were taken from the NRC-sponsored Eastern and Central United States Seismic Characterization Program [Ref C-3] and are shown in Figure C-18. On these plots are shown the 15%, 50%, 85%, and the mean hazard curves. The median curve and the mean curve were input, and random realizations for the Monte Carlo study were generated assuming a lognormal distribution for any given peak ground acceleration.

A second set of hazard curves was obtained from the commercial power industry-sponsored Electrical Power Research Institute's Seismic Hazard Methodology Development program for the Eastern United States [Ref C-4].

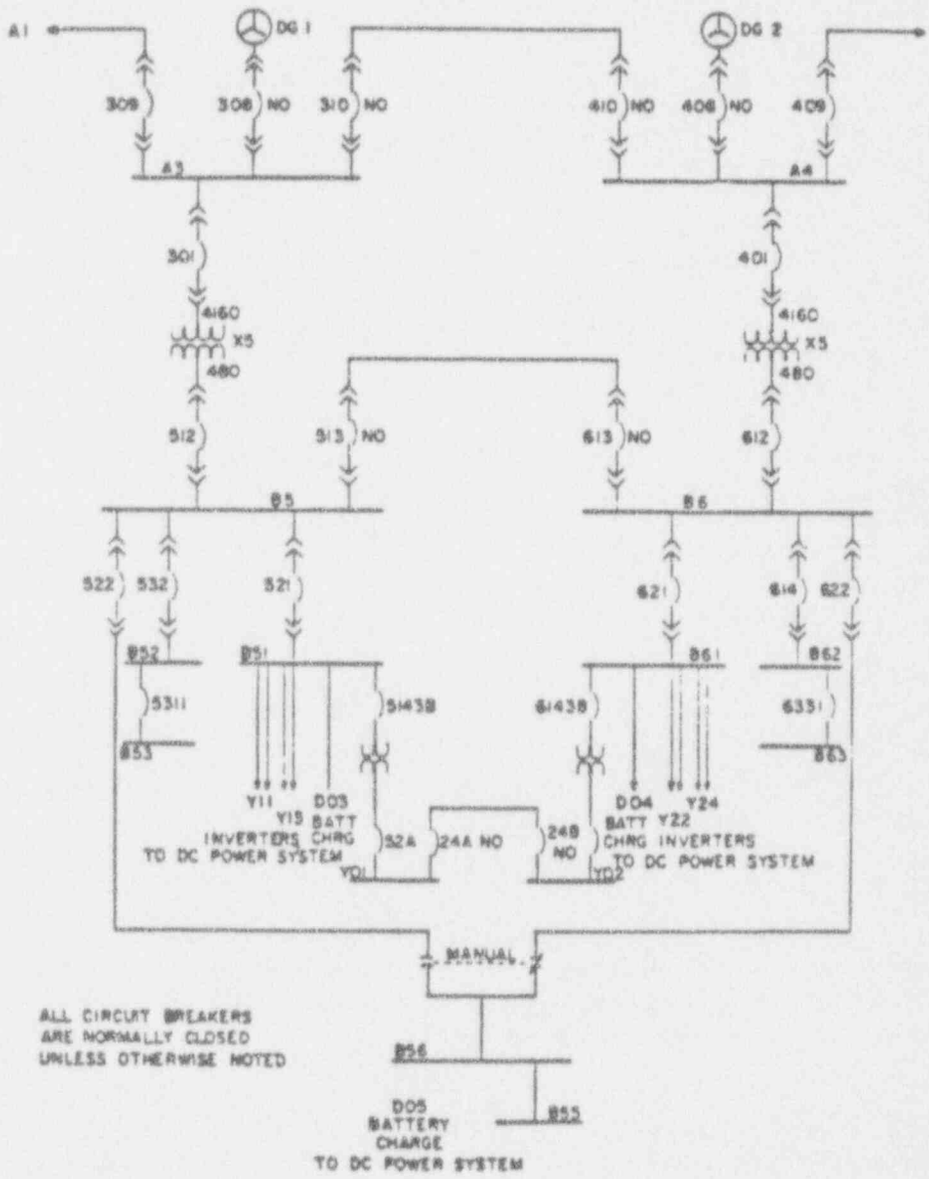

Figure C-13 Emergency AC Electrical System

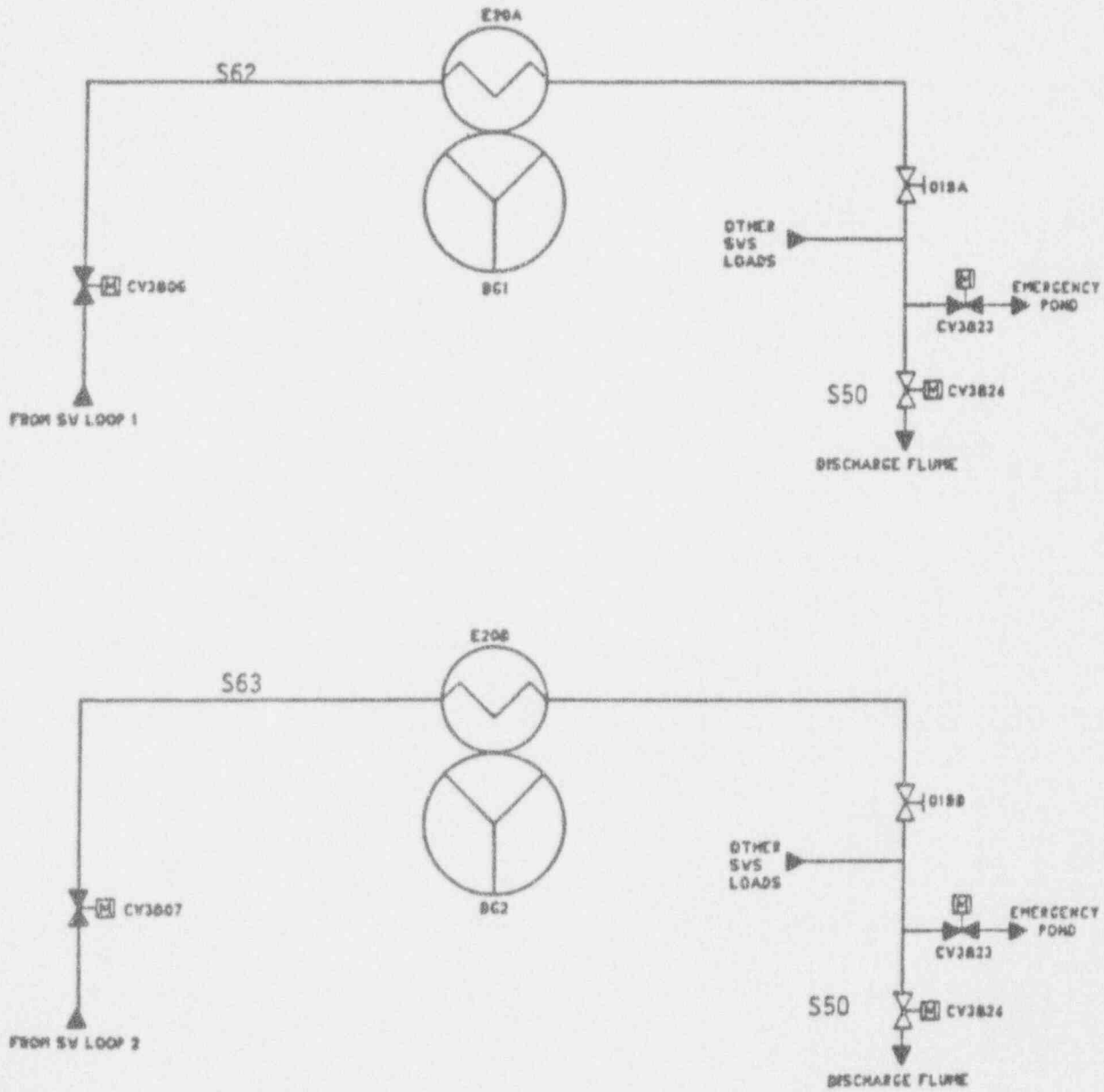

Figure C-14 Pipe Segments for Service Water Cooling of Diesel Generators

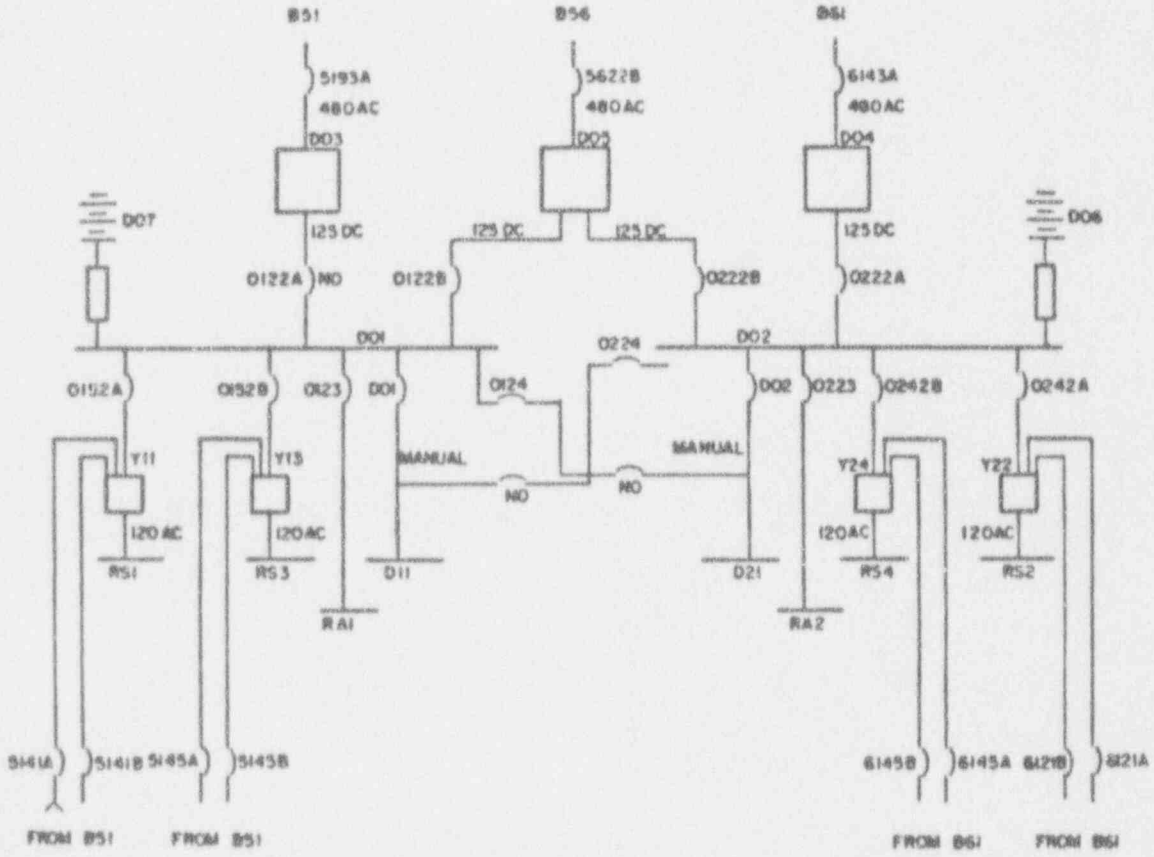

Figure C-15 DC Power System

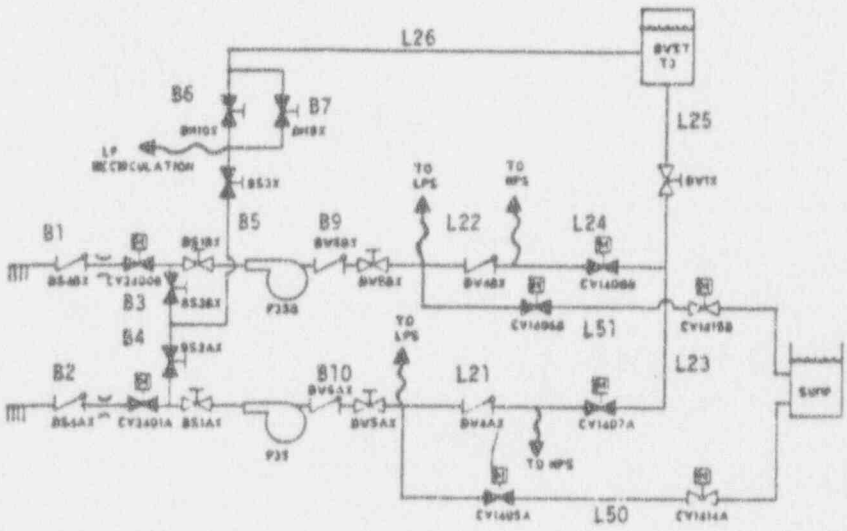

Figure C-16 Pipe Segments for the Reactor Building Spray Injection/Recirculation Systems

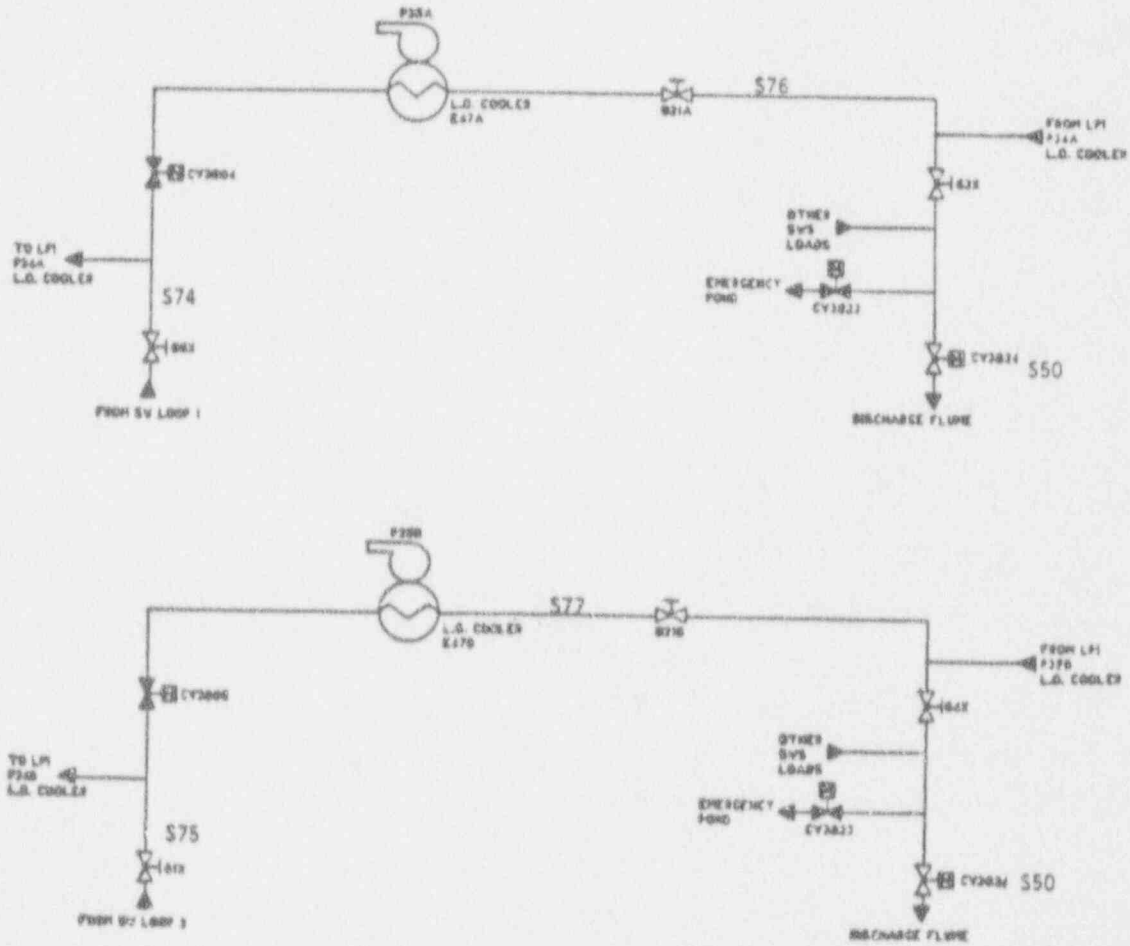

Figure C-17 Pipe Segments for Reactor Building
Spray Pumps Lube Oil Cooling

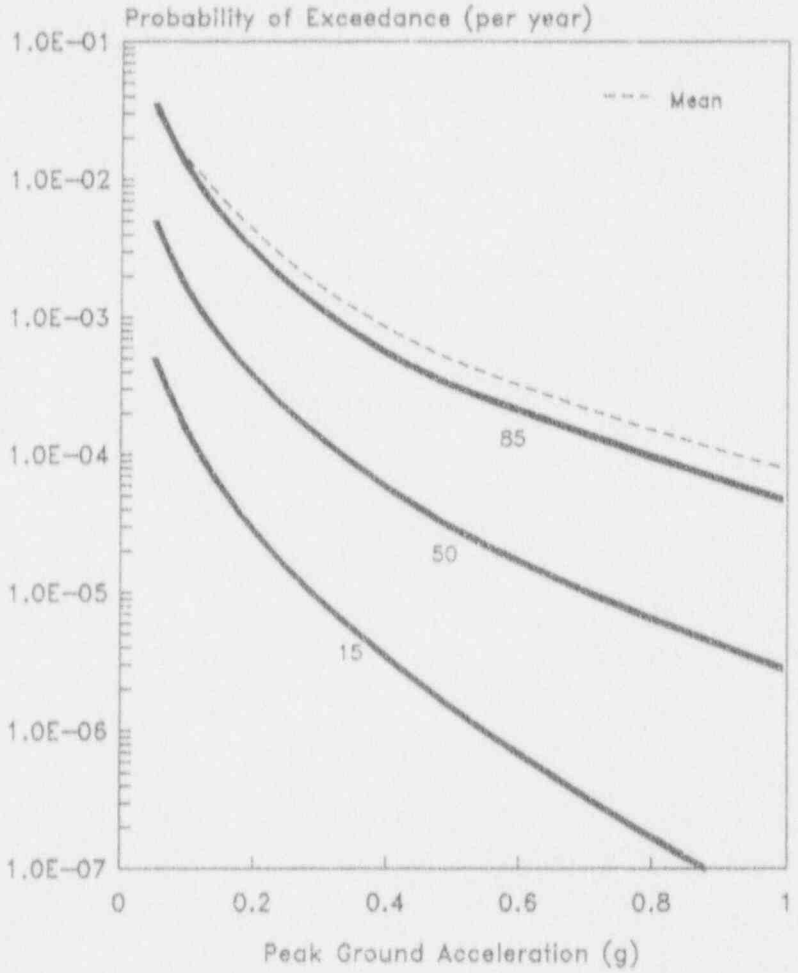

Figure C-18 ANO-1 LLNL Hazard Curves: Mean, Median, 85th and 15th Percentile Curves

The corresponding hazard curves are shown in Figure C-19. These were also fit with a lognormal model for each peak ground acceleration value in the uncertainty analysis.

C.3 RESPONSE CALCULATIONS

This chapter will describe and summarize:

- the site and earthquake characteristics that provide the starting point in the best-estimate soil-structure analysis of the ANO structures
- the probabilistic response analysis of the reactor building and the auxiliary building with and without degraded shear wall stiffness, and
- the in-structure responses that define the response of components identified on the Boolean expressions for the LOCA and transient accident sequences analyzed.

C.3.1 Site Layout and Foundation Description

The Arkansas Nuclear One site in its natural state is an area where clay and silty clay deposits overlie bedrock consisting of Pennsylvanian McAlester formation shale. Thickness of the clay overburden varies from 13 to 24 feet at the site. Hard fine grained sandstone of the Harthshorne formation underlie the shale and was encountered at a depth of 150 ft. Basemats of the structures of concern to this study were embedded and founded on the Pennsylvanian McAlester shale. For this study, seismic response analyses of the reactor and auxiliary building were performed. Figure C-20 illustrates the general plant layout and shows relative location of these structures. Figure C-21 shows grade and foundation elevations for the ANO reactor and auxiliary buildings.

C.3.2 Soil Properties and Earthquake Definition

The initial step in performing a probabilistic response analysis involves two inter-related tasks, whose objectives are to:

- define soil properties as a function of excitation level over the range of earthquakes to be considered, i.e., as defined by the seismic hazard curve, and
- define the input motion for the determination of seismic responses of structures and components for this range of earthquakes.

Three earthquake levels were considered and defined by their peak ground acceleration in the horizontal direction--0.20g (SSE), 0.40G (2SSE), and 0.60g (3SSE). They are denoted acceleration ranges 1, 2, and 3 in

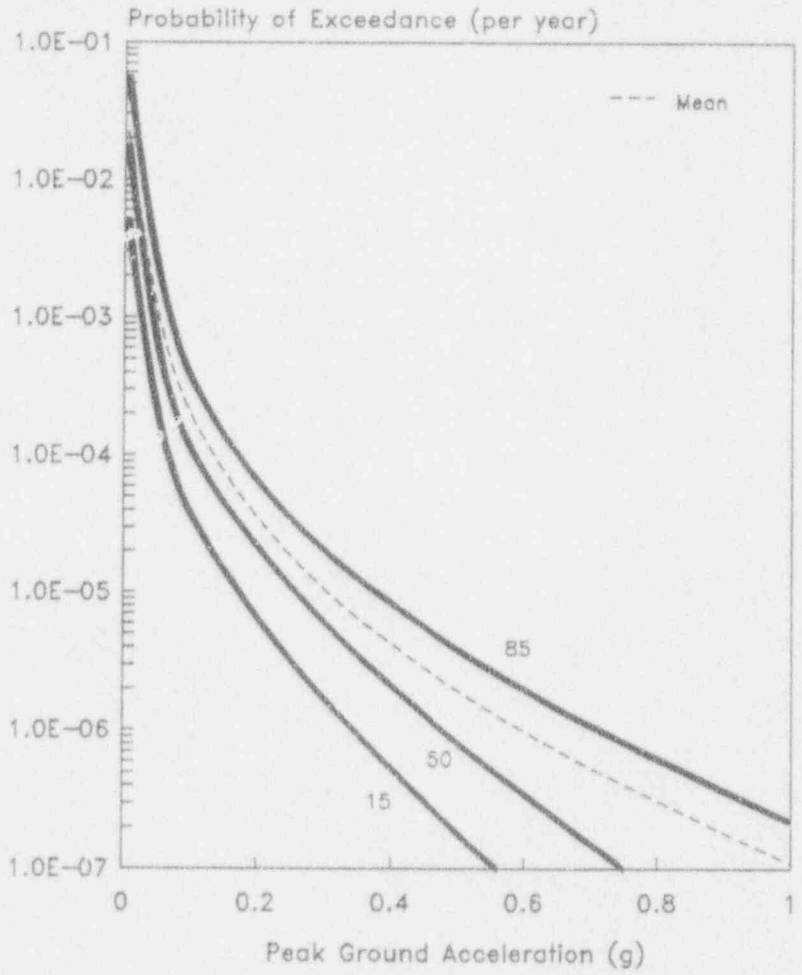

Figure C-19 ANO-1 EPRI Hazard Curves: Mean, Median, 85th and 15th Percentile Curves

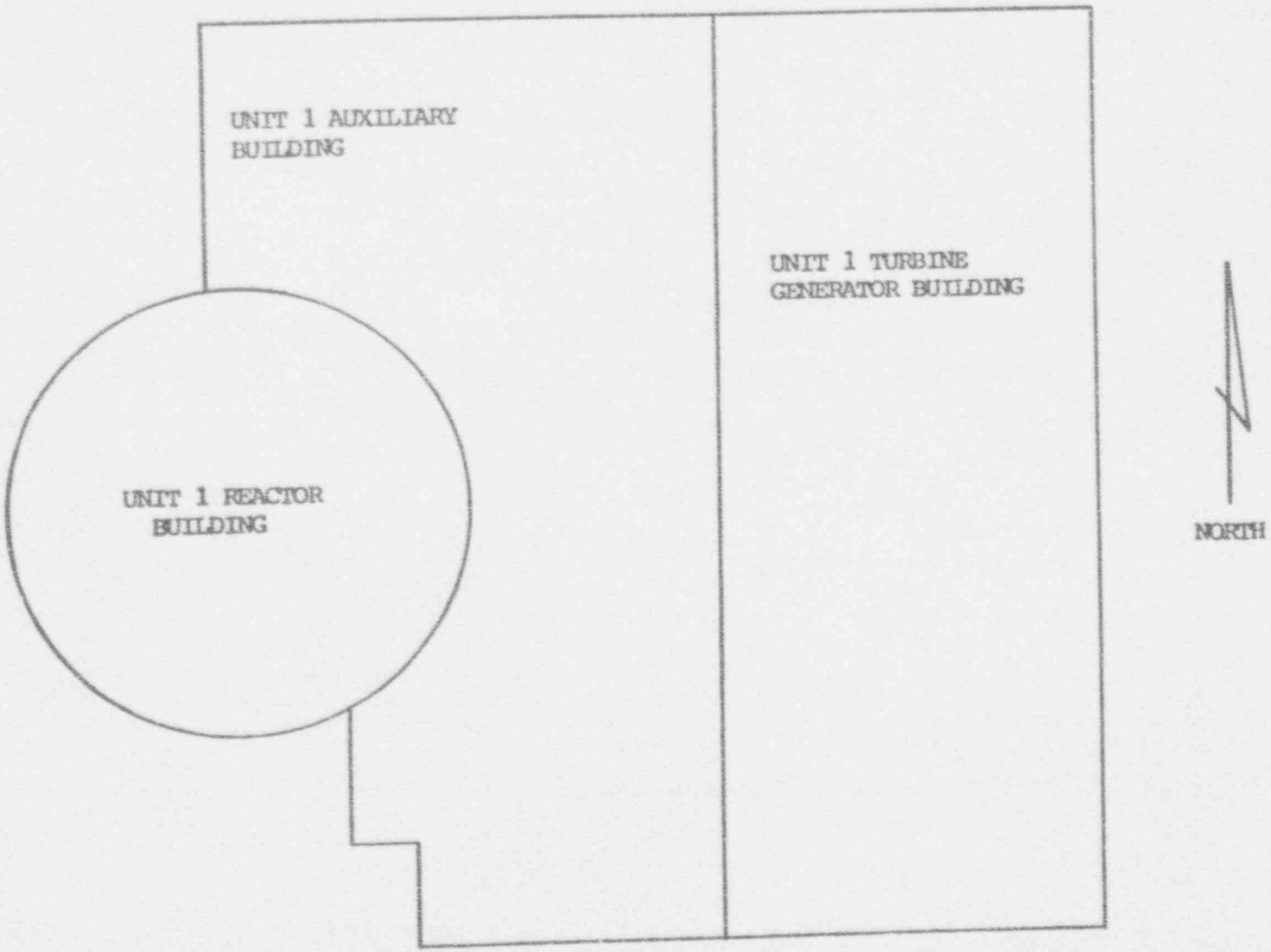

Figure C-20 ANO-1 General Plant Layout

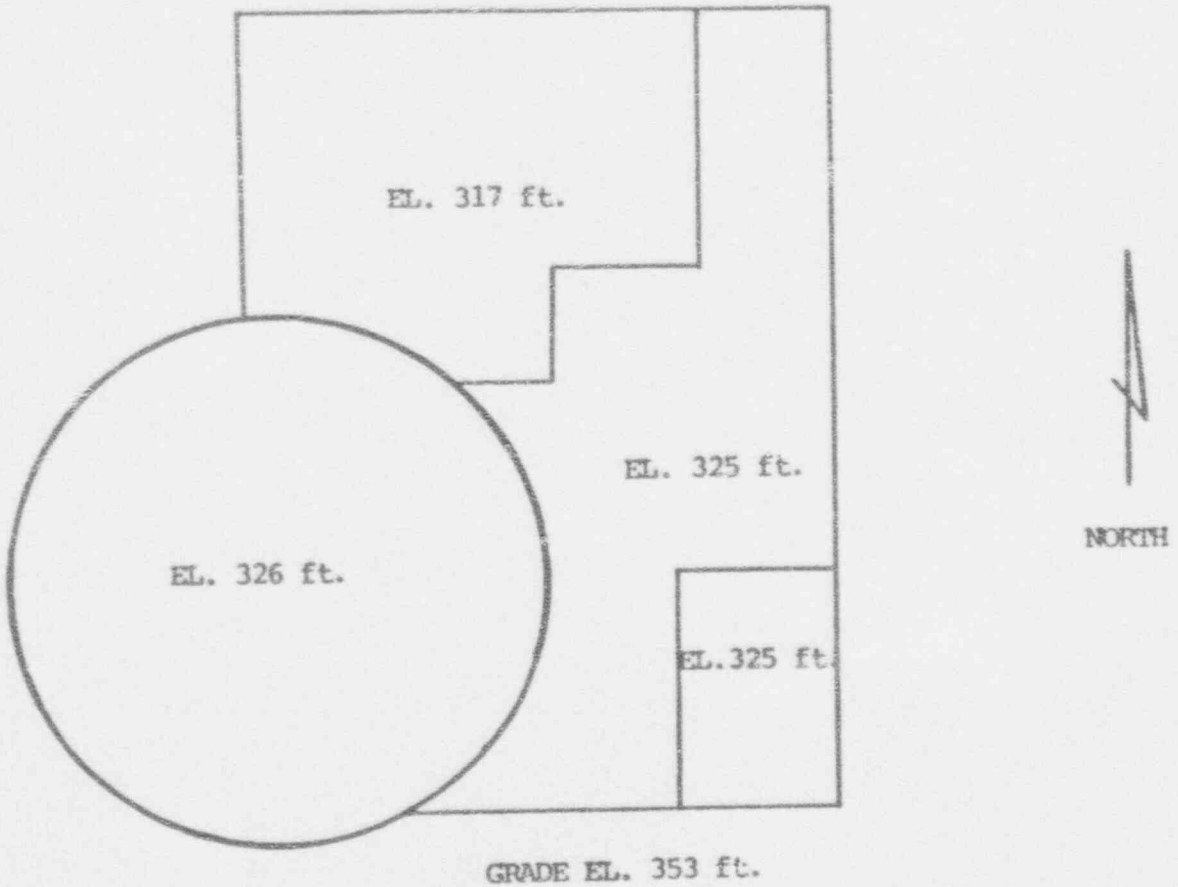

Figure C-21 ANO-1 Grade and Foundation Elevations for Reactor and Auxiliary Buildings

subsequent discussions. These earthquake levels were treated explicitly--input motions and seismic response for other levels defined by the hazard curve can then be interpolated from the results.

In general, soil properties such as shear modulus and damping are a function of soil strain and consequently a function of earthquake acceleration. With higher excitation levels, soil shear modulus tends to decrease while soil damping tends to increase. The ANO-1 soil properties are characteristic of a rock site. For such stiff soils, the degradation in shear modulus is small and there is little local site amplification of the earthquake ground motion. For this reason, a single nominal soil shear modulus was used in the analyses of the ANO-1 structures for all three excitation levels However, nominal soil damping did vary from one acceleration level to another. Table C-1 lists the nominal soil properties used.

The frequency characteristics of the free-field ground motion were defined by a best-estimate median response spectra associated with rock and presented in Reference C-6. For our probabilistic response analysis, a single artificial acceleration time history scaled to the appropriate peak ground acceleration whose response spectra approximated this best-estimate spectra defined the free-field motion. Figure C-22 compares the median rock spectra from Reference C-6 with the response spectra generated from the artificial time history for 5% damping. A single time history (rather than an ensemble of motions) was selected to model the free-field motion. A more thorough approach is to define an ensemble of motions at the free-field to describe the frequency characteristics of the motion--their median response spectra closely approximating the median of Reference C-6. Following the TAP A-45 analyses, however, a single time history is chosen for our purposes. This is deemed adequate because, first, the SSI analysis (to be discussed later) includes variability in soil properties which does introduce variability in the input motion to the structures. Second, the objective of this effort is to predict median seismic response and not the entire response distribution. Hence, a smaller number of samples is required and a complete specification of variability in the free-field motion is not necessary.

C.3.3 Structural Models

Three separate buildings were modeled for ANO-1; the Reactor Building, the Auxiliary Building and the Intake Structure. All three models used in the dynamic analysis were 2-D lumped mass models taken from the original ANO-1 FSAR [C-5]. Since these models were only developed for one horizontal component of direction, a similar model was developed for its perpendicular horizontal component. These new models were developed from as-built drawings obtained at the plant site.

The material properties for these structures came directly from specimen tests that were performed during the construction of all three structures for both the concrete and reinforcing steel used. These properties were used to determine the original stiffness, and reduced stiffnesses were then determined based on the model shown in Chapter 3 of the main report.

Table C-1

Nominal Soil Properties for ANO-1 Analyses

	Acceleration Range 1 (0.2g)	Acceleration Range 2 (0.4g)	Acceleration Range 3 (0.6g)
Shear Modulus	3.85 E7 lbs/ft^2	3.85 E7 lbs/ft^2	3.85 E7 lbs/ft^2
Damping	7%	8.5%	10%

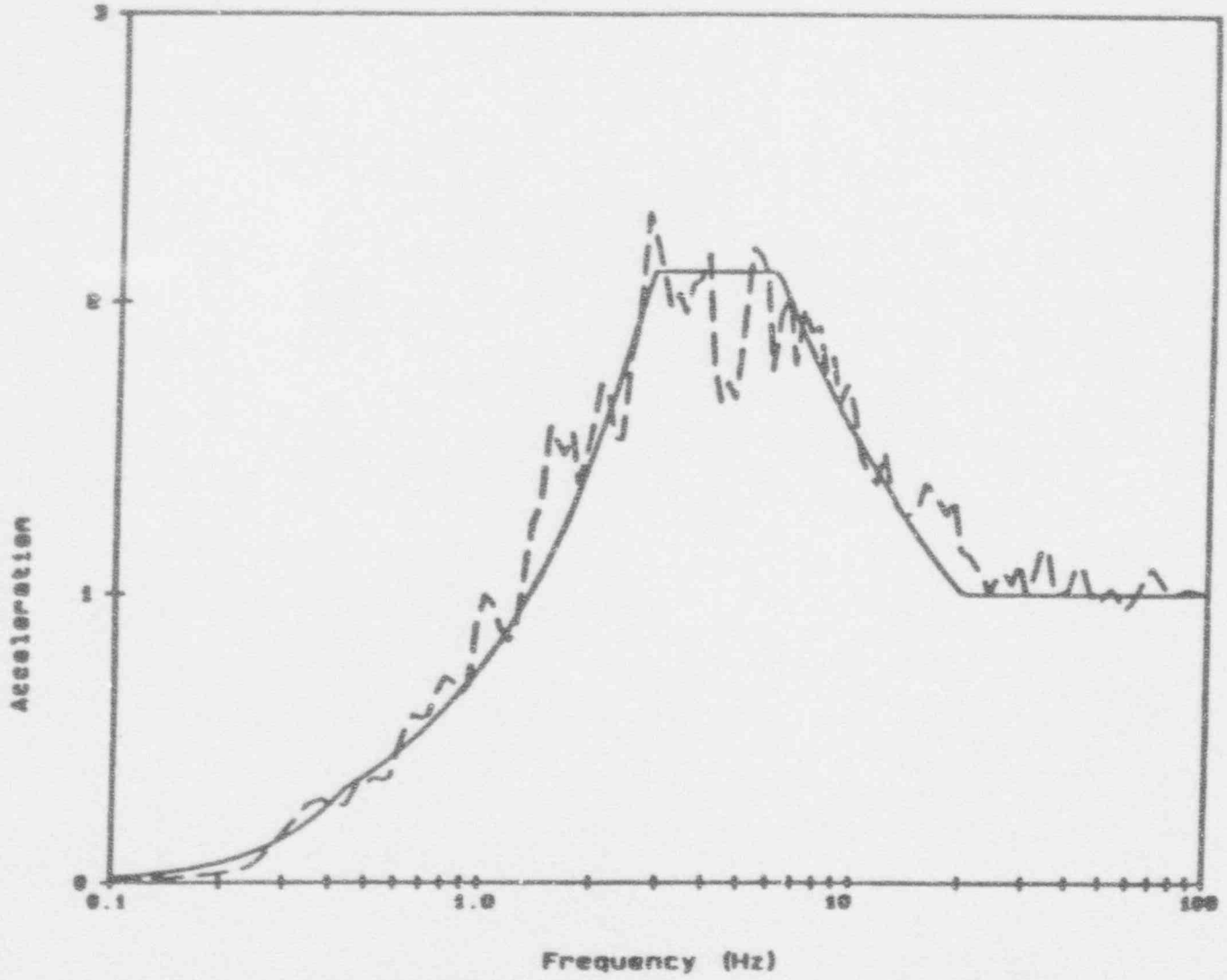

Figure C-22 Comparison of Ground Motion Spectra (Median on rock outcrop from Ref C-6) with Spectra from Artificial Time History

The reduction in stiffnesses for the structural models' beam elements was performed in such a way that only shear deformation contribution to each element stiffness was reduced, and the bending deformation contribution was unchanged. That is, the term GA_s was reduced (where G is the shear modulus and A_s is the shear area) but EI (where E is Young's Modulus and I is the cross-section area moment of inertia) was unchanged.

Reactor Building

The reactor building is a reinforced concrete building, circular in plan (≠61.75 ft. radius). The building is supported on a 8.5 ft. thick reinforced concrete mat at elevation 326 ft. and extends in height to elevation 535 ft. Grade is at 353 ft.

A fixed-base model excluding the soil springs was reconstructed from the data given in the FSAR. Figure C-23 shows the model and correlates node points and floor elevations. The internal structure and containment shell are modeled without any coupling between them. Only the containment internal structure had its stiffness reduced for this study. The containment shell stiffness was not changed because (a) the shear wall stiffness reduction data is not directly applicable and (b) containment shell structures were explicitly excluded from the scope of this study. In addition, response points associated with safety related components of concern are all located within the internal structure of the Reactor Building. The internal structures fundamental mode of vibration has a frequency of 12.18 Hz in the X- direction and 12.47 Hz in the Y-direction.

Auxiliary Building

The auxiliary building is a reinforced concrete building, rectangular in plan (143 ft. x 175 ft.). The building is supported on mat foundations at elevations 335 ft. and 317 ft. An equivalent depth of embedment based on surface area at the two depths is 27 ft. The amount of embedment is significant for the SSI analyses.

As for the reactor building, a fixed-base model of the auxiliary building excluding the soil springs was reconstructed from the data and used for the probabilistic response analyses. Figure C-24 shows the model and correlates node points and floor elevations. The auxiliary building fundamental modes of vibration have lowest natural frequencies of 13.29 Hz in the X-direction and 13.24 Hz in the Y-direction.

Intake Structure

The intake structure is a reinforced concrete building, rectangular in plan (78 ft. x 109 ft.). The structure is supported on a sloping mat foundation from elevations 312 ft. to 319 ft.

As for the other structures, a fixed-base model of the intake structure excluding the soil springs was reconstructed from the data and used for the probabilistic response analyses. Figure C-25 shows the model and correlates node points and floor elevations. The intake structure

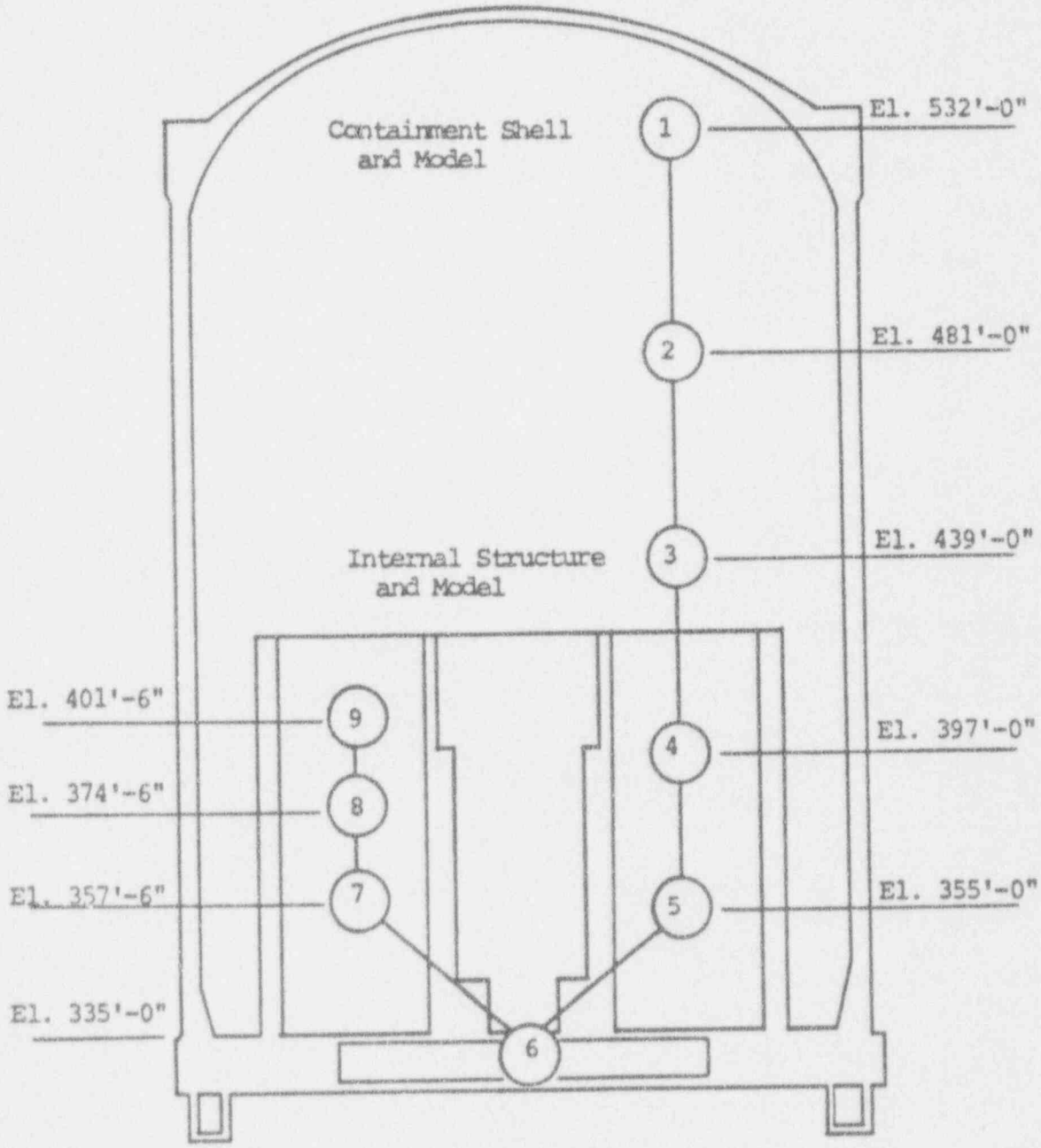

Figure C-23 ANO-1 Reactor Building Structural Model

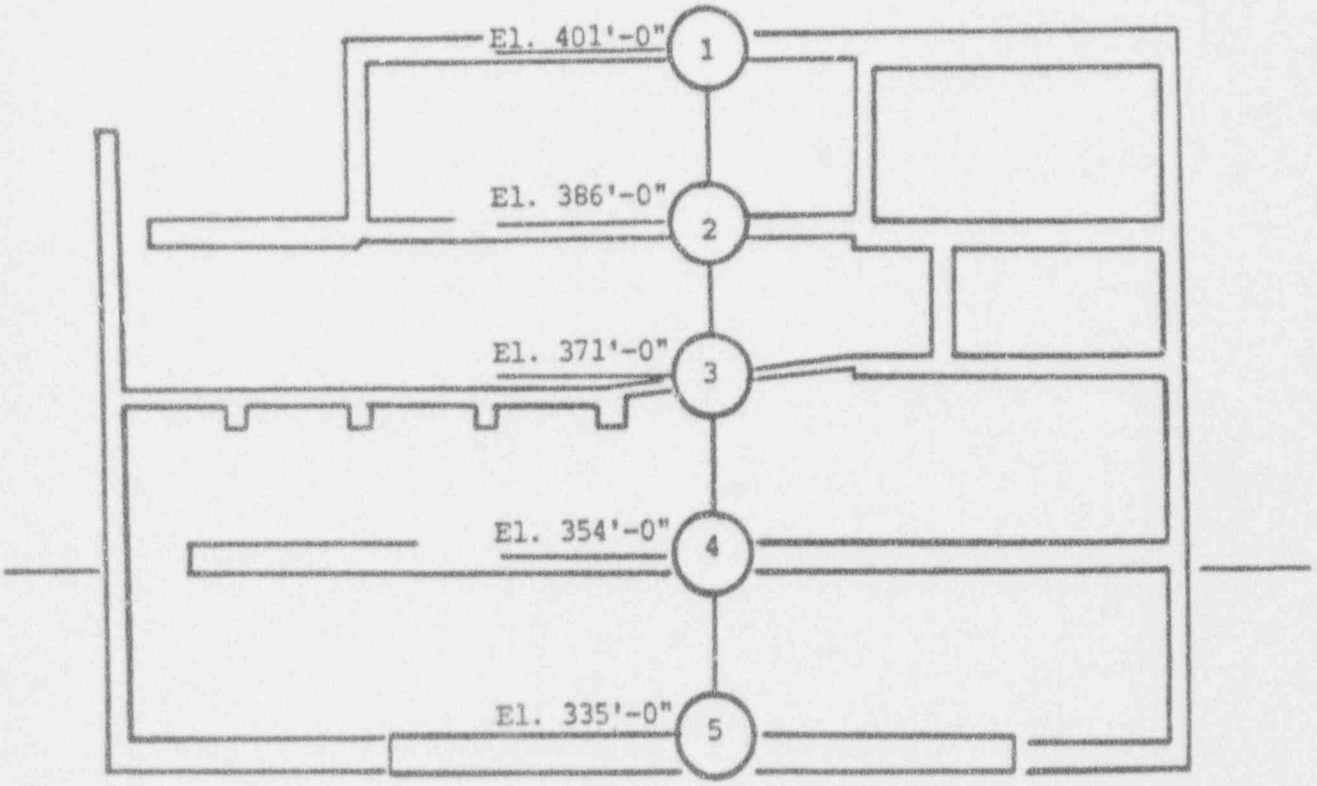

Figure C-24 ANO-1 Auxiliary Building Structural Model

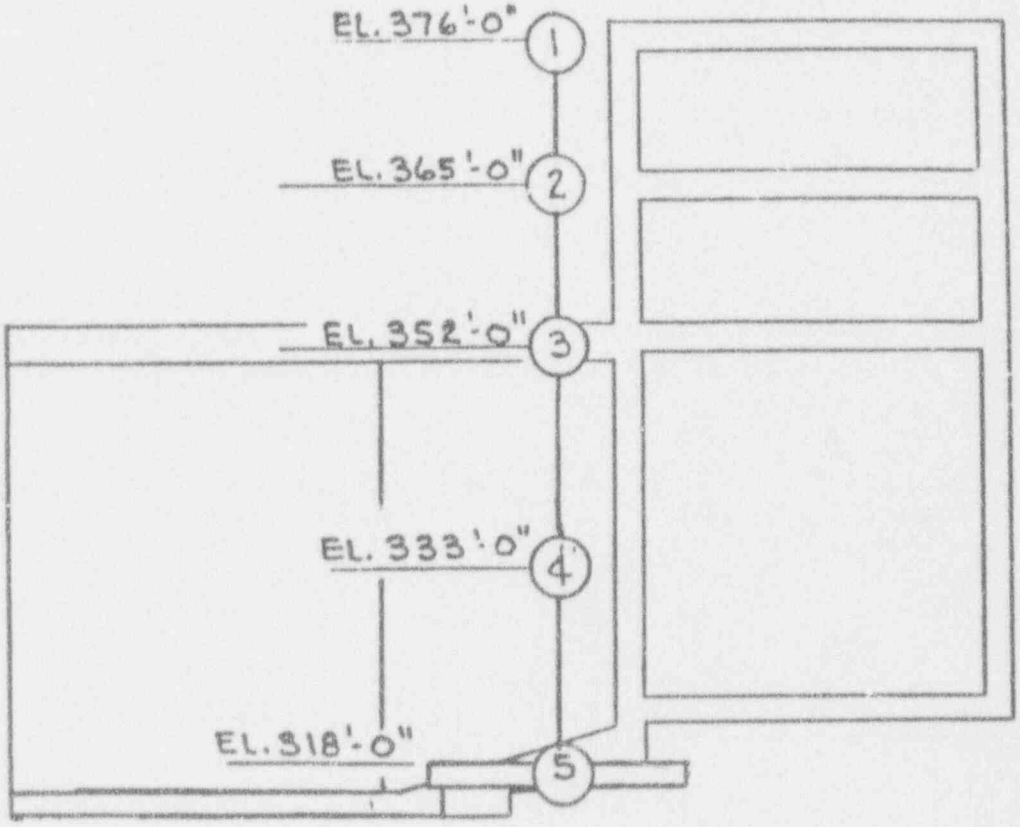

Figure C-25 ANO-1 Intake Structure Structural Model

fundamental modes of vibration have lowest natural frequencies of 18.31 Hz in the X-direction and 19.11 Hz in the Y-direction.

C.3.4 Probabilistic Response Analysis

In recognition of the importance of the effects of embedment and soil-structure interaction, probabilistic response analyses were performed on the reactor building (containment shell and internals) and the auxiliary building to generate median responses for the seismic PRA. The methodology used is that of SMACS [Ref. C-7] as implemented in the computer program CLASSI [Ref. C-8] utilizing the substructure approach. The substructure approach to SSI is composed of the following elements: specification of the free-field ground motion; calculation of the dynamic characteristics of the structures; determination of the foundation impedances and analysis of the coupled soil-structure system.

The seismic input variability is normally introduced by considering an ensemble of earthquake motions. For this study, only the one artificial earthquake motion described earlier was used. Note that a series of ten earthquake simulations for each acceleration range were performed but that each used the identical free-field input motion as a starting point.

Soil-structure interaction and structure response variability are introduced through a limited number of parameters--soil shear modulus, soil damping, structure frequency and modal damping. Variability in SSI was incorporated through modeling soil shear modulus and material damping as random variables with log-normal distributions--medians corresponding to the nominal values of Table C-1 and coefficients of variation of 0.4 and 0.5, respectively. Variability in structure dynamic behavior was also modeled by treating structure frequency and modal damping as random variables. Nominal values of structure frequencies were those calculated in the eigenvalue extraction analysis for the structure model. Nominal values of structure damping were taken to to be 0.07, 0.085, and 0.10 (fractions of critical damping) for the three seismic acceleration ranges considered here. These were based on published damping values and assumed stress levels achieved.

Parameter variations in each step of the response analysis were selected to represent random variability, and not to include modeling uncertainty. The assumed parameter variability corresponds to that detailed in the SSMRP response calculations made for the Zion Nuclear Power Plant [Reference C-9]. The parameter values for each of the ten simulations were selected from the probability distributions by dividing the distributions into equally probable segments, sampling from each segment, and combining the samples by a Latin hypercube experimental design.

The responses calculated from the simulations are combined to estimate median responses conditional on the occurrence of an earthquake described by the hazard curve parameter, i.e., peak ground acceleration.

Reactor Building Responses

For each of the ten earthquake simulations at each of the internal structures nodes, acceleration time histories and corresponding in-structure response spectra at 5% damping were calculated. These spectra were then combined into mean responses for all nodes in the internal structure model (nodes 7-9). Figures C-25 thru C-28 presents median horizontal in-structure spectra for the three seismic acceleration levels using reduced stiffnesses. Each graph shows an overplot of the median free-field response spectra at 1 SSE. These spectra formed the basis for determining the response of critical components housed at the various elevations in the internal structure.

Auxiliary Building Responses

For each of the earthquake simulations acceleration time histories and corresponding in-structure response spectra at 5% damping were calculated. These spectra were then combined into median responses for all nodes. Figures C-29 thru C-31 presents mean horizontal spectra for the three seismic acceleration levels using reduced stiffnesses for three nodes 2,3 and 5. Each plot shows an overplot of the median free-field response spectra at 1 SSE. These spectra formed the basis for determining the response of critical components housed in the auxiliary building.

Intake Structure Responses

For each of the earthquake simulations acceleration time histories and corresponding in-structure response spectra at 5% damping were calculated. These spectra were then combined into median responses for all nodes. Figures C-32 thru C-34 presents mean horizontal spectra for the three seismic acceleration levels using reduced stiffnesses for three nodes 2,3 and 5. Each plot shows an overplot of the median free-field response spectra at 1 SSE. These spectra formed the basis for determining the response of critical components housed in the intake structure.

C.3.4.1 Responses in Terms of Peak Ground Acceleration

From the pairs of response spectra (generated with and without stiffness reduction effects) at the three pga levels (0.2g, 0.4g, and 0.6g), one can construct plots of any particular spectral acceleration response (at any point in the structures being modeled) as a function of pga. The difference between these plots shows the effect of stiffness reduction directly. This was done for the locations of all equipment modeled on the accident sequence expressions (for the spectral acceleration corresponding to the equipment of interest).

These plots of the response point spectral accelerations versus peak ground acceleration for responses corresponding to critical components are shown on Figures C-35 through C-41. (Note that the spectral acceleration is identified in the caption on each plot.) It can be seen that a nearly linear relation exists up to peak ground accelerations of

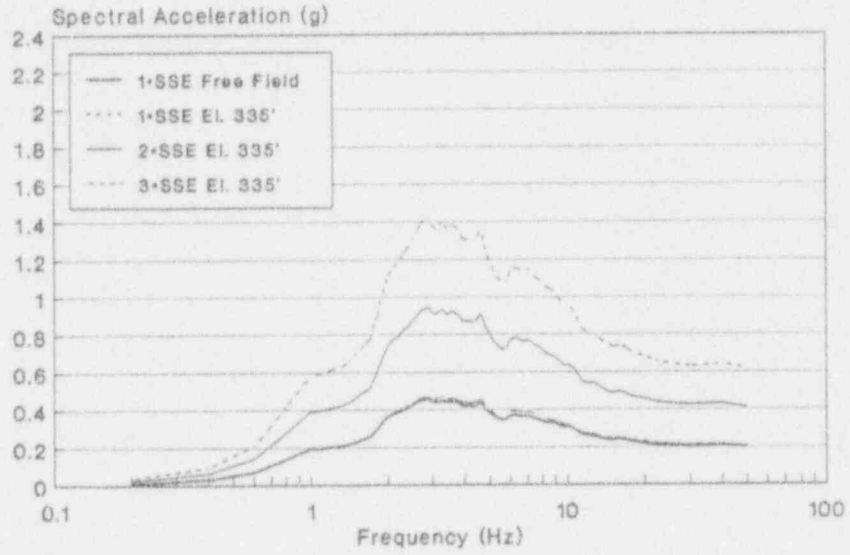

N-S Direction
5% Spectral Damping
SSE = 0.20g

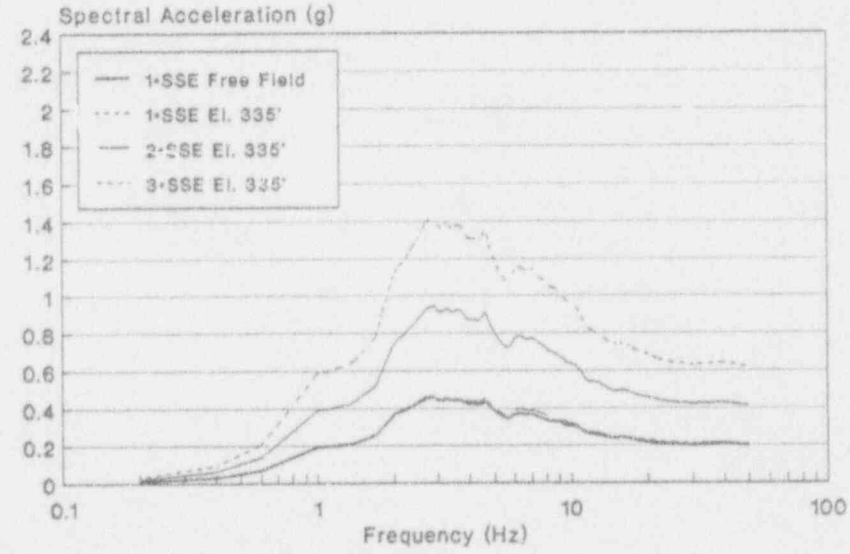

E-W Direction
5% Spectral Damping
SSE = 0.20g

Figure C-26 ANO-1 Reactor Internals Responses, El. 335'

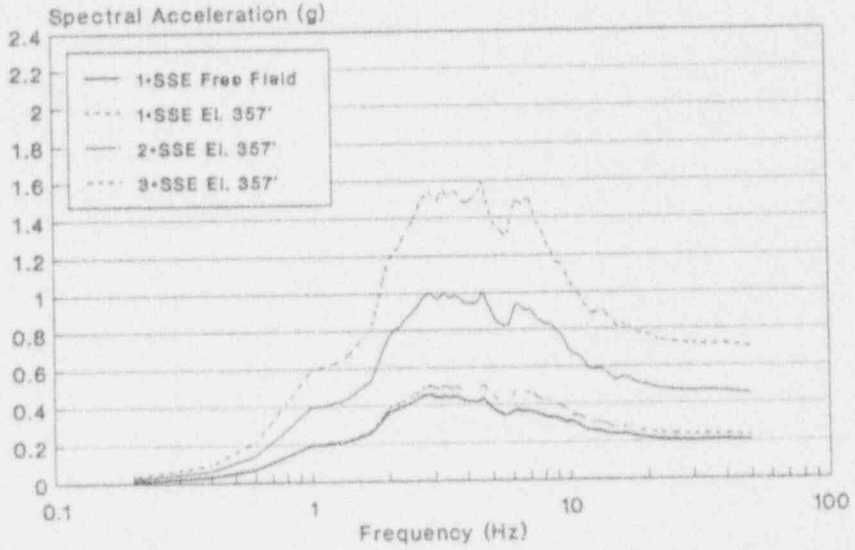

N-S Direction
5% Spectral Damping
SSE = 0.20g

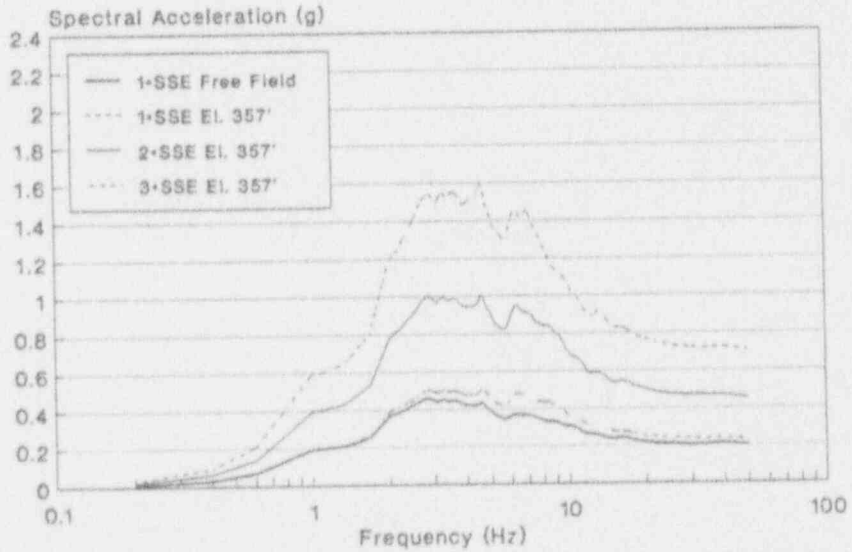

E-W Direction
5% Spectral Damping
SSE = 0.20g

Figure C-27 ANO-1 Reactor Internals Responses, El. 357'

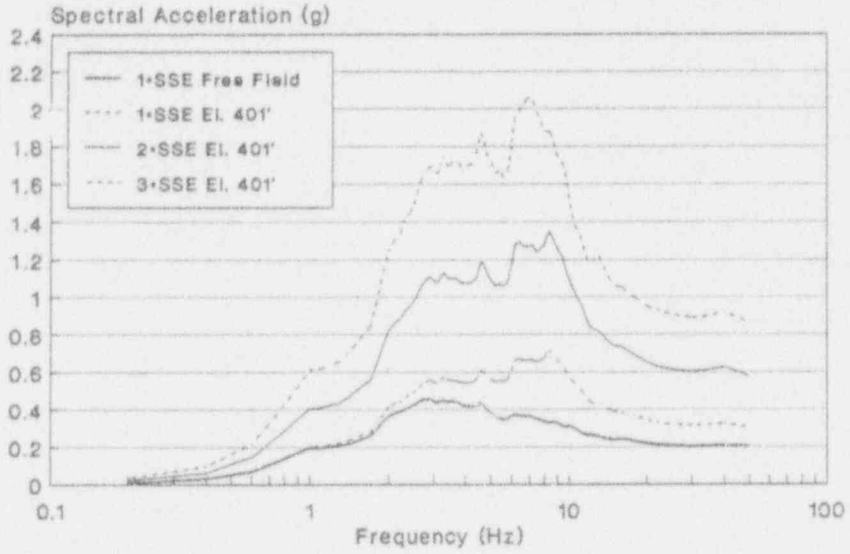

N-S Direction
5% Spectral Damping
SSE = 0.20g

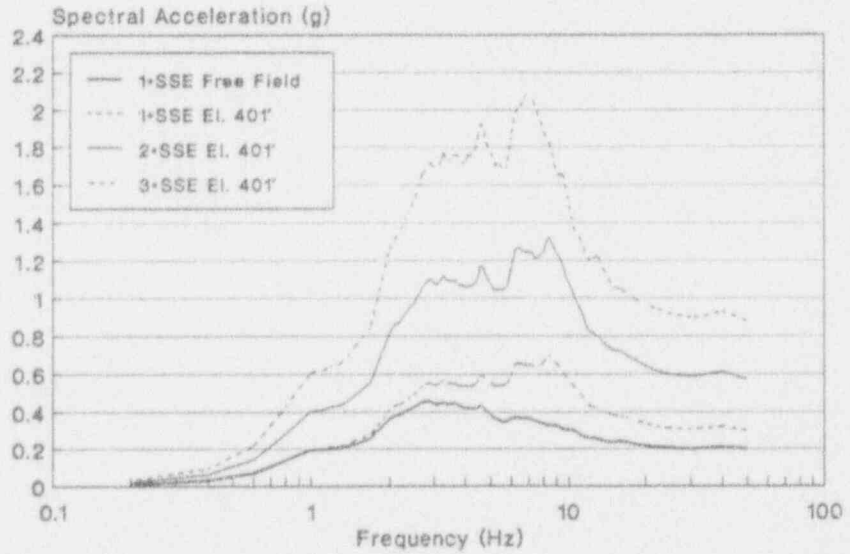

E-W Direction
5% Spectral Damping
SSE = 0.20g

Figure C-28 ANO-1 Reactor Internals Responses, El. 401'

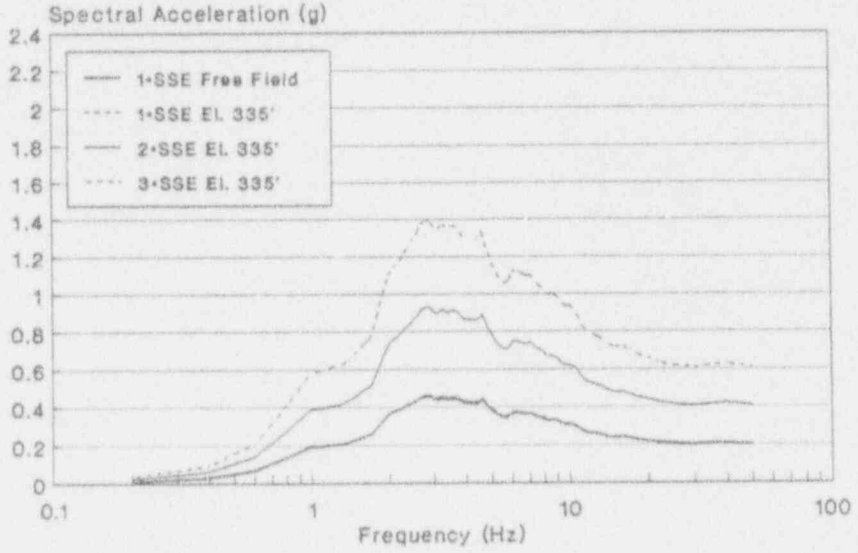

N-S Direction
5% Spectral Damping
SSE = 0.20g

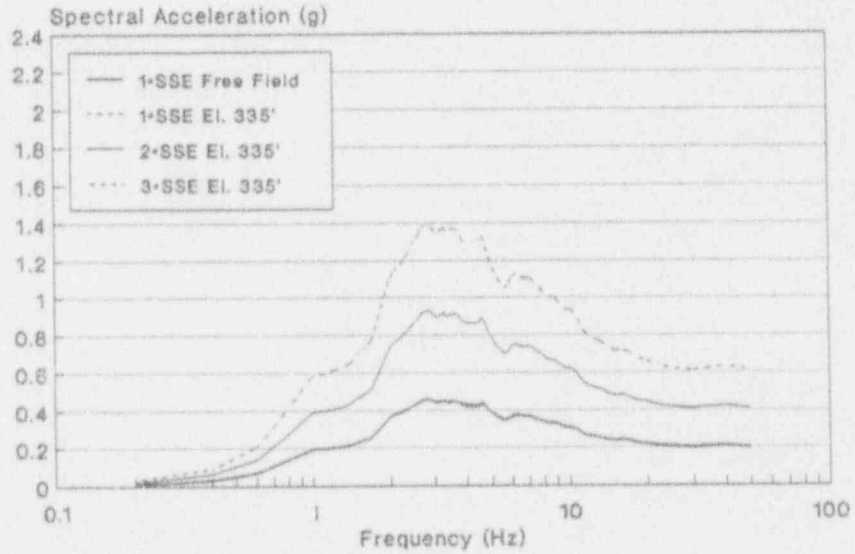

E-W Direction
5% Spectral Damping
SSE = 0.20g

Figure C-29 ANO-1 Auxiliary Building Responses, El. 335'

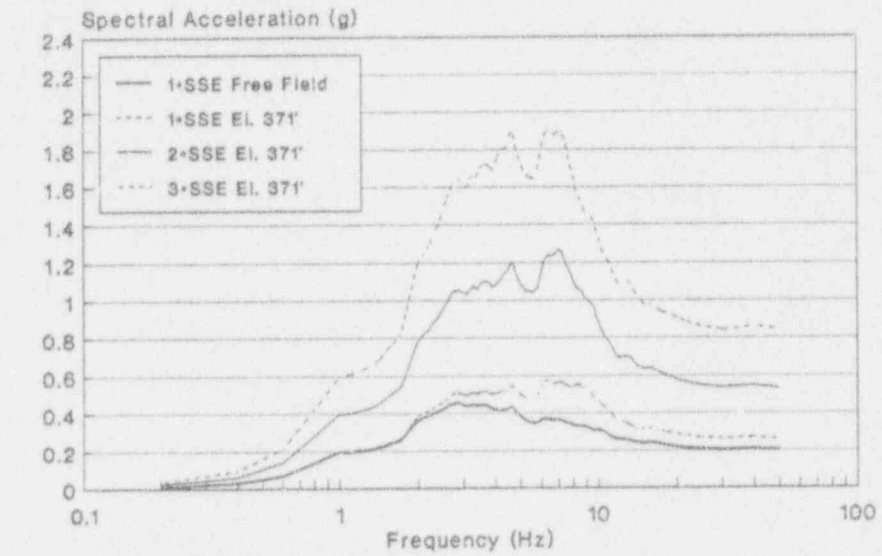

N-S Direction
5% Spectral Damping
SSE = 0.20g

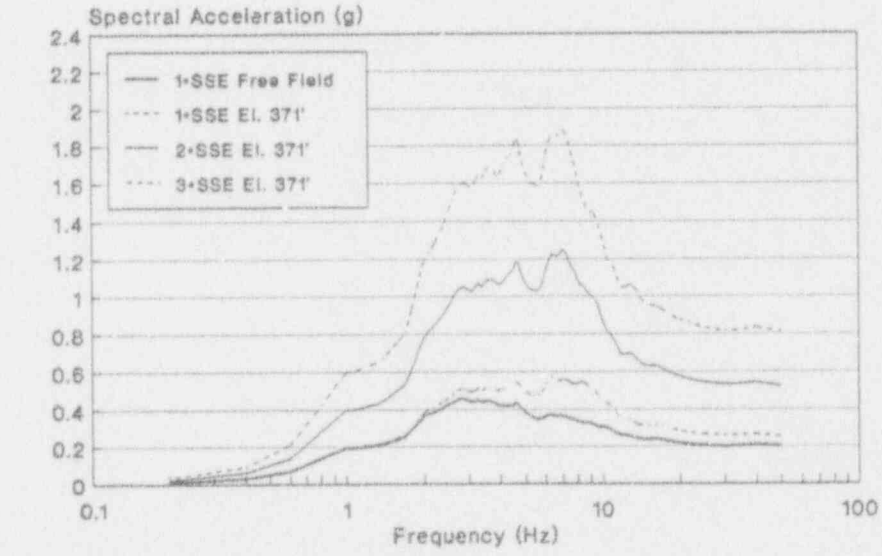

E-W Direction
5% Spectral Damping
SSE = 0.20g

Figure C-30 ANO-1 Auxiliary Building Responses, El. 371'

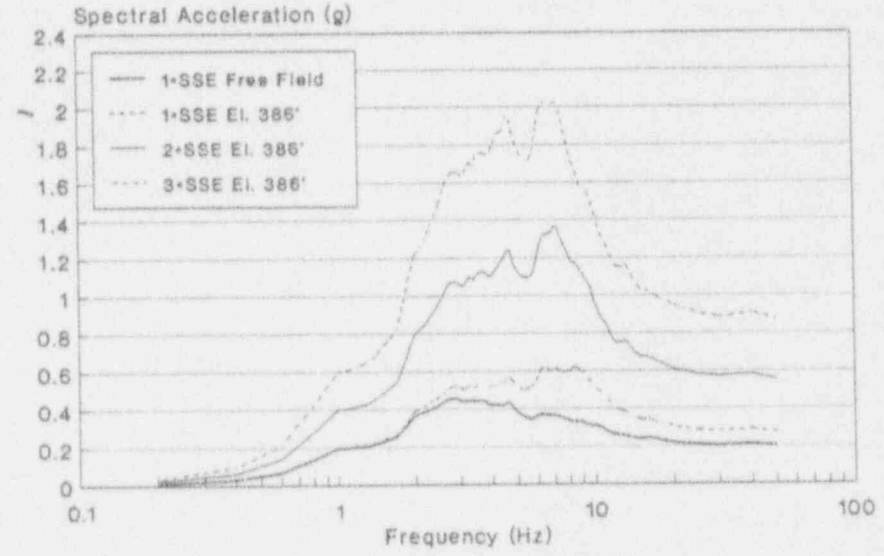

N-S Direction
5% Spectral Damping
SSE = 0.20g

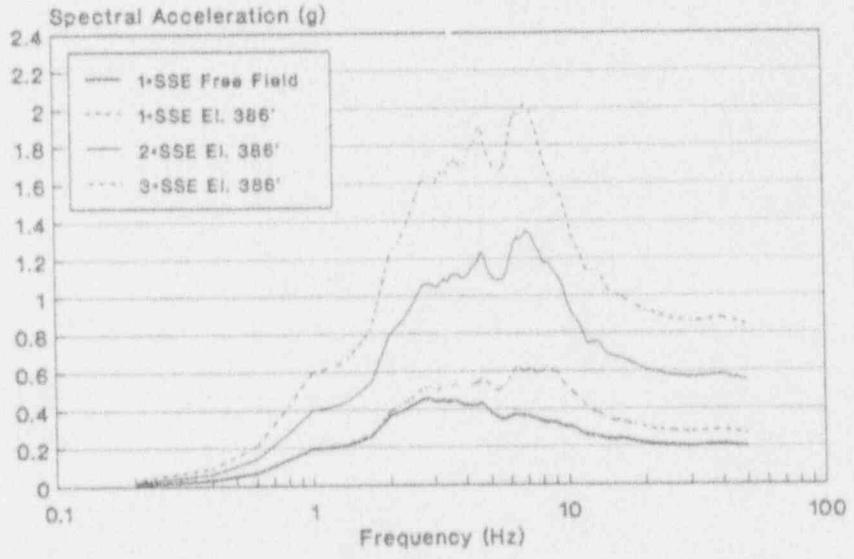

E-W Direction
5% Spectral Damping
SSE = 0.20g

Figure C-31 ANO-1 Auxiliary Building Responses, El. 386'

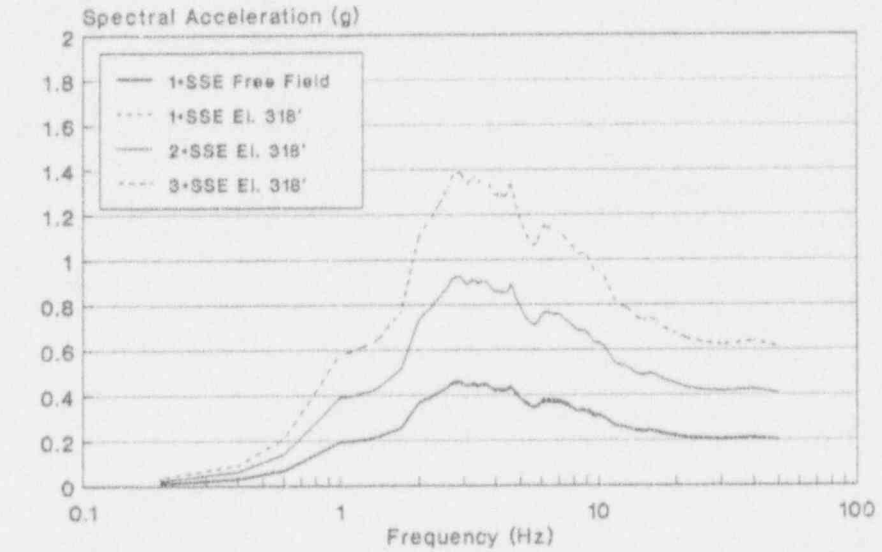

NW-SE Direction
5% Spectral Damping
SSE = 0.20g

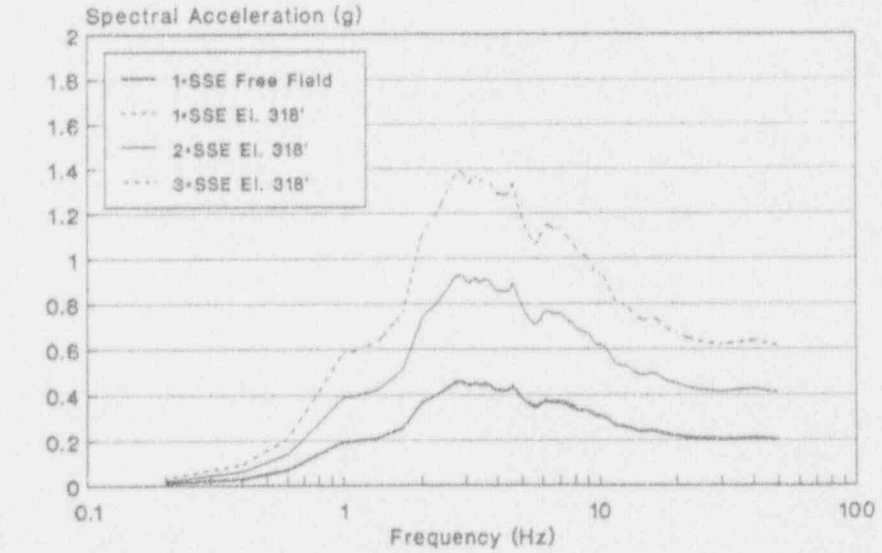

NE-SW Direction
5% Spectral Damping
SSE = 0.20g

Figure C-32 ANO-1 Intake Structure Responses, El. 318'

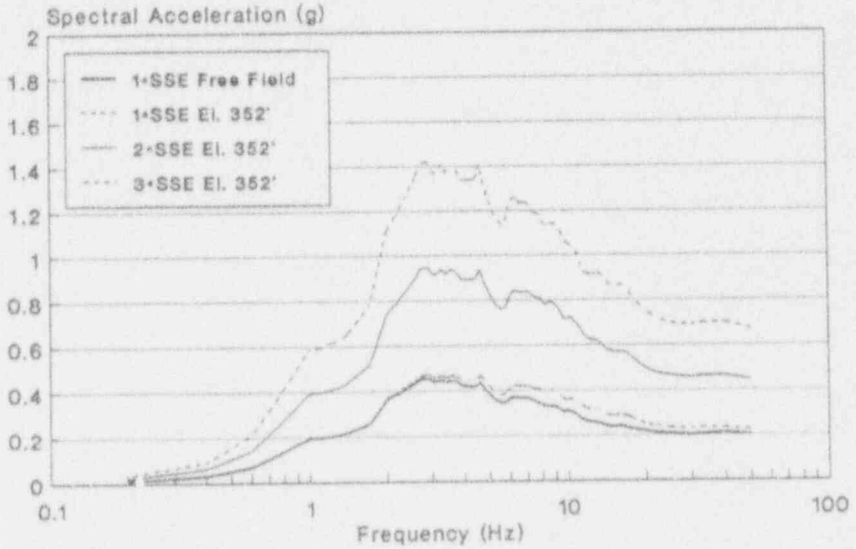

NW-SE Direction
5% Spectral Damping
SSE = 0.20g

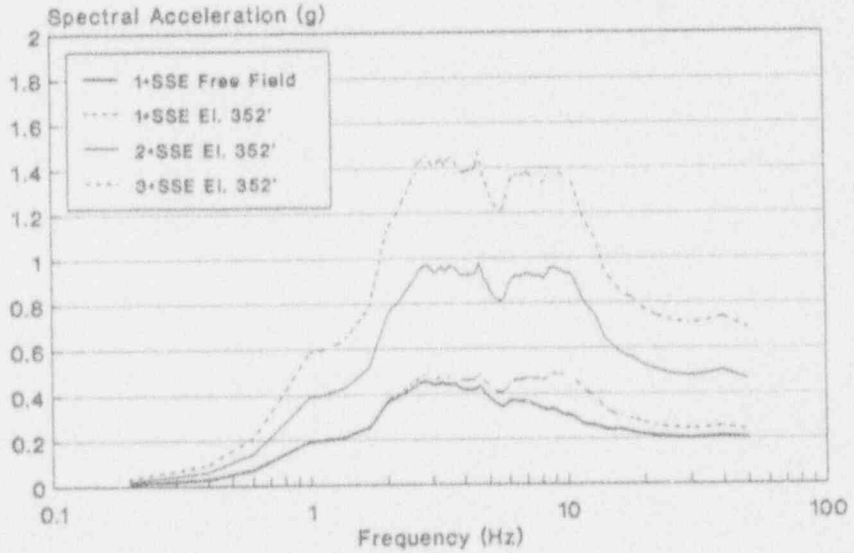

NE-SW Direction
5% Spectral Damping
SSE = 0.20g

Figure C-33 ANO-1 Intake Structure Responses, El. 352'

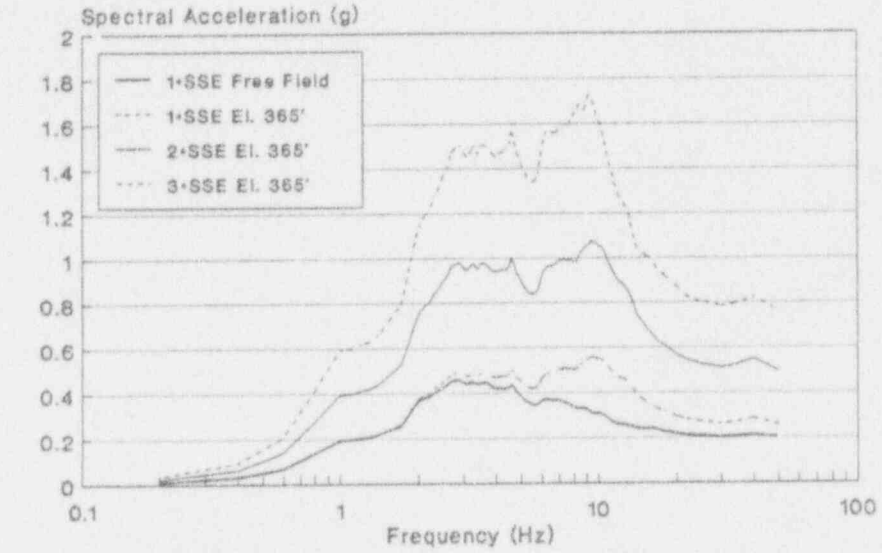

NW-SE Direction
5% Spectral Damping
SSE = 0.20g

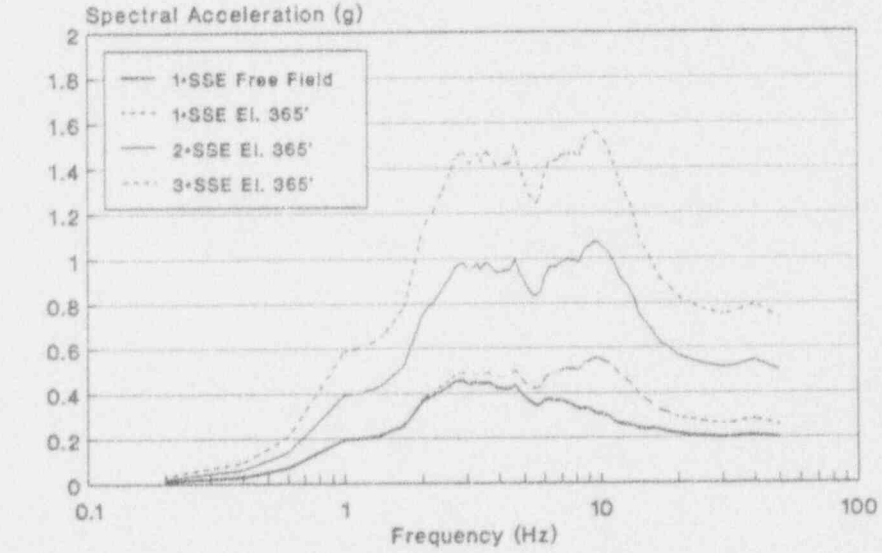

NE-SW Direction
5% Spectral Damping
SSE = 0.20g

Figure C-34 ANO-1 Intake Structure Responses, El. 365'

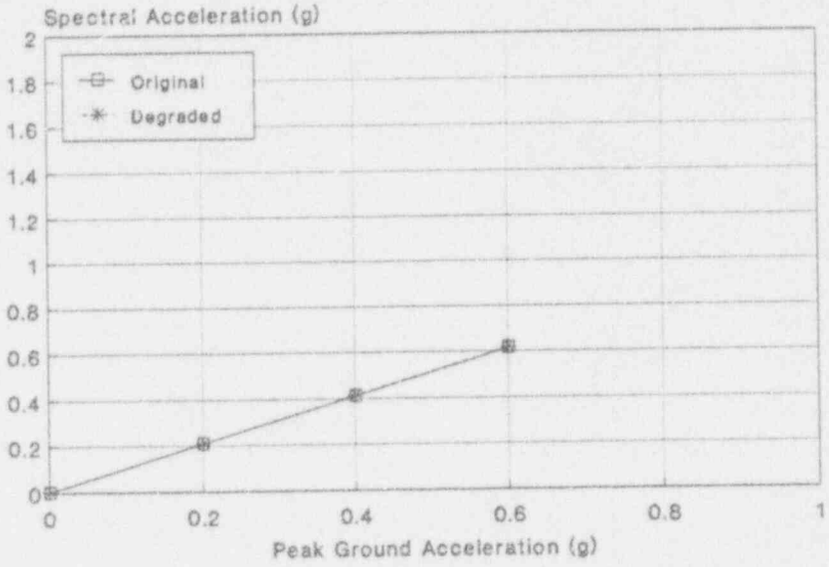

Figure C-35 ANO-1 Median Responses Reactor Internals El. 335', ZPA

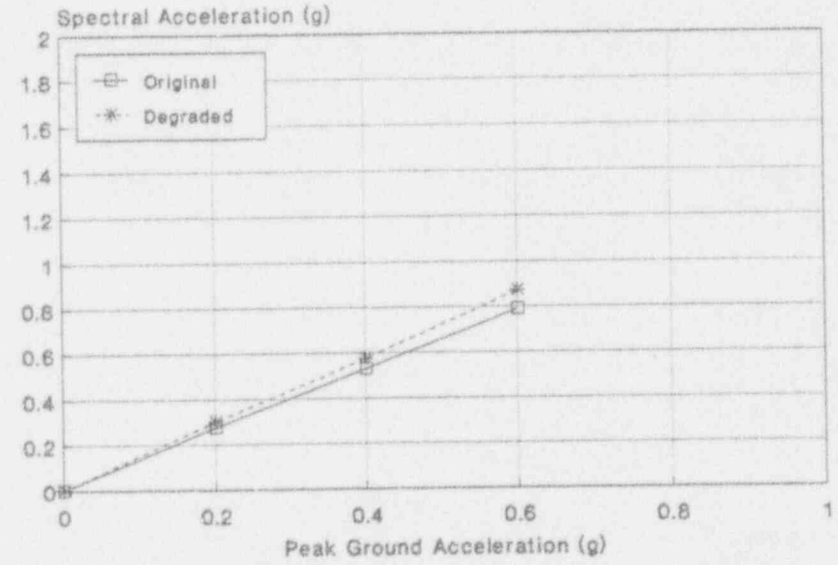

Figure C-36 ANO-1 Median Responses Reactor Internals El. 401', ZPA

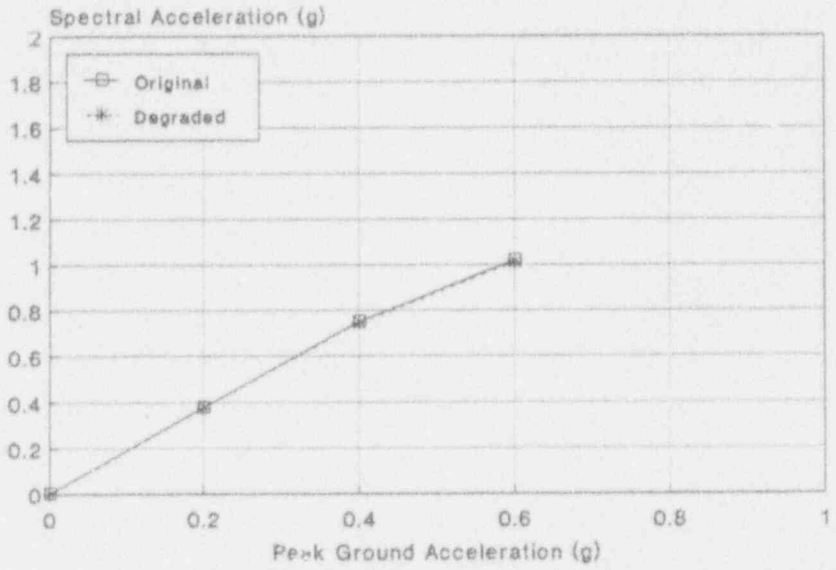

Figure C-37 ANO-1 Median Responses Auxiliary Building El. 335', 7 Hz

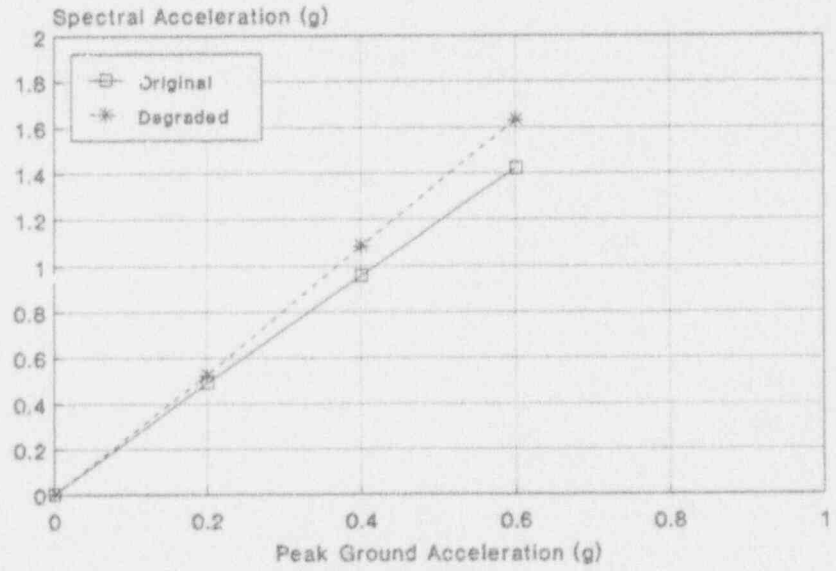

Figure C-38 ANO-1 Median Responses Auxiliary Building El. 371', 5-10 Hz

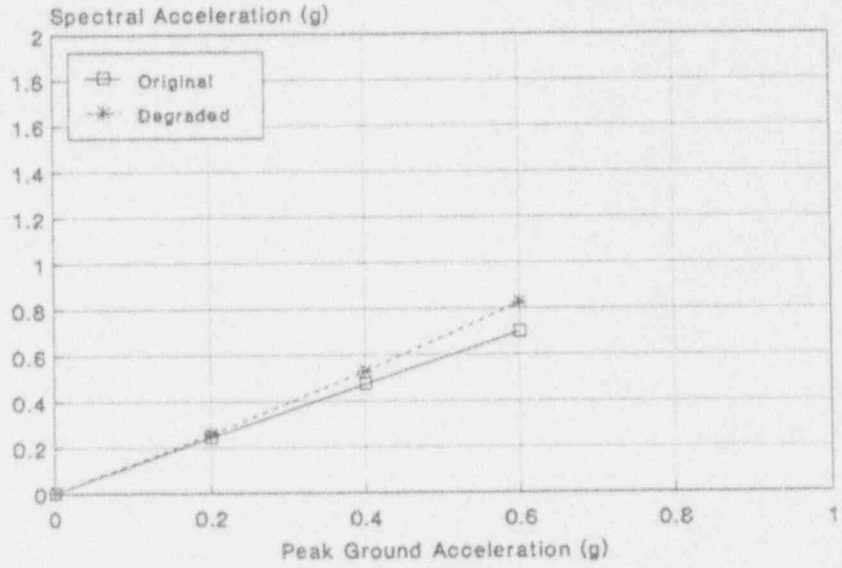

Figure C-39 ANO-1 Median Responses Auxiliary Building El. 371', ZPA

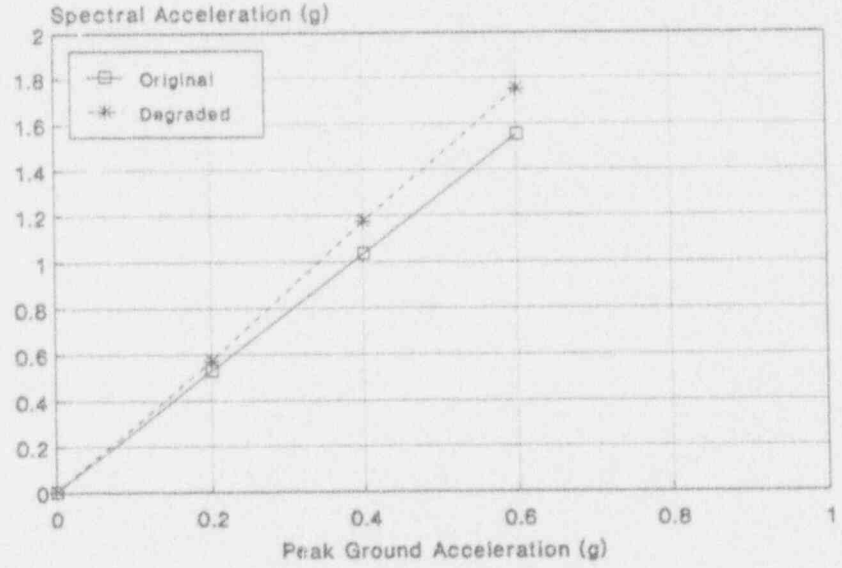

Figure C-40 ANO-1 Median Responses Auxiliary Building El. 386', 5-10 Hz

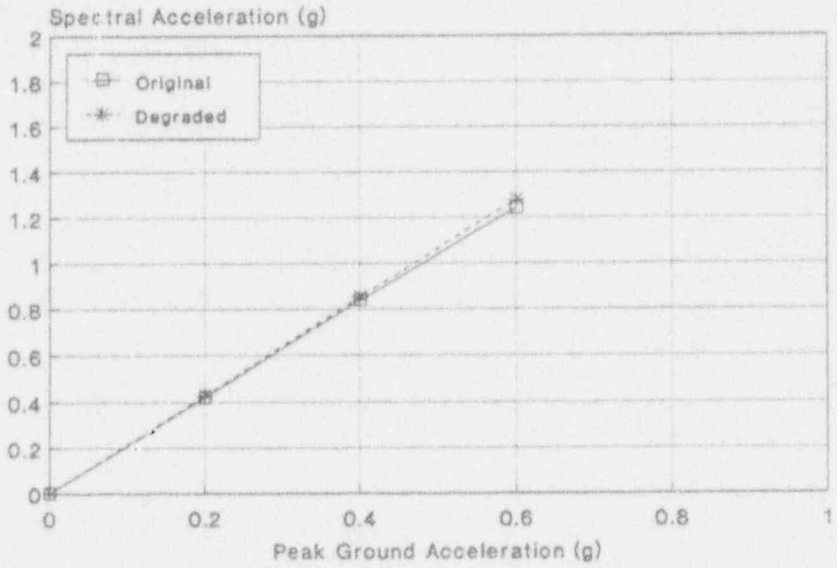

Figure C-41 ANO-1 Median Responses Intake Structure El. 352', 5 Hz

0.60g. Furthermore, for those curves which show some non-linearity at higher acceleration levels, a linear relation provides a conservative estimate of the local response. Such behavior was first recognized in the SSMRP studies. Inasmuch as the bulk of the risk is generally due to earthquake levels only up to the 4 SSE level, it can be seen that relating local response to peak ground acceleration in a linear fashion is appropriate for the ANO-1 analysis.

These plots also show some changes between using original and reduced stiffnesses. At the lowest elevations, there is no change in responses. For upper floors, the response is always higher for the reduced stiffness case, particularly in the 5-10 Hz range. This was most apparent in the Auxiliary building where responses were as much as 20% higher. This was primarily caused by the shifting of the 1st modal frequency down into a higher range of earthquake energies. The Auxiliary building subjected to an SSE earthquake had a fundamental frequency of about 11.2 Hz when original stiffnesses were used. Using reduced stiffnesses and the same SSE input, the frequency dropped to 10.2 Hz. Furthermore, at the highest earthquake input (3 SSE), the fundamental frequency dropped down to about 8.2 Hz.

However, the Reactor internal structure and the Intake structure did not experience as great a increase in response as did the Auxiliary Building. In the case of the Reactor internals, the fundamental frequency was 10.7 using original stiffnesses at the SSE, and only dropped to 10.0 for reduced stiffnesses at both the SSE and 2 SSE levels of input. This is because the internals are primarily made up of very thick concrete walls, resulting in lower shear stresses during an earthquake, and a delaying any significant reductions in stiffness.

Similarly, the Intake structure experienced only a small increase in response. In this case, it was the result of a much higher fundamental frequency, 16 Hz using original stiffnesses at 1 SSE. After reducing the stiffnesses, the frequency only dropped to 14.7 Hz at 1 SSE, and at 3 SSE the frequency only dropped to about 13 Hz. Although this is a significant drop in frequency, the lowest level (13 Hz) is still well above most of the earthquake energies.

C.3.4.2 Variability in Response

Variability in responses (floor slab and spectral accelerations) is assigned based on the detailed SSMRP response calculations made for the Zion Nuclear Power Plant [C-9]. In this evaluation, an attempt was made to accurately compute the responses of walls and floor slabs in the Zion structures, moments in the important piping systems, accelerations of all important valves, and the spectral accelerations at each safety system component (pump, electrical bus, motor control center,, etc.). Correlation between the responses of all components was computed directly from the dynamic response calculations. Detailed summary plots showed that the random uncertainty in the various responses could be reasonably approximated as follows:

Response Type	β random
Peak Ground Acceleration	0.25
Floor Zero Period Accelerations	0.35
Floor Spectral Accelerations	0.45

where β is the standard deviation of the logarithm of the response. The modeling (systematic) variability was taken as 0.3 for all responses.

C.3.4.3 Correlation Between Responses

Generic rules for estimating correlations between the various responses were also derived from SSMRP response calculations for the Zion plant. These rules are summarized in Table C-2. By use of this table, the correlation between any pair of responses can be determined. These correlations are used in evaluating the probabilities for cut sets involving dependent failures.

C.4 SEISMIC FRAGILITIES

The equipment seismic fragilities used in the TAP A-45 study were used in the present study (with two exceptions discussed later). However, in the TAP A-45 study, no building fragilities were developed, and hence a complete set of structural fragilities was developed in this program.

In general, equipment failure is taken as either loss of pressure boundary integrity or loss of operability. Failure (fragility) is characterized by a cumulative distribution function which describes the probability that failure has occurred given a value of loading. Loading may be described by local spectral acceleration or moment, depending on the component failure mode. The fragilities are related to the local response to permit an accurate assessment of the effect of earthquake-induced correlation in the evaluation of the accident sequences.

C.4.1 Generic Fragilities

A generic data base of fragility functions for seismically-induced failures was developed in the SSMRP [Ref. C-10]. As a first step, all components were grouped into generic categories. For example, all motor operated valves located on piping with diameters between 2-1/2 and 8 inches were placed into a single generic category, and similarly, all motor control centers were placed into another generic category. The generic categories are shown on Table C-3. The median failure accelerations and both random and systematic uncertainties (expressed as standard deviations of the logarithms of the fragility) are listed in Table C-4.

Table C-2

Rules for Assigning Response Correlation $\rho_{R_1 R_2}$

1. Components on the same floor slab, and sensitive to the same spectral frequency range (i.e., ZPA, 5-10 Hz or 5 Hz) will be assigned response correlation = 1.0.

2. Components on different floor slabs, sensitive to different ranges of spectral acceleration will be assigned response correlation = 0.5.

3. Components on different floor slabs (but in the same building) and sensitive to the same spectral frequency range will be assigned response correlation = 0.75.

4. Components on the ground surface (outside tanks, etc.) shall be treated as if they were on the grade floor of an adjacent building.

5. "Ganged" valve configurations (either parallel or series) will have response correlation = 1.0.

6. All other configurations will have response correlation = 0.0.

Table C-3

Generic Component Categories

Fragility Category	Component Class	Typical Components	Frequency (Hz)
1	LOSP	Ceramic Insulators	ZPA
2	Relays		5-10
3	Circuit Breakers		5-10
4	Batteries		ZPA
5	Battery Racks		ZPA
6	Inverters		5-10
7	Transformers	4 kV to 480 V and 480 to 120 V	10
8	Motor Control Centers	Control for ESF Pumps and Valves	5-10
9	Aux. Relay Cabinets		5-10
10	Switchgear (Including Transformers, Buses and Breakers)	416 V and 480 V	5-10
11	Cable Trays		ZPA
12	Control Panels and Racks	RPS Process Control	5-10
13	Local Instruments	Misc. Pressure & Temperature Sensors	5-35
14	Diesel Generators	4160 ac Emergency Power Units	22
15	Horizontal Motors	Motor-Generator Sets	ZPA
16	Motor-Driven Pumps and Compressors	AFWS, RHR, SIS, Charging Pumps, Lube Oil Pumps, Diesel Starting Compressors	7
17	Large Vertical, Centrifugal Pumps (Motor-Drive)	Service Water Pumps	5
18	Large Motor-Operated Valves (10")		ZPA
19	Small Motor-Operated Valves (10")		ZPA
20	Large Pneumatic/Hydraulic Valves	Includes MSIV, ADP, and PORV	ZPA
21	Large Check and Relief Valves		ZPA
22	Miscellaneous Small Valves (8")		ZPA
23	Large Horizontal Vessels & Heat Exchangers	Pressurizer Relief Tank, CCW Heat Exchangers	ZPA
24	Small to Medium Heat Exchangers and Vessels	Boron Injection Tank	20
25	Large Vertical Storage Vessels with Formed Heads	RHR Heat Exchanger, Accumulator Tank	ZPA
26	Large Vertical Flat-Bottomed Storage Tanks	CST, RWST	
27	Air Handling Units	Containment Fan Coolers	5

Table C-4

Generic Component Fragilities, in Units of Gravity (g)

Category	Generic Component	Median*	B_U	B_R
1	Ceramic Insulators	0.25	0.25	0.25
2	Relays	3.00	0.48	0.75
3	Circuit Breakers	7.63	0.48	0.74
4	Batteries	0.80	0.40	0.39
5	Battery Racks	2.29	0.31	0.39
6	Inverters	2.00	0.26	0.35
7	Dry Transformers	8.80	0.28	0.30
8	Motor Control Centers	7.63	0.48	0.74
9	Auxiliary Relay Cabinets	7.63	0.48	0.74
10	Switchgear	6.43	0.29	0.66
11	Cable Trays	2.23	0.34	0.19
12	Control Panels and Racks	11.50	0.48	0.74
13	Local Instruments	7.68	0.20	0.35
14	Diesel Generators	1.00	0.25	0.31
15	Horizontal Motors	12.10	0.27	0.31
16	Motor-Driven Pumps and Compressors	2.80	0.25	0.27
17	Large Vertical Centrifugal Pumps	2.21	0.22	0.32
18	Large Motor-Operated Valves (10 in.)	6.50	0.26	0.60
19	Small Motor-Operated Valves (10 in.)	3.83	0.26	0.35
20	Large Pneumatic/Hydraulic Valves	6.50	0.26	0.35
21	Large Relief, Manual, and Check Valves	8.90	0.20	0.35
22	Miscellaneous Small Valves	12.50	0.33	0.43
23	Large Horizontal Vessels and Heat Exchangers	3.0	0.30	0.53
24	Small to Medium Vessels and Heat Exchangers	1.84	0.25	0.45
25	Large Vertical Vessels With Formed Heads	1.46	0.20	0.35
26	Large Vertical Tanks With Flat Bottoms	0.45	0.25	0.35
27	Air Handling Units	6.90	0.27	0.61

R = Random Uncertainty.

U = Systematic Uncertainty.

*All medians in terms of spectral acceleration at 5% damping.

Fragilities for electrical components represent a special problem in that there is a wide variety of electrical gear found within a plant. Because, in most cases, circuits are protected by time delay circuits and because, in most cases, chatter of relays would not cause a change in the state of the system being controlled, the TAP A-45 program chose not to include relay chatter as a failure mode for electrical gear but rather included only circuit breaker trip.

C.4.2 Site Specific Component Fragilities

During the TAP A-45 plant visit (April 1986), the following components were identified as requiring plant-specific fragility derivations:

1) BWST, CST
2) 4160 VAC Switchgear
3) 480 VAC Switchgear

Originally, a median fragility level of 0.4g was assigned to the BWST. However, since then, the BWST was replaced, and thus we assumed a relatively strong median fragility of M_f=1.0g, which is more typical of modern, well designed tanks.

The 4160 VAC switchgear and 480 VAC switchgear were observed during the original Tap A-45 plant visit not to be anchored. Based on these observations, site-specific fragilities were developed for all the 4160 VAC and 480 VAC switchgear. A median fragility for both these cabinets was determined to be 0.324g. For this study, it has been assumed that the anchorages have been upgraded, raising the assumed capacity to 0.7g. The site-specific fragilities are summarized on Table C-5.

C.4.3 Structural Fragilities

The ANO-1 structural fragilities were derived in terms of factors which account for structure ultimate strength and inelastic energy absorption capability. The basic techniques used to determine the median values and associated variabilities of the terms were essentially those described in Section 2.5 of the main report.

The structures were considered to fail functionally when inelastic deformations of the structure under seismic load are estimated to be sufficient to potentially interfere with the operability of safety-related equipment attached to the structure. The element and system ductility limits chosen for structures were estimated to correspond to the onset of significant structural damage. This was believed to represent a conservative bound on the level of inelastic structural deformation which might interfere with the operability of components housed within the structure.

In order to determine the structural fragilities at ANO-1, it was necessary to develop a complete structural model for each structure

Table C-5

ANO-1 Site Specific Fragilities

Component	Failure Mode	Median Base Acceleration at Failure	Random Uncertainty	Modeling Uncertainty
4160 VAC Switchgear	Sliding & tipping due to minimal anchorage	0.7g	0.4	0.3
480 VAC Switchgear	Sliding & tipping due to minimal anchorage	0.7g	0.4	0.3
BWST	Buckling (Est)	1.0g	0.3	0.29
CST	Buckling (Est)	1.0g	0.3	0.29

(including every load-resisting shear wall). Since only stick models were available in the FSAR data, the necessary models were developed from as-built drawings that were obtained directly from the plant as part of this study. After determining maximum floor loads from a time history analysis of each structure, the resulting shear forces in each wall, including any torsional effects, could then be computed. A total shear force and overturning moment was then computed for each elevation. In addition, using the drawings, the ultimate capacity of each wall could be determined. The loads and capacities then provide the necessary factors used to determine the structural fragility for each structure as described in Section 2.5 of the main report.

Determination of structural fragilities utilizes seismic responses which depend on the assumed stiffnesses of the structural model. To account for the reduction of stiffness with shear stress (i.e., with acceleration) further considerations are required. The approach described below was used to incorporate this effect.

First, we identify bounding ground motion cases for which structural response is essentially linear. The lower bound case will always be the 1*SSE case. The upper bound case will be the one corresponding to the highest ground motion level for which stresses are still "approximately elastic". Based upon the force-deflection curve corresponding to the specified stiffness-NBSS relationship, the structure can be considered "approximately elastic" so long as shear stresses are all less than about 300 psi. Hence the use of linear elastic analysis in this process is valid. This corresponds to a stiffness reduction factor of 0.33 from the model described in Section 3.2 of the main report.

Then, for the lower and upper bound ground motion cases identified above, structural fragilities were determined using the following guidelines:

1. The strength factor based on the original stiffness were scaled by the ratio of the median load for the bounding case to the median load from the original stiffness evaluation. (This scaling was performed for the governing shear wall element.)

2. The inelastic energy absorption factor for the bounding case considered was determined using the corresponding frequency for the dominant mode resulting from the reduced stiffness calculation.

3. Median damping values of 7% and 8.5% have been specified for the 1*SSE and 2*SSE cases. Damping factors were included in the fragilities to account for the difference in response associated with a median damping of 10% at structural failure. (Variability associated with damping was not included in the fragility, since this is included in the response variability.)

The median accelerations at failure for the two bounding cases was compared. So long as they were not significantly different, a single fragility was selected which is thus representative of the range of frequency reduction expected at failure.

The resulting fragilities for both original and reduced stiffnesses of the ANO-1 structures are listed in Table C-6. In general, several potential failure modes were investigated for each structure. Fragilities for the governing failure modes are reported. These failure modes are typically associated with structural failure which would result in damage to the safety-related equipment located in the building.

Both the original and reduced stiffness structural fragilities listed in Table C-6 are typical of fragilities for similar structures at other Nuclear Power Plants. As can be seen, the effect of reduced stiffness was minor. At most, the median capacity was reduced by 10%. This is expected to have a minor effect on the total core damage frequency due to the already high structural fragilities (i.e., > 1.4g).

C.5 CORE DAMAGE AND RISK COMPUTATIONS

C.5.1 Initiating Events

The initiating events considered for the seismic analysis for ANO-1 were:

- Reactor Vessel Rupture (ECCS ineffective)
- Large LOCA [A_2] (pipe break between 13.5" < ID < 36.0")
- Large LOCA [A_1] (pipe break between 10.0" < ID < 13.5")
- Medium LOCA [M_2] (pipe break between 4.0" < ID < 10.0")
- Medium LOCA [M_1] (pipe break between 1.66"< ID < 4.0")
- Small LOCA (pipe break between 1.2" < ID < 1.66")
- Small-Small LOCA (pipe break between ID < 1.2")
- Intake Structure Failure
- Type 2 Transient (PCS initially inoperable)
- Type 3 Transient (PCS initially available)

The reactor vessel rupture event was computed based on the probability of failure of the supports of the reactor vessel itself, or failure of the Reactor Internal Structure or Auxiliary Building. The frequency for the large LOCA event was computed based on the failure of the supports of the steam generators and the reactor coolant pumps. Failures of the piping were not included as a review of their capacity showed that they were significantly higher than the pump or steam generator support failures and hence, would make negligible contribution to the initiating event frequency.

The small-small, small and medium LOCA initiating events were computed

Table C-6

Summary of Structural Fragilities for ANO-1

Structure	Element	Original[1] A_m(g)	B_R	B_U	Reduced[2] A_m(g)	B_R	B_U	Effect of Failure
Reactor Internals	N-S Shear Walls	3.3	0.06	0.21	3.0	0.06	0.21	Vessel Rupture Initiating Event
Auxiliary Building Building	N-S Shear Walls	1.5	0.09	0.23	1.4	0.10	0.23	Included in RVR initiating event leading directly core damage
Intake Structure	E-W Shear Walls	2.4	0.07	0.27	2.4	0.08	0.27	Seal LOCA with Station Blackout

1. These fragilities are based on loads from analyses using original stiffnesses.

2. These fragilities are based on loads from analyses including shear wall stiffness degradation.

3. B_R and B_U do not include response variability.

based on the failure of piping in the reactor coolant loop. The fragility for the pipe failures was generated from the calculations of piping failures for pipes considered in the SSMRP Zion analysis. (In addition, transfers from the transient tree based on stuck open relief valves are considered. Two stuck open relief valves are equivalent to a medium LOCA whereas one stuck open relief valve is equivalent to a small LOCA.)

The Intake Structure Failure initiating event was computed based on the fragility of the structure. When the structure fails, it will result in a Seal LOCA with station blackout.

The frequency of the Type 2 transient initiating event (in which loss of offsite power is implied) is computed based on the failure of ceramic insulators. These have a relatively low median failure level, and are the dominant cause of seismically-induced loss of offsite power.

Finally, the Type 3 transient initiating event probability is computed from the condition that the sum of the initiating event probabilities considered must be unity. The hypothesis is that, given an earthquake above the Operating Basis Earthquake (OBE), at least one the initiating events will occur. At the least, the operators must manually shut the plant down for inspection following an OBE level earthquake.

C.5.2 Event Trees

The event trees developed for the internal event analyses in IREP and the TAP A-45 programs were used directly. They are repeated here for ease of subsequent discussion as Figures C-42 through C-49.

C.5.3 Accident Sequences

The accident sequence expressions (in terms of component failure basic events) developed in the TAP A-45 program for the small-small, small, T_2 and T_3 initiators were used directly. This is appropriate since very conservative screening was used in that program in solving the fault trees and event trees for the accident sequences in terms of the basic failure events. That is, screening failure probabilities were developed for each component on the fault trees for use in the screening process, and these probabilities were based on very conservative estimates of the seismic response that the components could experience. These bounding response estimates were more than adequate to encompass the increases in responses which were found (due to degrading the shear wall stiffnesses) in this program. Thus the accident sequence expressions developed in the TAP A-45 program were directly useable in the context of this shear wall degradation study. A total of 15 accident sequences were obtained from the TAP A-45 ANO-1 final report [Ref. C-2]. (These accident sequences were quantified with the point estimate seismic hazard curve used in the original TAP A-45 analysis of ANO-1, and the TAP A-45 results were reproduced. This verifies that the sequences were properly extracted and coded for the current re-evaluation and uncertainty analyses described below.)

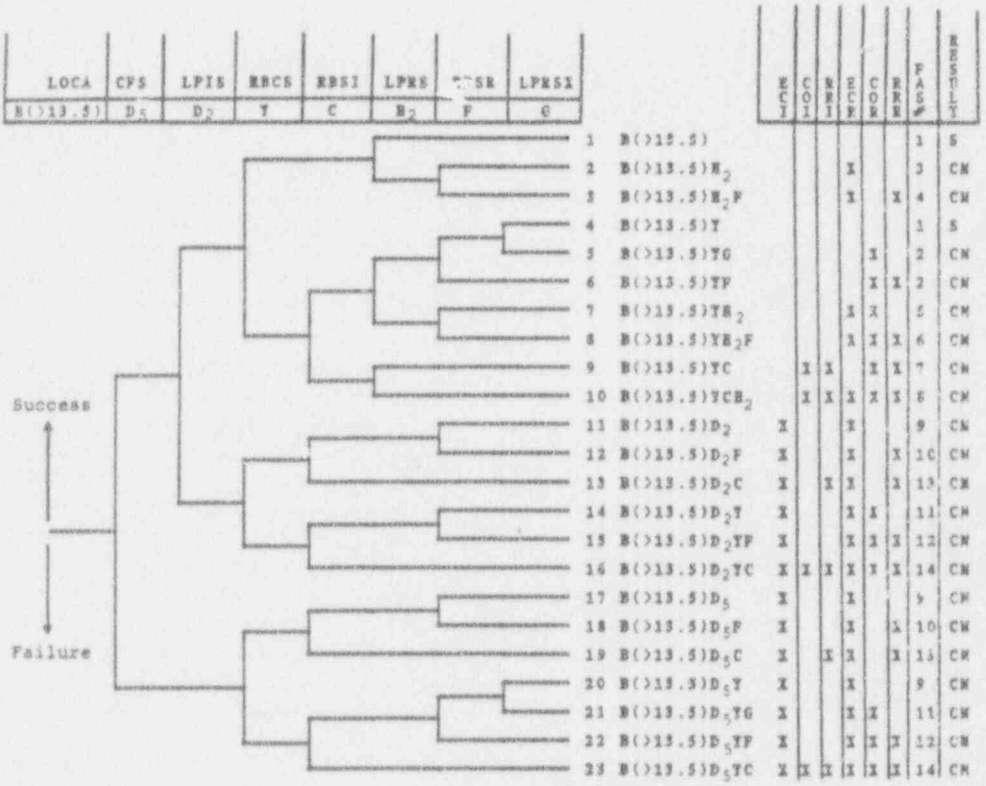

Figure C-42 ANO-1 Large LOCA Event Tree [A_2]
(Breaks 13.5" < ID < 36")

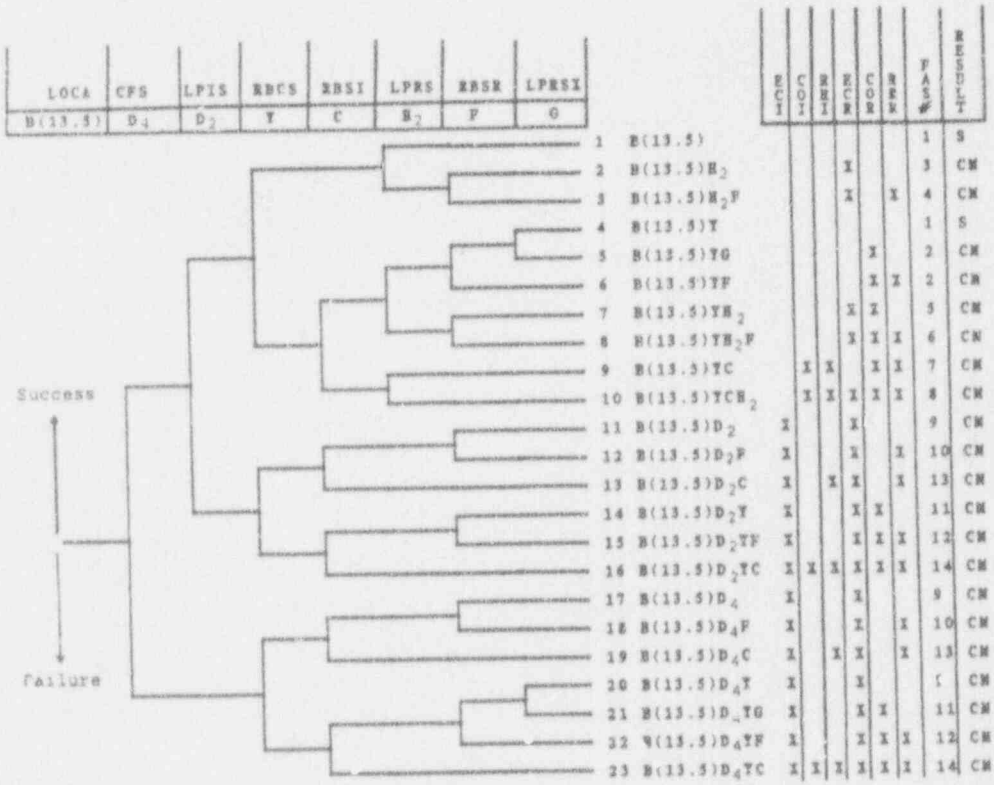

Figure C-43 ANO-1 Large LOCA Event Tree [A_1]
(Breaks 10" < ID < 13.5")

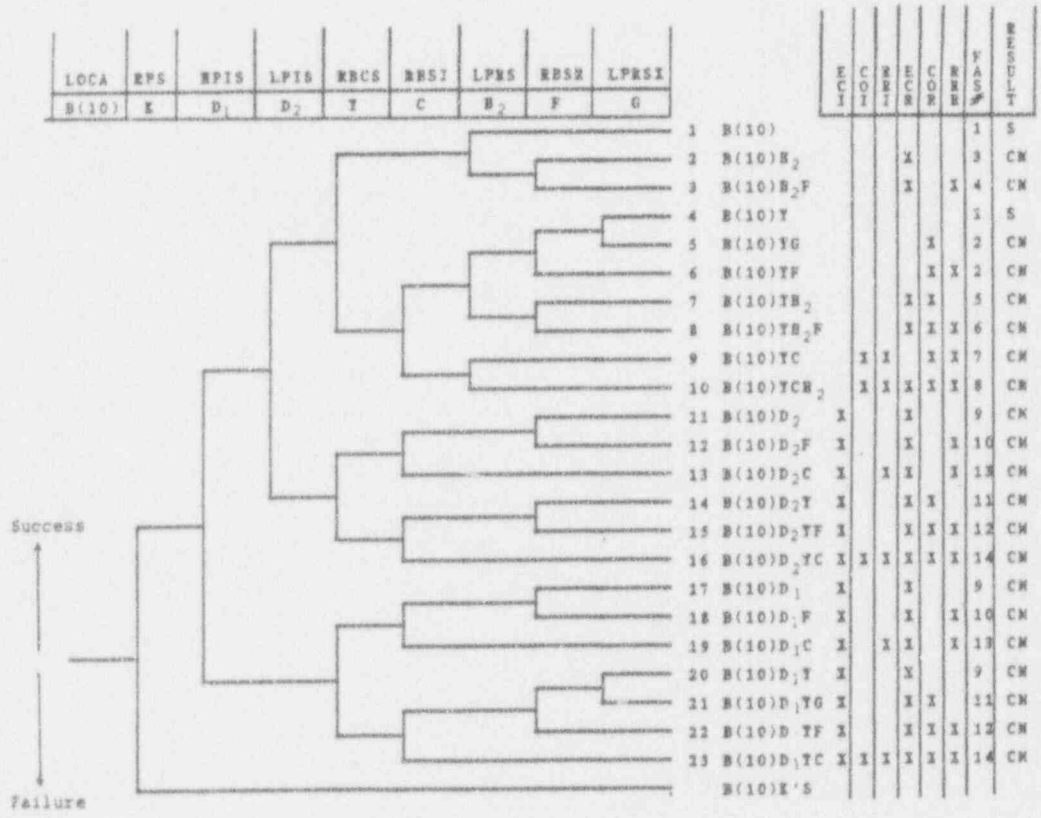

Figure C-44 ANO-1 Medium LOCA Event Tree [M_2]
(Breaks 4" < ID < 10")

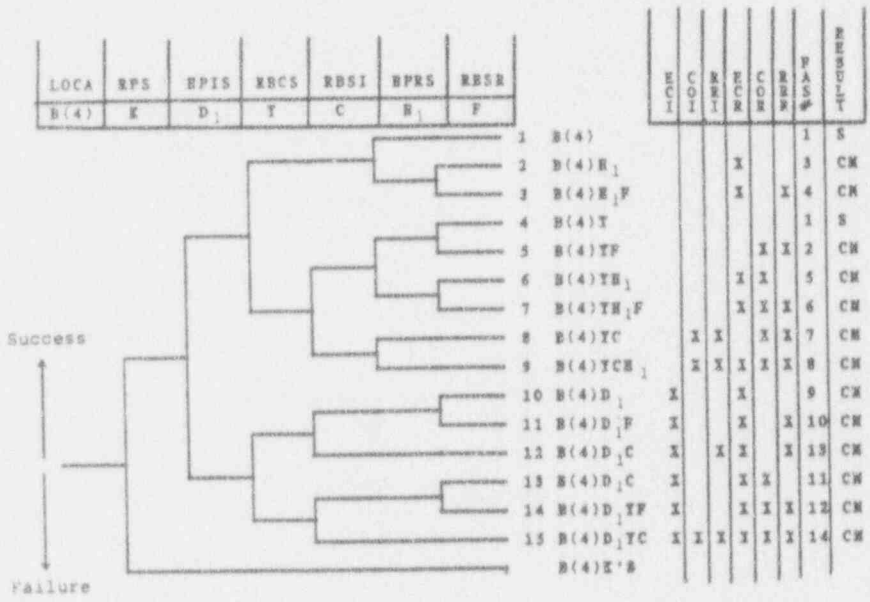

Figure C-45 ANO-1 Medium LOCA Event Tree [M_1]
(Breaks 1.66" < ID < 4")

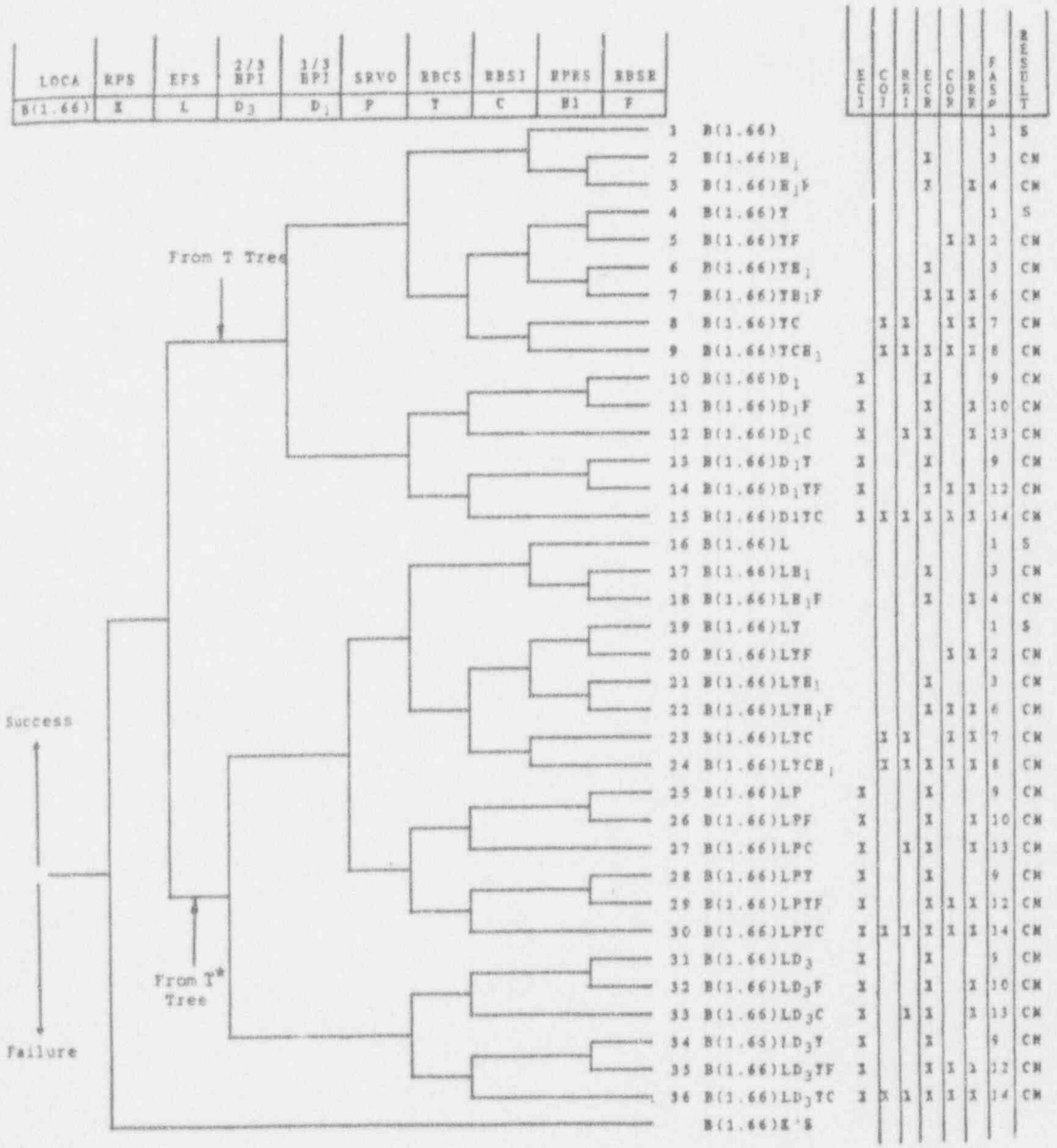

Figure C-46 ANO-1 Small LOCA Event Tree [S_2]
(Breaks 1.2" < ID < 1.66")

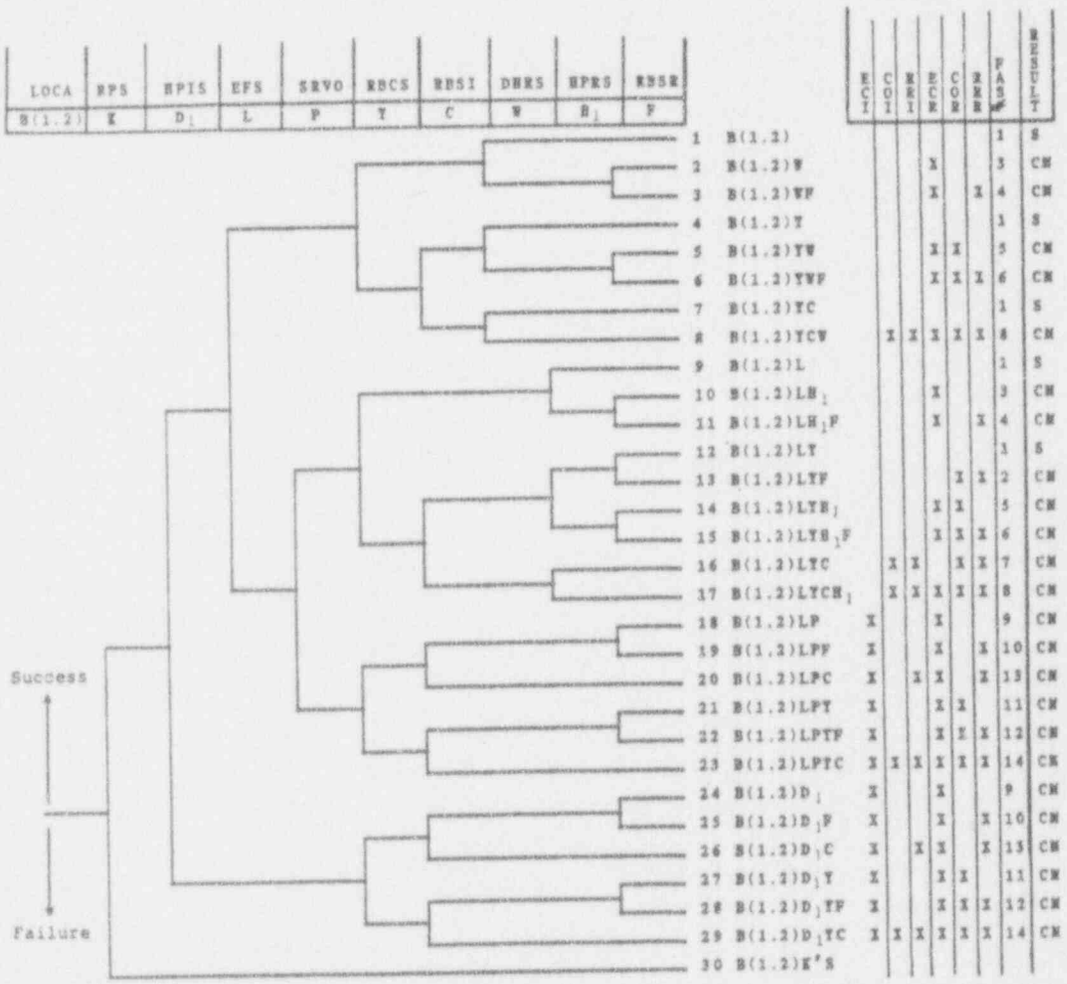

Figure C-47 ANO-1 Small-Small LOCA Event Tree [S_3]
(Breaks 0.38" < ID < 1.2")

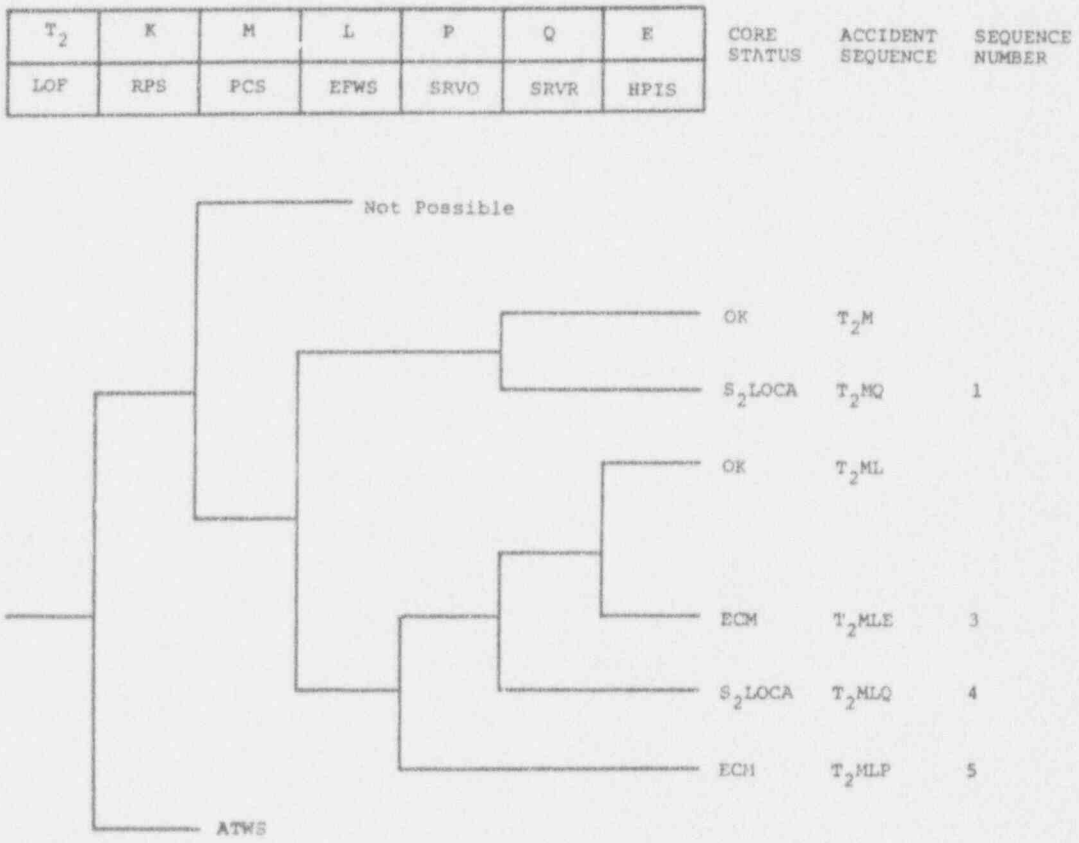

Figure C-48 Transient Type 2 Event Tree [T_2]
(PCS initially inoperable)

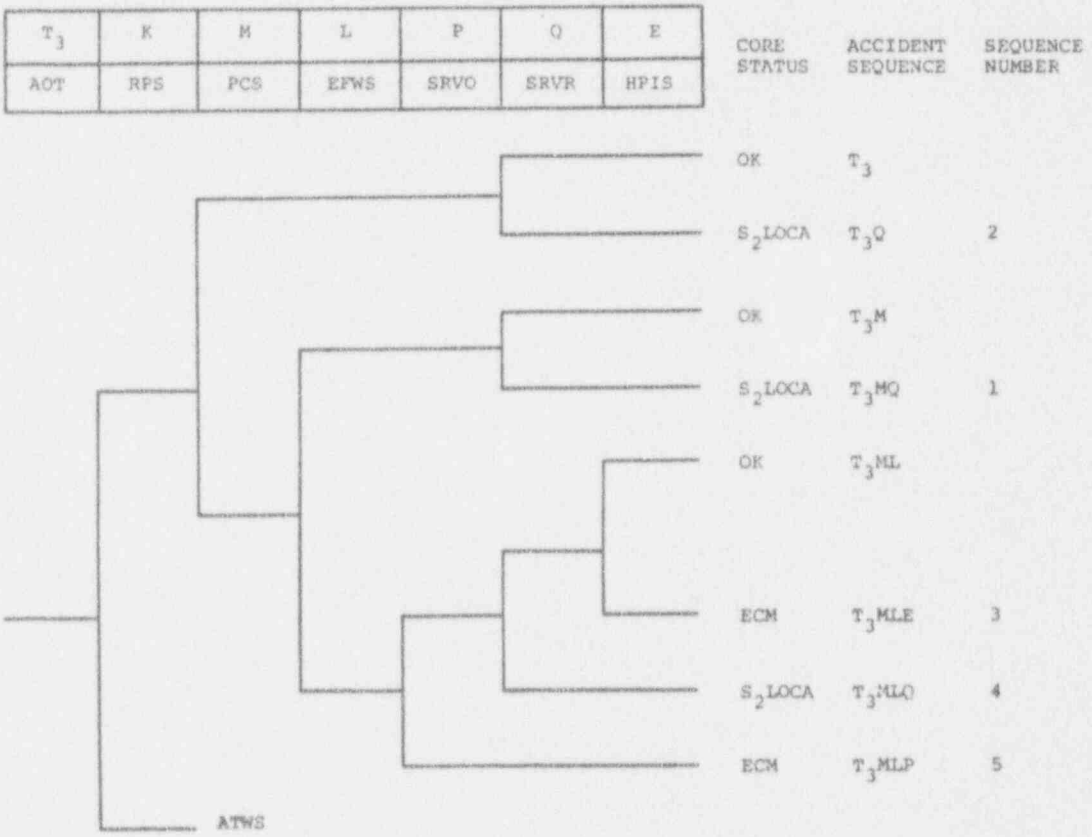

Figure C-49 Transient Type 3 Event Tree [T_3]
(PCS initially available)

In order to perform a complete seismic PRA for this shear wall degradation study of ANO-1, accident sequences for MLOCA, LLOCA, and RVR initiating events were needed, since these were not in the scope of the TAP A-45 program. These were obtained from the sequences developed in the IREP program, whose final report [Ref. C-1] listed success criteria for each of these events and accident sequence expressions for the LOCA events. These were reviewed, and then used directly. This is appropriate, since the sequences and component dependencies for the LLOCA and RVR events are quite simple and easily verified by reference to the reported LOCA success criteria. A total of 6 additional accident sequences were obtained from the IREP ANO-1 final report [C-1].

Taken together, a total of 21 accident sequences corresponding to the 8 initiating events were evaluated in this study. These 21 sequences are presented in Table C-7 along with identification of the Boolean sequences that were solved for each accident sequence. (The number of Booleans solved using the SETS code is less than the number of accident sequences because several accident sequences may utilize the same Boolean expression even though the initiating event may be different.) Also identified on this table are the complement expressions which must be included in the numerical sequence quantification at high PGA levels at which success probabilities may be significantly less than unity. The multiplier expression column lists those events specified by algebraic equations rather than by Boolean logical expressions. Table C-8 describes the abbreviations used for the accident sequences in Table C-7. The actual equations for the Boolean expressions, systems and complement events are listed at the end of this report (ANO-1 Appendix - Input Files).

C.5.4 Accident Sequence Quantification

To evaluate the effect of including degraded shear wall stiffnesses in the seismic PRA of ANO-1, the accident sequences described above were quantified both with and without the stiffness reduction. In each case, a complete uncertainty analysis was performed on the accident sequences using a true Monte Carlo analysis. Thus, the expression for the unconditional accident sequence frequencies (and for core damage frequency), shown as below:

$$ACC_j = \int P(ACC_j, PGA) f_{eq}(PGA) d(PGA)$$

where

$P(ACC_j, PGA)$ is the conditional frequency of accident sequence j as a function of PGA, and

$f_{eq}(PGA)$ is the probability distribution function for the hazard curve,

was randomly sampled varying the hazard curve parameters, the random failure frequencies, and the seismic response and fragility parameters.

Table C-7

Seismic Accident Sequences for ANO-1

	Accident Sequence		Multiplier Expression	Boolean Expression	Complement Factor
	Vessel Rupture				
1.	RVR-1		1	1	1
	Large LOCA				
2.	A2-LOCA-1	$A_2\ \bar{D}_5\ D_2$	1	BOOL 9	$\bar{D}_5$
3.	A2-LOCA-2	$A_2\ D_5$	1	1	1
	Intermediate LOCA				
4.	M2-LOCA-1	$M_2\ \bar{K}\ \bar{D}_1\ D_2$	1	BOOL 8	$\bar{K}\ \bar{D}_1$
5.	M2-LOCA-2	$M_2\ \bar{K}\ D_1$	1	BOOL 4	$\bar{K}$
6.	M1-LOCA-1	$M_1\ \bar{K}\ D_1$	1	BOOL 4	$\bar{K}$
	Small LOCA				
7.	SLOCA-1	$S_2\ M\ \bar{L}\ H_1\ H_2$	1	BOOL 1	$\bar{L}$
8.	SLOCA-2	$S_2\ M\ \bar{L}\ D_1\ \bar{X}\ H_2$	1	BOOL 2	$\bar{L}\ \bar{X}$
9.	SLOCA-3	$S_2\ M\ \bar{L}\ D_1\ \bar{X}\ D_2$	1	BOOL 3	$\bar{L}\ \bar{X}$
10.	SLOCA-4	$S_2\ M\ \bar{L}\ D_1\ X$	1	BOOL 4	$\bar{L}$
11.	SLOCA-5	$S_2\ M\ L\ H_1$	1	BOOL 5	1
12.	SLOCA-7	$S_2\ M\ L\ D_1$	1	BOOL 6	1
	Intake Structure				
13.	INTK-1	INTK	1	1	1
	Small-Small LOCA				
7.	SSLOCA-1	$S_3\ M\ \bar{L}\ H_1\ H_2$	1	BOOL 1	$\bar{L}$
8.	SSLOCA-2	$S_3\ M\ \bar{L}\ D_1\ \bar{X}\ H_2$	1	BOOL 2	$\bar{L}\ \bar{X}$
9.	SSLOCA-3	$S_3\ M\ \bar{L}\ D_1\ \bar{X}\ D_2$	1	BOOL 3	$\bar{L}\ \bar{X}$
10.	SSLOCA-4	$S_3\ M\ \bar{L}\ D_1\ X$	1	BOOL 4	$\bar{L}$
11.	SSLOCA-5	$S_3\ M\ L\ H_1$	1	BOOL 5	1
12.	SSLOCA-7	$S_3\ M\ L\ D_1$	1	BOOL 6	1
	Loss of Feedwater Transient				
20.	T2-2	$T_2\ M\ L\ \bar{P}\ \bar{Q}\ E$	1	BOOL 6	$\bar{P}\ \bar{Q}$
	Other Transient				
21.	T3-2	$T_3\ M\ L\ \bar{P}\ \bar{Q}\ E$	1	BOOL 6	$\bar{P}\ \bar{Q}$

Table C-8

Safety Systems Nomenclature

D_1	- Failure of the High Pressure Injection System (HPIS)
D_2	- Failure of the Low Pressure Injection System (LPIS)
D_4	- Failure of the Core Flood System (CFS) 1 of 2 Tanks
D_5	- Failure of the Core Flood System (CFS) 2 of 2 Tanks
E	- Failure of the High Pressure Injection System (HPIS) with operator initiation
H_1	- Failure of the High Pressure Recirculation System (HPRS)
H_2	- Failure of the Low Pressure Recirculation System (LPRS)
K	- Failure of the Reactor Protection System (RPS)
L	- Failure of the Emergency Feedwater System (EFWS)
M	- Failure of the Power Conversion System (PSC)
P, P_1	- Failure of Safety Relief Valves (SRVs) to open
Q	- Failure of SRVs to close
X	- Failure of Secondary Blowdown (SBD)

From the accumulated values of accident sequence frequency and core damage frequency, exact statistics on their distributions are directly obtainable. The result is an estimate of the mean annual frequency of each accident sequence as well as of the total core damage plus a description of the distributions associated with these estimates.

In addition, a mean point estimate quantification (for which all random parameters were set to their mean values and a single quantification was made for each case. This allows for an efficient evaluation of each individual component's importance to the total core damage frequency and a determination of the relative contribution of different earthquake levels to the total. (Experience has shown that such mean point estimate calculations yield results which are very close to the actual mean results obtained from the full uncertainty analysis.)

C.5.4.1 Core Damage Frequency Results Without Stiffness Reduction

The 21 accident sequences were fully quantified using component random failures and the seismic fragilities and responses plus their associated random and systemic variabilities. Based on this quantification, five dominant sequences were identified. These dominant sequences are (in order of importance):

T2-2 (41%)
M1-LOCA-1 (14%)
SSLOCA-3 (10%)
SSLOCA-7 (8%)
SLOCA-3 (5%)

The percentage contributions were taken from the Monte Carlo uncertainty results. The total mean core damage frequency for the ANO-1 base case was computed to be 1.07E-3 per year using the LLNL seismic hazard curves and 8.78E-6 per year using the EPRI hazard curves. The relative contributions of the accident sequences are shown in Table C-9. Table C-10 shows the various percentiles of distribution from the Monte Carlo analysis for both sets of hazard curves. Relative importance of the basic events to these results are presented in the point estimate results presented below.

The largest contributor to the core damage frequency is the transient sequence:

$$\text{T2-2} = T_2\ M\ L\ \bar{P}\ \bar{Q}\ E$$

in which the emergency feedwater system (L) fails and the PCS (M) fails due to the initiator. The second greatest contributor is the Intermediate LOCA sequence:

$$\text{M1-LOCA-1} = M_1\ \bar{K}\ D_1$$

in which the RPS (K) is assumed to succeed and the HPIS (D_1) fails to provide flow to the reactor vessel from at least one of three high

Table C-9

Accident Sequence and Total Core Damage Mean Frequencies
for ANO-1 with Original Stiffnesses
(Monte Carlo Uncertainty Analysis)

		Mearf Frequency (per year)	
Accident Sequence		LLNL Hazard	EPRI Hazard
1	RVR-1	1.25E-5	5.73E-8
2	A2-LOCA-1	5.95E-6	4.04E-8
3	A2-LOCA-2	3.80E-7	2.24E-9
4	M2-LOCA-1	5.68E-7	5.67E-9
5	M2-LOCA-2	3.92E-5	1.99E-7
6	M1-LOCA-1	1.56E-4	1.21E-6
7	SLOCA-1	1.29E-5	1.03E-7
8	SLOCA-2	1.64E-5	1.17E-7
9	SLOCA-3	6.90E-5	5.87E-7
10	SLOCA-4	2.42E-6	2.09E-8
11	SLOCA-5	5.87E-6	3.60E-8
12	SLOCA-7	4.27E-5	2.63E-7
13	INTK-1	6.02E-7	2.10E-9
14	SSLOCA-1	2.19E-5	1.77E-7
15	SSLOCA-2	2.87E-5	2.04E-7
16	SSLOCA-3	1.30E-4	1.11E-6
17	SSLOCA-4	4.56E-6	3.95E-8
18	SSLOCA-5	8.88E-6	5.52E-8
19	SSLOCA-7	7.14E-5	4.46E-7
20	T2-2	4.28E-4	3.80E-6
21	T3-2	1.51E-5	3.05E-7
	TOTAL	1.07E-3	8.78E-6

Table C-10

Accident Sequence Frequency Distribution Percentiles
for ANO-1 with Original Stiffnesses
(Monte Carlo Uncertainty Analysis)

	LLNL Hazard	EPRI Hazard
Mean	1.07E-3	8.78E-6
Var	3.45E-5	2.34E-10
5%	1.62E-6	3.83E-7
50%	7.70E-5	3.78E-6
95%	3.21E-3	3.39E-5

pressure pumps, taking suction from the BWST. The third largest contributor to the core damage frequency is the SSLOCA-3, given by:

$$SSLOCA\text{-}3 = S_3\ M\ \bar{L}\ D_1\ \bar{X}\ D_2$$

which includes the failure of both the HPIS (D_1) and LPIS (D_2) and the failure of these systems is dominated by failure of electrical busses. SLOCA-3 is the fifth highest contributor and involves the same event trees but a lower initiating event than the Small-Small LOCA. The forth highest contributor to core damage frequency is the SSLOCA-7, and is given by:

$$SSLOCA\text{-}7 = S_3\ M\ L\ D_1$$

in which failure is similar to T_2-2 and involves the same cutsets.

Mean Point Estimate

The mean point estimate is based on using the mean values for all variables. Table C-11 presents the mean core damage contributions at seven intervals over the LLNL hazard curve for each accident sequence. Table C-12 presents the mean core damage contributions for the EPRI hazard curve. The right hand column presents the total contribution of each accident sequence to the total core damage frequency of 1.14E-3 for the LLNL hazard curves and 8.85E-6 for the EPRI hazard curves. As can be seen, the incremental contributions from the LOCA events do not become significant until the higher acceleration levels. The reactor vessel rupture sequence does not make a significant contribution until the highest PGA increment.

An important thing to note from Table C-11 is the sum of the accident sequence contributions at each earthquake level, as shown at the bottom of each column on the table. The contributions are seen to be small at the first increment, increasing to a maximum at the third and forth earthquake increment, and then decreasing at higher earthquake levels. This indicates that the bulk of the risk is occurring in the range of 0.2 g to 0.6 g which roughly corresponds to the range of 1-3 SSE. Further, this shows that the bulk of the risk has been captured by integrating over the range 0.1 g to 0.8 g.

Basic Event Importance

The importance of the basic seismic failure events was evaluated by setting the seismic failure probability to zero in the mean point estimate calculation, which gives a measure of the net reduction in core damage frequency that would occur if that component could never fail due to seismic shaking.

Results of these calculations for both sets of hazard curves are shown in Table C-13. It can be seen that the largest reduction occurs for the 4kV and 480V electrical busses. This is again because they have a low

Table C-11

Total Accident Sequence Frequency Increments
LLNL Seismic Hazard Curves for ANO-1 with Original Stiffnesses
(Mean Point Estimate Calculation)

	0.10-0.20g	0.20-0.30g	0.30-0.40g	0.40-0.50g	0.50-0.60g	0.60-0.70g	0.70-0.80g	TOTAL
1	3.5E-09	8.4E-08	4.6E-07	1.3E-06	2.4E-06	3.6E-06	4.5E-06	1.2E-05
2	8.7E-09	2.3E-07	7.1E-07	1.3E-06	1.7E-06	1.9E-06	1.9E-06	7.6E-06
3	1.6E-12	3.4E-10	5.4E-09	2.8E-08	8.0E-08	1.6E-07	2.5E-07	5.3E-07
4	4.2E-08	1.3E-07	7.9E-09	1.2E-10	9.4E-13	0.0E+00	0.0E+00	1.7E-07
5	1.2E-07	1.7E-06	3.6E-06	4.8E-06	5.2E-06	5.1E-06	4.6E-06	2.5E-05
6	3.5E-06	2.4E-05	3.3E-05	3.2E-05	2.8E-05	2.3E-05	1.7E-05	1.6E-04
7	1.8E-07	1.6E-06	4.3E-06	5.5E-06	4.6E-06	2.9E-06	1.5E-06	2.1E-05
8	1.3E-07	1.5E-06	4.1E-06	5.6E-06	4.8E-06	2.9E-06	1.5E-06	2.0E-05
9	3.5E-06	1.8E-05	1.7E-05	1.1E-05	6.3E-06	3.2E-06	1.5E-06	6.1E-05
10	1.4E-07	6.4E-07	5.9E-07	3.8E-07	2.1E-07	1.1E-07	5.2E-08	2.1E-06
11	2.7E-09	2.8E-08	2.2E-07	9.0E-07	2.0E-06	2.9E-06	3.1E-06	9.2E-06
12	8.5E-08	1.9E-06	8.1E-06	1.3E-05	1.3E-05	8.9E-06	5.7E-06	5.0E-05
13	7.3E-13	3.9E-10	5.5E-09	2.4E-08	5.9E-08	9.8E-08	1.3E-07	3.1E-07
14	3.8E-07	3.2E-06	8.0E-06	9.8E-06	7.7E-06	4.5E-06	2.2E-06	3.6E-05
15	2.6E-07	2.9E-06	7.7E-06	1.0E-05	8.0E-06	4.6E-06	2.2E-06	3.6E-05
16	7.3E-06	3.6E-05	3.3E-05	2.0E-05	1.1E-05	5.0E-06	2.3E-06	1.1E-04
17	2.9E-07	1.3E-06	1.1E-06	6.8E-07	3.6E-07	1.7E-07	7.7E-08	4.0E-06
18	5.6E-09	5.6E-08	4.2E-07	1.6E-06	3.4E-06	4.6E-06	4.7E-06	1.5E-05
19	1.8E-07	3.7E-06	1.5E-05	2.4E-05	2.1E-05	1.4E-05	8.5E-06	8.7E-05
20	6.8E-06	6.4E-05	1.4E-04	1.3E-04	7.6E-05	3.7E-05	1.7E-05	4.7E-04
21	3.2E-06	5.5E-06	4.0E-06	1.5E-06	4.0E-07	9.1E-08	2.1E-08	1.5E-05
	2.6E-05	1.7E-04	2.8E-04	2.7E-04	1.9E-04	1.2E-04	7.9E-05	1.14E-03

Table C-12

Total Accident Sequence Frequency Increments
EPRI Seismic Hazard Curves for ANO-1 with Original Stiffnesses
(Mean Point Estimate Calculation)

	0.10-0.20g	0.20-0.30g	0.30-0.40g	0.40-0.50g	0.50-0.60g	0.60-0.70g	0.70-0.80g	TOTAL
1	6.3E-11	9.5E-10	3.9E-09	9.0E-09	1.4E-08	1.8E-08	2.2E-08	6.9E-08
2	1.6E-10	2.7E-09	6.1E-09	8.9E-09	1.0E-08	9.5E-09	9.3E-09	4.7E-08
3	3.0E-14	3.9E-12	4.6E-11	2.0E-10	4.8E-10	8.1E-10	1.3E-09	2.8E-09
4	7.6E-10	1.4E-09	6.7E-11	8.5E-13	5.6E-15	0.0E+00	0.0E+00	2.2E-09
5	2.2E-09	2.0E-08	3.1E-08	3.4E-08	3.1E-08	2.6E-08	2.3E-08	1.7E-07
6	6.4E-08	2.8E-07	2.8E-07	2.3E-07	1.7E-07	1.1E-07	8.6E-08	1.2E-06
7	3.3E-09	1.8E-08	3.6E-08	3.9E-08	2.7E-08	1.4E-08	7.4E-09	1.5E-07
8	2.3E-09	1.6E-08	3.5E-08	3.9E-08	2.8E-08	1.5E-08	7.4E-09	1.4E-07
9	6.3E-08	2.0E-07	1.5E-07	7.9E-08	3.7E-08	1.6E-08	7.5E-09	5.5E-07
10	2.5E-09	7.3E-09	5.0E-09	2.7E-09	1.3E-09	5.5E-10	2.6E-10	2.0E-08
11	4.9E-11	3.2E-10	1.9E-09	6.3E-09	1.2E-08	1.5E-08	1.5E-08	5.1E-08
12	1.5E-09	2.1E-08	6.9E-08	9.4E-08	7.5E-08	4.5E-08	2.8E-08	3.3E-07
13	1.3E-14	4.4E-12	4.7E-11	1.7E-10	3.5E-10	4.9E-10	6.3E-10	1.7E-09
14	6.9E-09	3.7E-08	6.9E-08	6.9E-08	4.6E-08	2.3E-08	1.1E-08	2.6E-07
15	4.8E-09	3.3E-08	6.6E-08	7.0E-08	4.8E-08	2.3E-08	1.1E-08	2.6E-07
16	1.3E-07	4.0E-07	2.8E-07	1.4E-07	6.3E-08	2.5E-08	1.1E-08	1.1E-06
17	5.3E-09	1.4E-08	9.5E-09	4.8E-09	2.1E-09	8.7E-10	3.8E-10	3.7E-08
18	1.0E-10	6.4E-10	3.6E-09	1.1E-08	2.0E-08	2.3E-08	2.3E-08	8.2E-08
19	3.2E-09	4.2E-08	1.3E-07	1.7E-07	1.3E-07	7.1E-08	4.2E-08	5.8E-07
20	1.2E-07	7.3E-07	1.2E-06	9.1E-07	4.5E-07	1.8E-07	8.4E-08	3.7E-06
21	5.8E-08	6.3E-08	3.4E-08	1.1E-08	2.4E-09	4.6E-10	1.0E-10	1.7E-07
	4.7E-07	1.9E-06	2.4E-06	1.9E-06	1.2E-06	6.3E-07	3.9E-07	8.85E-06

Table C-13

Dominant Component Contributions to Mean Core Damage at ANO-1
..equency Ranked by Risk Reduction Potential

Component	Percent Reduction if not Failed	
	LLNL Hazard	EPRI Hazard
4kV and 480V Busses	65%	70%
Ceramic Insulators	37%	38%
CST	12%	12%

fragility due to the lack of adequate anchorage and also because these busses have a significant risk reduction potential inasmuch as all off site power and on site emergency power is fed through these busses. The second largest reduction comes from the ceramic insulators. This occurs, of course, because the ceramic insulators are the basis for the loss of off site power and all the T_1 transient sequences. Failure of the CST is the third leading contributor to core damage. All other components and structures had risk reduction potentials of less than 2 percent.

C.5.4.2 Core Damage Frequency Results With Stiffness Reduction

The seismic risk at the ANO-1 plant with reduced stiffnesses was recalculated in exactly the same fashion, except that now the responses derived using the degraded shear wall stiffness model were used. The same initiating events, component fragilities, and accident sequence definitions were used. The same interval of integration over the hazard curve (0.1g to 0.8g) was used. The only difference was the floor responses were different based on the reduced shear wall stiffness as discussed in section C.3.4 and structural fragilities also changed as discussed in section C.4.3

The results of this requantification using Monte Carlo uncertainty estimates are summarized in Tables C-14 and C-15. The same dominant accident sequences were identified, although the percentage contributions were slightly different:

T2-2 (41%)
M1-LOCA-1 (13%)
SSLOCA-3 (12%)
SSLOCA-7 (7%)
SLOCA-3 (6%)

Based on the complete uncertainty analysis, the mean core damage frequency was computed to be 1.15E-3 using the LLNL hazard curves and 9.61E-6 for the EPRI hazard curves. This is an 8% and 10% increase over the case with no frequency reduction (1.07E-3 for LLNL and 8.78E-6 for EPRI). The mean frequencies of the original accident sequences are shown on Table C-9.

Mean Point Estimate

A point estimate calculation with all values set equal to their mean values was also made. Tables C-16 and C-17 present the total accident sequence frequencies at 7 different intervals over the LLNL and EPRI hazard curves respectively, again for the mean point estimate case. These tables may be compared directly to Table C-11 and C-12 for the base cases using original stiffnesses.

Table C-14

Accident Sequence and Total Core Damage Mean Frequencies
for ANO-1 with Reduced Stiffnesses
(Monte Carlo Uncertainty Analysis)

Accident Sequence		Mean Frequency (per year) LLNL Hazard	EPRI Hazard
1	RVR-1	1.81E-5	7.94E-8
2	A2-LOCA-1	5.87E-6	4.05E-8
3	A2-LOCA-2	3.69E-7	2.19E-9
4	M2-LOCA-1	3.69E-7	4.18E-9
5	M2-LOCA-2	3.91E-5	2.03E-7
6	M1-LOCA-1	1.57E-4	1.26E-6
7	SLOCA-1	1.37E-5	1.06E-7
8	SLOCA-2	1.70E-5	1.22E-7
9	SLOCA-3	7.28E-5	6.42E-7
10	SLOCA-4	2.54E-6	2.27E-8
11	SLOCA-5	6.53E-6	4.04E-8
12	SLOCA-7	4.49E-5	2.83E-7
13	INTK-1	5.76E-7	2.04E-9
14	SSLOCA-1	2.34E-5	1.84E-7
15	SSLOCA-2	2.98E-5	2.12E-7
16	SSLOCA-3	1.38E-4	1.22E-6
17	SSLOCA-4	4.82E-6	4.32E-8
18	SSLOCA-5	9.94E-6	6.24E-8
19	SSLOCA-7	7.54E-5	4.81E-7
20	T2-2	4.67E-4	4.23E-6
21	T3-2	1.82E-5	3.68E-7
	TOTAL	1.15E-3	9.61E-6

Table C-15

Accident Sequence Frequency Distribution Percentiles
for ANO-1 with Reduced Stiffnesses
(Monte Carlo Uncertainty Analysis)

	LLNL Hazard	EPRI Hazard
Mean	1.15E-3	9.61E-6
Var	3.82E-5	2.62E-10
5%	1.87E-6	4.55E-7
50%	8.61E-5	4.31E-6
95%	3.46E-3	3.78E-5

Table C-16

Total Accident Sequence Frequency Increments
LLNL Seismic Hazard Curves for ANO-1 with Reduced Stiffnesses
(Mean Point Estimate Calculation)

	0.10-0.20g	0.20-0.30g	0.30-0.40g	0.40-0.50g	0.50-0.60g	0.60-0.70g	0.70-0.80g	TOTAL
1	4.0E-09	1.2E-07	6.6E-07	1.8E-06	3.3E-06	4.7E-06	5.8E-06	1.6E-05
2	1.1E-08	2.4E-07	7.1E-07	1.3E-06	1.7E-06	1.9E-06	1.8E-06	7.6E-06
3	1.6E-12	3.4E-10	5.4E-09	2.8E-08	7.9E-08	1.6E-07	2.5E-07	5.2E-07
4	4.2E-08	5.6E-08	1.3E-09	6.5E-12	0.0E+00	0.0E+00	0.0E+00	9.8E-08
5	1.7E-07	1.8E-06	3.6E-06	4.8E-06	5.2E-06	5.0E-06	4.5E-06	2.5E-05
6	4.8E-06	2.6E-05	3.3E-05	3.2E-05	2.8E-05	2.2E-05	1.7E-05	1.6E-04
7	1.8E-07	1.7E-06	4.7E-06	6.1E-06	4.9E-06	3.0E-06	1.5E-06	2.2E-05
8	1.5E-07	1.6E-06	4.4E-06	5.9E-06	4.9E-06	2.9E-06	1.5E-06	2.1E-05
9	4.8E-06	1.9E-05	1.7E-05	1.1E-05	6.2E-06	3.1E-06	1.5E-06	6.3E-05
10	1.9E-07	6.8E-07	5.9E-07	3.8E-07	2.1E-07	1.1E-07	5.0E-08	2.2E-06
11	2.7E-09	3.1E-08	2.6E-07	1.0E-06	2.3E-06	3.4E-06	3.5E-06	1.1E-05
12	1.2E-07	2.4E-06	9.4E-06	1.4E-05	1.3E-05	8.8E-06	5.6E-06	5.3E-05
13	7.3E-13	4.9E-10	5.9E-09	2.5E-08	6.1E-08	1.0E-07	1.3E-07	3.2E-07
14	3.9E-07	3.4E-06	8.8E-06	1.1E-05	8.3E-06	4.7E-06	2.2E-06	3.9E-05
15	3.2E-07	3.3E-06	8.4E-06	1.0E-05	8.2E-06	4.6E-06	2.2E-06	3.7E-05
16	1.0E-05	3.8E-05	3.3E-05	2.0E-05	1.0E-05	5.0E-06	2.2E-06	1.2E-04
17	4.0E-07	1.3E-06	1.1E-06	6.8E-07	3.6E-07	1.7E-07	7.5E-08	4.1E-06
18	5.7E-09	6.3E-08	4.9E-07	1.9E-06	3.9E-06	5.4E-06	5.2E-06	1.7E-05
19	2.5E-07	4.8E-06	1.8E-05	2.6E-05	2.1E-05	1.4E-05	8.4E-06	9.2E-05
20	9.8E-06	8.3E-05	1.6E-04	1.4E-04	7.7E-05	3.6E-05	1.6E-05	5.2E-04
21	4.6E-06	7.1E-06	4.6E-06	1.6E-06	4.0E-07	9.0E-08	2.0E-08	1.9E-05
	3.6E-05	2.0E-04	3.1E-04	2.9E-04	2.0E-04	1.3E-04	8.0E-05	1.23E-03

Table C-17

Total Accident Sequence Frequency Increments
EPRI Seismic Hazard Curves for ANO-1 with Reduced Stiffnesses
(Mean Point Estimate Calculation)

	0.10-0.20g	0.20-0.30g	0.30-0.40g	0.40-0.50g	0.50-0.60g	0.60-0.70g	0.70-0.80g	TOTAL
1	7.1E-11	1.3E-09	5.7E-09	1.3E-08	2.0E-08	2.4E-08	2.9E-08	9.2E-08
2	2.0E-10	2.7E-09	6.1E-09	8.9E-09	1.0E-08	9.4E-09	9.1E-09	4.6E-08
3	2.9E-14	3.9E-12	4.6E-11	2.0E-10	4.7E-10	8.0E-10	1.2E-09	2.7E-09
4	7.5E-10	6.3E-10	1.1E-11	4.6E-14	0.0E+00	0.0E+00	0.0E+00	1.4E-09
5	3.0E-09	2.1E-08	3.1E-08	3.4E-08	3.1E-08	2.5E-08	2.2E-08	1.7E-07
6	8.7E-08	2.9E-07	2.8E-07	2.3E-07	1.7E-07	1.1E-07	8.4E-08	1.2E-06
7	3.3E-09	1.9E-08	4.0E-08	4.3E-08	3.0E-08	1.5E-08	7.4E-09	1.6E-07
8	2.8E-09	1.9E-08	3.8E-08	4.1E-08	2.9E-08	1.5E-08	7.2E-09	1.5E-07
9	8.6E-08	2.2E-07	1.5E-07	7.9E-08	3.7E-08	1.6E-08	7.3E-09	5.9E-07
10	3.4E-09	7.7E-09	5.0E-09	2.7E-09	1.3E-09	5.4E-10	2.5E-10	2.1E-08
11	5.0E-11	3.6E-10	2.2E-09	7.4E-09	1.4E-08	1.7E-08	1.7E-08	5.8E-08
12	2.2E-09	2.7E-08	8.0E-08	1.0E-07	7.6E-08	4.5E-08	2.8E-08	3.6E-07
13	1.3E-14	5.5E-12	5.0E-11	1.8E-10	3.6E-10	5.0E-10	6.3E-10	1.7E-09
14	7.0E-09	3.9E-08	7.5E-08	7.7E-08	5.0E-08	2.4E-08	1.1E-08	2.8E-07
15	5.8E-09	3.7E-08	7.1E-08	7.4E-08	4.9E-08	2.3E-08	1.1E-08	2.7E-07
16	1.8E-07	4.4E-07	2.8E-07	1.4E-07	6.2E-08	2.5E-08	1.1E-08	1.1E-06
17	7.2E-09	1.5E-08	9.5E-09	4.8E-09	2.1E-09	8.6E-10	3.8E-10	4.0E-08
18	1.0E-10	7.1E-10	4.2E-09	1.3E-08	2.4E-08	2.7E-08	2.6E-08	9.5E-08
19	4.6E-09	5.5E-08	1.5E-07	1.8E-07	1.3E-07	7.1E-08	4.2E-08	6.3E-07
20	1.8E-07	9.4E-07	1.4E-06	9.8E-07	4.6E-07	1.8E-07	8.2E-08	4.2E-06
21	8.4E-08	8.1E-08	3.9E-08	1.1E-08	2.4E-09	4.5E-10	1.0E-10	2.2E-07
	6.5E-07	2.2E-06	2.6E-06	2.0E-06	1.2E-06	6.3E-07	4.0E-07	9.77E-06

The incremental contributions from each of the accident sequences remained about the same when using reduced stiffnesses. Similarly, the contribution and ranking of each earthquake level also was not affected. The bulk of the risk occurred in the 1-3 SSE range, assuring that by integrating from 0.1g to 0.8g we have again captured the bulk of the risk at ANO-1.

Basic Event Importance

The importance of the basic seismic failure events was not re-evaluated using reduced stiffnesses. It was assumed they would not be greatly affected by this. The 4kV and 480V electrical busses should again dominate the risk reduction potential, followed by the ceramic insulators leading to LOSP and then the CST. No new contributors are expected to have risk reduction potentials of more than 2%.

C.5.4.3 Summary of Results

Although the percent increase in core damage frequency due to the stiffness reduction was small (~8%), the magnitude of increase itself (8.0E-5 using LLNL hazard curves) is quite significant. This increase in core damage frequency is due primarily to the increased values of response for the 5-10 Hz range of the Auxiliary building at elevations 371' and 386' respectively. These are the locations at which all the vital 480V and 4kV AC switchgear cabinets are located. Both these responses have been significantly increased over the case with no stiffness reduction. Since these switchgear cabinets still have a moderately low fragility and still contribute significantly to core damage, raising the response will result in a higher probability of losing all vital AC power and leading to a higher total core damage frequency at ANO-1.

C.6 DETERMINISTIC IMPACTS

C.6.1 Deterministic Response Analysis

To assess the impact of the frequency reduction model on the deterministic design calculations for ANO-1, a set of "design-like" structural response calculations was performed. These calculations are as close to the original design calculation methods as could be determined from the ANO-1 Final Safety Analysis Report [C-5]. However, we did not seek to obtain the original design calculational results themselves. Instead, we performed two sets of calculations using the FSAR guidance. The first set of calculations utilized the "design-like" models with as-calculated stiffnesses. This "design-like" calculation involved using a single synthetic time history scaled to the SSE at ANO-1 and using the same damping values as was used in the original design analysis. The second set of calculations used the same structural models but incorporated a stiffness reduction of 25% of the shear wall stiffness.

A deterministic time history analysis was performed both on the original models and the reduced stiffness models using a single synthetic time history based on a spectrum shape derived from NUREG/CR-0098 [C-11] having a pga of 0.2g (1*SSE). Figure C-50 shows response spectra for this time history for several values of spectral damping. (Structural damping was taken as 5% for both sets of calculations.)

C.6.2 Deterministic Results for ANO-1

Acceleration response spectra at various nodal locations throughout all the structures comparing the undegraded response to the reduced stiffness response are plotted in the following figures:

Reactor Building	Figs. C-51 thru C-53
Auxiliary Building	Figs. C-54 thru C-56
Intake Structure	Figs. C-57 thru C-59

These responses appear much more jagged and have sharper peaks, since these were based on a single time history, as compared to the median spectra generated in the probabilistic response analysis. It can be seen from these spectra that some very significant shifts in peak values and frequencies are present. Most notably, the Auxiliary Building experienced a significant increase in the 10 Hz range in both directions at the upper floor elevations. In addition, the Intake Structure experienced a significant increase in the 13 Hz range in both directions for the upper floor elevations when reduced stiffnesses were modeled.

Tables C-18 through C-20 show a comparison of story shear and moment loads listed by floor elevation (that is, the shear and moment values just under the floor slabs at these elevations) for the original and reduced stiffness models described above when subjected to the synthetic time history at 1 SSE. Note that the values listed are net total forces and moments for that elevation and have not yet been distributed to the individual walls at that elevation.

In general, it can be seen that there is a maximum increase in loads of about 20% due to the stiffness reduction. Since there is very little assumed torsion in any of these structures, the same increase would apply to loads in the individual walls. Thus, from a design viewpoint, the stiffness reduction does result in a significant increase in net loads, but this increase (20%) is probably well within the range of conservatism implicit in the original design calculations.

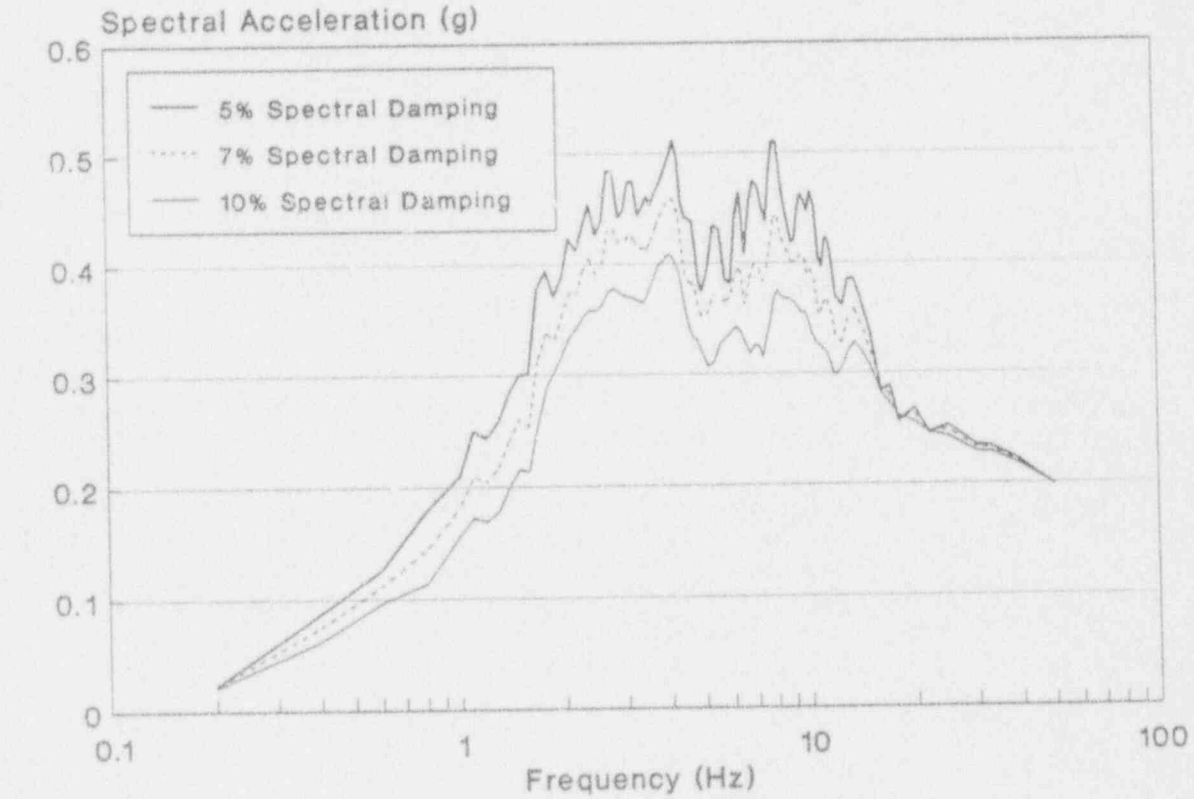

PGA = 0.2g (1•SSE)

Figure C-50 NUREG/CR-0098 Scaled Ground Motion Input Spectra

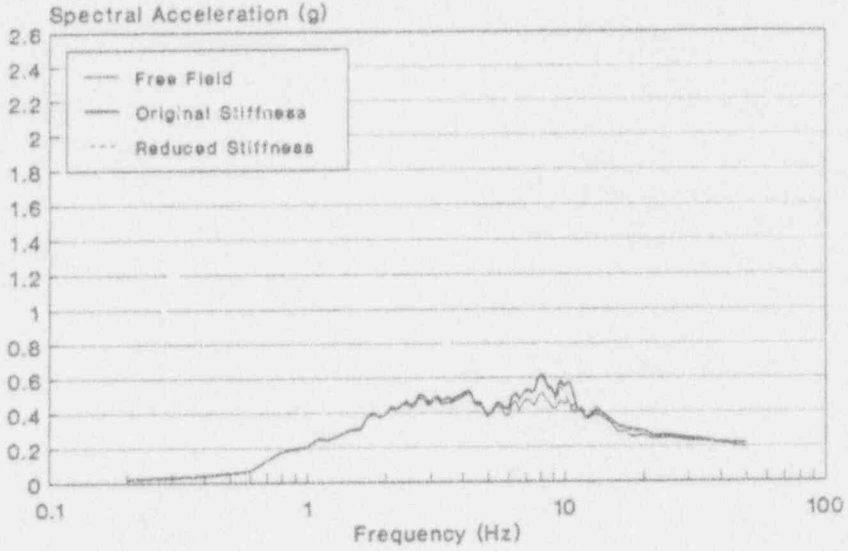

N-S Direction, El. 335'
5% Spectral Damping
PGA = 0.20g

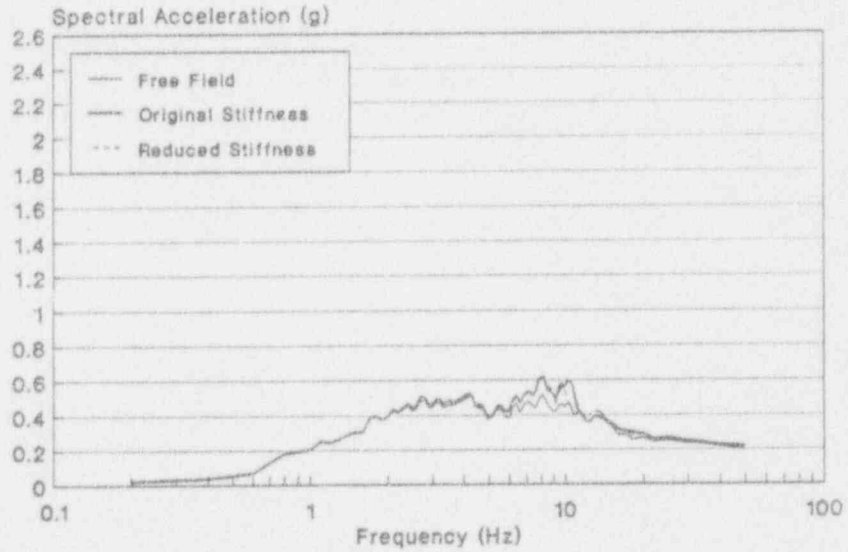

E-W Direction, El. 335'
5% Spectral Damping
PGA = 0.20g

Figure C-51 ANO-1 Deterministic Analysis, Reactor Building, El. 335'

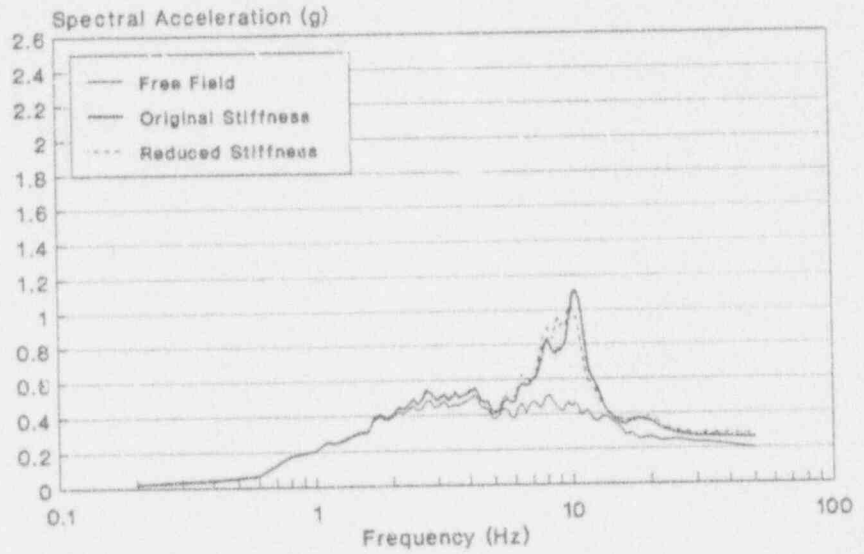

N-S Direction, El. 357'
5% Spectral Damping
PGA = 0.20g

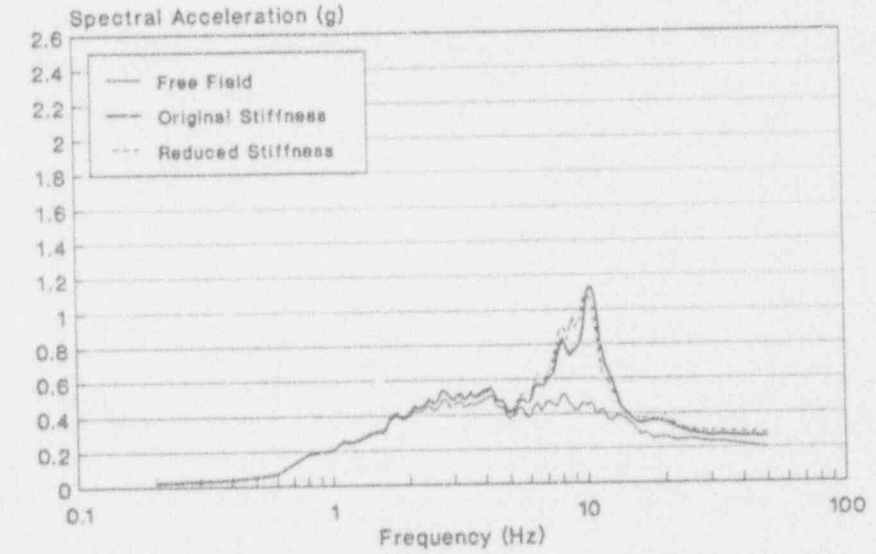

E-W Direction, El. 357'
5% Spectral Damping
PGA = 0.20g

Figure C-52 ANO-1 Deterministic Analysis, Reactor Building, El. 357'

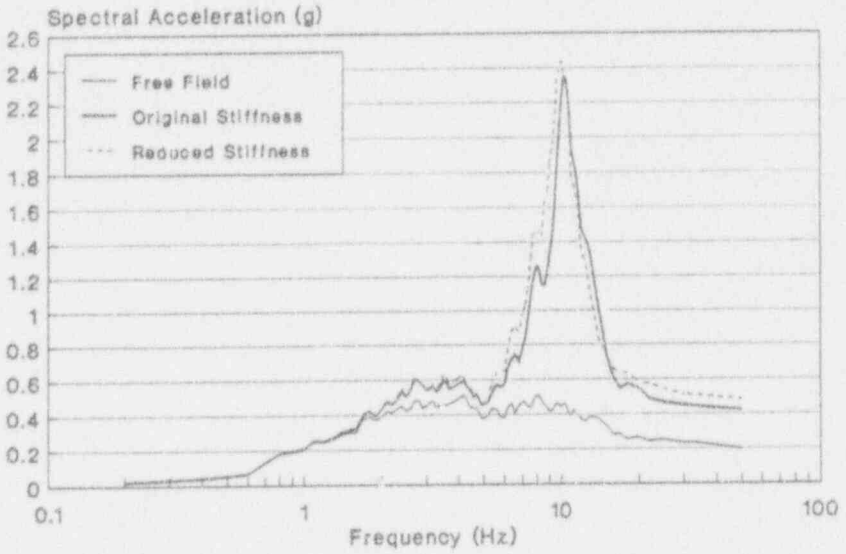

N-S Direction, El. 401'
5% Spectral Damping
PGA = 0.20g

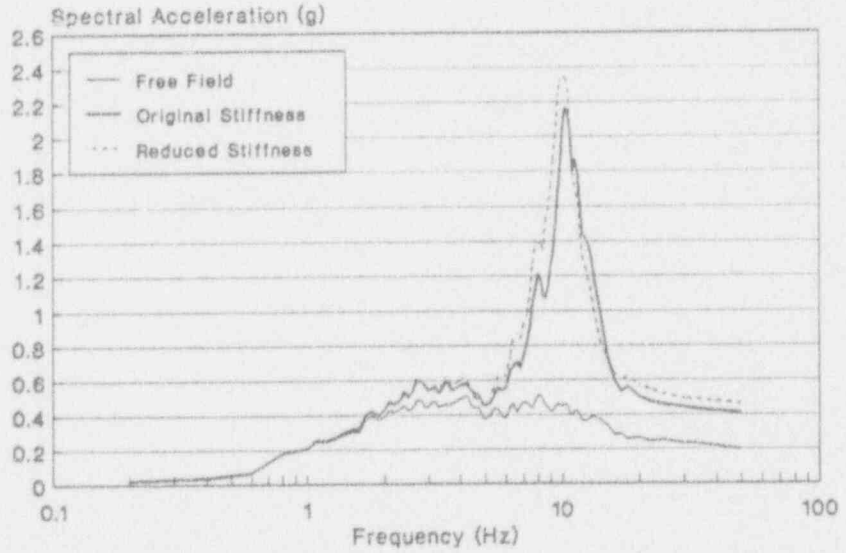

E-W Direction, El. 401'
5% Spectral Damping
PGA = 0.20g

Figure C-53 ANO-1 Deterministic Analysis, Reactor Building, El. 401'

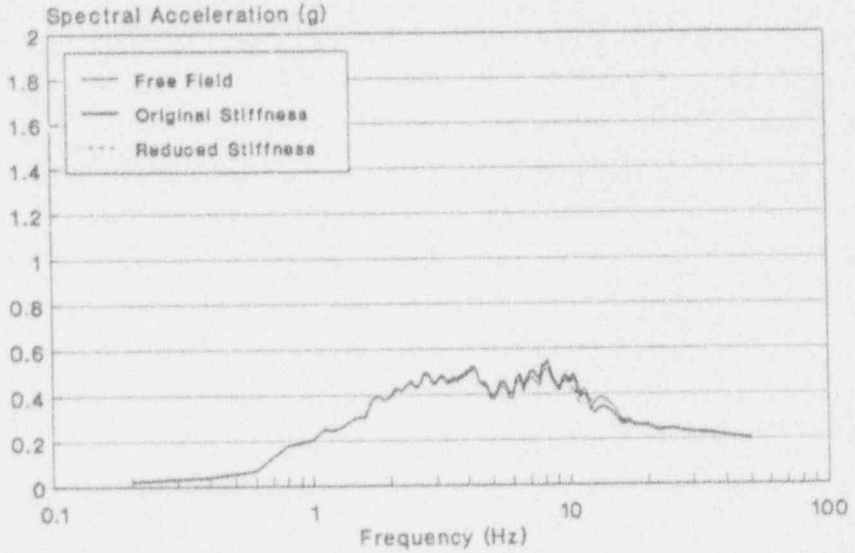

N-S Direction, El. 335'
5% Spectral Damping
PGA = 0.20g

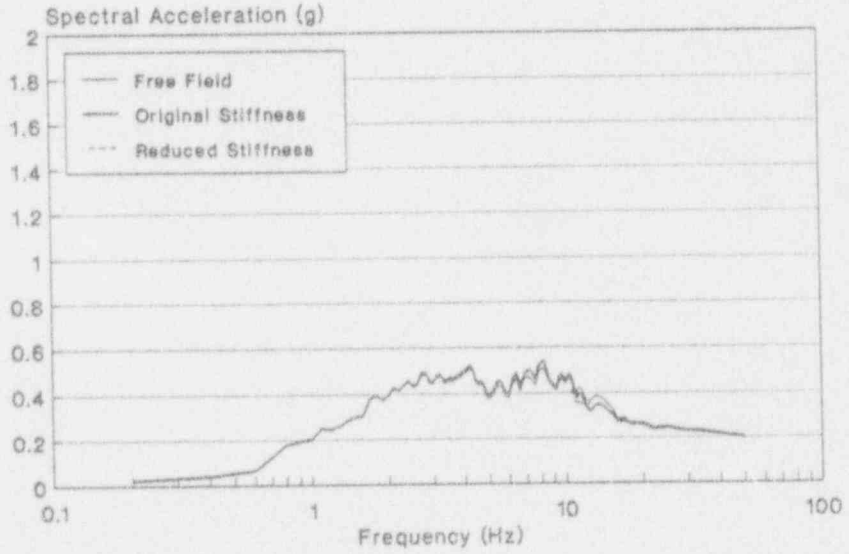

E-W Direction, El. 335'
5% Spectral Damping
PGA = 0.20g

Figure C-54 ANO-1 Deterministic Analysis, Auxiliary Building, El. 335'

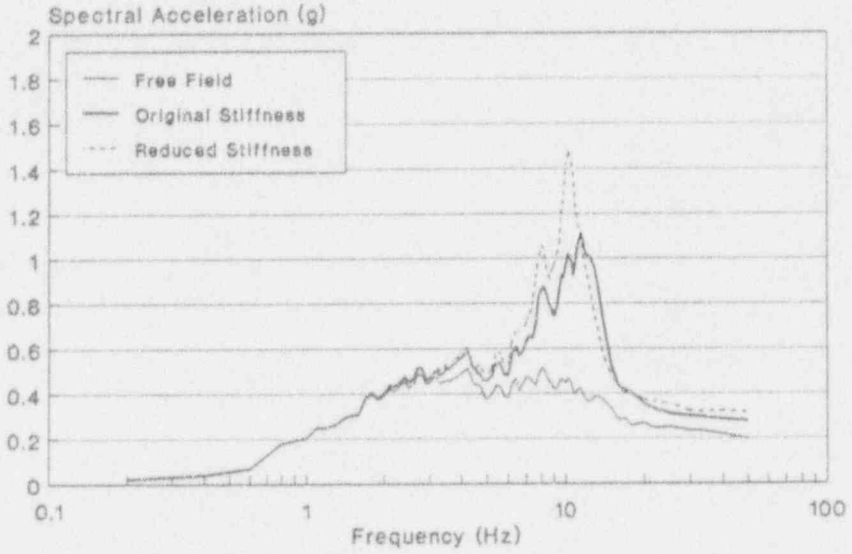

N-S Direction, El. 371'
5% Spectral Damping
PGA = 0.20g

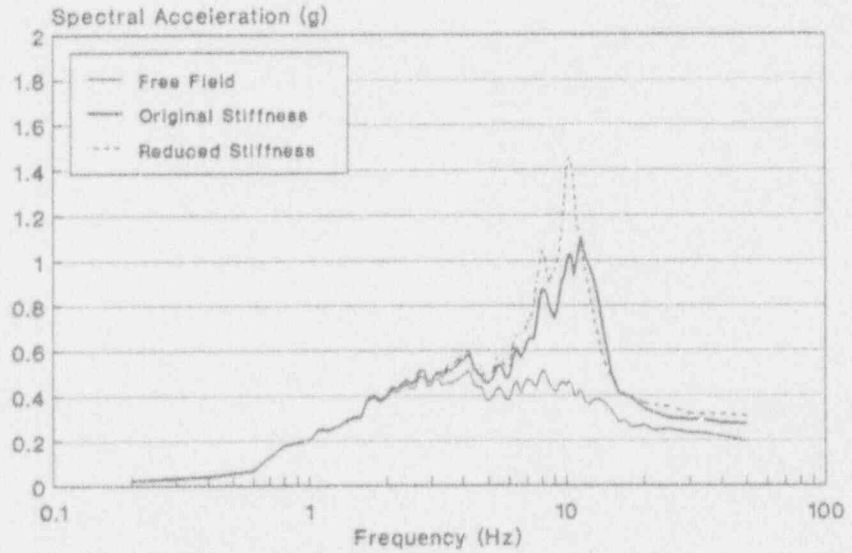

E-W Direction, El. 371'
5% Spectral Damping
PGA = 0.20g

Figure C-55 ANO-1 Deterministic Analysis, Auxiliary Building, El. 371'

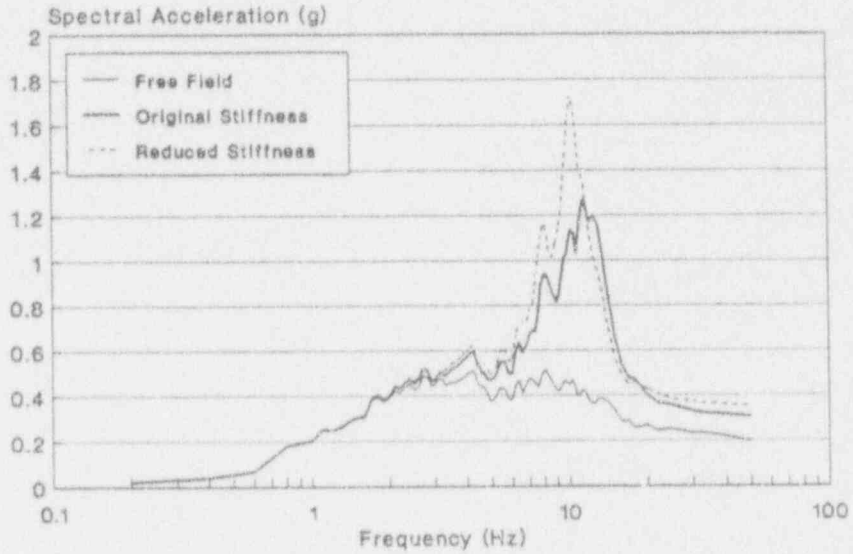

N-S Direction, El. 386'
5% Spectral Damping
PGA = 0.20g

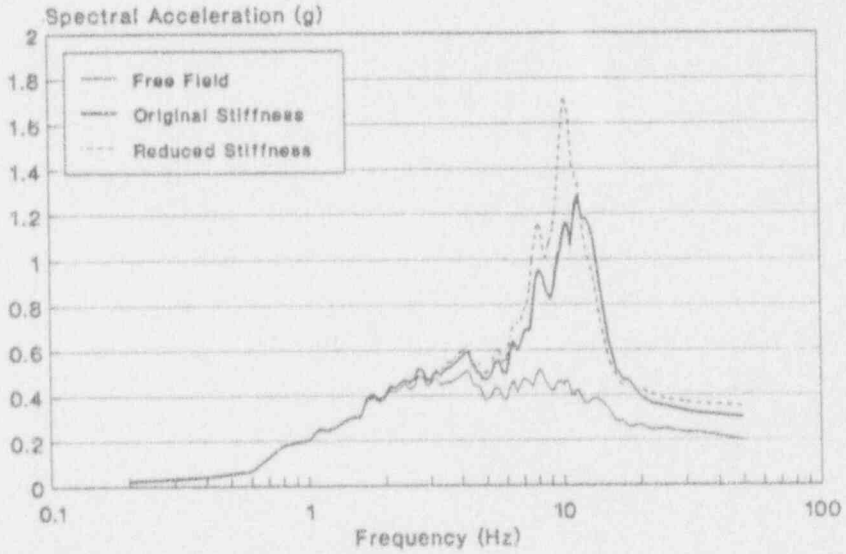

E-W Direction, El. 386'
5% Spectral Damping
PGA = 0.20g

Figure C-56 ANO-1 Deterministic Analysis, Auxiliary Building, El. 386'

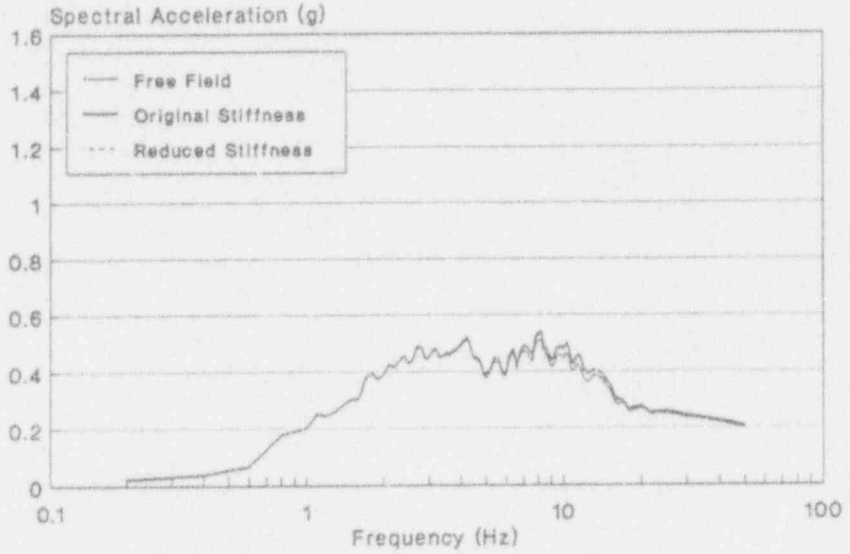

NW-SE Direction, El. 318'
5% Spectral Damping
PGA = 0.20g

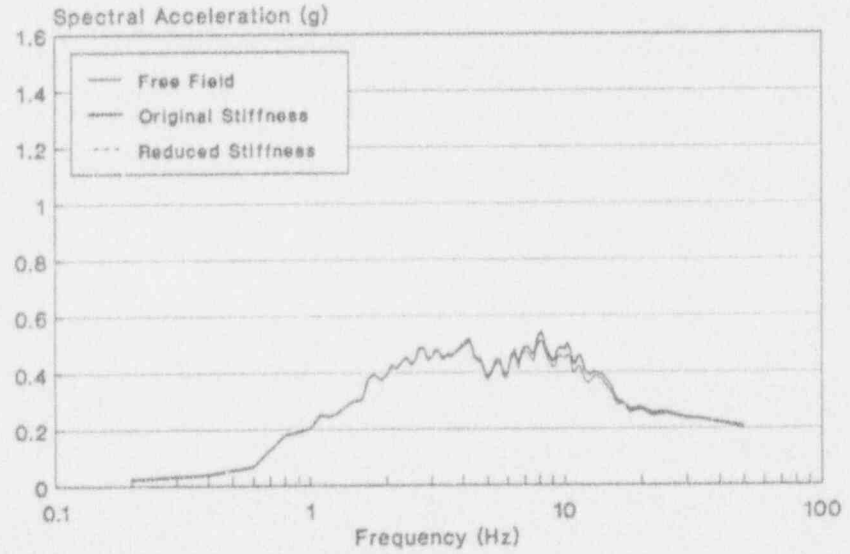

NE-SW Direction, El. 318'
5% Spectral Damping
PGA = 0.20g

Figure C-57 ANO-1 Deterministic Analysis, Intake Structure, El. 318'

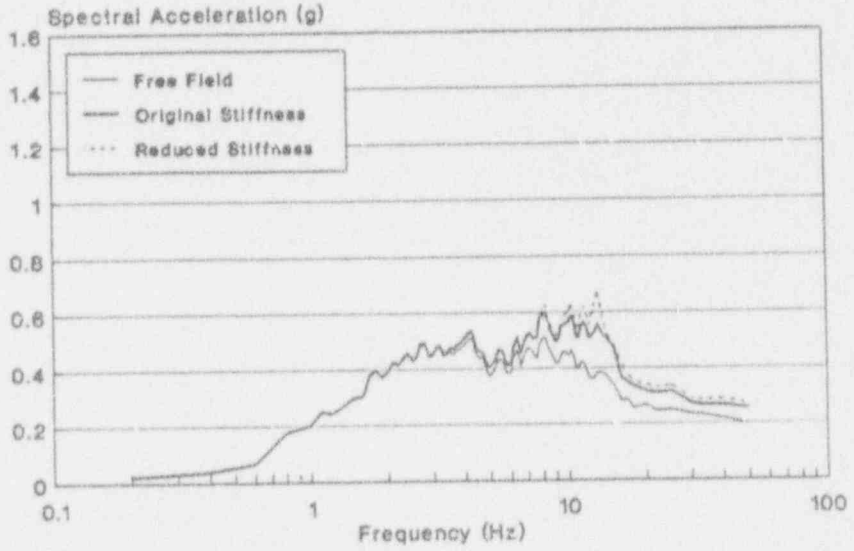

NW-SE Direction, El. 352'
5% Spectral Damping
PGA = 0.20g

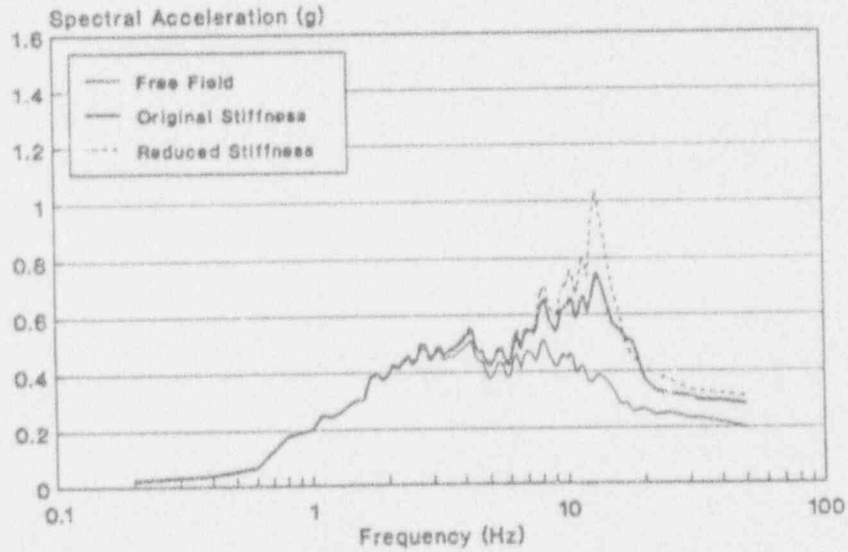

NE-SW Direction, El. 352'
5% Spectral Damping
PGA = 0.20g

Figure C-58 ANO-1 Deterministic Analysis, Intake Structure, El. 352'

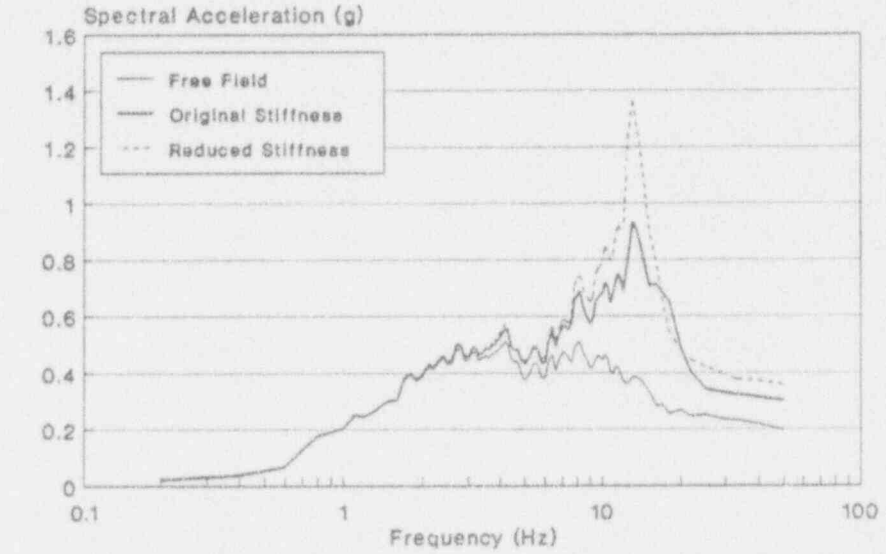

NW-SE Direction, El. 365'
5% Spectral Damping
PGA = 0.20g

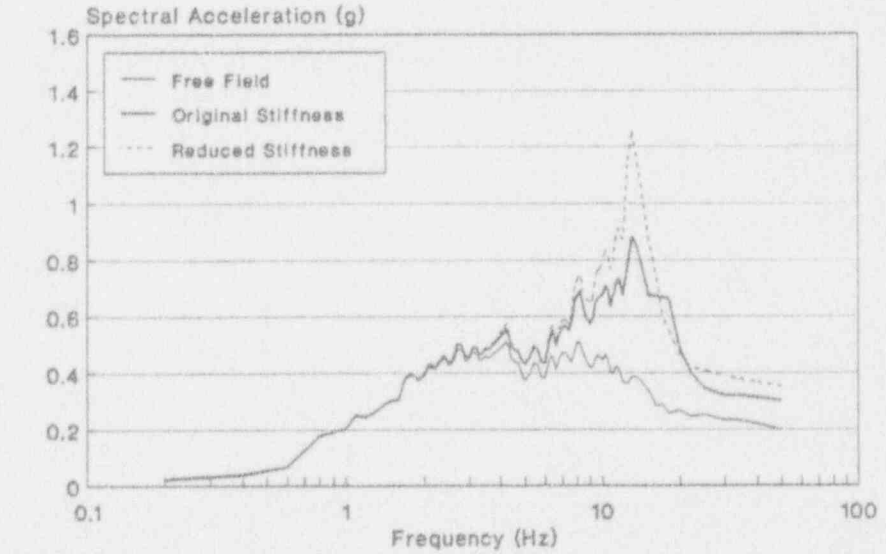

NE-SW Direction, El. 365'
5% Spectral Damping
PGA = 0.20g

Figure C-59 ANO-1 Deterministic Analysis, Intake Structure, El. 365'

Table C-18

Forces between Floor Levels of ANO-1 Reactor Building

Original Stiffnesses

Elev.	$Shear_X$(kip)	$Shear_Y$(kip)	$Moment_X$(kip-ft)	$Moment_Y$(kip-ft)
Internals:				
335'	261	260	12,730	12,560
357'	204	202	6,864	6,703
374'	126	121	3,404	3,275

Reduced Stiffnesses

Elev.	$Shear_X$(kip)	$Shear_Y$(kip)	$Moment_X$(kip-ft)	$Moment_Y$(kip-ft)
Internals:				
335'	298	298	14,700	14,550
357'	236	235	7,994	7,839
374'	148	143	3,991	3,848

Table C-19

Forces between Floor Levels of ANO-1 Auxiliary Building

Original Stiffnesses

Elev.	$Shear_X$(kip)	$Shear_Y$(kip)	$Moment_X$(kip-ft)	$Moment_Y$(kip-ft)
335'	327	323	13,560	13,420
354'	241	239	7,342	7,293
371'	155	154	3,236	3,229
386'	61	61	909	914

Reduced Stiffnesses

Elev.	$Shear_X$(kip)	$Shear_Y$(kip)	$Moment_X$(kip-ft)	$Moment_Y$(kip-ft)
335'	360	358	15,030	14,980
354'	269	268	8,192	8,185
371'	173	174	3,616	3,626
386'	68	68	1,016	1,024

Table C-20

Forces between Floor Levels of ANO-1 Intake Structure

Original Stiffnesses

Elev.	$Shear_X$(kip)	$Shear_Y$(kip)	$Moment_X$(kip-ft)	$Moment_Y$(kip-ft)
318'	77	84	2,595	2,776
333'	52	57	1,431	1,509
352'	24	23	435	418
365'	12	11	130	122

Reduced Stiffnesses

Elev.	$Shear_X$(kip)	$Shear_Y$(kip)	$Moment_X$(kip-ft)	$Moment_Y$(kip-ft)
318'	85	94	2,909	3,126
333'	59	65	1,631	1,717
352'	28	26	511	485
365'	14	13	154	143

C.7 REFERENCES

C-1. G.J. Kolb, Interim Reliability Evaluation Program: Analysis of the Arkansas Nuclear One - Unit 1 Nuclear Power Plant, NUREG/CR-2787, SAND82-0978, Vol. 1, June 1982.

C-2. W.R. Cramond, et. al., Shutdown Decay Heat Removal Analysis of a Babcock and Wilcox Pressurized Water Reactor, NUREG/CR-4713, SAND86-1832, March 1987.

C-3. D.L. Bernreuter, et. al., Seismic Hazard Characterization of 69 Nuclear Plant Sites East of the Rocky Mountains, NUREG/CR-5250, October, 1988.

C-4. Electric Power Research Institute, Seismic Hazard Methodology for the Central and Eastern United States, EPRI NP-4726, Vols 1-10, July, 1986.

C-5. Arkansas Nuclear One - Unit 1 Nuclear Power Plant Final Safety Analysis Report, April, 1971.

C-6. N.M. Newmark, A Study of Vertical and Horizontal Earthquake Spectra, Directorate of Licensing, US Atomic Energy Commission, WASH-1255, UC-11, 1973.

C-7. J.J. Johnson, et. al., Phase I Final Report - SmACS - Seismic Methodology Analysis Chain with Statistics (Project VIII), NUREG/CR-2015, Vol. 9, UCRL-53021, July 1981.

C-8. H.L. Wong, et. al., Soil-Structure Interaction: A linear Continuum Mechanics Approach (CLASSI), Dept. of Civil Engineering, University of Southern California, CE79-03, 1980.

C-9. M.P. Bohn, et al., Application of the SSMRP Methodology to the Seismic Risk at the Zion Nuclear Power Plant, Lawrence Livermore National Laboratory, Livermore, CA, UCRL-53483, NUREG/CR-3428, 1983.

C-10. L.E. Cover, et al., Handbook of Nuclear Power Plant Seismic Fragilities, NUREG/CR-3558, December 1983.

C-11. N.M. Newmark, et. al., Development of Criteria for Seismic Review of Selected Nuclear Power Plants, NUREG/CR-0098, 1978.

ATTACHMENT TO APPENDIX C

FILES FOR ANO-1 SEISMIC ANALYSIS

Fragility Files

Response Files

Accident Sequence Expressions

Cross-Reference File

ANO-1 FRAGILITIES FILE (ORIGINAL STIFFNESS CASE)

No.	M_F	β_{fr}	β_{fu}	Category
1	0.25	0.25	.25	CERAMIC INSULATORS
2	4.00	0.48	.75	RELAY CHATTER
3	7.63	0.48	.74	CIRCUIT BREAKER TRIP
4	2.50	0.40	.39	BATTERIES
5	2.29	0.31	.39	BATTERY RACKS
6	2.00	0.26	.35	INVERTORS
7	8.80	0.28	.30	TRANSFORMERS
8	7.63	0.48	.74	MOTOR CONTROL CENTER
9	7.63	0.48	.66	AUX RELAY CABINET
10	6.43	0.29	.66	SWITCHGEAR
11	2.23	0.34	.19	CABLE TRAYS
12	11.50	0.46	.74	CONTROL PANELS AND RACKS
13	7.68	0.20	.35	LOCAL INSTRUMENTS
14	1.00	0.25	.31	DIESEL GENERATOR
15	12.10	0.27	.31	MOTORS-HORIZONTAL
16	2.80	0.25	.27	MOTOR-DRIVEN PUMPS & COMPRESSORS
17	2.21	0.22	.32	LG. VERT. M-D. CENTRIF PUMP
18	6.50	0.26	.60	LMOV
19	4.83	0.26	.60	SMALL MOV & AOVs
20	6.50	0.26	.34	LG. PNEUM/HYD VALVE
21	8.90	0.20	.35	LG. MANUAL,CHECK,RELIEF VALVE
22	12.50	0.33	.43	MISC. SMALL VALVES
23	3.00	0.30	.53	LG. HORIZ. VESSELS
24	1.84	0.25	.45	SM-MED HEAT EXCHANGERS & VESSELS
25	1.46	0.20	.35	LG. VERT VESSELS w/ FORMED HEADS
26	0.45	0.35	.29	LG. VERT. FLAT BOTTOMED TANKS
27	2.4e6	0.18	.33	PIPING (MASTER FRAGITITY)
28	6.90	0.27	.61	AIR HANDLING UNITS
29	2.45	0.24	.3	STEAM GENERATOR (ZION-SSMRP)
30	2.65	0.24	.3	REACTOR COOLANT PUMP (ZION-SSMRP)
31	0.78	0.521	.3	SSLOCA FIT (SSMRP)
32	0.95892	0.50	.3	SLOCA FIT (SSMRP)
33	1.4967	0.4681	.3	MLOCA FIT (SSMRP)
34	1.8286	0.40764	.3	ALOCA FIT (MONTE CARLO SG&RCP-ZION)
35	2.2701	0.39086	.3	RVR FIT (MONTE CARLO SG&RCP-ZION)
36	0.70	0.40	.3	ELEC CABINET SLIDING/TIPPING
37	1.00	0.30	.29	BWST (ANO-1)
38	1.00	0.30	.29	CST (ANO-1)
39	0.537	0.305	.3	AFWS FIT
40	2.00	0.42	.23	ACCUMULATORS
41	3.30	0.06	.21	REACTOR INTERNAL STRUCTURE (ANO-1)
42	1.50	0.09	.23	AUXILIARY BUILDING (ANO-1)
43	2.40	0.07	.27	INTAKE STRUCTURE (ANO-1)

ANO-1 FRAGILITIES FILE (REDUCED STIFFNESS CASE)

No.	M_F	β_{fr}	β_{fu}	Category
1	0.25	0.25	.25	CERAMIC INSULATORS
2	4.00	0.48	.75	RELAY CHATTER
3	7.63	0.48	.74	CIRCUIT BREAKER TRIP
4	2.50	0.40	.39	BATTERIES
5	2.29	0.31	.39	BATTERY RACKS
6	2.00	0.26	.35	INVERTORS
7	8.80	0.28	.30	TRANSFORMERS
8	7.63	0.48	.74	MOTOR CONTROL CENTER
9	7.63	0.48	.66	AUX RELAY CABINET
10	6.43	0.29	.66	SWITCHGEAR
11	2.23	0.34	.19	CABLE TRAYS
12	11.50	0.46	.74	CONTROL PANELS AND RACKS
13	7.68	0.20	.35	LOCAL INSTRUMENTS
14	1.00	0.25	.31	DIESEL GENERATOR
15	12.10	0.27	.31	MOTORS-HORIZONTAL
16	2.80	0.25	.27	MOTOR-DRIVEN PUMPS & COMPRESSORS
17	2.21	0.22	.32	LG. VERT. M-D. CENTRIF PUMP
18	6.50	0.26	.60	LMOV
19	4.83	0.26	.60	SMALL MOV & AOVs
20	6.50	0.26	.34	LG. PNEUM/HYD VALVE
21	8.90	0.20	.35	LG. MANUAL,CHECK,RELIEF VALVE
22	12.50	0.33	.43	MISC. SMALL VALVES
23	3.00	0.30	.53	LG. HORIZ. VESSELS
24	1.84	0.25	.45	SM-MED HEAT EXCHANGERS & VESSELS
25	1.46	0.20	.35	LG. VERT VESSELS w/ FORMED HEADS
26	0.45	0.35	.29	LG. VERT. FLAT BOTTOMED TANKS
27	2.4e6	0.18	.33	PIPING (MASTER FRAGITITY)
28	6.90	0.27	.61	AIR HANDLING UNITS
29	2.45	0.24	.3	STEAM GENERATOR (ZION-SSMRP)
30	2.65	0.24	.3	REACTOR COOLANT PUMP (ZION-SSMRP)
31	0.78	0.521	.3	SSLOCA FIT (SSMRP)
32	0.95892	0.50	.3	SLOCA FIT (SSMRP)
33	1.4967	0.4681	.3	MLOCA FIT (SSMRP)
34	1.8286	0.40764	.3	ALOCA FIT (MONTE CARLO SG&RCP-ZION)
35	2.2701	0.39086	.3	RVR FIT (MONTE CARLO SG&RCP-ZION)
36	0.70	0.40	.3	ELEC CABINET SLIDING/TIPPING
37	1.00	0.30	.29	BWST (ANO-1)
38	1.00	0.30	.29	CST (ANO-1)
39	0.537	0.305	.3	AFWS FIT
40	2.00	0.42	.23	ACCUMULATORS
41	3.00	0.06	.21	REACTOR INTERNAL STRUCTURE (ANO-1)
42	1.40	0.10	.23	AUXILIARY BUILDING (ANO-1)
43	2.40	0.08	.27	INTAKE STRUCTURE (ANO-1)

ANO-1 RESPONSE MULTIPLE FILE (ORIGINAL STIFFNESS CASE)

No.	F_1	F_2	β_{rr}	β_{ru}	Response
1	2.02	-0.00898	0.35	.25	RB/335, 5 HZ
2	1.97	-0.02378	0.35	.25	7
3	1.60	-0.01369	0.35	.25	10
4	1.03	-0.00607	0.35	.25	ZPA
5	1.83	-0.01960	0.35	.25	5-10
6	2.21	-0.02385	0.35	.25	RB/357.5, 5 HZ
7	2.27	-0.05030	0.35	.25	7
8	1.82	-0.07075	0.35	.25	10
9	1.12	-0.03929	0.35	.25	ZPA
10	2.11	-0.05105	0.35	.25	5-10
11	2.61	-0.05788	0.35	.25	RB/401.5, 5 HZ
12	3.03	-0.09600	0.35	.25	7
13	2.92	-0.12430	0.35	.25	10
14	1.37	-0.07459	0.35	.25	ZPA
15	2.97	-0.10363	0.35	.25	5-10
16	1.99	-0.00551	0.35	.25	AB/335, 5 HZ
17	1.88	-0.00647	0.35	.25	7
18	1.53	0.00102	0.35	.25	10
19	1.03	-0.00305	0.35	.25	ZPA
20	1.76	-0.00569	0.35	.25	5-10
21	2.35	-0.01996	0.35	.25	AB/371, 5 HZ
22	2.56	-0.05442	0.35	.25	7
23	2.28	-0.07511	0.35	.25	10
24	1.20	-0.04213	0.35	.25	ZPA
25	2.45	-0.05683	0.35	.25	5-10
26	2.43	-0.02190	0.35	.25	AB/386, 5 HZ
27	2.73	-0.05980	0.35	.25	7
28	2.58	-0.08946	0.35	.25	10
29	1.27	-0.04731	0.35	.25	ZPA
30	2.65	-0.06529	0.35	.25	5-10
31	1.92	0.0	0.35	.25	YARD, 5 HZ
32	1.84	0.0	0.35	.25	7
33	1.55	0.0	0.35	.25	10
34	1.00	0.0	0.25	.25	ZPA
35	1.72	0.0	0.35	.25	5-10
36	2.10	-0.00298	0.35	.25	INTAKE/352, 5 HZ
37	1.00	0.0	0.00	.25	RESPONSE FOR RVR & ALOCA IE
38	1.00	0.0	0.00	.25	RESPONSE FOR M- & S-LOCA IE
39	6.00	0.0	0.25	.25	PIPING RESPONSE
40	1.25	0.0	0.25	.25	RESPONSE FOR BWST

ANO-1 RESPONSE MULTIPLE FILE (REDUCED STIFFNESS CASE)

No.	F_1	F_2	β_{rr}	β_{ru}	Response
1	2.01	-0.00838	0.35	.25	RB/335, 5 HZ
2	1.95	-0.01703	0.35	.25	7
3	1.60	-0.00242	0.35	.25	10
4	1.03	-0.00817	0.35	.25	ZPA
5	1.81	-0.01242	0.35	.25	5-10
6	2.29	0.05452	0.35	.25	RB/357.5, 5 HZ
7	2.34	0.08950	0.35	.25	7
8	1.79	-0.01951	0.35	.25	10
9	1.14	0.04681	0.35	.25	ZPA
10	2.14	0.00564	0.35	.25	5-10
11	2.78	0.07667	0.35	.25	RB/401.5, 5 HZ
12	3.27	0.08508	0.35	.25	7
13	2.85	-0.12082	0.35	.25	10
14	1.50	-0.04672	0.35	.25	ZPA
15	3.14	-0.06104	0.35	.25	5-10
16	1.98	-0.01884	0.35	.25	AB/335, 5 HZ
17	1.87	-0.01168	0.35	.25	7
18	1.56	0.00401	0.35	.25	10
19	1.03	-0.01401	0.35	.25	ZPA
20	1.75	-0.01443	0.35	.25	5-10
21	2.49	0.22456	0.35	.25	AB/371, 5 HZ
22	2.82	0.29305	0.35	.25	7
23	2.30	-0.07790	0.35	.25	10
24	1.28	0.13025	0.35	.25	ZPA
25	2.62	0.08810	0.35	.25	5-10
26	2.60	0.22297	0.35	.25	AB/386, 5 HZ
27	3.06	0.26768	0.35	.25	7
28	2.58	-0.12612	0.35	.25	10
29	1.36	0.09092	0.35	.25	ZPA
30	2.87	0.05397	0.35	.25	5-10
31	1.92	0.0	0.35	.25	YARD, 5 HZ
32	1.84	0.0	0.35	.25	7
33	1.55	0.0	0.35	.25	10
34	1.00	0.0	0.25	.25	ZPA
35	1.72	0.0	0.35	.25	5-10
36	2.13	-0.00278	0.35	.25	INTAKE/352, 5 HZ
37	1.00	0.0	0.00	.25	RESPONSE FOR RVR & ALOCA IE
38	1.00	0.0	0.00	.25	RESPONSE FOR M- & S-LOCA IE
39	6.00	0.0	0.25	.25	PIPING RESPONSE
40	1.25	0.0	0.25	.25	RESPONSE FOR BWST

Boolean for S(1)

```
    Bool(1) =
SWSV-02-03-CM +
SWSV-40-41-CM +
LPRSV-CM +
BATTD07-ZBT * SWS3841-NCC +
BATTD07-ZBT * LPR1406B-VCC +
BATTD06-ZBT * SWS3803-VCC +
BATTD06-ZBT * LPR1405A-VCC +
BATTD07-ZBT * SWS3802-VCC +
BATTD06-ZBT * SWS3840-NCC +
BATTD06-ZBT * LPI1428A-NOC +
BATTD07-ZBT * LPR1415B-VOC +
BATTD07-ZBT * LPI1429B-NOC +
BATTD06-ZBT * LPR1414A-VOC +
LF-SWS-VCH4B * SWS3802-VCC +
LF-SWS-VCH4A * SWS3840-NCC +
LF-SWS-VCH4B * SWS3841-NCC +
LF-SWS-VCH4B * LPR1406B-VCC +
LF-SWS-VCH4A * SWS3803-VCC +
LF-SWS-VCH4A * LPR1405A-VCC +
LF-SWS-VCH4B * LPR1415B-VOC +
LF-SWS-VCH4B * LPI1429B-NOC +
LF-SWS-VCH4A * LPR1414A-VOC +
LF-SWS-VCH4A * LPI1428A-NOC +
DG1-GEN * SWS3841-NCC +
DG1-GEN * SWS3802-VCC +
DG2-GEN * SWS3840-NCC +
DG1-GEN * LPR1406B-VCC +
DG2-GEN * SWS3803-VCC +
DG2-GEN * LPR1405A-VCC
```

Boolean for S(2)

```
    Bool(2) =
DG1-GEN * SWS3802-VCC * HPIP36CB-PMD +
DG1-GEN * LPR1406B-VCC * HPIP36CB-PMD +
LPI1407A-VCC * B62-480VAC +
B62-480VAC * SWSOP4BA-PMD +
BATTD07-ZBT * SWS3810B-VCC * LPR1406B-VCC +
BATTD07-ZBT * SWS3810B-VCC * SWS3802-VCC +
BATTD07-ZBT * LPR1415B-VOC * SWS3810B-VCC +
LPI1407A-VCC * B62-480VAC +
LF-SWS-VCH4B * SWS3802-VCC * SWS3810B-VCC +
LF-SWS-VCH4B * LPR1406B-VCC * SWS3810B-VCC +
LF-SWS-VCH4B * LPR1415B-VOC * SWS3810B-VCC +
DG1-GEN * SWS3802-VCC * SWS3810B-VCC +
```

```
DG1-GEN * LPR1406B-VCC * SWS3810B-VCC +
DG1-GEN * LPR1415B-VOC * SWS3810B-VCC +
SWSV-02-03-CM * HPSV-CM +
LPRSV-CM * HPSV-CM +
LPSV-CM * HPSV-CM +
SWS3806A-VCC * SWS3802-VCC * SWS3810B-VCC +
LPI1407A-VCC * LPR1406B-VCC * SWS3810B-VCC +
LPI1407A-VCC * SWS3802-VCC * SWS3810B-VCC +
SWS3806A-VCC * LPR1406B-VCC * SWS3810B-VCC +
SWS3643A-VOO * SWS3802-VCC * SWS3810B-VCC +
SWS3643A-VOO * LPR1406B-VCC * SWS3810B-VCC +
SWS3806A-VCC * LPR1415B-VOC * SWS3810B-VCC +
SWS3646A-VOC * SWS3802-VCC * SWS3810B-VCC +
LPR1406B-VCC * SWS3645A-VOC * SWS3810B-VCC +
LPR1406B-VCC * SWS3644A-VOC * SWS3810B-VCC +
LPI1407A-VCC * LPR1415B-VOC * SWS3810B-VCC +
LPR1406B-VCC * SWS3646A-VOC * SWS3810B-VCC +
SWS3644A-VOC * SWS3802-VCC * SWS3810B-VCC +
SWS3645A-VOC * SWS3802-VCC * SWS3810B-VCC +
SWS3643A-VOO * LPR1415B-VOC * SWS3810B-VCC +
BATTD06-ZBT * LPR1414A-VOC * HPSV-CM +
BATTD07-ZBT * LPR1415B-VOC * HPSV-CM +
BATTD07-ZBT * SWSV-08-10-CM * LPR1415B-VOC +
LPR1415B-VOC * SWS3646A-VOC * SWS3810B-VCC +
LPR1415B-VOC * SWS3645A-VOC * SWS3810B-VCC +
LPR1415B-VOC * SWS3644A-VOC * SWS3810B-VCC +
BATTD07-ZBT * LPR1406B-VCC * HPIP36CB-PMD +
BATTD07-ZBT * SWS3802-VCC * HPIP36CB-PMD +
BATTD07-ZBT * LPR1415B-VOC * HPIP36CB-PMD
```

Boolean for S(3)

```
    Bool(3) =
B5-480VAC * B6-480VAC +
B6-480VAC * A3-4160VAC +
B6-480VAC * B51-480VAC +
B5-480VAC * A4-4160VAC +
A3-4160VAC * A4-4160VAC +
A4-4160VAC * B51-480VAC +
B5-480VAC * B61-480VAC +
A3-4160VAC * B61-480VAC +
B51-480VAC * B61-480VAC +
A3-4160VAC * B62-480VAC +
DG-CM +
SWSP-CM +
HPSIV-CM +
SWSV-06-07-CM +
SWS3824-VOC +
BATTD06-ZBT * DG1-GEN +
BATTD07-ZBT * DG2-GEN +
BATTD07-ZBT * LF-SWS-VCH4A +
```

```
BATTD06-ZBT * LF-SWS-VCH4B +
LF-SWS-VCH4A * LF-SWS-VCH4B +
LF-SWS-VCH4B * DG2-GEN +
LF-SWS-VCH4A * DG1-GEN +
BATTD06-ZBT * SWS3806A-VCC +
BATTD06-ZBT * LPI1407A-VCC +
BATTD07-ZBT * LPI1408B-VCC +
BATTD07-ZBT * SWS3807B-VCC +
BATTD06-ZBT * SWS3820A-VOO +
BATTD06-ZBT * SWS3643A-VOO +
BATTD06-ZBT * SWS3645A-VOC +
BATTD06-ZBT * SWS3644A-VOC +
BATTD07-ZBT * SWS3641B-VOC +
BATTD06-ZBT * SWS3646A-VOC +
LF-SWS-VCH4B * SWSOP4CB-PAC +
LF-SWS-VCH4A * SWSOP4BA-PAC
```

Boolean for S(4)

```
    Bool(4) =
B51-480VAC * B62-480VAC +
B5-480VAC * B62-480VAC +
HPSV-CM +
BATTD07-ZBT * SWS3810B-VCC
```

Boolean for S(5)

```
    Bool(5) =
DG1-GEN * LPIOP34B-PMD * EFWOP7AX-PTD +
DG1-GEN * EFWOP7AX-PTD * SWS3802-VCC +
DG1-GEN * EFWOP7AX-PTD * LPR1406B-VCC +
DG1-GEN * EFWOP7AX-PTD * SWS3841-NCC +
DG1-GEN * EFWOP7AX-PTD * SWS3821-VCC +
BATTD07-ZBT * EFWOP7AX-PTD * SWS3802-VCC +
BATTD07-ZBT * EFWOP7AX-PTD * LPR1406B-VCC +
BATTD07-ZBT * EFWOP7AX-PTD * SWS3841-NCC +
BATTD07-ZBT * EFWOP7AX-PTD * SWS3821-VCC +
SWSV-02-03-CM * CST-TNK +
LPRSV-CM * CST-TNK +
SWSV-21-22-CM * CST-TNK +
SWSV-40-41-CM * CST-TNK +
BATTD07-ZBT * SWS3841-NCC * EFWOOY2B-VCC +
BATTD07-ZBT * SWS3802-VCC * EFWOOY2B-VCC +
BATTD07-ZBT * SWS3821-VCC * EFWOOY2B-VCC +
BATTD07-ZBT * LPR1406B-VCC * EFWOOY2B-VCC +
BATTD06-ZBT * LPR1405A-VCC * CST-TNK +
BATTD07-ZBT * SWS3841-NCC * CST-TNK +
BATTD07-ZBT * SWS3821-VCC * CST-TNK +
BATTD06-ZBT * SWS3840-NCC * CST-TNK +
BATTD06-ZBT * SWS3822-VCC * CST-TNK +
```

```
BATTD06-ZBT * SWS3803-VCC * CST-TNK +
BATTD06-ZBT * SWS3808A-VCC * CST-TNK +
BATTD07-ZBT * SWS3802-VCC * CST-TNK +
BATTD07-ZBT * LPR1406B-VCC * CST-TNK +
BATTD07-ZBT * SWS3841-NCC * EFW2802B-VOC +
BATTD07-ZBT * SWS3802-VCC * EFW2802B-VOC +
BATTD07-ZBT * SWS3821-VCC * EFW2802B-VOC +
BATTD07-ZBT * LPR1415B-VOC * EFWOOY2B-VCC +
BATTD07-ZBT * LPR1406B-VCC * EFW2802B-VOC +
BATTD07-ZBT * LPI1429B-NOC * EFWOOY2B-VCC +
LF-SWS-VCH4B * LPIOP34B-PMD * EFWOP7AX-PTD +
LF-SWS-VCH4B * SWS3841-NCC * EFWOP7AX-PTD +
LF-SWS-VCH4B * SWS3821-VCC * EFWOP7AX-PTD +
LF-SWS-VCH4B * SWS3802-VCC * EFWOP7AX-PTD +
LF-SWS-VCH4B * LPR1406B-VCC * EFWOP7AX-PTD
```

Boolean for S(7) & T(2)

```
    Bool(6) =
BATT-CM +
CST-TNK * BWST-TNK +
A3-4160VAC * B6-480VAC * EFWOP7AX-PTD +
A3-4160VAC * A4-4[illegible]AC * EFWOP7AX-PTD +
A3-4160VAC * B61-480VAC * EFWOP7AX-PTD +
A3-4160VAC * B62-480VAC * EFWOP7AX-PTD +
B51-480VAC * B61-480VAC * CST-TNK +
B51-480VAC * B6-480VAC * CST-TNK +
B5-480VAC * B61-480VAC * CST-TNK +
B5-480VAC * B6-480VAC * CST-TNK +
A3-4160VAC * B61-480VAC * CST-TNK +
A3-4160VAC * B6-480VAC * CST-TNK +
B51-480VAC * A4-4160VAC * CST-TNK +
B51-480VAC * B62-480VAC * CST-TNK +
B5-480VAC * A4-4160VAC * CST-TNK +
B5-480VAC * B62-480VAC * CST-TNK +
A3-4160VAC * A4-4160VAC * CST-TNK +
A3-4160VAC * B62-480VAC * CST-TNK +
A3-4160VAC * B61-480VAC * EFW2802B-VOC +
A3-4160VAC * B6-480VAC * EFW2802B-VOC +
A3-4160VAC * A4-4160VAC * EFW2802B-VOC +
A3-4160VAC * B62-480VAC * EFW2802B-VOC +
A3-4160VAC * BWST-TNK * EFW2802B-VOC +
DG-CM * EFWOP7AX-PTD +
SWSP-CM * EFWOP7AX-PTD +
LF-DC-Y22DC * SWS3824-VOC * LF-DC-Y11DC +
LF-DC-Y22 * SWS3824-VOC * LF-DC-Y11 +
LF-DC-Y22DC * SWS3824-VOC * LF-DC-Y11 +
LF-DC-Y22 * SWS3824-VOC * LF-DC-Y11DC +
BATTD07-ZBT * LF-DC-Y22DC * SWS3824-VOC +
BATTD06-ZBT * SWS3824-VOC * LF-DC-Y11DC +
BATTD07-ZBT * LF-DC-Y22 * SWS3824-VOC +
```

```
BATTD06-ZBT * SWS3824-VOC * LF-DC-Y11 +
SWS3824-VOC * CST-TNK +
SWS3824-VOC * EFW2802B-VOC +
DG-CM * CST-TNK +
DG-CM * EFW2802B-VOC
```

Boolean for LPIS (1 out of 2 trains)
and WITHOUT common cutsets in Bool(4)

```
    Bool(7) =
BWST-TNK +
LOSP * BATT-CM +
LOSP * DG-CM +
B62-480VAC * LF-SWS-VCH4B +
B51-480VAC * LF-SWS-VCH4A +
A3-4160VAC * LF-SWS-VCH4A +
B5-480VAC * LF-SWS-VCH4A +
A4-4160VAC * LF-SWS-VCH4B +
B61-480VAC * LF-SWS-VCH4B +
B6-480VAC * LF-SWS-VCH4B +
LF-SWS-VCH4A * LPI1407A-VCC +
SWS3840-NCC * LF-SWS-VCH4A +
A4-4160VAC * LPI1407A-VCC +
A4-4160VAC * SWS3840-NCC +
LPI1407A-VCC * LPI1408B-VCC +
LF-SWS-VCH4B * LPI1408B-VCC +
SWS3840-NCC * LPI1408B-VCC +
B51-480VAC * LPI1408B-VCC +
A3-4160VAC * LPI1408B-VCC +
B5-480VAC * LPI1408B-VCC +
SWS3841-NCC * LPI1407A-VCC +
SWS3841-NCC * LF-SWS-VCH4B +
SWS3841-NCC * SWS3840-NCC +
B51-480VAC * SWS3841-NCC +
A3-4160VAC * SWS3841-NCC +
B5-480VAC * SWS3841-NCC +
B61-480VAC * LPI1407A-VCC +
B61-480VAC * SWS3840-NCC +
B6-480VAC * LPI1407A-VCC +
B6-480VAC * SWS3840-NCC +
B62-480VAC * SWS3643A-VOO +
LF-SWS-VCH4A * SWS3820A-VOO +
LF-SWS-VCH4A * SWS3643A-VOO +
A4-4160VAC * SWS3820A-VOO +
A4-4160VAC * SWS3643A-VOO +
LPI1408B-VCC * SWS3643A-VOO +
SWS3841-NCC * SWS3643A-VOO +
B61-480VAC * SWS3643A-VOO +
B6-480VAC * SWS3643A-VOO +
B62-480VAC * SWS3644A-VOC +
SWS3645A-VOC * LF-SWS-VCH4A +
```

```
SWS3646A-VOC * LF-SWS-VCH4A +
SWS3644A-VOC * LF-SWS-VCH4A +
LPI1428A-NOC * LF-SWS-VCH4A +
SWS3641B-VOC * SWS3820A-VOO +
SWS3641B-VOC * SWS3643A-VOO +
SWS3641B-VOC * LPI1407A-VCC +
SWS3641B-VOC * LF-SWS-VCH4B +
SWS3641B-VOC * SWS3840-NCC +
SWS3641B-VOC * SWS3645A-VOC +
SWS3641B-VOC * SWS3646A-VOC +
SWS3641B-VOC * SWS3644A-VOC +
LPI1428A-NOC * SWS3641B-VOC +
B51-480VAC * SWS3641B-VOC +
A3-4160VAC * SWS3641B-VOC +
B5-480VAC * SWS3641B-VOC +
A4-4160VAC * SWS3645A-VOC +
A4-4160VAC * SWS3646A-VOC +
A4-4160VAC * SWS3644A-VOC +
A4-4160VAC * LPI1428A-NOC +
SWS3645A-VOC * LPI1408B-VCC +
SWS3646A-VOC * LPI1408B-VCC +
SWS3644A-VOC * LPI1408B-VCC +
LPI1428A-NOC * LPI1408B-VCC +
SWS3645A-VOC * SWS3841-NCC +
SWS3646A-VOC * SWS3841-NCC +
SWS3644A-VOC * SWS3841-NCC +
LPI1428A-NOC * SWS3841-NCC +
LPI1429B-NOC * SWS3643A-VOO +
LPI1429B-NOC * LPI1407A-VCC +
LPI1429B-NOC * LF-SWS-VCH4B +
LPI1429B-NOC * SWS3840-NCC +
LPI1429B-NOC * SWS3645A-VOC +
LPI1429B-NOC * SWS3646A-VOC +
LPI1429B-NOC * SWS3644A-VOC +
LPI1428A-NOC * LPI1429B-NOC +
B51-480VAC * LPI1429B-NOC +
A3-4160VAC * LPI1429B-NOC +
B5-480VAC * LPI1429B-NOC +
B62-480VAC * SWS3645A-VOC +
B61-480VAC * SWS3645A-VOC +
B61-480VAC * SWS3646A-VOC +
B61-480VAC * SWS3644A-VOC +
B61-480VAC * LPI1428A-NOC +
B6-480VAC * SWS3645A-VOC +
B6-480VAC * SWS3646A-VOC +
B6-480VAC * SWS3644A-VOC +
B6-480VAC * LPI1428A-NOC +
B62-480VAC * SWS3646A-VOC +
SWSOP4CB-PAC * SWS3820A-VOO +
SWSOP4CB-PAC * SWS3643A-VOO +
SWSOP4CB-PAC * LPI1407A-VCC +
SWSOP4CB-PAC * SWS3840-NCC +
```

```
SWSOP4CB-PAC * SWSOP4BA-PMD +
SWSOP4CB-PAC * SWSOP4BA-PAC +
SWSOP4CB-PAC * SWS3645A-VOC +
SWSOP4CB-PAC * SWS3646A-VOC +
SWSOP4CB-PAC * SWS3644A-VOC +
LPI1428A-NOC * SWSOP4CB-PAC +
B51-480VAC * SWSOP4CB-PAC +
A3-4160VAC * SWSOP4CB-PAC +
B5-480VAC * SWSOP4CB-PAC +
SWS3641B-VOC * SWSOP4BA-PMD +
SWS3641B-VOC * SWSOP4BA-PAC +
A4-4160VAC * SWSOP4BA-PMD +
A4-4160VAC * SWSOP4BA-PAC +
SWSOP4BA-PMD * LPI1408B-VCC +
SWSOP4BA-PAC * LPI1408B-VCC +
B62-480VAC * SWSOP4BA-PAC +
SWSOP4BA-PMD * SWS3841-NCC +
SWSOP4BA-PAC * SWS3841-NCC +
LPI1429B-NOC * SWSOP4BA-PMD +
LPI1429B-NOC * SWSOP4BA-PAC +
B61-480VAC * SWSOP4BA-PMD +
B61-480VAC * SWSOP4BA-PAC +
B6-480VAC * SWSOP4BA-PMD +
B6-480VAC * SWSOP4BA-PAC +
SWSOP4BA-PMD * LF-SWS-VCH4A +
DG1-GEN * DG2-GEN * LOSP +
B51-480VAC * DG2-GEN * LOSP +
A3-4160VAC * DG2-GEN * LOSP +
B5-480VAC * DG2-GEN * LOSP +
DG1-GEN * B61-480VAC * LOSP +
DG1-GEN * A4-4160VAC * LOSP +
DG1-GEN * B6-480VAC * LOSP +
DG1-GEN * B62-480VAC * LOSP +
B51-480VAC * B62-480VAC * BATT-CM +
B5-480VAC * B62-480VAC * BATT-CM +
LOSP * BATTD07-ZBT * BATTD06-ZBT +
DG1-GEN * LOSP * BATTD06-ZBT +
B51-480VAC * LOSP * BATTD06-ZBT +
A3-4160VAC * LOSP * BATTD06-ZBT +
B5-480VAC * LOSP * BATTD06-ZBT +
DG2-GEN * LOSP * BATTD07-ZBT +
B61-480VAC * LOSP * BATTD07-ZBT +
A4-4160VAC * LOSP * BATTD07-ZBT +
B6-480VAC * LOSP * BATTD07-ZBT +
B62-480VAC * LOSP * BATTD07-ZBT +
B51-480VAC * B62-480VAC * BATTD07-ZBT +
B5-480VAC * B62-480VAC * BATTD07-ZBT +
LOSP * BATTD06-ZBT * LF-SWS-VCH4B +
DG2-GEN * LOSP * LF-SWS-VCH4B +
LOSP * BATTD07-ZBT * LF-SWS-VCH4A +
DG1-GEN * LOSP * LF-SWS-VCH4A +
LOSP * BATTD06-ZBT * LPI1407A-VCC +
```

```
    SWS3840-NCC * LOSP * BATTD06-ZBT +
    SWS3806A-VCC * LOSP * BATTD06-ZBT +
    SWS3807B-VCC * LOSP * LPI1407A-VCC +
    SWS3807B-VCC * LOSP * LF-SWS-VCH4B +
    SWS3807B-VCC * LOSP * BATTD07-ZBT +
    SWS3807B-VCC * SWS3840-NCC * LOSP +
    SWS3806A-VCC * SWS3807B-VCC * LOSP +
    DG1-GEN * SWS3807B-VCC * LOSP +
    B51-480VAC * SWS3807B-VCC * LOSP +
    A3-4160VAC * SWS3807B-VCC * LOSP +
    B5-480VAC * SWS3807B-VCC * LOSP +
    DG2-GEN * LOSP * LPI1407A-VCC +
    DG2-GEN * SWS3840-NCC * LOSP +
    SWS3806A-VCC * DG2-GEN * LOSP +
    LOSP * BATTD07-ZBT * LPI1408B-VCC +
    SWS3841-NCC * LOSP * BATTD07-ZBT +
    SWS3806A-VCC * LOSP * LPI1408B-VCC +
    SWS3806A-VCC * LOSP * LF-SWS-VCH4A +
    SWS3806A-VCC * SWS3841-NCC * LOSP +
    SWS3806A-VCC * B61-480VAC * LOSP +
    SWS3806A-VCC * A4-4160VAC * LOSP +
    SWS3806A-VCC * B6-480VAC * LOSP +
    SWS3806A-VCC * B62-480VAC * LOSP +
    DG1-GEN * LOSP * LPI1408B-VCC +
    DG1-GEN * SWS3841-NCC * LOSP +
    LOSP * BATTD06-ZBT * SWS3820A-VOO +
    LOSP * BATTD06-ZBT * SWS3643A-VOO +
    SWS3807B-VCC * LOSP * SWS3820A-VOO +
    SWS3807B-VCC * LOSP * SWS3643A-VOO +
    DG2-GEN * LOSP * SWS3820A-VOO +
    DG2-GEN * LOSP * SWS3643A-VOO


Boolean for LPIS (2 out of 2 trains)
and WITHOUT common cutsets in Bool(4)

        Bool(8) = Bool(7) +
    B61-480VAC * BATTD06-ZBT * SWS3820A-VOO +
    B61-480VAC * BATT-CM * SWS3820A-VOO +
    B6-480VAC * BATTD06-ZBT * SWS3820A-VOO +
    B6-480VAC * BATT-CM * SWS3820A-VOO


Boolean for LPIS (2 out of 2 trains)
and WITH common cutsets in Bool(4)

        Bool(9) = Bool(8) +
    A3-4160VAC * B62-480VAC +
    B51-480VAC * A4-4160VAC +
    A3-4160VAC * A4-4160VAC +
    B5-480VAC * A4-4160VAC +
    B51-480VAC * B61-480VAC +
```

```
    A3-4160VAC * B61-480VAC +
    B5-480VAC * B61-480VAC +
    B51-480VAC * B6-480VAC +
    A3-4160VAC * B6-480VAC +
    B5-480VAC * B6-480VAC +
    LF-SWS-VCH4A * LF-SWS-VCH4B +
    SWS3824-VOC +
    SWSOP4CB-PAC * LF-SWS-VCH4B +
    SWSOP4BA-PAC * LF-SWS-VCH4A



        PCS   = 8.6E-02
        X     = 3.3E-02
        AFW   = AFWS-FIT
        CFS1  = 2.0*(ACCUM-1) - ACCUM-2
        CFS2  = ACCUM-2
        RPS   = 0.0
        PBAR    = 1.0
        QBAR    = 1.0
        XBAR    = 1.0 - X
        AFWBAR  = 1.0 - AFW
        CFS1BAR = 1.0 - CFS1
        CFS2BAR = 1.0 - CFS2
        RPSBAR  = 1.0 - RPS

RVR
        ACC(1) = IE(1)

A2 LOCA
        ACC(2) = IE(2)*CFS1BAR*BOOL(9)
        ACC(3) = IE(2)*CFS1

M2 LOCA
        ACC(4) = IE(3)*RPSBAR*(1.-BOOL(4))*BOOL(8)
        ACC(5) = IE(3)*RPSBAR*BOOL(4)

M1 LOCA
        ACC(6) = IE(4)*RPSBAR*BOOL(4)

SLOCA
        ACC(7)  = IE(5)*BOOL(1)*AFWBAR
        ACC(8)  = IE(5)*BOOL(2)*XBAR*AFWBAR
        ACC(9)  = IE(5)*BOOL(3)*XBAR*AFWBAR
        ACC(10) = IE(5)*BOOL(4)*X*AFWBAR
        ACC(11) = IE(5)*BOOL(5)
        ACC(12) = IE(5)*BOOL(6)

Intake Structure  (Seal LOCA w/ Station Blackout)
        ACC(13) = IE(6)
```

```
SSLOCA
        ACC(14) = IE(7)*BOOL(1)*AFWBAR
        ACC(15) = IE(7)*BOOL(2)*XBAR*AFWBAR
        ACC(16) = IE(7)*BOOL(3)*XBAR*AFWBAR
        ACC(17) = IE(7)*BOOL(4)*X*AFWBAR
        ACC(18) = IE(7)*BOOL(5)
        ACC(19) = IE(7)*BOOL(6)

T2 TRANSIENT
        ACC(20) = IE(8)*PBAR*QBAR*BOOL(6)

T3 TRANSIENT
        ACC(21) = IE(9)*PCS*PBAR*QBAR*BOOL(6)
```

ANO-1 CROSS REFRENCE FILE

P_{random}	Basic Event	EF	N_{frag}	N_{resp}	N_{corr}	No.
0.00E+00	LOSP	3.0	1	34		1
0.00E+00	BWST-TNK	1.001	37	40		2
0.00E+00	CST-TNK	1.001	38	34		3
6.00E-05	A3-4160VAC	1.001	36	25		4
6.00E-05	A4-4160VAC	1.001	36	25		5
8.40E-05	B5-480VAC	1.001	36	25		6
3.00E-05	B51-480VAC	1.001	36	25		7
8.40E-05	B6-480VAC	1.001	36	25		8
3.00E-05	B61-480VAC	1.001	36	30		9
3.00E-05	B62-480VAC	1.001	36	30		10
1.80E-03	BATTD06-ZBT	1.001	4	24		11
1.80E-03	BATTD07-ZBT	1.001	4	24		12
4.40E-04	BATT-CM	1.001	4	24	2	13
3.80E-02	DG1-GEN	1.001	14	24		14
3.80E-02	DG2-GEN	1.001	14	24		15
1.50E-03	DG-CM	1.001	14	24	2	16
3.60E-05	EFW2802B-VOC	1.001	19	39		17
3.60E-05	EFW2902B-VOC	1.001	19	39		18
8.00E-03	EFWOOY2B-VCC	1.001	19	39		19
3.50E-02	EFWOP7AX-PTD	1.001	16	17		20
5.70E-03	HPIP36CB-PMD	1.001	16	17		21
4.00E-04	HPSIV-CM	1.001	19	39	2	22
1.00E-04	HPSV-CM	1.001	19	39	4	23
2.40E-03	LF-DC-Y11	1.001	6	25		24
1.00E-04	LF-DC-Y11DC	1.001	3	25		25
2.40E-03	LF-DC-Y22	1.001	6	25		26
1.00E-04	LF-DC-Y22DC	1.001	3	25		27
1.90E-02	LF-SWS-VCH4A	1.001	28	36		28
1.90E-02	LF-SWS-VCH4B	1.001	28	36		29
8.00E-03	LPI1407A-VCC	1.001	19	39		30
8.00E-03	LPI1408B-VCC	1.001	19	39		31
3.60E-05	LPI1428A-NOC	1.001	19	39		32
3.60E-05	LPI1429B-NOC	1.001	19	39		33
8.70E-03	LPIOP34B-PMD	1.001	16	17		34
8.00E-03	LPR1405A-VCC	1.001	19	39		35
8.00E-03	LPR1406B-VCC	1.001	19	39		36
3.60E-05	LPR1414A-VOC	1.001	19	39		37
3.60E-05	LPR1415B-VOC	1.001	19	39		38
4.00E-04	LPRSV-CM	1.001	19	39	2	39
4.00E-04	LPSV-CM	1.001	19	39	2	40
3.60E-05	SWS3641B-VOC	1.001	19	39		41
3.00E-03	SWS3643A-VOO	1.001	19	39		42
3.00E-03	SWS3644A-VOC	1.001	19	39		43
3.60E-05	SWS3645A-VOC	1.001	19	39		44
3.60E-05	SWS3646A-VOC	1.001	19	39		45
8.00E-03	SWS3802-VCC	1.001	19	39		46
8.00E-03	SWS3803-VCC	1.001	19	39		47
8.00E-03	SWS3806A-VCC	1.001	19	39		48

P_{random}	Basic Event	EF	N_{freq}	N_{resp}	N_{corr}	No.
8.00E-03	SWS3807B-VCC	1.001	19	39		49
8.00E-03	SWS3808A-VCC	1.001	19	39		50
8.00E-03	SWS3810B-VCC	1.001	19	39		51
3.00E-03	SWS3820A-VOO	1.001	19	39		52
8.00E-03	SWS3821-VCC	1.001	19	39		53
8.00E-03	SWS3822-VCC	1.001	19	39		54
3.60E-05	SWS3824-VOC	1.001	19	39		55
8.00E-03	SWS3840-NCC	1.001	19	39		56
8.00E-03	SWS3841-NCC	1.001	19	39		57
8.70E-03	SWSOP4BA-PAC	1.001	17	36		58
8.70E-03	SWSOP4BA-PMD	1.001	17	36		59
8.70E-03	SWSOP4CB-PAC	1.001	17	36		60
1.00E-05	SWSP-CM	1.001	17	36	2	61
4.00E-04	SWSV-02-03-CM	1.001	19	39	2	62
4.00E-04	SWSV-06-07-CM	1.001	19	39	2	63
4.00E-04	SWSV-08-10-CM	1.001	19	39	2	64
4.00E-04	SWSV-21-22-CM	1.001	19	39	2	65
4.00E-04	SWSV-40-41-CM	1.001	19	39	2	66
0.00E+00	IE-RVR	3.0	35	37		67
0.00E+00	IE-ALOCA	3.0	34	37		68
0.00E+00	IE-MLOCA	3.0	33	38		69
0.00E+00	IE-SLOCA	3.0	32	38		70
0.00E+00	IE-SSLOCA	3.0	31	38		71
0.00E+00	AFWS FIT	3.0	39	34		72
0.00e+00	ACCUM-1	3.0	40	4		73
0.00e+00	ACCUM-2	3.0	40	4	2	74
0.00E+00	REACTOR-BLDG	3.0	41	34		75
0.00E+00	AUX-BLDG	3.0	42	34		76
0.00E+00	INTAKE-STRCT	3.0	43	34		77

DISTRIBUTION:

U. S. Nuclear Regulatory Commission
Attn: Roger M. Kenneally
Office of Nuclear Regulatory Research
Mail Stop NL/S-217A
Washington, D.C. 20555

EQE Engineering
Attn: Alejandro P. Asfura
44 Montgomery Street, Suite 3200
San Francisco, CA 94104
(3 copies)

Internal SNL:
MS0736 N. R. Ortiz (6400)
MS0744 W. A. von Riesemann (6403)
MS0737 M. P. Bohn (6449)
MS0737 E. W. Klamerus [15] (6449)
MS0899 Technical Library [5] (7141)
MS0619 Technical Publications (7151)
MS9018 Central Technical Files (8523-2)

NRC FORM 335 (2-89) NRCM 1102, 3201, 3202

U.S. NUCLEAR REGULATORY COMMISSION

BIBLIOGRAPHIC DATA SHEET

(See instructions on the reverse)

1. REPORT NUMBER (Assigned by NRC, Add Vol., Supp., Rev., and Addendum Numbers, if any.)

NUREG/CR-5407
SAND93-0234

2. TITLE AND SUBTITLE

Assessment of the Impact of Degraded Shear Wall Stiffnesses on Seismic Plant Risk and Seismic Design Loads

3. DATE REPORT PUBLISHED

MONTH	YEAR
February	1994

4. FIN OR GRANT NUMBER

A1851

5. AUTHOR(S)

E.W. Klamerus, M.P. Bohn/ SNL

J.J. Johnston, A.P. Asfura, D.J. Doyle/ EQE

6. TYPE OF REPORT

Technical

7. PERIOD COVERED (Inclusive Dates)

8. PERFORMING ORGANIZATION – NAME AND ADDRESS (If NRC, provide Division, Office or Region, U.S. Nuclear Regulatory Commission, and mailing address; if contractor, provide name and mailing address.)

Sandia National Laboratories
Albuquerque, New Mexico 87185

Subcontractor:
EQE Engineering, Inc.
44 Montgomery Street
San Fransisco, CA 94104

9. SPONSORING ORGANIZATION – NAME AND ADDRESS (If NRC, type "Same as above"; if contractor, provide NRC Division, Office or Region, U.S. Nuclear Regulatory Commission, and mailing address.)

Division of Engineering
Office of Nuclear Regulatory Research
U.S. Nuclear Regulatory Commission
Washington, D.C. 20555

10. SUPPLEMENTARY NOTES

11. ABSTRACT (200 words or less)

Test results sponsored by the USNRC have shown that reinforced shear wall (Seismic Category I) structures exhibit stiffnesses and natural frequencies which are smaller than those calculated in the design process. The USNRC has sponsored Sandia National Labs to perform an evaluation of the effects of the reduced frequencies on several existing seismic PRAs in order to determine the seismic risk implications inherent in these test results. This report presents the results for the re-evaluation of the seismic risk for three nuclear power plants; the Peach Bottom Atomic Power Station, the Zion Nuclear Power Plant, and Arkansas Nuclear One - Unit 1 (ANO-1). Increases in core damage frequencies for seismic initiated events at Peach Bottom were 25 to 30 percent (depending on whether LLNL or EPRI hazard curves were used). At the ANO-1 site, the corresponding increases in plant risk were 10 percent (for each set of hazard curves). Finally, at Zion, there was essentially no change in the computed core damage frequency when the reduction in shear wall stiffness was included. In addition, an evaluation of deterministic "design like" structural dynamic calculations with and without the shear stiffness reductions was made. Deterministic loads calculated for these two cases typically increased on the order of 10 to 20 percent for the affected structures.

12. KEY WORDS/DESCRIPTORS (List words or phrases that will assist researchers in locating the report.)

Probabilistic Risk Assessment (PRA)
External Events
Seismic Analysis
Stiffness Reduction
Deterministic Analysis

13. AVAILABILITY STATEMENT

unlimited

14. SECURITY CLASSIFICATION

(This Page)
unclassified
(This Report)
unclassified

15. NUMBER OF PAGES

16. PRICE

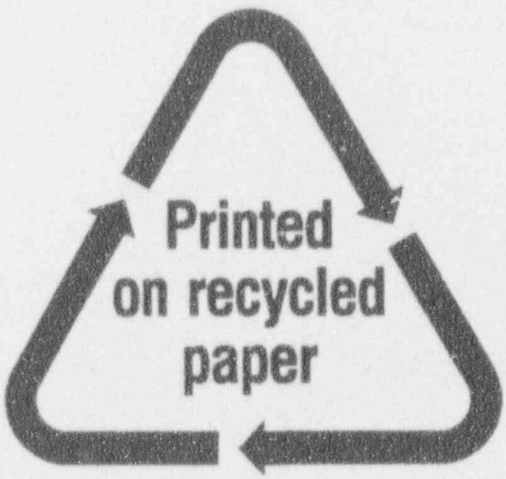

Federal Recycling Program

UNITED STATES
NUCLEAR REGULATORY COMMISSION
WASHINGTON, D.C. 20555-0001

OFFICIAL BUSINESS
PENALTY FOR PRIVATE USE, $300

SPECIAL FOURTH-CLASS RATE
POSTAGE AND FEES PAID
USNRC
PERMIT NO. G-67